The Octopaminergic Modulatory Circuitry of the *Drosophila* Larval Mushroom Body Calyx

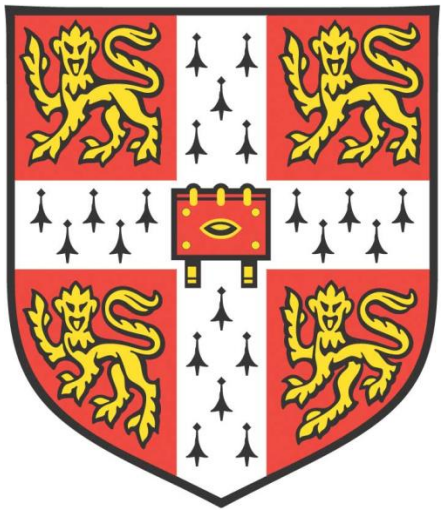

Jin Yan Hilary Wong

Fitzwilliam College

Department of Genetics

University of Cambridge

This dissertation is submitted for the degree of Doctor of Philosophy.

2018

Abstract

The Octopaminergic Modulatory Circuitry of the *Drosophila* Larval Mushroom Body Calyx

Jin Yan Hilary WONG

How are neuromodulatory networks organised to adapt sensory discrimination for different contexts? I hypothesised that neurons within a sensory circuit express different neuromodulatory receptors for differential modulation. Here I aimed to use the simple and genetically amenable *Drosophila* larval Mushroom Body (MB) calyx, a higher order processing area involved in learned odour discrimination, as a model to map octopamine (OA) neuromodulatory circuitry.

I first identified olfactory projection neurons (PNs), a GABAergic feedback neuron and cholinergic extrinsic neurons as putative postsynaptic partners to OA neurons in the MB calyx using GFP reconstitution across synaptic partners.

Next, I used novel EGFP-tagged OA receptors generated from recombination-mediated cassette exchange with MiMIC insertions in receptor genes to visualise endogenous expression patterns of OA receptors. Most notably, this is the first report of α2-adrenergic-like OA receptor localisation in any insect.

For the first time, I showed that the α1-adrenergic-like OAMB localised to PN presynaptic terminals in the calyx; while Octβ1R localised diffusely in the calyx, resembling the innervation pattern of MB neuron dendrites. I detected EGFP-tagged Octα2R and Octβ2R in some PN cell bodies but not in neuron terminals – suggesting that Octα2R and Octβ2R may be expressed in some PNs, provided the misfolded fusion proteins are retained in the cell bodies of the neurons they are normally expressed in. Furthermore, I found that Octα2R and $GABA_AR$ fusion proteins localised to OA cell bodies but not to neuronal terminals, suggesting that OA neurons are subjected to inhibition, again given that these are not artefacts of the fusion proteins.

To obtain tools to study OA modulation in the larval calyx, I then confirmed the expression patterns of driver lines that more specifically labelled calyx-innervating OA and extrinsic neurons, and tested the efficacy of three OAMB receptor knockdown lines.

This initial attempt of mapping OA receptors, while subjected to further verification and development, is consistent with my hypothesis that a single neuromodulatory source can regulate multiple neuronal types in the same circuit through the distribution of different types of neuromodulatory receptors. This provides a new perspective in how the anatomical organisation of neuromodulation within a sensory network may translate to flexible outputs.

Acknowledgements

I would like to express my sincerest gratitude to my supervisor Dr. Liria Masuda-Nakagawa for this invaluable opportunity; and her patience and guidance throughout this PhD journey. I also thank my second supervisor, Dr. Cahir O'Kane, whose sound advice has helped shape this thesis, and for generating many of the fly stocks used in this study. My thanks extend to past and present members of the Masuda-Nakagawa group, especially Angela Wan for optimising the single cell GRASP protocol and analysis used in this thesis, as well as her constant support and reassurance; and Alex McLachlan for always providing constructive feedback and for our delightful scientific discussions.

I am incredibly grateful to the *Drosophila* microinjection team at the Department of Genetics Fly Facility, especially Sang Chan, Kadri Oras and Glynnis Johnson for generating OA receptor protein traps for this study. I am also extremely thankful to Prof. Alfonso Martinez-Arias, Dr. David Turner and the Martinez-Arias group for equipment access; Dr. Nick Dzhindzhev, Dr. George Tzolovsky, Dr. Zhiang Guo, Liv Grant, Dr. Megan Oliva, Dr. Juan Jose Perez-Moreno, Dr. Sean Munro and Dr. Nadine Muschalik for protocols and reagents; as well as all the members of the Fly Facility, especially Dr. Simon Collier and Huai Xue Lin.

I thank all the members of the Department of Genetics for their help and encouragement. Special thanks to Anood, Eliška, Ali, Ayesha, Melissa, Jennifer, Yan, Ash, Alexis, Claire, Andy and Dr. Marisa Segal. I also acknowledge my advisor Prof. Steve Russell and my graduate tutor Dr. Jonathan Cullen for their generous help; and Dr. David Coomes and Mrs. Sue Free for their kindness.

I would also like to show my greatest appreciation to the Medical Research Council for funding my PhD studentship; and the Cambridge Philosophical Society and Fitzwilliam College for additional funding.

I further thank my examiners Dr. Matthias Landgraf and Prof. Kevin Moffat for taking the time to read this thesis, for a challenging viva discussion and for providing invaluable comments to this final version.

Finally, I thank my family and friends for their continuous and unconditional support through the ups and downs of my PhD experience: my parents, grandparents and sister for their love and understanding; Sylvia and Stan, for their wisdom and generosity; Francis, Timo, Kaka, Helen and Victor for general emotional support, Ján and Mischa for their boundless positivity and for believing that I could do this; and last but not least, Alessio, Yi Lei, Beth, Monica, Cat and Andrea – I couldn’t have finished without you.

Table of Contents

List of Figures

List of Tables

List of Abbreviations

A	Anterior
ACh	Acetylcholine
AL	Antennal lobe
AmOA1	*Apis mellifera* octopamine receptor 1
APL	Anterior paired lateral neuron
BDSC	Bloomington *Drosophila* Stock Center
BF	Bright field
Brp	Bruchpilot
Ca^{2+}	Calcium
cAMP	Cyclic adenosine monophosphate
CB	Cell body or cell bodies
chGFP	Chicken anti-GFP
CNS	Central nervous system
Cnx99a	Anti-calnexin99A
CPM	Centroposterior medial compartment
CREB	cAMP response element-binding protein
CS	*Canton-S*
CS-	Conditional stimulus unpaired with unconditional stimulus
CS+	Conditional stimulus paired with unconditional stimulus
D	Dorsal
DA	Dopamine or Dopaminergic
DGRC	*Drosophila* Genomics Resource Center/Kyoto Stock Center
Dlg	Discs large
dsRNA	Double stranded RNA
EGFP	Enhanced Green Fluorescent Protein
EGFP-F/R	EGFPdo-Seq-F/R
EM	Electron microscopy
ER	Endoplasmic reticulum
FLP	Flippase
FRT	Flippase recognition target
GDP	Gene Disruption Project
GRASP	GFP reconstitution across synaptic partners
HCN	Hyperpolarisation-activated, cyclic nucleotide-gated cation channel
iACT	Inner antenna-cerebral tract
K^+	Potassium
KC	Kenyon Cell
L	Lateral
L1	First instar larval
L3	Third instar larval
LB	Luria Broth
lb	Labial
LH	Lateral horn
lon	Larval optic neuropil

M	Medial
MB	Mushroom body
md	Mandibular
MiMIC	*Minos*-mediated integration cassette
MiR/L	MiMIC insertion sequences Left/Right
ML	Mushroom body medial lobe
mPN	Multiglomerular projection neuron
mx	Maxillary
N/No.	Number
NA	Noradrenaline or Noradrenergic
NA	Numerical aperture
Na^+	Sodium
N/A	Not available/applicable
NGS	Normal goat serum
NPF	Neuropeptide F
OA	Octopamine or Octopaminergic
OAMB	Octopamine receptor in mushroom bodies
Octα2R	α2-adrenergic-like octopamine receptor
OctβR	β-adrenergic-like octopamine receptors
OriF/R	Orientation-MiL-F/R
P	Posterior
PBS	Phosophate buffered saline
PBT	Phosophate buffered saline with 0.3% Triton-X
PCR	Polymerase chain reaction
PCT	Protocerebral tract neurons
Ped	Pedunculus
PKA	Protein kinase A
PKC	Protein kinase C
PN	Projection neuron
Post	Postsynaptic
Pre	Presynaptic
ratGFP	Rat anti-GFP
rbGFP	Rabbit anti-GFP
Rdl	Resistant to dieldrin ($GABA_AR$ Subunit)
RMCE	Recombinase-mediated cassette exchange
RNAi	RNA interference
SA	Splice acceptor
SD	Splice donor
S.D.	Standard deviation
S.E.M.	Standard error of the mean
shRNA	Short hairpin RNA
siRNA	Short interfering RNA
SOC	Super optimal broth with catabolite repression
SOG/SEZ	Suboesophageal ganglion/Subesophageal zone
spGFP	Split GFP
sVM	SOG ventral median
sVPM	SOG ventral paired median neuron
sVUM	SOG ventral unpaired median neuron
TA	Tyramine or Tyraminergic

Tdc	Tyrosine decarboxylase
TM	Transmembrane domain
Tβh	Tyramine beta-hydroxylase
uPN	Uniglomerular projection neuron
US	Unconditional stimulus
V	Ventral
VL	Mushroom body vertical lobe
VDRC	Vienna *Drosophila* Resource Center

Chapter 1. Introduction

1.1. Neuromodulation of higher order sensory discrimination circuits

1.1.1. Sensory discrimination in the higher brain

Animals are constantly exposed to sensory information in their environment. Therefore, they need to learn to recognise sensory cues that are biologically relevant to their survival, such as signals for food, mates or danger; and disregard other stimuli present in the background. Before an animal can learn to associate a stimulus with its appropriate valence, it must first be able to perceive the difference between two or more sensory stimuli – a process known as sensory discrimination. Sensory discrimination is also required for identifying a novel stimulus, which could signal unpredictability or danger, from previously experienced stimuli.

In order for an animal to discriminate between sensory stimuli, each stimulus must have a unique representation in the brain. Sensory stimuli are represented in the higher brain by populations of highly selective neurons which fire in response to a limited number of stimuli. Only a few neurons in the population respond to each stimulus, generating non-overlapping representations for a large number of stimuli, which allows for successful discrimination between similar cues. This is known as selective and sparse coding, and can be observed across a variety of sensory systems: from odours in the insect olfactory learning centre (Perez-Orive et al., 2002), to vocalisations in the zebra finch auditory cortex (Schneider and Woolley, 2013), and face recognition in the human medial temporal lobe (Quian Quiroga et al., 2005).

Selectivity is driven by the convergence of sensory inputs onto higher brain neurons from broadly responsive input neurons. In mammalian and insect olfactory systems, anatomical and physiological data have proposed that the spiking of a higher brain neuron requires the simultaneous activation of multiple olfactory inputs (Perez-Orive et al., 2002; Masuda-Nakagawa et al., 2005; Franks and Isaacson, 2006; Gruntman and Turner, 2013).

Inhibition is also required for maintaining neuronal selectivity and sparse coding in sensory representations. Global synaptic inhibition by odour-responsive GABAergic interneurons required to maintain sparse odour

representations is conserved in mammals and insects (Poo and Isaacson, 2009; Papadopoulou et al., 2011). In *Drosophila*, blocking such GABAergic inhibition reduces sparseness and increases overlap in odour response, resulting in impaired odour discrimination behaviour (Lin et al., 2014).

1.1.2. Context-dependent adaptation of sensory discrimination

While sparse and selective coding mechanisms allow a large number of stimuli to be represented in the higher brain, there is still a physical limit to the number of stimuli that can be differentiated. However, it is not necessary for an animal to be able to discriminate all the stimuli they encounter at all times. For example, the ability to recognise the smell of food is more important to a hungry animal than to a satiated animal. Therefore, it is important that sensory circuits can be adapted depending on the physiological state and external context of the animal.

In humans, attention and reward can enhance the ability to successfully discriminate visual, somatosensory and auditory cues (Gutnisky et al., 2009; Baldassi and Simoncini, 2011; Aton, 2013). Pairing an odour with reward allows rats to discriminate odours that they were previously unable to spontaneously discriminate, that is to recognise a novel odour from a previously habituated odour (Linster et al., 2001, 2002). Fruit flies are only able to discriminate a rewarded odour when they are starved, suggesting that sensory discrimination is also modulated by satiety states (Krashes and Waddell, 2008).

Animals are also capable of generalising their responses to a previously learned stimulus to a novel stimulus that is perceptually similar. This is important for producing the most appropriate response to a novel stimulus, and also ensures that the correct responses to learned stimuli are reproduced despite noisy backgrounds.

Whether an animal generalises or discriminates particular stimuli depends on how the stimuli are presented. This is manifested behaviourally in different associative learning tasks. When a conditional stimulus (CS+) is paired with an unconditional stimulus (US), an untrained stimulus perceptually similar to the CS+ could elicit the same response as that of the CS+, resulting in generalisation. However, when the other similar stimulus is explicitly unpaired from the reward (CS-) in a differential training task, the animal would instead

learn to discriminate between the two similar stimuli (Mishra et al., 2010; Chen et al., 2011a).

Both generalisation and discrimination behaviours can be predicted by the activation pattern of a population of highly selective neurons in the *Drosophila* learning centre (Campbell et al., 2013); but the decorrelation of odour representations only occurs in differential training tasks required for discrimination (Barth et al., 2014). This suggests the same cue could be differentially represented in the brain depending on the context it was presented in and result in alternative behavioural responses.

1.1.3. Neuromodulators confer context

Neuromodulators are chemicals that can alter neuronal excitability and synaptic strength in neural circuits. Classical neuromodulators include acetylcholine, dopamine, serotonin, noradrenaline and its insect counterpart octopamine, histamine, adenosine, and numerous neuropeptides (Brezina, 2010). Although each neuromodulatory system is associated with particular general functions, for example dopamine with reward or noradrenaline with arousal; they are in fact closely interconnected and share overlapping and/or antagonistic functions (Brezina, 2010; Sara and Bouret, 2012).

As the activity of neuromodulatory neurons varies with the internal states or external environments of the animal, they are ideal for conferring contextual information to sensory circuits. Internal signals such as arousal or satiety can change neuromodulatory activity. Mammalian noradrenergic neurons are inactive in sleep, show tonic activity in quiet wake and increase phasic firing in active wake and stressful states (Table 1.1; Rajkowski et al., 1994; Atzori et al., 2016). In *Drosophila*, dopamine levels increase in response to starvation (Inagaki et al., 2012), and this increases sugar sensitivity in starved flies (Inagaki et al., 2014). Starvation in *Drosophila* also increases expression of the short neuropeptide F receptor whose signalling mediates starvation-mediated food search behaviour (Root et al., 2011). External signals such as food, mates or stress also influence neuromodulator levels and activity. Serotonin concentration increases when female mice are interacting with male mice, or when they are placed in a mildly stressful restricted arena

Arousal State	NA Tonic Firing	NA Phasic Firing	Receptor Activation
Sleep	N/A	N/A	None
Quiet Wake	Low	High	α2-adrenoceptor
Active Wake	Intermediate	Intermediate	α1-adrenoceptor
Fight-or-Flight (Stress)	High	Low	β-adrenoceptor

Table 1.1. A model for the relationship between arousal state, noradrenergic neuron firing and receptor activation proposed in Atzori et al. (2016). The relationship between arousal state and the firing modes of noradrenergic neurons in the locus coeruleus, based on electrophysiological data from primates and rodents. State-dependent functions of noradrenaline (NA) are mediated by the concentration-dependent activation of different types of adrenoceptors.

(Hanson and Hurley, 2014). In cockroaches and locusts, octopamine concentration in the haemolymph increases in response to stressful stimuli (Davenport and Evans, 1984). Furthermore, light intensity can regulate the membrane potentials and spontaneous firing rates of *Drosophila* neurons that express the neuropeptide PDF (Sheeba et al., 2008). The wide range of contexts that can be communicated to neural circuits by various neuromodulatory systems could therefore allow animals to adapt and generate the best response under constantly changing circumstances.

1.1.4. Neuromodulation of sensory discrimination pathways

Neuromodulatory systems have widespread projections in the brain, including many sensory processing regions in the higher brain. Retrograde tracing has shown that cholinergic and noradrenergic neurons innervated the mouse primary visual, auditory and somatosensory cortices (Kim et al., 2016). Noradrenergic innervation has also been observed in the mammalian piriform cortex (Linster & Hasselmo, 2001) and amygdala (Sara & Bouret, 2012) – higher brain structures involved in olfactory processing. Moreover, the fly olfactory learning centre known as the mushroom body (MB) (Heisenberg et al., 1985; Heisenberg, 2003) is also immunoreactive for dopamine, serotonin, octopamine, and the neuropeptide sNPF (Nässel et al., 2008; Pech et al., 2013). In fact, putative synaptic contacts have been observed between intrinsic MB neurons with dopaminergic, serotonergic and octopaminergic neurons; suggesting that MB neurons are heavily subjected to neuromodulation (Pech et al., 2013).

There is also direct evidence linking neuromodulation to higher order sensory discrimination pathways. Learned odour discrimination in rats is disrupted by pharmacologically blocking muscarinic acetylcholine receptors (Fletcher and Wilson, 2002). Optogenetically inducing the release of the neuropeptide oxytocin improved the ability of rats to recognise the smell from a familiar conspecific versus a novel one (Oettl et al., 2016). The representation of tones in the rodent primary auditory cortex, and therefore auditory discrimination behaviour, can be altered by pairing tones with dopaminergic activation (Aton, 2013). In the mouse auditory thalamus, blocking adenosine

production or A1-adenosine receptor signalling can also affect cortical auditory representation and improve discrimination (Blundon et al., 2017).

In fact, a single neuromodulator, such as noradrenaline, may impair or improve discrimination in different sensory pathways. Blocking adrenoceptors in the rat anterior piriform cortex impaired odour discrimination (Shakhawat et al., 2015). In the mouse visual cortex, systemic injection of α1-adrenoceptor agonists induced long term depression in the inputs to excitatory cortical neurons, leading to impaired visual discrimination (Treviño et al., 2012). On the other hand, noradrenaline injection at the guinea pig auditory cortex improved discrimination between natural vocalisations by decorrelating firing patterns in auditory cortical neurons that had previously showed increased activity in response to noradrenaline (Gaucher and Edeline, 2015). The diverse effects of a specific neuromodulator, therefore, make it challenging to understand its functions and mechanisms.

Furthermore, much of our understanding of neuromodulation of sensory discrimination pathways has been through studying the effects of applying agonists and antagonists against neuromodulatory receptors. However, it is difficult to control spatial and temporal specificity of injected drugs to match the physiological activity of neuromodulators – which can act both tonically and phasically depending on the context, and also affect longer range targets. Moreover, there is a large heterogeneity of neuronal types in a given brain region, such that activating neuromodulatory receptors on all neurons simultaneously would obscure the neural mechanisms in which individual neurons affect the overall circuitry.

This issue of temporal specificity could be partially resolved by the activation of neuromodulatory neurons using electrophysiology and optogenetics. Electrophysiological recording and calcium imaging can also be used to monitor how neuromodulation affects neuronal activity. While these methods have been used to study individual synapses, it is still extremely challenging to generate a network-level understanding of neuromodulation in the higher brain without the knowledge of the anatomical connections or neuromodulatory targets in a sensory discrimination circuit. For this reason, little is known about how neuromodulation regulates component neurons within a sensory discrimination circuit, and how this could affect the circuit as a whole.

1.2. The Drosophila larval olfactory system as a model for sensory processing

Here I aimed to study octopamine modulation of the *Drosophila* larval olfactory pathway in order to investigate the anatomical organisation of sensory discrimination circuitry subjected to neuromodulation in the higher brain. In this section, I will first outline the model system, along with its similarities and differences to mammalian systems, followed by why it is a good model for studying sensory neuromodulation.

1.2.1. The mushroom body – the insect olfactory learning centre

The Mushroom Bodies (MBs) are higher brain sensory processing centres in insects – most well-known for their involvement in odour discrimination learning – which is impaired when the MBs are absent (Heinsenberg et al., 1985; Heisenberg, 2003). In the MBs, the sparse and selective activity of the population of intrinsic MB neurons (Kenyon Cells or KCs) is thought to maintain non-overlapping odour representations and underlie odour discrimination (Perez-Orive et al., 2002; Gruntman and Turner, 2013; Lin et al., 2014). KC dendrites receive olfactory inputs at the MB calyx, where the sparseness and selectivity of KCs is thought to be regulated (Masuda-Nakagawa et al., 2005, 2014; Lin et al., 2014). KC axons project to the MB lobes, where the convergence of CS+/CS- and US required for associative olfactory learning is thought to occur (Schwaerzel et al., 2003; Aso et al., 2014; Hige et al., 2015). The structure of the *Drosophila* larval MBs are shown in Figures 1.1 and 1.2; while the innervation pattern of fly larval KCs is shown in Figure 1.3.

The MB is often considered to be analogous to the mammalian olfactory cortex, in particular the piriform cortex, as they share anatomical and functional principles of sensory coding (Wilson and Sullivan, 2011). Odour representations in the MB and piriform cortex both rely on the sparse and distributed population response of their intrinsic neurons – KCs and pyramidal neurons respectively (Perez-Orive et al., 2002; Turner et al., 2008; Stettler and Axel, 2009). In both instances, this is facilitated by the random convergence of olfactory inputs from second order projection neurons, projection neurons in insects and mitral/tufted cells in mammals (Masuda-Nakagawa et al., 2005; Stettler and Axel, 2009; Caron et al., 2013; Gruntman and Turner, 2013). This sparse activation pattern

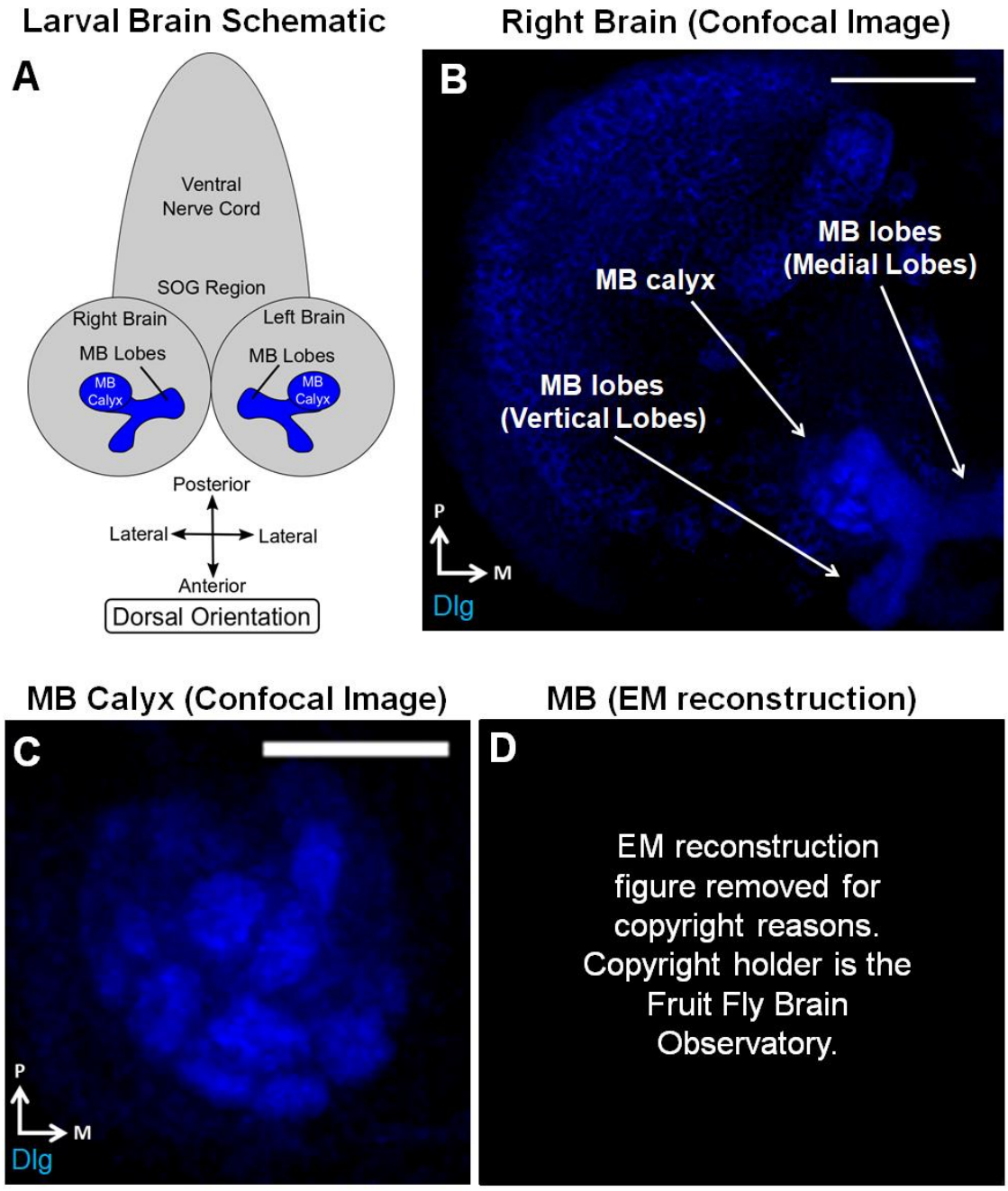

Figure 1.1. The *Drosophila* larval Mushroom Body visualised from the dorsal orientation. **(A)** Schematic of the *Drosophila* third instar larval brain visualised from the dorsal orientation. The Mushroom Bodies (MBs) are labelled and indicated in blue. **(B-C)** Confocal projection of the right third instar larval brain lobe **(B)** and MB calyx **(C)** from the dorsal orientation, where posterior (P) is up and medial (M) is right. Neuropils are labelled by anti-Discs Large (Dlg) and shown in blue. **(D)** The first instar larval MB reconstructed from electron microscopy (EM) data oriented dorsally. **Figure 1.1D** is obtained from https://neuronlp.larva.fruitflybrain.org/. Abbreviations: SOG, suboesophageal ganglion. Scale bar: 50 µm in **(B)** and 20 µm in **(C)**.

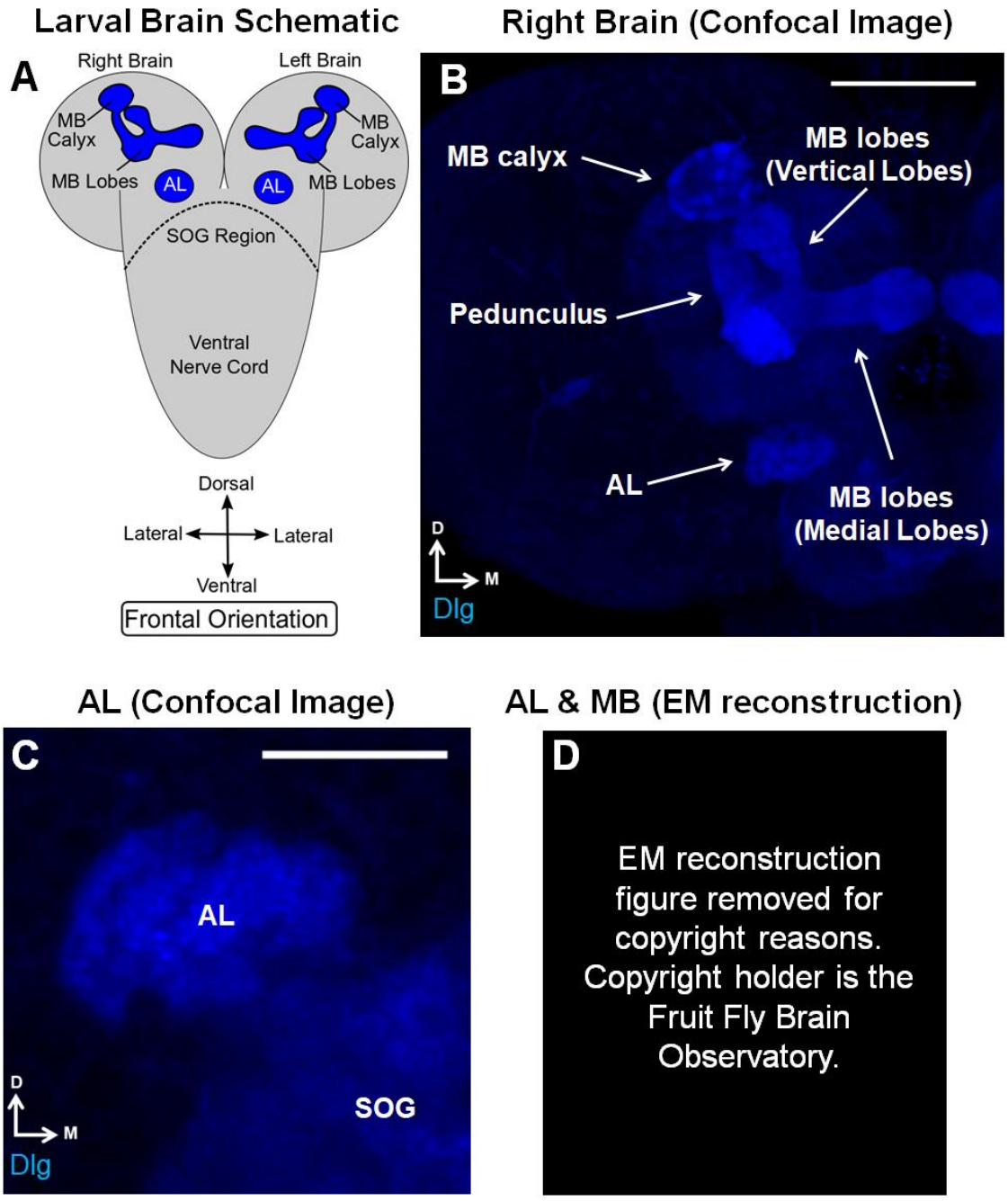

Figure 1.2. The *Drosophila* larval Mushroom Body and Antennal Lobe visualised from the frontal orientation. (A) Schematic of the *Drosophila* third instar larval brain visualised from the frontal orientation. The MBs and Antennal Lobes (ALs) are labelled and indicated in blue. **(B-C)** Confocal projection of the right third instar larval brain lobe **(B)** and AL **(C)** from the frontal orientation, where dorsal (D) is up and medial (M) is right. Neuropils are labelled by anti-Dlg and shown in blue. **(D)** The first instar larval MB and AL reconstructed from EM data oriented frontally. **Figure 1.2D** is obtained from https://neuronlp.larva.fruitflybrain.org/. Abbreviations: iACT, inner antenna-cerebral tract; SOG, suboesophageal ganglion. Scale bar: 50 μm in **(B)** and 20 μm in **(C)**.

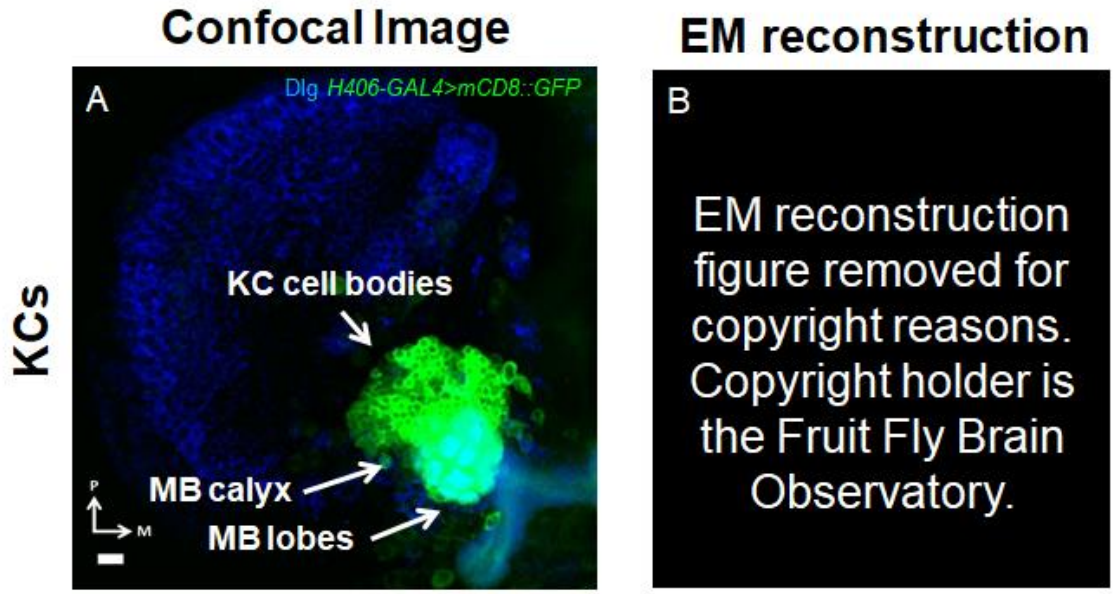

Figure 1.3. Innervation pattern of larval KCs. (A) Confocal projection of the third instar larval brain lobe oriented dorsally; where posterior (P) is up and medial (M) is right. Larval KCs are visualised using KC driver *H406-IT.GAL4>UAS-mCD8::GFP* in green, and MB neuropils are labelled by anti-Dlg in blue. Scale bar: 10 µm. **(B)** Innervation pattern of KCs in the first instar larval MB reconstructed from EM data. **Figure 1.3B** is obtained from https://neuronlp.larva.fruitflybrain.org/. Abbreviations: KC, Kenyon Cell.

is further regulated by global inhibition by GABAergic interneurons in the piriform cortex and insect MBs (Poo and Isaacson, 2009; Papadopoulou et al., 2011; Lin et al., 2014; Masuda-Nakagawa et al., 2014). Moreover, both the MB and piriform cortex receive extensive neuromodulatory inputs: most notably aminergic and peptidergic inputs to the MB; and cholinergic and noradrenergic inputs to the piriform cortex (Heuer et al., 2012; Pech et al., 2013; Linster and Cleland, 2016). On the other hand, it is unknown whether the compartmentally discrete innervation pattern of extrinsic input and output neurons observed in the MB (Aso et al., 2014) applies to the mammalian olfactory cortex. However, this may be due to the lack of tools for distinguishing individual neuronal types in mammalian cortices, as opposed to the tools currently available to study the fly MBs. Nevertheless, the shared coding principles with the mammalian olfactory cortex suggest that the insect MB may be a useful model for studying principles of the broad anatomical principles of neuromodulation in sensory circuitries.

1.2.2. The *Drosophila* larval olfactory pathway

While the MBs are integral to olfactory learning in both adults and larval *Drosophila* (Heisenberg et al., 1985), the number of KCs in *Drosophila* – around 2,500 in adults and 600 in larvae – is considerably lower than that of other insects, for example 170,000 in honeybees and 200,000 in cockroaches (Heisenberg, 2003; Ramaekers et al., 2005). The numerical simplicity of the fruit fly MB, together with the extensive genetic tools available for its manipulation (Section 1.2.8), are the main reasons why the *Drosophila* olfactory pathway is such an attractive model system.

In addition to the conserved coding principles between the fly MB and the mammalian olfactory cortex discussed above, the olfactory pathway in the fly adult and larvae also share a similar architecture to that of the mammalian olfactory system (Fig. 1.4; Tanaka et al., 2004; Ramaekers et al., 2005):

In fly larvae, odours are first detected by 21 olfactory sensory neurons at the dorsal organ. This is analogous to the peripheral detection of odours at the olfactory epithelium in mammals and the antenna in fly adults. Each olfactory sensory neuron expresses a single type of odour receptor, and projects to a

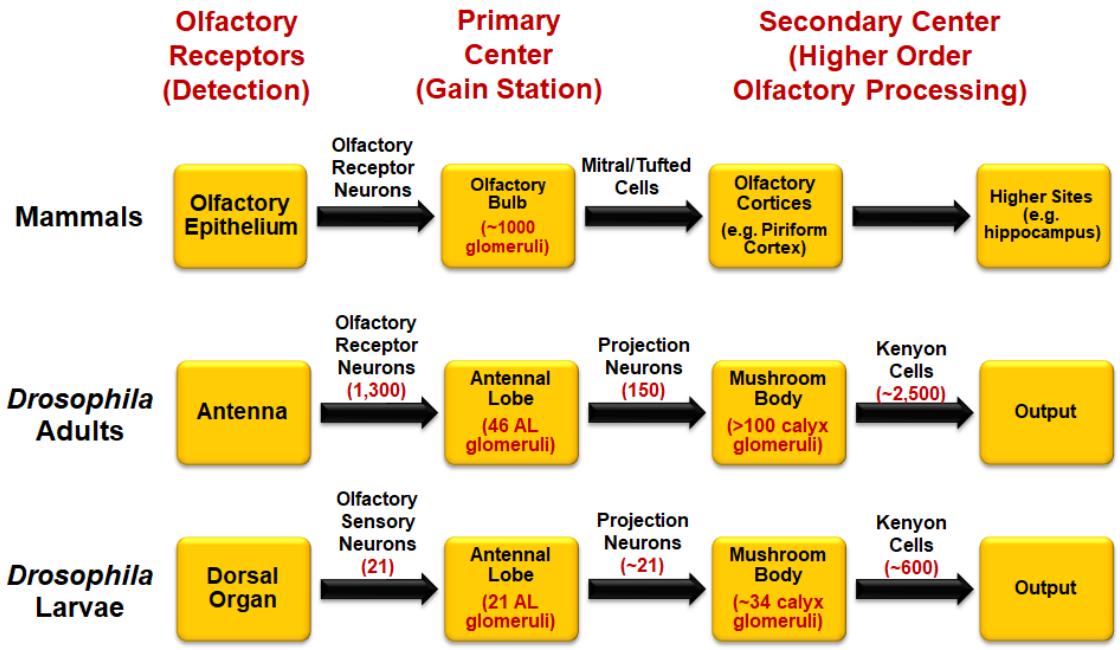

Figure 1.4. Mammals, *Drosophila* adults and larvae share a conserved pathway for odour recognition. Odours are first detected by olfactory receptors on olfactory receptor neurons in the periphery. Olfactory information from the same type of olfactory receptors converges at glomeruli in the primary olfactory center, and then delivered to secondary and higher olfactory processing regions by projection neurons. Estimated numbers of neurons and glomeruli involved at each step shown in brackets. Figure redrawn from data in Ramaekers et al. (2005) and Masuda-Nakagawa et al. (2005).

single glomerulus in the Antennal Lobe (AL) – the primary olfactory centre analogous to the mammalian olfactory bulb. Larval olfactory projection neurons (PNs), analogous to mitral/tufted cells, then carry olfactory information from a single AL glomerulus to 1-2 glomeruli in the MB calyx stereotypically (Fig. 1.5A-B). KCs integrate information from multiple PNs by sending dendrites to around 6 calyx glomeruli non-stereotypically (Masuda-Nakagawa et al., 2005, 2009). This is comparable to the convergence of olfactory inputs from mitral/tufted cells to pyramidal neurons in the piriform cortex (Stettler and Axel, 2009). Moreover, a single GABAergic APL neuron activated by KC output at the MB lobes sends feedback inhibition to KC dendrites at the MB calyx (Fig. 1.5C-D; Lin et al., 2014; Masuda-Nakagawa et al., 2014). This feedback inhibition motif is also observed in GABAergic interneurons in the piriform cortex (Poo and Isaacson, 2009). This suggests that many features of the olfactory pathway are conserved between mammals and *Drosophila* larvae.

Besides KCs, PNs and the GABAergic APL neuron, the larval MB calyx is also innervated by cholinergic MB output neurons known as Odd/Odd-like neurons discussed below (Slater et al., 2015) and neuromodulatory octopaminergic (OA) neurons discussed in the following section (Honjo and Furukubo-Tokunaga, 2009; Selcho et al., 2014).

Clonal analysis revealed that there are 2 or 3 calyx-innervating Odd neurons, all of which have cell bodies located dorso-posterior to the calyx and innervate the centroposterior medial compartment (CPM) – a neuropil surrounding the MB lobes (Fig. 1.5E-F; Slater et al., 2015). Odd neurons are postsynaptic in the larval MB calyx, appear to form putative synapses with PNs, and are involved in odour intensity discrimination (Slater et al., 2015). However, as the *Odd-GAL4* line used in Slater et al. (2015) labels many KCs in addition to Odd neurons (L. Masuda-Nakagawa, personal communication), it is unclear whether the putative synapses with PNs and the olfactory behaviours observed are attributed to Odd neurons or KCs. Odd-like neurons labelled in the *OK263-GAL4* driver are similar in morphology and innervation pattern to Odd neurons (Slater et al., 2015; M.T., Part II Report 2015; L. Masuda-Nakagawa, personal communication). Therefore, neurons that show similar morphology and innervation to Odd neurons are described as Odd-like neurons in this study.

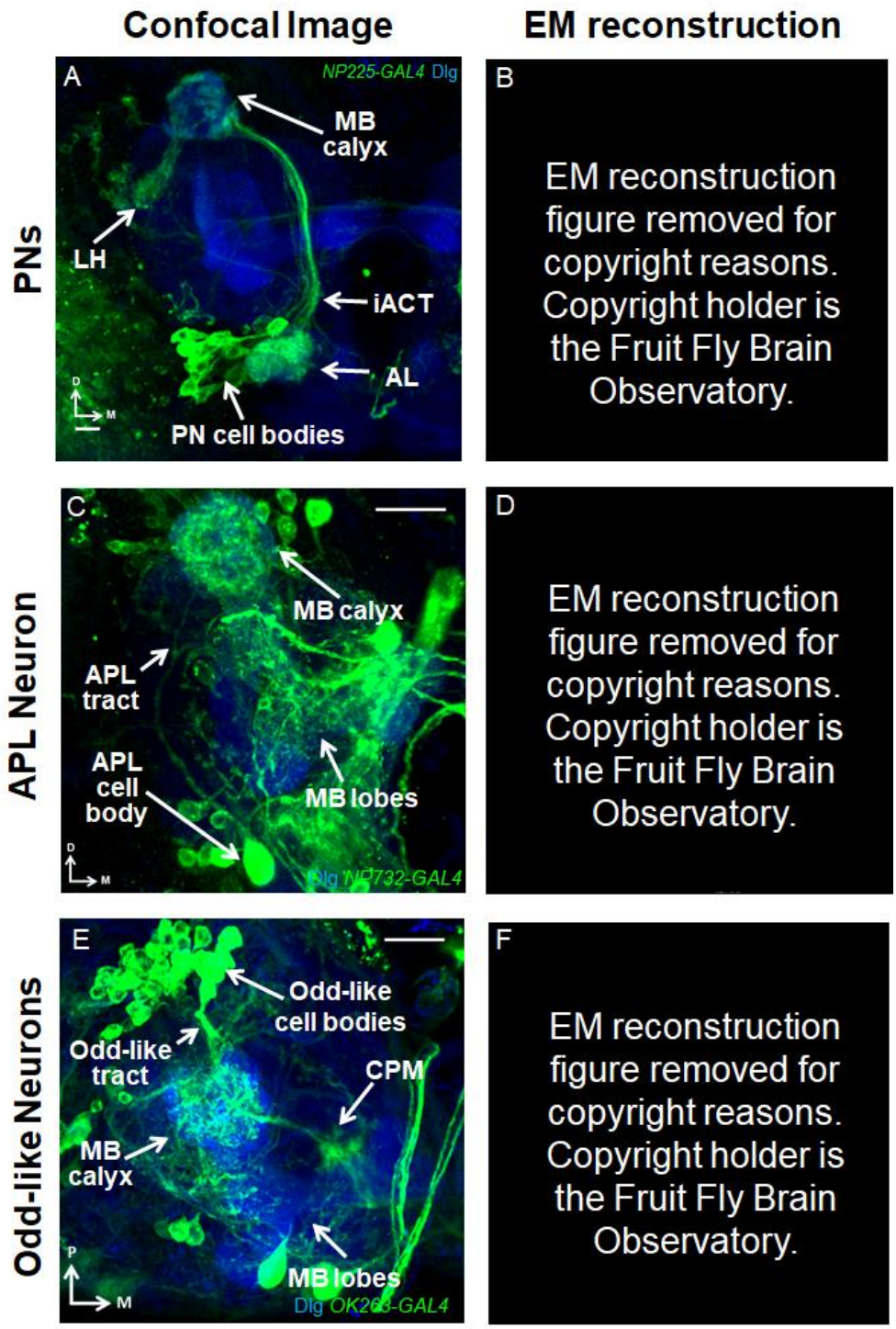

Figure 1.5. Innervation patterns of PNs, the APL neuron and Odd-like neurons in the larval brain. (A,C,E) Confocal projections of the third instar larval brain lobe. Neuropils labelled by anti-Dlg is blue. Medial (M) is right; dorsal (D) is up for **(A,C)** and posterior (P) is up for **(E)**. **(A)** A subset of PNs labelled by *NP225-GAL4* (green) innervating the Antennal Lobe (AL), the MB calyx via the inner antenna-cerebral tract (iACT), and the lateral horn (LH) which is associated with innate olfactory behaviour. **(C)** The APL neuron labelled in *NP732-GAL4* (green) innervates the MB calyx and lobes. **(E)** Odd-like neurons labelled by *OK263-GAL4* (green) innervate the MB calyx and the centroposterior medial compartment (CPM), a neuropil around the MB lobes. **(B,D,F)** Innervation patterns of a subset of PNs **(B)**, the APL neuron **(D)** and Odd-like neurons **(F)** in the first instar larval MB reconstructed from EM data. **Figure 1.5E** was imaged from a sample prepared by Magdalene Ting. **Figures 1.5B,D,F** are obtained from https://neuronlp.larva.fruitflybrain.org/. Scale bar: 10 μm for **(A)**, 50 μm for **(C,E)**.

1.2.3. OA neurons in the larval MB calyx

Like other higher sensory processing centres, the larval MB calyx is subjected to neuromodulatory inputs. While the adult calyx shows immunoreactivity to octopamine, dopamine, serotonin and neuropeptide sNPF (Nässel et al., 2008; Pech et al., 2013), the larval MB calyx appears to only receive octopaminergic and peptidergic neuromodulatory innervation (Nässel et al., 2008; Honjo and Furukubo-Tokunaga, 2009; Selcho et al., 2014). As the larval MB calyx shows little immunoreactivity against serotonin (Huser et al., 2012), no innervation of dopaminergic neurons labelled by *TH-GAL4* (Honjo and Furukubo-Tokunaga, 2009) or other *GAL4* lines labelling dopaminergic pPAM neurons (Rohwedder et al., 2016); OA neurons are most likely the main source of aminergic neuromodulation in the larval MB calyx.

Not only is OA innervation of the MB calyx conserved between adult and larval *Drosophila*, it is conserved across insects, including in honeybees, locusts, blowflies, cockroaches and moths (Bräunig and Burrows, 2004; Dacks et al., 2005; Sinakevitch et al., 2005; Sinakevitch and Strausfeld, 2006; Selcho et al., 2014). This suggests a functionally conserved role for OA neuromodulation of the MB calyx circuitry. Yet, it is still unclear what the functions and mechanisms of OA neuromodulation are in the MB calyx, and how this in turn affects odour discrimination.

OA innervation of the larval MB calyx was first observed using the *Tdc2-GAL4* line, which labels OA- and tyramine (TA)-positive neurons in the *Drosophila* brain (Cole et al., 2005; Busch et al., 2009; Honjo and Furukubo-Tokunaga, 2009). I have previously confirmed that the *Tdc2* processes innervating the larval calyx are immunoreactive against OA (Fig. 1.6A-C; H.W., MPhil Thesis 2014). This suggested that the neuromodulator OA is released in the larval MB calyx.

Clonal analysis has since revealed two types of OA neurons innervating the larval MB calyx – sVUMmd1 and sVUMmx1 neurons – collectively known as the sVUM1 neurons (Selcho et al., 2014). sVUM1 cell bodies are located at the ventral median of the suboesophageal ganglion (SOG) region (also known as the subesophageal zone, SEZ), where sVUMmd1 is in the mandibular (md)

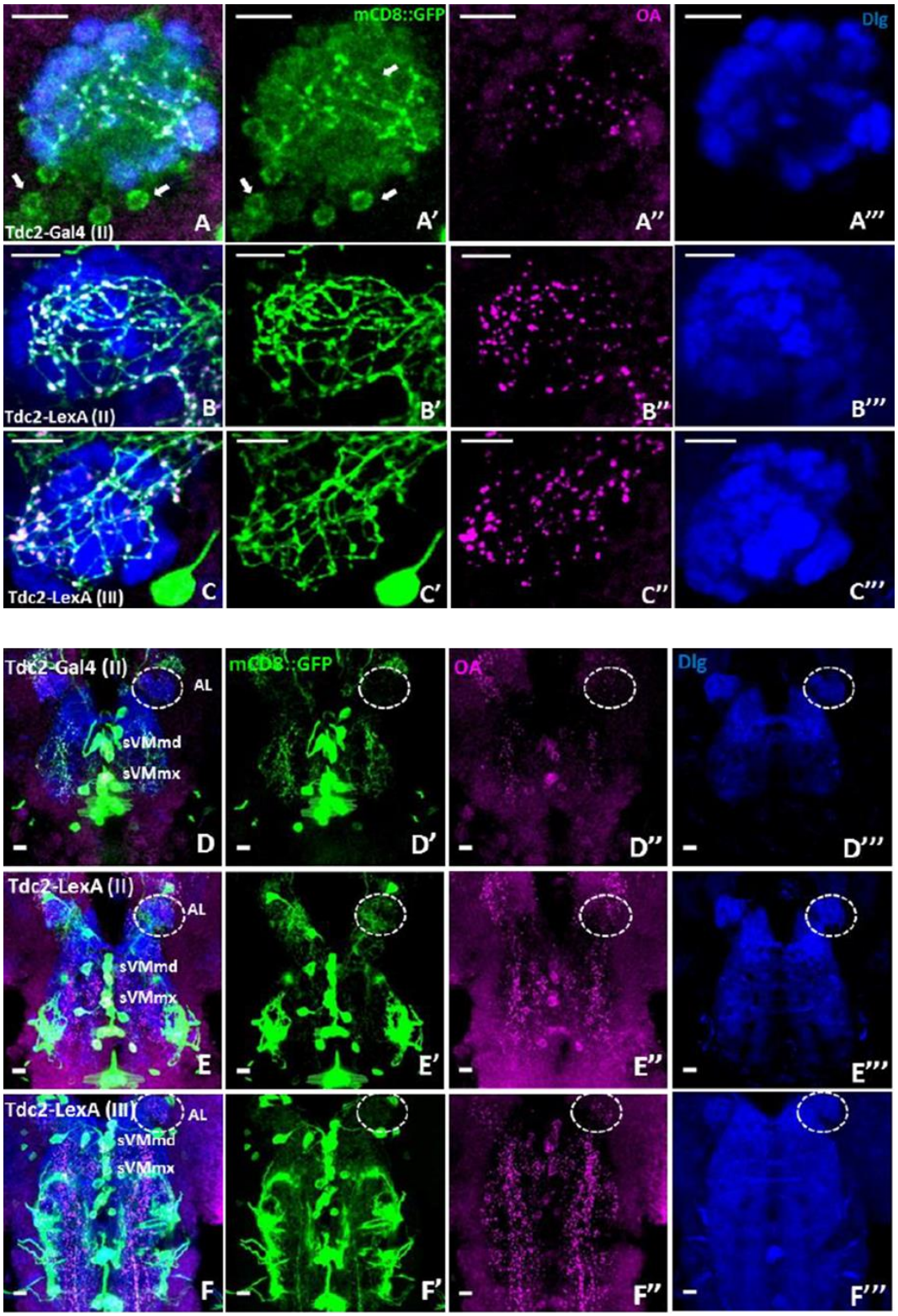

Figure 1.6. Calyx-innervating OA neurons and their cell body location in the larval brain. mCD8::GFP driven by *Tdc2-GAL4* or *Tdc2-LexA* is green, anti-OA is magenta and anti-Dlg is blue. **(A,D)** *Tdc2-GAL4>UAS-mCD8::GFP*, **(B,E)** *Tdc2-LexA(II)>LexAOp-mCD8::GFP* and **(C,F)** *Tdc2-LexA(III)>LexAOp-mCD8::GFP*. **(A-C)** are confocal projections of the calyx, where medial is right and anterior is up. Arrows indicate KC cell bodies. **(D-F)** are confocal projections of the ventral SOG, where anterior is up and medial is at the vertical midline. SOG ventral median mandibular (sVMmd) and SOG ventral median maxillary (sVMmx) cell body clusters, and Antennal Lobe (AL) as labelled. Scale bar: 10 µm. From Fig. 14 in H.W., MPhil Thesis (2014).

cluster and sVUMmx1 is in the maxillary (mx) cluster (Fig. 1.6D-F; Selcho et al., 2014). In addition to the MB calyx, sVUM1 neurons also innervate the AL and the SOG (Selcho et al., 2014). The innervation pattern of the sVUM1 neurons is shown in Fig. 1.7. Electron microscopy (EM) reconstruction data show that sVUMmd1 and sVUMmx1 (named OAN-a1 and OAN-a2 respectively) have non-overlapping innervation patterns in the first instar larval (L1) MB calyx (Fig. 1.7D; Eichler et al., 2017; https://neuronlp.larva.fruitflybrain.org/). However, it is unknown whether sVUMmd1 and sVUMmx1 are functionally equivalent.

Tdc2 processes colocalise with postsynaptic markers at the SOG region, but predominantly colocalise with presynaptic markers in the calyx (H.W., L.M.N., unpublished). This suggests that sVUM1 neurons receive inputs at the SOG region, where the primary gustatory centre is located (Colomb et al., 2007); and send outputs to modulate the calyx. This is in agreement with the presynaptic terminals of sVUM1 neurons observed in the L1 calyx using EM (Eichler et al., 2017). EM data also revealed that sVUM1 neurons contained both small clear vesicles and dense core vesicles in their L1 calyx terminals – suggesting that sVUM1 neurons may release OA or possible co-transmitters both synaptically and via volume transmission (Eichler et al., 2017). On the other hand, it is unclear whether sVUM1 neurons are pre- and/or post-synaptic in the AL. While both pre- and post-synaptic markers are observed at the AL (H.W., L.M.N., unpublished), the *Tdc2-GAL4* line used to assess polarity labels tyraminergic lAL neurons as well as the sVUM1 neurons in the AL (Selcho et al., 2014).

The OA-VUMa2 neurons in adult flies and the VUMmx neurons in honeybees share the same innervation pattern as larval sVUM1 neurons (Hammer, 1993; Kreissl et al., 1994; Hammer and Menzel, 1998; Busch et al., 2009). This suggests that these neurons may have conserved functions in olfactory processing in the MB calyx – possibly in olfactory rewarding learning, in which honeybee VUMmx neurons are involved in (Hammer, 1993; Hammer and Menzel, 1998).

1.2.4. Connectivity of OA neurons in the larval MB calyx

To identify the potential synaptic partners of sVUM1 neurons in the calyx, I

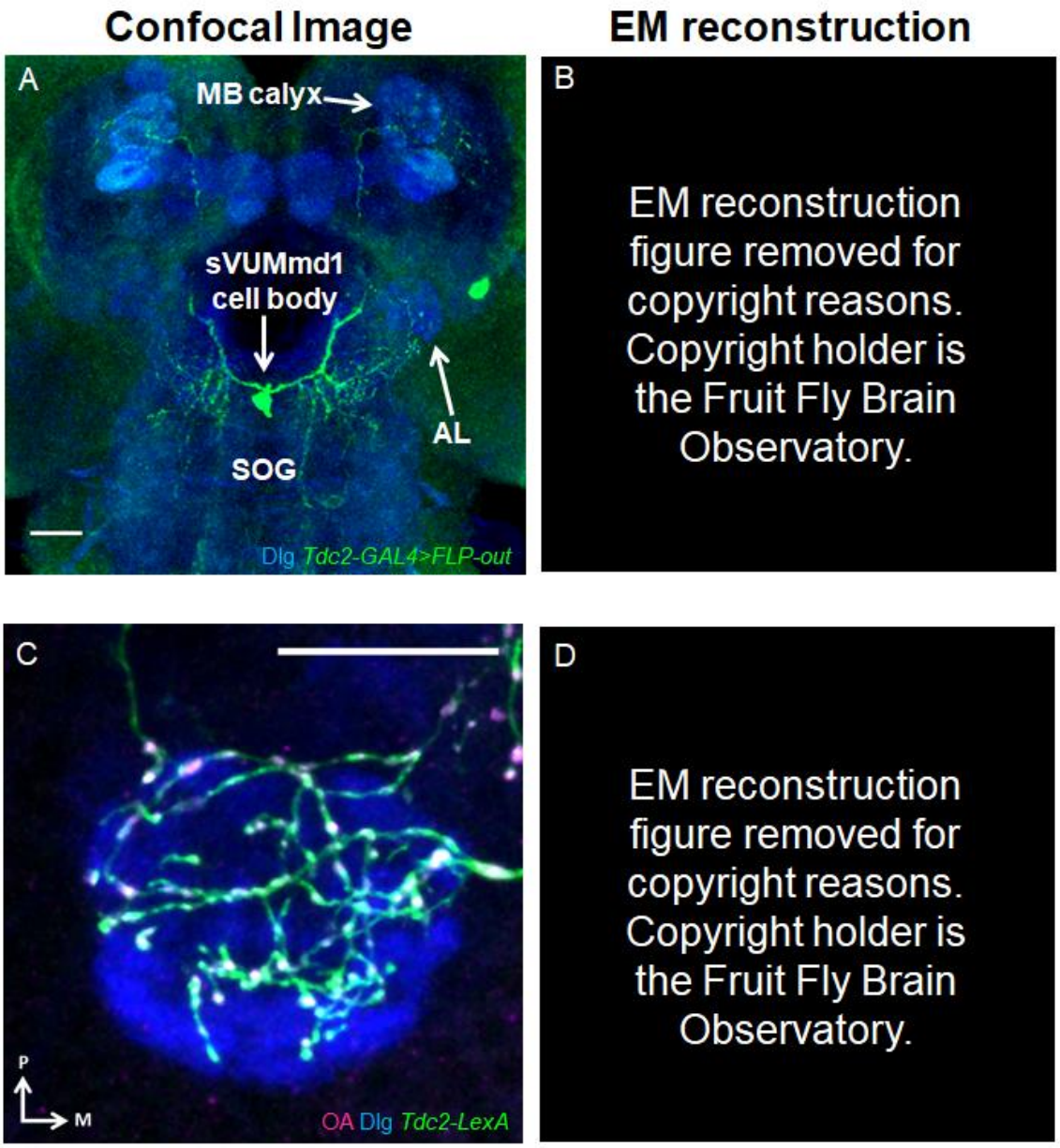

Figure 1.7. Innervation pattern of octopaminergic sVUM1 neurons in the larval brain. (A) Confocal projection of the third instar larval brain lobe and SOG oriented ventrally; where anterior is up and medial is at the vertical mid-line. A sVUM1 neuron clone is visualised using *Tdc2-GAL4>FLP-out* in green. Anti-Dlg is blue. **(C)** Confocal projection of the dorsal MB calyx, where posterior (P) is up and medial (M) is right. sVUM1 neurons are labelled by *Tdc2-LexA* (green), anti-OA is magenta and anti-Dlg is blue. **(B,D)** Innervation pattern of sVUM1 neurons – sVUMmd1 (blue) and sVUMmx1 (green) in the first instar larval brain **(B)** and MB calyx **(D)** reconstructed from EM data. **Figures 1.7B,D** are obtained from https://neuronlp.larva.fruitflybrain.org/. Scale bar: 20 μm. Abbreviations: AL, antennal lobe; SOG, suboesophageal ganglion.

previously conducted GFP reconstitution across synaptic partners (GRASP) (Gordon and Scott, 2009) as part of my MPhil Thesis. I found that while sVUM1 neurons had very few synaptic connections with KCs, there were putative synaptic connections between sVUM1 neurons and PNs, the APL neuron, and Odd-like neurons (Fig. 1.8; H.W., MPhil Thesis 2014). Using the single cell GRASP method (Karuppudurai et al., 2014) to isolate GRASP signals from neuronal clones, my colleague additionally found that sVUMmd1 and sVUMmx1 neurons both individually formed putative synapses with Odd-like neurons (A.W., MPhil Thesis 2015). This suggested that OA signalling from sVUM1 neurons modulate PNs, the APL neuron and Odd-like neurons in the calyx circuitry. As PNs and the APL neuron synapse with KCs (Masuda-Nakagawa et al., 2014), sVUM1 signalling may be indirectly modulating odour representations in KCs via these two types of neurons.

Interestingly, the limited GRASP connections observed between KCs and sVUM1 neurons in the larval calyx is contrary to the dense GRASP signals observed between KCs and OA neurons in the adult MB calyx (Zhou et al., 2012; Pech et al., 2013). Moreover, EM data from the first instar larva indicated that there were synaptic connections between KCs and sVUM1 neurons (Eichler et al., 2017), most likely in the L1 calyx – the only neuropil both KCs and sVUM1 neurons innervate. Therefore, it is unclear whether the limited GRASP between KCs and sVUM1 neurons in the third instar larval (L3) calyx is a developmental anomaly or an experimental artefact. On the other hand, sVUM1 connectivity with Odd-like neurons is consistent with L1 EM data (Eichler et al., 2017; Https://neuronlp.larva.fruitflybrain.org/); although connections between sVUM1 neurons and non-KC calyx-innervating neurons have not been explicitly explored in the L1 or adult calyx.

It is also unclear how neuromodulatory neurons are connected in mammalian sensory cortices, such as the piriform cortex. The connectivity of sVUM1 neurons with multiple potential synaptic partners in the larval MB calyx suggests that neuromodulation may affect a heterogeneous population of interconnected cortical neurons, which will have consequences in our understanding of the neuromodulatory circuitry and output. However, different types of cortical neurons cannot be easily identified or manipulated currently.

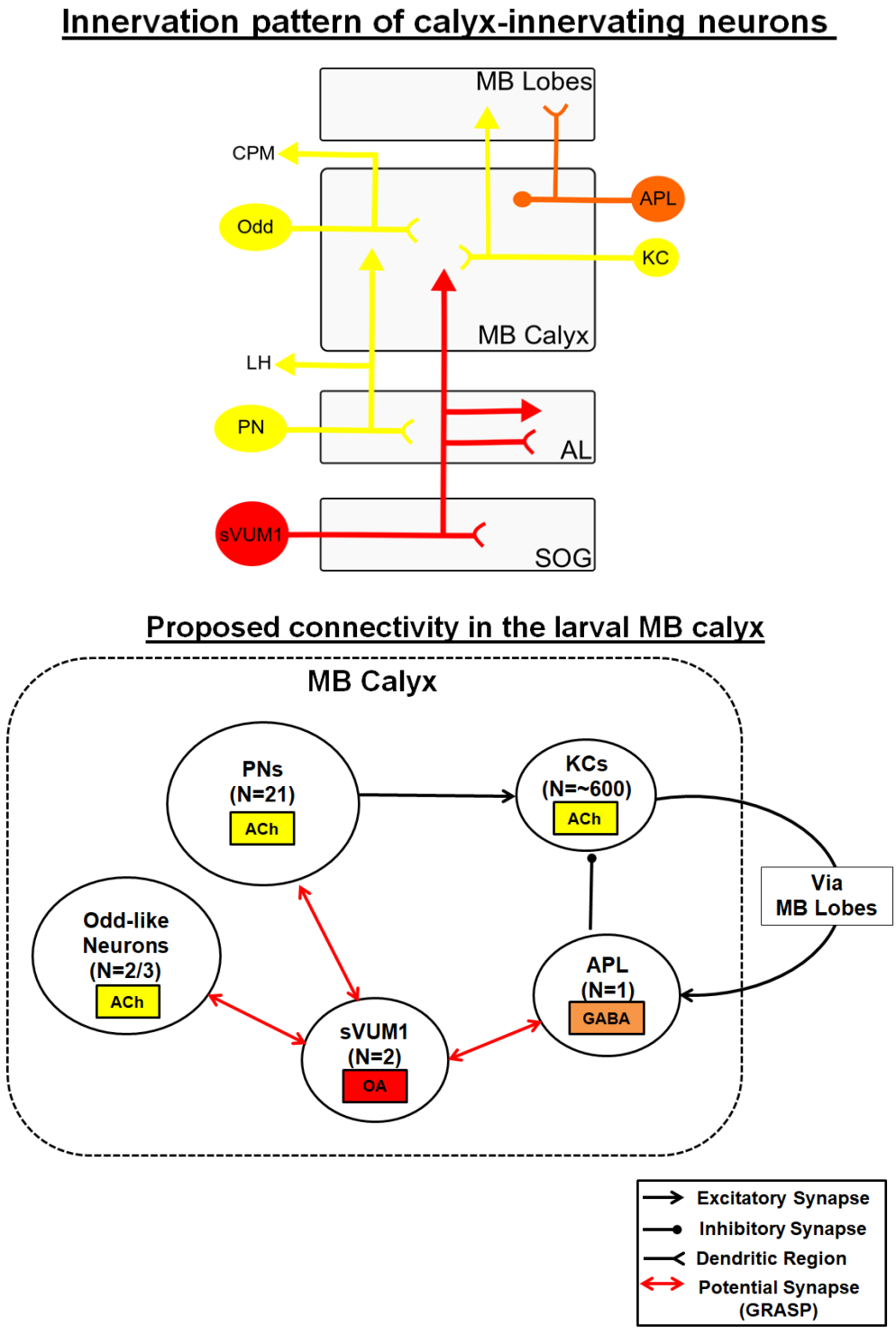

Figure 1.8. **Calyx-innervating neurons and their connectivity in the larval MB calyx.** Summary schematic of the known innervation patterns and connectivity of calyx-innervating neurons in the larval MB calyx based on data from Masuda-Nakagawa et al., 2005, 2014; Selcho et al., 2014; Slater et al., 2015; Barnstedt et al., 2016; H.W., MPhil Thesis 2014. Putative synapses identified using GRASP (H.W., MPhil Thesis 2014) are indicated with double-ended arrows as the direction of neurotransmission is unknown. Approximate numbers of each neuronal type are as indicated. Main neurotransmitter for each neuronal type are as labelled: Acetylcholine (ACh) in yellow, GABA in orange and OA in red. Abbreviations: AL, antennal lobe; CPM, centroposterior medial compartment; KC, Kenyon Cell; LH, lateral horn; MB, mushroom body; N, number; OA, octopamine; PN, projection neuron.

This is why understanding neuromodulatory networks in a well-characterised and simpler model like the *Drosophila* larval MB calyx may be beneficial.

1.2.5. Towards an OA neuromodulatory connectome in the larval MB calyx

While GRASP and EM data are useful in studying connectivity in the larval MB calyx, they are not without limitations. GRASP can only be used to detect membrane contacts but not actual synapses. Moreover, the direction of neurotransmission is not specified at GRASP contacts. Therefore, it is unclear whether potential synaptic partners identified in this method are indeed subjected to OA signalling by sVUM1 neurons, or are in fact providing inputs to the sVUM1 neurons. There are slightly more information collected using EM data; which can reveal the location of pre- and post-synapses as well as that of dense core vesicles which are related to volume transmission (Meinertzhagen and Lee, 2012). However, the process of obtaining EM data is difficult, labour-intensive and time-consuming. For example, the current data we have on the L1 connectivity are obtained from a single larva (Berck et al., 2016; Eichler et al., 2017). Therefore, it is unclear whether the connectivity obtained can be replicated and thus representative of the L1 brain. There are also other reasons why synaptic connectivity data may still be insufficient in mapping the OA neuromodulatory circuitry in the MB calyx.

sVUM1 neurons display immunoreactivity to both OA and its precursor TA (Selcho et al., 2014), which itself is a neurotransmitter that has been shown to modulate larval locomotion (Saraswati et al., 2004). OA neurons also contain large dense core vesicles (Grygoruk et al., 2014; Eichler et al., 2017), traditionally associated with neuropeptide co-transmission (Karhunen et al., 2001; Nässel, 2009). As OA neurons in locusts co-label with FMFRamide and locustatachykinin-related peptides (Stevenson and Pflüger, 1994; Vitzthum and Homberg, 1998), this suggests that OA neurons in *Drosophila* may also co-release neuropeptides. Hence, even if synapses are observed between sVUM1 neurons and their postsynaptic partners, it is possible that these neurons may be modulated by other neurotransmitters co-released by sVUM1 neurons such as TA or neuropeptides rather than OA.

Synaptic connectivity is also unable to reflect the potential extrasynaptic signalling of neuromodulators (Agnati et al., 1995; Brezina, 2010). Extrasynaptic

release sites and receptors have been observed for various neuromodulators (Trueta and De-Miguel, 2012). A diffusion model for dopamine in the substantia nigra pars compacta and striatum proposed that dopamine can act on receptors 2-8 μm from its release site (Rice and Cragg, 2008); suggesting that neuromodulators are capable of long-range diffusion to reach non-synaptic targets. While extrasynaptic OA transmission in *Drosophila* has not yet been studied, extrasynaptic OA receptors in *C.elegans* (Bentley et al., 2016) and extrasynaptic NA varicosities in the mammalian cortices (Descarries et al., 1977) have been well-documented. Additionally, OA can persist and travel for long distances as a neurohormone in the extracellular fluid of other insects (Goosey and Candy, 1980; Adamo et al., 1995). Feeding OA to *Tβh* mutant flies defective in OA synthesis can also rescue impaired olfactory reward learning (Schwaerzel et al., 2003), suggesting that ingested OA can travel long distances to reach its brain targets. The large dense core vesicles in *Drosophila* OA neurons express the vesicular monoamine VMAT (Grygoruk et al., 2014), which suggests that OA may also be loaded into dense core vesicles. Dense core vesicles are associated with extrasynaptic release, as EM data show that they are often localised outside of active zones (Zhu et al., 1986; Karhunen et al., 2001; Trueta and De-Miguel, 2012). This is supported by EM observations which show that sVUM1 terminals in the L1 calyx have both clear vesicles associated with synaptic transmission, as well as dense core vesicles associated with volume transmission (Eichler et al., 2017). Together, this suggests that OA may be released extrasynaptically via dense core vesicles. Thus, OA in the calyx may be able to diffuse to and act on neurons that do not synapse with sVUM1 neurons.

Another characteristic of neuromodulation that cannot be revealed through synaptic connectivity is that a single neuromodulator is able to activate multiple types of neuromodulatory receptors – which are usually G-protein coupled receptors. For example, noradrenergic activation of β-adrenoceptors increases intracellular cAMP, while activating α2-adrenoceptors decreases cAMP levels. Therefore, the expression of β-adrenoceptors versus α2-adrenoceptors would result in different, or even antagonising, effects on neuronal and synaptic activity (Hein et al., 1999; Marzo et al., 2009).

Therefore, to fully understand the anatomical organisation of the calyx OA neuromodulatory circuitry, it is not only necessary to confirm synaptic connectivity, but also to map all the possible OA receptors on calyx-innervating neurons to determine potential targets of sVUM1 signalling.

1.2.6. *Drosophila* as a model organism

The fruit fly *Drosophila melanogaster* is a well-established model organism for studying sensory neuromodulation (Taghert and Nitabach, 2012; Kim et al., 2017; Sayin et al., 2018). As laboratory animals, they are small, cheap, easy to maintain and can reproduce in large numbers within a short time period. While the fly brain is thought to contain a million-fold fewer neurons than the human brain (Venken et al., 2011b), flies are still capable of displaying complex cognitive behaviours, most notably the ability to learn and form associative memories (Heisenberg et al., 1985). The *Drosophila* olfactory learning pathway has been particularly well-characterised (Schwaerzel et al., 2003; Burke et al., 2012); especially in our understanding of how dopaminergic neuromodulation in the fly olfactory learning centre facilitates innate and learned olfactory behaviours (Cohn et al., 2015; Hige et al., 2015; Aso and Rubin, 2016). Neuromodulation of other behaviours, such as feeding, locomotion, courtship and aggression, have also been extensively studied in fruit flies (Andrews et al., 2014; Inagaki et al., 2014; Yang et al., 2015; Schlegel et al., 2016).

As discussed in Sections 1.2.1 & 1.2.2., the *Drosophila* olfactory pathway is also a useful model because of its shared sensory coding principles with mammals, suggesting strong degrees of functional conservation. Moreover, the fruit fly shares many gene orthologues with mammals, including those for neuromodulatory receptors (Evans and Maqueira, 2005). In fact, mutations in fly orthologues have been used to model human diseases such as hereditary spastic paraplegia (Summerville et al., 2016).

That said, the main attraction with working with fruit flies is the extensive toolkit and resources that are available and in development. Like many other organisms, the fruit fly genome has been fully sequenced and easily accessible online. The Flybase project (Gramates et al., 2017), in particular, provides an extensive online database that contains information on genes, sequences and reagents in *Drosophila*. There are also large-scale projects aimed at

reconstructing the synaptic connectivity of the entire fly brain from EM images, which would be useful for understanding neuromodulatory circuitry. This has begun to come into fruition for the olfactory learning centres in both adults (Takemura et al., 2017) and first instar larvae (Berck et al., 2016; Eichler et al., 2017). So far, comparable efforts of generating a full connectome have only been made in the far simpler *C.elegans* (Bentley et al., 2016); which does not have a central nervous system. Most importantly, *Drosophila* is one of the most genetically tractable organisms available (Venken et al., 2011b), which I will discuss in Section 1.2.8.

1.2.7. The *Drosophila* larva as a model organism

Like adult flies, *Drosophila* larvae are also able to learn to discriminate between different odours (Scherer et al., 2003). As discussed in Sections 1.2.1. and 1.2.2., the *Drosophila* larval olfactory pathway is not only well characterised, but also shares a similar structure and conserved coding principles to that of fly adults and mammals, albeit with fewer neurons and potentially less redundancy (Fig. 1.4; Masuda-Nakagawa et al., 2005; Ramaekers et al., 2005). Therefore, fly larvae present a numerically simple model system for elucidating the fundamental circuitry organisation of complex behaviours such as odour discrimination.

In fact, the larval central nervous system (CNS) has been widely used to study the mechanisms of olfactory processing, reward learning and state-dependent neuromodulation (Masuda-Nakagawa et al., 2005; Schroll et al., 2006; Kreher et al., 2008; Selcho et al., 2009; Zhang et al., 2013a). Thus, experimental methods and behavioural assays, including associative olfactory learning, discrimination and generalisation tasks, in the fly larvae are very well-established (Chen et al., 2011a; Honjo et al., 2012; Pauls et al., 2014). Furthermore, genetic tools available in fruit flies (Section 1.2.8) are applicable to both adult and larval stages.

Besides its numerical simplicity, fly larvae have two intrinsic advantages over adult flies: they are easier to handle experimentally as they do not fly; and their optical transparency is useful for optogenetic stimulation and imaging (Schroll et al., 2006; Honjo et al., 2012). It is disadvantageous that fly larvae are immature organisms whose neural circuits are still developing, although it can

also be argued that they are animals with their own specific needs independent of adult flies.

1.2.8. Genetic tools in *Drosophila*

The main advantage of using *Drosophila* as a model organism to study neural circuitry is undoubtedly the wealth of genetic tools that are available; compared to both mammals and other invertebrates, including classical neuromodulation models such as honeybees and crustaceans (Marder, 2012).

1.2.8.1. Transcriptional driver lines

The most valuable tools in *Drosophila* are binary transcriptional drivers, such as the *GAL4* and *LexA* systems (Brand and Perrimon, 1993; Lai and Lee, 2006), for tissue-specific expression of reporters and effectors. The large number of transcriptional driver lines developed in *Drosophila* (Hayashi et al., 2002; Jenett et al., 2012) label many different neuronal types with various degrees of specificity.

This allows for highly specific genetic manipulation not yet possible in most other models. For example, there are only a few tissue-specific transgenic mouse strains, such as *ChAT-Cre*, *VGAT-ChR2-EYFP* (Zhang et al., 2016) or *ArcCreERT2* (Root et al., 2011), most of which label large populations of neurons. Otherwise, tissue-specific expression in rodents involves infecting neurons in a particular region non-specifically with adeno-associated virus vectors encoding the effector of choice (Root et al., 2011; Akerboom et al., 2013). Even in honeybees, visualising ORNs and PNs require neurobiotin injection, which lacks specificity and cannot ensure the same neurons are labelled for each experiment (Sinakevitch et al., 2017).

The expression pattern of *Drosophila* lines can be further refined through clonal analysis and genetic intersection to probe the morphology and function respectively of very specific subsets of neurons, sometimes even at a single neuron resolution (Lee and Luo, 1999; Wong et al., 2002; Venken et al., 2011b). This level of specificity is ideal for studying the effects of neuromodulation on component neurons in a sensory circuit.

While these methods are available, there is still much work to be done in obtaining specific drivers for neurons of interest. Currently, the lines used to investigate OA function in the MBs also label additional OA neurons that do not show MB innervation (Burke et al., 2012; Selcho et al., 2014) – making it difficult to isolate the functions of individual neurons, such as sVUM1 neurons. Therefore, it is necessary to obtain alternative drivers that label these neurons of interest. These lines may either be more specific; or can be used with an existing line that shares expression only in the neurons of interest to generate a genetic intersection to specifically label neurons expressed in both driver lines (Venken et al., 2011b).

1.2.8.2. Tools for visualising and manipulating neurons

To visualise neuronal morphology and innervation patterns, transcriptional drivers can be used to drive fluorescent reporters such as mCD8::GFP (Lee and Luo, 1999; Pfeiffer et al., 2010). The innervation patterns of single neurons labelled within a transcriptional driver can also be resolved using the multicolour FLP-out technique (Nern et al., 2015) developed from the mammalian Brainbow system (Livet et al., 2007). The polarity of specific neurons can be identified by tissue-specific expression of synaptic markers fused to fluorescent proteins, such as n-syb::GFP and DenMark for pre- and post-synaptic sites respectively (Sweeney et al., 1995; Nicolaï et al., 2010).

Gentically encoded functional imaging tools for measuring neuronal activity are also well-established in *Drosophila*. These include the calcium indicator GCaMP (Tian et al., 2009), cAMP sensors (Shafer et al., 2008), and synapto-pHluorin to assay neurotransmitter release (Ng et al., 2002). These tools make it easier to visualise activity in specific neurons, compared to the more traditional electrophysiological methods, with which is more difficult to consistently record from the same neurons; and can reflect cellular effects of neuronal or receptor activation, such as change in cAMP levels.

On the other hand, effectors can be used for activating or blocking neuronal activity, overexpression or genetic rescue in a mutant background. In particular, there are many thermogenetic and optogenetic techniques developed in *Drosophila* for conditional neuronal manipulation. These include temperature-sensitive inhibition and activation of neurons by shibire^{ts} and dTrpA1

respectively (Kitamoto, 2001; Rosenzweig et al., 2005), as well as light-sensitive ion channels such as the ChR2 channelrhodopsin (Schroll et al., 2006); all of which have been previously used to study the mechanisms of olfactory learning (Schwaerzel et al., 2003; Schroll et al., 2006; Burke et al., 2012). While optogenetics are available in some vertebrate models, such as rodents and zebrafish (Boyden et al., 2005; Akerboom et al., 2013), it remains challenging to restrict tissue-specific expression patterns to neurons of interest. *Drosophila* larvae offer the additional advantage of optical transparency for effective optogenetic manipulation in freely behaving animals; and unlike mammalian models, require no surgical procedures (Schroll et al., 2006).

There are also large collections of RNAi fly stocks for tissue-specific knockdown of gene expression from the *Drosophila* transgenic RNAi Project and the Vienna *Drosophila* Resource Center (Dietzl et al., 2007; Ni et al., 2008; Perkins et al., 2015). This is particularly useful for studying the functions of proteins such as neuromodulatory receptors in specific neurons *in vivo*, compared to the widespread and potentially off-target actions of pharmacological manipulation of neuromodulators and their receptors in mammalian systems.

1.2.8.3. Tools for studying neuronal connectivity

To understand neural connectivity, two or more transcriptional driver systems can be used together to investigate the anatomical or physiological interaction between two or more populations of neurons (Lai and Lee, 2006). This could be used to determine whether the two lines label the same neurons, or whether different neurons labelled by the two drivers innervated the same region, through colocalisation of two fluorescent reporters.

Dual transcriptional driver systems can also be used to identify putative synaptic connections with the GRASP method (Gordon and Scott, 2009). Here, the split GFP halves are expressed at the membranes of two neuronal populations labelled by a *GAL4* line and a *LexA* line respectively, such that GFP signal is only detected when split GFP is reconstituted at membrane contacts between these neurons, indicating at potential synapses. The single-cell GRASP method developed based on the FLP-out technique can even identify potential synapses between single neuronal clones (Wong et al., 2002;

Karuppudurai et al., 2014). This provides a high throughput method for mapping potential synaptic connections, and offers an economical and convenient alternative to EM. While GRASP has been adapted for the mouse brain (Feng et al., 2014), it is reliant on the successful injection of viral vectors due to the lack of transcriptional driver lines in mice – a time-consuming and technically challenging task that also lacks the specificity compared to the single neuron resolution capable in *Drosophila* models.

1.2.8.4. Tools for visualising endogenous protein localisation

Like many other organisms, CRISPR/Cas9-mediated genome editing methods have been rapidly developing in *Drosophila* (Gratz et al., 2013; Yu et al., 2014). This is particularly useful for visualising the endogenous expression patterns of proteins especially if specific antibodies are not yet available, such as neuromodulatory receptors.

There are also insertion line collections in *Drosophila* that can be used to generate protein traps, such as the *Minos*-mediated integration cassette (MiMIC) collection (Venken et al., 2011a). The MiMIC construct is a *Minos* transposon carrying a gene trap flanked by two *attP* sites, which has been inserted in random locations of the *Drosophila* genome. When MiMIC is inserted in a coding region intron, it can be replaced with a protein trap containing a fluorescent reporter through *φC31* integrase-mediated *attP-attB* recombination. This introduces an artificial exon encoding the fluorescent reporter within the protein of interest (Venken et al., 2011a; Nagarkar-jaiswal et al., 2015).

While CRISPR knock-in in *Drosophila* was still at its early stages of development (Gratz et al., 2013; Xue et al., 2014), the MiMIC recombinase-mediated cassette exchange (RMCE) method already had an established protocol, produced a higher frequency of successful knock-in recombinants and could be readily converted to different fluorescent reporters or gene-specific binary factor protein traps (Venken et al., 2011a; Diao et al., 2015; Gnerer et al., 2015; Nagarkar-jaiswal et al., 2015). On the other hand, CRISPR allowed for targeted reporter insertion at any genomic location, and should be used if no suitable MiMIC line is available.

1.3. OA and noradrenergic modulation of olfactory discrimination

1.3.1. OA as the insect counterpart of noradrenaline

OA is a major biogenic amine often considered to be the insect analogue of the vertebrate neuromodulator noradrenaline (NA). This is predominantly due to the strong sequence similarities shared between OA receptors and mammalian adrenergic receptors (Maqueira et al., 2005; Qi et al., 2017). OA and NA also share similar chemical structures, although they are synthesised through slightly different biochemical pathways. While OA is synthesised from tyrosine using the enzymes tyrosine decarboxylase (Tdc) and tyramine-β-hydroxylase (Tβh) via TA, which can also act as a neurotransmitter; NA is instead synthesised from tyrosine via dopamine and dopamine-β-hydroxylase (Roeder, 1999).

While trace levels of OA have been detected in vertebrates, NA is absent from invertebrates. Instead, OA takes on many similar functions to NA in invertebrate nervous systems, such as arousal, motivation, learning and memory (Roeder, 1999). Notably, OA and NA may share conserved functions in modulating olfactory processing pathways. Similar to OA innervation of the insect AL and MB (Sinakevitch et al., 2005; Busch et al., 2009; Selcho et al., 2014), noradrenergic (NA) fibres innervate their counterparts, the olfactory bulb and the piriform cortex respectively, where adrenergic receptors have also been identified (Shipley and Ennis, 1996).

1.3.2. Noradrenergic modulation of higher olfactory processing

Previous studies have shown that NA modulation acts on olfactory cortical neurons and affects olfactory learning and discrimination behaviours. *In vivo* activation of NA neurons increases odour responses of pyramidal cells in the piriform cortex (Bouret & Sara, 2002); while *in vitro* application of NA reduces excitatory synaptic potentials in the same neurons (Hasselmo et al., 1997). The late phase of cortical olfactory adaptation in the piriform cortex can also be blocked by activating β-adrenoceptors (Best and Wilson, 2004). Behaviourally, β-adrenoceptor activation in the anterior piriform cortex can substitute as an unconditional stimulus for olfactory preference learning in rat pups (Morrison et al., 2013). A more recent report showed for the first time that injecting

adrenergic receptor antagonists in the anterior piriform cortex impaired odour discrimination (Shakhawat et al., 2015).

While many of the above studies do not differentiate between the types of the receptors activated and neuronal types they are activated on, NA modulation in the same pathway could result in opposite outcomes dependent on the type of receptor activated. For example, injecting β-adrenoceptor antagonists in the olfactory bulb improves odour discrimination, while α1-adrenoceptor antagonists impairs odour discrimination (Mandairon et al., 2008). Moreover, NA application more strongly suppressed synaptic potentials at layer Ib of the piriform cortex (where pyramidal cells form reciprocal synapses) than in layer Ia (input region from olfactory bulb) (Hasselmo et al., 1997). This suggests that NA modulation is more sensitive at particular synapses. Therefore, receptor localisation, receptor affinity and local concentration of NA could all be contributing to differential effects of NA within a circuit.

At the moment, as neuronal subtypes in the cortical regions of mammals remain elusive and difficult to isolate or manipulate, it is challenging to elucidate the organisation of the NA signalling network in the mammalian olfactory cortex. Therefore, studying OA circuits in the simpler and genetically tractable *Drosophila* larvae could shed light on conserved circuit mechanisms for noradrenergic-like neuromodulation of odour discrimination.

1.3.3. The role of octopamine in the MB calyx

Besides being a potentially conserved source of neuromodulation in the insect MB calyx, the main motivation for studying OA signalling arises from its known involvement in olfactory learning behaviours in the MBs. Traditionally, OA signalling in the MBs was proposed to convey the sugar reward signal required for associative olfactory learning to KCs (Schwaerzel et al., 2003). It was first discovered in honeybees that activation of a calyx-innervating OA neuron can be paired with an odour to form an artificial reward memory (Hammer, 1993). This was followed by studies in *Drosophila* larvae and adults that showed pairing OA activation with odours produced artificial appetitive memories (Schroll et al., 2006; Burke et al., 2012). Conversely, the lack of OA impaired olfactory reward memory in flies and larvae (Schwaerzel et al., 2003; Selcho et al., 2014).

Recent studies have refuted the classical model for associative olfactory learning in the MBs: in which OA conveys reward, while dopamine (DA) conveys punishment. Firstly, the disruption of OA signalling impairs reward memory formation only with sweet but non-nutritious sugars in adult and larval *Drosophila* (Burke et al., 2012; Selcho et al., 2014); suggesting that OA neurons only convey the sweetness aspect of reward rather than a general reward signal. This was supported by the discovery of rewarding dopaminergic (DA) neurons in adult and larval *Drosophila* that showed broader reward signalling than OA neurons (Burke et al., 2012; Rohwedder et al., 2016). Moreover, these rewarding DA neurons appeared to be downstream of OA neurons that do not appear to innervate adult fly MBs (Burke et al., 2012). Furthermore, the odour-paired activation of MB-innervating neurons OA-VPM3, OA-VPM4 and OA-VUMa2 (analogous to the larval sVUM1 neurons and the honeybee VUMmx neuron) was insufficient to induce appetitive learning (Burke et al., 2012). This is further complicated by the role of neuropeptide F (NPF) in appetitive olfactory behaviours: NPF signalling is required on DA neurons innervating the MB for appetitive memory in starved adult flies (Krashes et al., 2009); while activating dNPF neurons in fly larvae inhibited appetitive olfactory learning (Rohwedder et al., 2015). However, there is no evidence that NPF and OA share the same signalling pathway. Overall, these results suggested that OA neurons innervating the MBs may not be involved in reward US signalling at all; but instead have an alternative role in olfactory processing in the MBs.

There is also more evidence suggesting that associative olfactory learning occurs at the MB lobes rather than the MB calyx. This idea was first proposed by Schwaerzel et al. (2003) who observed that cAMP machinery required for olfactory memory formation localised to the MB lobes but not to the MB calyx. In *Drosophila* larvae, DA neurons required for associative learning did not appear to innervate the larval MB calyx (Honjo and Furukubo-Tokunaga, 2009; Rohwedder et al., 2016). On the other hand, the tiled innervation patterns of reinforcing DA neurons and MB output neurons in the MB lobe compartments identified in adult flies provide an anatomical framework for associative learning (Aso et al., 2014). This anatomical model was supported by the observation that pairing activation of an aversive DA neuron with an odour resulted in synaptic depression at KC output synapses at the MB lobes, but did not affect KC odour

responses (Hige et al., 2015). This has now led to the revised model that only DA neurons are responsible for modulating KC output synapses at the MB lobes for associative olfactory learning.

For these reasons, it is unlikely that OA neurons in the MB calyx are involved in signalling reward for associative learning. Nevertheless, the conserved OA inputs to the MB calyx indicated functional significance for OA modulation of the system. One of the hypotheses is that, similar to NA modulation of the piriform cortex, OA could be modulating odour responses of KC populations in the larval calyx that could be manifested in odour discrimination behaviour.

As the calyx is the MB input region, it is likely that OA is modulating inputs to the MB at the calyx. This is supported by putative synaptic connections between sVUM1 neurons with PNs and the APL neuron (H.W., MPhil Thesis 2014), which both provide input to KCs in the calyx (Fig. 1.8). The output of the APL neuron in the calyx, in particular, has been known to control the sparseness of KC activation which is required for maintaining odour discrimination of similar odours (Lin et al., 2014). Therefore, OA signalling in the calyx could in turn affect how odours are represented by KCs, underlying a context-dependent change in odour discrimination ability.

1.4. Adrenoceptors and OA receptors in olfactory processing

The diverse actions of neuromodulators are mediated by receptors that are coupled to different cellular pathways (Nadim and Bucher, 2014). Therefore, to understand the OA neuromodulatory circuitry in the larval MB calyx, it is necessary to map the receptors that are involved.

In mammals, there are three main types of adrenoceptors that respond to NA – α1-, α2- and β-adrenoceptors. Each receptor type is coupled to a different G-protein: α1-adrenoceptor with the excitatory G_q protein, which leads to the increase of IP3 and intracellular calcium levels; α2-adrenoceptor with the inhibitory $G_{i/o}$ protein which decreases cAMP levels; and β-adrenoceptor with the excitatory G_s protein, which increases cAMP. The three types of adrenoceptors respond to NA with different affinities: α2-adrenoceptors shows the highest affinity to NA, followed by α1-adrenoceptors and finally β-adrenoceptors (Ramos and Arnsten, 2007; Atzori et al., 2016). Therefore, the

context-dependent fluctuation of NA concentration would activate different types of adrenoceptors (Table 1.1), producing differential effects on its cellular targets correspondingly. All three types of adrenoceptors also localise to the piriform cortex, suggesting that they may have functional roles in modulating higher olfactory responses (Shipley and Ennis, 1996).

OA receptors in *Drosophila* and other insects are classified with reference to adrenoceptor types based on their sequence similarities and signalling properties. To date, five OA receptors in *Drosophila* have been identified, based on their preferential activation by OA. These include the α1-adrenergic-like octopamine receptor in mushroom bodies (OAMB) (Han et al., 1998), the α2-adrenergic-like Octα2R (CG18208) (Qi et al., 2017), and three β-adrenergic-like octopamine receptors – Octβ1R, Octβ2R and Octβ3R (Evans and Maqueira, 2005; Maqueira et al., 2005). In addition, there are also three known TA receptors that may be activated by OA, despite being preferentially activated by the OA precursor TA (Saudou et al., 1990; Bayliss et al., 2013).

I will discuss the known physiology and functions of OA receptors in *Drosophila*, their known roles in olfactory processing in the MB, and hypothesise how they might contribute to the larval MB calyx olfactory circuitry.

1.4.1. α1-adrenergic-like OAMB receptor

OAMB is the first cloned OA receptor in *Drosophila*. It is considered to be α1-adrenergic-like as its transmembrane domains show 52-55% sequence identity to human α1-adrenoceptors (Han et al., 1998; Evans and Maqueira, 2005). OAMB activation in cultured cells predominantly increases intracellular calcium levels, suggesting that like α1-adrenoceptors, it is also coupled to the G_q pathway (Han et al., 1998; Balfanz et al., 2005; Morita et al., 2006). A higher OA concentration can also increase intracellular cAMP in OAMB-expressing cells (Han et al., 1998; Balfanz et al., 2005; Morita et al., 2006). Although some papers have claimed that cAMP increase is only observed in the OAMB-K3/DmOA1A isotype but not the OAMB-AS/DmOA1B isotype (Lee et al., 2003, 2009; Balfanz et al., 2005); there is actually a slightly greater increase in cAMP upon OAMB-AS/DmOA1B compared to OAMB-K3/DmOA1A activation at the same OA concentration, when the same transfection protocol and cAMP assay was used (Balfanz et al., 2005).

OAMB was first named due to its enrichment in the *Drosophila* adult MBs, including in KC cell bodies (Han et al., 1998). Later studies showed that *oamb* mutants failed to form appetitive olfactory memories in adult flies (Burke et al., 2012; Kim et al., 2013). Knocking down OAMB in dopaminergic PAM neurons impaired reward olfactory learning (Burke et al., 2012), while the specific expression of OAMB in KCs in *oamb* mutants rescued the learning impairment (Kim et al., 2013). This suggests that OAMB could be involved in reward learning on both KCs and reinforcing dopaminergic neurons.

However, it is unclear if and how OAMB expression on KCs fits into the current model of associative olfactory learning which depends on DA modulation of KC output synapses. For example, does OAMB mediate an additional component of the reward signal conveyed by direct OA signalling to the MBs? Alternatively, does OAMB affect associative learning by conveying a non-reinforcing signal such as the novelty of a stimulus or the physiological state of the animal? Nevertheless, the presence of OA innervation in both the MB calyx and lobes suggests that OAMB is likely mediating OA signalling to KCs, even though its function is controversial; and this is likely to be conserved in larval KCs.

In addition, the OAMB homologue AmOA1 localises to GABAergic feedback neurons in the MB calyx in honeybees (Sinakevitch et al., 2013). α1-adrenergic modulation in the mammalian olfactory bulb also increases the activity of inhibitory granule cells (Nai et al., 2009). This suggests that OAMB could be expressed in the GABAergic larval APL neuron, which maintains the sparse responses of KCs required for similar odour discrimination (Lin et al., 2014; Masuda-Nakagawa et al., 2014), and modulate inibition from the APL neuron to KCs in the larval MB calyx.

On a cellular level, OAMB activation is most likely to increase the excitability of neurons it is expressed on. Upon OA activation, OAMB-transfected rat cortical neurons in culture showed enhanced calcium response during depolarisation, increased spiking frequency in response to current injection and increased membrane resistance. The increase of membrane resistance is a result of OAMB suppression of leak currents, which would result in prolonged depolarisation (Morita et al., 2006). OAMB activation also inhibits Ca^{2+}-dependent-K^{+} currents carried by Slowpoke channels in *Drosophila* pars

intercerebralis neurons (Crocker et al., 2010). This is consistent with α1-adrenergic modulation of potassium currents in mammals (Marzo et al., 2009).

Based on the known functions of α1-adrenoceptors, OAMB may also control presynaptic neurotransmitter release, especially from PNs or the APL neuron in the calyx. α1-adrenoceptors at the rodent prefrontal cortex enhance presynaptic glutamate release (Zhang et al., 2013b; Luo et al., 2015); while blocking α1-adrenoceptors decreases cocaine-induced dopamine release in the rat nucleus accumbens (Mitrano et al., 2012). On the other hand, α1-adrenoceptor activation paired with intense visual stimulation induces long term depression at input synapses to the rat visual cortex, resulting in reduced orientation-specific visual discrimination (Treviño et al., 2012).

1.4.2. α2-adrenergic-like Octα2R receptor

Until recently, it was unclear whether *Drosophila* expressed an α2-adrenergic-like OA receptor. Protein-BLAST (States and Gish, 1994) with the human α2-adrenergic receptor sequence revealed an uncharacterised putative aminergic receptor CG18208 that showed high levels of sequence similarity (44-52%) with human α2 receptors. However, it was not until last year that the CG18208 receptor was cloned and assayed for OA activation. CG18208 in transfected CHO cells preferentially responds to OA and higher concentrations of serotonin, resulting in a decrease of intracellular cAMP levels, similar to the physiological effects of the α2-adrenoceptor (Qi et al., 2017). CG18208 has now been renamed as Octα2R due to its sequence similarity and comparative pharmacological properties to the human α2-adrenoceptor (Qi et al., 2017).

This is the second α2-adrenergic-like OA receptor that has been identified in insects, following the characterisation of the CsOA3 receptor in the rice stem borer. While CsOA3 is also preferentially activated by OA and decreases intracellular cAMP in response, its activation also elicits a calcium increase. Unlike Octα2R, CsOA3 does not respond to serotonin activation (Wu et al., 2014). Two other α2-adrenergic-like receptors have been identified through sequence similarity to flour beetles and honeybees; although neither has been characterised (Wu et al., 2014; Qi et al., 2017).

As Octα2R activation decreases intracellular cAMP levels, this suggests that it is probably coupled to the inhibitory $G_{i/o}$ pathways like α2-adrenoceptors.

This suggests that like NA, OA signalling in *Drosophila* could also exert inhibitory cellular effects. However, little else is known about the function, physiology and localisation of Octα2R in *Drosophila*, or that of the other α2-adrenergic-like OA receptors in insects.

Therefore, possible functions of Octα2R-mediated signalling in the larval MB calyx can only be predicted from the known effects of α2-adrenoceptors. Octα2R activation could reduce excitatory postsynaptic currents in neurons, such as the action of α2-adrenoceptor agonists in the rat medial prefrontal cortex (Yi et al., 2013); or cause hyperpolarisation and a decrease in firing in neurons, similar to α2-adrenoceptor action in granule cells in the mammalian olfactory bulb (Nai et al., 2010). Alternatively, Octα2R may also be able to enhance neuronal responses, as α2-adrenoceptor-induced decrease of cAMP could block hyperpolarisation-activated cyclic nucleotide gated cation (HCN) channels, and enhance both glutamatergic and cholinergic responses in the prefrontal cortex (Zhang et al., 2013b). Moreover, Octα2R may also act as an auto-inhibitory receptor on OA neurons; as the activation of α2-adrenoceptors caused hyperpolarisation and decreased input resistance in rat NA neurons (Williams et al., 1985).

α2-adrenoceptors are also important for controlling neurotransmitter release, both as inhibitory autoreceptors on NA neurons, but also regulating DA and serotonin release (Scheibner et al., 2001; Bucheler et al., 2002). This suggests that Octα2R may regulate OA signalling at sVUM1 terminals, or modulate neurotransmitter release of other presynaptic terminals at the larval MB calyx. Furthermore, α2-adrenoceptors in the rat piriform cortex also regulate the number of neurons which express plasticity markers (Vadodaria et al., 2017); suggesting that α2-adrenoceptors and its analogue Octα2R could be contributing to structural plasticity in neural circuits as well.

1.4.3. β-adrenergic-like Octβ1R, Octβ2R and Octβ3R receptors

Three β-adrenergic-like OA receptors (OctβRs) have been identified in *Drosophila* – Octβ1R, Octβ2R and Octβ3R – as their transmembrane domains showed 48-57% sequence similarity to human β-adrenoceptors (Maqueira et al., 2005). All three OctβRs are probably coupled to the excitatory G_s pathway, as *in vitro* activation of OctβRs increases cAMP levels (Balfanz et al., 2005;

Maqueira et al., 2005). The three receptors respond to similar ranges of OA concentration, but they have slightly different pharmacological profiles to other drugs (Maqueira et al., 2005). Moreover, their transcripts show different patterns of localisation in the *Drosophila* brain (Ohhara et al., 2012). Octβ1R also couples to the inhibitory G_o pathway which inhibits cAMP levels at the larval neuromuscular junction in the regulation of synaptic growth (Koon and Budnik, 2012); and might therefore mediate inhibitory signals as well.

While there are contradictory reports as to whether any of the OctβRs are localised to the *Drosophila* MBs, at least Octβ2R and Octβ3R have been implicated in olfactory memory formation (Burke et al., 2012; Wu et al., 2013; Walkinshaw et al., 2015). Octβ2R knockdown in the α'β' KCs failed to form anesthesia-resistant aversive olfactory memory (Wu et al., 2013). Octβ2R is also required for the artificial implantation of appetitive olfactory memories by activating *Tdc2-GAL4* neurons in satiated flies but not for hungry flies (Burke et al., 2012). This indicates that Octβ2R may be differentially required for appetitive olfactory memory formation depending on the satiety state of the animals. However, artificial reward memory fails to form in hungry flies upon *Tdc2-GAL4* activation when Octβ2R is knocked down in the dopaminergic MB-MP1 neurons (Burke et al., 2012). As activating the MB-MP1 neuron induces aversive memory (Aso et al., 2010), this suggests Octβ2R may be negatively modulating MB-MP1 neurons in appetitive memory formation. Nevertheless, this suggests that Octβ2R plays an important role in the adult MB olfactory memory circuitry – a role that may be shared in larvae. On the other hand, a RNAi screen revealed that pan-neural RNAi knockdown of Octβ3R improved aversive learning (Walkinshaw et al., 2015). However, it is not known what neurons Octβ3R may be acting on.

The role of β-adrenoceptors in olfactory processing is likely to be conserved in mammals. In the rat brain, β2-adrenoceptor transcripts are localised to olfactory and memory centres including the olfactory bulb, piriform cortex and hippocampus (Nicholas et al., 1993). Pharmacological studies have also shown the requirement of β-adrenoceptors in olfactory dishabituation in the rat piriform cortex (Best and Wilson, 2004), odour preference learning in rat pups (Harley et al., 2006; Morrison et al., 2013); and modulation of odour

discrimination in the mammalian olfactory bulb (Doucette et al., 2007; Mandairon et al., 2008).

The only reports of the cellular actions of OctβRs in *Drosophila* neurons are at the NMJ, where Octβ1R and Octβ2R have opposing roles in controlling synaptopod and synaptic bouton growth of glutamatergic and OA motorneurons (Koon et al., 2011; Koon and Budnik, 2012). $G_o\alpha$/+; *octβ1R/+* transheterozygote mutants showed a non-additive increase of boutons, suggesting that Octβ1R and $G_o\alpha$ are likely to act in the same pathway (Koon and Budnik, 2012). Disrupting the cAMP/CREB pathway in OA motorneurons prevents OA-induced synaptic growth, similar to the *octβ2R* mutant phenotype (Koon et al., 2011). In an *octβ1R* mutant background, where increased synaptic growth occurred, *rut* mutations (lacking adenyl cyclase required for cAMP production) and *dnc* overexpression (overexpressing phosphodiesterase required for cAMP breakdown) decreased synaptic growth – the same phenotype observed in *rut* mutation and *dnc* expression in a WT background. This suggested that *rut* and *dnc* were downstream to Octβ1R. Furthermore, the number of synaptopods in *octβ1R; octβ2R* double mutants reverted to wild type levels (Koon and Budnik, 2012). Overall, this suggests that Octβ1R and Octβ2R both act in the same cAMP pathway to regulate synaptic growth at the NMJ; where Octβ2R is probably coupled to G_s and increases cAMP levels, while Octβ1R is coupled to G_o and decreases cAMP.

More generally, cAMP signalling is known to regulate neuronal excitability and synaptic plasticity. cAMP activates protein kinase A (PKA), which can regulate the activity of Na^+ and K^+ channels, including inhibiting slowpoke (a voltage-gated calcium-dependent potassium channel) to prolong depolarisation (Gordon et al., 1990; Zhou et al., 2002). PKA phosphorylation of synapsin, which increases synaptic vesicles at the active zone (Michels et al., 2011), and the transcription factor CREB required for protein synthesis (Perazzona et al., 2004), are both important in synaptic plasticity and memory formation in *Drosophila*. cAMP can also activate HCN channels in a PKA-independent pathway resulting in synaptic potentiation (Pedarzani and Storm, 1995; Cheung et al., 2006). Therefore, OctβR activation on calyx-innervating neurons is likely to increase neuronal excitability and induce synaptic potentiation via cAMP signalling mechanisms.

1.5. Aims

While there have been many examples of context-dependent neuromodulation of higher sensory pathways, the lack of knowledge in the anatomical organisation of neuromodulatory circuits have impeded our understanding of the circuit mechanisms behind. Therefore, in this project, I endeavored to construct a neuromodulatory map of a higher order sensory discrimination pathway using the relatively simple model of OA signalling in the *Drosophila* larval MB calyx as a framework for identifying and testing the circuit mechanisms of neuromodulation.

Here, I aimed to address the following questions to build a neuromodulatory connectome for the larval MB calyx through identifying calyx-innervating neurons that express OA receptors:

1) What are the potential postsynaptic targets of OA neurons in the larval MB calyx?

I previously identified PNs, the APL neuron and Odd-like neurons as putative synaptic partners of sVUM1 neurons using GRASP (H.W., MPhil Thesis 2014). However, as the GRASP method detects membrane contacts rather than actual synapses, it is unclear whether these neurons form functional synapses with sVUM1 neurons and what the direction of synaptic neurotransmission would be. Moreover, as sVUM1 neurons may co-release TA or neuropeptides, potential synaptic connections do not necessarily indicate OA signalling from sVUM1 neurons.

Therefore, in Chapter 3, I aimed to supplement classical GRASP (Gordon and Scott, 2009) experiments with anti-OA labelling to identify GRASP sites that coincide with OA release, in order to clarify the identity of postsynaptic OA targets in the calyx. In the same chapter, I also aimed to examine single cell GRASP connectivity (Karuppudurai et al., 2014) between sVUM1 neurons and APL neurons using a method optimised in the lab (A.W., MPhil Thesis 2015). This would show whether both sVUMmd1 and sVUMmx1 neurons form putative synapses with the APL neuron, but also identify GRASP sites that colocalise with sVUM1 presynaptic terminals using the single cell GRASP construct.

2) Which of the different OA receptor types localise to putative postsynaptic targets of sVUM1 neurons in the larval MB calyx?

Neuromodulators act on slow metabotropic receptors which can mediate a wide range of downstream effects in target neurons – allowing for a large degree of flexibility in neuromodulation. As discussed in Section 1.4, the effects of OA signalling in calyx-innervating neurons are strongly dependent on the type of OA receptors they express, the secondary signalling mechanisms they are coupled to, as well as the downstream effectors found within each neuron.

To understand how OA signalling from sVUM1 neurons may be mediated on their potential postsynaptic targets, I aimed to determine which of the five known OA receptors in *Drosophila* they express using novel protein traps of OA receptors generated by MiMIC recombinase-mediated cassette exchange in Chapters 4-6. I would first determine whether the localisation pattern of EGFP-tagged OA receptors resembled that of the target neurons, followed by whether they colocalised with molecular markers or neurotransmitter immunolabelling of these neuronal types.

3) Are OA receptors localised to neurons that do not form putative synapses with sVUM1 neurons in the larval MB calyx?

As there is evidence suggesting that neuromodulators, including the OA sVUM1 neurons are able to act extrasynaptically, I aimed to determine whether OA receptors localise to the calyx terminals of KCs. This is because KCs only showed few putative synapses with sVUM1 neurons according to GRASP results in the larval MB calyx, and is therefore a possible candidate for extrasynaptic OA receptor localisation. In Chapters 4-6, I examined whether EGFP-tagged OA receptors localised to KC cell bodies and in a diffuse manner in the larval MB calyx, which would suggest receptor localisation to KC dendrites.

4) Do sVUM1 neuron terminals express modulatory receptors in the larval MB calyx?

The α2-adrenoceptor is a presynaptic autoreceptor in mammals (Langer, 1980). This suggests that the analogous Octα2R may play a similar role in OA neurons in *Drosophila*. Moreover, Octβ1R and Octβ2R are required on OA Type II motorneurons for regulating synaptic growth (Koon et al., 2011; Koon and Budnik, 2012), suggesting that OA neurons may express OA receptors and are therefore subjected OA modulation. There is also pharmacological evidence showing the presence of a presynaptic OA autoreceptor in locust neurons (Howell and Evans, 1998). Therefore, I aimed to determine whether any of the Octβ1R, Octβ2R or Octα2R localised to sVUM1 neurons in Chapters 5-6, using anti-OA labelling to identify sVUM1 cell bodies in the SOG and OA terminals in the larval calyx.

In addition to autoregulation, sVUM1 neurons may be regulated by other calyx-innervating neurons, for example, the APL neuron which is also presynaptic in the calyx (Masuda-Nakagawa et al., 2014). Therefore, I aimed to determine whether sVUM1 neurons were subjected to GABAergic inhibition by examining GABA receptor localisation to the calyx terminals of sVUM1 neurons in Chapter 7 using MiMIC protein traps with anti-OA to label sVUM1 neurons.

5) What are the genetic tools that can be used to validate the sVUM1 neuromodulatory circuitry?

To test the functionality of the sVUM1 connections identified in the neuromodulatory and anatomical map, and to understand the function of sVUM1 modulation in the larval MB calyx, it is essential to have the appropriate tools for genetic manipulation of specific subsets of neurons.

To test the function of OA receptors in the larval MB calyx circuitry, it is necessary to have genetic tools for OA receptor knockdown on specific types of calyx-innervating neurons. In Chapter 4, I aimed to identify the strongest available *UAS-OAMB-RNAi* line for OAMB knockdown in calyx-innervating neurons by comparing the signal intensity of EGFP-tagged OAMB receptors in knockdown versus non-knockdown calyces.

It is also useful to have specific transcriptional driver lines to study the functions of sVUM1 neurons and their effects on other calyx-innervating neurons. While the *Tdc2-GAL4* (Cole et al., 2005) driver line has been traditionally used to study OA neurons, it labels almost all the OA- and TA-positive neurons in the larval CNS – a total of around 80 neurons (Selcho et al., 2012). Therefore, to isolate the function of the calyx-innervating sVUM1 neurons, it is necessary to obtain more specific sVUM1 driver lines. In Chapter 8, I aimed to conduct anti-OA labelling of Janelia *GAL4/LexA* lines (Jenett et al., 2012; L. Masuda-Nakagawa, personal communication) to confirm that they labelled sVUM1 neurons. I also examined the expression pattern of a specific driver line for sVUM1 neurons generated using genetic intersection (C. O'Kane, L. Masuda-Nakagawa, personal communication). In addition, I aimed to confirm the expression patterns of specific calyx-innervating neuron drivers identified from the Janelia *GAL4/LexA* collection (Jenett et al., 2012; L. Masuda-Nakagawa, personal communication).

Chapter 2. Materials and Methods

2.1. Fly Stocks

Flies were raised on standard cornmeal medium at 25°C and subjected to a 12 hour day/night cycle unless stated otherwise. Fly stocks used are listed in Table 2.1.

MiMIC lines with insertions in a coding region intron of receptor genes were selected from the MiMIC collection (Venken et al., 2011a; http://flypush.imgen.bcm.tmc.edu/pscreen/). EGFP-tagged receptor lines were identified from the MiMIC RMCE collection (Nagarkar-Jaiswal et al., 2015; http://flypush.imgen.bcm.tmc.edu/pscreen/rmce/).

GAL4-LexA double construct lines and the intersectional line used in this study were generated by Dr. Cahir O'Kane.

2.2. FRT-GRASP

Flies used in the FRT-GRASP experiment were raised at 18°C. FRT-GRASP crosses were set up in vials containing half the amount of cornmeal medium. The progeny was heat shocked 24-30 hours after egg laying at 37°C for 15 minutes using a water bath (Grant Instruments); and subsequently kept at room temperature until dissection. Optimal heat shock conditions were established by Angela Wan (A.W., MPhil Thesis 2015).

2.3. Verification of MiMIC insertion lines

The location of the MiMIC insertion site within OA receptor protein isotypes was identified by aligning receptor protein sequences to genomic sequences using tblastn (Altschul et al., 1990) hosted on Flybase (http://flybase.org/blast/). TMHMM software (Sonnhammer et al., 1998; http://www.cbs.dtu.dk/services/TMHMM/) was used to predict the transmembrane domains (TM) of receptor proteins.

PCR reactions were carried out to verify the 5' and 3' flanking ends of MiMIC insertions in MiMIC lines (Table 2.1) using the primers listed in Table 2.2.

***GAL4/LexA* lines**			
Genotype	**Source**	**Reference**	**Notes**
NP732-GAL4	DGRC 112307	Masuda-Nakagawa et al., 2014	APL neuron line
NP2631-GAL4	DGRC 104266	Masuda-Nakagawa et al., 2014	APL neuron line
NP225-GAL4	DGRC 112095	Tanaka et al., 2004	PN line
H500-IT.GAL4	Hilary Wong	H.W., MPhil Thesis 2014; Venken et al., 2011	KC line
OK263-GAL4	COK, LMN		Odd-like neuron line
Tdc2-GAL4 (II)	Gift from Scott Waddell	Cole et al., 2005	OA neuron line
Tdc2-LexA (II)	Gift from Scott Waddell	Burke et al., 2012	OA neuron line
Tdc2-LexA (III)	Gift from Scott Waddell	Burke et al., 2012	OA neuron line
R68B12-GAL4	BDSC 39463	Jenett et al., 2012	Odd-like screen
R68B12-LexA	BDSC 54095	Jenett et al., 2012	Odd-like screen
R68C01-GAL4	BDSC 39464	Jenett et al., 2012	Odd-like screen
R74G04-GAL4	BDSC 47742	Jenett et al., 2012	Odd-like screen
R76B09-GAL4	BDSC 46962	Jenett et al., 2012	Odd-like screen
R76C06-GAL4	BDSC 39925	Jenett et al., 2012	Odd-like screen
NP7088-GAL4	DGRC 105362	Tanaka et al., 2008	sVUM1 screen
R34A11-GAL4	BDSC 49767	Jenett et al., 2012	sVUM1 screen
R34A11-LexA	BDSC 52755	Jenett et al., 2012	sVUM1 screen
R43E08-GAL4	BDSC 47929	Jenett et al., 2012	sVUM1 screen
R57F09-LexA	BDSC 54716	Jenett et al., 2012	sVUM1 screen
R61E08-GAL4	BDSC 39273	Jenett et al., 2012	sVUM1 screen
R68A08-GAL4	BDSC 39450	Jenett et al., 2012	sVUM1 screen
R76G06-GAL4	BDSC 39940	Jenett et al., 2012	sVUM1 screen
R76G07-GAL4	BDSC 48331	Jenett et al., 2012	sVUM1 screen
R76G11-GAL4	BDSC 48333	Jenett et al., 2012	sVUM1 screen
R76H01-LexA	BDSC 54075	Jenett et al., 2012	sVUM1 screen
R76H03-LexA	BDSC 54954	Jenett et al., 2012	sVUM1 screen
R76H04-GAL4	BDSC 41306	Jenett et al., 2012	sVUM1 screen
R77B01-GAL4	BDSC 46977	Jenett et al., 2012	sVUM1 screen
R83G11-GAL4	BDSC 46764	Jenett et al., 2012	sVUM1 screen
R83H01-GAL4	BDSC 40368	Jenett et al., 2012	sVUM1 screen

Table 2.1A. List of fly stocks used in this study. Sources: BDSC, Bloomington *Drosophila* Stock Center; COK, Cahir O'Kane; DGRC, Kyoto Stock Center; LMN, Liria Masuda-Nakagawa.

MiMIC lines (Venken et al., 2011)		
Genotype	**Source**	**Notes**
Mi{y$^{+mDint2}$=MIC}CG18208^{MI10227}	BDSC 53233	*MI10227*
Mi{y$^{+mDint2}$=MIC}OAMB^{MI12417}	BDSC 57940	*MI12417*
Mi{y$^{+mDint2}$=MIC}Octβ1R^{MI05807}	BDSC 42119	*MI05807*
Mi{y$^{+mDint2}$=MIC}Octβ2R^{MI13416}	BDSC 59133	*MI13416*
Mi{y$^{+mDint2}$=MIC}Octβ3R^{MI06217}	BDSC 43050	*MI06217*
MiMIC RMCE lines (Venken et al., 2011; Nagarkar-Jaiswal et al., 2015)		
Genotype	**Source**	**Notes**
Mi{PT-GFSTF.1}OAMB$^{MI12417\text{-}GFSTF.1}$	Fly Facility	*OAMB::EGFP*
Mi{PT-GFSTF.2}Octβ1R$^{MI05807\text{-}GFSTF.2}$	BDSC 60236	*Octβ1R::EGFP*
Mi{PT-GFSTF.2}Octβ2R$^{MI13416\text{-}GFSTF.2}$	Fly Facility	*Octβ2R::EGFP*
Mi{PT-GFSTF.0}Octβ3R$^{MI06217\text{-}GFSTF.0}$	Fly Facility	*Octβ3R::EGFP (Phase 0)*
Mi{PT-GFSTF.1}Octβ3R$^{MI06217\text{-}GFSTF.1}$	BDSC 60245	*Octβ3R::EGFP (Phase 1)*
Mi{PT-GFSTF.0}CG18208$^{MI10227\text{-}GFSTF.0}$	Fly Facility	*CG18208::EGFP*
Mi{PT-GFSTF.0}Rdl$^{MI02620\text{-}GFSTF.0}$	BDSC 59796	*Rdl::EGFP*
Mi{PT-GFSTF.0}GABA-B-R1$^{MI01930\text{-}GFSTF.0}$	BDSC 60522	*GABA-B-R1::EGFP*

Table 2.1B. List of fly stocks used in this study. Sources: BDSC, Bloomington *Drosophila* Stock Center; Fly Facility, The University of Cambridge Department of Genetics Fly Facility.

Other lines			
Genotype	**Source**	**Reference**	**Notes**
UAS-mCD8::GFP (III)	BDSC 5130	Lee and Luo, 1999	
13XLexAOp-mCD8::GFP (III)	BDSC 32203	Pfeiffer et al., 2010	
10XUAS-IVS-mCD8::RFP (II)	BDSC 32219	Pfeiffer et al., 2010	
10XUAS-IVS-mCD8::RFP, 13XLexAOp2-mCD8::GFP (X)	BDSC 32229	Pfeiffer et al., 2010	
UAS-Chrimson::mVenus (III)	BDSC 55136	Klapoetke et al., 2014	Reporter for intersectional lines
LexAOp-CD4::spGFP11; UAS-CD4::spGFP1-10	LMN	Masuda-Nakagawa et al., 2014	GRASP line
LexAOp2-IVS>stop>spGFP11::CD4::HA-T2A-Brp::mCherry, UAS-spGFP1-10::CD4, UAS-HRP::CD2	Gift from Marco Gallio	Karuppudurai et al., 2014	FRT-GRASP line
hsFLP	BDSC 1929		Heat shock-induced Flippase (FLP)
LexAOp-FLP		Shang et al., 2008	
FRT-GAL80	BDSC 38879	Bohm et al., 2010	
VALIUM10-Luciferase (III)	BDSC 35788	Ni et al., 2011	RNAi control
VALIUM20-EGFP.shRNA.3 (III)	BDSC 41560	Neumüller et al., 2012	GFP-RNAi
P{GD696}v2861(II)	VDRC 2861	Burke et al., 2012	*UAS-OAMB-RNAi (v2861)*
P{KK111456}VIE-260B (II)	VDRC 106511	Zhang et al., 2013a	*UAS-OAMB-RNAi (v106511)*
P{TRiP.JF01732}attP2	BDSC 31233	Deady and Sun, 2015	*UAS-OAMB-dsRNA (B31233)*
UAS-Sec61β::tdTom (II)	Gift from O'Kane lab	Summerville et al., 2016	ER marker
Canton-S	Gift from John Carlson		Wild type control
PBac{IT.GAL4}S576 (III)	Shershah Assadullah	Gohl et al., 2011	PCR negative control
CyO/If; TM6B/MKRS			Double balancer

Table 2.1C. List of fly stocks used in this study. Sources: BDSC, Bloomington *Drosophila* Stock Center; LMN, Liria Masuda-Nakagawa; VDRC, Vienna Stock Center.

Primer	Sequence
Orientation-MiL-F (OriF)	GCGTAAGCTACCTTAATCTCAAGAAGAG
Orientation-MiL-R (OriR)	CGCGGCGTAATGTGATTTACTATCATAC
EGFPdo-Seq-F (EGFP-F)	GGATGACGGCACCTACAAGAC
EGFPdo-Seq-R (EGFP-R)	GTGGCTGTTGAAGTTGTACTC
MiMIC-5R	CTTGAGATTAAGGTAGCTTACGC
MiMIC-3F	TGCAGGTCGACGAATTCAAC
MI12417-5F	CCACAATCAACGTCCTGCTC
MI12417-3R	GATTATCGCCACCACAGAGTC
MI05807-5F	TCCTTTCATTCCCGAGCACC
MI05807-3R	CTCGTTAACAATCGCTCGCC
MI13416-5F1	CGGAGTCACTGAGTAATGGCG
MI13416-5F2	ATGGCGAGTGGTATGAGCAG
MI13416-5F3	GTGCTCTAGATGGCGAGTGG
MI13416-5F4	ACCGAGGCTCATTAACACAG
MI13416-5F5	GAGGCTCATTAACACAGCGC
MI13416-3R	GCTGCCTCATTGAACTCCAG
MI06217-5F	GCAGGAGAACAGCGACAGTC
MI06217-3R	CCTGTCTCTGGAAGTAGGTCG
MI10227-5F	TCATGATCACGGCAGTCTGG
MI10227-3R	ACACTCGGAATGTAGCCAGC

Table 2.2. List of primers and sequences used in this study. Orientation-MiL-F, Orientation-MiL-R, EGFPdo-Seq-F and EGFPdo-Seq-R were previously used in Venken et al. (2011a). The remaining primers were designed using Primer3 software (Untergasser et al., 2007; http://primer3.ut.ee/).

2.4. Generation and validation of EGFP-tagged receptor lines

OAMB::EGFP, *Octβ2R::EGFP*, *Octβ3R::EGFP (Phase 0)* and *CG18208::EGFP* recombinant stocks were generated using MiMIC recombinase-mediated cassette exchange, as described in Venken et al. (2011a), by the University of Cambridge Department of Genetics Fly Facility for this study.

In brief, embryos from the selected MiMIC lines were injected with an EGFP-FlAsH-StrepII-TEV-3xFlag plasmid of the appropriate splice phase (Table 2.3; Venken et al., 2011a) and a helper φC31-integrase (Fig. 2.1). Injected embryos were left to hatch into adult flies and subsequently crossed to a double balancer stock in a *y w* background. RMCE events were identified by the loss of the *yellow*$^{+}$ phenotype encoded by the MiMIC construct in the F1 progeny. Finally, recombinant flies were balanced to establish a stock (Fig. 2.1; Venken et al., 2011a).

Four PCR reactions (PCR1, PCR2, PCR3 and PCR4) were carried out to characterise the insertion orientation of the EGFP cassette in each of the recombinant stocks, as described in Venken et al. (2011a). The following primer pairs were used: Orientation-MiL-F (OriF)/EGFPdo-Seq-R (EGFP-R) for PCR1, OriF/EGFPdo-Seq-F (EGFP-F) for PCR2, Orientation-MiL-R (OriR)/EGFP-R for PCR3 and OriR/EGFP-F for PCR4. Primer sequences are listed in Table 2.2.

2.5. Molecular methods

2.5.1. Plasmid preparation

Plasmids for MiMIC injections were obtained from the *Drosophila* Genomic Resource Center (DGRC) (Table 2.3). 1 µl of plasmid DNA (1-100 ng/ µl) was added to 50 µl of DN5α competent cells (gift from Liv Grant, Glover Group). The cells were incubated on ice for 30 minutes, heat shocked at 42ºC for 45 seconds in a water bath (Fisher Scientific) and then placed on ice for another 2 minutes. 250 µl of warm sterile SOC medium (2% Tryptone, 0.5% Yeast extract, 10mM NaCl, 2.5mM KCl, 10mM $MgCl_2$, 20mM glucose; Genetics Media Service) was added to the cells and then placed at 37ºC for 1 hour in a shaking incubator (Innova44 Incubator Shaker). Transformed bacteria were plated onto

MiMIC line	Splice Phase	Plasmid	Plasmid Source
Mi{y$^{+mDint2}$=MIC}OAMB^{MI12417}	1	pBS-KS-attB1-2-PT-SA-SD-1-EGFP-FlAsH-StrepII-TEV-3xFlag	DGRC 1306
Mi{y$^{+mDint2}$=MIC}Octβ2R^{MI13416}	2	pBS-KS-attB1-2-PT-SA-SD-2-EGFP-FlAsH-StrepII-TEV-3xFlag	DGRC 1314
Mi{y$^{+mDint2}$=MIC}Octβ3R^{MI06217}	0	pBS-KS-attB1-2-PT-SA-SD-0-EGFP-FlAsH-StrepII-TEV-3xFlag	DGRC 1298
Mi{y$^{+mDint2}$=MIC}CG18208^{MI10227}			

Table 2.3. List of plasmids used to generate MiMIC RMCE stocks in this study. DGRC, *Drosophila* Genomic Resource Center.

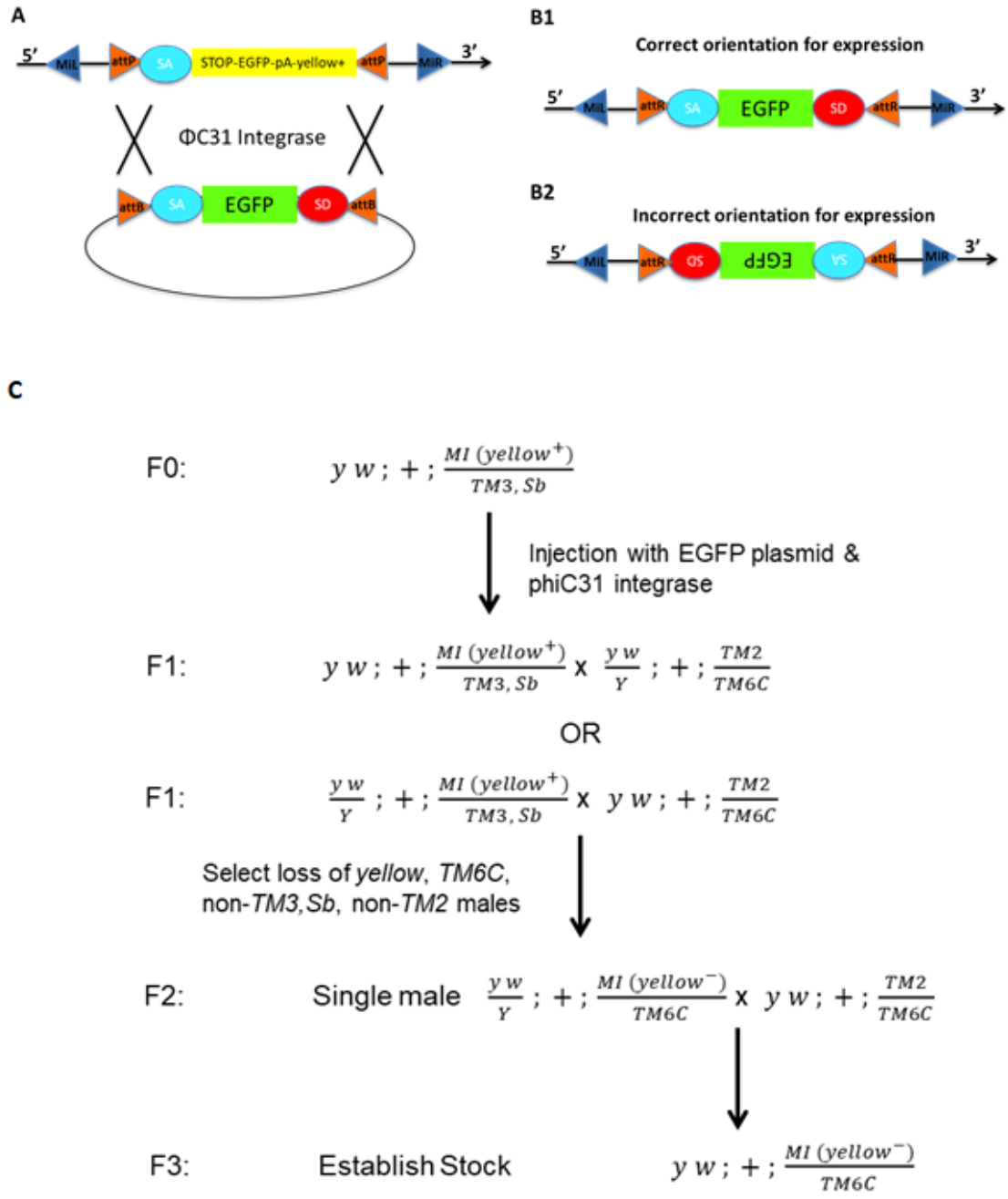

Figure 2.1. Generation of EGFP protein traps using MiMIC φC31-integrase-mediated cassette exchange. (A) Schematic for the generation of EGFP protein traps through MiMIC RMCE. **(B)** Possible EGFP cassette orientations after recombination. **(C)** Crossing scheme for MiMIC cassette exchange on the third chromosome. Abbreviations: MiL/R, MiMIC insertion sequences Left/Right; SA, splice acceptor site; SD, splice donor site. Figure reproduced from protocol described in Venken et al. (2011).

1.5% LB agar plates (1% NaCl, 1% Tryptone, 0.5% Yeast extract, 1.5% Agar; Genetics Media Service) with 100 µg/ ml ampicillin (Melford Labs, A0104), and incubated at 37°C overnight in a static incubator (Raven incubator).

A single colony of transformed bacteria was inoculated in 5 ml of LB medium (1% NaCl, 1% Tryptone, 0.5% Yeast extract; Genetics Media Service) with 100 µg/ ml ampicillin to form a starter culture. This was incubated for 8 hours at 37°C in the shaker. 25 µl of the starter culture was then inoculated with 25 ml of LB medium and incubated overnight at 37°C in the shaker. The resulting cells were harvested by centrifugation at 6000 x *g* for 15 minutes at 4ºC. Plasmid DNA was then purified from the cells using the Qiagen Plasmid Midi Kit (Qiagen 12143), dissolved in autoclaved milliQ water to use at a concentration of 0.4 µg/ µl, $OD_{260/280}$: 1.8-1.9.

2.5.2. DNA extraction

Genomic DNA was extracted from 15-30 flies (1-7 days after eclosion) and homogenised in fly homogenisation buffer (100 mM Tris-HCl, 8.5; 80 mM NaCl, Sigma, 31434; 5% Sucrose, Sigma, S0389; 0.5% SDS, Sigma, L4509; 50 mM NaEDTA, Sigma, ED2SS, pH 8.0). The homogenate was incubated with RNase A (Roche, 10109142001) for 1 hour at 37°C, followed by Proteinase K (Roche, 03115887001) for 1 hour at 50°C, and purified with phenol-chloroform (Sigma, 77617) and chloroform (Sigma, C2432). DNA was then precipitated with 0.6 volumes of isopropanol (Sigma, 59304) and washed with 75% ethanol (Sigma, E7023), dried overnight at room temperature and resuspended in 10 mM Tris-HCl pH 8.0 (Sigma, T6066).

2.5.3. PCR and sequencing

For each PCR reaction (20 µl), 0.4 µl or 1 µl genomic DNA, 1 µl of each 10 µM primer (Sigma), 2µl 10X PCR buffer (Qiagen, 203203), 0.4 µl 10 µM dNTP mix (Roche, 11581295001), 0.08 µl 5 U/µl HotStarTaq DNA polymerase (Qiagen, 203203) and 15.1 µl or 14.5 µl milliQ water were used. PCR cycling was conducted with a G-Storm Thermal Cycler (GS4) and the following conditions were used: initial denaturation at 95°C for 15 minutes, 40 cycles of denaturation at 94°C for 30s, annealing at 60°C for 30s and elongation at 72°C for 1 min, followed by a final elongation step at 72°C for 10 minutes. PCR products were

loaded together with 6X DNA gel loading dye (ThermoFisher, R0611) onto a 1% Agarose Gel (Ultrapure Agarose, Invitrogen, 16500500; 1X TBE buffer, Invitrogen, 15581044) with GelRed (Biotium, 41003-T) for gel electrophoresis. 100 bp DNA ladder was used as a marker (Invitrogen, 15628019).

PCR products were purified using the Qiaquick PCR Purification Kit (Qiagen, 28104); and sequenced at the Department of Biochemistry Sequencing Facility (University of Cambridge). The sequenced products were aligned to *Drosophila melanogaster* and MiMIC sequences using nucleotide BLAST (Altschul et al., 1990; https://blast.ncbi.nlm.nih.gov/Blast.cgi?PAGE_TYPE=BlastSearch).

2.6. Immunohistochemistry

Third instar wandering stage larvae (144-176 hours after egg laying) were dissected in cold PBS (Sigma, P4417), fixed in 4% Formaldehyde (Polysciences, 18814)/PEM buffer (0.1 M PIPES, Sigma, P1851; 2 mM EGTA, Sigma E3889; 1 mM $MgSO_4$; NaOH) for 2 hours at 4°C, washed for 3x10 minutes (or 4x15 minutes) in 0.3% Triton-X (Sigma, T8787) in PBS (PBT) and incubated in 10% NGS (Vector Labs, S-1000) in 0.3% PBT for 1 hour at room temperature. Brains were incubated in primary antibody in 10% NGS-0.3% PBT at 4°C for 2-3 days on a mini disk rotor (Biocraft, BC-710), washed for 3x15 minutes with 0.3% PBT and further incubated in secondary antibody in blocking solution at 4°C for 2-3 days on the mini disk rotor. Brains were finally washed for 15 minutes with PBT, followed by 3x10 minutes with PBS, and left in 50% Glycerol/PBS at 4°C for at least one overnight prior to imaging. Primary and secondary antibodies used are listed in Table 2.4.

To reduce background staining levels of the polyclonal chicken anti-GFP (Abcam, Ab13970) and polyclonal rabbit anti-GFP (Invitrogen, A11122), the antibodies were pre-incubated with *MI12417* larval brains which did not express GFP. 50 *MI12417* larval brains were incubated in 1:20 anti-GFP in 10% NGS in 0.3% PBT at 4°C for 1 overnight. A further 50 *MI12417* larval brains were added to the antibody solution and further incubated at 4°C for 2 overnights. The antibody solutions were then used at a final concentration of 1:1000 or 1:2000.

Primary Antibodies			
Antibody	**Host**	**Source**	**Working Dilution**
Anti-GFP	Rat, monoclonal	Nacalai 440426 (Clone GF090R)	1:1000
Anti-GFP	Chicken, polyclonal	Abcam, Ab13970	1:1000/1:2000
Anti-GFP	Rabbit, polyclonal	Invitrogen, A11122	1:1000/1:2000
Anti-GFP	Rabbit, polyclonal	Abcam, Ab6556	1:1000
Anti-GFP	Rabbit, polyclonal	Abcam, Ab290	1:800
Anti-DsRed	Rabbit, polyclonal	Clontech, 632496	1:1000
Anti-GABA	Rabbit, polyclonal	Sigma, A2052	1:1000
Anti-Octopamine (OA)	Rabbit, polyclonal	MoBiTec, 1003GE	1:1000
Anti-Discs Large (Dlg)	Mouse, monoclonal	DSHB, 4F3	1:200
Anti-Calnexin99A	Mouse, monoclonal	Gift from Munro Lab (Riedel et al., 2016)	1:10
Secondary Antibodies			
Antibody	**Host**	**Source**	**Working Dilution**
Anti-Rat Alexa 488	Goat, polyclonal	Invitrogen, A11006	1:200
Anti-Chicken Alexa 488	Goat, polyclonal	Invitrogen, A11039	1:200
Anti-Rabbit Alexa 488	Goat, polyclonal	Invitrogen, A11034	1:200
Anti-Rabbit Alexa 568	Goat, polyclonal	Invitrogen, A11036	1:200
Anti-Mouse Alexa 647	Goat, polyclonal	Invitrogen, A21236	1:200

Table 2.4. List of antibodies used in this study.

2.7. Mounting, confocal imaging and image analysis

Mounting and orientation of brains for image uptake were as described in the supplemental information in Masuda-Nakagawa et al. (2009). Schematics of larval brains orientations are shown in Fig. 1.1 and 1.2. The larval MB calyx was imaged from the dorsal orientation (Fig. 1.1), the larval AL was imaged from the frontal orientation (Fig. 1.2), and the larval SOG was imaged from the ventral orientation (Fig. 1.7A-B). Specific calyx-innervating neurons are imaged from the same orientations as shown in Figures 1.3, 1.5 and 1.7.

Imaging was conducted using a Zeiss LSM710 Confocal Microscope with a 40X oil, NA 1.3 objective or with a 20X air, NA 0.8 objective. Images were processed using ImageJ software (Schneider et al., 2012; https://imagej.nih.gov/ij/download.html). All brains are shown in the right brain orientation. The intensity within a region of interest was quantified by measuring the mean grey value using the Analyse function on ImageJ. For a single calyx or AL, this was averaged across multiple confocal optical slices. Statisical descriptions were conducted using Microsoft Excel.

2.8. L1 connectivity data and analysis

L1 connectivity data were obtained from the NeuroNLP.larva server (https://neuronlp.larva.fruitflybrain.org/) maintained by the Fruit Fly Brain Observatory, where published EM reconstruction data from Berck et al. (2016) and Eichler et al. (2017) are compiled. L1 images were taken directly from NeuroNLP.larva website. The number of sVUM1 synapses with calyx-innervating neurons was manually quantified and analysed from data available from the website.

Chapter 3. GRASP connectivity of sVUM1 neurons in the larval MB calyx

3.1. Introduction

To understand how the octopaminergic neuromodulatory circuitry is organised in the larval MB calyx, it is necessary to first identify the neurons postsynaptic to the octopaminergic sVUM1 neurons in the calyx.

Using the GFP reconstitution across synaptic partners (GRASP) method (Gordon and Scott, 2009), I had previously identified olfactory PNs, the APL neuron and Odd-like neurons as putative synaptic partners of sVUM1 neurons in the larval MB calyx (Fig. 3.1; H.W., MPhil Thesis 2014). In addition, I observed limited GRASP between sVUM1 neurons and KCs in the calyx (H.W., MPhil Thesis 2014), suggesting that sVUM1 neurons and KCs were unlikely to synapse there.

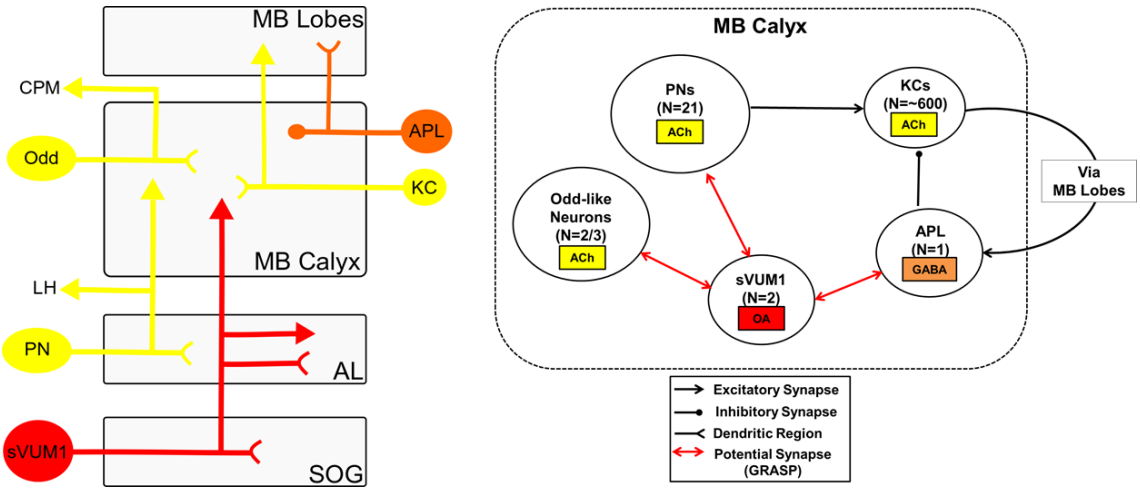

Figure 3.1. Summary diagram of sVUM1 connectivity in the larval MB calyx. Adapted from Fig. 1.8. in Chapter 1. Abbreviations: ACh, acetylcholine; AL, antennal lobe; CPM, centroposterior medial compartment; KC, Kenyon Cell; LH, lateral horn; MB, mushroom body; N, number; OA, octopamine; PN, projection neuron.

However, there were several limitations to these results:

Firstly, the GRASP method detects the split-GFP reconstitution at the plasma membranes of two neuronal populations, rather than actual synaptic connections (Feinberg et al., 2008; Gordon and Scott, 2009). Therefore, GRASP may also detect membrane contacts that do not form synapses.

Secondly, for the same reasons, GRASP is unable to detect the direction of neurotransmission. Therefore, it is unclear whether PNs, the APL neuron and Odd-like neurons are pre- and/or post-synaptic to sVUM1 neurons; and hence predict whether they are subjected to OA neuromodulation. This particularly applies to PNs and the APL neuron, as they are also predominantly presynaptic in the larval MB calyx (Masuda-Nakagawa et al., 2005, 2014; L. Masuda-Nakagawa, personal communication).

Thirdly, the *Tdc2-GAL4* line previously used to investigate KC-sVUM1 connections in the larval calyx labels KCs (H.W., MPhil Thesis 2014). Therefore, it was unclear whether the limited GRASP signal detected is between KC-sVUM1 or KC-KC, considering the complementary splitGFP halves are both expressed in KCs. Moreover, the limited GRASP between KC-sVUM1 was contrary to what was expected from KC-OA GRASP results in the adult MB calyx (Zhou et al., 2012; Pech et al., 2013) and KC-sVUM1 synapses reconstructed from L1 EM data (Eichler et al., 2017). Given the experimental constraints, it cannot be confirmed whether the low number of possible KC-sVUM1 contacts observed is an artefact.

Finally, it was unclear whether one or both of the sVUM1 neurons – sVUMmd1 and sVUMmx1 – are responsible for the GRASP signals observed. EM data revealed that sVUMmd1 and sVUMmx1 show non-overlapping innervation in the L1 calyx (Fig. 1.7D; Eichler et al., 2017; https://neuronlp.larva.fruitflybrain.org/). This suggested that sVUMmd1 and sVUMmx1 may not share the same synaptic partners. Using the single cell GRASP method to restrict one of the splitGFP components to single cell clones generated by heat shock-induced FLP recombination (Karuppudurai et al., 2014), my colleague found that both sVUM1 neurons showed GRASP with Odd-like neurons in the larval calyx (A.W., MPhil Thesis 2015). However, it is unclear whether this applies to other putative synaptic partners of sVUM1 neurons.

With the above concerns in mind, I aimed to provide evidence for possible postsynaptic partners to sVUM1 neurons subjected to OA signalling in this chapter. I examined whether GRASP between sVUM1 neurons and each of its putative synaptic partners colocalised with anti-OA, with the assumption that GRASP localised to OA terminals suggested that these sites were postsynaptic to OA transmission from sVUM1 neurons. To confirm whether KCs are potential postsynaptic partners of sVUM1 neurons in the L3 calyx, I repeated the KC-sVUM1 GRASP experiment using transcriptional drivers that specifically label KCs and sVUM1 neurons in the calyx respectively, using anti-OA to label OA terminals. In addition, I aimed to determine whether sVUMmd1 and/or sVUMmx1 neurons synapse with the APL neuron, by using the single cell GRASP method developed by Karuppudurai et al. (2014) and optimised for use with sVUM1 neurons by Angela Wan (A.W., MPhil Thesis 2015).

3.2. Results

3.2.1. sVUM1 GRASP with PNs, APL and Odd-like neurons colocalised with OA puncta

To determine whether PNs, the APL neuron and Odd-like neurons are putative postsynaptic partners to sVUM1 neurons, I examined whether their GRASP signals with sVUM1 neurons colocalised with OA puncta in the larval MB calyx.

To visualise potential synaptic contacts between PNs and sVUM1 neurons, I expressed one part of the splitGFP using *NP225-GAL4*, which labels the majority of olfactory PNs (Masuda-Nakagawa et al., 2005), and the complementary part of the splitGFP using *Tdc2-LexA* (Burke et al., 2012), which labels the OA sVUM1 neurons in the larval MB calyx (H.W., MPhil Thesis 2014). Many of the GRASP signals between PNs and sVUM1 neurons colocalised with OA labelling (n=16; Fig. 3.2, filled arrowheads).

The extent of colocalisation for individual puncta varied: some GRASP signals only localised to the periphery of OA puncta (Fig. 3.2C), while other GRASP signals showed more complete colocalisation (Fig. 3.2D,G). There may be a functional consequence for the differences observed in colocalisation patterns. For example, GRASP puncta localised to the periphery

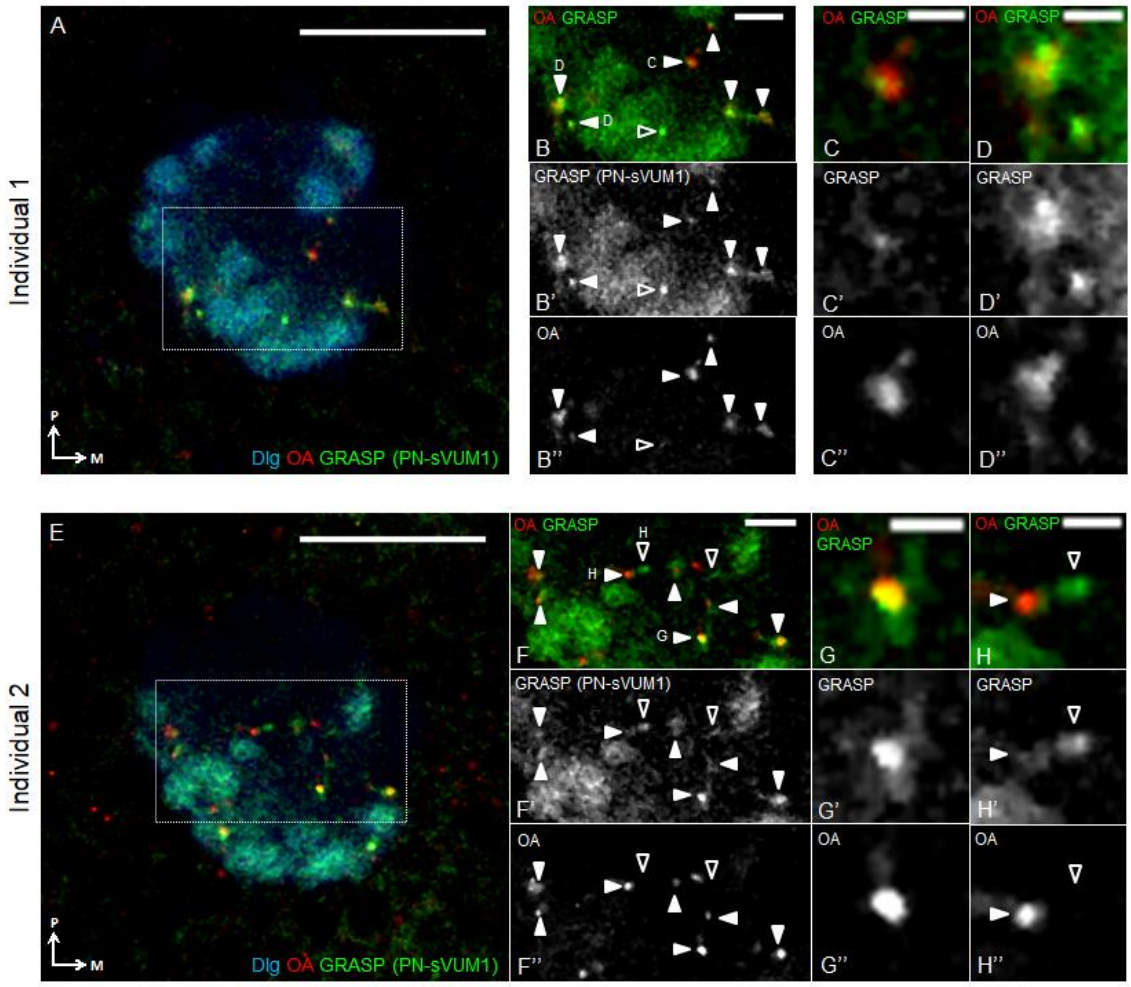

Figure 3.2. Some PN-sVUM1 GRASP puncta colocalised with OA terminals. Single confocal optical sections of the calyx from two *NP225-GAL4/LexAOp-CD4::spGFP11; Tdc2-LexA/UAS-CD4::spGFP1-10* individuals. Green is PN-sVUM1 GRASP, red is anti-OA and blue is anti-Dlg. **(B,F)** are magnified from the rectangular box in **(A)** and **(E)** respectively. **(C-D)** and **(G-H)** are magnified puncta labelled in **(B)** and **(F)** respectively. Filled arrowheads indicate GRASP-OA colocalisation, and empty arrowheads indicate GRASP puncta negative for OA. Medial (M) is right, posterior (P) is up. Scale bar: 20 μm for **(A,E)**, 5 μm for **(B,F)** and 2 μm for **(C-D,G-H)**.

of OA boutons may suggest these OA boutons have additional non-PN synaptic partners or are bi-directional synapses; although these possibilities cannot be validated at this resolution. Some GRASP signals do not colocalise with OA boutons (Fig. 3.2B,F,H, empty arrowheads). These could be sites where PNs are presynaptic to sVUM1 neurons, where sVUM1 neurons release a non-OA neurotransmitter to the postsynaptic PN, or non-synaptic membrane contacts detected as false positives with the GRASP method.

16 ± 2.1 out of 24 ± 2.6 GRASP signals overlapped with OA puncta (n=16; Fig. 3.2, filled arrowheads; Table 3.1). As this accounted for around 65% of total GRASP signals, this suggested that PNs are possible postsynaptic partners of sVUM1 neurons in the calyx. As *NP225-GAL4* labels most of the 21 olfactory PNs (Masuda-Nakagawa et al., 2005), if GRASP signals are evenly distributed across PNs, this suggested each PN has approximately one postsynapse with sVUM1 neurons in the calyx.

Next, I expressed the two halves of the splitGFP in the APL neuron using the *NP2631-GAL4* driver (Masuda-Nakagawa et al., 2014), and in sVUM1 neurons labelled by *Tdc2-LexA*. 29 ± 2.6 out of 40 ± 3.2 (around 72%) GRASP puncta colocalised with OA boutons (n=9; Fig. 3.3., filled arrowheads; Table 3.2), where the APL neuron is probably postsynaptic to OA neurotransmission from sVUM1 neurons. I also observed variable patterns of GRASP-OA colocalisation (Fig. 3.3C-D, G-H), similar to those in PN-sVUM1 GRASP.

There were also GRASP signals that did not overlap with OA boutons (Fig. 3.3, empty arrowheads). This is consistent with the 50% of APL-sVUM1 GRASP signals that colocalised with GABA boutons (H.W., MPhil Thesis 2014); and suggested that sVUM1 neurons were probably postsynaptic to the APL neuron at these sites, if the same logic was applied. The percentages of GRASP-OA puncta and GRASP-GABA puncta out of total GRASP signals – 72% and 50% respectively – add up to more than 100%. Therefore, some GRASP signals may be at sites that are presynaptic for both GABA and OA. This suggested the presence of axo-axonal synapses between sVUM1 neurons and the APL neuron, as well as the possibility of bi-directional synapses.

I then validated whether GRASP between Odd-like neurons labelled in *OK263-GAL4* (L. Masuda-Nakagawa, personal communication) and sVUM1

PN-sVUM1 GRASP	GRASP	OA	GRASP-OA overlap	%overlap/ OA	%overlap/ GRASP
Individual 1	24	88	15	17%	63%
Individual 2	19	81	14	17%	74%
Individual 3	15	79	8	10%	53%
Individual 4	17	74	12	16%	71%
Individual 5	15	69	8	12%	53%
Individual 6	18	84	12	14%	67%
Individual 7	12	82	8	10%	67%
Individual 8	22	79	17	22%	77%
Individual 9	32	80	23	29%	72%
Individual 10	29	71	18	25%	62%
Individual 11	15	69	4	6%	27%
Individual 12	41	90	25	28%	61%
Individual 13	21	65	15	23%	71%
Individual 14	47	83	35	42%	74%
Individual 15	37	78	30	38%	81%
Individual 16	24	70	16	23%	67%
N	16	16	16	16	16
Mean	24	78	16	21%	65%
S.D.	10.3	7.3	8.4	0.1	0.1
S.E.M.	2.6	1.8	2.1	0.0	0.0

Table 3.1. Numbers of PN-sVUM1 GRASP and OA puncta in *NP225-GAL4;Tdc2-LexA>GRASP* calyces. Abbreviations: GRASP-OA overlap, GRASP puncta colocalised with OA labelling; %overlap/OA = number of puncta positive for both GRASP and OA divided by total number of OA puncta*100%; %overlap/GRASP = number of puncta positive for both GRASP and OA divided by total number of GRASP puncta*100%; N, number; S.D., standard deviation; S.E.M., standard error of the mean.

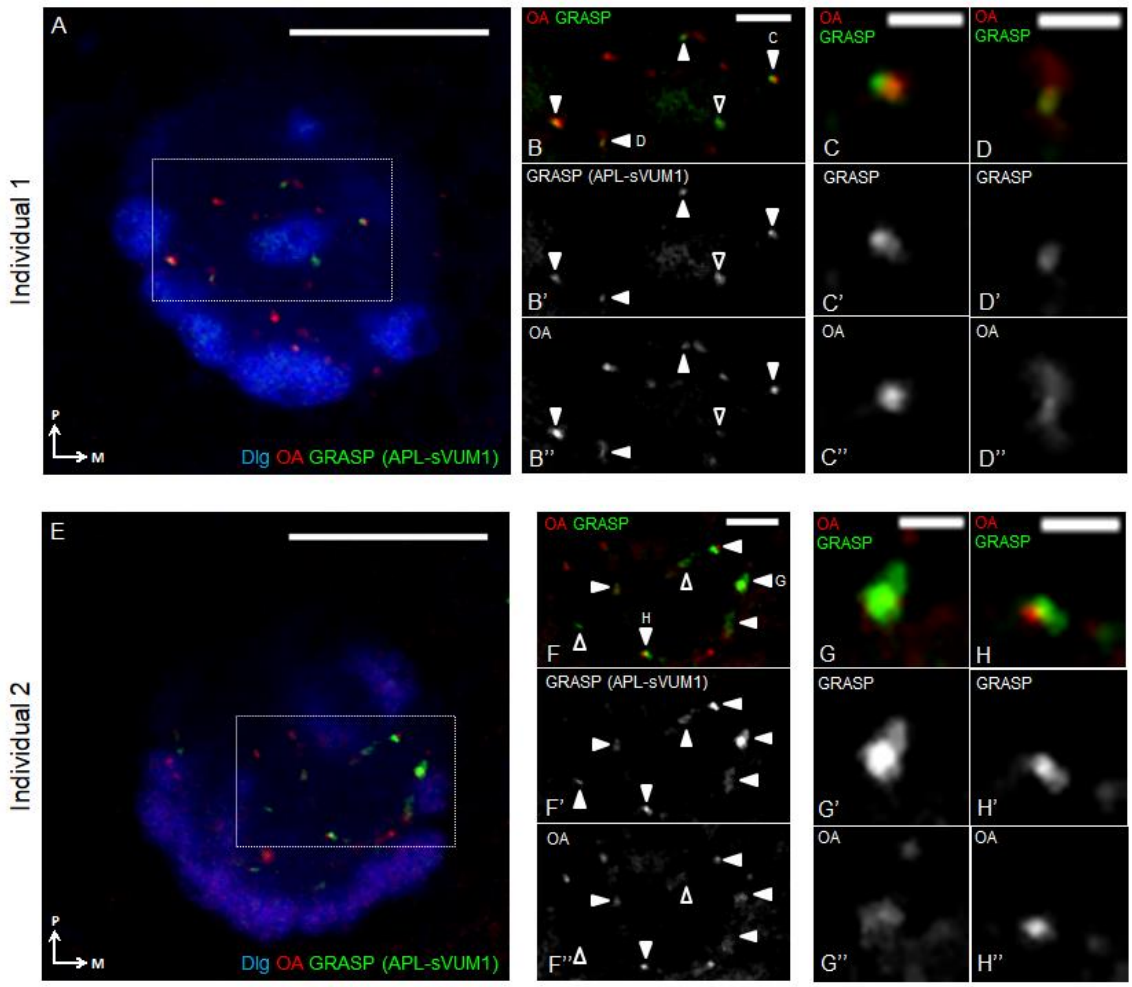

Figure 3.3. Many APL-sVUM1 GRASP puncta colocalised with OA terminals. Single confocal optical sections of the calyx from two *NP2631-GAL4/LexAOp-CD4::spGFP11; Tdc2-LexA/UAS-CD4::spGFP1-10* individuals. Green is APL-sVUM1 GRASP, red is anti-OA and blue is anti-Dlg. **(B,F)** are magnified from the rectangular box in **(A)** and **(E)** respectively. **(C-D)** and **(G-H)** are magnified puncta labelled in **(B)** and **(F)** respectively. Filled arrowheads indicate GRASP-OA colocalisation, and empty arrowheads indicate GRASP puncta negative for OA. Medial (M) is right, posterior (P) is up. Scale bar: 20 µm for **(A,E)**, 5 µm for **(B,F)** and 2 µm for **(C-D,G-H)**.

APL-sVUM1 GRASP	GRASP	OA	OA overlap	%overlap/ OA	%overlap/ GRASP
Individual 1	29	43	23	53%	79%
Individual 2	43	56	31	55%	72%
Individual 3	42	53	27	51%	64%
Individual 4	46	59	33	56%	72%
Individual 5	47	60	30	50%	64%
Individual 6 - Left Calyx	45	55	32	58%	71%
Individual 6 - Right Calyx	20	37	13	35%	65%
Individual 7 - Left Calyx	50	55	40	73%	80%
Individual 7 - Right Calyx	40	47	34	72%	85%
N	9	9	9	9	9
Mean	40	52	29	56%	72%
S.D.	9.6	7.7	7.7	0.1	0.1
S.E.M.	3.2	2.6	2.6	0.0	0.0

Table 3.2. Numbers of APL-sVUM1 GRASP and OA puncta in *NP2631-GAL4;Tdc2-LexA>GRASP* calyces. Abbreviations as Table 3.1.

neurons labelled in *Tdc2-LexA* colocalised with OA. 19 ± 1.4 out of 26 ± 1.8 (around 75%) GRASP signals between Odd-like neurons and sVUM1 neurons colocalised with OA (n=19; Fig. 3.4, filled arrowheads; Table 3.3) – indicating that Odd-like neurons were putative postsynaptic partners to sVUM1 neurons. Again, there are varying degrees of GRASP-OA overlap at specific puncta (Fig. 3.4C,F). The GRASP puncta that do not overlap with OA (Fig. 3.4, empty arrowheads) are probably not synaptic sites, as Odd-like neurons are predominantly postsynaptic in the larval calyx (L. Masuda-Nakagawa, personal communication). However, these may reflect Odd-like-sVUM1 synaptic connections in which sVUM1 neurons release non-OA neurotransmitters, such as TA or neuropeptides.

The above results suggested that PNs, the APL neuron and Odd-like neurons are all putative postsynaptic partners to sVUM1 neurons in the larval calyx. However, it is important to consider the large variation in the number of OA boutons observed between the three GRASP experiments, although this number remains relatively consistent (SEM < 3) within an experiment. This may be due to natural variation of OA boutons in different fly genotypes, or may be variations in the experimental conditions, such as antibody labelling batches. This may have led to over- or under-estimation of the number of OA boutons. Therefore, it is more beneficial to consider the relative rather than absolute number of GRASP-OA puncta out of the total GRASP puncta, with GRASP and OA puncta acting as internal controls for each other within a single calyx.

3.2.2. KCs showed limited GRASP with sVUM1 neurons in the calyx

To confirm that KCs were unlikely to be postsynaptic partners of sVUM1 neurons in the calyx, I expressed the two halves of splitGFP in KCs, using the *H500-IT.GAL4* KC driver which I generated and characterised (H.W., MPhil Thesis 2014), and in sVUM1 neurons using *Tdc2-LexA*. Unlike the *Tdc2-GAL4* driver previously used for this experiment, *Tdc2-LexA* does not label KCs in the larval calyx (H.W., MPhil Thesis 2014). Therefore, this ensures that any GRASP signals observed between *H500-IT.GAL4* and *Tdc2-LexA* are attributed to KC-sVUM1 GRASP in the calyx.

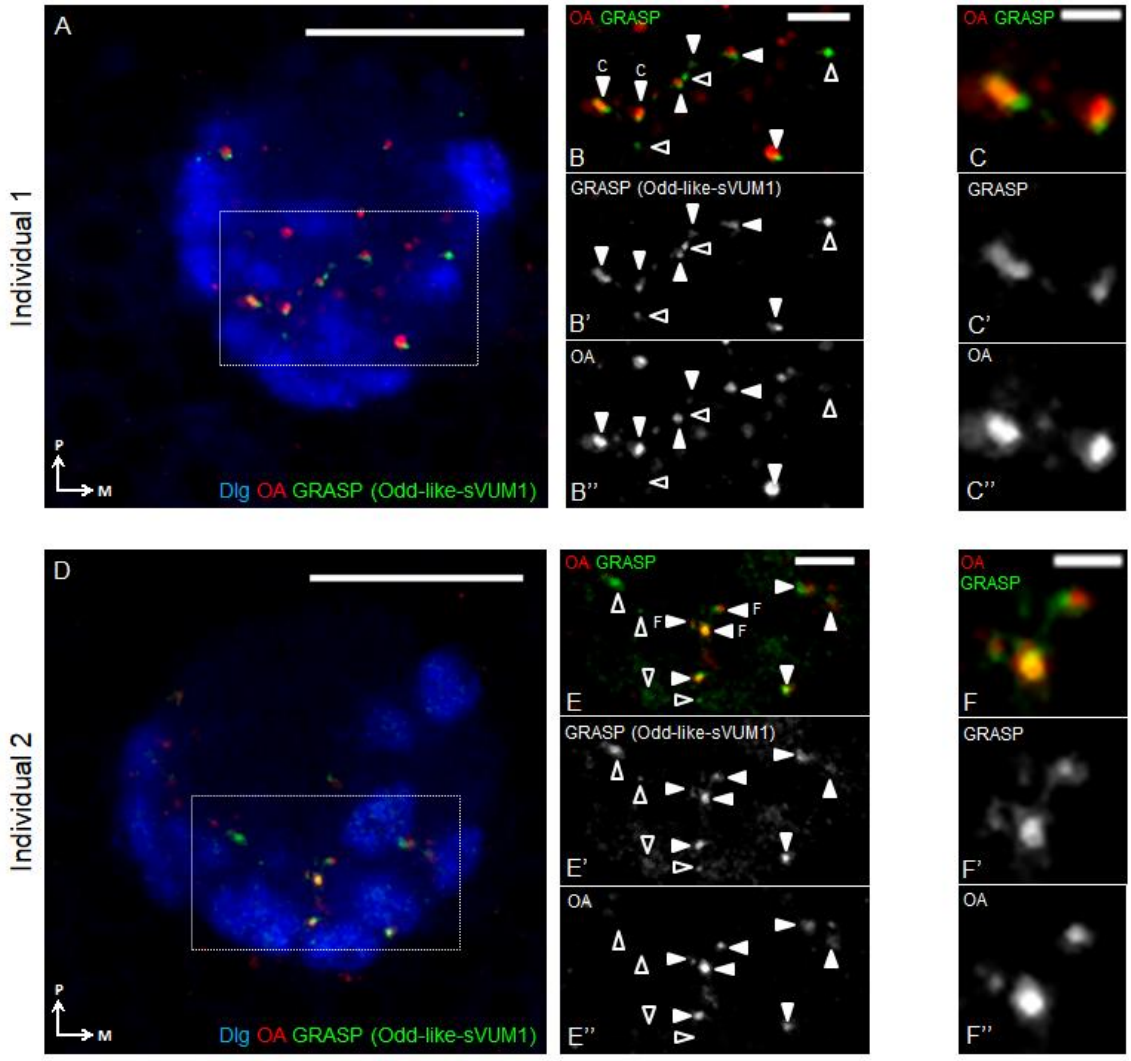

Figure 3.4. Many Odd-like-sVUM1 GRASP puncta colocalised with OA terminals. Single confocal optical sections of the calyx from two *OK263-GAL4/LexAOp-CD4::spGFP11; Tdc2-LexA/UAS-CD4::spGFP1-10* individuals. Green is Odd-like-sVUM1 GRASP, red is anti-OA and blue is anti-Dlg. **(B,E)** are magnified from the rectangular box in **(A)** and **(D)** respectively. **(C,F)** are magnified puncta labelled in **(B)** and **(E)** respectively. Filled arrowheads indicate GRASP-OA colocalisation, and empty arrowheads indicate GRASP puncta negative for OA. Medial (M) is right, posterior (P) is up. Scale bar: 20 µm for **(A,D)**, 5 µm for **(B,E)** and 2 µm for **(C,F)**.

Odd-like-sVUM1 GRASP	GRASP	OA	OA overlap	%overlap/ OA	%overlap/ GRASP
Individual 1	19	48	13	28%	70%
Individual 2	31	31	20	64%	63%
Individual 3	17	26	14	54%	84%
Individual 4	18	30	16	53%	89%
Individual 5	33	53	23	43%	71%
Individual 6	15	25	12	47%	77%
Individual 7	24	38	22	58%	92%
Individual 8	21	33	16	48%	74%
Individual 9	12	39	10	25%	78%
Individual 10	36	51	28	55%	78%
Individual 11	21	44	16	37%	79%
Individual 12 - Left Calyx	27	47	17	36%	63%
Individual 12 - Right Calyx	30	48	17	35%	57%
Individual 13 - Left Calyx	38	44	30	68%	79%
Individual 13 - Right Calyx	37	46	26	57%	71%
Individual 14 - Left Calyx	27	42	23	54%	83%
Individual 14 - Right Calyx	28	43	17	39%	61%
Individual 15 - Left Calyx	32	52	25	49%	78%
Individual 15 - Right Calyx	32	58	27	47%	84%
N	19	19	19	19	19
Mean	26	42	19	47%	75%
S.D.	7.7	9.4	5.9	0.1	0.1
S.E.M.	1.8	2.2	1.4	0.0	0.0

Table 3.3. Numbers of Odd-like-sVUM1 GRASP and OA puncta in *OK263-GAL4;Tdc2-LexA>GRASP* calyces. Abbreviations as Table 3.1.

I consistently observed 10 or less KC-sVUM1 GRASP puncta in larval calyces (n=16; Fig. 3.5, arrowheads); where 10 out of 16 calyces showed less than 5 GRASP puncta each (Table 3.4). This is consistent to the number of GRASP signals observed using *Tdc2-GAL4* and *MB247-LexA* drivers (H.W., MPhil Thesis 2014). 3 ± 0.7 out of 4 ± 0.8 (or around 82%) GRASP puncta colocalised with OA boutons (Fig. 3.5, filled arrowheads; Table 3.4) – suggesting KCs were likely to have few postsynaptic contacts with sVUM1 neurons in the calyx.

Neither *H500-IT.GAL4>GRASP* (n=2; Fig. 3.6A) nor *Tdc2-LexA>GRASP* (n=4; Fig. 3.6B) showed GRASP puncta on their own. Moreover, both *H500-IT.GAL4* and *Tdc2-LexA* were present in the *H500-IT.GAL4;Tdc2-LexA* line used for KC-sVUM1 GRASP, and specifically label KCs and sVUM1 neurons in the calyx respectively (Fig. 3.6C-D). These controls validate the GRASP signals observed in Fig. 3.5 result from splitGFP reconstitution between KCs and sVUM1 neurons in the larval calyx.

3.2.3. sVUMmd1 and sVUMmx1 clones both showed GRASP with the APL neuron

To determine whether one or both sVUM1 neurons are responsible for the GRASP observed with the APL neuron, I expressed spGFP1-10 in the APL neuron using *NP2631-GAL4, and LexAOp2-IVS>stop>spGFP11::CD4::HA-T2A-Brp::mCherry* in *Tdc2-LexA* neurons to generate sVUMmd1 and sVUMmx1 clones driving spGFP11 upon heat shock-induced FLP-out (Karuppudurai et al., 2014). The optimal heat shock conditions to generate sVUM1 clones and method to identify sVUMmd1 and sVUMmx1 clones were established by Angela Wan (A.W., MPhil Thesis 2015).

I identified five individuals that labelled *Tdc2-LexA* clones innervating the larval calyx – all of which showed between 1-8 GRASP puncta per calyx (Fig. 3.7, 3.8; Table 3.5). To distinguish between sVUMmd1 and sVUMmx1 clones, I measured the perpendicular distance between the cell body of the clone to the AL from the ventral orientation. This distance is 26.91 ± 3.89 µm for sVUMmd cell bodies and 49.27 ± 5.64 µm for sVUMmx cell bodies (A.W., MPhil Thesis 2015). From this data, I also observed that the SOG bifurcation point for

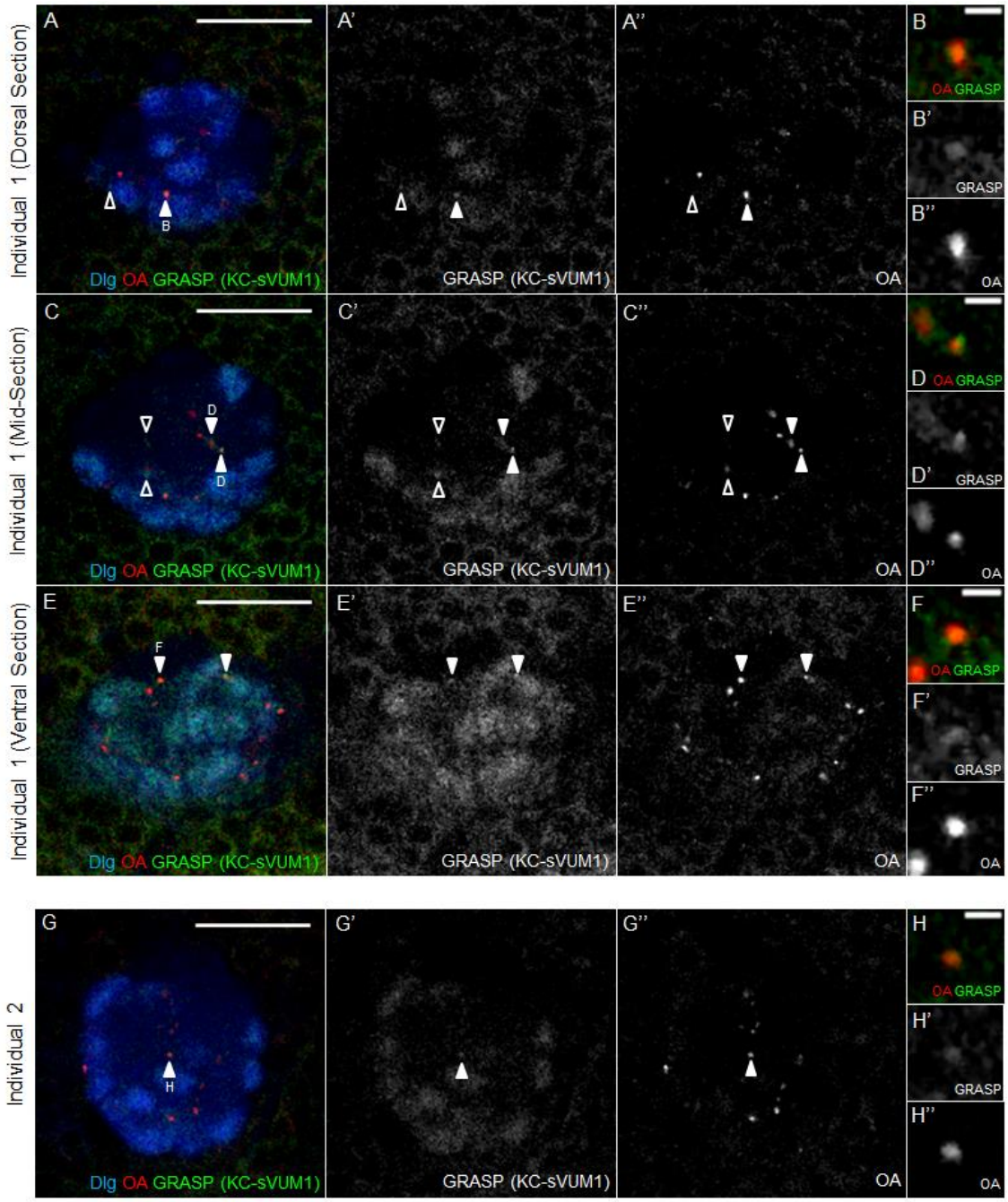

Figure 3.5. Few GRASP puncta between KCs and sVUM1 neurons. Single confocal optical sections of the calyx from two *Tdc2-LexA/LexAOp-CD4::spGFP11; H500-IT.GAL4/UAS-CD4::spGFP1-10* individuals. Green is KC-sVUM1 GRASP, red is anti-OA and blue is anti-Dlg. **(B,D,F,H)** are magnified puncta labelled in **(A,C,E,G)** respectively. Filled arrowheads indicate GRASP-OA colocalisation, and empty arrowheads indicate GRASP puncta negative for OA. Medial (M) is right, posterior (P) is up. Scale bar: 20 µm for **(A,C,E,G)** and 2 µm for **(B,D,F,H)**.

KC-sVUM1 GRASP	GRASP	OA	OA overlap	%overlap/ OA	%overlap/ GRASP
Individual 1	1	70	1	1%	100%
Individual 2	0	69	0	0%	N/A
Individual 3	2	72	2	3%	100%
Individual 4	10	57	7	12%	70%
Individual 5 - Left Calyx	1	70	0	0%	0%
Individual 5 - Right Calyx	2	74	1	1%	20%
Individual 6 - Left Calyx	5	95	5	5%	100%
Individual 6 - Right Calyx	8	89	7	8%	88%
Individual 7 - Left Calyx	7	67	7	10%	100%
Individual 7 - Right Calyx	9	84	8	10%	89%
Individual 8 - Left Calyx	1	88	1	1%	100%
Individual 8 - Right Calyx	4	55	4	0%	100%
Individual 9 - Left Calyx	4	71	3	4%	75%
Individual 9 - Right Calyx	7	67	7	10%	100%
Individual 10 - Left Calyx	0	52	0	0%	N/A
Individual 10 - Right Calyx	2	61	2	3%	100%
N	16	16	16	16	14
Mean	4	71	3	4%	82%
S.D.	3.3	12.4	3.0	0.0	0.3
S.E.M.	0.8	3.1	0.7	0.0	0.1

Table 3.4. Numbers of KC-sVUM1 GRASP and OA puncta in *Tdc2-LexA; H500-IT.GAL4>GRASP* calyces. Abbreviations as Table 3.1.

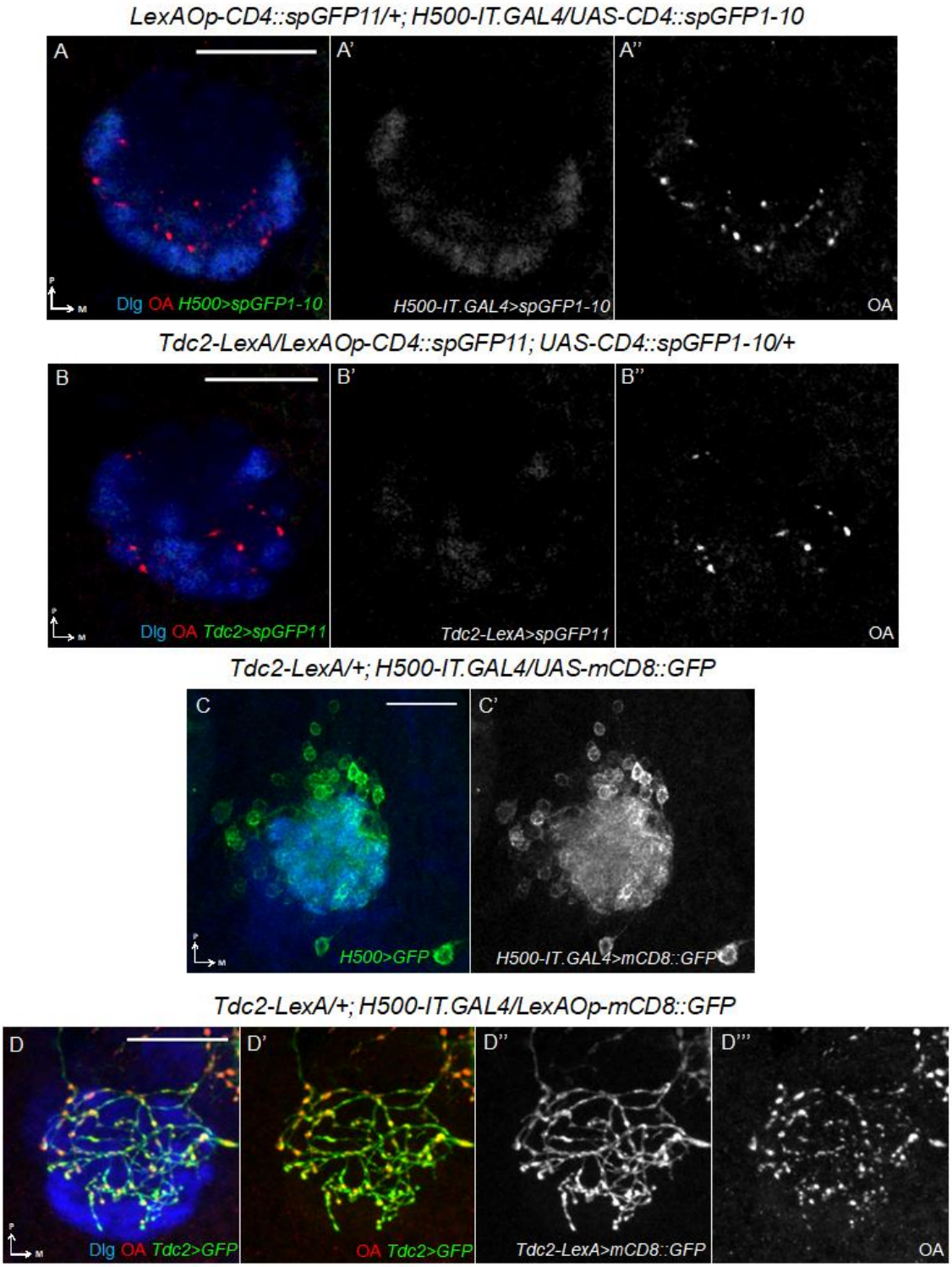

Figure 3.6. Negative and positive controls for KC-sVUM1 GRASP. (A-B) are single representative confocal optical sections of the calyx. No GRASP puncta observed in *H500-IT.GAL4>GRASP* (green) **(A)** or *Tdc2-LexA>GRASP* (green) **(B)** negative control calyces. **(C-D)** are confocal projections of the calyx. *H500-IT.GAL4;Tdc2-LexA>UAS-mCD8::GFP* (green) **(C)** and *H500-IT.GAL4;Tdc2-LexA>LexAOp-mCD8::GFP* (green) **(D)** validate the presence of KC driver *H500-IT.GAL4* and sVUM1 driver *Tdc2-LexA* respectively in the *H500-IT.GAL4;Tdc2-LexA* construct used for KC-sVUM1 GRASP. Red is anti-OA and blue is anti-Dlg. Medial (M) is right, posterior (P) is up. Scale bar: 20 µm.

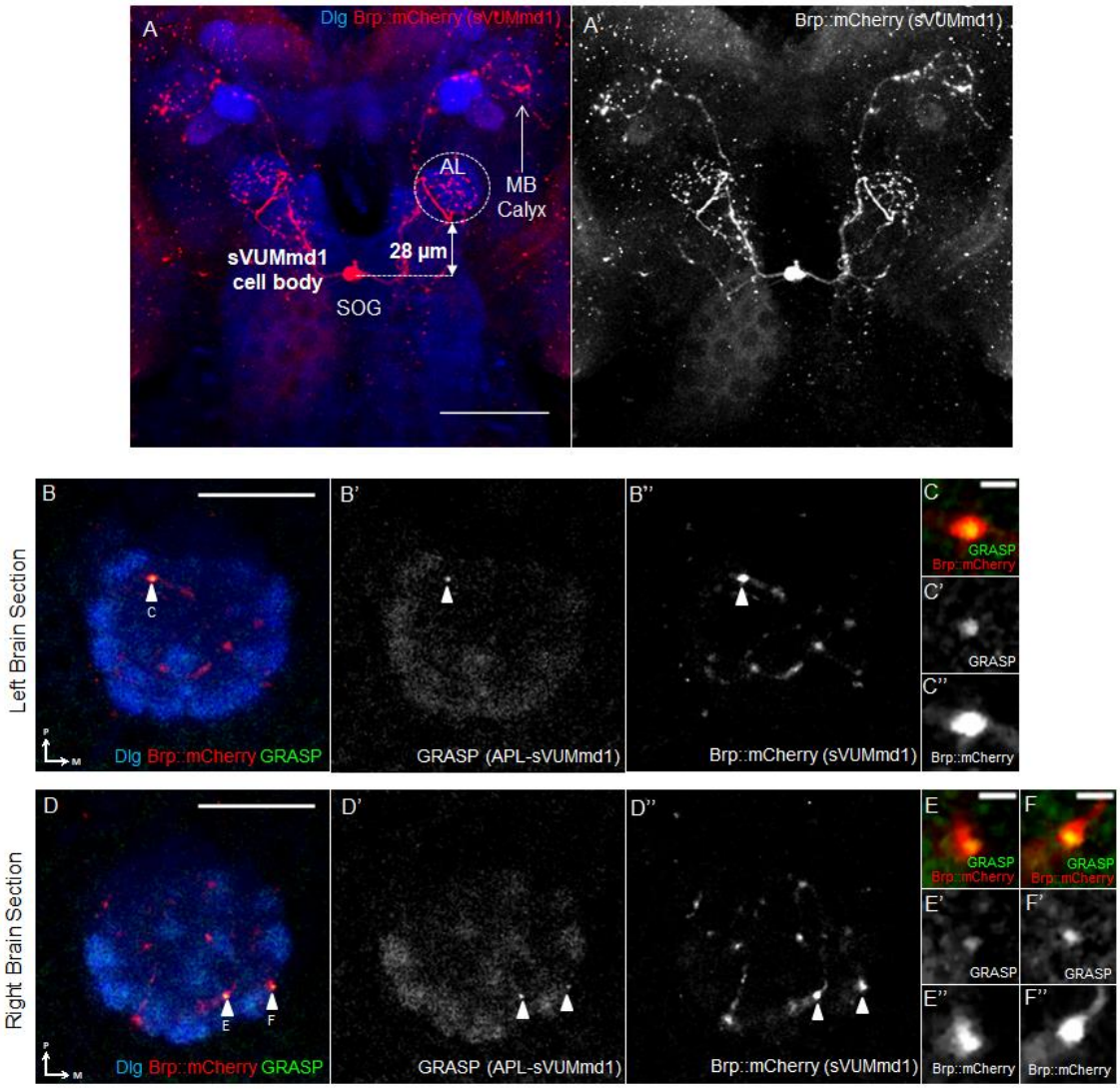

Figure 3.7. GRASP puncta observed between APL and sVUMmd1 clone. (A) Confocal projection of the ventral larval brain and SOG of *hsFLP; Tdc2-LexA/NP2631-GAL4; LexAOp2-IVS>stop>spGFP11::CD4::HA-T2A-Brp::mCherry, UAS-spGFP1-10::CD4, UAS-HRP::CD2*. Anterior is up, medial is at vertical mid-line. FLP-out clone is labelled with Brp::mCherry (red), anti-Dlg is blue. The perpendicular distance from the bottom end of the AL and the sVUMmd1 cell body is indicated. **(B,D)** Single confocal optical sections of the calyx from the same individual. Medial (M) is right and posterior (P) is up. Green is APL-sVUMmd1 GRASP. **(C,E-F)** are magnified puncta from **(B)** and **(D)** respectively. Filled arrowheads indicate GRASP-Brp::mCherry colocalisation. Scale bar: 50 µm for **(A)**, 20 µm for **(B,D)** and 2 µm for **(C,E)**.

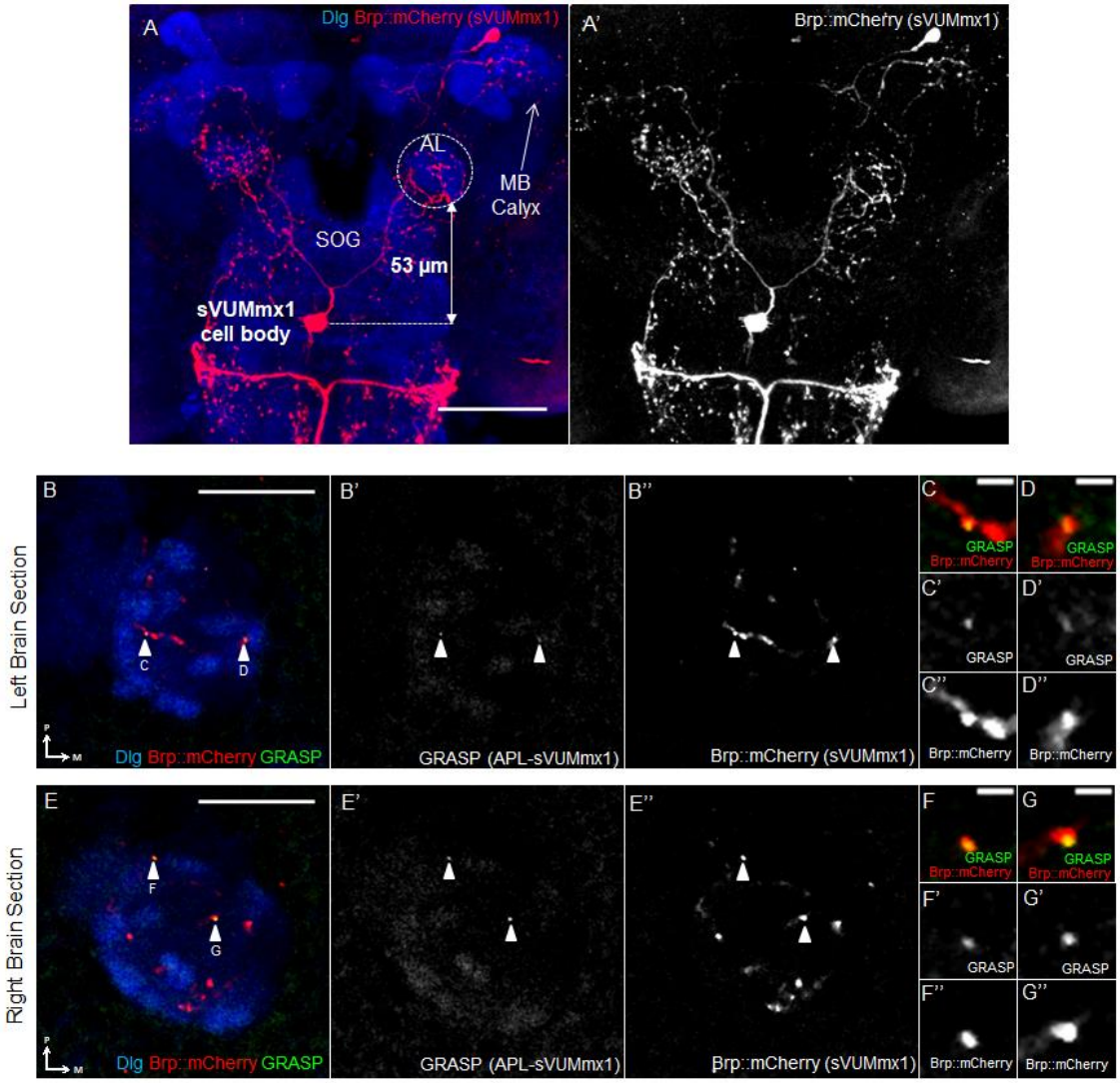

Figure 3.8. GRASP puncta observed between APL and sVUMmx1 clone. (A) Confocal projection of the ventral larval brain of *hsFLP; Tdc2-LexA/NP2631-GAL4; LexAOp2-IVS>stop>spGFP11::CD4::HA-T2A-Brp::mCherry, UAS-spGFP1-10::CD4, UAS-HRP::CD2*. Anterior is up, medial is at vertical mid-line. FLP-out clone is labelled with Brp::mCherry (red), anti-Dlg is blue. The perpendicular distance from the bottom end of the AL and the sVUMmx1 cell body is indicated. **(B,E)** Single confocal optical sections of the calyx from the same individual. Medial (M) is right and posterior (P) is up. Green is APL-sVUMmx1 GRASP. **(C-D,F-G)** are magnified puncta from **(B)** and **(E)** respectively. Filled arrowheads indicate GRASP-Brp::mCherry colocalisation. Scale bar: 50 µm for **(A)**, 20 µm for **(B,E)** and 2 µm for **(C-D,F-G)**.

	Distance from AL (μm)	No. of GRASP puncta		sVUM1 clone
		Left Calyx	Right Calyx	
Individual 1	28	1	4	sVUMmd1
Individual 2	53	2	2	sVUMmx1
Individual 3	51	3	2	sVUMmx1
Individual 4	53	7	8	sVUMmx1
Individual 5	31 & 51 (2 Cell Bodies)	8	7	Undetermined

Table 3.5. Numbers of APL-sVUMmd1 and APL-sVUMmx1 GRASP puncta in *NP2631-GAL4;Tdc2-LexA>FRT-GRASP* calyces. Distance from AL is calculated from the bottom tip of the AL to the sVUM cell body. Abbrevations: No., number.

sVUMmd neurons was more horizontal while that for sVUMmx neurons was V-shaped. Using these two criteria, I identified one individual that labelled a sVUMmd1 clone (Fig. 3.7) and three individuals that each labelled a sVUMmx1 clone (Fig. 3.8; Table 3.5). The fifth individual labelled two cell bodies – one in the sVUMmd cluster and another in the sVUMmx cluster – and therefore it was not possible to distinguish whether it labelled sVUMmd1 and/or sVUMmx1 (Table 3.5).

Both sVUMmd1 (n=1; Fig. 3.7B-F) and sVUMmx1 (n=3; Fig. 3.8B-G) clones showed GRASP with the APL Neuron. All of the GRASP puncta colocalised with Brp::mCherry puncta (Fig. 3.7B-F, 3.8B-G), which labelled presynaptic terminals of sVUM1 clones. This suggested the APL neuron was postsynaptic to both sVUMmd1 and sVUMmx1 clones at these sites.

The maximum sum of GRASP signals detected for sVUMmd1 and sVUMmx1 clones with the APL neuron is 12 per calyx (Table 3.5) – less than half of the average number of APL-sVUM1 GRASP signals that colocalised with OA (Table 3.2). The reason for this discrepancy is unclear. However, I speculate that this could be due to the lower expression levels of the spGFP components as these larvae were raised at room temperature rather than 25ºC following the heat shock treatment to induce clones. An alternative speculation is that the heat shock treatment itself affected the development of sVUM1 and/or APL synaptic terminals, such that they showed fewer GRASP contacts. There is also a large variation in the number of GRASP signals detected per calyx (Table 3.5). This is probably due to a small sample size, which was caused by the low frequency – 2.7% at optimal heat shock conditions – for generating unambiguous sVUM1 clones (A.W., MPhil Thesis 2015).

3.3. Discussion

3.3.1. OA colocalisation with sVUM1 GRASP

To identify postsynaptic partners of sVUM1 neurons in the larval calyx, I used anti-OA labelling to identify sVUM1 terminals where OA is released. I assumed that 1) OA is mainly released at the presynaptic terminals of sVUM1 neurons; 2) GRASP-OA colocalisation indicated higher probability of synaptic contact; and 3) neurons that show GRASP-OA colocalisation with sVUM1 neurons are putatively postsynaptic to sVUM1 neurons. However, there may be alternative interpretations for GRASP-OA colocalisation or the lack thereof.

OA boutons may not necessarily indicate pre-synaptic terminals of sVUM1 neurons, because OA can be released extrasynaptically via volume transmission as evidenced by the dense core vesicles observed in fly OA neurons (Grygoruk et al., 2014; Eichler et al., 2017). However, OA-GRASP contacts suggest that these neurons are in close enough proximity to receive OA signalling, whether it is via synaptic or non-synaptic transmission. Moreover, even if OA-GRASP colocalisation accurately marks presynaptic sVUM1 terminals, their GRASP partners could instead be modulating presynaptic OA release from sVUM1 neurons. This is probable when sVUM1 GRASP partners are also predominantly presynaptic in the calyx, such as PNs or the APL neuron. It is also possible that these GRASP contacts show bi-directional axo-axonal transmission. These different connectivity scenarios may be one of the reasons for the variable degree of overlap between GRASP and OA puncta.

While the absolute number of GRASP puncta detected vary depending on the putative synaptic partner, the percentage of GRASP-OA contacts out of total GRASP signals ranges between 65-82% (Fig. 3.9; Table 3.1, 3.2, 3.3, 3.4). There are several interpretations as to why some GRASP signals do not overlap with OA: 1) Some of the GRASP signals are not synaptic contacts, but are due to neuronal tracts crossing over each other; 2) Some GRASP puncta instead localised to the presynaptic terminals of the GRASP partners, such as GRASP-GABA colocalisation observed in APL-sVUM1 GRASP (H.W., MPhil Thesis 2014), indicating that sVUM1 neurons may sometimes be postsynaptic; and 3) GRASP puncta may be localised to sVUM1 terminals in which alternative neurotransmitters, such as neuropeptides, are released instead of OA.

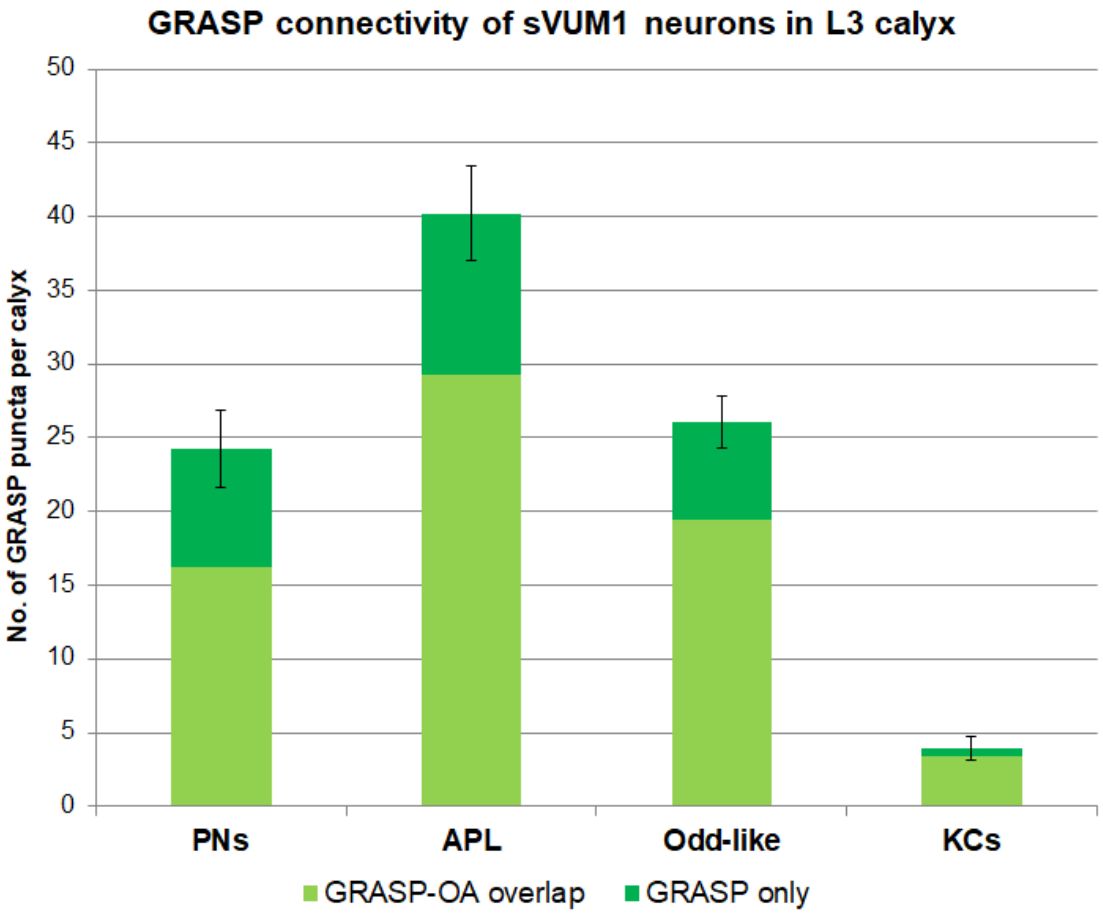

Figure 3.9. Numbers of GRASP puncta between sVUM1 neurons and their putative synaptic partners in the third instar larval calyx. Light green indicates the number of GRASP-OA puncta, while dark green indicates the number of GRASP puncta that did not colocalise with OA. Error bars indicate standard error of the mean (S.E.M.). Abbreviations: L3, third instar larval; No., number.

3.3.2. Putative postsynaptic targets of sVUM1 neurons in the calyx

Based on GRASP-OA colocalisation, PNs, the APL neuron and Odd-like neurons are putative postsynaptic partners of sVUM1 neurons in the calyx (Fig. 3.10). Consistent with previous results (H.W., MPhil Thesis 2014), KCs showed limited GRASP with sVUM1 neurons, most of which overlapped with OA; suggesting that very few KCs are postsynaptic to sVUM1 neurons. To determine the distribution of OA synapses between its multiple putative postsynaptic partners, I quantified the percentage of OA-GRASP puncta out of total OA boutons. The APL neuron and Odd-like neurons showed the largest share of putative OA synapses at around 56% and 47% respectively (Table 3.2, 3.3). This was followed by PNs at around 21% (Table 3.1), while KCs showed the smallest share at around 4% (Table 3.4). This suggested that the APL and Odd-like neurons were probably the main targets of OA signalling from sVUM1 neurons in the calyx.

The single APL neuron shows the largest absolute number and share of OA-GRASP contacts with sVUM1 neurons (Fig. 3.9; Table 3.2). This suggested that the APL neuron is strongly modulated by OA signalling by sVUM1 neurons in the calyx. APL-sVUM1 GRASP also colocalised with GABA (H.W., MPhil Thesis 2014), suggesting that sVUM1 neurons are reciprocally modulated by the APL neuron in the calyx (Fig. 3.10). As both sVUM1 neurons and the APL neuron are predominantly presynaptic in the calyx (Masuda-Nakagawa et al., 2014; L. Masuda-Nakagawa, personal communication), their synapses are likely to be axo-axonal and/or bi-directional. This suggested that the APL neuron inhibited OA release from sVUM1 terminals, while sVUM1 modulated GABA release from APL terminals, in the larval MB calyx. This provides an avenue for sVUM1-mediated control of the APL feedback inhibition onto KCs, and therefore the sparseness of odour representations in the MBs. However, whether OA signalling increases or decreases APL activity depends on the type of OA receptors expressed on the APL neuron.

Another instance of axo-axonal modulation by sVUM1 neurons is likely to be at PN terminals in the calyx. As putative postsynaptic partners to sVUM1 neurons, sVUM1 signalling may modulate neurotransmitter release from

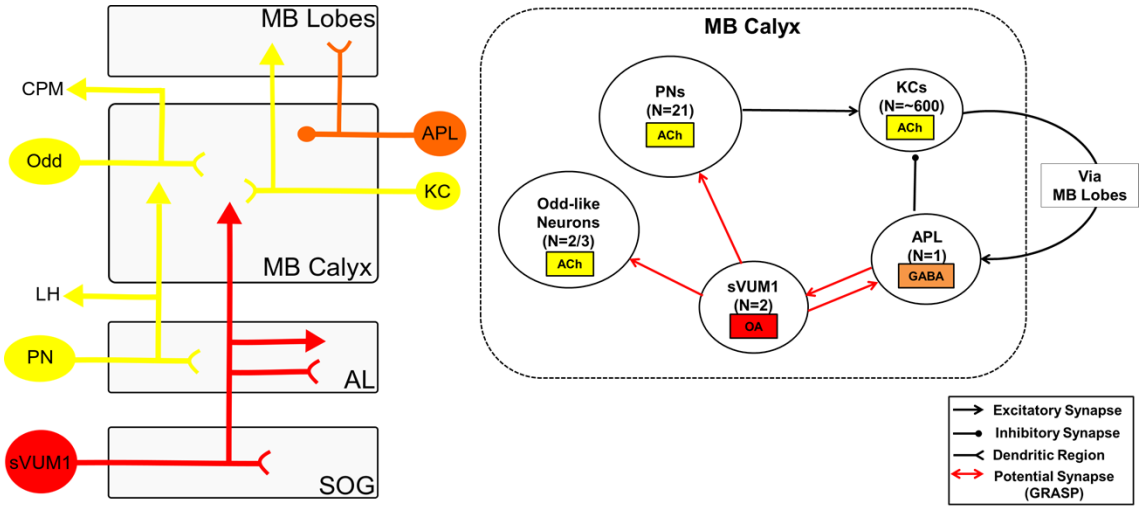

Figure 3.10. Revised sVUM1 connectivity diagram of the larval MB calyx. Abbreviations: ACh, acetylcholine; AL, antennal lobe; CPM, centroposterior medial compartment; KC, Kenyon Cell; LH, lateral horn; MB, mushroom body; N, number; OA, octopamine; PN, projection neuron.

presynaptic terminals of PNs onto KCs, which would also affect odour representations in KCs. If all PNs labelled by the *NP225-GAL4* line show GRASP with sVUM1 neurons, they would each share one synapse with one of the sVUM1 neurons. Alternatively, only a subset of PNs may synapse with sVUM1 neurons.

Odd-like neurons also show a large share of OA-GRASP contacts. This is expected as Odd-like neurons are postsynaptic in the calyx (Slater et al., 2015). As there are two or three Odd-like neurons in the larval calyx (Slater et al., 2015; Eichler et al., 2017), they may each form more than one synapse with sVUM1 neurons. This suggests that the activity of Odd-like neurons may be regulated by sVUM1 neurons.

Limited GRASP contacts were observed between KCs and sVUM1 neurons using two different set of drivers suggested very few KCs – out of a larval population of around 600 (Ramaekers et al., 2005) – synapse with sVUM1 neurons. As mentioned above, KC activity may still be modulated by sVUM1 signalling via PNs and the APL neuron. Alternatively, KCs may also receive OA signalling via non-synaptic transmission if they expressed extrasynaptic OA receptors.

3.3.3. GRASP connectivity of sVUMmd1 and sVUMmx1 neurons

While sVUMmd1 and sVUMmx1 neurons innervate the same neuropils, they show largely non-overlapping innervation patterns (Fig. 3.11A-B), suggesting that they may not share the same synaptic partners. The evidence so far contradicts this prediction, as both sVUMmd1 and sVUMmx1 clones show single cell GRASP with Odd-like neurons (A.W., MPhil Thesis 2015) and the APL neuron in the calyx. This is in agreement with EM data from the L1 brain – which additionally show that sVUMmd1 and sVUMmx1 neurons each have similar number of synapses with PNs (Fig. 3.11C).

While sVUMmd1 and sVUMmx1 may show equivalent connectivity in the larval calyx, it is still unclear whether they are functionally redundant, as they may receive inputs from different neurons outside the MB, for which data are not yet available. In fact, ablating all the sVUM neurons in the mandibular (md) segment versus those in the maxillary (mx) segment in fly larvae resulted in

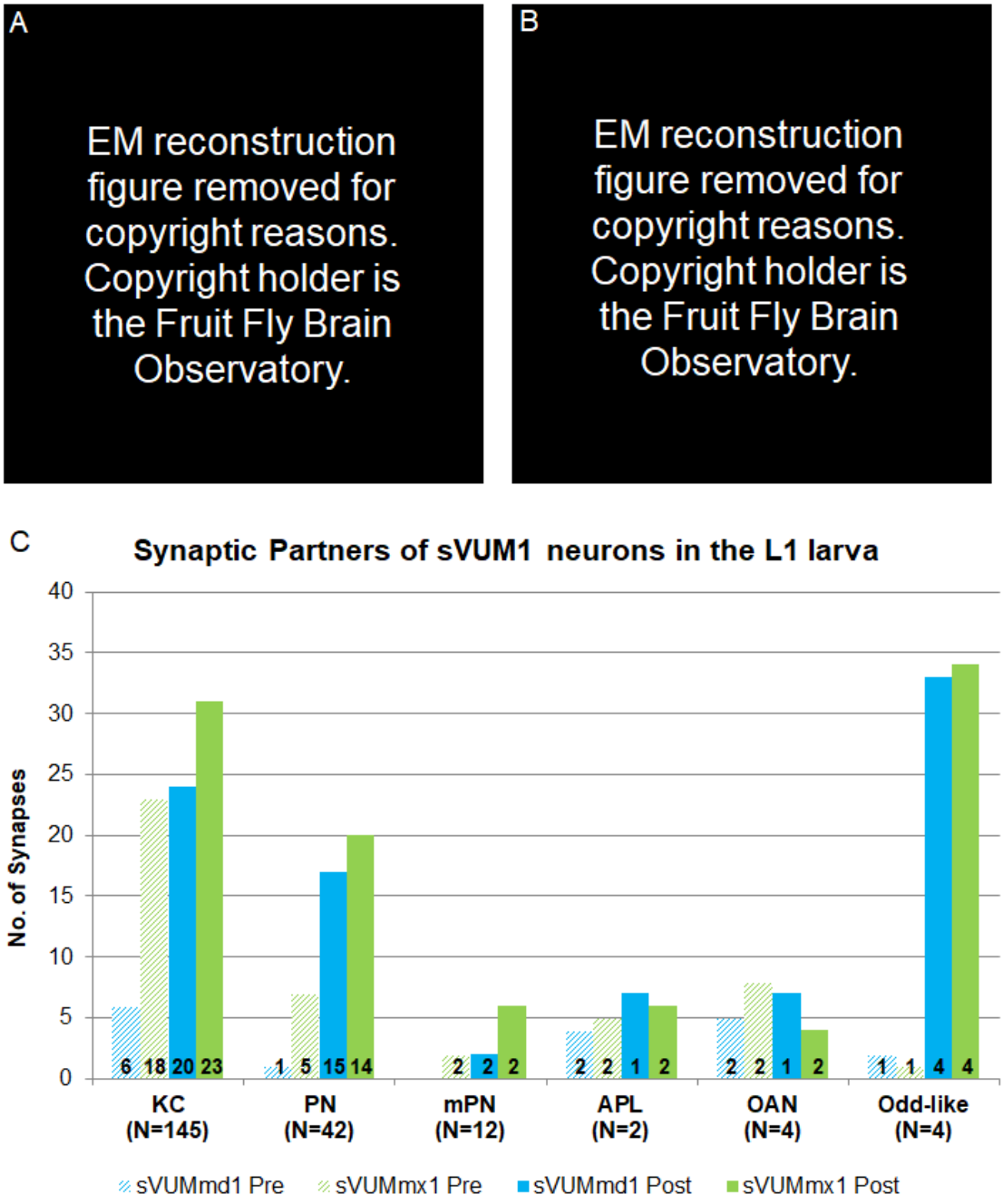

Figure 3.11. Synaptic connectivity of sVUM1 neurons in the first instar larval brain. (A-B) Innervation pattern of sVUMmd1 (blue) and sVUMmx1 (green) neurons in the first instar larval (L1) brain **(A)** and MB calyx **(B)** reconstructed from EM data. **(C)** Synaptic connectivity of sVUM1 neurons in the L1 larva based on EM data. The bar graph represents the total number of synapses between sVUMmd1 (blue) or sVUMmx1 (green) neurons and their synaptic partners in both of the brain lobes in the L1 brain. The numbers immediately above the x-axis indicate the number of neurons from each neuronal type that synapse with sVUM1 neurons; e.g. 6 KCs are presynaptic to sVUMmd1 neurons. The total number of each neuronal type is labelled below the x-axis, e.g. N=145 for KCs. **Figure 3.11** is generated from data and images obtained from https://neuronlp.larva.fruitflybrain.org/ Abbreviations: AL, antennal lobe; mPN, multiglomerular PN; N/No., number; OAN, OA neurons; Pre, presynaptic partner; Post, postsynaptic partner; SOG, suboesophageal ganglion.

opposing satiety state-dependent feeding behaviours (Zhang et al., 2013a) – suggesting that there may be functional differences between OA neurons in the two segments.

On the other hand, the OA-VUMa2 neurons in the adult brain which innervate the same neuropils as the sVUM1 neurons (Busch et al., 2009; Selcho et al., 2014) are similarly divided into md and mx subtypes based on the locations of their cell bodies (Busch and Tanimoto, 2010). However, there is no evidence to suggest they show different connectivity patterns or functions.

3.3.4. OA connectivity in the first instar larval and adult calyces

The main difference between OA connectivity in the L3 compared to L1 and adult calyces is the lack of putative KC-OA synapses. Strong and dense GRASP signals have been observed between OA neurons and KCs in the adult calyx (Zhou et al., 2012; Pech et al., 2013); while more recent EM data have shown that L1 KCs synapse with sVUM1 neurons (Fig. 3.11C; Eichler et al., 2017). This difference may be due to changes in neuronal connectivity over development: KCs initially form synapses with OA neurons in the L1 stage, these synapses get pruned at the L3 stage and regrown in adults. While the lineage of OA neurons is unclear, this could be linked to the pruning of larval KCs after the L3 stage that eventually become γ KCs, or the birth of the adult specific α/β KCs (Lee et al., 1999). In the adult, there are also two additional types of OA neurons innervating the calyx besides the sVUM1 analogue OA-VUMa2 that do not have larval analogues (Busch et al., 2009); and therefore may instead be responsible for the OA-KC GRASP observed in the adult calyx. As a neuromodulator, OA may be required for functions specific to individual developmental stages. For example, courtship behaviour requires OA function in the adult MB (Zhou et al., 2012), but this circuit would be unnecessary in the third instar larvae, which is why third instar larvae may lack some of the connections found in the adult brain. Nevertheless, as third instar larvae are still capable of odour discrimination, this suggests that limited KC-OA synapses are not crucial for this conserved behaviour.

Besides KCs, there is little evidence for other synaptic partners of OA neurons in the adult calyx. However, EM reconstruction data in the first instar larva (Berck et al., 2016; Eichler et al., 2017) show that a subset of PNs, the

APL neuron and Odd-like neurons are all postsynaptic to sVUM1 neurons; while the APL neuron is also presynaptic to sVUM1 neurons (Fig. 3.11C). This is consistent with my deductions from GRASP-OA/GABA colocalisation experiments in the L3 calyx. This suggests that much of the sVUM1 synaptic connectivity is already in place at the L1 stage. Additionally, L1 EM data show that 1) sVUM1 neurons synapse with multiglomerular PNs (mPNs); 2) five PNs are presynaptic to the sVUMmx1 neuron; and 3) sVUMmd1 and sVUMmx1 neurons have reciprocal connections with each other (Fig. 3.11C). This suggests strong interconnectivity between sVUM1 neurons with each other and other calyx-innervating neurons. However, we currently only have EM reconstruction data for one single larva (Berck et al., 2016; Eichler et al., 2017). This may not be representative of larval connectivity, as we do not know how synaptic connectivity may vary between individuals, or how this changes when larvae mature from L1 to L3 stages.

3.3.5. Alternative methods to identify sVUM1 target neurons

While GRASP is a convenient and high throughput method to identify putative synaptic partners of specific neurons, the main concern is that it does not directly detect synapses. Classical GRASP relies on the reconstitution of splitGFP fused to the human membrane protein CD4 (Feinberg et al., 2008; Gordon and Scott, 2009), such that CD4::spGFP is localised to the plasma membrane of the neurons they are expressed in, not just at synaptic terminals. Therefore, GRASP signals may be observed in the absence of synapses, such as when neuronal tracts cross over, provided that plama membrane-tethered spGFP halves are in close enough contact to reconstitute. This is also why GRASP cannot be used to detect the direction of neurotransmission.

Synaptic markers, such as Bruchpilot::mCherry in the FRT-GRASP construct (Karuppudurai et al., 2014), or neurotransmitter labelling, such as anti-OA used in this chapter, can be used to determine whether GRASP signals localised to synaptic terminals. spGFP can also be tethered to a synaptic marker, such as synaptobrevin (Karuppudurai et al., 2014), to ensure spGFP localisation to synaptic terminals.

While these methods may improve the probability of identifying synaptic connections using GRASP, it is still not possible to directly visualise synapses

using confocal microscopy. Synaptic clefts are around 100 nm in the central nervous system (Feinberg et al., 2008), postsynaptic sites are less than 100 nm in size, while the diameter of synaptic vesicles are 5-30 nm (Meinertzhagen and Lee, 2012) – all of which are beyond the resolving limit of confocal microscopes, which is around 150-200 nm for a numerical aperture of 1.3. Currently, EM is the only method at a sufficiently high resolution (around 2 nm) for visualising synapses in the fly brain (Meinertzhagen and Lee, 2012).

Recent connectomics projects are utilising EM data to systematically reconstruct the synaptic connectivity of the fly adult and L1 brains (Berck et al., 2016; Eichler et al., 2017; Takemura et al., 2017; Zheng et al., 2018). These projects have generated large amounts of data on the connectivity of neurons innervating the MBs already, including that of sVUM1 neurons in the L1 larva (Fig. 3.11; Eichler et al., 2017); and are expected to become extremely useful resources upon their completion.

As an unbiased method to map synapses, EM data can be used to identify novel synaptic partners that have not been previously identified. However, this may result in large amounts of data that we cannot yet interpret, as it is difficult to acquire the appropriate tools to characterise these neurons based on their morphology. Moreover, EM reconstruction and tracing is a time-consuming and labour-intensive task. The current data are generated from a single L1 larval brain and a single adult brain (Berck et al., 2016; Eichler et al., 2017; Takemura et al., 2017; Zheng et al., 2018); and cannot take into account of individual variability.

In the context of understanding neuromodulatory circuitry, EM connectivity data can show the location of dense core vesicles associated with volume transmission, for example in sVUM1 neurons in the L1 larva (Meinertzhagen and Lee, 2012; Eichler et al., 2017); but it cannot reveal their downstream extrasynaptic targets. The only comprehensive way of identifying all possible targets of neuromodulatory neurons is to identify where their receptors are localised. Therefore, in the following chapters, I aimed to identify the neurons subjected to OA signalling by the sVUM1 neurons in the calyx by systematically mapping OA receptor localisation.

Chapter 4. Expression of α1-adrenergic-like OAMB receptors in calyx-innervating neurons

4.1. Introduction

OAMB is a strong candidate for mediating OA signal in the larval MB calyx circuitry, based on its expression pattern in the adult MB (Han et al., 1998), and its known function in appetitive olfactory learning (Burke et al., 2012; Kim et al., 2013).

OAMB localisation to the MB calyx is likely to be conserved across insects, including in fly larvae. Based on immunostaining data, OAMB is enriched in the adult fly MB calyx (Han et al., 1998). Its honeybee homologue AmOA1 is similarly localised to the olfactory region (lip) of the honeybee calyx (Sinakevitch et al., 2011). Indeed, mRNA transcripts of α1-adrenoceptors localise to the rat piriform cortex and amygdala (Domyancic & Morilak, 1997). This suggests that α1-adrenoceptor localisation to higher brain olfactory centres may be conserved from insects to mammals, and therefore may share conserved functions in modulating olfactory processing circuits.

oamb mutants cannot form appetitive olfactory memories in adult flies (Burke et al., 2012; Kim et al., 2013); which suggests that OAMB may be required on neurons in the MB olfactory learning circuitry. Kim et al. (2013) showed that driving OAMB expression in αβ and γ KCs was sufficient for rescuing the learning impairment in an *oamb* mutant background. However, this rescue phenotype may be due to ectopic rather than native OAMB expression in KCs, as the group did not show whether OAMB knockdown specifically in KCs impaired learning. Burke et al. (2012) claimed that OAMB is instead required in dopaminergic PAM neurons, which convey sugar reinforcement signals from upstream OA neurons to the MBs, as OAMB-RNAi in PAM neurons significantly impaired reward learning. While it is uncertain whether appetitive olfactory learning in adult flies requires OAMB on KCs, PAM neurons or both, OAMB expression in neurons involved in olfactory processing or learning is likely to be conserved in the larval MB circuitry.

To understand whether and how OA signalling in the larval MB calyx is mediated by OAMB (Fig. 4.1), I aimed to address the following questions:

1) Is OAMB expressed in any of the putative postsynaptic partners of sVUM1 neurons?

Kim et al. (2013) observed that the OAMB localised to MB extrinsic neurons innervating the adult fly calyx and not in KCs, but did not show data in support. This suggested that OAMB is likely to be expressed in non-KC neurons in the larval calyx as well. Therefore, as potential postsynaptic partners of the OA sVUM1 neurons, PNs, the APL neuron and Odd-like neurons (Chapter 3) are all candidates for OAMB expression in the larval calyx.

While it is not known which of the above neurons express OAMB in *Drosophila*, this could be predicted from the localisation of its honeybee homologue AmOA1. AmOA1 immunoreactivity colocalised with anti-GABA, but not with a uniglomerular PN marker at the lip (olfactory region) of the honeybee calyx (Sinakevitch et al., 2013). This suggested that AmOA1 was expressed in GABAergic PCT feedback neurons but not uniglomerular PNs. If the function of α1-adrenergic-like OA receptors in insect MB calyces is conserved, this suggests that OAMB is probably expressed in the larval GABAergic APL neuron but not larval olfactory PNs, the *Drosophila* counterparts of the PCT neurons and uniglomerular PNs respectively.

Therefore, I aimed to determine whether OAMB localised to larval PNs, APL and Odd-like neurons.

2) Is OAMB localised to the presynaptic terminals of calyx-innervating neurons?

α1-adrenoceptors are primarily enriched in the axon terminals of dopamine neurons in rats based on electron microscopy data (Mitrano et al., 2012). Several electrophysiological studies have also shown that presynaptic α1 receptors are involved in modulating glutamate and GABA release in the hypothalamus and prefrontal cortex (Chen et al., 2006; Luo et al., 2015; Zhang et al., 2013b). This suggests the α1-adrenergic-like OAMB may also be expressed in presynaptic terminals of calyx-innervating neurons, such as that of

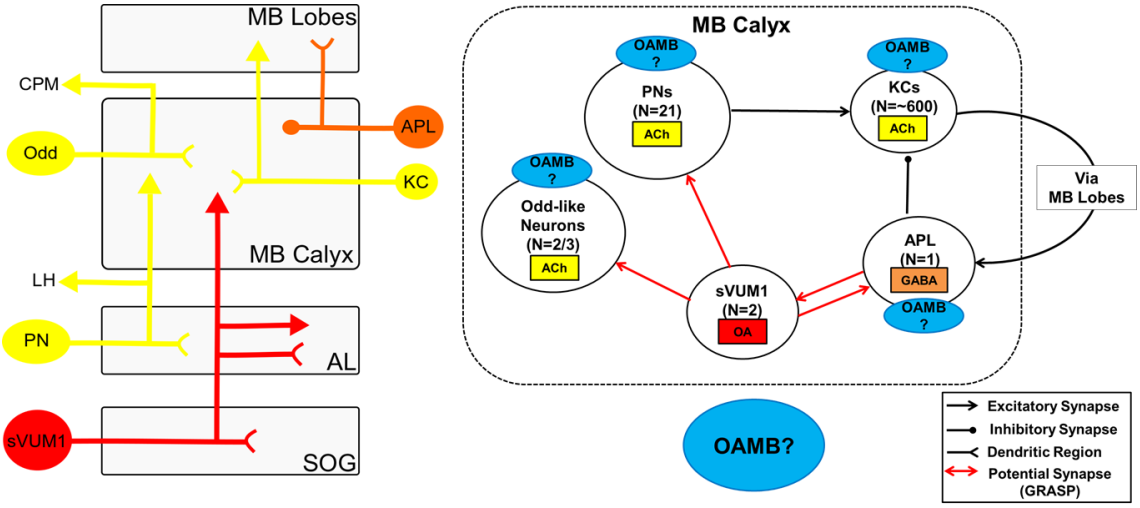

Figure 4.1. Hypothetical OAMB localisation pattern in larval MB calyx circuitry. Abbreviations: ACh, acetylcholine; AL, antennal lobe; CPM, centroposterior medial compartment; KC, Kenyon Cell; LH, lateral horn; MB, mushroom body; N, number; OA, octopamine; PN, projection neuron.

PNs and the APL neuron, which are predominantly presynaptic in the calyx (Masuda-Nakagawa et al., 2014). The subcellular localisation of OAMB to presynaptic terminals is expected to have functional consequences in regulating neurotransmitter release machinery. For example, it may enhance the probability of neurotransmitter release and increase the number of synaptic vesicles, as in the case of α1-adrenoceptor regulation of glutamate release in rat medial prefrontal cortex neurons (Luo et al., 2015).

Here I aimed to determine whether OAMB localised to the presynaptic terminals of PNs and the APL neuron in the larval MB calyx.

3) Is OAMB expressed on KCs extrasynaptically in the larval calyx?

OAMB transcripts observed in KC cell bodies in adult flies (Han et al., 1998), and anti-AmOA1 signal in honeybee KCs (Sinakevitch et al., 2011) suggests that OAMB localisation to KCs may be conserved in larvae. However, few synaptic connections between sVUM1 neurons and KCs in the larval calyx were detected using GRASP (H.W., MPhil Thesis 2014).

Here I aimed to determine whether OAMB localised to KC dendrites in the larval MB calyx, and therefore whether KCs express extrasynaptic OA receptors in the larval calyx in response to sVUM1 signalling.

OAMB expression has previously been examined using mRNA *in situ* hybridisation (Han et al., 1998) and promoter-*GAL4* lines (El-Kholy et al., 2015; Huetteroth et al., 2015; Watanabe et al., 2017). However, neither of these methods can show the subcellular localisation of OAMB. Additionally, promoter-GAL4 lines may not accurately reflect the endogenous expression pattern of OAMB. There is a large variation in the neurons labelled in two GAL4 lines generated from different promoter fragments of the *OAMB* gene (Watanabe et al., 2017); and a third *OAMB-GAL4* line generated using the complete promoter region of *OAMB* (El-Kholy et al., 2015). Even when the complete promoter region of *OAMB* was used to generate an *OAMB-GAL4* line, this line still cannot guarantee endogenous *OAMB* expression which may be regulated by distal enhancer elements outside of the promoter region.

Anti-OAMB antibodies (Han et al., 1998; Lee et al., 2009; Kim et al., 2013) have also been used to determine OAMB localisation. However, it is difficult to differentiate between signal and background in adult fly brains stained with anti-OAMB, due to the poor signal-to-noise ratio and high background staining in *oamb* hypomorphic and null mutant controls (Kim et al., 2013). This suggests that the anti-OAMB antibodies are not specific. Anti-OAMB shows a much better signal when it is overexpressed using the *GAL4/UAS* system (Kim et al., 2013), suggesting that endogenous OAMB expression in the adult MB may be too low to be robustly visible with anti-OAMB.

Here I used newly generated EGFP-tagged OAMB receptors to visualise the endogenous localisation pattern of OAMB. As the *EGFP* sequence was inserted along with RNA splicing signals in a coding intron of the *OAMB* gene, EGFP was expressed as an artificial exon under the control of the same promoters and regulators as *OAMB*. Therefore, EGFP was translated as a fusion with the OAMB protein, and should report the subcellular localisation of the OAMB protein. EGFP-tagged OAMB was used to report OAMB localisation in specific neurons identified using *GAL4* lines or neurotransmitter antibody labelling, as well as to measure OAMB levels after RNAi or protein knockdown in specific neurons.

4.2. Results

4.2.1. Selection and generation of an EGFP-tagged OAMB line

To visualise OAMB expression in the larval MB calyx, I selected the *MI12417* line from the MiMIC collection to generate an EGFP-tagged OAMB receptor stock. The MI12417 insertion is in a coding region intron of the *OAMB* gene (Venken et al., 2011a; Fig. 4.2, 4.3A). By aligning cDNA and protein sequences of *OAMB*, I mapped the location of the MI12417 insertion in coding region intron 3 of the *OAMB* gene to amino acid position 338 (Fig. 4.3) in all OAMB protein isotypes. Amino acid position 338 was in the intracellular domain between TM V and VI for all OAMB isotypes according to the TM prediction software TMHMM (Fig. 4.4).

Insertion MI12417

Gene Information

Affected Gene(s)
Oamb

Position	Oamb - coding intron
Phase	Oamb-RB:1, Oamb-RC:1, Oamb-RD:1, Oamb-RE:1, Oamb-RF:1

Release 6 Annotation

Scaffold	Coordinate	Strand	Site	GBrowse Link
3R	20697059	-	92F6	3R:20697059

FlyBase Annotation	Transposon
FBti0162526	Mi{MIC}

Stock Availability

Donor/Collection	Stockcenter Designation	Stock No.
GDP	Bloomington	57940

Flanking Sequence

MI12417-3' (KG961362)	TAATATGTCTTCCCTGTTAGCATGTTCTGTTTGCAATTTTCTATTTTCTT AGGTTTTTGTCGTTTCAGGCCTCACTGGTCCCCAAAGACTCTGTGGTGGC GATAATCCCCGGGAGCAGATTCCGTTTGAAGTCGGGAGCCCCCATTAGAC TGGCACTGGGTGTTTATTTTAATATGTGGCCCATTACTTGGCCAGGGCCA CAGCGCACTTTCTTCCGCGTGATC

Figure 4.2. ***MI12417*** **insertion stock listed on the Gene Disruption Project Database**. (http://flypush.imgen.bcm.tmc.edu/pscreen/details.php?line=MI12417).

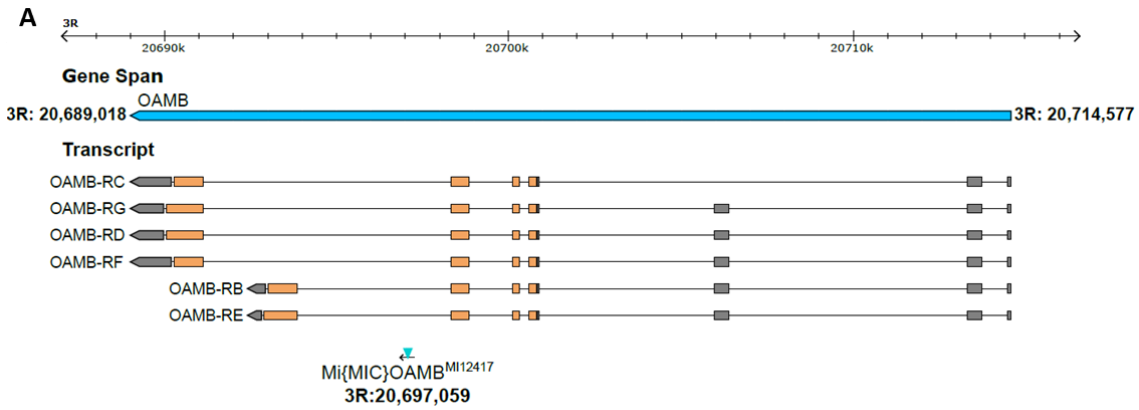

B1. OAMB-PB tblastn alignment to *Drosophila* sequences

```
Exon 3
Query:   284     PWKCELTNDRGYVLYSALGSFYIPMFVMLFFYWRIYRAAVRTTRAINQGFKTTKG     338
                 PWKCELTNDRGYVLYSALGSFYIPMFVMLFFYWRIYRAAVRTTRAINQGFKTTKG
20698497         PWKCELTNDRGYVLYSALGSFYIPMFVMLFFYWRIYRAAVRTTRAINQGFKTTKG     20698333

Exon 4
Query:   338     GSPRESGNNRVDESQLILRIHRGRPCSTPQRTPLSVHSMSSTLSVNSNGGGGGAVASGLG         397
                 GSPRESGNNRVDESQLILRIHRGRPCSTPQRTPLSVHSMSSTLSVNSNGGGGGAVASGLG
20693849         GSPRESGNNRVDESQLILRIHRGRPCSTPQRTPLSVHSMSSTLSVNSNGGGGGAVASGLG         20693670
```

B2. OAMB-PC tblastn alignment to *Drosophila* sequences

```
Exon 3
Query:   284     PWKCELTNDRGYVLYSALGSFYIPMFVMLFFYWRIYRAAVRTTRAINQGFKTTKG     338
                 PWKCELTNDRGYVLYSALGSFYIPMFVMLFFYWRIYRAAVRTTRAINQGFKTTKG
20698497         PWKCELTNDRGYVLYSALGSFYIPMFVMLFFYWRIYRAAVRTTRAINQGFKTTKG     20698333

Exon 4
Query:   338     GSKGIGSRFEEQRLTLRIHRGRGSNQQDSMHSNGSTQSTTTTLGTPSPERLSKYATRRLH         397
                 GSKGIGSRFEEQRLTLRIHRGRGSNQQDSMHSNGSTQSTTTTLGTPSPERLSKYATRRLH
20691108         GSKGIGSRFEEQRLTLRIHRGRGSNQQDSMHSNGSTQSTTTTLGTPSPERLSKYATRRLH         20690929
```

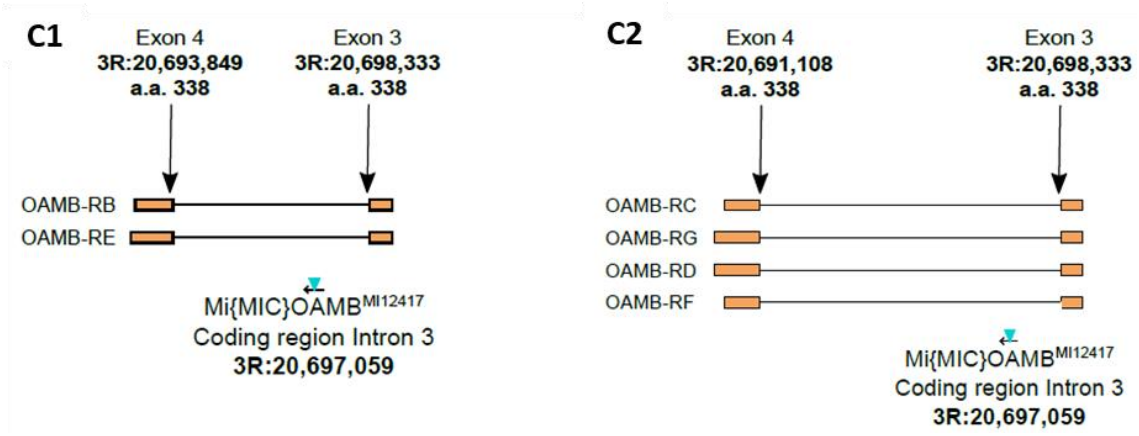

Figure 4.3. MI12417 insertion was in coding region intron 3 of the *OAMB* gene. (A) Map of MI12417 insertion site relative to *OAMB* gene and transcripts (Adapted from GBrowse). **(B)** Amino acid coordinates for the MI12417 insertion site based on tblastn alignment with *OAMB* transcripts. **(C)** Magnified map of MI12417 insertion in coding region intron 3 of *OAMB* transcripts with genomic and amino acid coordinates.

A

OAMB-PB TMHMM Predictions

WEBSEQUENCE	TMHMM2.0	outside	1	21
WEBSEQUENCE	TMHMM2.0	TMhelix	22	44
WEBSEQUENCE	TMHMM2.0	inside	45	56
WEBSEQUENCE	TMHMM2.0	TMhelix	57	79
WEBSEQUENCE	TMHMM2.0	outside	80	93
WEBSEQUENCE	TMHMM2.0	TMhelix	94	116
WEBSEQUENCE	TMHMM2.0	inside	117	136
WEBSEQUENCE	TMHMM2.0	TMhelix	137	159
WEBSEQUENCE	TMHMM2.0	outside	160	293
WEBSEQUENCE	TMHMM2.0	TMhelix	294	316
WEBSEQUENCE	TMHMM2.0	inside	317	523
WEBSEQUENCE	TMHMM2.0	TMhelix	524	546
WEBSEQUENCE	TMHMM2.0	outside	547	555
WEBSEQUENCE	TMHMM2.0	TMhelix	556	578
WEBSEQUENCE	TMHMM2.0	inside	579	637

MI12417 insertion site: a.a. 338

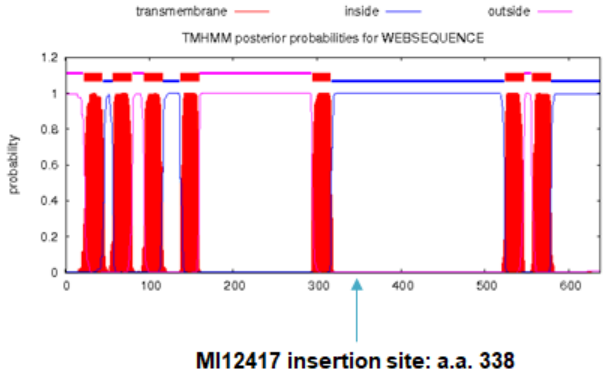

MI12417 insertion site: a.a. 338

B

OAMB-PC TMHMM Predictions

WEBSEQUENCE	TMHMM2.0	outside	1	21
WEBSEQUENCE	TMHMM2.0	TMhelix	22	44
WEBSEQUENCE	TMHMM2.0	inside	45	56
WEBSEQUENCE	TMHMM2.0	TMhelix	57	79
WEBSEQUENCE	TMHMM2.0	outside	80	93
WEBSEQUENCE	TMHMM2.0	TMhelix	94	116
WEBSEQUENCE	TMHMM2.0	inside	117	136
WEBSEQUENCE	TMHMM2.0	TMhelix	137	159
WEBSEQUENCE	TMHMM2.0	outside	160	293
WEBSEQUENCE	TMHMM2.0	TMhelix	294	316
WEBSEQUENCE	TMHMM2.0	inside	317	520
WEBSEQUENCE	TMHMM2.0	TMhelix	521	543
WEBSEQUENCE	TMHMM2.0	outside	544	552
WEBSEQUENCE	TMHMM2.0	TMhelix	553	575
WEBSEQUENCE	TMHMM2.0	inside	576	645

MI12417 insertion site: a.a. 338

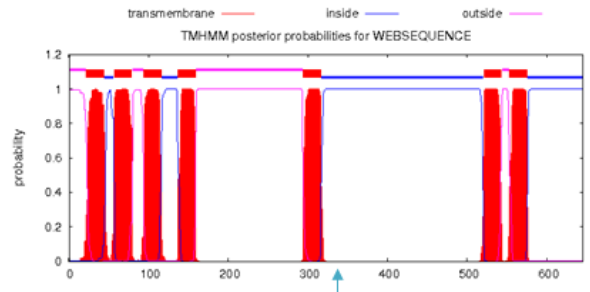

MI12417 insertion site: a.a. 338

Figure 4.4. MI12417 insertion was between TM V and VI of OAMB proteins. MI12417 insertion site relative to TMHMM predictions of TMs for OAMB isotypes: OAMB-PB **(A)** and OAMB-PC **(B)**.

Therefore, a protein trap generated from *MI12417* should not disrupt any TMs to cause protein mislocalisation.

To verify the MI12417 insertion site, I conducted PCR reactions against the 5' and 3' flanking ends of the MiMIC insertion (Fig. 4.5A). PCR products were detected for the *MI12417* stock but not for the non-MiMIC negative control (Fig. 4.5B). The sequenced PCR products contained both MiMIC sequences and flanking *OAMB* genomic sequences (Fig. S1, S2). This confirmed the location of the MI12417 insertion in a coding region intron of *OAMB*.

4.2.2. Validation of *OAMB::EGFP* lines

Nine *OAMB::EGFP* recombinant stocks were recovered after introducing the EGFP reporter cassette to the *MI12417* line. As the EGFP reporter must be inserted in the same direction as the *OAMB* gene for expression, I determined the EGFP insertion orientation of the nine recombinant stocks using PCR reactions described in Venken et al. (2011a). Products observed for PCR1 and PCR4 reactions predicted correct EGFP insertion orientation for expression, while products for PCR2 and PCR3 reactions did not (Fig. 4.6A).

Robust bands for PCR1 and PCR4 reactions were observed for six of the recombinant stocks (Fig. 4.6B). These stocks were therefore expected to express EGFP (Table 4.1). Two stocks produced strong bands for PCR2 and PCR3 reactions (Fig. 4.6B2), and were thus not expected to express EGFP (Table 4.1). One stock produced only a band for PCR1 but not for the other three PCR reactions (Fig. 4.6B3). As it was unclear whether EGFP was correctly inserted in this stock, it was not assayed for expression (Table 4.1).

EGFP signal was detected in the MB calyces of non-fixed L3 brains for the six *OAMB::EGFP* stocks that contained EGFP in the correct orientation for expression, namely *Stocks 2, 4, 5, 7, 8* and *9,* but not in the two stocks that did not (Fig. 4.6, 4.7; Table 4.1). To visualise endogenous expression of OAMB receptors in the larval MB calyx, I used *OAMB::EGFP Stock 9* because it contained the EGFP cassette in the correct orientation (Fig. 4.6B3) and expressed OAMB::EGFP signal in the MB calyx (Fig. 4.7F). This stock was henceforth designated as *OAMB::EGFP*.

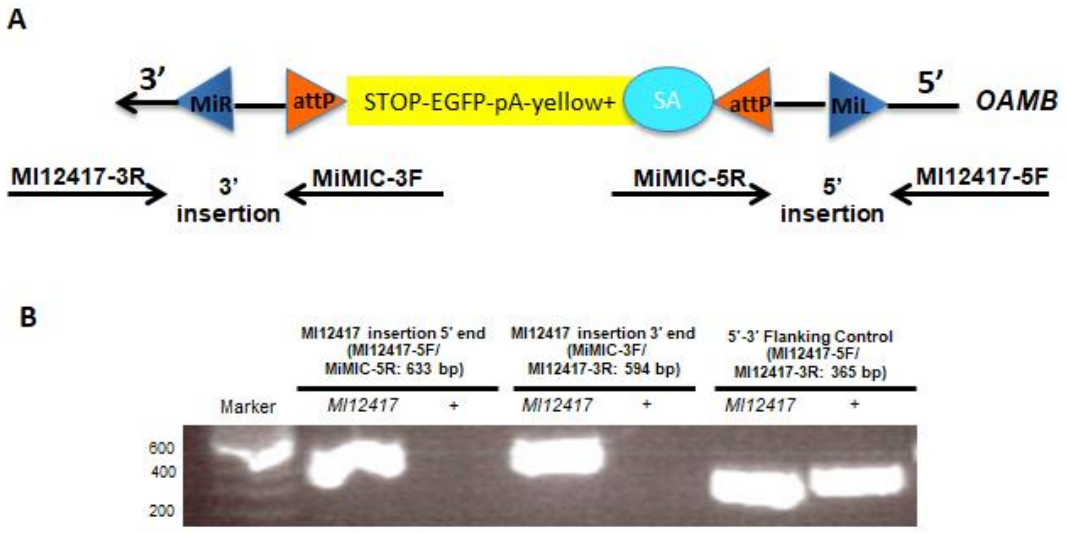

Figure 4.5. PCR verification of MI12417 insertion in the *OAMB* gene. (A) Primers designed against 5' and 3' insertion flanking ends for validating MI12417 insertion in the *OAMB* gene. **(B)** PCR products were detected for 5' and 3' MI12417 insertion ends with *MI12417* DNA but not with non-MiMIC control *S576-IT.GAL4* (denoted as +) DNA. PCR products detected using primers against *OAMB* genomic flanking sequences (5'-3' flanking control) suggested the absence of the MiMIC construct in the negative control, and heterozygosity of the MI12417 insertion cassette in the *MI12417* stock. Abbreviations: MiL/R, MiMIC insertion sequences Left/Right; SA, splice acceptor site; pA, polyA sequence; yellow+, yellow+ phenotype marker for MiMIC cassette.

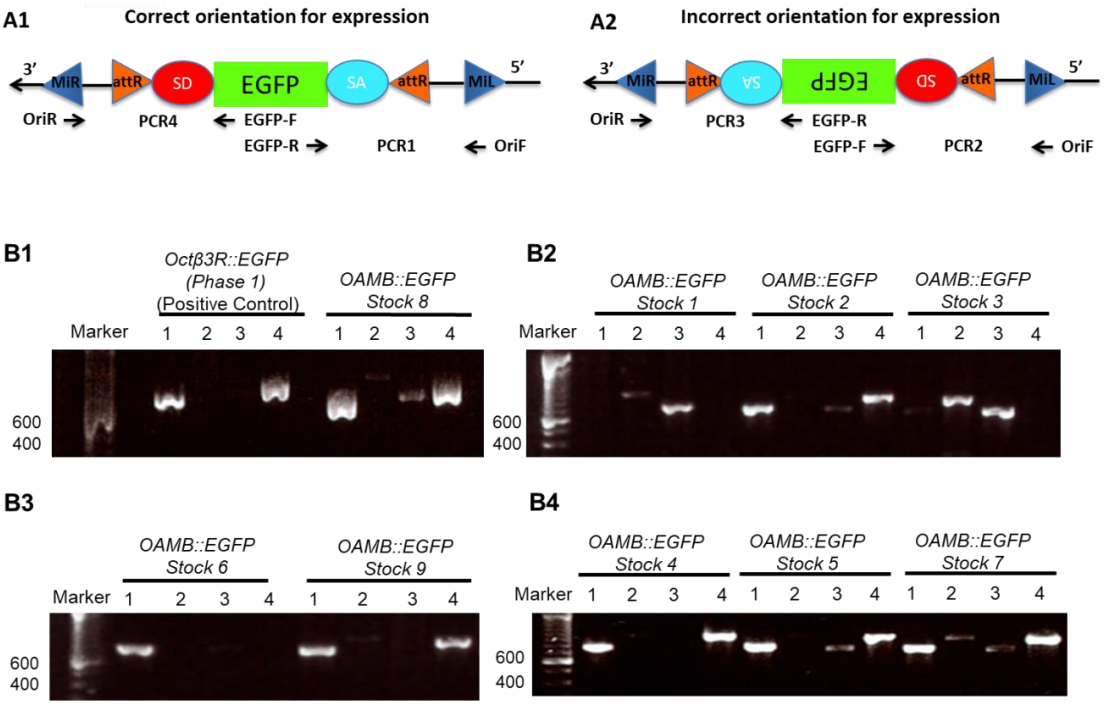

Figure 4.6. PCR validation of EGFP orientation in recombinant *OAMB::EGFP* stocks. (A1) Products for PCR1 and PCR4 indicated EGFP cassette in the correct orientation for expression. **(A2)** Products for PCR2 and PCR3 indicated EGFP cassette in the incorrect orientation for expression. **(B)** Results for PCR reactions 1-4 for *OAMB::EGFP Stock 8* **(B1)**, *Stocks 1, 2, 3* **(B2)**, *Stocks 6, 9* **(B3)**, and *Stocks 4, 5, 7* **(B4)**. *Octβ3R::EGFP (Phase 1)* (BDSC 60245, Venken et al., 2011a; Nagakar-Jaiswal et al., 2015) was used as a positive control for PCR1 and PCR4 reactions **(B1)**. Abbreviations: MiL/R, MiMIC sequences Left/Right; SA, splice acceptor site; SD, splice donor site; OriF, Orientation-MiL-F; OriR, Orientation-MiL-R; EGFP-F, EGFPdo-Seq-F; EGFP-R, EGFPdo-Seq-R.

Stock	PCR1	PCR2	PCR3	PCR4	Figure (PCR)	Expected expression	Observed Expression	Figure (Expression)
OAMB::EGFP Stock 1	-	++	++	-	4.6B2	No	No	4.7G
OAMB::EGFP Stock 2	++	-	+	++	4.6B2	Yes	Yes	4.7A
OAMB::EGFP Stock 3	+	++	++	-	4.6B2	No	No	4.7H
OAMB::EGFP Stock 4	++	-	-	++	4.6B4	Yes	Yes	4.7B
OAMB::EGFP Stock 5	++	-	+	++	4.6B4	Yes	Yes (weak)	4.7C
OAMB::EGFP Stock 6	++	-		-	4.6B3	Unknown	N/A	N/A
OAMB::EGFP Stock 7	++	+	+	++	4.6B4	Yes	Yes	4.7D
OAMB::EGFP Stock 8	++	+	+	++	4.6B1	Yes	Yes	4.7E
OAMB::EGFP Stock 9	++	+	-	++	4.6B3	Yes	Yes	4.7F

Table 4.1. Six out of nine recombinant *OAMB::EGFP* stocks contained EGFP in the correct orientation for expression. PCR products from each of the PCR reactions (PCR1, PCR2, PCR3 and PCR4) were scored as follows: -, no bands observed; +, weak band observed; ++, strong band observed. PCR results were used to determine whether OAMB::EGFP expression was expected (Expected Expression). This correlated with stocks that expressed OAMB::EGFP (Observed Expression).

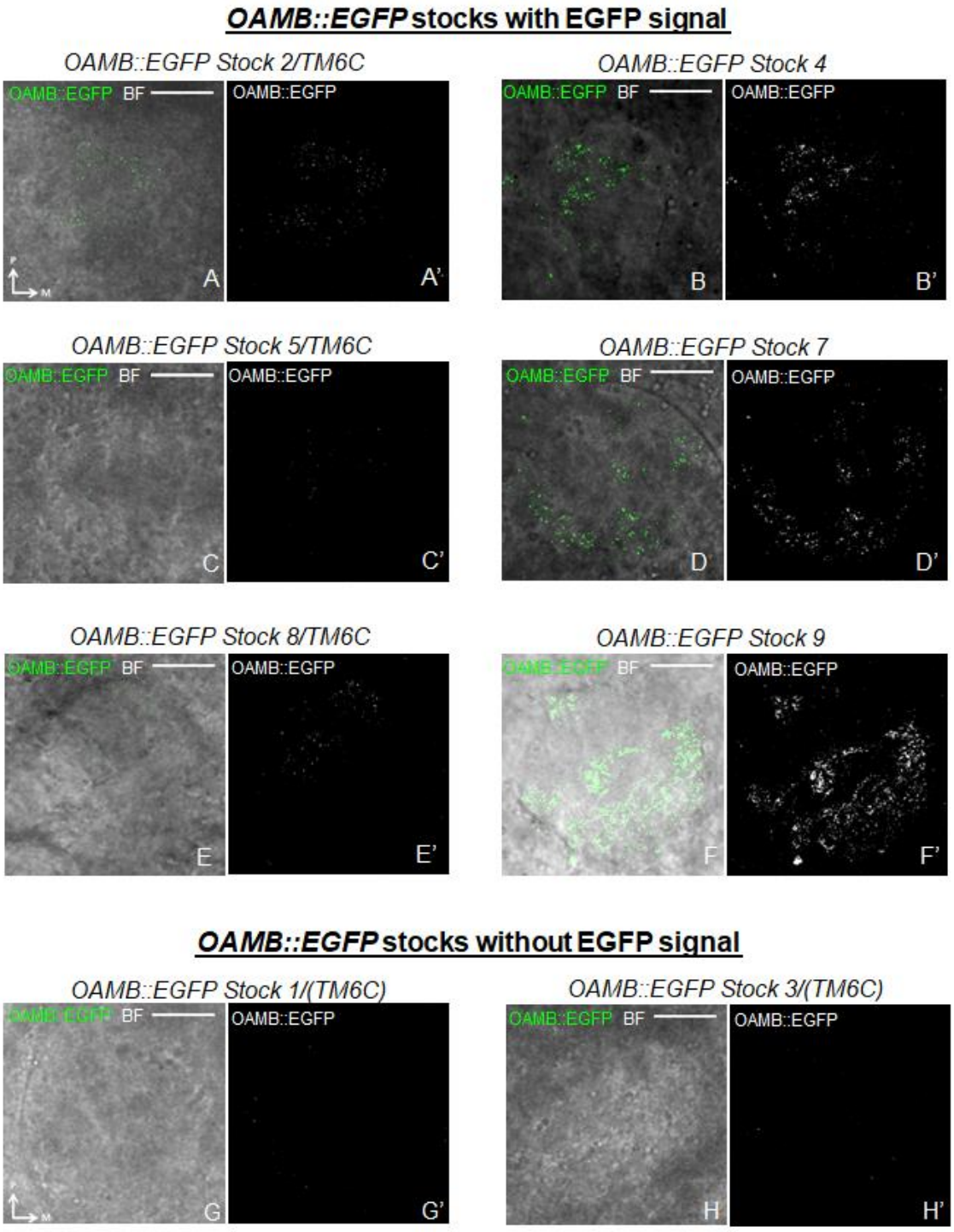

Figure 4.7. Six *OAMB::EGFP* stocks showed EGFP expression in *Drosophila* larval MB calyx. Single confocal optical sections of the calyx of non-fixed third instar larval *OAMB::EGFP* brains. White is bright field (BF) and green is OAMB::EGFP. **(A-F)** Six *OAMB::EGFP* stocks with EGFP signal: *OAMB::EGFP Stock 2/TM6C* **(A)**, *OAMB::EGFP Stock 4* **(B)**, *OAMB::EGFP Stock 5/TM6C* **(C)**, *OAMB::EGFP Stock 7* **(D)**, *OAMB::EGFP Stock 8/TM6C* **(E)**, *OAMB::EGFP Stock 9* **(F)**. Individuals heterozygous for *OAMB::EGFP* (with TM6C balancers) showed a weaker signal **(A,C,E)** than individuals homozygous for *OAMB::EGFP* (without TM6C balancers) **(B,D,F)**. **(G-H)** Two *OAMB::EGFP* stocks without EGFP signal: *OAMB::EGFP Stock 1/(TM6C)* **(G)**, *OAMB::EGFP Stock 3/(TM6C)* **(H)**. Medial (M) is right, posterior (P) is up. Scale bar: 20 μm.

A previous study suggested that *MI12417* is an *oamb* mutant stock, as the MI12417 insertion did not complement *oamb* mutant phenotypes in egg laying following chromosomal deletions in its homologous regions (Deady and Sun, 2015). Consistent with this, I observed that the *MI12417* stock was homozygous infertile, as no viable progeny was produced by homozygous *MI12417* flies. This supported the claim that OAMB protein function was disrupted in the *MI12417* stock.

Homozygous infertility of *MI12417* flies was not reverted to wild type in *OAMB::EGFP*, even though it contained the EGFP cassette in the correct orientation for expression. This suggested *OAMB::EGFP* produced an OAMB::EGFP fusion that was not a functional OAMB protein.

4.2.3. Visualisation of EGFP-tagged receptors with antibody labelling

To visualise OAMB localisation to neuropils and specific neurons, I conducted immunolabelling using GFP antibody to amplify the EGFP signal and Discs large (Dlg) antibody to label neuropil structures.

Monoclonal rat anti-GFP (Nacalai, 440426, clone GF090R) – an antibody that our lab previously used to visualise mCD8::GFP and GRASP in the larval MB calyx (Masuda-Nakagawa et al., 2014) – failed to detect OAMB::EGFP signals in *OAMB::EGFP* calyces relative to the wild type *CS* negative control (Fig. 4.8A-B). This was unexpected as I observed OAMB::EGFP signal in the calyces of non-fixed *OAMB::EGFP* brains (Fig. 4.7F). Rat anti-GFP also did not recognise GABA-B-R1::EGFP signals in the calyces of *GABA-B-R1::EGFP* larvae (Fig. 4.8C) – another protein trap line generated using the MiMIC RMCE method that should contain EGFP signals in the larval calyx (Chapter 7) – compared to *CS* negative control (Fig. 4.8D).

As a positive control, *Tdc2-GAL4>mCD8::GFP* was detected by rat anti-GFP in the larval calyx (Fig. 4.8E). This suggested that the rat anti-GFP was functional, but did not recognise the EGFP protein tag used in protein traps generated by MiMIC RMCE. This may be because this EGFP tag did not contain the epitope recognised by the rat anti-GFP GF090R clone.

Therefore, the signal observed in *OAMB::EGFP*, *GABA-B-R1::EGFP* and negative control *CS* brains in the GFP channel (Fig. 4.8A-D) is likely to be

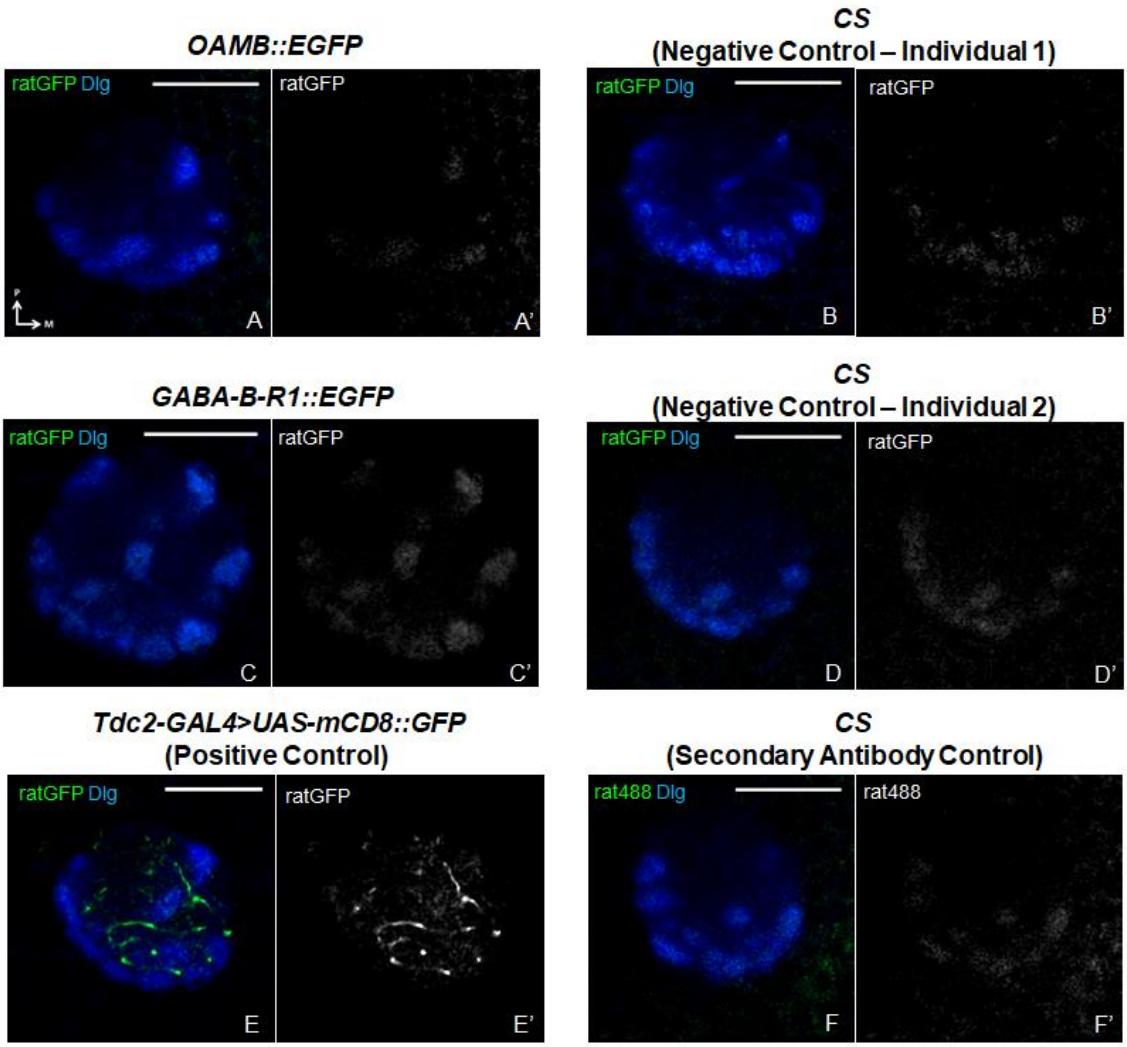

Figure 4.8. Monoclonal rat anti-GFP did not recognize EGFP-tagged receptors. Single confocal optical sections of the calyx from larvae of the following genotypes: *OAMB::EGFP/(TM6C)* **(A)**, *CS* **(B,D,F)**, *GABA-B-R1::EGFP/(SM6a)* **(C)** and *Tdc2-GAL4/+; UAS-mCD8::GFP/+* **(E)**. Blue is neuropil marker anti-Dlg. Green is rat anti-GFP (440426, clone GF090R; ratGFP) in **(A-E)**. Anti-GFP is omitted in **(F)**, where green is instead anti-rat Alexa 488 (rat488). Medial (M) is right, posterior (P) is up. Scale bar: 20 µm.

background signal that may have been caused by non-specific antibody binding that was only detected when high laser conditions were applied during confocal imaging. A similar background signal was also observed when rat anti-GFP was omitted in a secondary antibody control *CS* brain also taken at high laser power conditions (Fig. 4.8F). This suggested that this may be due to non-specific binding of the anti-rat Alexa 488 secondary antibody.

To increase the probability of detecting the EGFP protein tag, I tested two polyclonal GFP antibodies which can recognise multiple epitopes on GFP proteins: a polyclonal rabbit anti-GFP (Invitrogen, A11122), used by Nagarkar-Jaiswal et al. (2015) to visualise EGFP-tagged proteins generated from MiMIC RMCE; and a polyclonal chicken anti-GFP (Abcam, ab13970). Both rabbit and chicken anti-GFP were able to detect clear EGFP signals in the calyces of *OAMB::EGFP* and *GABA-B-R1::EGFP* larvae relative to *MI12417* or *CS* negative controls (Fig. 4.9, 4.10). EGFP localisation patterns appeared to be consistent within the same genotype regardless of whether rabbit or chicken anti-GFP was used. This suggested that the rabbit anti-GFP (A11122) and chicken anti-GFP (Ab13970) can both detect EGFP protein traps generated from MiMIC lines.

I chose to use chicken anti-GFP in favor of rabbit anti-GFP in the following sections for visualising EGFP protein traps unless stated otherwise, as chicken anti-GFP could be used in conjunction with other rabbit antibodies including rabbit anti-DsRed and rabbit anti-OA for co-labelling calyx-innervating neurons.

4.2.4. OAMB::EGFP localisation to larval MB calyx glomeruli

OAMB::EGFP larvae showed GFP localisation to calyx glomeruli (Fig. 4.11A-F), but not in the negative controls (Fig. 4.11G-L). EGFP localisation to synaptic regions suggested that GFP had been successfully fused to OAMB to form a correctly folded protein. This fusion was therefore designated as OAMB::EGFP.

However, OAMB::EGFP did not localise to all MB calyx glomeruli labelled with the neuropil marker anti-Dlg. By examining the slices of the confocal stack using ImageJ, I estimated the number of calyx glomeruli that did not contain OAMB::EGFP signal and their general positions. Out of 34 MB calyx

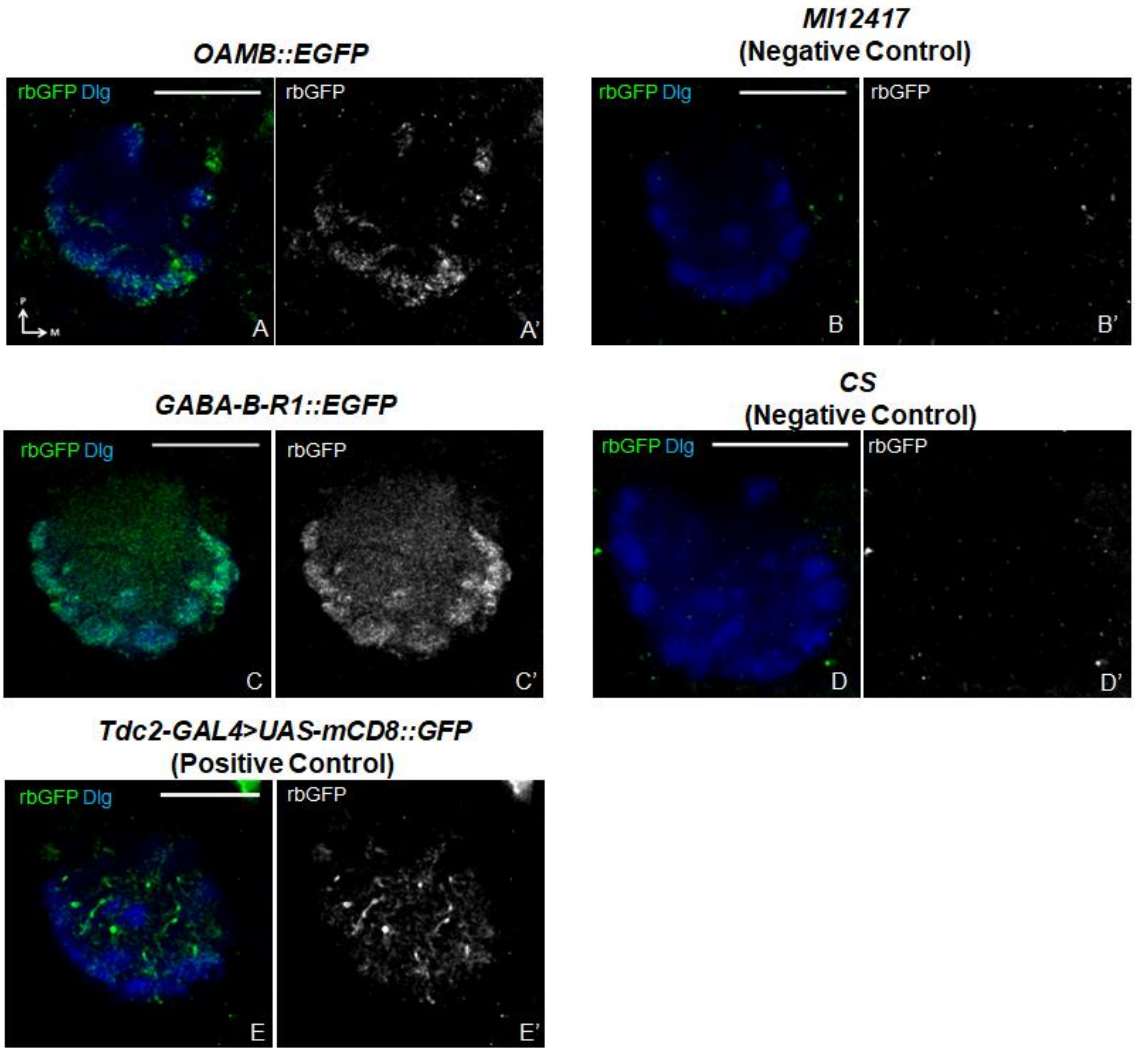

Figure 4.9. EGFP-tagged receptors could be labelled using polyclonal rabbit anti-GFP. Single confocal optical sections of the calyx from larvae of the following genotypes: *OAMB::EGFP* **(A)**, *MI12417/(TM3,Sb)* **(B)**, *GABA-B-R1::EGFP/(SM6a)* **(C)**, *CS* **(D)**, and *Tdc2-GAL4/+; UAS-mCD8::GFP/+* **(E)**. Blue is anti-Dlg and green is polyclonal rabbit anti-GFP (LifeTech A11122; rbGFP). Medial (M) is right, posterior (P) is up. Scale bar: 20 µm.

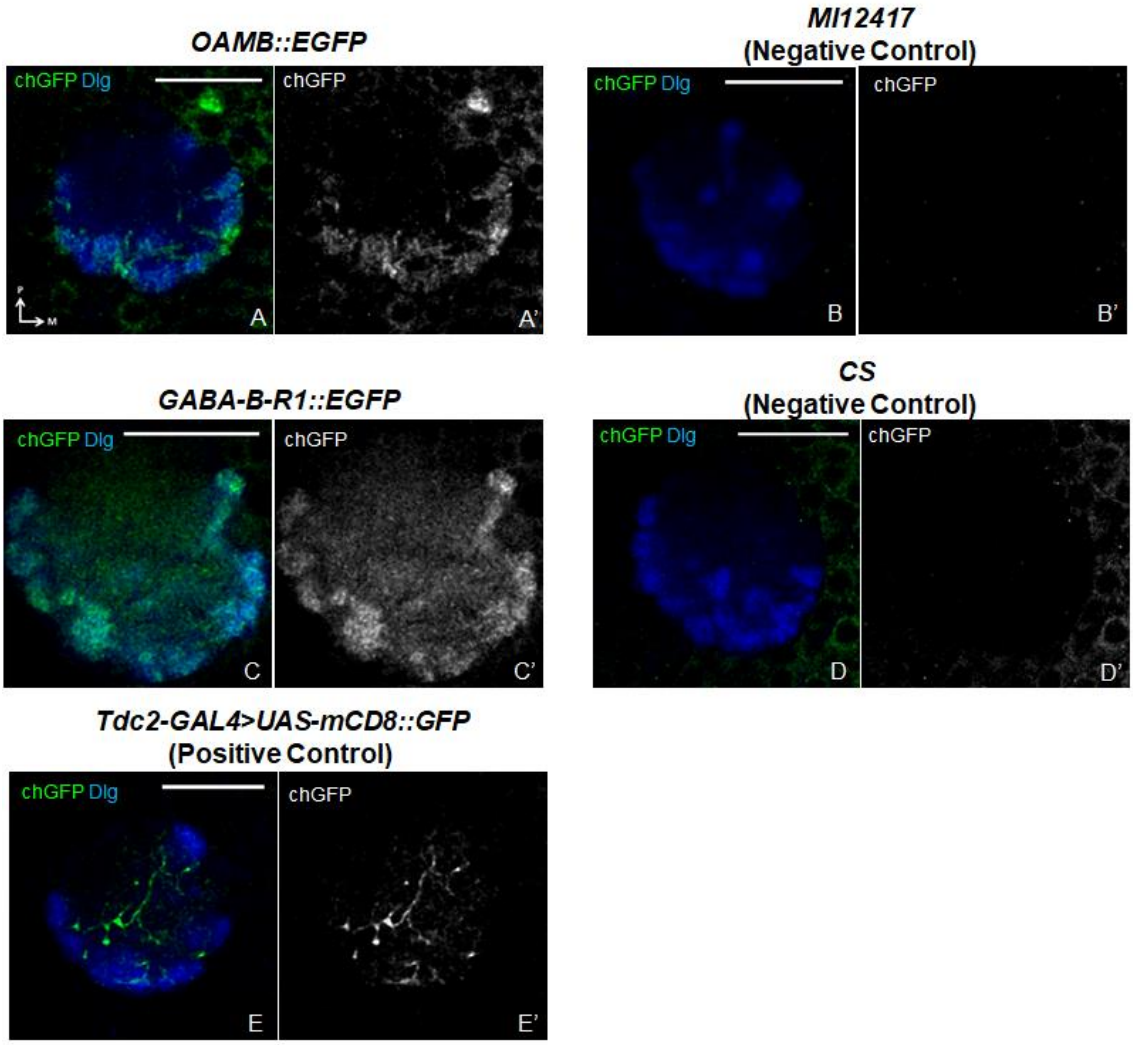

Figure 4.10. EGFP-tagged receptors could be labelled using polyclonal chicken anti-GFP. Single confocal optical sections of the calyx from larvae of the following genotypes: *OAMB::EGFP* **(A)**, *MI12417/(TM3,Sb)* **(B)**, *GABA-B-R1::EGFP/(SM6a)* **(C)**, *CS* **(D)**, and *Tdc2-GAL4/+; UAS-mCD8::GFP/+* **(E)**. Blue is anti-Dlg and green is polyclonal chicken anti-GFP (Abcam Ab13970; chGFP). Medial (M) is right, posterior (P) is up. Scale bar: 20 µm.

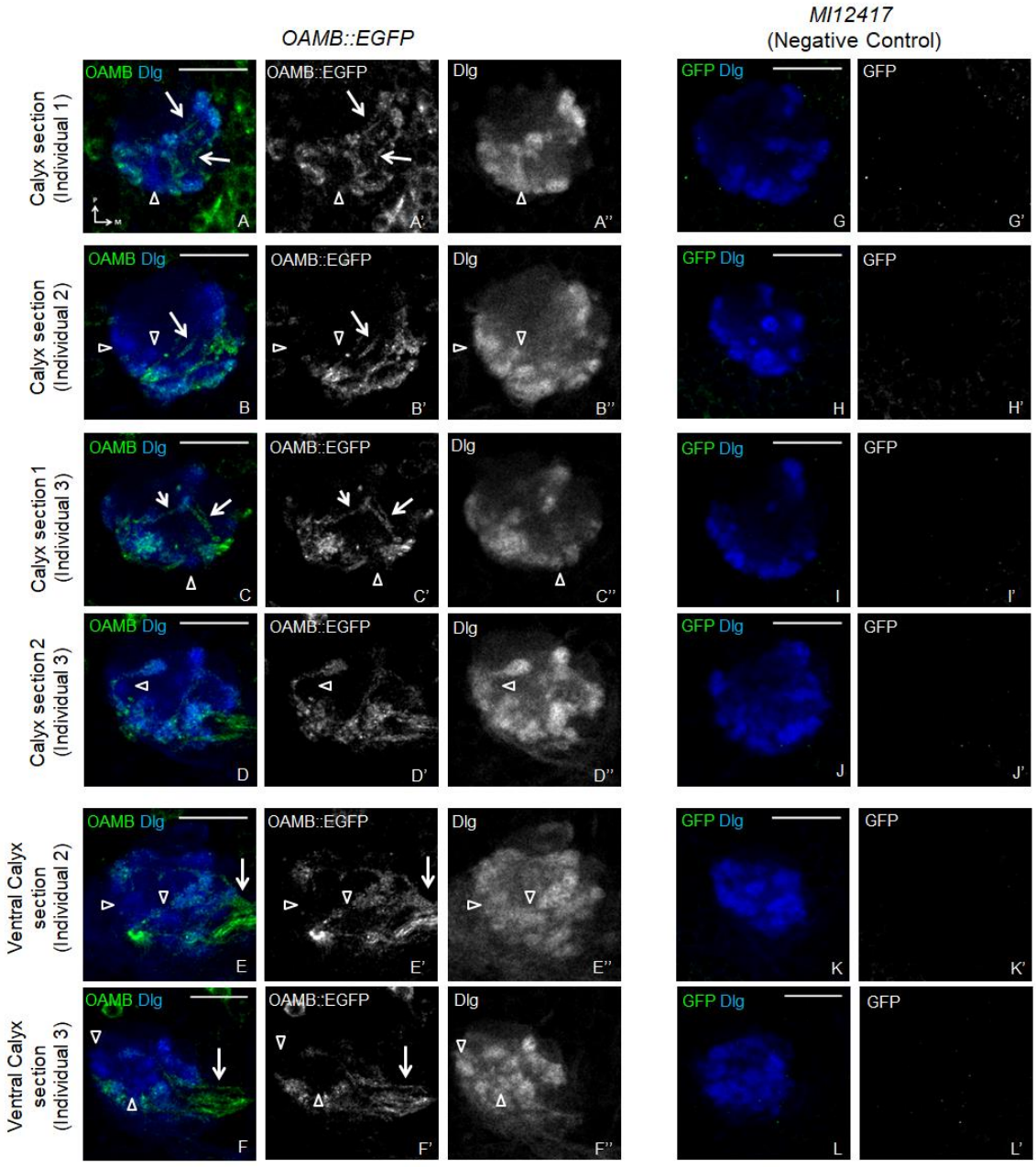

Figure 4.11. OAMB::EGFP localised to many but not all MB calyx glomeruli. Single confocal optical sections of the calyx from three *OAMB::EGFP* individuals **(A-F)**, with *MI12417* parental line negative controls **(G-L)**. Green is OAMB::EGFP and blue is anti-Dlg. OAMB::EGFP-negative calyx glomeruli are indicated with empty arrowheads. OAMB::EGFP-positive tracts are indicated with arrows. Medial (M) is right and posterior (P) is up. Scale bar: 20 µm.

glomeruli (Masuda-Nakagawa et al., 2005), I estimated that around 6 (n=11) calyx glomeruli did not contain EGFP (Table 4.2). This suggested that OAMB::EGFP was present in around 28 calyx glomeruli – 80% of the total number of glomeruli.

The calyx glomeruli that did not contain OAMB::EGFP (Fig. 4.11, empty arrowheads; Table 4.2) varied in position, but often included an anterior glomerulus (n=4; Fig. 4.11A,C), 1-2 lateral glomeruli (n=9; Fig. 4.11B,D) and several ventral glomeruli (n=11; Fig. 4.11E-F). As olfactory PNs innervate calyx glomeruli stereotypically (Masuda-Nakagawa et al., 2009), I expected that the glomerular localisation of OAMB::EGFP will also be stereotyped. Therefore, this variation is most likely caused by the difficulty of precisely orienting the fly larval calyx for imaging and the subsequent quantification of the number of glomeruli.

Most of the OAMB::EGFP-positive glomeruli are likely to be innervated by olfactory PNs, which are responsible for innervating around two-thirds of all the calyx glomeruli (Masuda-Nakagawa et al., 2005). This will be validated using a PN marker in Section 4.2.5. The neurons that innervate the remaining one-third of calyx glomeruli have not yet been characterised. They are most likely to be multiglomerular PNs – PNs which innervate more than one AL glomerulus, three of which innervate the L1 calyx (Berck et al., 2016); or non-olfactory PNs, such as thermosensory and photosensory PNs that send inputs to KCs, but whose calyx innervation patterns are unknown (Eichler et al., 2017). Therefore, OAMB::EGFP localisation may be associated with the neuronal type innervating calyx glomeruli – probably mainly olfactory PNs, but may also include PNs of specific modalities.

There may also be some calyx glomeruli at the L3 stage that are not yet innervated by any larval PNs; but are innervated by later-born adult PNs. This is possible as some adult-specific PNs that have not yet developed processes are already present in third instar larvae (Das et al., 2013). It would not be necessary for OAMB to localise to calyx glomeruli that are not innervated by any neurons. Hence, the possible lack of PN innervation may explain why some calyx glomeruli are OAMB::EGFP-negative; and possibly why this number is variable, if some of the PN processes are being developed at this stage.

Individual	OAMB-negative glomeruli	Positions of OAMB-negative glomeruli
Individual 1	5	1 dorsoposterior, 3 anterior, 1 ventrolateral
Individual 2	6	1 anterior, 1 lateral, 4 ventral
Individual 3	5	1 lateral, 4 ventral
Individual 4	7	1 anterior, 1 lateral, 5 ventral
Individual 5	7	1 posteromedial, 2 lateral, 4 lateral
Individual 6	5	1 lateral, 1 anterior, 3 ventral
Individual 7	7	1 anterior, 2 lateral, 4 ventral
Individual 8	5	5 ventral
Individual 9	7	1 lateral, 6 ventral
Individual 10	7	1 dorsoposterior, 1 lateral, 5 ventral
Individual 11	5	1 lateral, 4 ventral

Table 4.2. Estimated numbers and positions of OAMB::EGFP-negative calyx glomeruli in *OAMB::EGFP* brains.

I also observed tracts in the inter-glomerular region (Fig. 4.11A-C, arrows). These tracts entered the calyx medially (Fig. 4.11E-F, arrows) and terminated in calyx glomeruli; resembling the inner antennocerebral tracts (iACT) described in Masuda-Nakagawa et al. (2005) in which PNs innervate the MB calyx.

4.2.5. OAMB::EGFP was expressed in olfactory projection neurons

OAMB::EGFP signal in calyx glomeruli and medial tracts entering the calyx matched the axonal innervation pattern of calyx glomeruli by PNs via the iACT (Masuda-Nakagawa et al., 2005). To establish whether OAMB was expressed in PNs, I examined whether OAMB::EGFP signal colocalised with PNs labelled by *NP225-GAL4* (Tanaka et al., 2004; Masuda-Nakagawa et al., 2005) in the larval calyx and AL.

OAMB::EGFP signal was observed in all calyx glomeruli expressing *NP225-GAL4* (n=7; Fig. 4.12, arrows; Table 4.3). OAMB::EGFP further localised to 8 ± 0.7 *NP225*-negative calyx glomeruli identified using anti-Dlg staining (Fig. 4.12, arrowheads; Table 4.3). This suggested that OAMB::EGFP localised to the presynaptic terminals of all the olfactory PNs labelled by *NP225-GAL4*, as well as to the terminals of neurons that innervated calyx glomeruli but were not labelled by *NP225-GAL4*.

OAMB::EGFP was also found in all AL glomeruli and in inter-glomerular regions of the AL (n=5; Fig. 4.13A-F; Table 4.4). This suggested that OAMB::EGFP may also localise to PN dendrites innervating AL glomeruli, as well as other neurons innervating the inter-glomerular regions of the AL.

To confirm OAMB expression in PNs, I examined whether larval olfactory PN cell bodies were positive for OAMB::EGFP. It has been previously observed using another larval PN driver line, *GH146-GAL4*, that PN cell bodies are located dorso-anteriorally to the larval AL (Ramaekers et al., 2005). In addition to larger dorsoanterior cell bodies of primary PNs innervating the AL, *GH146-GAL4* also labelled smaller cell bodies of secondary adult-specific PNs which did not innervate neuropils at the larval stage, as well as non-PN cell bodies located lateral to the AL (Ramaekers et al., 2005; Das et al., 2013). As *GH146-*

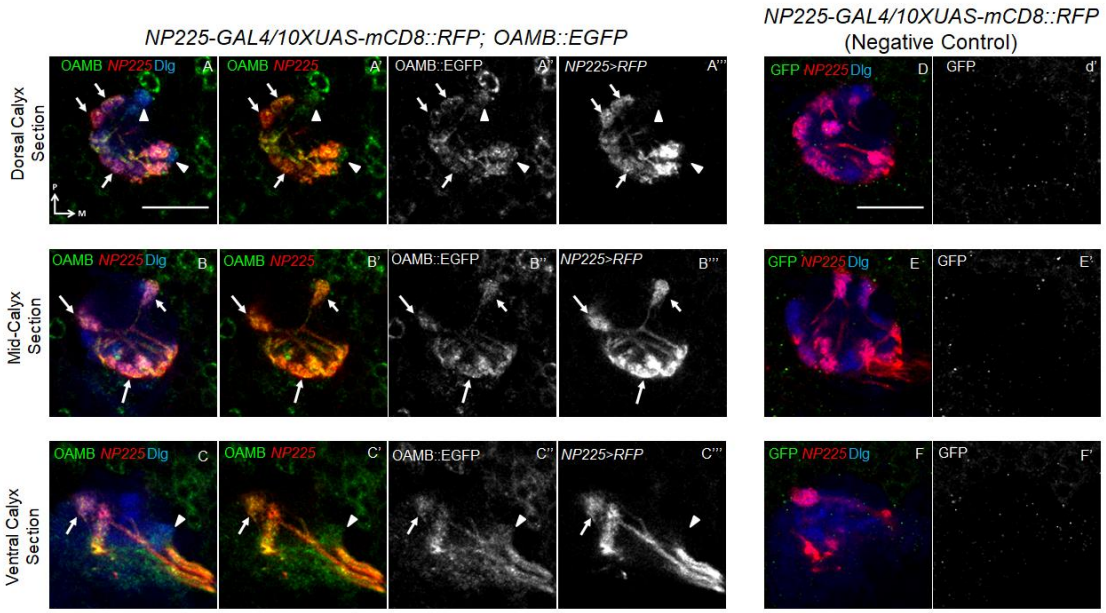

Figure 4.12. OAMB::EGFP colocalised with PN terminals labelled by *NP225-GAL4* in calyx glomeruli. Single confocal optical sections of the calyx of *NP225-GAL4/UAS-mCD8::RFP; OAMB::EGFP* **(A-C)** and negative control *NP225-GAL4/UAS-mCD8::RFP; TM6B/MKRS* **(D-F)**. Green is OAMB::EGFP, red is mCD8::RFP driven by PN driver *NP225-GAL4* and blue is anti-Dlg. Arrowheads indicate glomeruli or cell bodies positive for OAMB::EGFP but not *NP225*, and arrows indicate OAMB::EGFP and *NP225>RFP* colocalisation. Medial (M) is right, posterior (P) is up. Scale bar: 20 μm.

Genotype	Individual	OAMB+	NP225+	OAMB+/ NP225+	OAMB+/ NP225-	OAMB-/NP225+	OAMB-/NP225-	Total (Dlg)
NP225-GAL4/UAS-mCD8::RFP; OAMB::EGFP	Individual 1	30	25	25	5	0	6	36
	Individual 2	29	19	19	10	0	6	35
	Individual 3	30	23	23	7	0	5	35
	Individual 4	32	24	24	8	0	5	37
	Individual 5	30	20	20	10	0	5	35
NP225-GAL4/+; UAS-mCD8::RFP/OAMB::EGFP	Individual 6	31	22	22	9	0	3	34
	Individual 7	29	23	23	6	0	5	34
Statistical Description	N	7	7	7	7	7	7	7
	Mean	30	22	22	8	0	5	35
	S.D.	1.1	2.1	2.1	2.0	0.0	1.0	1.1
	S.E.M.	0.4	0.8	0.8	0.7	0.0	0.4	0.4

Table 4.3. Numbers of calyx glomeruli positive for OAMB::EGFP and *NP225-GAL4*. Abbreviations: OAMB+, OAMB::EGFP-positive; OAMB-, OAMB::EGFP-negative; NP225+, *NP225>RFP*-positive; NP225-, *NP225>RFP*-negative; Total, number of calyx glomeruli observed with neuropil marker anti-Dlg; N, number; S.D., standard deviation; S.E.M., standard error of the mean.

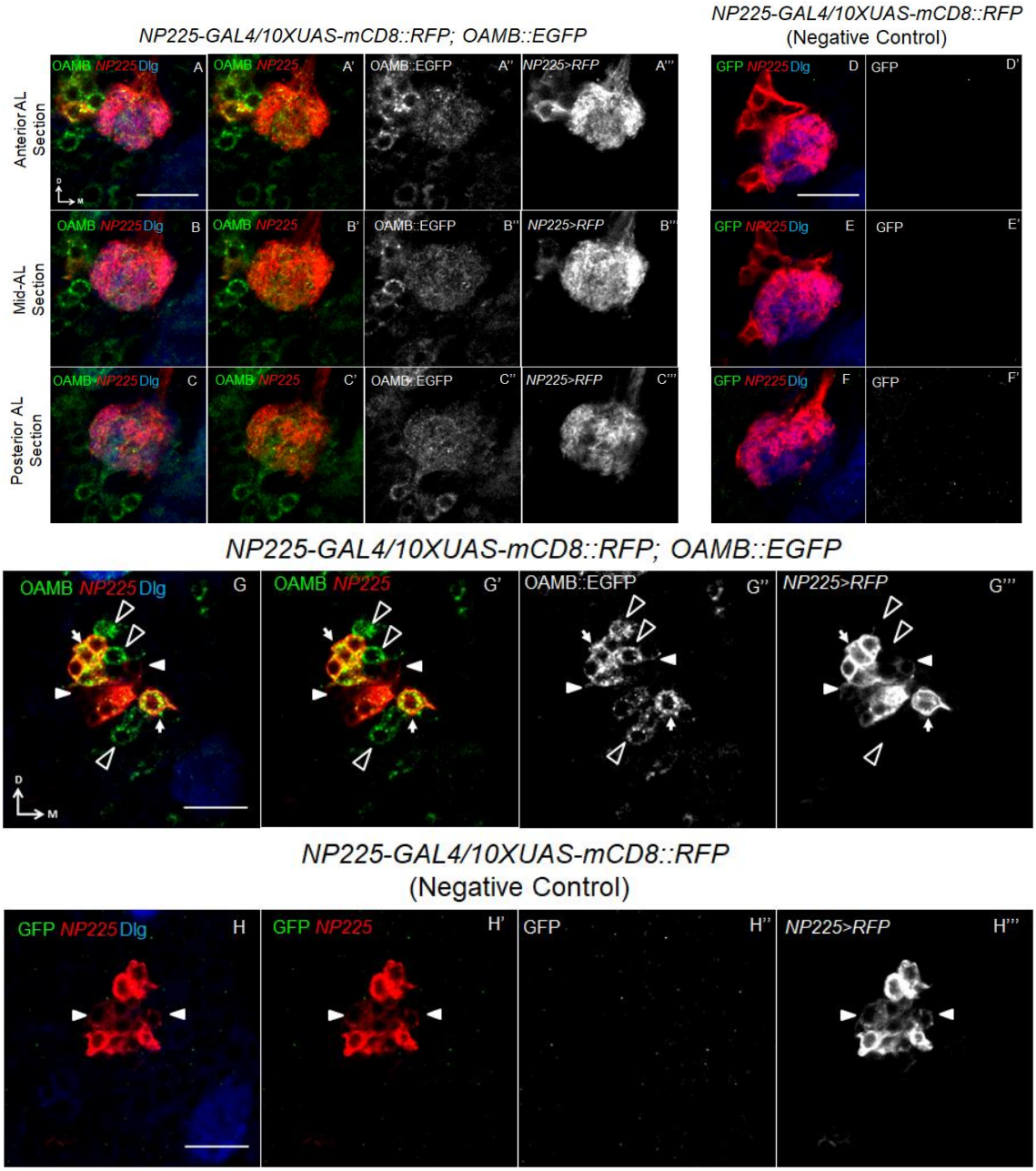

Figure 4.13. OAMB::EGFP colocalised with PN cell bodies and dendrites labelled by *NP225-GAL4*. Confocal optical sections of *NP225-GAL4/UAS-mCD8::RFP; OAMB::EGFP* **(A-C,G)** and negative control *NP225-GAL4/UAS-mCD8::RFP; TM6B/MKRS* **(D-F,H)**. Green is OAMB::EGFP, red is *NP225>RFP* and blue is anti-Dlg. **(A-F)** are confocal optical sections of the AL. **(G-H)** are confocal optical sections taken immediately anterior to the AL. Arrows indicate OAMB-*NP225* colocalisation. Filled arrowheads indicate cell bodies positive for *NP225* only, while empty arrowheads indicate cell bodies positive for OAMB::EGFP only. Medial (M) is right, dorsal (D) is up. Scale bar: 20 μm.

Genotype	Individual	OAMB-Glomeruli	NP225-Glomeruli	OAMB+/NP225+ Cell bodies
NP225-GAL4/UAS-mCD8::RFP; OAMB::EGFP	Individual 1	0	3	22
	Individual 2	0	5	21
	Individual 3	0	2	21
	Individual 4	0	4	20
	Individual 5	0	4	20
Statistical Description	N	5	5	5
	Mean	0	4	21
	S.D.	0.0	1.1	0.8
	S.E.M.	0.0	0.5	0.4

Table 4.4. Numbers of AL glomeruli and *NP225-GAL4* cell bodies positive for OAMB::EGFP. Abbreviations: OAMB+, OAMB::EGFP-positive; OAMB-, OAMB::EGFP-negative; NP225+, *NP225>RFP*-positive; NP225-, *NP225>RFP*-negative; N, number; S.D., standard deviation; S.E.M., standard error of the mean.

GAL4 labels 19 AL glomeruli (Masuda-Nakagawa et al., 2009), it is expected to label around 19 PNs. A similar number of PNs was expected to be labelled in *NP225-GAL4*, as both PN drivers label 23 calyx glomeruli (Masuda-Nakagawa et al., 2005, 2009).

Similar to *GH146-GAL4*, *NP225-GAL4* labelled two morphologically distinct types of cell bodies near the AL. The large (8-10 μm in diameter) strongly-labelled cell bodies that sent tracts to the AL, which were likely to be primary larval PNs, often colocalised with OAMB::EGFP (Figure. 4.13G; arrows). On the other hand, the smaller (4-5 μm in diameter) and weakly-labelled cell bodies which did not extend tracts were likely to be secondary PNs; and did not colocalise with OAMB::EGFP (Fig. 4.13G-H; filled arrowheads). This suggested that OAMB::EGFP was probably expressed in primary larval PNs but not secondary adult-specific PNs in the larval brain.

21 ± 0.4 *NP225*-positive cell bodies near the AL colocalised with OAMB::EGFP (n=5; Fig. 4.13G, arrows; Table 4.4). On the other hand, 4 ± 0.5 AL glomeruli were not labelled by *NP225-GAL4* (n=5; Table 4.4). As each PN innervates a single AL glomerulus, and there are 21 AL glomeruli in total, this suggested that around 17 PNs are labelled by *NP225-GAL4*. This further suggested that around 17 of the 21 cell bodies positive for both *NP225* and OAMB::EGFP were likely to be primary larval PN cell bodies. The remaining cell bodies are likely to be AL interneurons also labelled by *NP225-GAL4*.

As the OAMB::EGFP signal was strong in calyx glomeruli, it might have obscured OAMB::EGFP localisation to the terminals of other neurons besides PN axons, such as in KC dendrites. To confirm OAMB::EGFP localisation to the presynaptic terminals of PNs, and to determine whether this localisation obscured OAMB::EGFP localisation to other neurons, I selectively knocked down OAMB::EGFP using *EGFP-shRNA.3* (Neumüller et al., 2012) in PNs labelled by *NP225-GAL4*. In *NP225>EGFP-shRNA* knockdown calyces, 6 ± 0.5 calyx glomeruli were positive for OAMB::EGFP, compared to 31 ± 0.6 OAMB::EGFP-positive glomeruli in non-knockdown controls (n=4; Fig. 4.14; Table 4.5). This was consistent with the predicted number of calyx glomeruli for a complete knockdown of OAMB::EGFP by *NP225-GAL4>EGFP-shRNA* based

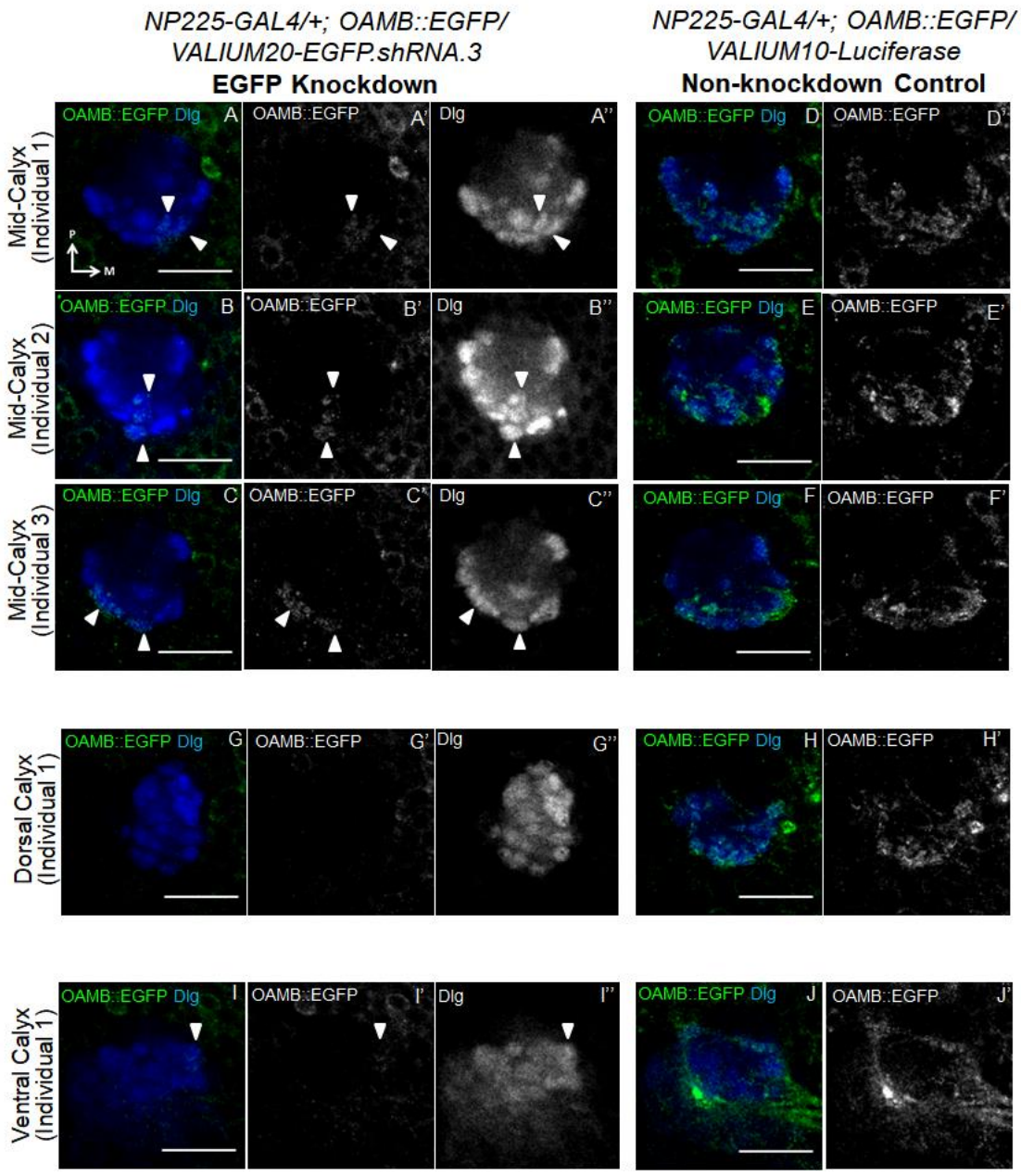

Figure 4.14. OAMB::EGFP signal selectively knocked down in calyx glomeruli labelled by *NP225-GAL4*. Confocal optical sections of the calyx of *NP225-GAL4/+; OAMB::EGFP/VALIUM20-EGFP-shRNA.3* **(A-C,G,I),** and non-knockdown control *NP225-GAL4/+; OAMB::EGFP/VALIUM10-Luciferase* **(D-F,H,J).** Green is OAMB::EGFP, blue is anti-Dlg. Filled arrowheads indicate OAMB::EGFP-positive calyx glomeruli in knockdown brains. Medial (M) is right and posterior (P) is up. Scale bar: 20 μm.

Individual	Knockdown Genotype	OAMB+	OAMB-	Total	Control Genotype	OAMB+	OAMB-	Total
Individual 1	*NP225-GAL4/+; OAMB::EGFP/VALIUM20-EGFP.shRNA.3*	7	28	35	*NP225-GAL4/+; OAMB::EGFP/VALIUM10-Luciferase*	31	4	35
Individual 2		5	31	36		31	5	36
Individual 3		7	29	36		32	4	36
Individual 4		6	30	36		29	7	36
Statistical Description	N	4	4	4	N	4	4	4
	Mean	6	30	36	Mean	31	5	36
	S.D.	1.0	1.3	0.5	S.D.	1.3	1.4	0.5
	S.E.M.	0.5	0.6	0.3	S.E.M.	0.6	0.7	0.3

Table 4.5. Numbers of OAMB::EGFP-positive calyx glomeruli in *NP225-GAL4>EGFP-shRNA* knockdown brains compared to non-knockdown controls. Abbreviations as Table 4.3.

on the numbers of calyx glomeruli that were positive for OAMB::EGFP and *NP225-GAL4* (Table 4.3). Therefore, this confirmed OAMB localised to the presynaptic terminals in the calyx of the majority of olfactory PNs.

In calyx glomeruli where OAMB::EGFP protein was knocked down by *NP225>EGFP-shRNA*, I did not observe any residual OAMB::EGFP signal (Fig. 4.14). This suggested that OAMB::EGFP was only expressed in olfactory PNs labelled by *NP225-GAL4* and not in other neuronal types innervating these particular glomeruli.

OAMB::EGFP signal in *NP225>EGFP-shRNA* knockdown ALs (n=4; Fig. 4.15A-B; Table 4.6) also appeared to be weaker than the non-knockdown controls (n=3; Fig. 4.15C-D; Table 4.6). This suggested that OAMB::EGFP localised to PN dendrites in the AL. The residual OAMB::EGFP signal observed in the AL was more likely due to OAMB::EGFP localisation to non-*NP225* neurons innervating the AL, rather than the efficacy of the *EGFP-shRNA* construct, as complete loss of OAMB::EGFP signal in knockdown larvae was observed in calyx glomeruli.

4.2.6. OAMB::EGFP did not localise to KCs in the calyx

As OAMB::EGFP was consistently absent in 5-6 calyx glomeruli (Table 4.2, 4.3), and there was no residual signal in *NP225*-calyx glomeruli where OAMB::EGFP was knocked down (Fig. 4.14); it was unlikely that OAMB localised to KC dendrites, which randomly arborise throughout calyx glomeruli (Masuda-Nakagawa et al., 2005).

To reconcile OAMB expression in adult KCs with the expected conservation of OAMB expression in larval KCs, I examined whether OAMB::EGFP was instead localised to the cell bodies or axons of larval KCs. Larval KC cell bodies are around 3-5 μm in diameter and are located dorsal to the calyx (Fig. 4.16A). OAMB::EGFP signal was observed in cell bodies that met these criteria in four out of eleven brains (Fig. 4.16B). The remaining seven brains only labelled cell bodies >5 μm in diameter which were too large to be KC cell bodies (Fig. 4.16C, empty arrowheads). Therefore, it was inconclusive as to whether KC cell bodies showed OAMB localisation. On the other hand, OAMB::EGFP signal was diffusely localised to the medial and vertical lobes of

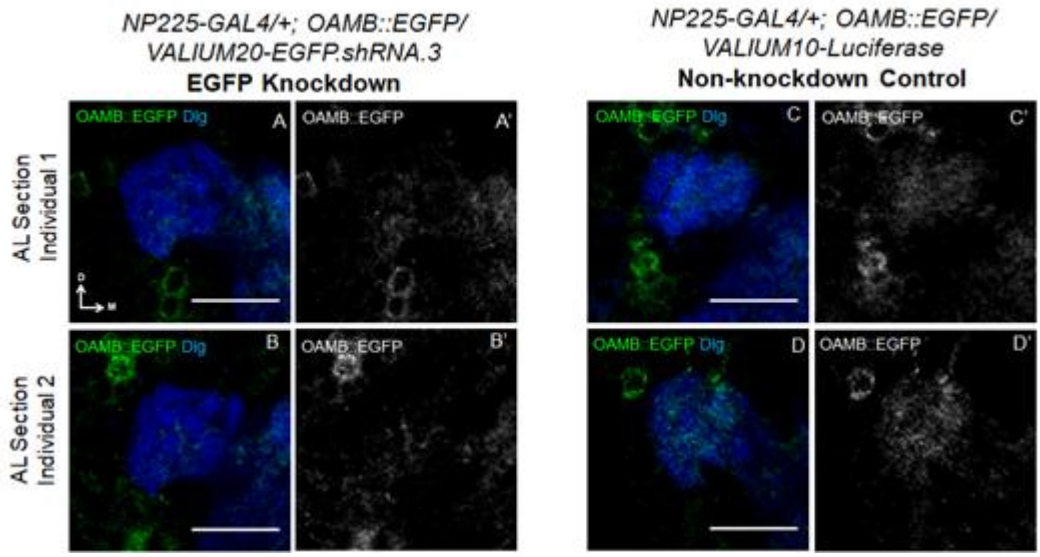

Figure 4.15. OAMB::EGFP signal partially knocked down in PN dendrites labelled by *NP225-GAL4*. Confocal optical sections of the AL of *NP225-GAL4/+; OAMB::EGFP/VALIUM20-EGFP-shRNA.3* **(A-B)**, and non-knockdown control *NP225-GAL4/+; OAMB::EGFP/VALIUM10-Luciferase* **(C-D)**. Green is OAMB::EGFP, blue is anti-Dlg. Medial (M) is right, dorsal (D) is up. Scale bar: 20 µm.

Individual	Knockdown Genotype	Mean Intensity	Control Genotype	Mean Intensity	% Knockdown/Non-Knockdown
Individual 1	*NP225-GAL4/+; OAMB::EGFP/VALIUM 20-EGFP.shRNA.3*	10.05	*NP225-GAL4/+; OAMB::EGFP/VALIUM 10-Luciferase*	27.12	37%
Individual 2		4.67		N/A	N/A
Individual 3		4.11		7.96	52%
Individual 4		2.83		12.56	23%

Table 4.6. Mean OAMB::EGFP intensity in *NP225>EGFP-shRNA* knockdown ALs compared to non-knockdown controls. Mean intensity is the calculated average of three mean grey values (ImageJ) of the AL taken at the mid-AL confocal optical slice and 10 confocal optical slices above and below it. % knockdown/non-knockdown = (mean intensity in knockdown brain)/(mean intensity in non-knockdown brain)*100%.

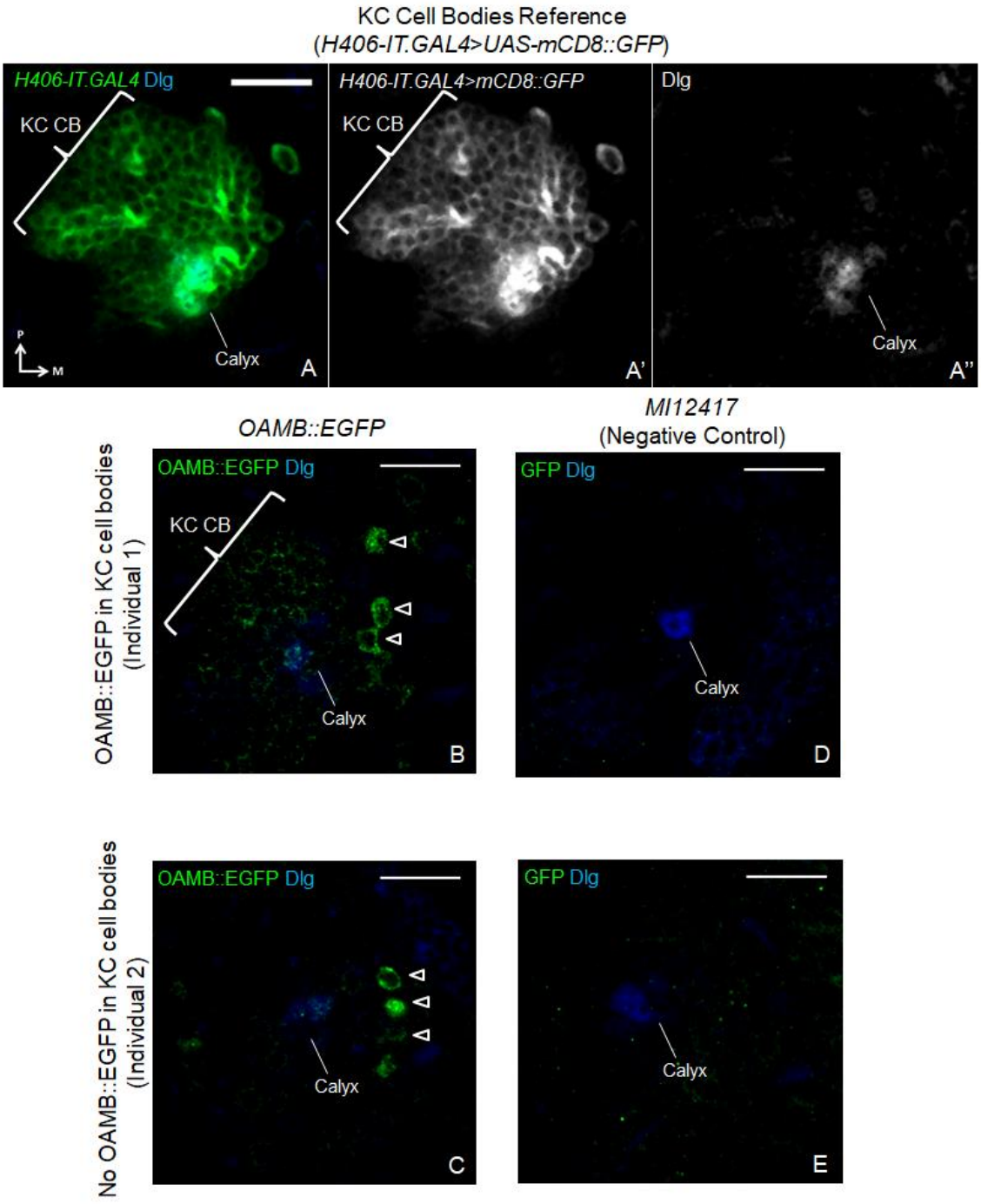

Figure 4.16. OAMB::EGFP localised to KC cell bodies in some but not all brains. Confocal optical sections taken immediately dorsal to the calyx, where KC cell bodies (CB) are located: *H406-IT.GAL4/UAS-mCD8::GFP* (green) as a KC cell bodies reference image **(A)**; two *OAMB::EGFP* (green) individuals **(B-C)**, with corresponding *MI12417* negative controls **(D-E)**. Blue is anti-Dlg. Non-KC cell bodies indicated with empty arrowheads. Medial (M) is right, posterior (P) is up. Scale bar: 20 µm.

the larval MB (n=7; Fig. 4.17), regardless of whether OAMB::EGFP signal localised to KC cell bodies (Fig. 4.16B-C). This suggested that OAMB may be localised to KC axons in the MB lobes, even though it did not localise to KC dendrites in the MB calyx.

4.2.7. OAMB::EGFP was not expressed in the GABAergic APL neuron

To determine whether OAMB was expressed in the GABAergic APL neuron, I visualised the colocalisation of OAMB::EGFP with anti-GABA, which labels all the presynaptic GABA boutons of the APL neuron – the only GABAergic neuron innervating the MB calyx (Masuda-Nakagawa et al., 2014). OAMB::EGFP-positive boutons in the calyx did not overlap with GABA-positive boutons (n=4; Fig. 4.18A-B, empty arrowheads). This suggested that OAMB did not localise to the presynaptic terminals of the APL neuron where GABA neurotransmitter is released.

The lack of colocalisation of OAMB::EGFP and the APL neuron marker *NP732-GAL4* (Masuda-Nakagawa et al., 2014) in the calyx (n=3; Fig. 4.18C-D, empty arrowheads), further suggested that OAMB did not localise to any APL neuronal processes in the calyx. This was consistent with the previous observation that *EGFP-shRNA* knockdown of OAMB::EGFP in PNs did not reveal additional extra-glomerular OAMB::EGFP localisation (Fig. 4.14) characteristic of APL innervation in the calyx (Fig. 4.18C).

Moreover, the APL cell body identified from its innervation of the calyx and MB lobes did not express OAMB::EGFP (n=3; Fig. 4.19); further suggesting that the APL neuron did not express OAMB.

4.2.8. OAMB::EGFP did not localise to Odd-like neurons in the calyx

To determine whether OAMB was expressed in Odd-like neurons, I examined OAMB colocalisation with *OK263-GAL4* (M.T., Part II Report 2015; L. Masuda-Nakagawa, personal communication). This line labelled a cluster of cell bodies located dorsal-posterior to the calyx, including calyx-innervating Odd-like neurons (Fig. 4.20A). OAMB::EGFP signal was observed in two *OK263*-positive cell bodies in the dorsal-posterior cluster (n=2; Fig. 4.20B-E, arrows).

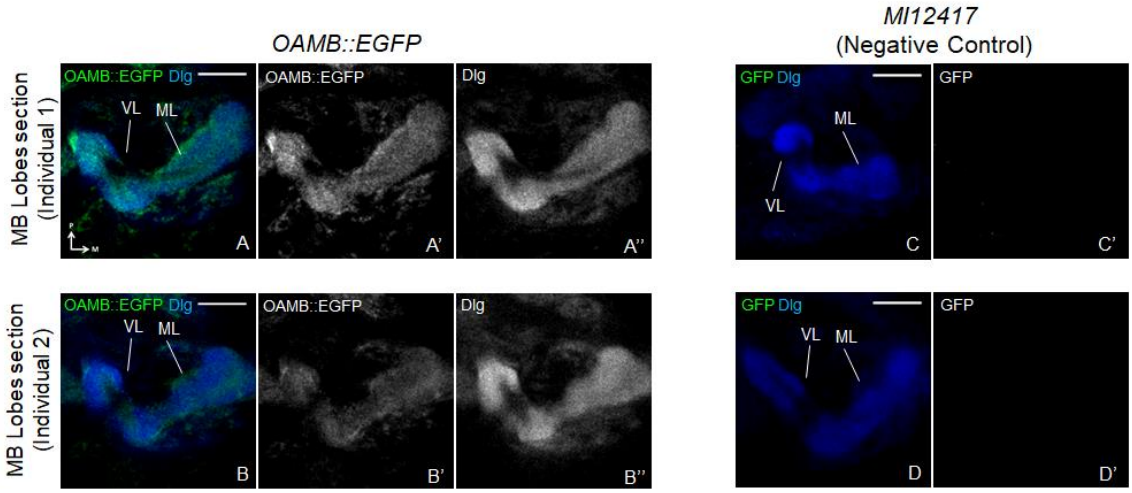

Figure 4.17. OAMB::EGFP localised to MB lobes. Confocal optical sections of the MB lobes of *OAMB::EGFP* **(A-B)** with corresponding *MI12417* negative controls **(C-D)** from the same individuals in Fig. 4.16. Green is OAMB::EGFP and blue is anti-Dlg. Medial (M) is right, posterior (P) is up. Scale bar: 20 µm. Abbreviations: VL, MB vertical lobe; ML, MB medial lobe.

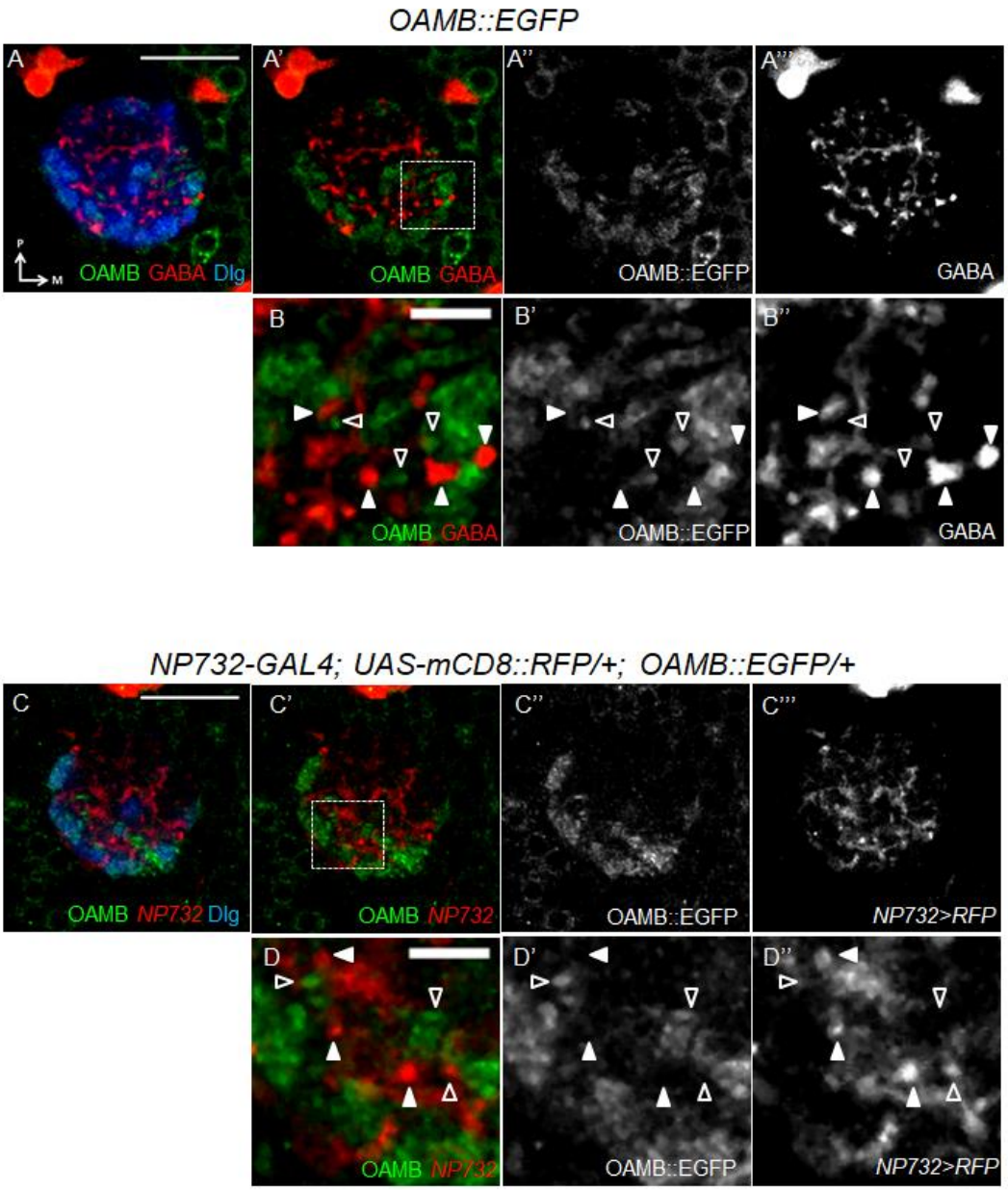

Figure 4.18. OAMB::EGFP did not colocalise with APL terminals in the calyx. (A-B) Confocal optical sections of the calyx of *OAMB::EGFP* (green), with anti-GABA (red) and anti-Dlg (blue) labelling. **(B)** Enlarged from dotted square in **(A)**. OAMB::EGFP puncta (empty arrowheads) did not overlap with GABA boutons (filled arrowheads). **(C-D)** Confocal optical section of the calyx of *NP732-GAL4; UAS-mCD8::RFP/+; OAMB::EGFP/+*. Green is OAMB::EGFP, red is *NP732>RFP* and blue is anti-Dlg. **(D)** Enlarged from dotted square in **(C)**. OAMB::EGFP puncta (empty arrowheads) did not overlap with *NP732* processes (filled arrowheads). Medial (M) is right, posterior (P) is up. Scale bar: 20 µm in **(A,C)** and 5 µm in **(B,D)**.

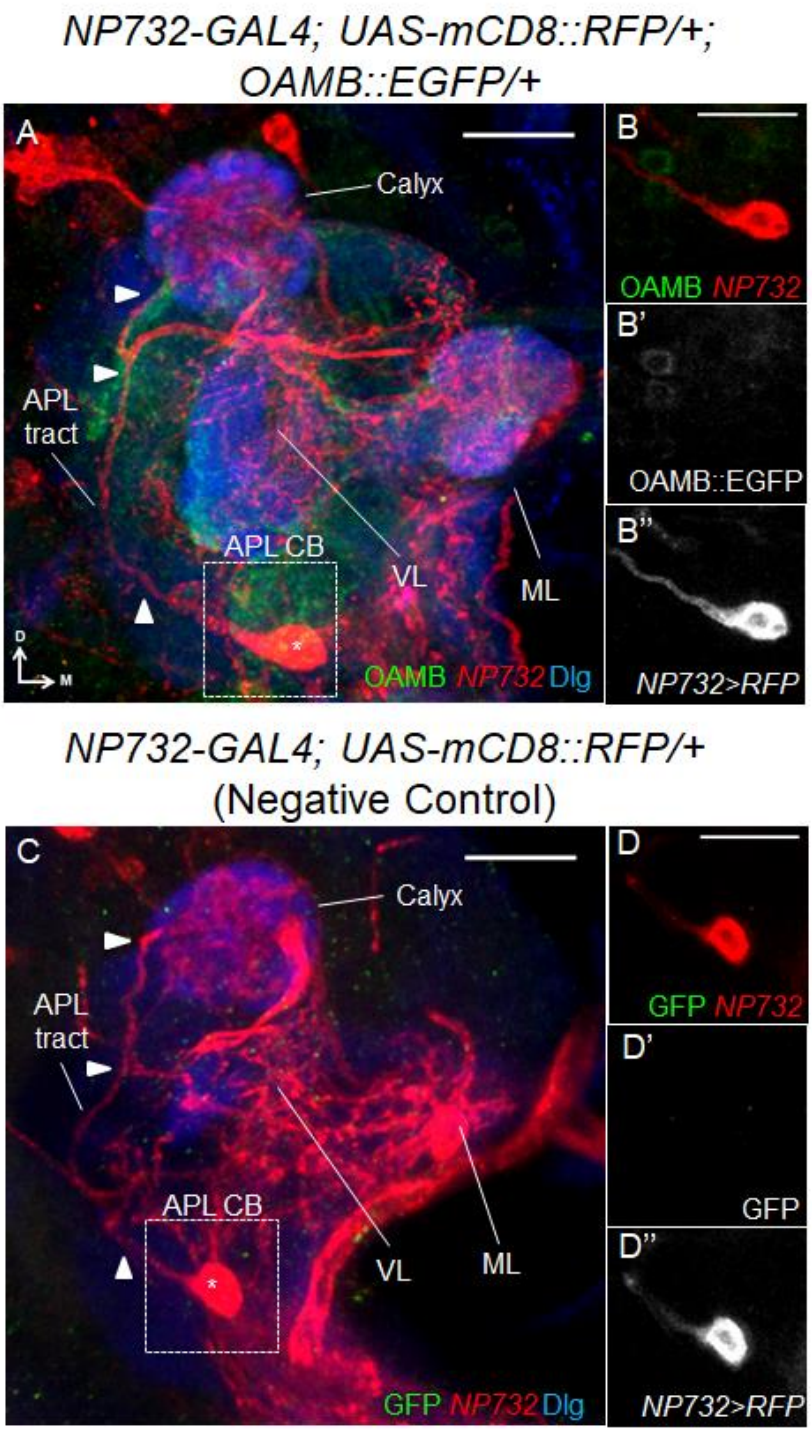

Figure 4.19. OAMB::EGFP did not colocalise with APL cell body. Confocal projections of the frontal brain lobe of *NP732-GAL4; UAS-mCD8::RFP/+; OAMB::EGFP/+* **(A-B)** and negative control *NP732-GAL4; UAS-mCD8::RFP/+; MKRS/TM6B* **(C-D)**. Green is OAMB::EGFP, red is *NP732>RFP* and blue is anti-Dlg. Asterisks indicate the APL cell body and arrowheads indicate the APL tract. **(B)** and **(D)** are confocal projections of the APL cell body taken from the dotted boxes in **(A)** and **(C)** respectively. Medial (M) is right, dorsal (D) is up. Abbreviations: VL, vertical lobe; ML, medial lobe; CB, cell body. Scale bar: 20 µm.

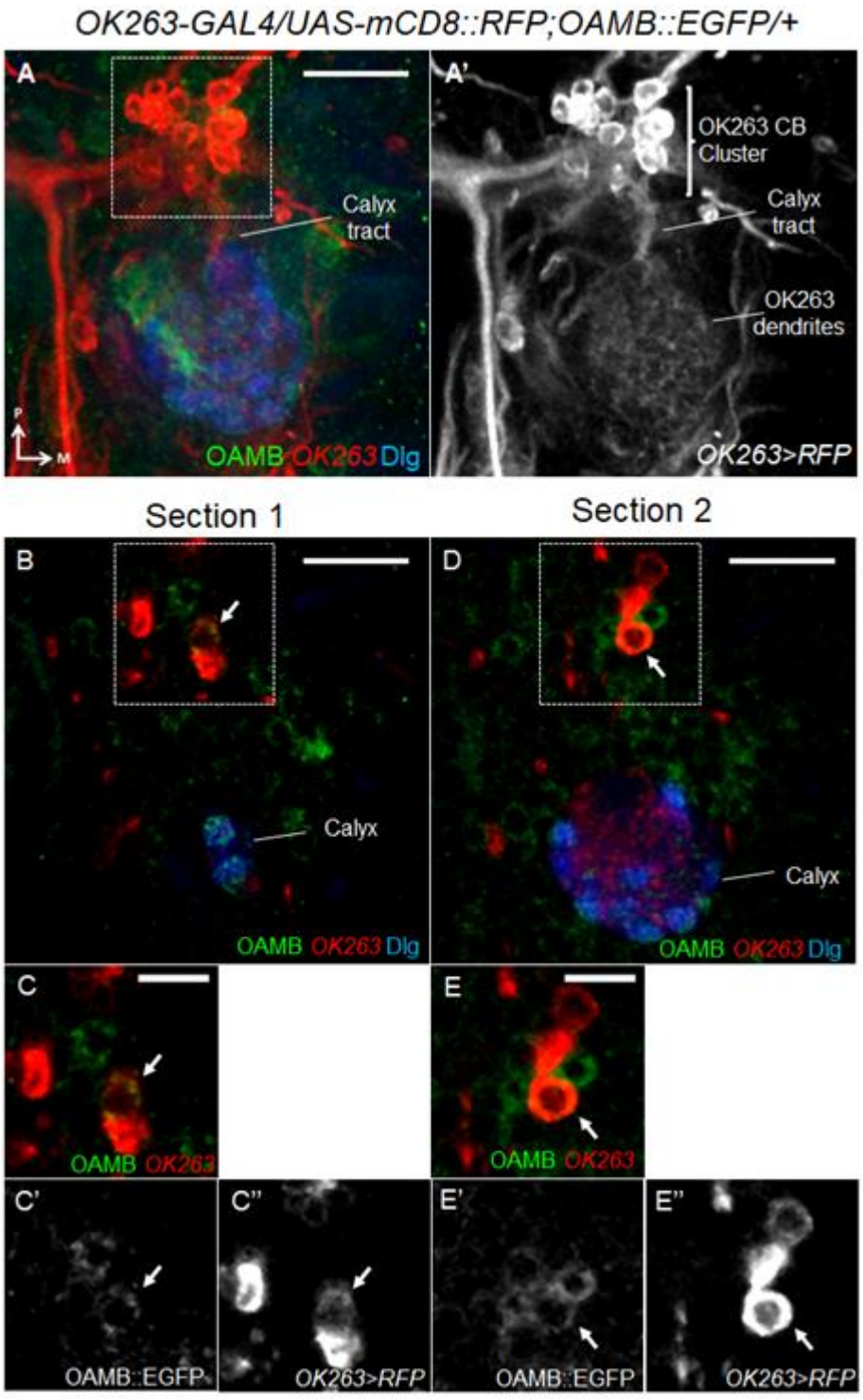

Figure 4.20. OAMB::EGFP colocalised with two cell bodies labelled by *OK263-GAL4*. Confocal projection **(A)** and two confocal optical sections **(B-E)** of the dorsal brain lobe of *OK263-GAL4/UAS-mCD8::RFP; OAMB::EGFP/+*. OAMB::EGFP is green, *OK263>RFP* is red and anti-Dlg is blue. Arrows indicate colocalisation of OAMB::EGFP and *OK263>RFP*. **(C,E)** are enlarged from the dotted squares in **(B,D)**. Dotted squares in **(A,B,D)** show the same region at different confocal optical slices. Medial (M) is right, posterior (P) is up. Abbreviations: CB, cell bodies. Scale bar: 20 µm in **(A,B,D)**; 10 µm in **(C,E)**.

However, as the tracts of these cell bodies merged together to form a single tract at the lateral edge of the pedunculus before entering the calyx (Fig. 4.20A), it was not possible to distinguish whether these OAMB-*OK263*-positive cell bodies projected to the calyx.

On the other hand, there was no overlap between OAMB::EGFP with OK263 dendrites in the calyx labelled by *OK263-GAL4* (n=2; Fig. 4.21A). This was again corroborated by the lack of extra-glomerular OAMB::EGFP signal characteristic of Odd-like innervation in calyces (Fig. 4.20A, 4.21A) in which OAMB::EGFP had been knocked down in PNs (Fig. 4.14). This suggested that OAMB did not localise to Odd-like dendrites in the calyx.

Furthermore, OAMB::EGFP signal did not localise to Odd-like axons innervating the neuropil around the medial lobe of the MB (n=2; Fig. 4.21B). As OAMB::EGFP did not localise to Odd-like processes in the calyx or MB lobes, the *OK263-GAL4* cell bodies expressing OAMB::EGFP signal probably did not belong to the calyx-innervating Odd-like neurons.

4.2.9. Testing RNAi lines for OAMB knockdown in PNs

To investigate the function of OAMB in PNs, it is necessary to be able to manipulate OAMB activity on specific neurons. One of the methods for tissue-specific knockdown OAMB function is through the use of RNAi. GFP-RNAi was previously used against OAMB::EGFP to show OAMB localisation to PN terminals in calyx glomeruli (Fig. 4.14). However, this method cannot be used to test OAMB function in PNs as the OAMB::EGFP fusion protein may itself be non-functional. Moreover, any non-EGFP-tagged OAMB proteins produced in a heterozygous animal will not be knocked down. Therefore, it was necessary to use *UAS-OAMB-RNAi* lines which targeted *OAMB* transcripts rather than EGFP sequences.

There are four *UAS-OAMB-RNAi* lines that have been previously used in the literature: Stocks *v2861* and *v106511* from the Vienna Stock Center; and stocks *UAS-OAMB-dsRNA (B31233)* and *UAS-OAMB-dsRNA (B31171)* from the Bloomington *Drosophila* Stock Center (Burke et al., 2012; Wu et al., 2013; Luo et al., 2014; Deady and Sun, 2015). All four of these lines encode dsRNA against fragments of the *OAMB* transcript. The efficacy of these lines have been

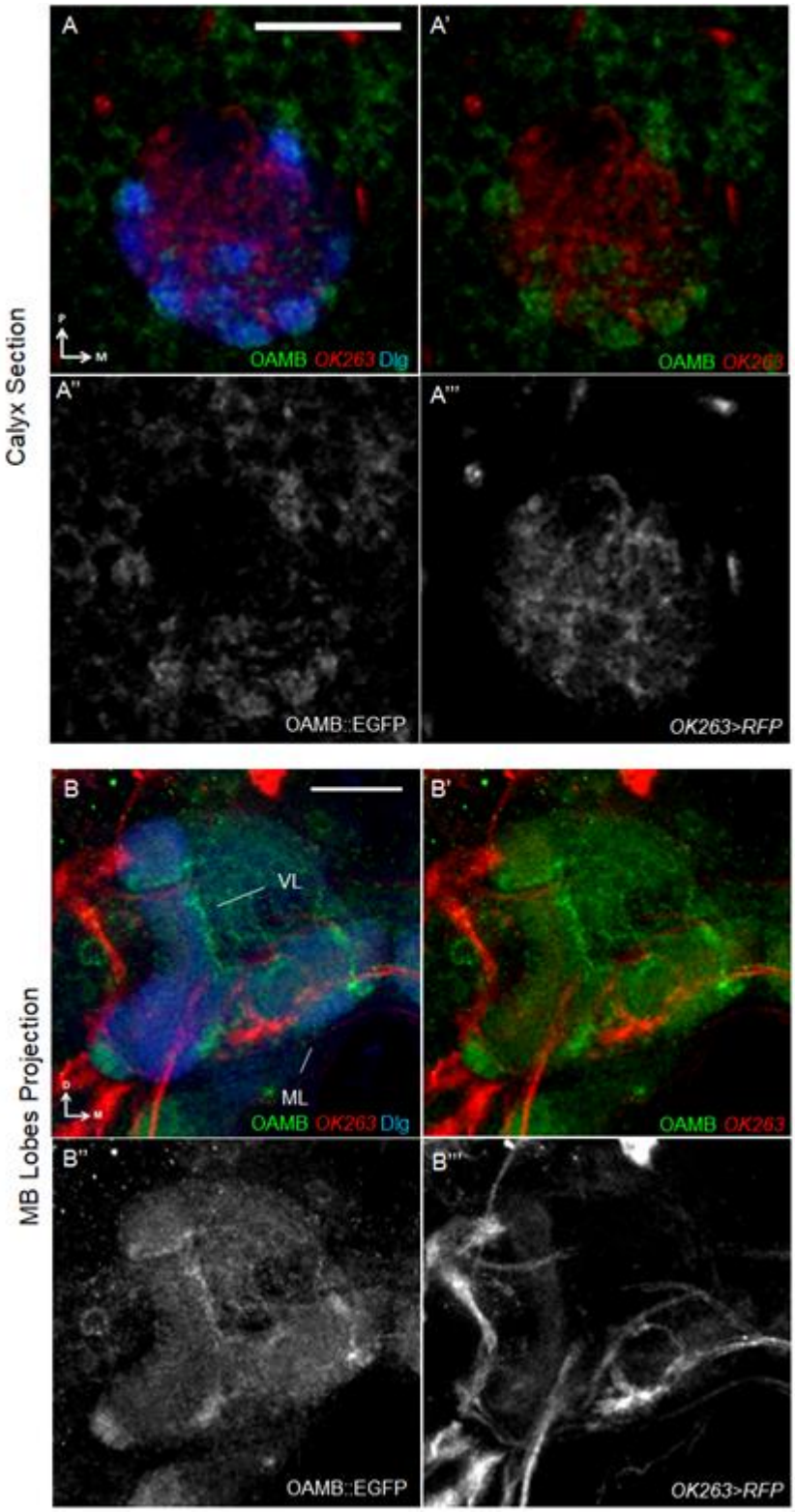

Figure 4.21. OAMB::EGFP did not colocalise with Odd-like neuronal processes. (A-B) *OK263-GAL4/UAS-mCD8::RFP; OAMB::EGFP/+* in MB calyx **(A)** and lobes **(B)**. OAMB::EGFP is green, *OK263>RFP* is red and anti-Dlg is blue. Medial (M) is right; posterior (P) is up for **(A)** and dorsal (D) is up for **(B)**. Abbreviations: VL, vertical lobe; ML, medial lobe. Scale bar: 20 μm.

compared in the context of ovulation phenotypes in Deady and Sun (2015), in which *v2861* showed the strongest phenotypes, followed by *v106511, B31233* and finally *B31171*.

To select the strongest OAMB RNAi line to study the function of OAMB expression on PNs, I used OAMB::EGFP intensity in calyx glomeruli as a quantifiable indicator for OAMB knockdown levels for three *UAS-OAMB-RNAi* lines: *v2861*, *v106511* and *B31233*. Using the ImageJ software, I measured the mean grey value of the GFP channel in calyx glomeruli marked as a region of interest. I was not able to differentiate between glomeruli based on whether they contained OAMB::EGFP originally or whether they expressed *NP225-GAL4*, and therefore chose to measure the intensity from all glomeruli marked with anti-Dlg for each confocal optical slice (Fig. 4.22, yellow dotted line). I took measurements from every fourth optical slice of the calyx for a total of 10 or 11 optical slices – which I then averaged to produce a mean intensity value. I then generated a knockdown percentage by comparing the mean intensity value for *NP225>OAMB-RNAi* knockdown brains with their non-knockdown controls.

I established a baseline reference using the *NP225>EGFP-shRNA* knockdown, because this line resulted in the strong knockdown of OAMB::EGFP signal in many calyx glomeruli, such that there were visibly less calyx glomeruli that contained OAMB::EGFP (Fig. 4.14; Table 4.5). Therefore, this served as a benchmark for near-complete knockdown of OAMB::EGFP signal. Table 4.7 shows the OAMB::EGFP intensity values for brains labelled with preincubated chicken anti-GFP – which were the antibody conditions used for *v2861* and *v106511* knockdown experiments. Table 4.8 shows the OAMB::EGFP intensity values for brains labelled with non-preincuabted chicken anti-GFP, matching the antibody conditions for the *B31233* knockdown experiment.

Although I used the same batch of antibodies and similar confocal conditions for the experimental and control individuals, they were not placed in the same tube during the immunolabelling process. Therefore, I also measured the intensity level of anti-Dlg labelling to serve as an internal control for variation between immunolabelling tubes as well as different individuals in the same tube. The average OAMB::EGFP intensity in *NP225>EGFP-shRNA* brains was around 20% to that of their corresponding non-knockdown *NP225>Luciferase*

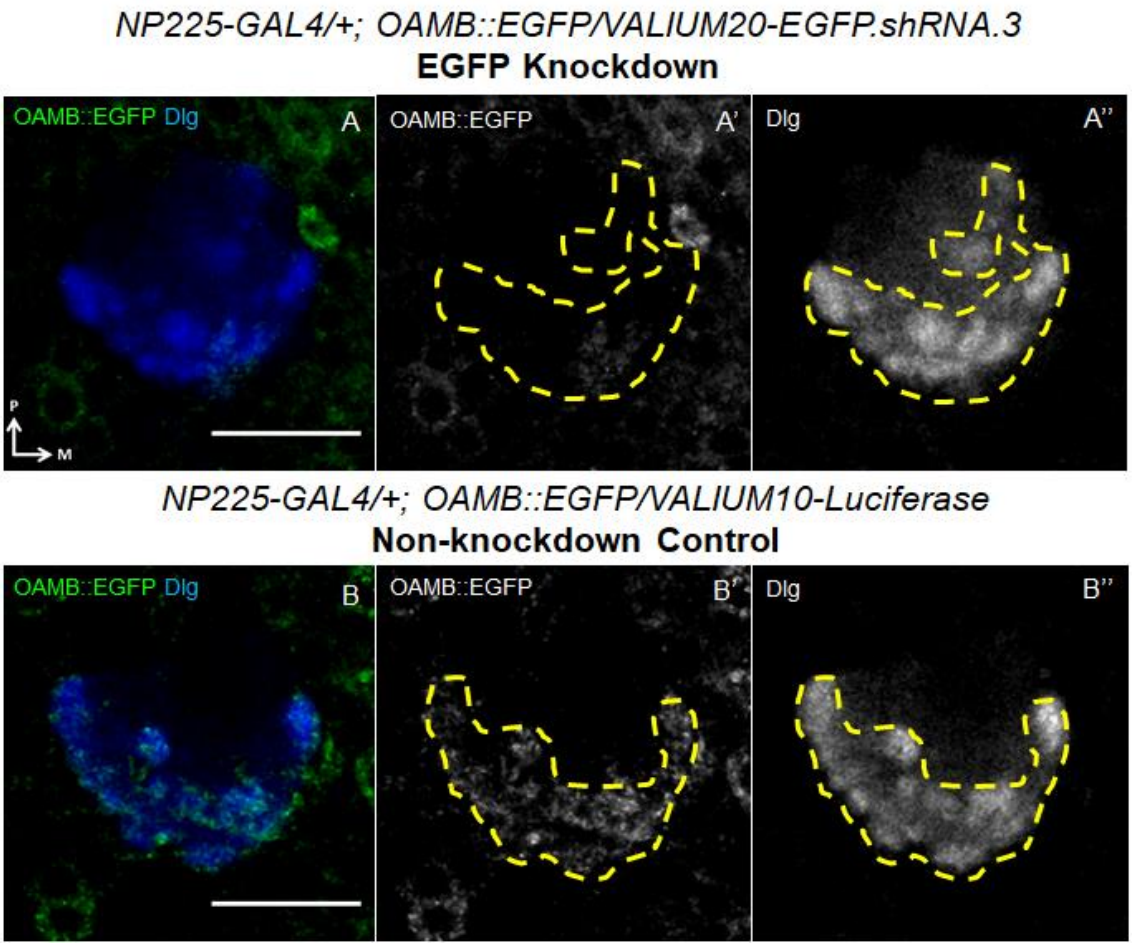

Figure 4.22. Quantification of OAMB::EGFP knockdown in calyx glomeruli. Confocal optical section of the calyx of *NP225-GAL4/+; OAMB::EGFP/VALIUM20-EGFP.shRNA.3* **(A)** and non-knockdown control *NP225-GAL4/+; OAMB::EGFP/VALIUM10-Luciferase* **(B)**. OAMB::EGFP is green, anti-Dlg is blue. Yellow dotted lines mark region of interest for measuring mean grey value for OAMB::EGFP. Medial (M) is right, posterior (P) is up. Scale bar: 20 µm.

Genotypes	*NP225-GAL4/+; OAMB::EGFP/VALIUM20 -EGFP-shRNA.3 (B41560)* **(EGFP Knockdown)**		*NP225-GAL4/+; OAMB::EGFP/VALIUM10 -Luciferase* **(Non-knockdown Control)**		**Knockdown/ Non-Knockdown (%)**	
Mean Intensity	**GFP**	**Dlg**	**GFP**	**Dlg**	**GFP**	**Dlg**
Individual 1	2.54	47.96	11.95	46.44	21%	103%
Individual 2	2.08	54.01	18.54	42.57	11%	127%
Individual 3	3.25	69.57	16.86	49.64	19%	140%
Individual 4	2.79	62.92	17.22	61.15	16%	103%
N	4	4	4	4		
Mean	2.67	58.61	16.14	49.95	17%	117%
S.D.	0.49	9.54	2.89	8.01		
S.E.M.	0.25	4.77	1.44	4.00		

Table 4.7. Mean OAMB::EGFP intensity in *NP225>EGFP-shRNA* brains (chicken anti-GFP, preincubated) compared to non-knockdown controls. Reference knockdown with similar antibody conditions for *NP225>v2861* and *NP225>v106511* knockdowns. Mean intensity is the average of 10 or 11 mean grey values (ImageJ) taken at every four confocal optical slices of the calyx where the mid-calyx is set as the middle confocal optical slice. Calyx glomeruli were selected as the region of interest. % knockdown/non-knockdown = (mean intensity in knockdown brain)/(mean intensity in non-knockdown brain)*100%. Abbreviations: N, number; S.D., standard deviation; S.E.M., standard error of the mean.

Genotypes	*NP225-GAL4/+; OAMB::EGFP/VALIUM20 -EGFP-shRNA.3 (B41560)* **(EGFP Knockdown)**		*NP225-GAL4/+; OAMB::EGFP/VALIUM10 -Luciferase* **(Non-knockdown Control)**		**Knockdown/ Non-Knockdown (%)**	
Mean Intensity	**GFP**	**Dlg**	**GFP**	**Dlg**	**GFP**	**Dlg**
Individual 1	4.88	72.60	20.43	78.62	24%	92%
Individual 2	4.21	67.67	23.29	78.75	18%	86%
Individual 3	3.15	69.50	20.23	60.30	16%	115%
Individual 4	1.99	72.56	9.28	64.21	21%	113%
N	4	4	4	4		
Mean	3.56	70.58	18.31	70.47	19%	100%
S.D.	1.27	2.42	6.18	9.62		
S.E.M.	0.63	1.21	3.09	4.81		

Table 4.8. Mean OAMB::EGFP intensity in *NP225>EGFP-shRNA* brains (chicken anti-GFP, non-preincubated) compared to non-knockdown controls. Reference knockdown with similar antibody conditions for *NP225>B31233* knockdown. Calculations and abbreviations as Table 4.7.

controls (n=8; Table 4.7, 4.8). On the other hand, the average anti-Dlg intensity in *NP225>EGFP-shRNA* brains was around 100% of their non-knockdown controls (Table 4.7, 4.8). This suggested that there was GFP knockdown in the experimental brains.

I did not observe detectable OAMB::EGFP knockdown in the calyx glomeruli of *NP225>v2861* brains (n=3; Fig. 4.23). Knockdown brains showed a mean OAMB::EGFP intensity of 11.3 ± 1.1 compared to 14.5 ± 1.9 in non-knockdown controls – that is, knockdown brains showed around 80% OAMB::EGFP signal of non-knockdown controls (n=3; Table 4.9). Individual 2 showed around 50% intensity compared to the corresponding non-knockdown control. However, after pooling the controls which were imaged at the same conditions, this individual was only around 65% of the averaged intensity of the non-knockdown control. Moreover, the percentage of experimental-to-control GFP intensity corresponded with that of anti-Dlg intensity (Table 4.9). Therefore, the difference in GFP intensity between experimental and control calyces were likely to be artefacts due to the individual variation in labelling.

As the *v106511* OAMB-RNAi line was maintained over the CyO balancer, I was not able to pre-screen *NP225>v106511* from CyO larvae in this experiment. Thus, only half of the progeny larvae dissected were expected to contain the *NP225>v106511* knockdown genotype. Three out of four *NP225>v106511 or CyO* brains did not show visibly lower OAMB::EGFP signals compared to the non-knockdown control (Fig. 4.24A-F). The remaining *NP225>v106511 or CyO* brain showed visibly lower OAMB::EGFP signals in calyx glomeruli than the non-knockdown controls (Fig. 4.24G-L). This was reflected in the OAMB::EGFP intensity values, where individual 3 showed a much lower mean intensity (5.6) than the other 3 individuals, and showed around 50% lower signal than the average of the non-knockdown controls (Table 4.10). The difference in GFP intensity between experimental and control was also much greater (47%) than the corresponding difference in anti-Dlg intensity (85%) (Table 4.10) – suggesting that the knockdown genotype, rather than labelling variability, was responsible for the decrease in GFP signal. This further suggested that from the four individuals, only individual 3 had the *NP225>v106511* knockdown genotype; and that *NP225>v106511* showed

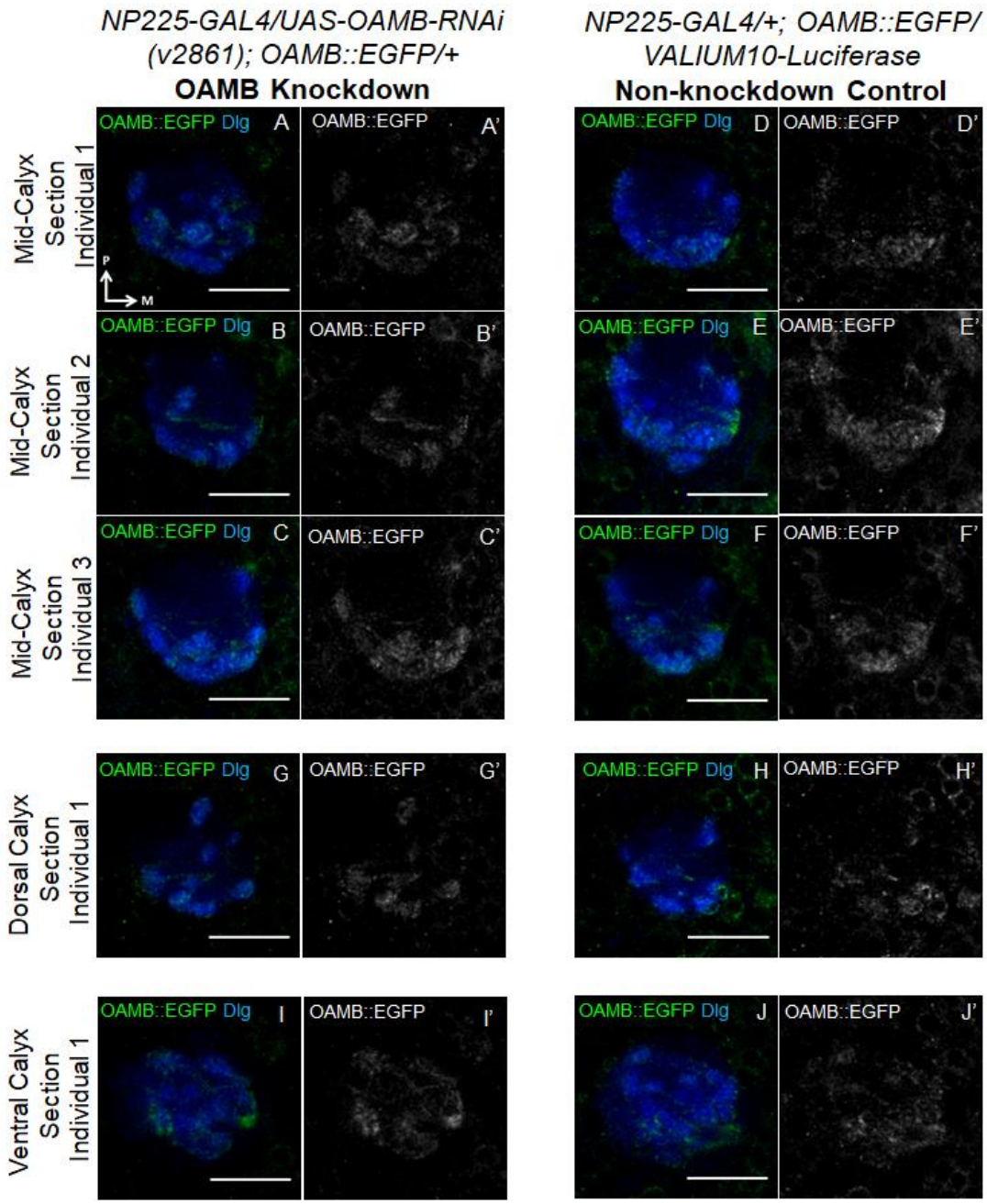

Figure 4.23. No detectable OAMB::EGFP knock down in calyx glomeruli of *NP225>v2861* brains. Confocal optical sections of the calyx from three *NP225-GAL4/UAS-OAMB-RNAi (v2861); OAMB::EGFP/+* individuals **(A-C,G,I)**, with non-knockdown control *NP225-GAL4/+; OAMB::EGFP/VALIUM10-Luciferase* **(D-F,H,J)**. Green is OAMB::EGFP, blue is anti-Dlg. Medial (M) is right and posterior (P) is up. Scale bar: 20 µm.

Genotypes	*NP225-GAL4/UAS-OAMB-RNAi (v2861); OAMB::EGFP/+* **(OAMB Knockdown)**		*NP225-GAL4/+; OAMB::EGFP/VALIUM10 -Luciferase* **(Non-knockdown Control)**		**Knockdown/ Non-Knockdown (%)**	
Mean Intensity	**GFP**	**Dlg**	**GFP**	**Dlg**	**GFP**	**Dlg**
Individual 1	10.31	44.57	12.03	60.23	86%	74%
Individual 2	9.91	45.17	18.26	72.98	54%	62%
Individual 3	13.52	50.77	13.06	50.34	104%	101%
N	3	3	3	3		
Mean	11.25	46.84	14.45	61.18	78%	77%
S.D.	1.98	3.42	3.34	11.35		
S.E.M.	1.14	1.97	1.93	6.55		

Table 4.9. Mean OAMB::EGFP intensity in *NP225>v2861* brains compared to non-knockdown controls. Calculations and abbreviations as Table 4.7.

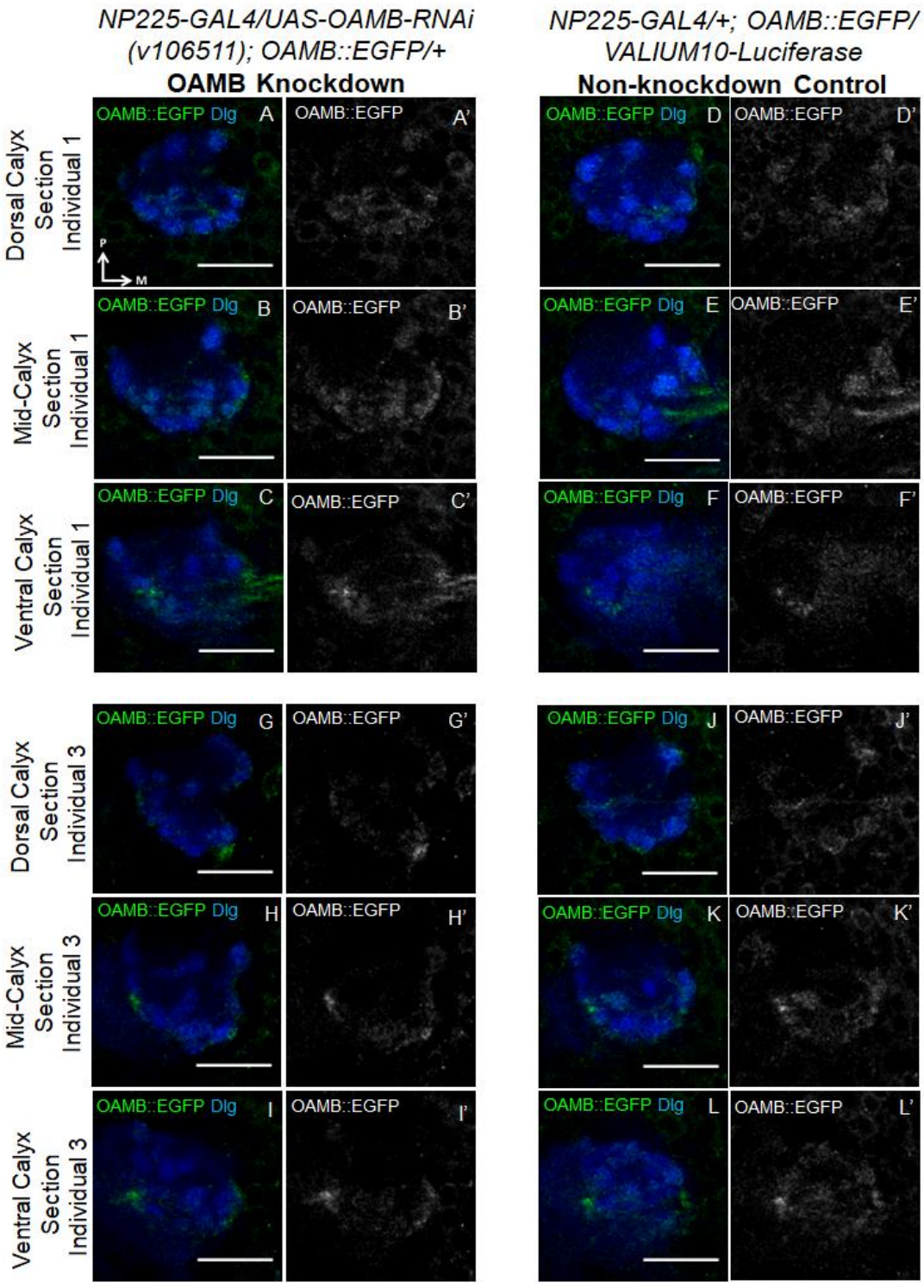

Figure 4.24. Variable levels of OAMB::EGFP knock down in calyx glomeruli of *NP225>v106511* brains. Confocal optical sections of the calyx from two *NP225-GAL4/UAS-OAMB-RNAi (v106511); OAMB::EGFP/+* individuals **(A-C,G-I)** and non-knockdown control *NP225-GAL4/+; OAMB::EGFP/VALIUM10-Luciferase* **(D-F,J-L)**. Individual 1 **(A-C)** did not show observable OAMB::EGFP knockdown, while individual 3 **(G-I)** showed partial OAMB::EGFP knockdown. Green is OAMB::EGFP, blue is anti-Dlg. Medial (M) is right and posterior (P) is up. Scale bar: 20 μm.

Genotypes	*NP225-GAL4/UAS-OAMB-RNAi (v106511); OAMB::EGFP/+* **(OAMB Knockdown)**		*NP225-GAL4/+; OAMB::EGFP/VALIUM10 -Luciferase* **(Non-knockdown Control)**		**Knockdown/ Non-Knockdown (%)**	
Mean Intensity	**GFP**	**Dlg**	**GFP**	**Dlg**	**GFP**	**Dlg**
Individual 1	13.81	53.54	12.97	69.15	106%	77%
Individual 2	11.50	66.18	9.15	56.90	126%	116%
Individual 3	5.59	47.53	12.02	55.80	47%	85%
Individual 4	8.72	52.38				
N	4	4	3	3		
Mean	9.91	54.91	11.38	60.61	87%	91%
S.D.	3.55	7.95	1.99	7.41		
S.E.M.	1.78	3.98	1.15	4.28		

Table 4.10. Mean OAMB::EGFP intensity in *NP225>v106511* brains compared to non-knockdown controls. Individual 3 may show partial knockdown (indicated in yellow in table; Fig. 4.24G-I). Calculations and abbreviations as Table 4.7.

partial knockdown of the OAMB::EGFP protein. However, more samples are required to confirm this result.

Finally, all of the *NP225>B31233* brains showed a comparable level of mean OAMB::EGFP intensities at 26.1 ± 5.0 to their corresponding non-knockdown controls at 20.5 ± 2.3 (n=5; Fig. 4.25; Table 4.11). As their anti-Dlg intensity levels were also comparable, this suggested that the *B31233* line did not have a clear effect on knocking down OAMB proteins.

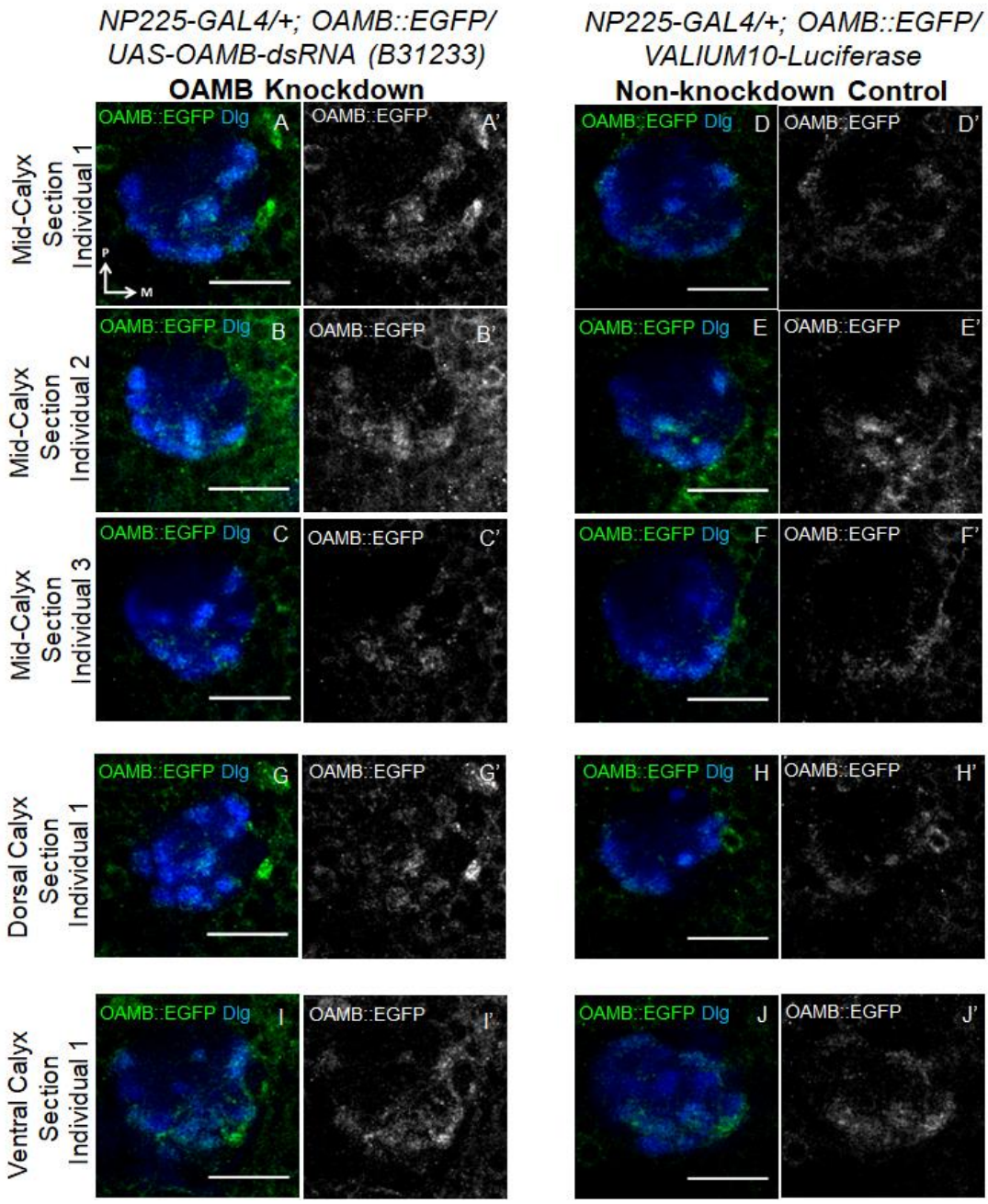

Figure 4.25. No observable OAMB::EGFP knock down in calyx glomeruli of *NP225>B31233* brains. Confocal optical sections of the calyx from three *NP225-GAL4/+; OAMB::EGFP/UAS-OAMB-dsRNA (B31233)* individuals **(A-C,G,I)**, with non-knockdown control *NP225-GAL4/+; OAMB::EGFP/VALIUM10-Luciferase* **(D-F,H,J)**. Green is OAMB::EGFP, blue is anti-Dlg. Medial (M) is right and posterior (P) is up. Scale bar: 20 µm.

Genotypes	*NP225-GAL4/+; OAMB::EGFP/VALIUM1-OAMB-dsRNA (B31233)* **(OAMB Knockdown)**		*NP225-GAL4/+; OAMB::EGFP/VALIUM10-Luciferase* **(Non-knockdown Control)**		**Knockdown/ Non-Knockdown (%)**	
Mean Intensity	**GFP**	**Dlg**	**GFP**	**Dlg**	**GFP**	**Dlg**
Individual 1	44.19	86.26	26.58	74.03	166%	117%
Individual 2	23.53	92.23	25.14	79.13	94%	117%
Individual 3	27.89	80.57	17.78	64.10	157%	126%
Individual 4	17.04	62.65	14.35	61.44	119%	102%
Individual 5	17.58	71.44	18.78	77.15	94%	93%
N	5	5	5	5		
Mean	26.05	78.63	20.52	71.17	127%	110%
S.D.	11.09	11.77	5.16	7.94		
S.E.M.	4.96	5.26	2.31	3.55		

Table 4.11. Mean OAMB::EGFP intensity in *NP225>B31233* brains compared to non-knockdown controls. Calculations and abbreviations as Table 4.7.

4.3. Discussion

Using a novel OAMB protein trap line, I have shown that the OAMB::EGFP fusion protein localised to the *Drosophila* larval MB calyx. This was consistent with *OAMB-GAL4* expression in the larval MB calyx (El-Kholy et al., 2015) – the only published study that investigated OAMB localisation in the larval brain. Although this suggested that *OAMB-GAL4* was expressed in some calyx-innervating neurons, unlike OAMB::EGFP fusion proteins, *OAMB-GAL4* cannot show whether OAMB localised to the calyx terminals of these neurons. Furthermore, while *OAMB-GAL4* is generated by *OAMB* promoter region fusion to *GAL4* sequences; EGFP is inserted within *OAMB* coding sequences in the OAMB::EGFP fusion protein, and hence subjected to endogenous regulation of *OAMB* expression. This suggests that OAMB::EGFP is theoretically more accurate for reflecting OAMB localisation patterns than *OAMB-GAL4* lines, and thus provide stronger evidence for OAMB localisation to larval calyx terminals.

OAMB::EGFP localisation in the larval calyx is also conserved with OAMB localisation to the adult *Drosophila* MB calyx (Han et al., 1998), and the homologue AmOA1 in the honeybee localising to the olfactory input region of the honeybee calyx (Sinakevitch et al., 2011), identified using antibody staining. However, the *Drosophila* OAMB antibody signal was weak and non-specific based on published images of the adult fly brain (Kim et al., 2013). This was also the case when anti-AmOA1 was used to visualise OAMB localisation in the *Drosophila* adult and larval brains (Sinakevitch et al., 2013; H.W., unpublished observations); although this was probably because an AmOA1 peptide sequence that did not perfectly match its homologous OAMB sequence was used to generate the antibody (Sinakevitch et al., 2011). As there are no other antibodies available, this suggests that it may be difficult to produce strong and specific OAMB antibodies.

Similar to anti-OAMB, there were also difficulties in visualising OAMB::EGFP, which was eventually overcome by optimising the immunolabelling protocol. This is one of the advantages of using a fusion protein instead of antibodies, as its signal can be amplified by anti-GFP. OAMB::EGFP signal in homozygous larvae can also be detected in non-fixed brains for live imaging, which is not possible when antibodies are used. On the other hand, anti-OAMB would not interfere with OAMB receptor expression, and

therefore less likely to affect normal OAMB function and localisation compared to the OAMB::EGFP fusion. Moreover, as anti-OAMB is not genetically encoded, it is not necessary to construct new fly lines to validate OAMB colocalisation with calyx-innervating neurons.

Nevertheless, conserved OAMB localisation to insect MB calyces suggests that OAMB is involved in mediating OA modulation of inputs to MB neurons.

4.3.1. OAMB localisation to PNs but not to APL or Odd-like neurons

From the three putative postsynaptic partners of sVUM1 neurons, I have shown that OAMB is expressed in PNs but not in the APL neuron or the calyx terminals of Odd-like neurons (Fig. 4.26). OAMB localisation to the calyx terminals of PNs suggests that PNs are able to receive OA signalling from sVUM1 neurons in the larval MB calyx, which supports the GRASP connectivity data (Chapter 3). On the other hand, the APL neuron and Odd-like neurons may express other OA receptors in order to respond to sVUM1 signalling (Chapters 5 & 6). It is also possible that the APL neuron may be modulating sVUM1 neurons in the calyx unidirectionally and therefore would not express any OA receptors.

This is the first report of OAMB expression in PNs in *Drosophila*; although it remains consistent with the unpublished result mentioned in Kim et al. (2013) that OAMB localised to non-KC extrinsic neurons in the adult MB calyx. Unlike OAMB, the honeybee α1-adrenergic-like receptor AmOA1 is localised to GABAergic PCT feedback neurons (analogous to larval APL neurons), but not to uniglomerular PNs (analogous to larval PNs), in the honeybee calyx (Sinakevitch et al., 2013). Therefore, should OAMB and AmOA1 activation have similar downstream effects on excitatory PNs and inhibitory feedback neurons respectively, it would result in opposite effects on the olfactory inputs to the fly larval calyx versus the honeybee calyx. This suggests that while OAMB localisation to the MB calyx may be conserved, it may not be mediating OA signalling in analogous neuronal types across insects.

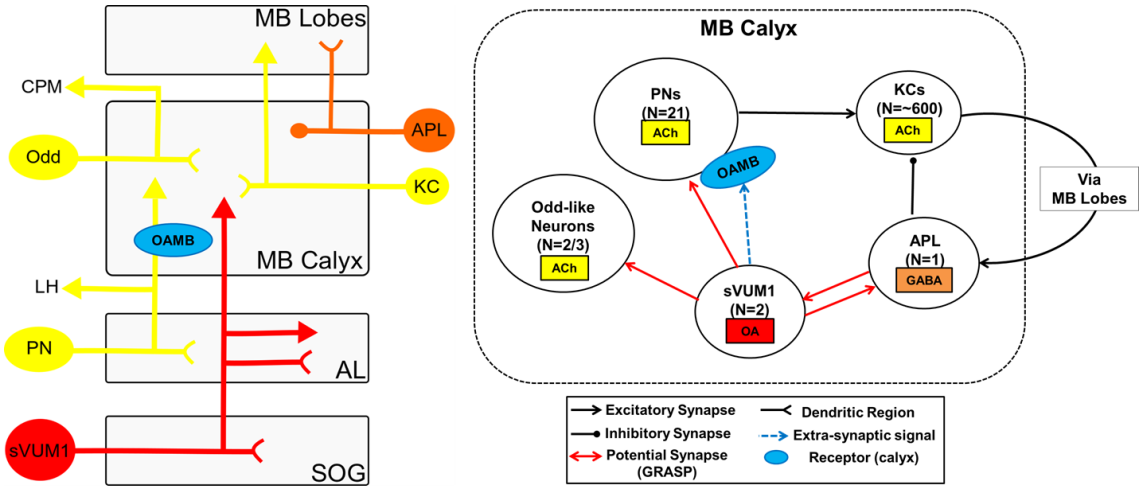

Figure 4.26. Proposed OAMB localisation pattern in larval MB calyx circuitry. Abbreviations: ACh, acetylcholine; AL, antennal lobe; CPM, centroposterior medial compartment; KC, Kenyon Cell; LH, lateral horn; MB, mushroom body; N, number; OA, octopamine; PN, projection neuron.

4.3.2. OAMB localisation to presynaptic terminals of olfactory PNs

OAMB::EGFP is localised to around 30 out of 35 larval calyx glomeruli. As the *NP225-GAL4* line labels olfactory PNs that innervate around 23 larval calyx glomeruli (Masuda-Nakagawa et al., 2005), OAMB::EGFP localisation on all *NP225-GAL4*-expressing glomeruli suggests that OAMB is likely to be expressed at the calyx terminals of most larval olfactory PNs. The remaining OAMB::EGFP-positive glomeruli are probably innervated by the two olfactory PNs not labelled by *NP225-GAL4* (Masuda-Nakagawa et al., 2009, 2010); as well as multiglomerular PNs and/or non-olfactory PNs (Eichler et al., 2017), although their larval calyx innervation patterns are not yet known. This suggests that OA signalling in the calyx broadly and non-specifically targets a diverse group of olfactory PNs, each bringing olfactory input from a single olfactory sensory neuron (Masuda-Nakagawa et al., 2005, 2009). This implies the effects of OA signalling in the calyx is not restricted to particular odour qualities, but instead target many olfactory inputs simultaneously, as well as potentially some non-olfactory inputs.

OAMB::EGFP localisation to larval calyx glomeruli suggests that OAMB is localised to the presynaptic terminals of olfactory PNs. This implies that OA could modulate olfactory inputs from PNs to KCs presynaptically. A possible method for presynaptic modulation is through the control of neurotransmitter release from PNs to KCs. For example, presynaptic α1-adrenoceptor

expression in the striatum and midbrain regulates dopaminergic transmission (Mitrano et al., 2012). α1-adrenoceptor activation has also been shown to increase glutamate release and decrease GABAergic input to hypothalamic neurons (Chen et al., 2006).

OAMB increases intracellular Ca^{2+} concentration in cultured cells (Han et al., 1998; Balfanz et al., 2005; Morita et al., 2006). It is possible this could enhance calcium-mediated exocytosis of neurotransmitters. For example, OA-induced increase of intracellular Ca^{2+} from the Endoplasmic Reticulum (ER) together with PKA activity can induce neuropeptide release at the *Drosophila* neuromuscular junction even when extracellular Ca^{2+} is absent (Shakiryanova et al., 2011). As OAMB is thought to be coupled to the G_q pathway, similar to its homologue α1-adrenoceptor, OAMB activation may also activate PKC via PLC/DAG activation. PKC is required for the presynaptic increase of the number of vesicles and probability of release in glutamate neurons of the rat medial prefrontal cortex (Luo et al., 2015). In the same system, presynaptic α1-adrenoceptor activation also activates presynaptic N-type Ca^{2+} channels, as adrenergic enhancement of glutamate release is reduced when these Ca^{2+} channels are blocked (Luo et al., 2015). This suggests that OAMB expression on PNs may result in OA-induced intracellular Ca^{2+} signalling, which then increases the release of acetylcholine by PNs on KCs, possibly via PKA or PKC-dependent pathways.

4.3.3. Possible OAMB localisation to olfactory PN dendrites

sVUM1 neurons are the only known OA neurons innervating the larval AL (Selcho et al., 2014), where olfactory PN dendrites are also located. As OAMB::EGFP signal was partially knocked down in the AL by *EGFP-shRNA* expression in the olfactory PN driver *NP225-GAL4*, this suggested that OAMB::EGFP localised to the olfactory PN dendrites arborising in AL glomeruli, as well as to some non-PN neurons innervating the AL. Therefore, olfactory PN dendrites and other AL-innervating neurons may also respond to modulation by sVUM1 signalling in the AL via OAMB.

If OAMB localised to olfactory PN dendrites, it would probably increase the neuronal excitability of olfactory PNs. OAMB activation increases spontaneous spiking in cultured rat cortical neurons (Morita et al., 2006). On the

other hand, OA reduction of outward hyperpolarising Ca^{2+}-dependent-K^{+} currents in *Drosophila* pars intercerebralis neurons is blocked in *oamb* mutants (Crocker et al., 2010). This suggests that OAMB expression on PN dendrites could reduce hyperpolarisation in PNs and/or increase PN firing; and would hence increase olfactory inputs from PNs to the MB.

4.3.4. Possible extrasynaptic localisation of OAMB

In agreement with the unpublished observation that anti-OAMB signal did not localise to KCs in the adult calyx discussed in Kim et al. (2013), OAMB receptors did not localise to KC dendrites in the MB calyx. This suggests that OAMB does not mediate extrasynaptic signalling from sVUM1 neurons to KCs in the larval MB calyx.

However, OAMB::EGFP signal is detected in the MB lobes and occasionally in KC cell bodies. This is consistent with anti-OAMB signal observed in the adult MB lobes (Han et al., 1998; Kim et al., 2013) and mRNA transcript localisation to KC cell bodies (Han et al., 1998). OAMB::EGFP signal in the MB lobes suggests that OAMB could be localised to KC axons in the larval MB lobes. This suggests that KC output may be presynaptic targets of OA signalling via OAMB. Alternatively, OAMB could be localised to extrinsic neurons innervating the larval MB lobes. Regardless, this does not provide evidence for extrasynaptic localisation of the OAMB receptor, as it is not known whether KCs or MB extrinsic neurons synapse with the OA neuron sVPM4, which innervates the MB lobes (Selcho et al., 2014).

On the other hand, OAMB::EGFP signal on PNs appears to be broader than putative sVUM1-PN connections observed through GRASP (Chapter 3). While sVUM1-PN GRASP signals localised to the interglomerular region of the calyx or at the periphery of calyx glomeruli, OAMB localised to the core and periphery of calyx glomeruli as well as the iACT. This suggests that there are many sites where PNs could respond to OA signal from sVUM1 neurons in the absence of a synaptic connection. Therefore, this supports the hypothesis that OA may act synaptically and extrasynaptically in the larval brain.

4.3.5. OAMB::EGFP localisation to other calyx-innervating neurons

In addition to PNs labelled by *NP225-GAL4*, OAMB::EGFP is observed in around five more calyx glomeruli than the total number of glomeruli expected to be innervated by all of the olfactory PNs. This implies that OAMB is localised to other non-characterised neurons which innervate the remaining calyx glomeruli.

OAMB may be expressed in multiglomerular olfactory PNs which innervate multiple AL glomeruli, three of which project to the calyx in the L1 brain (Berck et al., 2016), and have been shown by MARCM clonal analysis to innervate 1-2 calyx glomeruli in the third instar larvae (Das et al., 2013). While the role of multiglomerular PNs in the larval calyx is unclear, there is evidence from L1 connectomics data that they are post-synaptic to sVUM1 neurons (https://neuronlp.larva.fruitflybrain.org/; Eichler et al., 2017). Therefore, sVUM1 neurons may modulate multiglomerular PNs via OAMB.

OAMB may also be expressed in projection neurons which do not follow the canonical innervation pattern of olfactory PNs (Masuda-Nakagawa et al., 2009; Das et al., 2013). An example of non-canonical projection neurons could be the S370b neurons described by Angela Wan in her MPhil thesis (2015). S370b neurons innervate 1-2 AL glomeruli and 3-4 calyx glomeruli, but their cell bodies are located posterior to the AL in the SOG region. They also send a medial tract to the AL and a lateral tract to the calyx, rather than following the canonical iACT (A.W., MPhil Thesis 2015). As S370b neurons innervate both the AL and SOG, the primary olfactory and gustatory centres respectively (Colomb et al., 2007), they may be multimodal projection neurons that carry both odour and taste inputs to calyx glomeruli. Alternatively, S370b neurons may be the larval equivalents to the adult bilateral ventral projection neuron (biVPN) that delivers carbon dioxide input to the MB calyx, as they share similar morphology and innervation patterns (Bräcker et al., 2013). However, the functions of the larval S370b neurons are yet to be characterised.

Nevertheless, this suggests that some of the OAMB::EGFP-positive glomeruli may be innervated by non-olfactory PNs. In the L1 connectomics project, around 16 non-olfactory PNs, including thermosensory and photosensory PNs, have been identified by being downstream to known first order sensory neurons (Eichler et al., 2017). However, it is not clear whether and how these non-olfactory PNs innervate calyx glomeruli, especially the one-

third that are not already innervated by olfactory PNs (Masuda-Nakagawa et al., 2005). In adult flies, the carbon dioxide biVPN and possibly some gustatory PNs innervate the main adult calyx (Bräcker et al., 2013; Kirkhart and Scott, 2015); although most non-olfactory inputs appear to innervate the accessory calyces instead (Kirkhart and Scott, 2015; Vogt et al., 2016; Yagi et al., 2016). This suggests that the L3 calyx may also receive inputs from non-olfactory PNs – although this remains to be characterised in the future. As there are around 6 calyx glomeruli that are OAMB::EGFP-negative, it is possible that OAMB expression correlates PNs carrying inputs of specific modalities.

OAMB expression on non-olfactory PNs innervating calyx glomeruli would suggest that sVUM1 signalling also modulates non-olfactory inputs to KCs, probably by presynaptically increasing neurotransmitter release from non-olfactory PNs via the α1-adrenergic-like OAMB, similar to the mechanisms proposed in Section 4.3.2. in olfactory PNs.

4.3.6. OAMB knockdown efficacy of three *UAS-OAMB-RNAi* lines

After identifying OAMB localisation to PNs, I tested three OAMB RNAi lines to validate the most effective line for knocking down OAMB proteins in PNs for use in future functional and behavioural experiments.

By measuring OAMB::EGFP intensity I could quantify how each RNAi line knocked down OAMB::EGFP proteins at its area of interest – the calyx glomeruli labelled by *NP225-GAL4*. This is more representative than measuring the number of *OAMB* transcripts present after knockdown. However, it is important to consider that the levels of OAMB::EGFP proteins do not reflect the level of OAMB proteins that are not tagged by EGFP. This method was also impeded by the fact that *NP225-GAL4* did not label all the OAMB::EGFP-positive calyx glomeruli. Therefore, it was difficult to determine the glomeruli which expressed *NP225>OAMB-RNAi* from the glomeruli that did not. This may be resolved by co-expressing *UAS-mCD8::RFP* to identify *NP225*-positive glomeruli subjected to RNAi knockdown.

There was some variation of intensity levels within a genotype and antibody batch, despite the fact that the brains were dissected and imaged under the same conditions. I attempted to control for individual variation by comparing anti-Dlg intensity which should not be affected by EGFP knockdown.

However, it would have been better if knockdown and non-knockdown control larvae were immunolabelled in the same tube to ensure they were exposed to exactly the same antibody conditions. Other sources of variation are probably linked to the individual variability of *GAL4/UAS* expression, estimations in the quantification method or other human errors.

Additionally, there was a misrepresentation of *NP225>v106511* genotypes as I was not able to distinguish larvae that carried the *v106511* construct versus those that instead carried the *CyO* balancer. To resolve this problem, it would be necessary to rebalance the stock with a second chromosome balancer that is linked to a phenotype that can be selected against at the larval stage, for example *CyO::EGFP*.

Through comparing the OAMB::EGFP intensity ratio between knockdown with non-knockdown controls, *NP225>EGFP-shRNA* remained the strongest line for knocking down OAMB::EGFP signal, and therefore EGFP-tagged OAMB proteins, at around 80%. From the *UAS-OAMB-RNAi* lines, *v106511* showed the strongest knockdown of OAMB::EGFP signals at around 50%, provided that this can be consistently observed in more than one individual that definitely contains the *v106511* construct. This was followed by the *v2861* line at around 20%, while *B31233* did not show any OAMB::EGFP signal reduction at all. The efficacy of these OAMB RNAi lines in PNs was in a slightly different order to that previously observed in ovulation phenotypes by Deady and Sun (2015).

As none of these stocks appeared to show near complete knockdown of OAMB::EGFP signal, it is necessary to improve OAMB knockdown efficacy through additional measures. This could include using *UAS-Dicer* constructs to increase the efficiency of processing dsRNA into siRNA that are used to target mRNA transcripts. This was used alongside *UAS-OAMB-RNAi* lines in Deady and Sun (2015). An alternative method could be to raise the temperature to 29ºC to allow maximum *GAL4* expression levels – which was used to increase RNAi knockdown efficacy in Nagarkar-Jaiswal et al. (2015).

The OAMB RNAi line with the strongest knockdown in PNs can be used to study the function of OAMB in PNs. For example, whether OAMB knockdown in PNs have a phenotype for odour discrimination, or how the activity of PNs or KCs would be affected when OAMB is knocked down in PNs.

4.3.7. Functionality of the OAMB::EGFP fusion protein

As the EGFP cassette is inserted in the coding region intron of the *OAMB* gene, it should theoretically be translated as an artificial exon without affecting *OAMB* coding exon sequences. In fact, lethality caused by the MiMIC insertion is often reverted when the MiMIC gene trap is replaced with the EGFP protein trap; and that around 75% of resulting fusion proteins generated from this method are functional (Venken et al., 2011a; Nagarkar-jaiswal et al., 2015).

The *OAMB::EGFP* homozygote generated for this study is viable but sterile. As OAMB regulates normal ovulation (Lee et al., 2009; Deady and Sun, 2015), this suggests that the OAMB::EGFP fusion protein is not fully functional. This appears contradictory to the successful OAMB::EGFP localisation to neuronal terminals, because misfolded proteins are usually detected post-translation in the endoplasmic reticulum (ER), retained and later degraded (Sitia and Braakman, 2003). While OAMB::EGFP colocalised with ER markers (Section 6.3.4), there was no further evidence that this was at higher levels than expected from normal trafficking from the ER during translation to the plasma membrane. This suggests that OAMB::EGFP misfolding was probably not detected at the ER and its lack of functionality is not due to mislocalisation.

While the EGFP insertion site in the OAMB protein was not near any of the TMs, it was less than five amino acids away from two potential consensus sites for Protein Kinase C phosphorylation (Han et al., 1998). Therefore, EGFP insertion may disrupt normal OAMB function by preventing PKC phosphorylation, possibly via steric hindrance, while subcellular localisation is not affected.

Chapter 5. Expression of β-adrenergic-like OA receptors in calyx-innervating neurons

5.1. Introduction

The β-adrenergic-like OctβRs – Octβ1R, Octβ2R and Octβ3R – are another class of OA receptors that may mediate sVUM1 signalling in the larval calyx circuitry. Based on published literature, it is inconclusive as to whether any of the three OctβRs localised to the larval MB calyx. Despite this, the expression and function of OctβRs in the adult fly MB circuitry suggest that OctβRs could be involved in mediating OA modulation in the larval calyx as well.

In situ hybridisation with Octβ1R, Octβ2R and Octβ3R antisense probes showed that the three OctβRs were expressed in different subsets of cells in the larval brain lobes (Ohhara et al., 2012). However, the authors did not attempt to identify the cell bodies expressing the OctβRs. It is also unclear whether any *in situ* hybridisation signals was detected in the larval MBs, even though *OctβR* expression was not observed in the adult MBs (Ohhara et al., 2012).

Another group visualised OctβR expression in the larval CNS using promoter-*GAL4* lines containing the full promoter region for each of the OctβRs (El-Kholy et al., 2015). All three *OctβR-GAL4* lines showed expression in the brain lobes with distinctive patterns (El-Kholy et al., 2015). In particular, *Octβ3R-GAL4* showed strong signals in the MB calyx and lobes, suggesting that Octβ3R may be expressed in neurons innervating the MB. However, due to the variability of promoter-*GAL4* expression patterns (Chapter 8), these data may not accurately represent the endogenous expression of OctβRs in the larval brain.

Using cell-type-specific RNA sequencing, Octβ1R and Octβ2R transcripts have been detected in adult KCs (Crocker et al., 2016). Anti-Octβ2R has also been observed in α'β' KCs in the MB lobes (Wu et al., 2013). Indeed, Octβ2R knockdown using a pan-KC driver and a specific α'β' KC driver failed to form anesthesia-resistant aversive olfactory memory (Wu et al., 2013). This suggests that Octβ1R and Octβ2R are expressed in adult KCs, and that Octβ2R

is required in α'β' KCs for olfactory memory; which is expected to be conserved in larval KCs.

In adult flies, functional Octβ2R is also required for normal artificial olfactory reward memory implantation (Burke et al., 2012); whereas Octβ3R knockdown in neurons resulted in improved aversive olfactory memory (Walkinshaw et al., 2015). This suggests that the involvement of OctβRs in olfactory processing circuitry is likely to extend to the larval MB calyx circuitry.

By examining the endogenous expression patterns of Octβ1R, Octβ2R and Octβ3R using EGFP-tagged receptors generated from MiMIC insertion lines, I aimed to address the following questions to understand OctβR localisation to neurons in the larval MB calyx circuitry (Fig. 5.1):

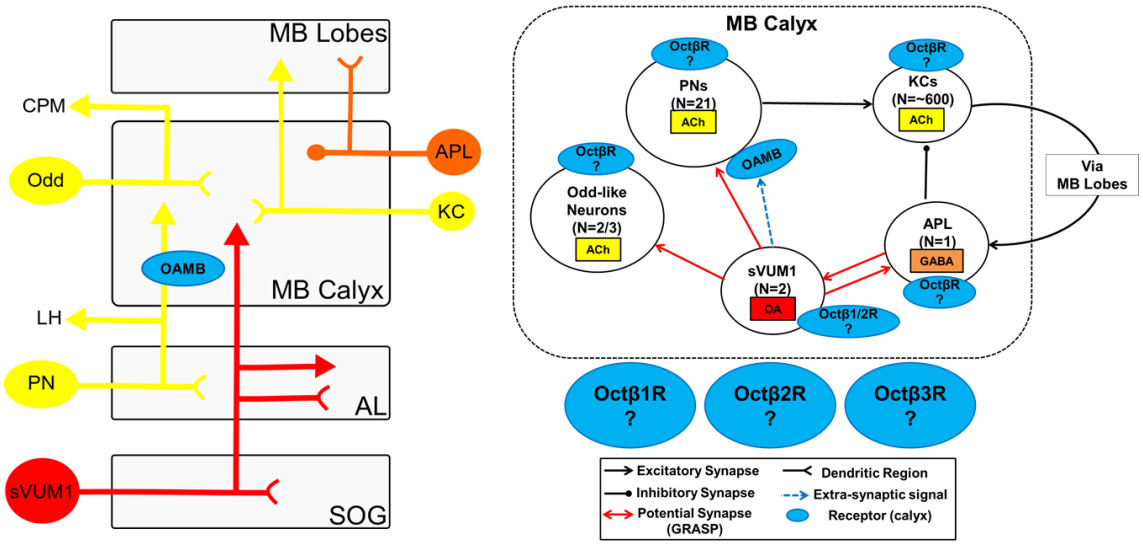

Figure 5.1. Hypothesised OctβR localisation pattern in larval MB calyx circuitry. Abbreviations: ACh, acetylcholine; AL, antennal lobe; CPM, centroposterior medial compartment; KC, Kenyon Cell; LH, lateral horn; MB, mushroom body; N, number; OA, octopamine; PN, projection neuron.

1) Are OctβRs expressed extrasynaptically in larval KC dendrites?

So far, there is no evidence that OA signalling from sVUM1 neurons in the larval calyx directly modulates KCs. KCs have very few synapses with sVUM1 neurons (Chapter 3; H.W., MPhil Thesis 2014), and KC dendrites did not express OAMB (Chapter 4). According to the literature, Octβ1R is expressed in adult KCs based on transcriptome analysis (Crocker et al., 2016), Octβ2R has

been identified in adult KCs both through transcriptome analysis and anti-Octβ2R immunostaining (Crocker et al., 2016; Wu et al., 2013), and *Octβ3R-GAL4* is strongly expressed in the larval MBs (El-Kholy et al., 2015). This suggests that larval KCs may express OA receptors, and thus facilitate extrasynaptic signalling from sVUM1 neurons in the calyx. Here I aimed to determine whether OctβRs are localised to larval KC dendrites.

2) Are OctβRs expressed in the putative postsynaptic partners of sVUM1 neurons?

While OAMB localised to PNs in the larval calyx, the other two putative postsynaptic partners of sVUM1 neurons identified by GRASP – the APL neuron and Odd-like neurons – did not express OAMB at their calyx terminals. In order to respond to OA signalling from sVUM1 neurons, they would need to express another type of OA receptor, which may be one of the OctβRs. In particular, Odd-like neurons may express Octβ2R, as two *Octβ2R-GAL4* lines generated from different promoter fragments of the *Octβ2R* gene both label Odd-like neurons (Chapter 8). Here I aimed to determine whether OctβRs localised to potential sVUM1 postsynaptic partners.

3) Are there Octβ1R- or Octβ2R-autoreceptors at the presynaptic terminals of sVUM1 neurons in the larval calyx?

Octβ1R and Octβ2R knockdown in Type II OA motorneurons using the *Tdc2-GAL4* line resulted in abnormal synaptic growth of OA terminals at the NMJ; suggesting that Octβ1R and Octβ2R might be acting as autoreceptors in OA neurons (Koon et al., 2011; Koon and Budnik, 2012). Using EGFP-tagged Octβ1R and Octβ2R, I aimed to determine whether Octβ1R and Octβ2R localised to the presynaptic terminals of sVUM1 neurons in the larval calyx, and consider the possibility of OA-OA communication or autoreceptor functions of Octβ1R and Octβ2R.

4) Are any of the OctβRs expressed in the same neurons as OAMB or each other?

As discussed above, Octβ1R and Octβ2R may colocalise in Type II OA motorneurons; especially since *octβ1R; octβ2R* double mutants have wild type levels of synaptic growth as opposed to the abnormal phenotypes observed in single mutants (Koon et al., 2011). This suggests that a single neuronal type may express more than one type of OA receptor. For example, PNs may express both OAMB and another OctβR. In this chapter, I aimed to investigate this possibility by examining OctβR localisation on calyx-innervating neurons.

5.2. Results

5.2.1. Octβ1R::EGFP localisation in the larval MB calyx circuitry

5.2.1.1. Selection and validation of an EGFP-tagged Octβ1R line

To visualise the endogenous expression pattern of Octβ1R in the larval MB calyx, I selected the *Octβ1R::EGFP* line (Fig. 5.2) from the MiMIC RMCE collection (Nagarkar-Jaiswal et al., 2015) generated from the *MI05807* MiMIC line (Fig. 5.3) by the Gene Disruption Project (Venken et al., 2011a).

MI05807 contained the MiMIC insertion within coding region intron 1 of the *Octβ1R* gene (Fig. 5.4). This corresponded to amino acid position 139 (Fig. 5.4B-C), and therefore the intracellular domain between TM I and II, in all of the Octβ1R protein isotypes (Fig. 5.5). This suggested that the Octβ1R::EGFP protein trap at this location should not disrupt TMs. PCR reactions conducted against the 5' and 3' flanking ends of the MI05807 insertion site (Fig. 5.6), and subsequent sequencing of these PCR products (Fig. S3, S4), confirmed the MI05807 insertion was in an *Octβ1R* coding region intron. I also confirmed using PCR that the EGFP cassette in the *Octβ1R::EGFP* stock was in the correct orientation for expression (Fig. 5.7).

The *Octβ1R::EGFP* stock was homozygous lethal (Fig. 5.2), suggesting that the Octβ1R::EGFP fusion produced was not a functional Octβ1R protein, and that functional Octβ1R proteins were essential for fly survival.

RMCE Line MI05807

Parental MI Line:

Insertion	Gene(s) Affected	Location	Position	Phase
MI05807	Octbeta1R [+]	3R:22511815 [+]	Octbeta1R-coding intron;	Octbeta1R-RA:2, Octbeta1R-RB:2, Octbeta1R-RC:2, Octbeta1R-RE:2

Gene Trap	Lethality
YES	viable

RMCE Line:

Insertion	Gene Target	Phase	Method	Tag
MI05807-GFSTF.2	Octbeta1R	2	injection	EGFP-FlAsH-StrepII-TEV-3xFLAG

Lethality	Fails to Complement
lethal	yes (stock used)

BDSC Stock No.
60236

Images (antibody staining)	
	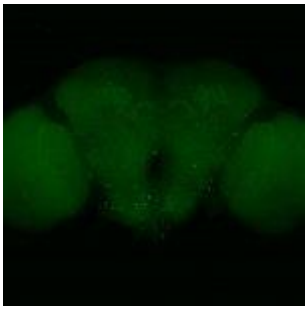

Figure 5.2. *Octβ1R::EGFP* recombinant stock listed on the Gene Disruption Project Database. (http://flypush.imgen.bcm.tmc.edu/pscreen/rmce/rmce.php?entry=RM00084).

Insertion MI05807

Gene Information

Affected Gene(s)
Octbeta1R

Position	Octbeta1R - coding intron
Phase	Octbeta1R-RA:2, Octbeta1R-RB:2, Octbeta1R-RC:2, Octbeta1R-RE:2

Release 6 Annotation

Scaffold	Coordinate	Strand	Site	GBrowse Link
3R	22511815	+	94B2	3R:22511815

FlyBase Annotation	Transposon
FBti0149079	Mi{MIC}

Stock Availability

Donor/Collection	Stockcenter Designation	Stock No.
GDP	Bloomington	42119

Flanking Sequence

MI05807-3' (JY137173)	TATAATCGGCTTTTGGGTAACGCCTCAATAACATTTTCGTGTTGCCTCTG ATGCGGGTGTTTTGCCTTTGTACTTTTTGGGCGCTTTAAGCTTGCTCCAA AAATGTAGACCTTTCGGGGCGTCAGTTTGTGGCCGTAATTAGGTTTGCGG GAGATGGTTTAATGTCCCAGTGAAATATGGCAAAATGGCGAGCGATTGTT AACGAGTTTAATAGATAAAGGTCGGATACACATAAAAAGAATATCCATGA TTGATGCAGTTTAAGAAGTTCCCATCCAAAGTTCCTTCATTCAAAAGTTT ATCTGGCACATTAATCCGTTTAGACGGAAAGCAAAACTTTCATTTGCGAT GTTGTGGTACGAAGAGTCAAGTTCCCGCAGATGTTATGGTTTTAAACATG AATTCCAACCGCCCATTCGGTTGCGGTTGTATCCGTGGAATGGCGTTATG TACGCCTGATTGTTTGGAAATCAGTGCGGACGGCCGATAAACGCATTTGC TGCTCCACATAGCGTATACGCCGCGTGCACCTAATTGACTTAACGTTTTG CGGTGCCACGCAACGTTGATGATC
MI05807-5' (JY137174)	GATCAAGTACGAGGAAGAGCCGGGAAAGTGTTTCCTCACTTTTCCTATTA ATTAGAGCTTTCCACGTTGGCTGCCTGCTGAAAGTGTCGACTCATAATTG TAATCAAACTTGACACCCAACAAGTTTCCTCCTTTCATTCCCGAGCACCC ACTATA

Figure 5.3. ***MI05807*** **insertion stock listed on the Gene Disruption Project Database**. (http://flypush.imgen.bcm.tmc.edu/pscreen/details.php?line=MI05807).

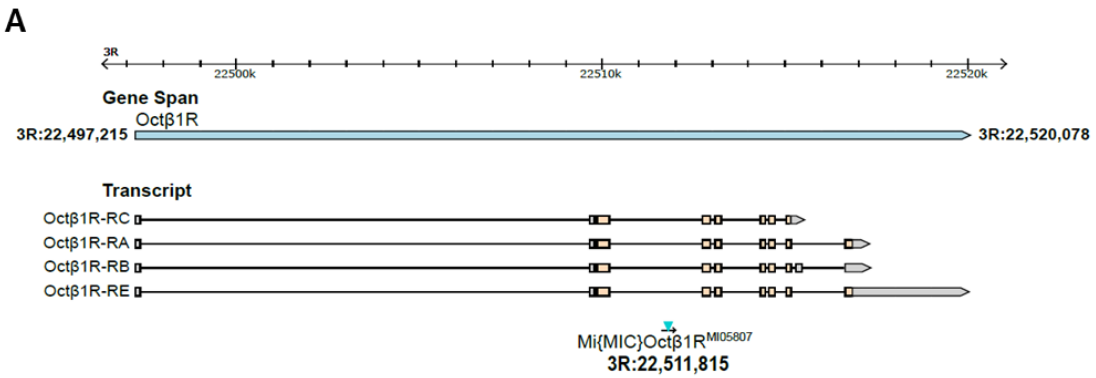

B. Octβ1R-PA tblastn alignment to *Drosophila* sequences

```
Exon 1
Query:   121     AILGNMLVIVSVMRHRKLR       139
                 AILGNMLVIVSVMRHRKLR
22510149         AILGNMLVIVSVMRHRKLR       22510205

Exon 2
Query:   139     RIITNYFVVSLAVADMLVALCAMTFNASVMISGKWMFGSVMCDMWNSFDVYFSTASIMHL        198
                  IITNYFVVSLAVADMLVALCAMTFNASVMISGKWMFGSVMCDMWNSFDVYFSTASIMHL
22512739         SIITNYFVVSLAVADMLVALCAMTFNASVMISGKWMFGSVMCDMWNSFDVYFSTASIMHL        22512918
```

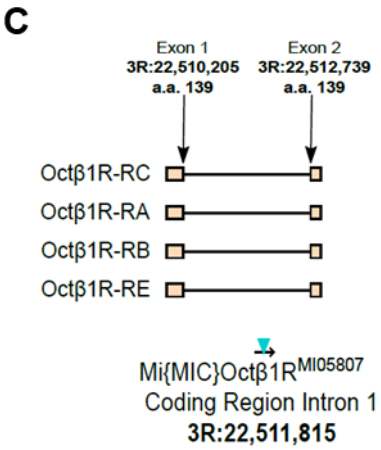

Figure 5.4. MI05807 insertion was in coding region intron 1 of the *Octβ1R* gene. (A) Map of MI05807 insertion site relative to *Octβ1R* gene and transcripts (Adapted from GBrowse). **(B)** Amino acid coordinates for the MI05807 insertion site based on tblastn alignment with *Octβ1R* transcripts. **(C)** Magnified map of MI05807 insertion in coding region intron 1 of *Octβ1R* transcripts with genomic and amino acid coordinates.

Octβ1R-PA TMHMM Predictions

WEBSEQUENCE	TMHMM2.0	outside	1	110
WEBSEQUENCE	TMHMM2.0	TMhelix	111	133
WEBSEQUENCE	TMHMM2.0	inside	134	144
WEBSEQUENCE	TMHMM2.0	TMhelix	145	167
WEBSEQUENCE	TMHMM2.0	outside	168	186
WEBSEQUENCE	TMHMM2.0	TMhelix	187	209
WEBSEQUENCE	TMHMM2.0	inside	210	228
WEBSEQUENCE	TMHMM2.0	TMhelix	229	251
WEBSEQUENCE	TMHMM2.0	outside	252	270
WEBSEQUENCE	TMHMM2.0	TMhelix	271	293
WEBSEQUENCE	TMHMM2.0	inside	294	350
WEBSEQUENCE	TMHMM2.0	TMhelix	351	373
WEBSEQUENCE	TMHMM2.0	outside	374	387
WEBSEQUENCE	TMHMM2.0	TMhelix	388	407
WEBSEQUENCE	TMHMM2.0	inside	408	508

MI05807 insertion site: a.a. 139

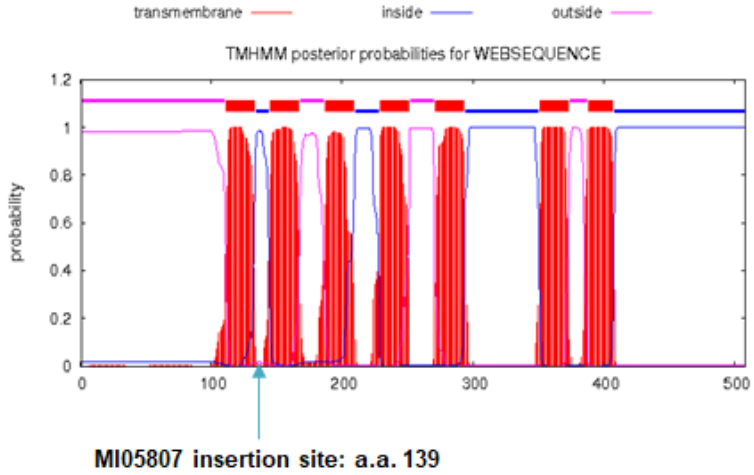

Figure 5.5. MI05807 insertion was between TM I and II of Octβ1R proteins. MI05807 insertion site relative to TM predictions (TMHMM) for the Octβ1R-PA isotype as a representative example.

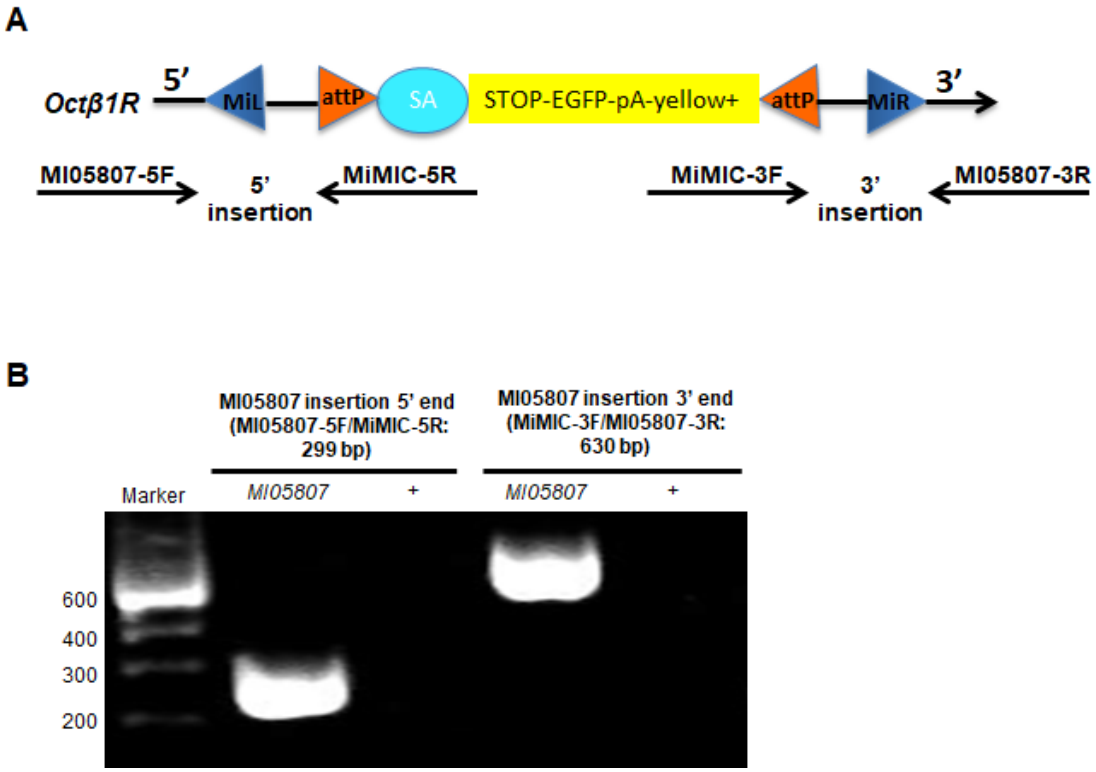

Figure 5.6. PCR verification of MI05807 insertion in the *Octβ1R* gene. (A) Primers designed against 5' and 3' insertion flanking ends for validating the MI05807 insertion in the *Octβ1R* gene. **(B)** PCR products were detected for 5' and 3' flanking ends with *MI05807* DNA but not with non-MiMIC control *S576-IT.GAL4* (denoted as +) DNA. Abbreviations: MiL/R, MiMIC insertion sequences Left/Right; SA, splice acceptor site; pA, polyA sequence; yellow+, yellow+ phenotype marker for MiMIC cassette.

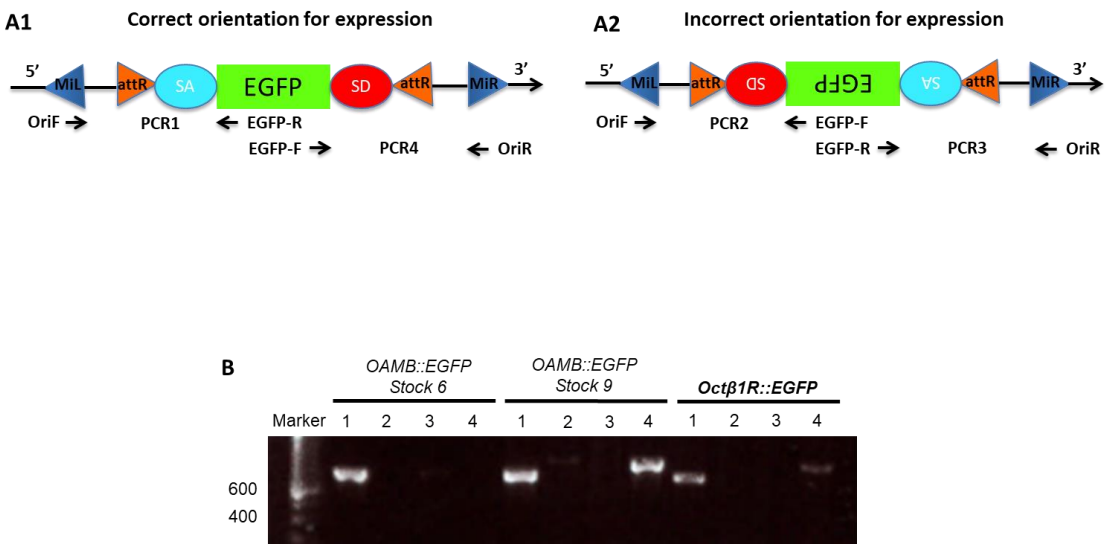

Figure 5.7. PCR validation of EGFP orientation in the *Octβ1R::EGFP* stock. (A1) Products for PCR1 and PCR4 indicated EGFP cassette in the correct orientation for expression. **(A2)** Products for PCR2 and PCR3 indicated EGFP cassette in the incorrect orientation for expression. **(B)** PCR results for PCR reactions 1-4 for *Octβ1R::EGFP*. It was loaded on the same gel as *OAMB::EGFP Stocks 6* and *9.* Abbreviations: MiL/R, MiMIC insertion sequences Left/Right; SA, splice acceptor site; SD, splice donor site; OriF, Orientation-MiL-F; OriR, Orientation-MiL-R; EGFP-F, EGFPdo-Seq-F; EGFP-R, EGFPdo-Seq-R.

5.2.1.2. Octβ1R::EGFP localisation in the larval MB calyx and dorsal cell bodies

Octβ1R::EGFP larvae showed a weak and diffuse smear throughout the calyx in both glomerular and inter-glomerular regions when compared to the *MI05807* parental line negative control (n=7; Fig. 5.8A-B). This pattern resembled that of KC dendrites which arborised randomly in the calyx. I also observed a localised signal at the ventral end of the calyx (Fig. 5.8C-D, arrowhead) stronger than that observed in the calyx, suggesting there was a higher density of Octβ1R proteins localised to this region. There were also more dorsal cell bodies that were less than 5 μm in diameter labelled in *Octβ1R::EGFP* larvae compared to the negative control (Fig. 5.8E-F); suggesting that Octβ1R::EGFP may localise to KC cell bodies.

As only weak Octβ1R::EGFP signals were observed using chicken anti-GFP (Ab13970), I tried to increase Octβ1R::EGFP signal by using an alternative anti-GFP antibody – a rabbit anti-GFP (A11122). Octβ1R::EGFP signals were stronger when visualised with rabbit anti-GFP, but showed a consistent pattern of localisation to the calyx, at the neuropil immediately ventral to the calyx and to small dorsal cell bodies (n=3; Fig. 5.9A-F), when compared to brains labelled with chicken anti-GFP (Fig. 5.8). Similar to chicken anti-GFP, rabbit anti-GFP also occasionally labelled few background cell bodies in the negative control (Fig. 5.8B,F; 5.9B,D,F).

The consistent observation of diffuse Octβ1R::EGFP signal in the calyx (Fig. 5.8A, 5.9A) in *Octβ1R::EGFP* brains labelled with either chicken or rabbit anti-GFP suggested Octβ1R may be expressed in KC dendrites in the calyx. This is further supported by the small (<5 μm in diameter) Octβ1R::EGFP-positive cell bodies observed dorsal to the calyx (Fig. 5.8E, 5.9E), which resemble KC cell bodies.

I also observed diffuse Octβ1R::EGFP signals in MB lobes (Fig. 5.9G-H; n=1 with rabbit anti-GFP; n=3 out of 6 with chicken anti-GFP). This suggested that Octβ1R might also localise to KC axons and/or MB extrinsic neurons innervating the MB lobes. This may be differentiated by determining whether the cell bodies of MB extrinsic neurons expressed Octβ1R::EGFP; and whether Octβ1R::EGFP signal can be knocked down when EGFP-RNAi is driven by a KC driver.

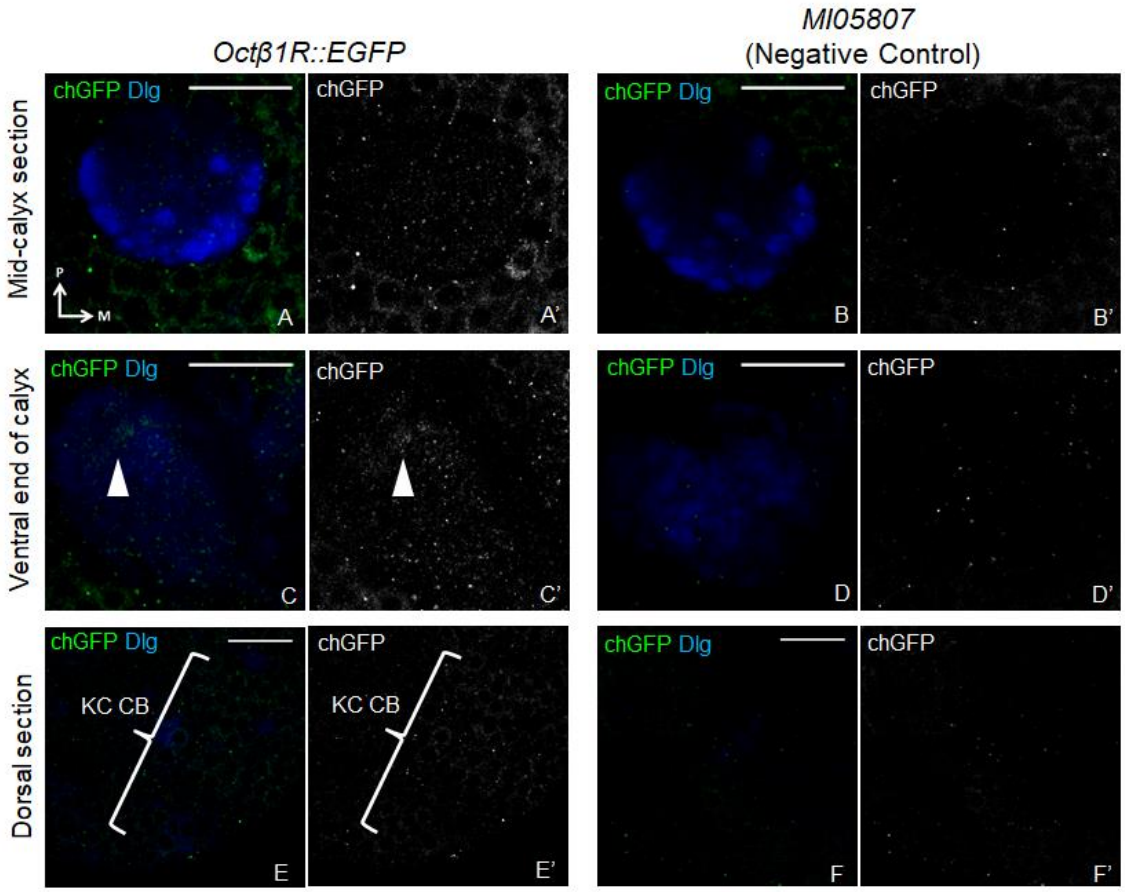

Figure 5.8. Octβ1R::EGFP localised diffusely to MB calyx and weakly to dorsal cell bodies in brains labelled with chicken anti-GFP. Single confocal optical sections of *Octβ1R::EGFP/TM6C,Sb Tb* **(A,C,E)** with *MI05807/TM3,Sb* parental line negative control **(B,D,F)**. Green is Octβ1R::EGFP visualized with chicken anti-GFP (chGFP, Ab13970) and blue is anti-Dlg. Localised signal at ventral end of calyx marked with arrowhead. Possible KC cell bodies (CB) are indicated. Medial (M) is right and posterior (P) is up. Scale bar: 20 μm.

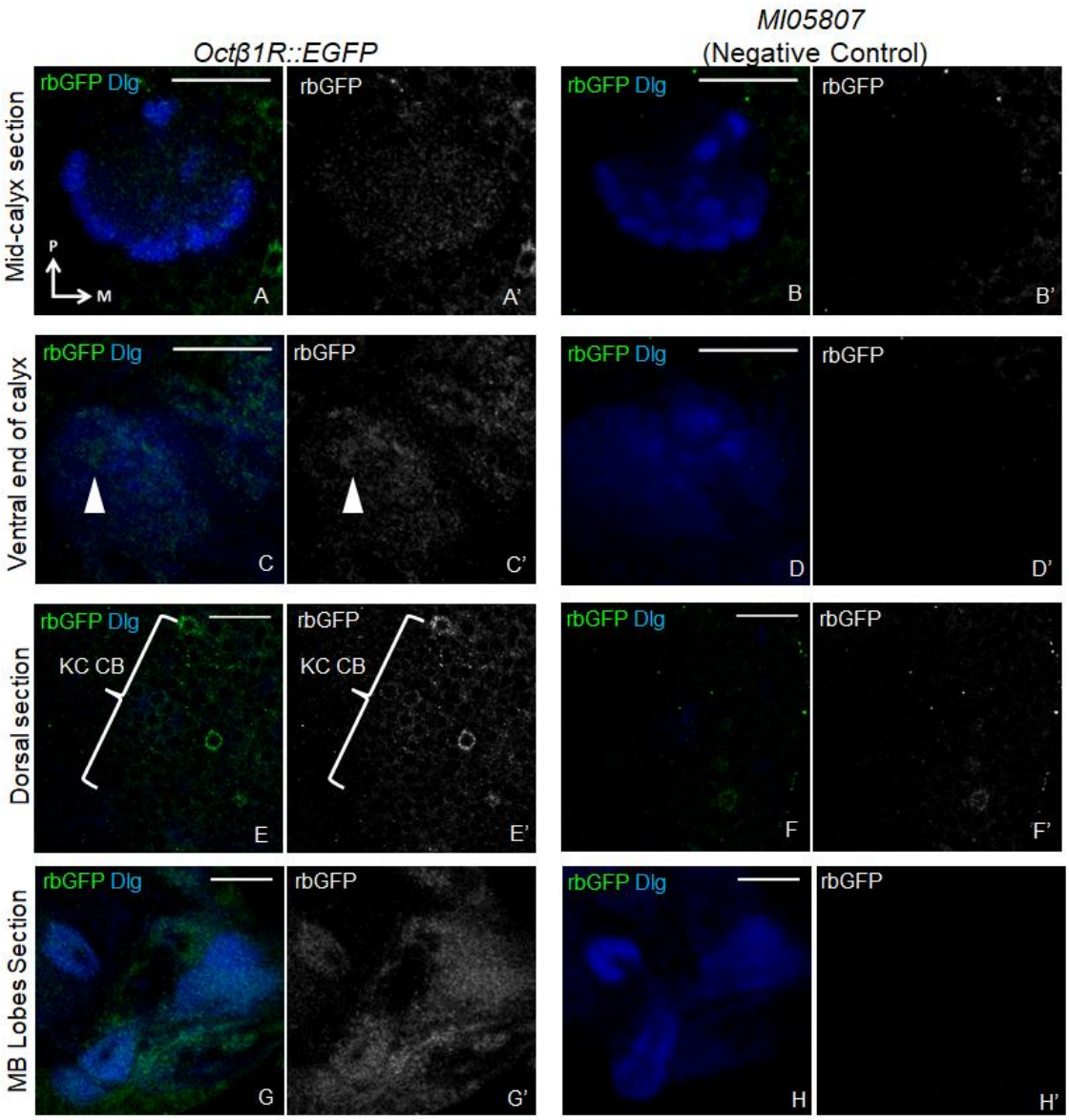

Figure 5.9. Octβ1R::EGFP localised diffusely in MB calyx and lobes and dorsal cell bodies in brains labelled with rabbit anti-GFP. Single confocal optical sections of *Octβ1R::EGFP/TM6C,Sb Tb* **(A,C,E,G)** with *MI05807/TM3,Sb* negative controls **(B,D,F,H)**. Green is Octβ1R::EGFP visualised with rabbit anti-GFP (rbGFP, A11122) and blue is anti-Dlg. Localised signal at ventral end of calyx marked with arrowhead. Possible KC cell bodies (CB) are indicated. Medial (M) is right and posterior (P) is up. Scale bar: 20 μm.

On the other hand, the diffuse pattern of Octβ1R::EGFP signal in the larval MB calyx suggested that Octβ1R was unlikely to be expressed in the calyx terminals of other calyx-innervating neurons. Octβ1R::EGFP did not show a distinctive glomerular pattern, which suggested that Octβ1R did not localise to PN presynaptic terminals in the calyx. As Octβ1R::EGFP did not localise to any interglomerular tracts in the calyx, Octβ1R was also unlikely to localise to APL neuron or Odd-like neuron terminals there. This also suggested that Octβ1R did not localise to the presynaptic terminals of sVUM1 neurons; and were therefore unlikely to act as autoreceptors in the calyx circuitry.

5.2.1.3. Octβ1R::EGFP localisation to AL and nearby cell bodies

To determine whether stronger Octβ1R::EGFP signal was observed elsewhere in the larval brain, I examined Octβ1R::EGFP localisation to the AL – where PNs and sVUM1 neurons also innervate.

I observed stronger Octβ1R::EGFP signal in cell bodies near the AL region as well as throughout the AL (Fig. 5.10), compared to the weak diffuse signal observed in the calyx (Fig. 5.8A, 5.9A). As Octβ1R::EGFP localised to all AL glomeruli (n=11; Fig. 5.10), this suggested that Octβ1R localised to the terminals of AL-innervating neurons which may include PN dendrites.

Some AL glomeruli showed stronger Octβ1R signal than others; for example, a medial AL glomerulus (Fig. 5.10B-E, arrowhead) showed a stronger signal than its neighbours. Based on the map of AL glomeruli, this AL glomerulus may be 35a, 42b, 67b or 74a (Masuda-Nakagawa et al., 2009). The cell bodies of PNs innervating three of these glomeruli (67b, 74a, 35a) are expected to be located more ventrally to the AL than most of the other PN cell bodies, including the PN innervating the 42b glomerulus (Berck et al., 2016). The 74a PN also innervates a ventral calyx glomerulus (Masuda-Nakagawa et al., 2010), which may match the stronger Octβ1R::EGFP signal observed at the ventral end of the calyx (Fig. 5.8C, 5.9C). The identity of this AL glomerulus needs to be verified with colocalisation with a specific PN marker.

I next examined Octβ1R::EGFP localisation to PN cell bodies labelled by *NP225-GAL4* (n=3; Fig. 5.11). Octβ1R::EGFP signal in cell bodies was weak (Fig. 5.11A-B), and background cell body labelling was occasionally observed

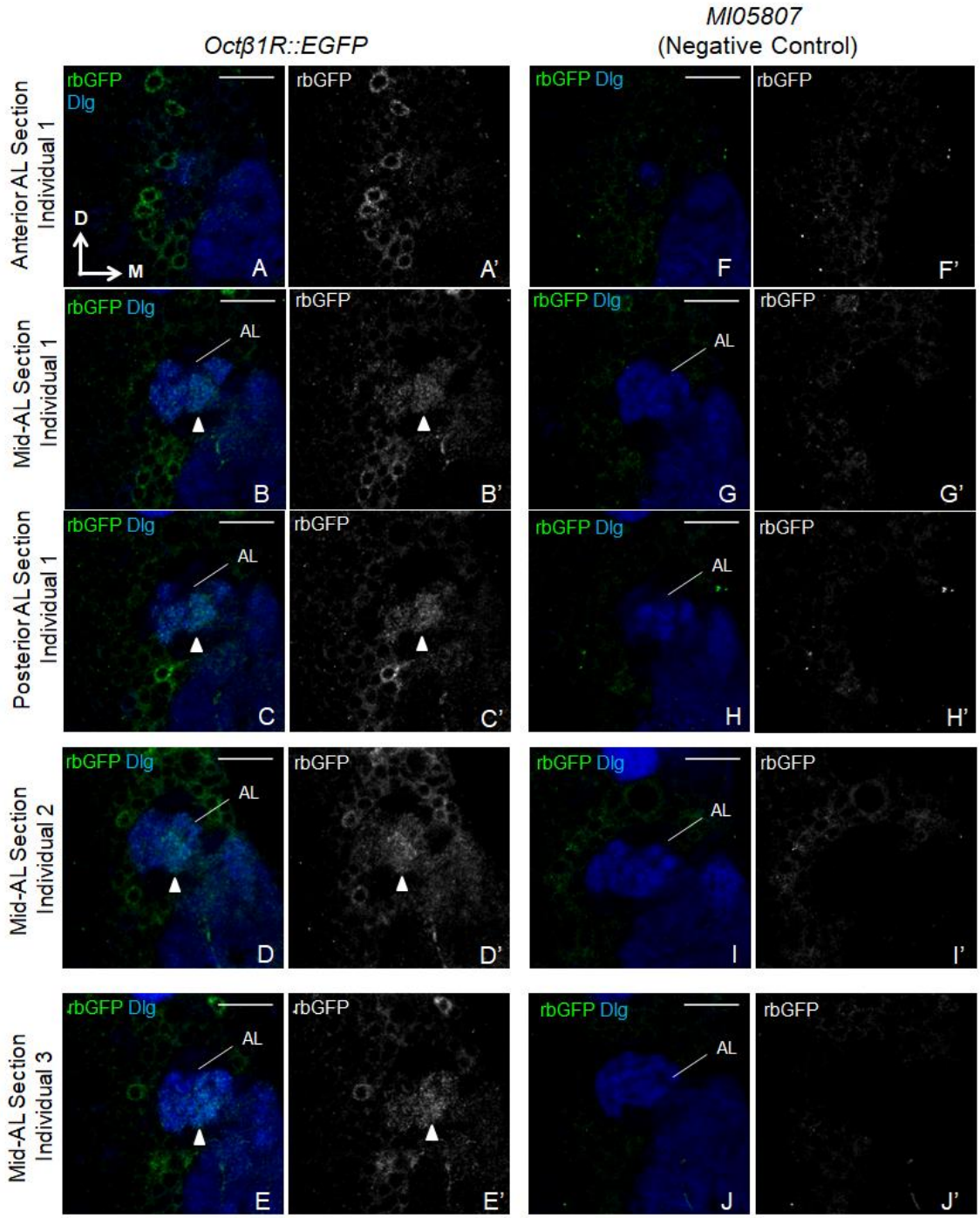

Figure 5.10. Octβ1R::EGFP localised to AL and nearby cell bodies. Single confocal optical sections of the AL from three *Octβ1R::EGFP/TM6C,Tb Sb* individuals **(A-E)**, with *MI05807/TM3,Sb* negative controls **(F-J)**. Green is Octβ1R::EGFP visualised with rabbit anti-GFP (rbGFP, A11122) and blue is anti-Dlg. Arrowhead indicates an AL glomerulus with stronger Octβ1R::EGFP signal. Medial (M) is right and dorsal (D) is up. Scale bar: 20 μm.

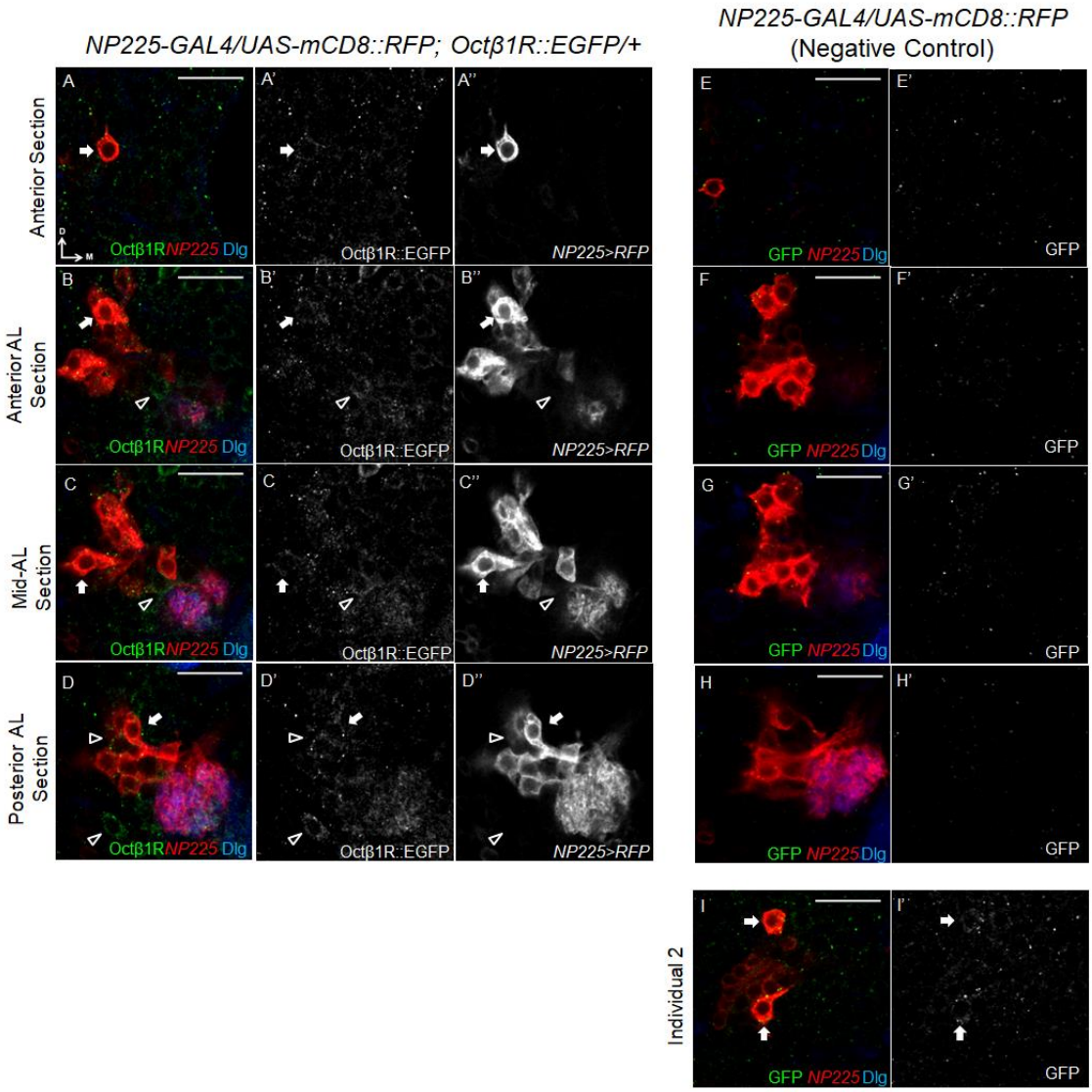

Figure 5.11. Octβ1R::EGFP colocalised with AL glomeruli and few cell bodies labelled by *NP225-GAL4*. Single confocal optical sections of the AL of *NP225-GAL4/UAS-mCD8::RFP; Octβ1R::EGFP/+* **(A-D)** and negative control *NP225-GAL4/UAS-mCD8::RFP; TM6B/MKRS* **(E-H)**. **(I)** is a second negative control individual. Green is Octβ1R::EGFP, red is *NP225>RFP* and blue is anti-Dlg. Arrows indicate Octβ1R-*NP225* colocalisation. Empty arrowheads indicate Octβ1R-positive cell bodies which did not express *NP225>RFP*. Medial (M) is right and dorsal (D) is up. Scale bar: 20 μm.

(Fig. 5.11I, arrows). Therefore, I first identified all the cell bodies that were Octβ1R::EGFP-positive relative to the background (Fig. 5.11A-D, arrows and empty arrowheads), and then determined whether they co-expressed *NP225>RFP* (Fig. 5.11A-D, arrows). I found that Octβ1R::EGFP and *NP225>RFP* colocalised in 5 ± 0.6 AL cell bodies (Fig. 5.11A-D; Table 5.1). However, the Octβ1R::EGFP signals observed in these cell bodies were very weak. As background GFP signals were observed in three cell bodies in one of the three negative controls (Fig. 5.11I, arrows; Table 5.1), it cannot be clearly concluded whether Octβ1R was expressed in PNs based on Octβ1R::EGFP localisation to PN cell bodies.

As each PN innervates one AL glomerulus (Masuda-Nakagawa et al., 2009), Octβ1R::EGFP signal should only be observed in around four AL glomeruli if Octβ1R only localised to PN dendrites in the AL. Instead, Octβ1R::EGFP localised to all AL glomeruli (Fig. 5.10) and many *NP225*-negative cell bodies nearby (Fig. 5.11A-D, empty arrowheads). This suggested that Octβ1R also localised to other neurons innervating AL glomeruli – potentially some of the GABAergic AL interneurons (Python and Stocker, 2002).

Octβ1R::EGFP signal colocalised with many GABA-positive cell bodies near the AL (n=2; Fig. 5.12, arrows) and with GABA immunoreactivity in the AL (Fig. 5.12). This suggested that Octβ1R localised to the terminals of GABAergic AL interneurons. Furthermore, this suggested that the medial AL glomeruli that showed stronger Octβ1R::EGFP signals (Fig. 5.10B-E, arrowhead) could be innervated by more than one-type of Octβ1R-expressing neurons.

5.2.2. Octβ2R::EGFP localisation in the larval MB calyx circuitry

5.2.2.1. Generation and validation of an EGFP-tagged Octβ2R line

To generate a novel *Octβ2R::EGFP* stock for visualising the endogenous expression pattern of Octβ2R in the larval MB calyx, I selected the *MI13416* line which contained the MiMIC insertion in a coding region intron of the *Octβ2R* gene (Venken et al., 2011a; Fig. 5.13, 5.14A). The MI13416 insertion site in coding region intron 1 of *Octβ2R* corresponded to amino acid position 185 (Fig. 5.14B-C) in all Octβ2R protein isotypes; and was predicted to be between TM I

Genotype	Individual	Octβ1R+/ NP225+	Control Genotype	Individual	Octβ1R+/ NP225+
NP225-GAL4/UAS-mCD8::RFP; Octβ1R::EGFP/+	Individual 1	4	*NP225-GAL4/UAS-mCD8::RFP*	Individual 1	0
	Individual 2	6		Individual 2	3
	Individual 3	5		Individual 3	0
Statistical Description	N	3	**Statistical Description**	N	3
	Mean	5		Mean	1
	S.D.	1.0		S.D.	1.7
	S.E.M.	0.6		S.E.M.	1.0

Table 5.1. Numbers of *NP225-GAL4* cell bodies positive for Octβ1R::EGFP. Abbreviations: Octβ1R +, Octβ1R::EGFP-positive; NP225+, *NP22>RFP*-positive; N, number; S.D., standard deviation; S.E.M., standard error of the mean.

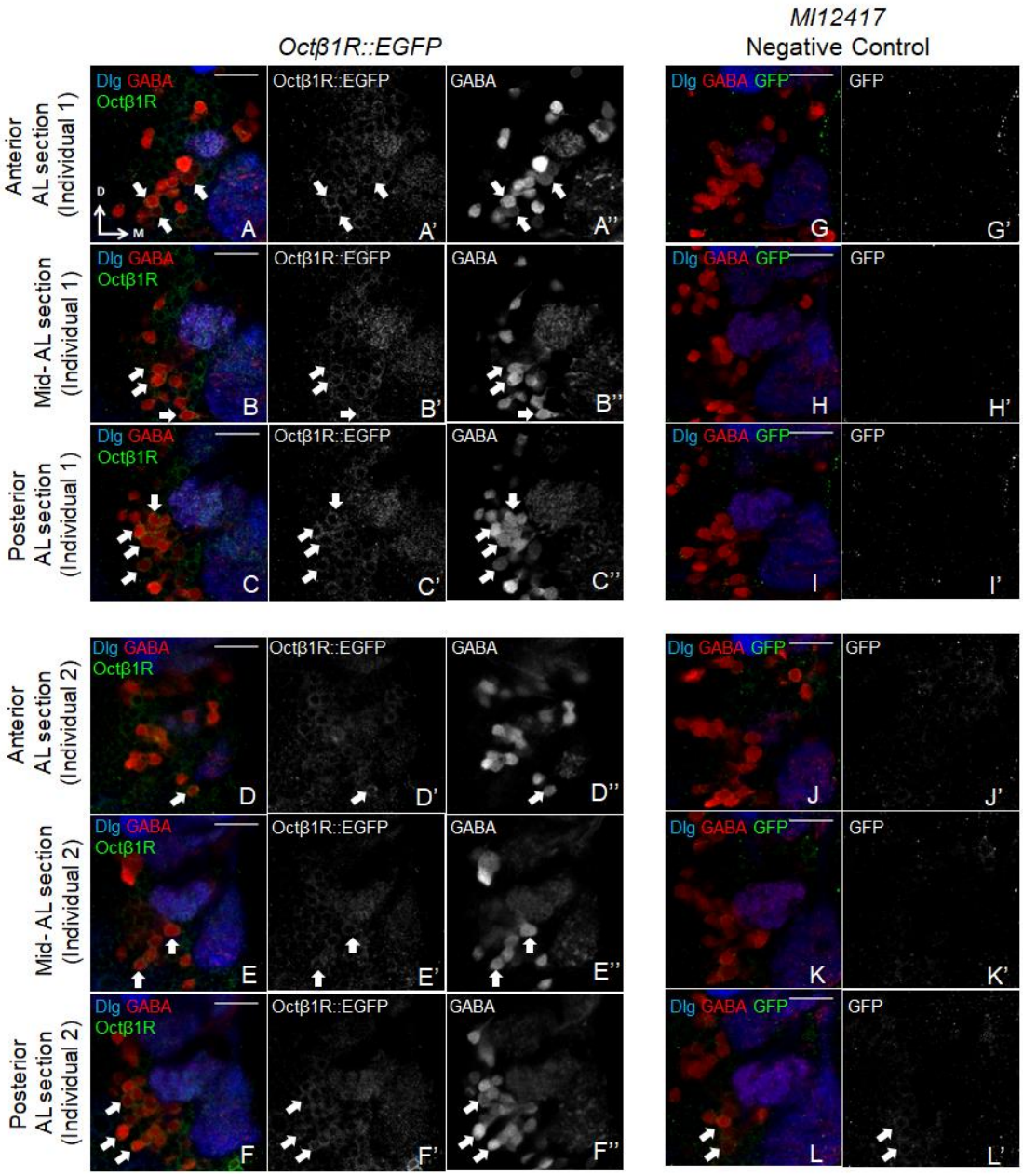

Figure 5.12. Octβ1R::EGFP colocalised with anti-GABA in AL and some nearby cell bodies. Single confocal optical sections of the AL from two *Octβ1R::EGFP/TM6C, Sb Tb* individuals **(A-F)** and negative control *MI12417* **(G-L)**. Green is Octβ1R::EGFP, red is anti-GABA and blue is anti-Dlg. Arrows indicate Octβ1R-GABA colocalisation. Medial (M) is right and dorsal (D) is up. Scale bar: 20 μm.

Insertion MI13416

Gene Information

Affected Gene(s)	Comments
Octbeta2R	Insertion is near the end of a copy of TE I-element that is within a coding intron of Octbeta2R gene. Mapped by unique segment of 3' flank

Position	Octbeta2R - coding intron
Phase	Octbeta2R-RA:2, Octbeta2R-RC:2, Octbeta2R-RD:2, Octbeta2R-RE:2, Octbeta2R-RF:2

Release 6 Annotation

Scaffold	Coordinate	Strand	Site	GBrowse Link
3R	12557762	-	87C1	3R:12557762

FlyBase Annotation	Transposon
FBti0166343	Mi{MIC}

Stock Availability

Donor/Collection	Stockcenter Designation	Stock No.
GDP	Bloomington	59133

Flanking Sequence

MI13416-3' (KO453971)	TATCTATCATAATAAATAAATAAATAAATATGTATATTTAGCAAGGGATA TACAAAAAATATTTTTCATTTATAAAGTTAACTTGAATGAAATTATTCGG TCGGTATATTACCATAATCGAGCAAAAGTTTTCGAGAGCAGTAAATGCTC AATTTTGATTGCAAACTTTTCCCATTTGGCTTAGTCAAAATGGTGAATGA AAGGCGGCCACCTGGAGTTCAATGAGGCAGCTGCACTCATCCGATTTGAA AGTCCTCGGCCAGCAACTGGTGCAAAATTCTAATTGGCACTCGGCTTGGA ATTCAATTTAAATAACAAAATAGCCATGAAGTGGTATAGGTTTGCCCAGA CGAGTGCGGTTGACCTAAGCATTTTCCTCCGCCCACTTGTTTCCCGTATA TATCAGATTTTCGTTCTGGCATCGGCTTAGCCCCCCTTGGGGTCGAAATC GTTCGACATCGTTCTCGATTCTTGACTGGCTTTTCAATTATACCCCCCGC TGGCAGCAGAATGCAATGGAGTCCAAACTGTCAACTCATACAAAAGAGTG GACCCCCACCATTCAACATCCCCGTCACGCATTCACTCATATGATATATC CTGATTAGCCCCCACGGGGTGCACGAAGGACCCCTCTCGCTTCGTGTGCT ATATGTATTGTTGGATATTGTCCTGTGATTGCTAACATCTCGTTCTCTTC TTCTCTTTGCAGAGTTATAACGAATTACTTTGTAGTTTCCTTAGCCATGG CTG

Figure 5.13. ***MI13416*** **insertion stock listed on the Gene Disruption Project Database**. (http://flypush.imgen.bcm.tmc.edu/pscreen/details.php?line=MI13416).

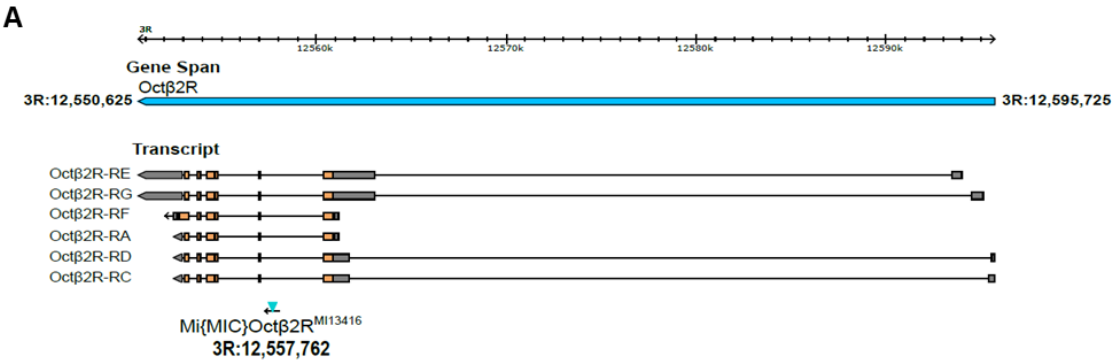

B. Octβ2R-PA tblastn alignment to *Drosophila* sequences

```
Exon 1
Query:   181   VRKLRVITNYFVVSLAMADIMVAI      204
               VRKLR +   F + L +     AI
12560414       VRKLRCVYVIFQLLLLLISCEKAI      12560343

Exon 2
Query:   185   RVITNYFVVSLAMADIMVAIMAMTFNFSVQVTGR   218
               RVITNYFVVSLAMADIMVAIMAMTFNFSVQVTGR
12557077       RVITNYFVVSLAMADIMVAIMAMTFNFSVQVTGR   12556976
```

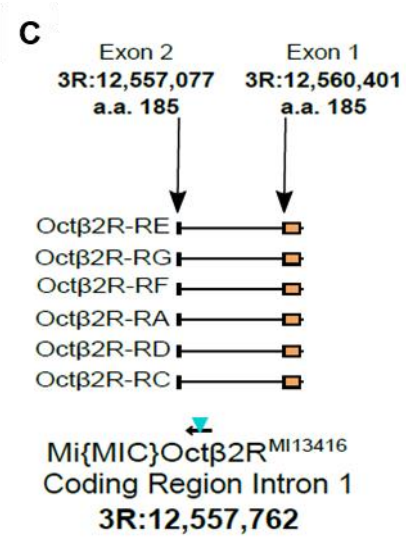

Figure 5.14. MI13416 insertion was in coding region intron 1 of the *Octβ2R* gene. (A) Map of MI13416 insertion site relative to *Octβ2R* gene and transcripts (Adapted from GBrowse). **(B)** Amino acid coordinates for the MI13416 insertion site based on tblastn alignment with *Octβ2R* transcripts. **(C)** Magnified map of MI13416 insertion in coding region intron 1 of *Octβ2R* transcripts with genomic and amino acid coordinates.

and II in all Octβ2R protein variants – one amino acid away from the TM II (Fig. 5.15). The proximity of the MI13416 insertion to a TM might potentially disrupt TM insertion and prevent the targeting of Octβ2R to membrane terminals.

I conducted PCR reactions to verify the MI13416 insertion site using primers against the 3' and 5' flanking ends of the insertion site (Fig. 5.16A). PCR products were obtained for the 3' flanking end, but not for the 5' end (Fig. 5.16B). To resolve this, I attempted to repeat the 5' flanking end PCR reactions with five different MI13416-5F primers. However, none of the MI13416-5F primers produced any PCR products with MiMIC-5R, which produced a robust product for the positive control using another MiMIC stock (Fig. 5.16C). This suggested that there was difficulty in designing suitable primers against genomic sequences at the 5' MI13416 insertion end.

Nevertheless, the sequenced PCR product for the 3' MI13416 insertion end aligned to both MiMIC sequences and *Octβ2R* sequences (Fig. S5). This confirmed that the MI13416 insertion was in a coding region intron of the *Octβ2R* gene. I observed an extra unidentified 26 bp sequence between the MiMIC and genomic sequences (Fig. S5A, green) which was also listed in the Gene Disruption Project website (Fig. 5.13).

Seventeen *Octβ2R::EGFP* recombinants stocks were recovered from introducing the EGFP cassette to the *MI13416* line. Only *Octβ2R::EGFP Stock 14* from the fourteen recombinant stocks validated showed robust bands for PCR1 and PCR4 reactions, but not for PCR2 and PCR3 reactions. This suggested *Stock 14* contained the EGFP reporter in the correct orientation for expression (Fig. 5.17; Table 5.2). Consistent with expectation, Octβ2R::EGFP signal was observed in the recombinant *Stock 14* but not in the negative control (Fig. 5.18). *Octβ2R::EGFP Stock 14* was henceforth designated as *Octβ2R::EGFP*.

5.2.2.2. Octβ2R::EGFP localised to cell bodies but not to larval MB calyx or other neuropils

In the *Octβ2R::EGFP* stock, Octβ2R::EGFP signal was detected in cell bodies around the larval MB calyx (Fig. 5.18, arrowheads), but not in the calyx itself

Octβ2R-PA TMHMM Predictions

WEBSEQUENCE	TMHMM2.0	outside	1	156
WEBSEQUENCE	TMHMM2.0	TMhelix	157	179
WEBSEQUENCE	TMHMM2.0	inside	180	185
WEBSEQUENCE	TMHMM2.0	TMhelix	186	208
WEBSEQUENCE	TMHMM2.0	outside	209	233
WEBSEQUENCE	TMHMM2.0	TMhelix	234	256
WEBSEQUENCE	TMHMM2.0	inside	257	268
WEBSEQUENCE	TMHMM2.0	TMhelix	269	291
WEBSEQUENCE	TMHMM2.0	outside	292	319
WEBSEQUENCE	TMHMM2.0	TMhelix	320	342
WEBSEQUENCE	TMHMM2.0	inside	343	408
WEBSEQUENCE	TMHMM2.0	TMhelix	409	431
WEBSEQUENCE	TMHMM2.0	outside	432	445
WEBSEQUENCE	TMHMM2.0	TMhelix	446	468
WEBSEQUENCE	TMHMM2.0	inside	469	536

MI13416 insertion site: a.a. 185

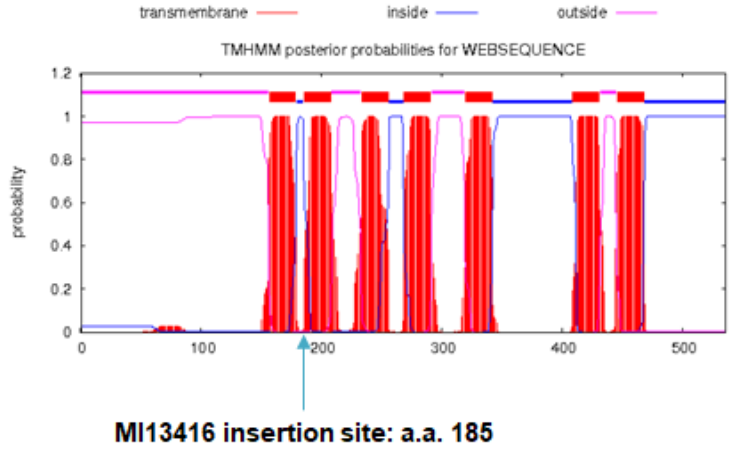

Figure 5.15. MI13416 insertion was between TM I and II of Octβ2R proteins. MI13416 insertion site relative to TM predictions (TMHMM) for the Octβ2R-PA isotype as a representative example.

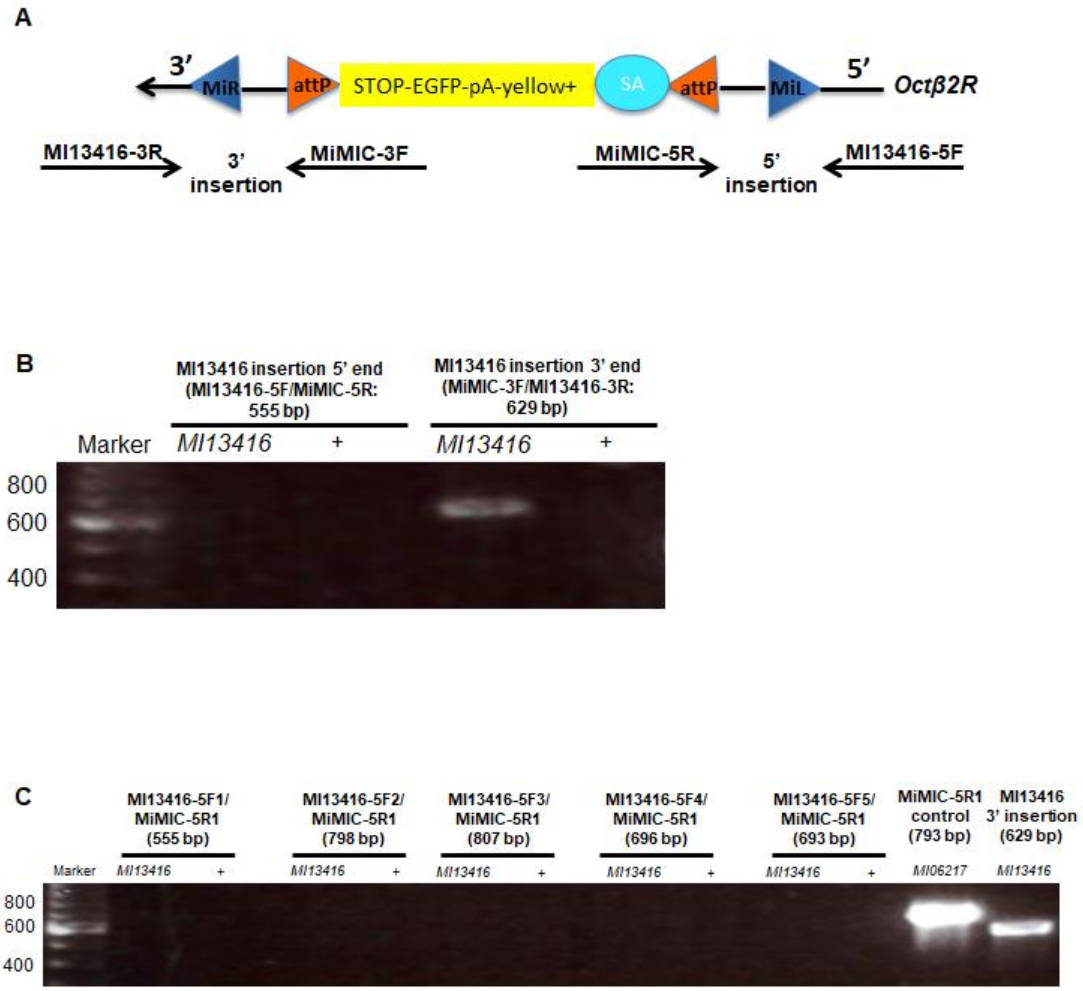

Figure 5.16. PCR verification of MI13416 insertion in the *Octβ2R* gene. (A) Primers designed against 5' and 3' insertion flanking ends for validating the MI13416 insertion in the *Octβ2R* gene. **(B)** PCR product detected for MI13416 3' but not 5' insertion end with *MI13416* DNA. No products were detected using non-MiMIC control *S576-IT.GAL4* (denoted as +) DNA. **(C)** No PCR products detected for MI13416 5' MiMIC insertion end using different MI13416-5F primers with MiMIC-5R1. Negative control: *CS* (denoted as +). MiMIC-5R1 positive control: MI06217 5' insertion end using *MI06217* DNA. *MI13416* DNA positive control: MI13416 3' insertion end. Abbreviations as Fig. 5.6.

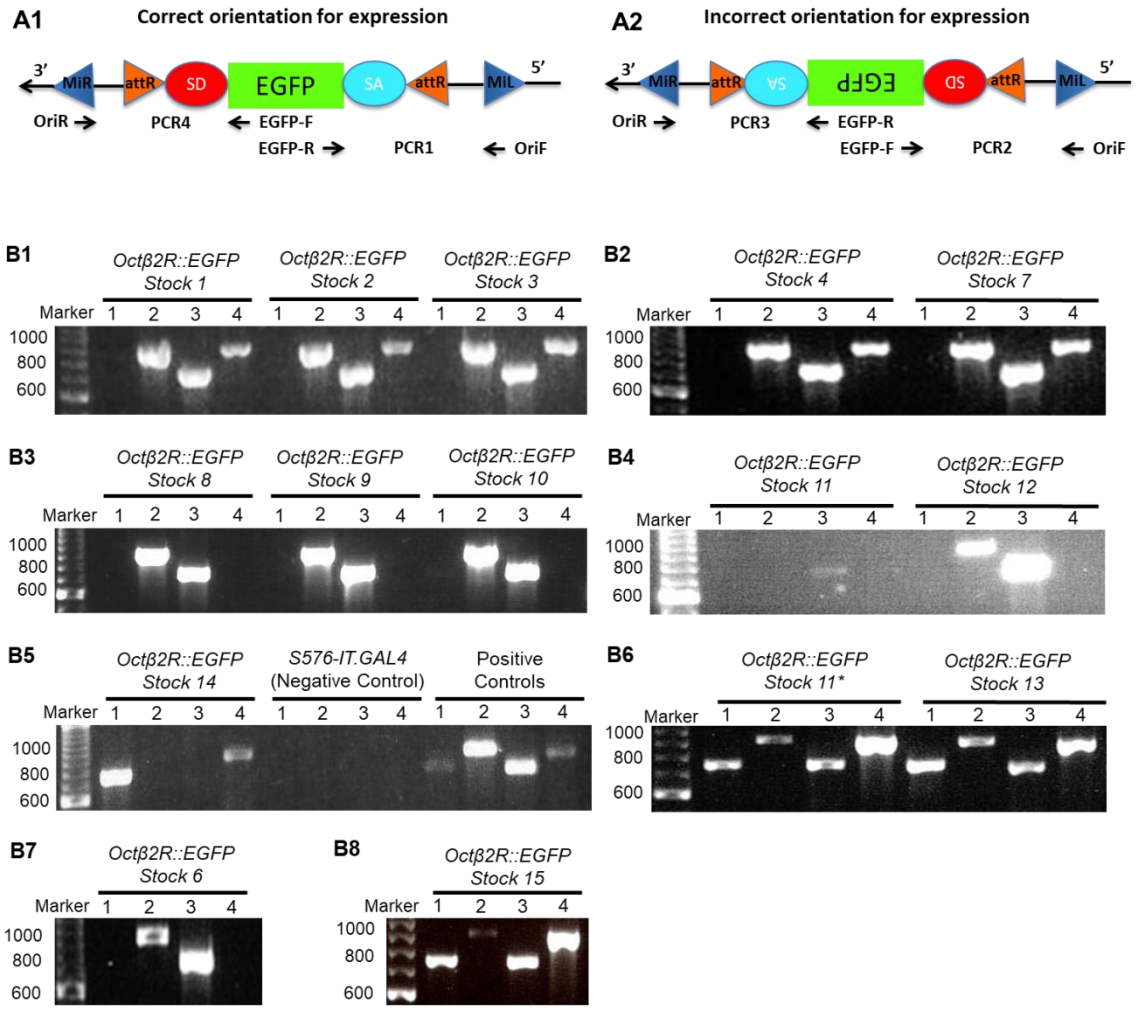

Figure 5.17. PCR validation of EGFP orientation in recombinant *Octβ2R::EGFP* stocks. (A1) Products for PCR1 and PCR4 indicated EGFP cassette in the correct orientation for expression. **(A2)** Products for PCR2 and PCR3 indicated EGFP cassette in the incorrect orientation for expression. **(B)** PCR results for PCR reactions 1-4 for *Octβ2R::EGFP Stocks 1, 2, 3* **(B1)**; *Stocks 4, 7* **(B2)**; *Stocks 8, 9, 10* **(B3)**; *Stocks 11, 12* **(B4)**; *Stock 14* **(B5)**; *Stocks 11(*repeated), 13* **(B6)**; *Stock 6* **(B7)**; and *Stock 15* **(B8)**. Abbreviations as Fig. 5.7.

Stock	PCR1	PCR2	PCR3	PCR4	Figure	Expected expression
Octβ2R::EGFP Stock 1	-	++	++	+	5.17B1	No
Octβ2R::EGFP Stock 2	-	++	++	+	5.17B1	No
Octβ2R::EGFP Stock 3	-	++	++	+	5.17B1	No
Octβ2R::EGFP Stock 4	-	++	++	+	5.17B2	No
Octβ2R::EGFP Stock 6	-	+	++	-	5.17B7	No
Octβ2R::EGFP Stock 7	-	++	++	+	5.17B2	No
Octβ2R::EGFP Stock 8	-	++	++	-	5.17B3	No
Octβ2R::EGFP Stock 9	-	++	++	-	5.17B3	No
Octβ2R::EGFP Stock 10	-	++	++	-	5.17B3	No
Octβ2R::EGFP Stock 11	+	+	+	++	5.17B4, 6	Maybe
Octβ2R::EGFP Stock 12	-	++	++	-	5.17B4	No
Octβ2R::EGFP Stock 13	+	+	+	++	5.17B6	Maybe
Octβ2R::EGFP Stock 14	**++**	**-**	**-**	**+**	**5.17B5**	**Yes**
Octβ2R::EGFP Stock 15	+	+	+	++	5.17B8	Maybe

Table 5.2. One out of fourteen recombinant *Octβ2R::EGFP* stocks contained EGFP in the correct orientation for expression. PCR products obtained for each of the PCR reactions (PCR1, PCR2, PCR3 and PCR4) were scored as follows: -, no bands observed; +, weak band observed; ++, strong band observed. PCR results were used to determine whether Octβ2R::EGFP expression was expected (Expected Expression).

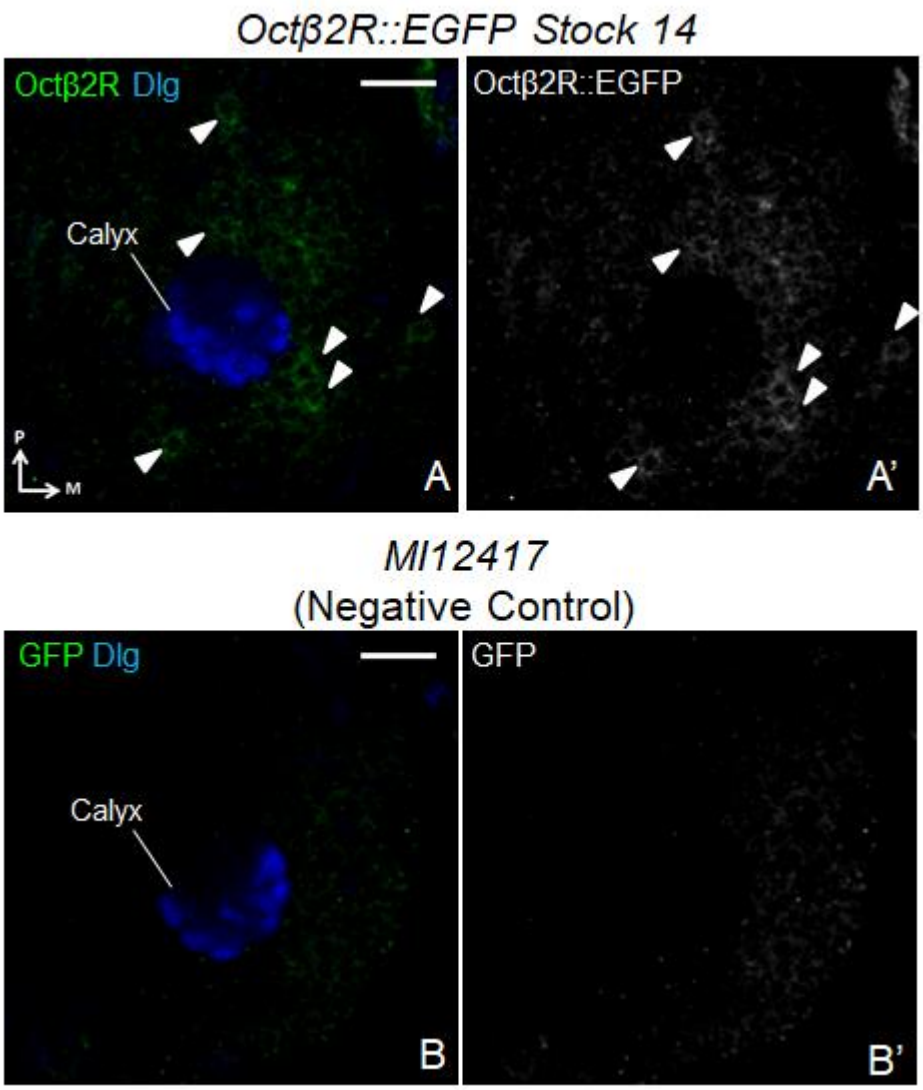

Figure 5.18. Octβ2R::EGFP signal in cell bodies in *Octβ2R::EGFP Stock 14*. Confocal optical sections of the dorsal brain of *Octβ2R::EGFP Stock 14* **(A)** with *MI12417* negative control **(B)**. Green is Octβ2R::EGFP and blue is anti-Dlg. Arrowheads indicate Octβ2R::EGFP-positive cell bodies. Medial (M) is right and posterior (P) is up. Scale bar: 20 μm.

(Fig. 5.18, 5.19). Octβ2R::EGFP signal was also absent in other major neuropils, including the MB lobes (Fig. 5.20A-B), AL (Fig. 5.20C-D) and SOG region (Fig. 5.20E-F); but present in cell bodies around these neuropils (Fig. 5.20). Furthermore, there were no neuronal tracts or processes positive for Octβ2R::EGFP (Fig. 5.18, 5.19, 5.20). This suggested that Octβ2R::EGFP was expressed in cell bodies, but not targeted to neuronal terminals. This might be because the close proximity of the MI13416 insertion to TM II disrupted TM insertion and subsequent targeting to the plasma membrane.

Therefore, the *Octβ2R::EGFP* line could be used to identify calyx-innervating neurons that expressed Octβ2R, but not the subcellular localisation of Octβ2R in those neurons. This could be achieved by determining whether *Octβ2R::EGFP*-positive cell bodies matched the approximate size and location of the cell bodies of calyx-innervating neurons; and subsequently through colocalisation with molecular markers that label these neurons.

5.2.2.3. Possible Octβ2R::EGFP localisation to KC and PN cell bodies

Few Octβ2R::EGFP-positive cell bodies around 3-5 μm in diameter were observed dorsal to the calyx (n=6; Fig. 5.21, filled arrowheads). The size and location of these cell bodies suggested that Octβ2R may be expressed in KC cell bodies. However, there were relatively few Octβ2R::EGFP-positive cell bodies smaller than 5 μm in diameter (around five in each of the confocal optical slices presented in Fig. 5.21) compared to hundreds of KC cell bodies expected in that region (Fig. 4.16A). This suggested that Octβ2R was either selectively expressed in a small number of KC cell bodies, or expressed in non-KC cell bodies of a similar size also located dorsal to the calyx.

To determine whether Octβ2R was expressed in PNs, I examined Octβ2R::EGFP colocalisation with *NP225-GAL4*-positive cell bodies near the AL (n=7; Fig. 5.22). 12 ± 1.1 cell bodies near the AL co-expressed Octβ2R::EGFP and *NP225>RFP* (Fig. 5.22A-D, arrows; Table 5.3), compared to 2 ± 1.0 *NP225>RFP*-positive cell bodies that showed background GFP signal in the negative control (Fig. 5.22E-H; Table 5.3). As *NP225-GAL4* labels the majority of a total of 21 PNs (Masuda-Nakagawa et al., 2005), this suggested that Octβ2R was expressed in around half of the PN cell bodies.

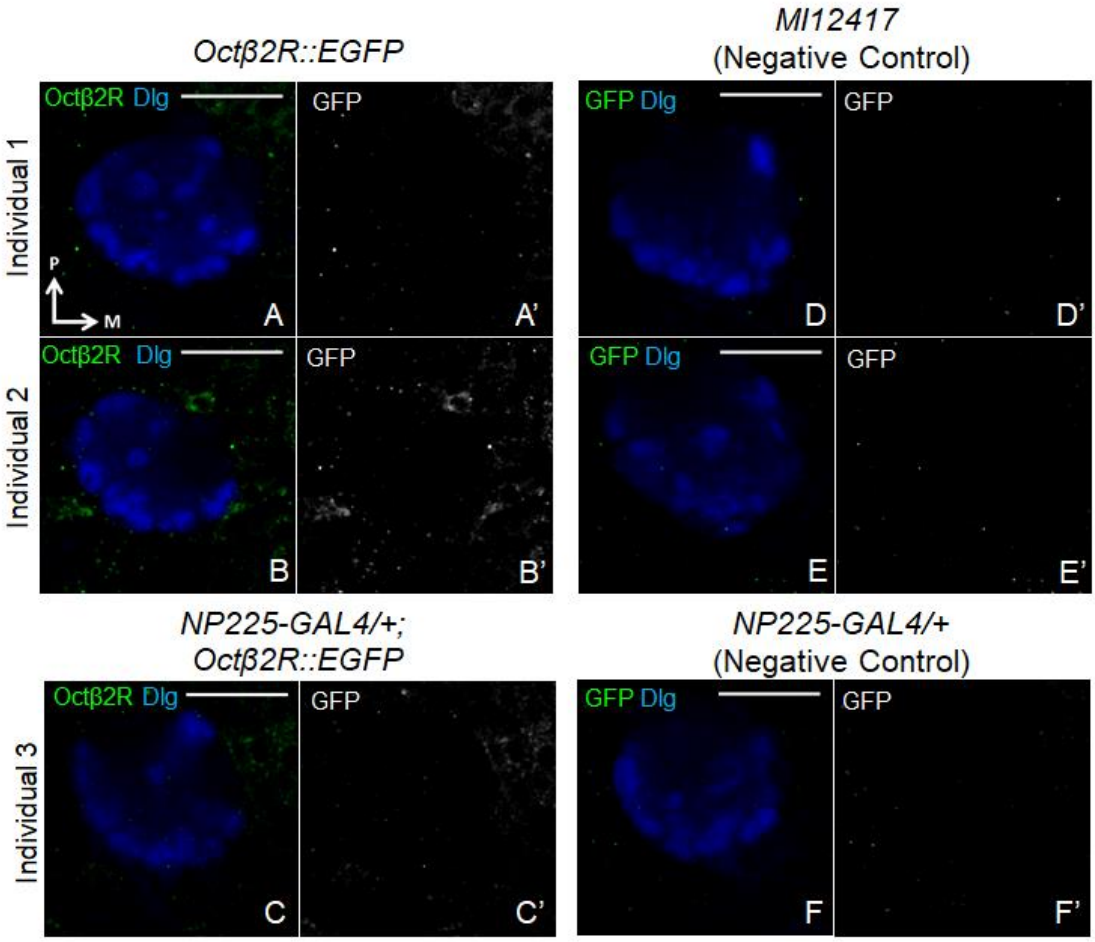

Figure 5.19. Octβ2R::EGFP signal was not observed in MB calyx. Single confocal optical sections of the calyx from three *Octβ2R::EGFP* individuals **(A-C)** with corresponding negative controls **(D-F)**. Green is Octβ2R::EGFP and blue is anti-Dlg. Medial (M) is right and posterior (P) is up. Scale bar: 20 μm.

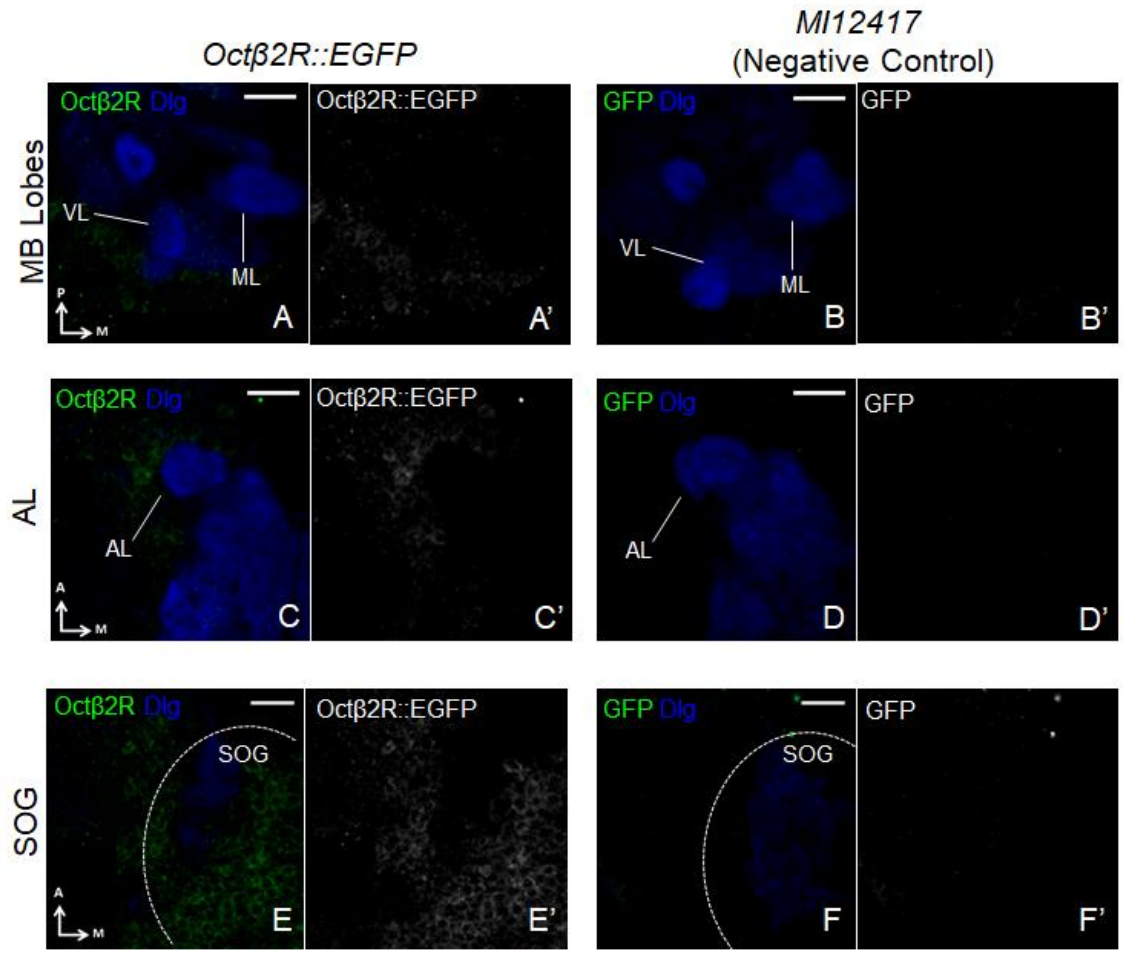

Figure 5.20. Octβ2R::EGFP signal localised to cell bodies but not major neuropils in the larval brain. Single confocal optical sections of the larval brain of *Octβ2R::EGFP* **(A,C,E)** with corresponding *MI12417* negative controls **(B,D,F)**. Green is Octβ2R::EGFP and blue is anti-Dlg. SOG is within the dotted area. Medial (M) is right. Posterior (P) is up for **(A-B)**; anterior (A) is up for **(C-F)**. Abbreviations: ML, medial lobe; VL, vertical lobe. Scale bar: 20 μm.

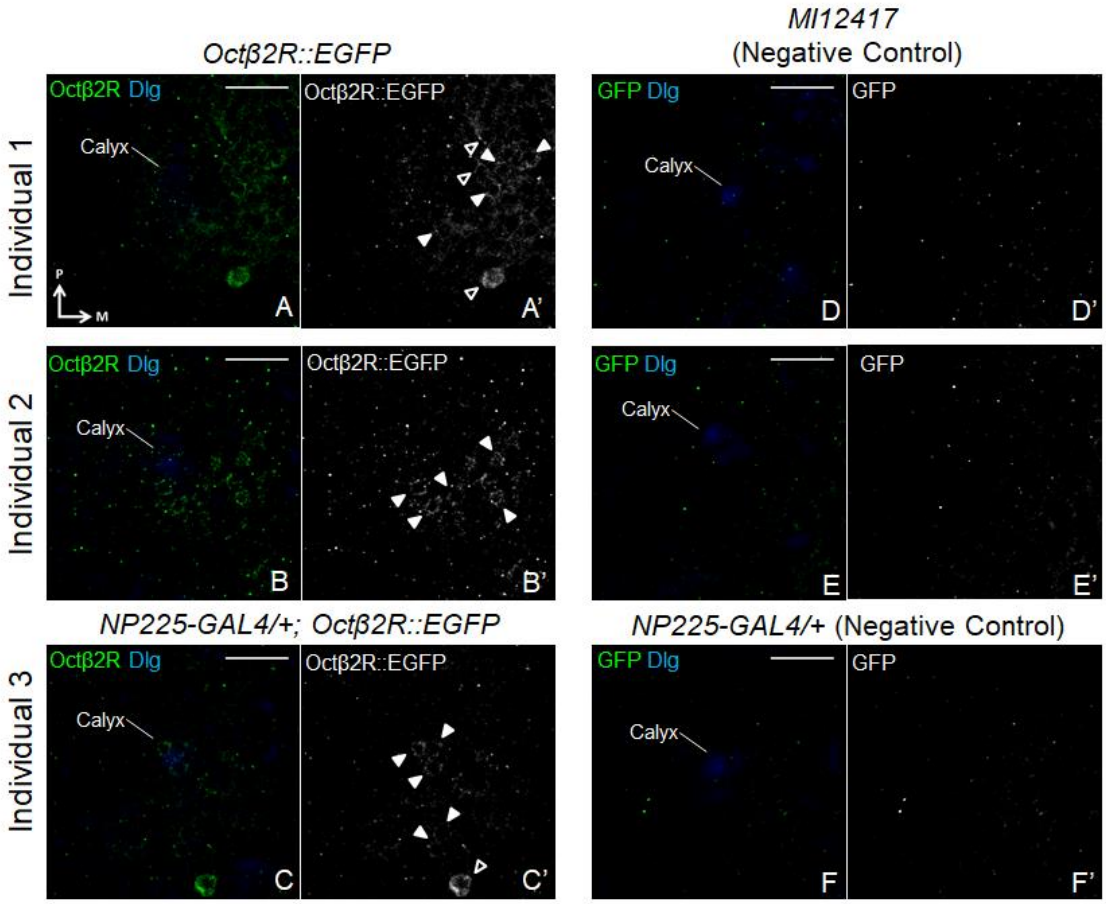

Figure 5.21. Octβ2R::EGFP localised to dorsal cell bodies. Single confocal optical sections taken immediately dorsal to the calyx from three *Octβ2R::EGFP* individuals **(A-C)** with corresponding negative controls **(D-F)**. Green is Octβ2R::EGFP and blue is anti-Dlg. Filled arrowheads indicate cell bodies <5 μm in diameter (around the size of KCs). Empty arrowheads indicate cell bodies >5 μm in diameter (larger than KCs). Medial (M) is right and posterior (P) is up. Scale bar: 20 μm.

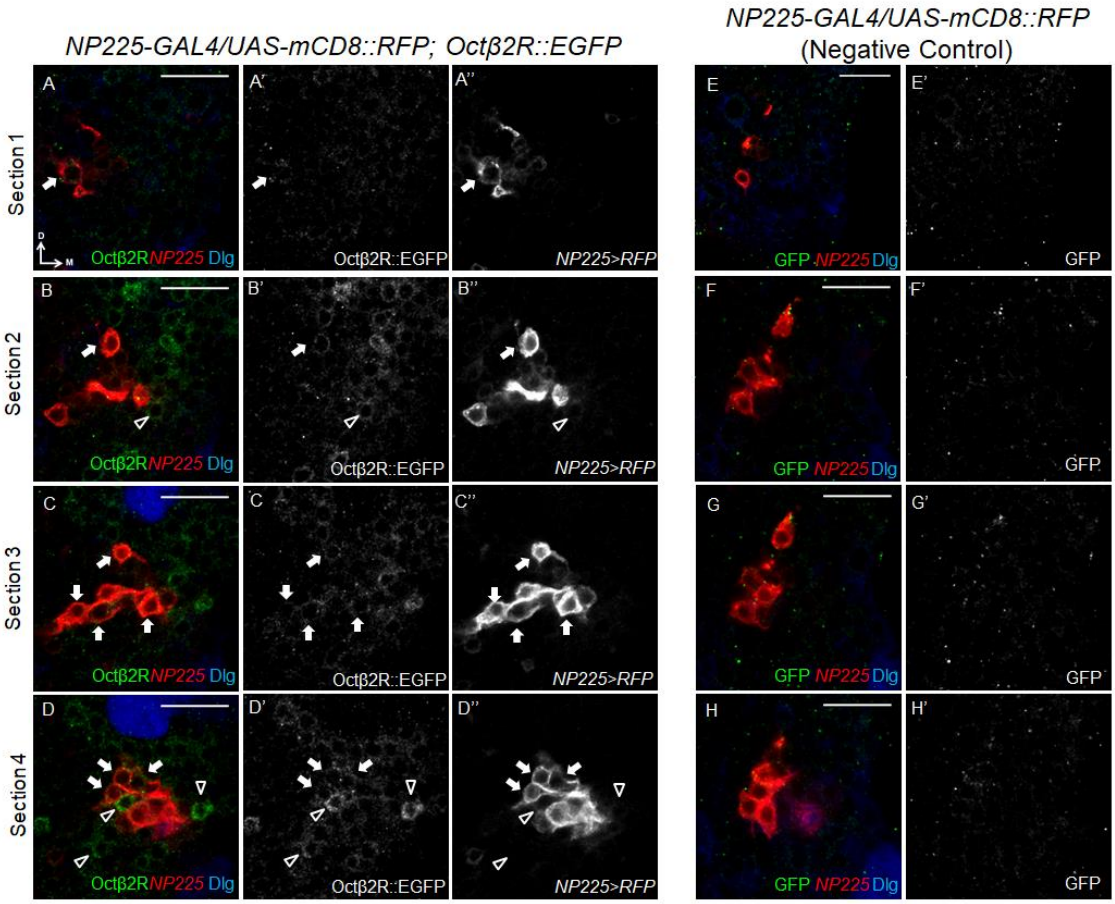

Figure 5.22. Octβ2R::EGFP colocalised with some PN cell bodies labelled by *NP225-GAL4*. Single confocal optical sections of the AL of *NP225-GAL4/UAS-mCD8::RFP; Octβ2R::EGFP* **(A-D)** and negative control *NP225-GAL4/UAS-mCD8::RFP; TM6B/MKRS* **(E-H)**. Green is Octβ2R::EGFP, red is *NP225>RFP* and blue is anti-Dlg. Arrows indicate Octβ2R-*NP225* colocalisation; while empty arrowheads indicate Octβ2R-positive cell bodies negative for *NP225>RFP*. Medial (M) is right and dorsal (D) is up. Scale bar: 20 μm.

Genotype	Individual	Octβ2R+/NP225+ Cell bodies	Control Genotype	Individual	Octβ2R+/NP225+ Cell bodies
NP225-GAL4/UAS-mCD8::RFP; Octβ2R::EGFP	Individual 1	15	*NP225-GAL4/UAS-mCD8::RFP*		
	Individual 2	12			
	Individual 3	11			
	Individual 4	13			
	Individual 5	8		Individual 1	3
	Individual 6	16		Individual 2	0
	Individual 7	10		Individual 3	3
Statistical Description	N	7	**Statistical Description**	N	3
	Mean	12		Mean	2
	S.D.	2.8		S.D.	1.7
	S.E.M.	1.1		S.E.M.	1.0

Table 5.3. Numbers of *NP225-GAL4* cell bodies positive for Octβ2R::EGFP. Abbreviations: Octβ2R+, Octβ2R::EGFP-positive; NP225+, *NP225>RFP*-positive; N, number; S.D., standard deviation; S.E.M., standard error of the mean.

5.2.2.4. Ambiguous Octβ2R::EGFP localisation to Odd-like and sVUM1 cell bodies

To determine whether Octβ2R was expressed in Odd-like neurons, I examined whether Octβ2R::EGFP localised to an Odd-like neuronal cell body labelled by *R68B12-GAL4*. *R68B12-GAL4* was made by fusing *GAL4* with a promoter fragment of the *Octβ2R* gene (Jenett et al., 2012); and therefore possibly labels some neurons that express Octβ2R. In Chapter 8, I showed that *R68B12-GAL4* labelled a calyx-innervating neuron that showed a similar innervation pattern to Odd neurons (Slater et al., 2015; L. Masuda-Nakagawa, personal communication). This Odd-like neuron cell body sends a clearly visible tract to the MB calyx.

Octβ2R::EGFP signal colocalised with the Odd-like neuron cell body labelled by *R68B12-GAL4* (n=3; Fig. 5.23A-B, filled arrowhead). However, GFP signal was also observed in the Odd-like neuron cell body in the negative control (Fig. 5.23C-D, arrowhead). This suggested that there may be bleed through of the *R68B12>RFP* signal to the GFP channel. Therefore, it was ambiguous as to whether Octβ2R::EGFP localised to the Odd-like neuron cell body labelled in this line.

Other cell bodies labelled by *R68B12-GAL4* did not show Octβ2R::EGFP signal or clear background labelling (Fig. 5.23A, C). On the other hand, a medial cell body (Fig. 5.23A, empty arrowhead) that did not colocalise with *68B12>RFP* was consistently observed in *Octβ2R::EGFP* but not negative control brains (Fig. 5.23C). This suggested that *Octβ2R::EGFP* and *R68B12-GAL4* did not share overlapping expression patterns other than the Odd-like neuron cell body, despite the fact that *R68B12-GAL4* is an *Octβ2R-GAL4* line.

As Octβ2R might be expressed in OA neurons at the NMJ (Koon et al., 2011), I next examined whether Octβ2R::EGFP localised to OA neuron cell bodies, visualised using anti-OA, at the SOG ventral median. Some OA-positive neurons colocalised with Octβ2R::EGFP (Fig. 5.24, arrows), but this was not consistent across individuals. Moreover, it was difficult to discern Octβ2R::EGFP signal from background labelling, and there was a large variability in the signal to noise ratio across different individuals (n=7; Fig. 5.24). Therefore, it was inconclusive from these data whether OA sVUM1 neurons, whose cell bodies are in the SOG region, express Octβ2R.

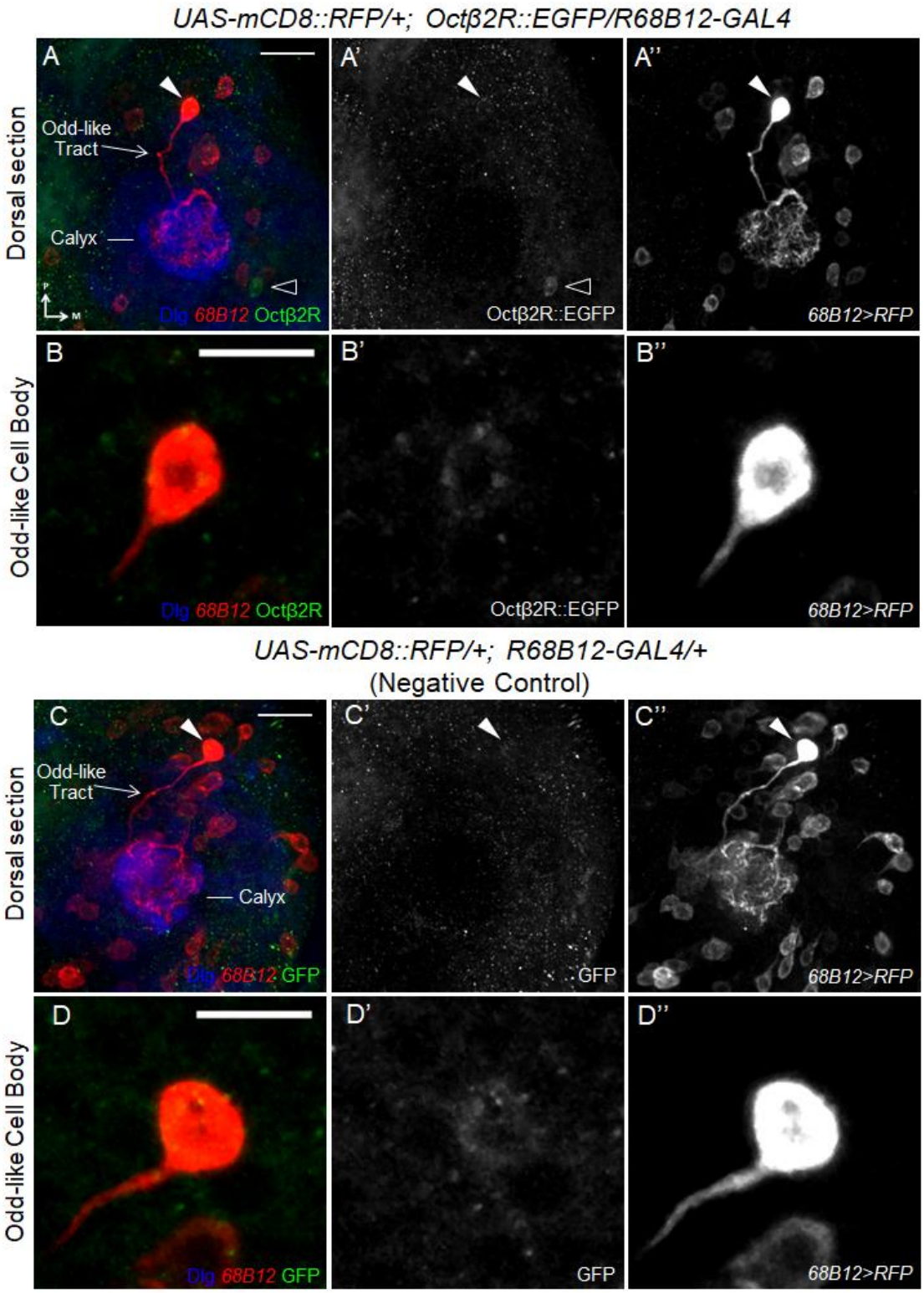

Figure 5.23. EGFP signal detected in Odd-like cell body labelled by *R68B12-GAL4* in *Octβ2R::EGFP* and negative control brains. Confocal projection of the brain lobe of *UAS-mCD8::RFP/+; Octβ2R::EGFP/R68B12-GAL4* **(A-B)** with *UAS-mCD8::RFP/+; R68B12-GAL4/+* negative control **(C-D)**. **(B,D)** are enlarged confocal projections of the Odd-like cell body. Green is Octβ2R::EGFP, red is *68B12>RFP* and blue is anti-Dlg. Filled arrowheads indicate Odd-like cell body; empty arrowhead indicates Octβ2R::EGFP-positive cell body that is *68B12*-negative. Medial (M) is right and dorsal (D) is up. Scale bar: 20 μm for **(A,C)**; 10 μm for **(B,D)**.

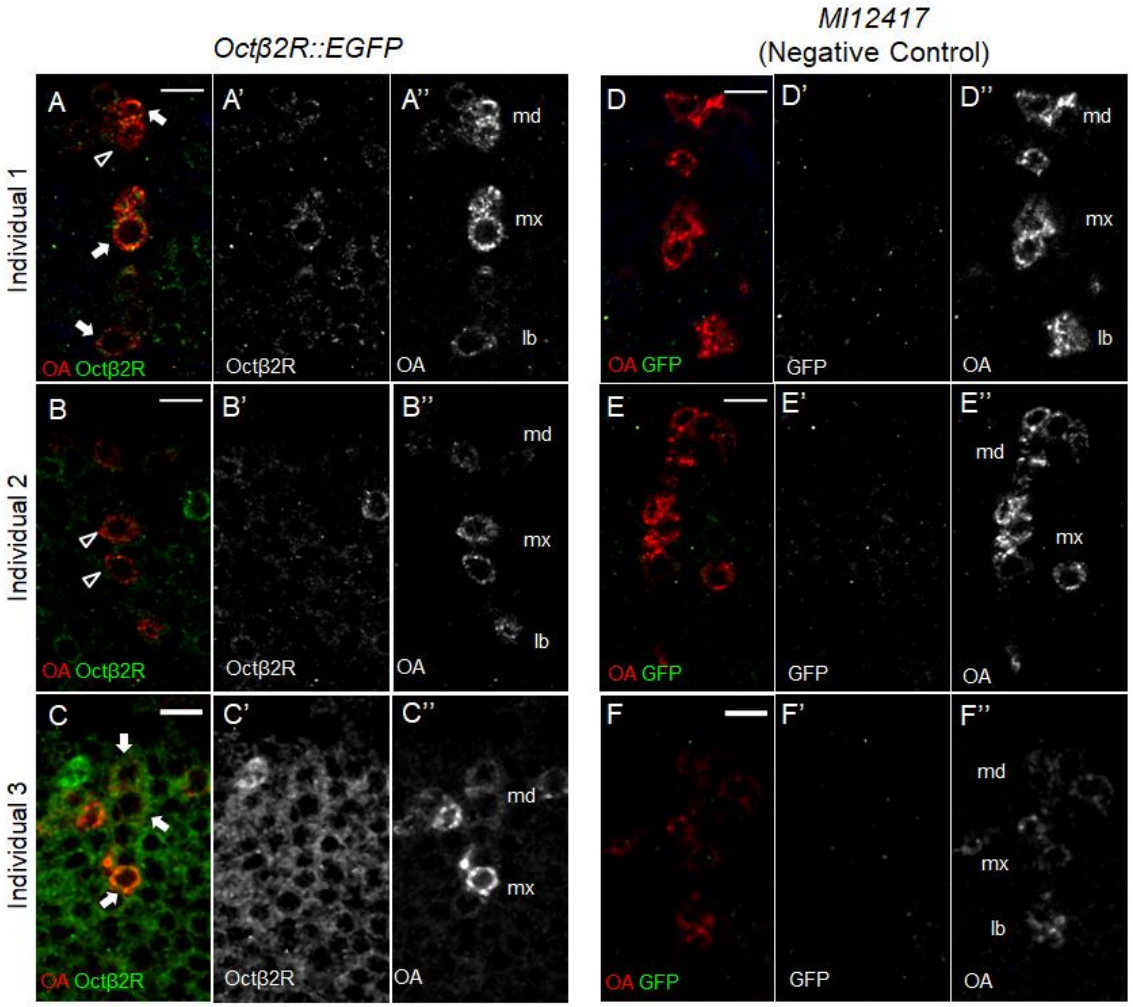

Figure 5.24. Octβ2R::EGFP may be localised to OA cell bodies at the SOG. Single confocal optical sections of the SOG from three *Octβ2R::EGFP* individuals **(A-C)** with *MI12417* negative controls **(D-F)**. Green is Octβ2R::EGFP and blue is anti-Dlg. Anterior is up and medial is at the vertical midline. Arrows indicate Octβ2R-*NP225* colocalisation; while empty arrowheads indicate OA-positive cell bodies negative for Octβ2R::EGFP. Abbreviations: lb, labial cluster; md, mandibular cluster; mx, maxillary cluster. Scale bar: 10 μm.

5.2.3. Octβ3R::EGFP localisation in the larval MB calyx circuitry

5.2.3.1. Selection, generation and validation of EGFP-tagged Octβ3R lines

To visualise Octβ3R expression in the larval brain, I selected the *MI06217* line from the MiMIC collection as it contained the MiMIC insertion in a coding region intron of the *Octβ3R* gene (Venken et al., 2011a; Fig. 5.25, 5.26). PCR reactions against the 5' and 3' flanking ends of the MI06217 insertion (Fig. 5.27), and the sequences of these PCR products (Fig. S6, S7), confirmed that the MI06217 insertion was in the *Octβ3R* gene.

Octβ3R encodes four transcriptional variants: *Octβ3R-RF* and *Octβ3R-RG* in the Phase 1 reading frame, and *Octβ3R-RJ* and *Octβ3R-RK* in the Phase 0 reading frame (Fig. 5.25, 5.26). In *Octβ3R-RF* and *Octβ3R-RG*, the MI06217 insertion was in coding region intron 5. This corresponded to amino acid position 1012 and 1013 respectively, and therefore the intracellular domain between TM V and VI in both protein isotypes (Fig. 5.28, 5.29). In *Octβ3R-RJ*, the *MI06217* insertion was in coding region intron 4, corresponding to amino acid position 351, and was therefore positioned in the intracellular domain between TM V and VI (Fig. 5.30). Finally, *Octβ3R-RK* did not encode a full length 7 TM receptor according to TMHMM predictions (Fig. 5.31), and was therefore not expected to be expressed.

I identified *Octβ3R::EGFP (Phase 1)* from the MiMIC RMCE collection (Nagarkar-Jaiswal et al., 2015; Fig. 5.32). Using PCR, I confirmed that the EGFP cassette was inserted in the correct orientation for expression in this stock (Fig. 5.33A, B1). This stock could be used to visualise the expression patterns of Octβ3R-PF and Octβ3R-PG, as it contained the EGFP cassette in the Phase 1 reading frame (Fig. 5.32)

To visualise the localisation of the Octβ3R-PJ protein, I introduced a Phase 0 EGFP cassette to the *MI06217* line to generate an *Octβ3R::EGFP (Phase 0)* protein trap. Nineteen *Octβ3R::EGFP (Phase 0)* recombinant stocks were recovered. Four out of the six recombinant stocks assayed showed stronger bands for PCR1 and PCR4 reactions than for PCR2 and PCR3 reactions; and

Insertion MI06217

Gene Information

Affected Gene(s)
Octbeta3R

Position	Octbeta3R - coding intron
Phase	Octbeta3R-RF:1, Octbeta3R-RG:1, Octbeta3R-RJ:0, Octbeta3R-RK:0

Release 6 Annotation

Scaffold	Coordinate	Strand	Site	GBrowse Link
3R	12515992	-	87B15	3R:12515992

FlyBase Annotation	Transposon
FBti0150501	Mi{MIC}

Stock Availability

Donor/Collection	Stockcenter Designation	Stock No.
GDP	Bloomington	43050

Flanking Sequence

MI06217-3' (JY252757)	TATATATATAATATAATGTATAGCATTTAGTTAGTTGCACCTGCAAACGA AGACAGAAAGGGACGACCTACTTCCAGAGACAGGGAGCCAACGATAATGA ATCTGAATCCATTCCCTTTTCGATC
MI06217-5' (JY252758)	GATCTTAAAATAAAGATACGAACTTTTACCATATTTAAATATAGTTCTTA CCTTGAAGAAAACTGTGAATTGTGTATTTAAGTTCCTTTCAAAAGCGGTG CGAATTTCTGAAAAATCATACAGTGTTTTAAAATGTATAGAACCTATAAA CCCTCATTGGAAAAGTAATACTCAAATGCTTCGAATGAAACTTTAGTTAA CTAGCTTACTATA

Figure 5.25. *MI06217* insertion stock listed on the Gene Disruption Project Database. (http://flypush.imgen.bcm.tmc.edu/pscreen/details.php?line=MI06217).

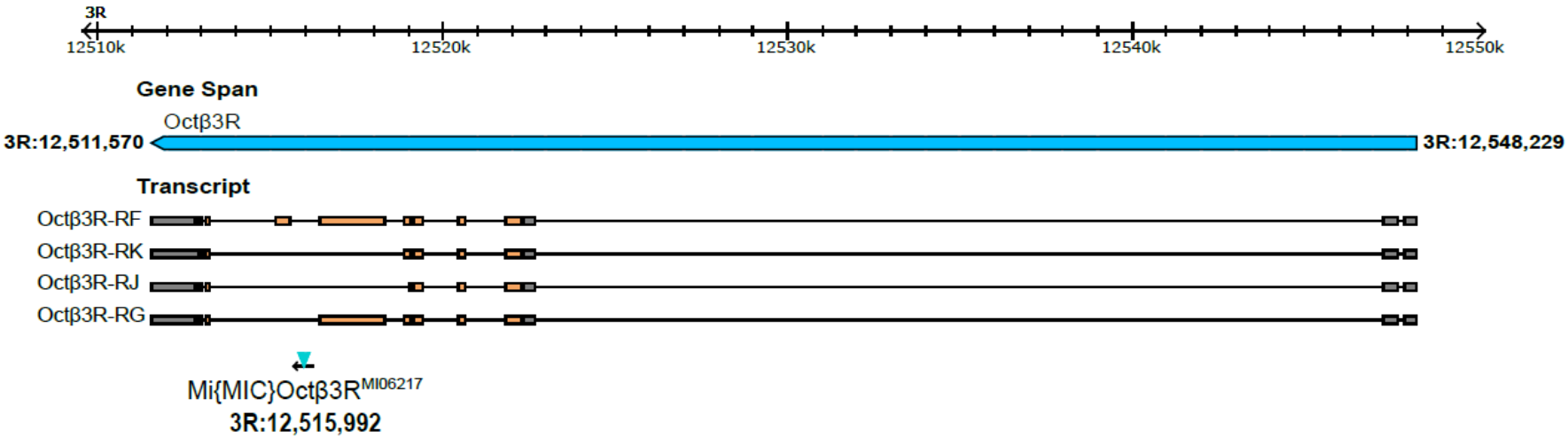

Figure 5.26. Map of MI06217 insertion relative to *Octβ3R* gene and transcripts. Adapted from GBrowse.

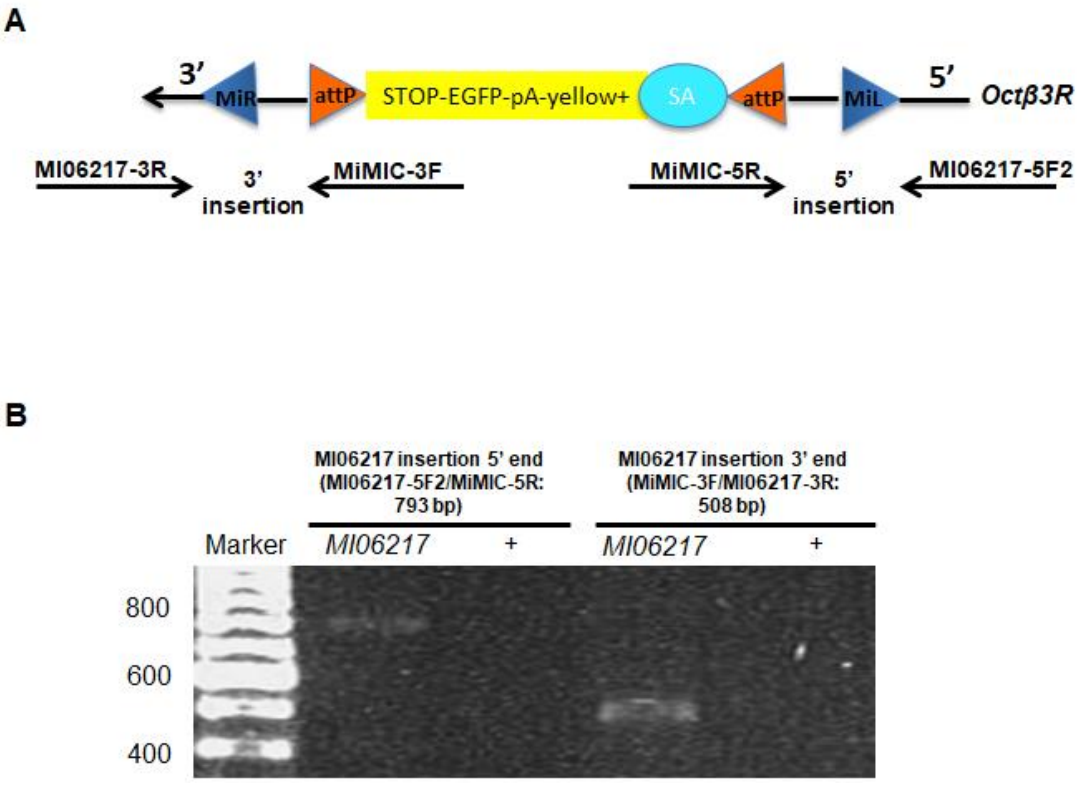

Figure 5.27. PCR verification of MI06217 insertion in the *Octβ3R* gene. (A) Primers designed against 5' and 3' insertion flanking ends for validating MI06217 insertion in the *Octβ3R* gene. **(B)** PCR products were detected for 5' and 3' MI06217 insertion ends for *MI06217* DNA but not for negative control *CS* (denoted as +) DNA. Abbreviations as Fig. 5.6.

A. Octβ3R-PF tblastn alignment to *Drosophila* sequences

```
Exon 4
Query:    989   INFSQENSDSRSYIPMGRV    1007
                INFSQENSDSRSYIPMGRV
12516522        INFSQENSDSRSYIPMGRV    12516466

Exon 5
Query:    1012  AKHEFSNKSSLIRRGGICIFVDEEEAEIIEQRPRGITFAAVPSPLPKCPLCGADISSTTG        1071
                A+HEFSNKSSLIRRGGICIFVDEEEAEIIEQRPRGITFAAVPSPLPKCPLCGADISSTTG
12515561        AEHEFSNKSSLIRRGGICIFVDEEEAEIIEQRPRGITFAAVPSPLPKCPLCGADISSTTG
        12515382
```

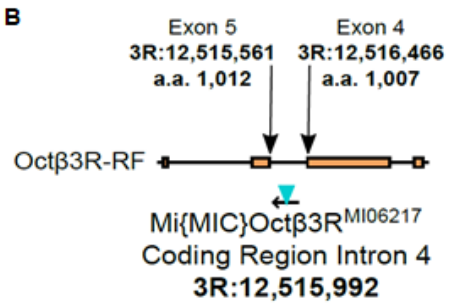

C

Octβ3R-PF TMHMM Predictions

```
WEBSEQUENCE    TMHMM2.0    outside      1    144
WEBSEQUENCE    TMHMM2.0    TMhelix    145    164
WEBSEQUENCE    TMHMM2.0    inside     165    176
WEBSEQUENCE    TMHMM2.0    TMhelix    177    199
WEBSEQUENCE    TMHMM2.0    outside    200    213
WEBSEQUENCE    TMHMM2.0    TMhelix    214    236
WEBSEQUENCE    TMHMM2.0    inside     237    256
WEBSEQUENCE    TMHMM2.0    TMhelix    257    279
WEBSEQUENCE    TMHMM2.0    outside    280    303
WEBSEQUENCE    TMHMM2.0    TMhelix    304    326
WEBSEQUENCE    TMHMM2.0    inside     327   1168   ← MI06217 insertion site: a.a. 1,012
WEBSEQUENCE    TMHMM2.0    TMhelix   1169   1191
WEBSEQUENCE    TMHMM2.0    outside   1192   1203
WEBSEQUENCE    TMHMM2.0    TMhelix   1204   1226
WEBSEQUENCE    TMHMM2.0    inside    1227   1256
```

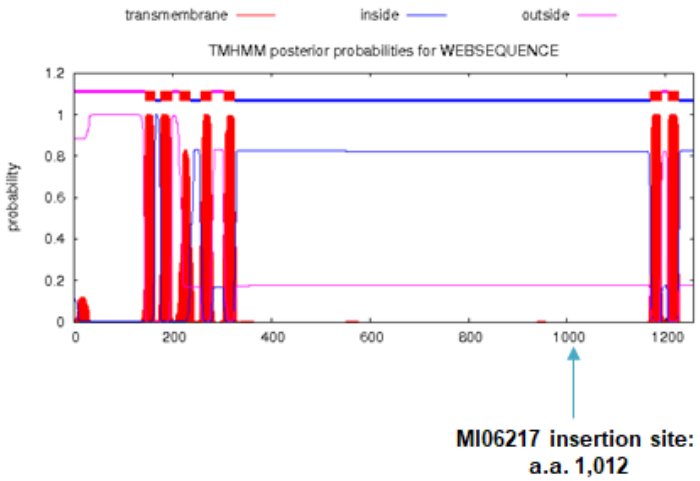

Figure 5.28. MI06217 insertion coordinates in *Octβ3R-RF* transcript and Octβ3R-PF protein isotype. (A) Amino acid coordinates for the MI06217 insertion site based on tblastn alignment with *Octβ3R-RF*. **(B)** Magnified map of MI06217 insertion in coding region intron 4 of *Octβ3R-RF* with genomic and amino acid coordinates. **(C)** MI06217 insertion was between TM V and VI based on TMHMM predictions for the Octβ3R-PF isotype.

A. Octβ3R-PG tblastn alignment to *Drosophila* sequences

```
Exon 4
Query:    989   INFSQENSDSRSYIPMGRVSTSSAS     1013
                INFSQENSDSRSYIPMGRVSTSSAS
12516522        INFSQENSDSRSYIPMGRVSTSSAS     12516448

Exon 5
Query:    1006  RVSTSSASGSVRPAKGWKAEHKAARTLGIIMGVFLLCWLPFFLW        1049
                ++S     GSVRPAKGWKAEHKAARTLGIIMGVFLLCWLPFFLW
12513273        KLSICPTGGSVRPAKGWKAEHKAARTLGIIMGVFLLCWLPFFLW        12513142
```

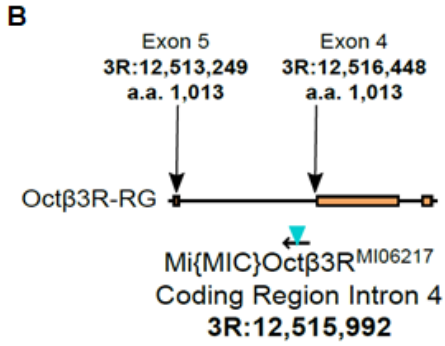

C **Octβ3R-PG TMHMM Predictions**

```
WEBSEQUENCE    TMHMM2.0    outside      1   144
WEBSEQUENCE    TMHMM2.0    TMhelix    145   164
WEBSEQUENCE    TMHMM2.0    inside     165   176
WEBSEQUENCE    TMHMM2.0    TMhelix    177   199
WEBSEQUENCE    TMHMM2.0    outside    200   213
WEBSEQUENCE    TMHMM2.0    TMhelix    214   236
WEBSEQUENCE    TMHMM2.0    inside     237   256
WEBSEQUENCE    TMHMM2.0    TMhelix    257   279
WEBSEQUENCE    TMHMM2.0    outside    280   303
WEBSEQUENCE    TMHMM2.0    TMhelix    304   326
WEBSEQUENCE    TMHMM2.0    inside     327  1030   <- MI06217 insertion site:
WEBSEQUENCE    TMHMM2.0    TMhelix   1031  1053      a.a. 1,013
WEBSEQUENCE    TMHMM2.0    outside   1054  1065
WEBSEQUENCE    TMHMM2.0    TMhelix   1066  1088
WEBSEQUENCE    TMHMM2.0    inside    1089  1118
```

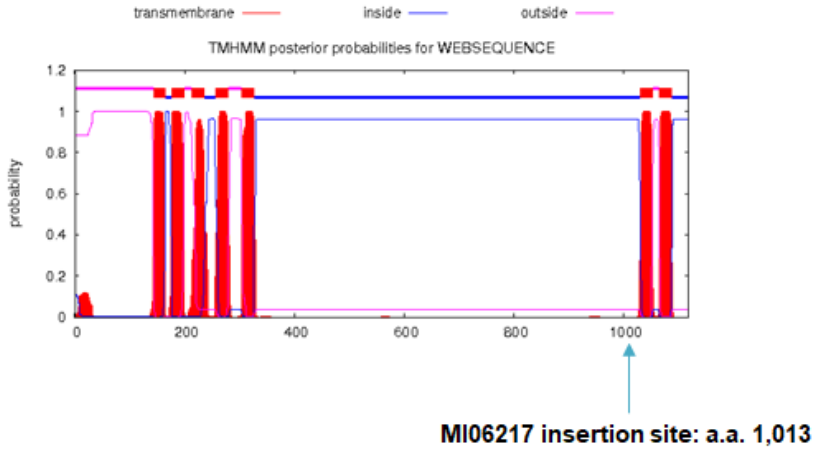

Figure 5.29. MI06217 insertion coordinates in *Octβ3R-RG* transcript and Octβ3R-PG protein isotype. (A) Amino acid coordinates for the MI06217 insertion site based on tblastn alignment with *Octβ3R-RG*. **(B)** Magnified map of MI06217 insertion in coding region intron 4 of *Octβ3R-RG* with genomic and amino acid coordinates. **(C)** MI06217 insertion was between TM V and VI based on TMHMM predictions for the Octβ3R-PG isotype.

A. Octβ3R-PJ tblastn alignment to *Drosophila* sequences

```
Exon 3
Query:    331    -----EAIRQRKALSRTSSNILLNSAE    352
                       EAIRQRKALSRTSSNILLNS
12519086         LWFSREAIRQRKALSRTSSNILLNSVH    12519006

Exon 4
Query:    350    SAEHKAARTLGIIMGVFLLCWLPFFLW    376
                  AEHKAARTLGIIMGVFLLCWLPFFLW
12513222         KAEHKAARTLGIIMGVFLLCWLPFFLW    12513142
```

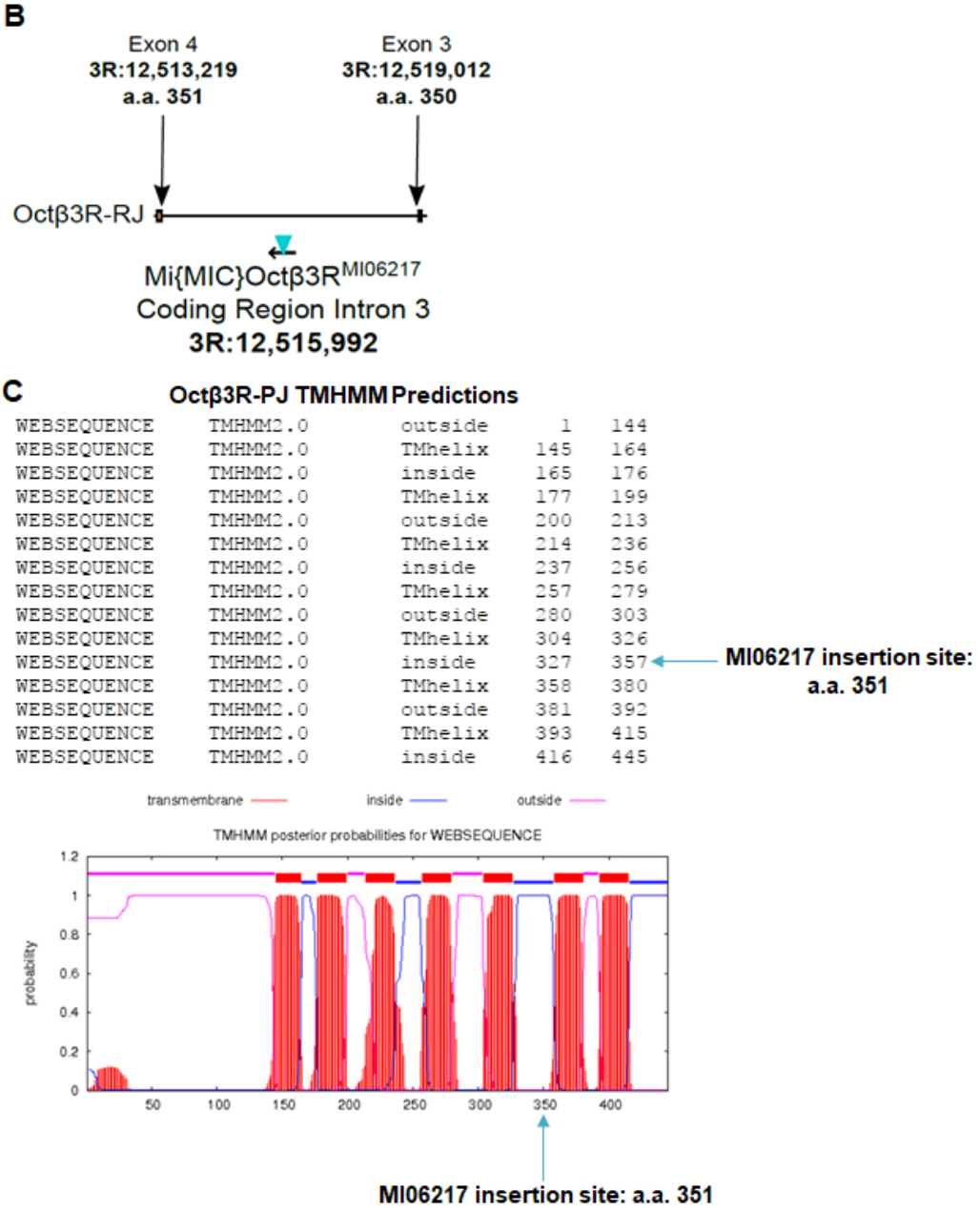

Figure 5.30. MI06217 insertion coordinates in *Octβ3R-RJ* transcript and Octβ3R-PJ protein isotype. (A) Amino acid coordinates for the MI06217 insertion site based on tblastn alignment with *Octβ3R-RJ*. **(B)** Magnified map of MI06217 insertion in coding region intron 3 of *Octβ3R-RJ* with genomic and amino acid coordinates. **(C)** MI06217 insertion was between TM V and VI based on TMHMM predictions for the Octβ3R-PJ isotype.

A. Octβ3R-PK tblastn alignment to *Drosophila* sequences

```
Exon 3
Query:    386   SNLEA          390
                SNLE
12518906        SNLEV          12518892

Exon 4
Query:    384   ALSNLEAVPCDRPKDGRPNTRPPAPWASSWASFCSAGCPSFCG          426
                +LS   +AVPCDRPKDGRPNTRPPAPWASSWASFCSAGCPSFCG
12513269        SLSAPQAVPCDRPKDGRPNTRPPAPWASSWASFCSAGCPSFCG          12513141
```

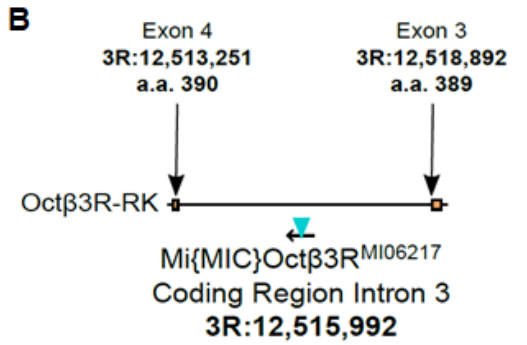

C **Octβ3R-PK TMHMM Predictions**

```
WEBSEQUENCE     TMHMM2.0        outside      1    144
WEBSEQUENCE     TMHMM2.0        TMhelix    145    164
WEBSEQUENCE     TMHMM2.0        inside     165    176
WEBSEQUENCE     TMHMM2.0        TMhelix    177    199
WEBSEQUENCE     TMHMM2.0        outside    200    213
WEBSEQUENCE     TMHMM2.0        TMhelix    214    236
WEBSEQUENCE     TMHMM2.0        inside     237    256
WEBSEQUENCE     TMHMM2.0        TMhelix    257    279
WEBSEQUENCE     TMHMM2.0        outside    280    303
WEBSEQUENCE     TMHMM2.0        TMhelix    304    326
WEBSEQUENCE     TMHMM2.0        inside     327    456
```

MI06217 insertion site: a.a. 390

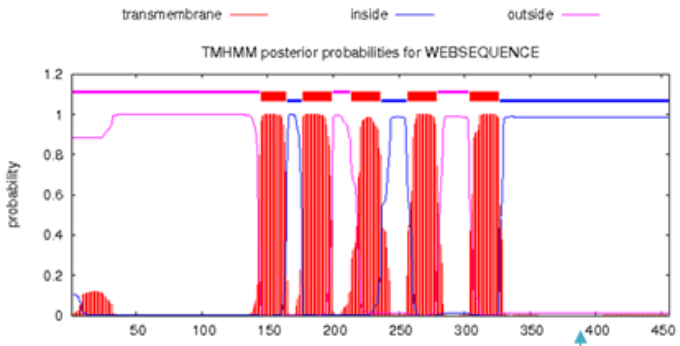

MI06217 insertion site: a.a. 390

Figure 5.31. MI06217 insertion coordinates in *Octβ3R-RK* transcript and Octβ3R-PK protein isotype. (A) Amino acid coordinates for the MI06217 insertion site based on tblastn alignment with *Octβ3R-RK*. **(B)** Magnified map of MI06217 insertion in coding region intron 3 of *Octβ3R-RK* with genomic and amino acid coordinates. **(C)** MI06217 insertion was after TM V in C-terminal based on TMHMM predictions for the Octβ3R-PK isotype.

RMCE Line MI06217

Parental MI Line:

Insertion	Gene(s) Affected	Location	Position	Phase
MI06217	Octbeta3R[-]	3R:12515992 [-]	Octbeta3R-coding intron;	Octbeta3R-RF:1, Octbeta3R-RG:1, Octbeta3R-RJ:0, Octbeta3R-RK:0

RMCE Line:

Insertion	Gene Target	Phase	Method	Tag
MI06217-GFSTF.1	Octbeta3R	1	injection	EGFP-FlAsH-StrepII-TEV-3xFLAG

Lethality	Fails to Complement
viable	

BDSC Stock No.
60245

Images (antibody staining)
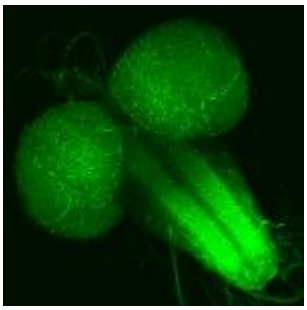

Figure 5.32. *Octβ3R::EGFP* recombinant stock listed on the Gene Disruption Project Database. (http://flypush.imgen.bcm.tmc.edu/pscreen/rmce/rmce.php?entry=RM00315).

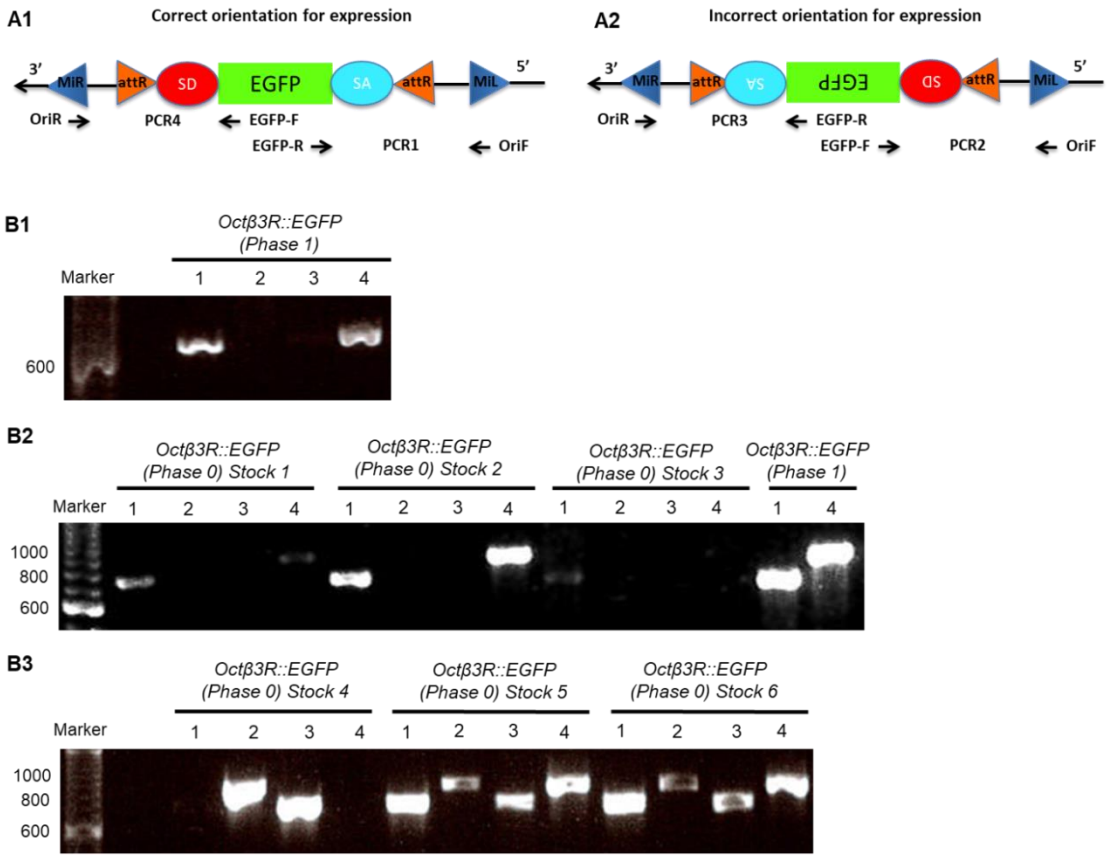

Figure 5.33. PCR validation of EGFP orientation for recombinant *Octβ3R::EGFP* stocks. **(A1)** Products for PCR1 and PCR4 indicated EGFP cassette in the correct orientation for expression. **(A2)** Products for PCR2 and PCR3 indicated EGFP cassette in the incorrect orientation for expression. **(B)** PCR results for PCR reactions 1-4 for *Octβ3R::EGFP (Phase 1)* **(B1)**, *Octβ3R::EGFP (Phase 0) Stocks 1, 2, 3*; with *Octβ3R::EGFP (Phase 1)* as positive control for PCR1 and PCR4 **(B2)**, *Octβ3R::EGFP (Phase 0) Stocks 4, 5, 6* **(B3)**. Abbreviations as Fig. 5.7.

therefore contained the EGFP cassette in the correct orientation for expression (Fig. 5.33A, B2-3; Table 5.4). As *Octβ3R::EGFP (Phase 0) Stock 2* had the most defined PCR results (Fig. 5.33B2; Table 5.4), I selected it for subsequent expression analyses and designated it as *Octβ3R::EGFP (Phase 0).*

5.2.3.2. No EGFP signal observed in *Octβ3R::EGFP (Phase 1)* stock

Octβ3R::EGFP (Phase 1) larvae did not show any EGFP signal in the larval MB calyx visualised using chicken anti-GFP (Ab13970) (n=3; Fig. 5.34) or rabbit anti-GFP (Ab6556) (n=3; Fig. 5.35). Some GFP-positive cell bodies were labelled in both *Octβ3R::EGFP (Phase 1)* brains and *MI06217* negative controls at similar levels of intensity (Fig. 5.34, 5.35). This suggested that these GFP-positive cell bodies were probably background labelling rather than signal.

No EGFP signal was observed elsewhere in either cell bodies or neuropils in the brain lobes of *Octβ3R::EGFP (Phase 1)* brains compared to negative controls (n=2; Fig. 5.36). Previous immunolabelling of *Octβ3R::EGFP (Phase 1)* larval brains conducted by the Gene Disruption Project also did not show defined Octβ3R::EGFP signals in cell bodies or neuropils; but instead showed homogeneous background labelling (Nagarkar-Jaiswal et al., 2015; Fig. 5.32). However, this was probably because the image was taken at low resolution, as the comparable image for *Octβ1R::EGFP* also did not show clear signals (Nagarkar-Jaiswal et al., 2015; Fig. 5.2), even though I observed Octβ1R::EGFP signal in the larval brain. This suggested that either the *Octβ3R::EGFP (Phase 1)* stock did not produce a functional or correctly targeted Octβ3R::EGFP protein, or that neither Octβ3R-PF nor Octβ3R-PG protein isotypes localised to the larval brain lobes.

To date, only one Octβ3R isotype has been cloned and functionally verified. This Octβ3R isotype was 440 amino acids in length and predicted to encode a seven TM receptor (Maqueira et al., 2005). This description fits only the Octβ3R-PJ protein isotype which is 445 amino acids in length; as both Octβ3R-PF and Octβ3R-PG were >1000 amino acids in length, and Octβ3R-PK only encoded five TMs. This suggested that it was probable that only the Octβ3R-PJ variant was functionally expressed. As no signals were observed using the *Octβ3R::EGFP (Phase 1)* stock, I focused the following

Stock	PCR1	PCR2	PCR3	PCR4	Figure	Expected expression
Octβ3R::EGFP (Phase 1)	**++**	**-**	**-**	**++**	**5.33B1, B2**	**Yes**
Octβ3R::EGFP (Phase 0) Stock 1	**+**	**-**	**-**	**+**	**5.33B2**	**Yes**
Octβ3R::EGFP (Phase 0) Stock 2	**++**	**-**	**-**	**++**	**5.33B2**	**Yes**
Octβ3R::EGFP (Phase 0) Stock 3	+	-	-	-	5.33B2	Maybe
Octβ3R::EGFP (Phase 0) Stock 4	-	++	++	-	5.33B3	No
Octβ3R::EGFP (Phase 0) Stock 5	**++**	**+**	**+**	**++**	**5.33B3**	**Yes**
Octβ3R::EGFP (Phase 0) Stock 6	**++**	**+**	**+**	**++**	**5.33B3**	**Yes**

Table 5.4. *Octβ3R::EGFP (Phase 1)* and four out of six recombinant *Octβ3R::EGFP (Phase 0)* stocks contained EGFP in the correct orientation for expression. PCR products obtained for each of the PCR reactions (PCR1, PCR2, PCR3 and PCR4) were scored as follows: -, no bands observed; +, weak band observed; ++, strong band observed. PCR results were used to determine whether Octβ3R::EGFP expression was expected (Expected Expression).

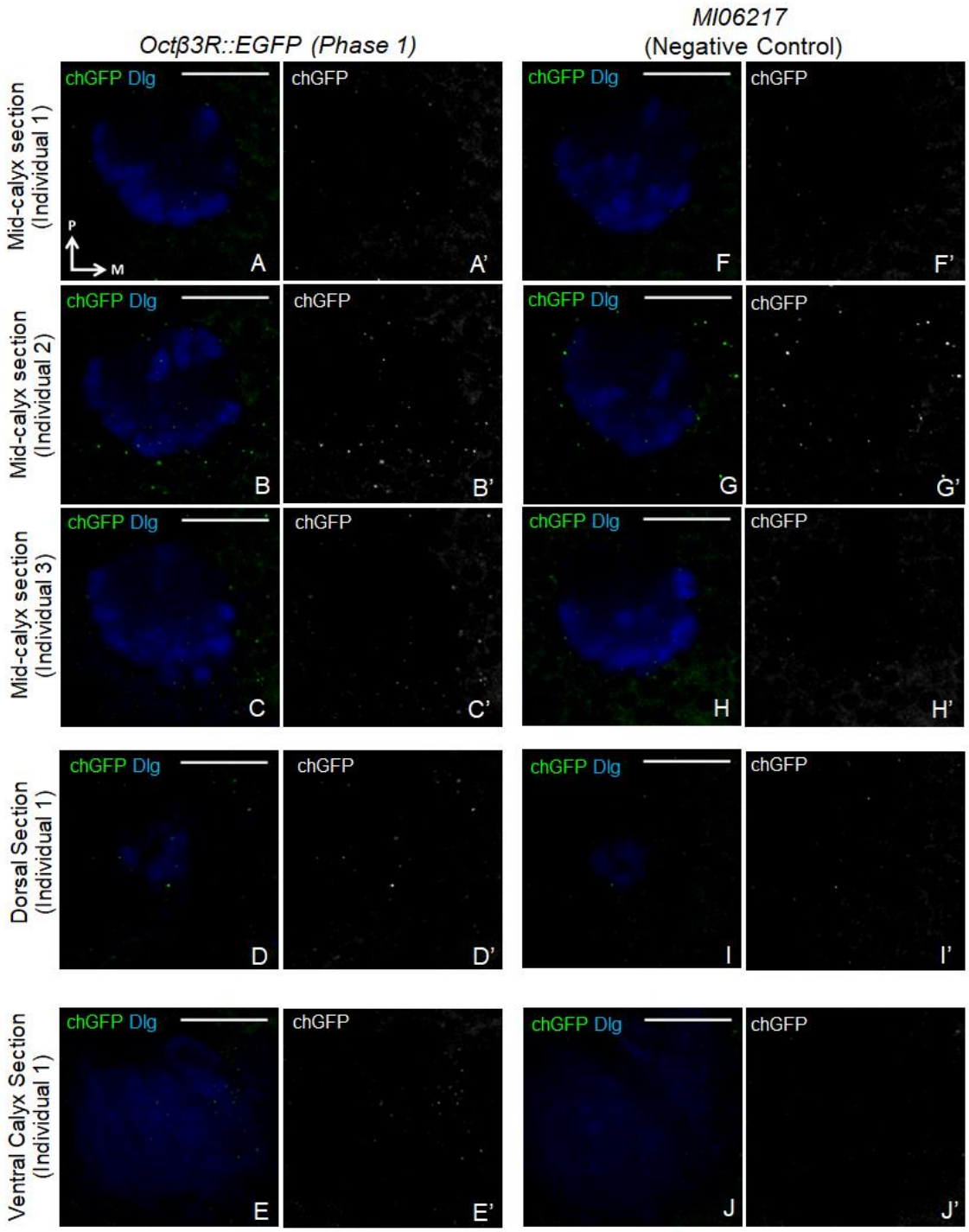

Figure 5.34. No EGFP signal observed in larval MB calyx in *Octβ3R::EGFP (Phase 1)* brains labelled with chicken anti-GFP. Single confocal optical sections of the calyx from three *Octβ3R::EGFP (Phase 1)* individuals **(A-E)**, with corresponding *MI06217* parental line negative controls **(F-J)**. Green is chicken anti-GFP (chGFP, Ab13970) and blue is anti-Dlg. Medial (M) is right and posterior (P) is up. Scale bar: 20 μm.

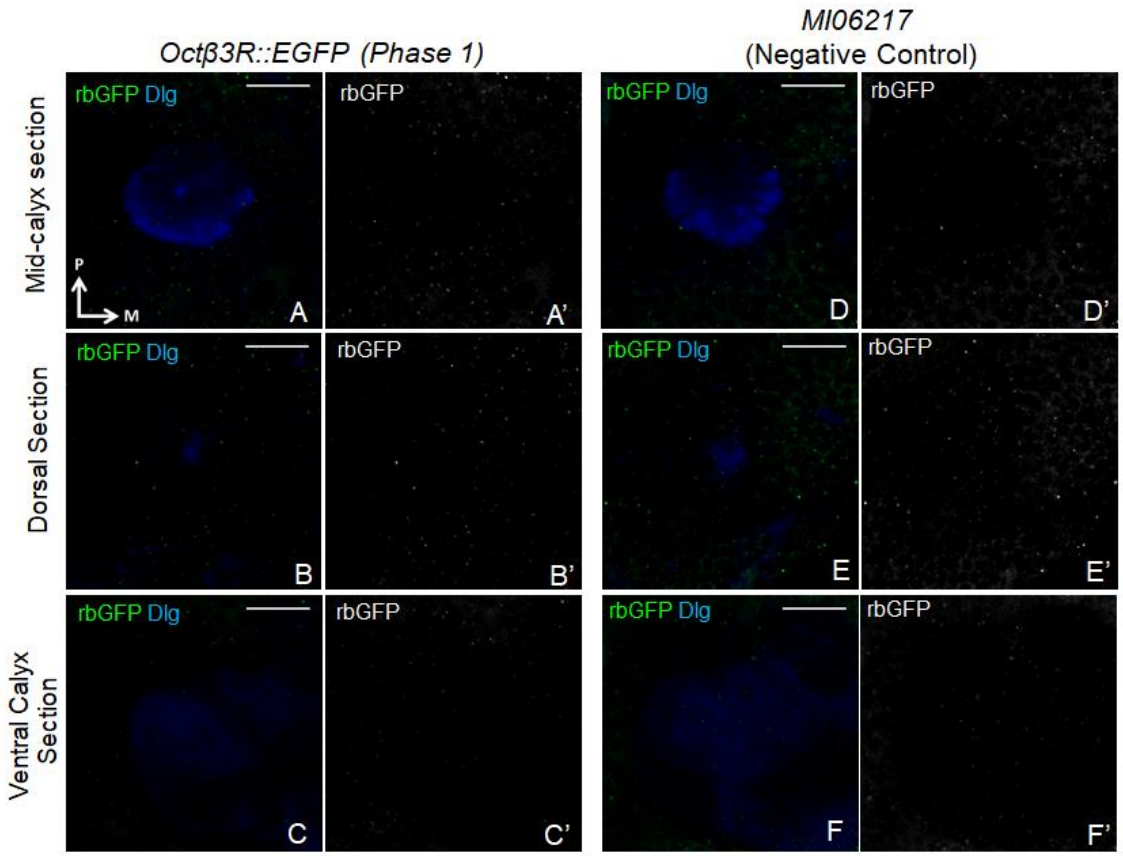

Figure 5.35. No EGFP signal observed in larval MB calyx in *Octβ3R::EGFP (Phase 1)* brains labelled with rabbit anti-GFP. Single confocal optical sections of the calyx of *Octβ3R::EGFP (Phase 1)* **(A-C)**, with *MI06217* parental line negative control **(D-F)**. Green is rabbit anti-GFP (rbGFP, Ab6556) and blue is anti-Dlg. Medial (M) is right and posterior (P) is up. Scale bar: 20 μm.

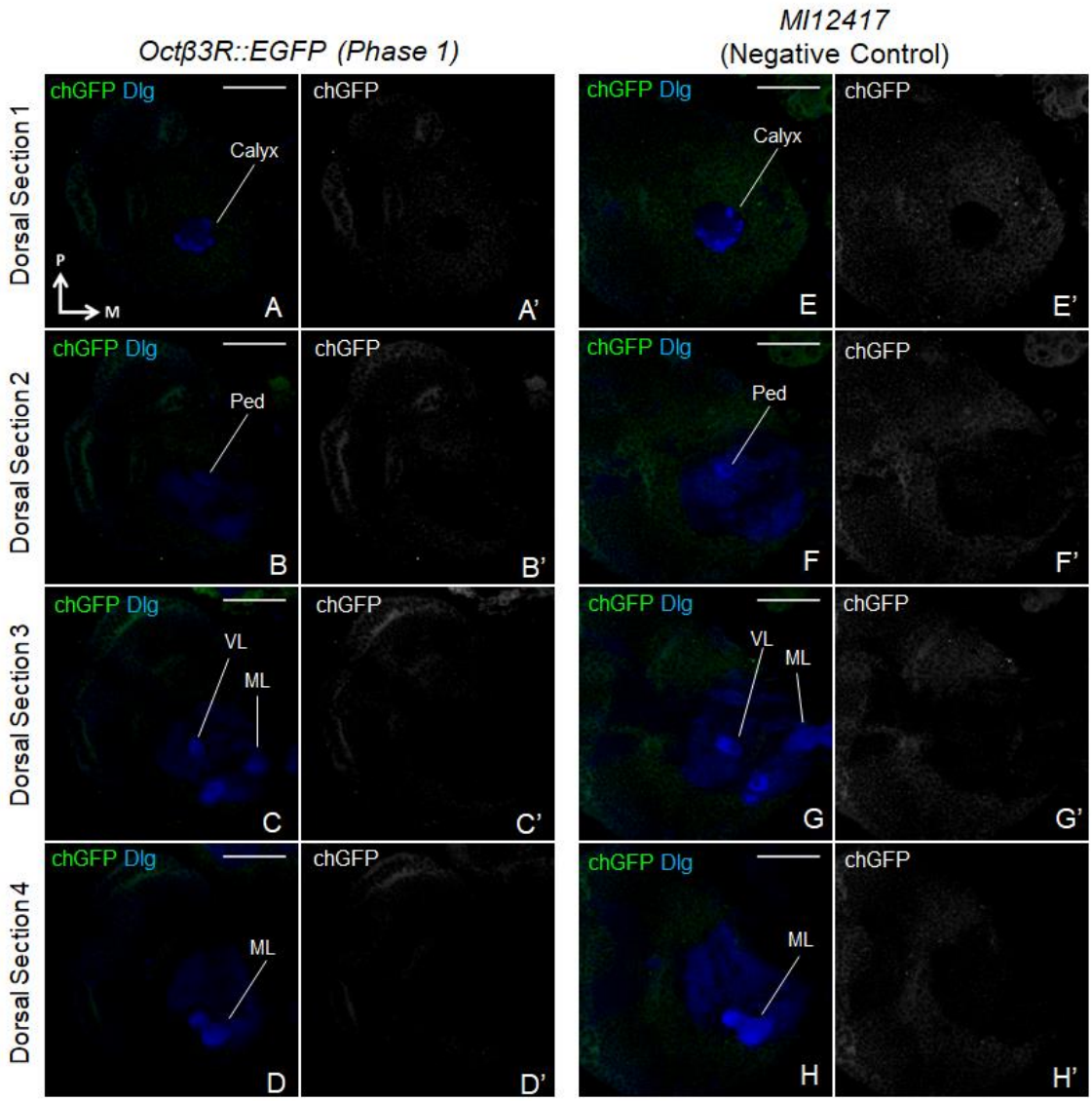

Figure 5.36. No EGFP signal observed in *Octβ3R::EGFP (Phase 1)* brain lobes. Single confocal optical sections of the dorsal larval brain of *Octβ3R::EGFP (Phase 1)* **(A-D)**, with corresponding *MI12417* negative control **(E-I)**. Green is chicken anti-GFP (chGFP, Ab13970) and blue is anti-Dlg. Medial (M) is right and posterior (P) is up. Scale bar: 50 μm. Abbreviations: ML, medial lobe; ped, pedunculus cross-section; VL, vertical lobe.

experiments on *Octβ3R::EGFP (Phase 0)*, which should reveal the expression pattern of the functional Octβ3R-PJ isotype.

5.2.3.3. No EGFP signal observed in *Octβ3R::EGFP (Phase 0)* stocks

Contrary to expectation, no EGFP signals were observed in *Octβ3R::EGFP (Phase 0)* larvae in the larval MB calyx (n=3; Fig. 5.37), AL (Fig. 5.38A-D) nor the SOG region (Fig. 5.38E-F). Similar to *Octβ3R::EGFP (Phase 1)* larvae, the GFP signals observed in cell bodies were comparable to background labelling of cell bodies in the negative control (Fig. 5.37, 5.38). Furthermore, I did not observe EGFP signals in the calyx, MB lobes, or in any nearby cell bodies using an alternative anti-GFP – the rabbit anti-GFP (A11122) – in *Octβ3R::EGFP (Phase 0)* larval brains (n=2; Fig. 5.39).

To ensure that this effect was not specific to the *Octβ3R::EGFP (Phase 0)* stock selected, I examined the expression patterns of two other *Octβ3R::EGFP (Phase 0)* recombinant stocks that contained EGFP in the correct orientation for expression: *Octβ3R::EGFP (Phase 0) Stock 1* and *Octβ3R::EGFP (Phase 0) Stock 5* (Fig. 5.33B2-3; Table 5.4). Neither of thse stocks showed any EGFP signals in the larval calyx, MB lobes nor nearby cell bodies besides background labelling that was also seen in negative controls (Fig. 5.40). These results showed that the *Octβ3R::EGFP (Phase 0)* stocks did not show Octβ3R::EGFP signal in the larval brain lobes. However, it was unclear why this was the case.

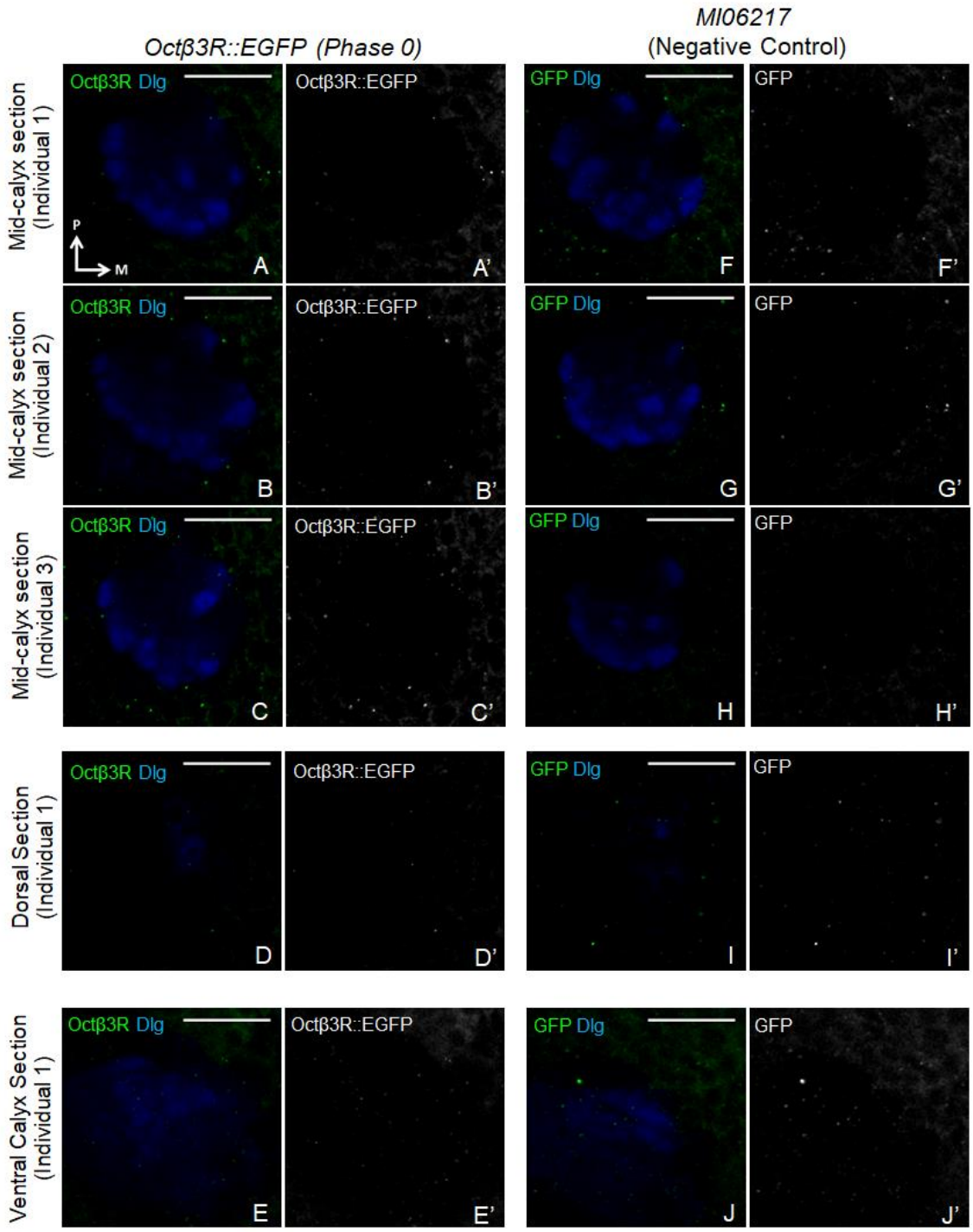

Figure 5.37. No EGFP signal observed in larval MB calyx in *Octβ3R::EGFP (Phase 0)* brains. Single confocal optical sections of the calyx from three *Octβ3R::EGFP (Phase 0)* individuals **(A-E)** with *MI06217* negative controls **(F-J)**. Green is chicken anti-GFP (chGFP, Ab13970) and blue is anti-Dlg. Medial (M) is right and posterior (P) is up. Scale bar: 20 μm.

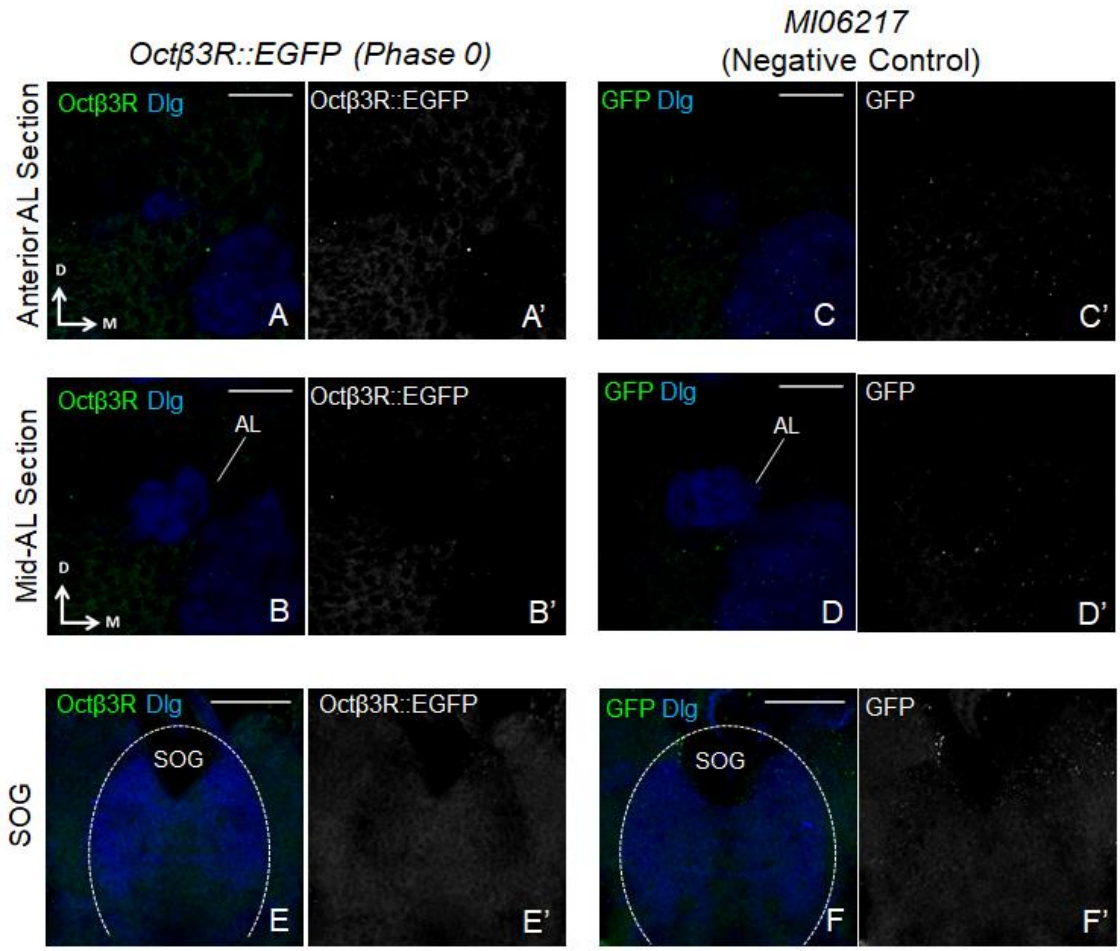

Figure 5.38. No EGFP signal observed in larval AL or SOG in *Octβ3R::EGFP (Phase 0)* brains. Single confocal optical sections of the larval brain of *Octβ3R::EGFP (Phase 0)* **(A-B,E)** with corresponding *MI06217* negative controls **(C-D,F)**. Green is chicken anti-GFP (chGFP, Ab13970) and blue is anti-Dlg. Medial (M) is right and dorsal (D) is up for **(A-D)**; and anterior is up, medial is at vertical midline for **(E-F)**. Scale bar: 20 μm.

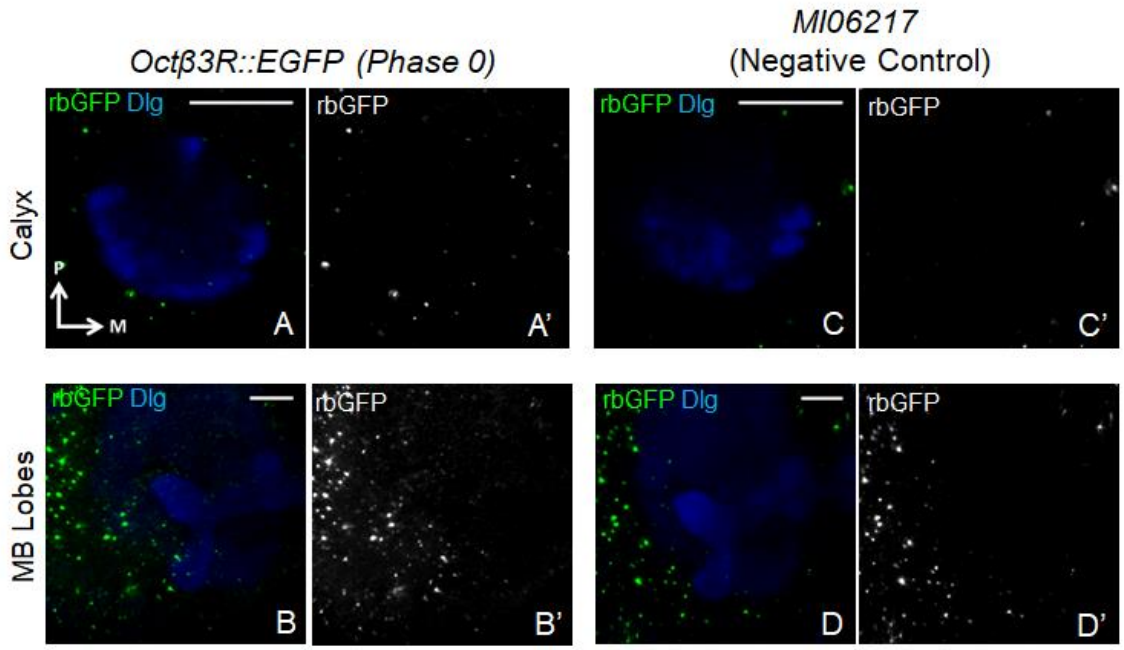

Figure 5.39. No EGFP signal observed in larval MB calyx or lobes in *Octβ3R::EGFP (Phase 0)* brains labelled with rabbit anti-GFP. Single confocal optical sections of the dorsal larval brain of *Octβ3R::EGFP (Phase 0)* **(A-B)** with *MI06217* negative controls **(C-D)**. Green is rabbit anti-GFP (rbGFP, A11122) and blue is anti-Dlg. Medial (M) is right and posterior (P) is up. Scale bar: 20 μm.

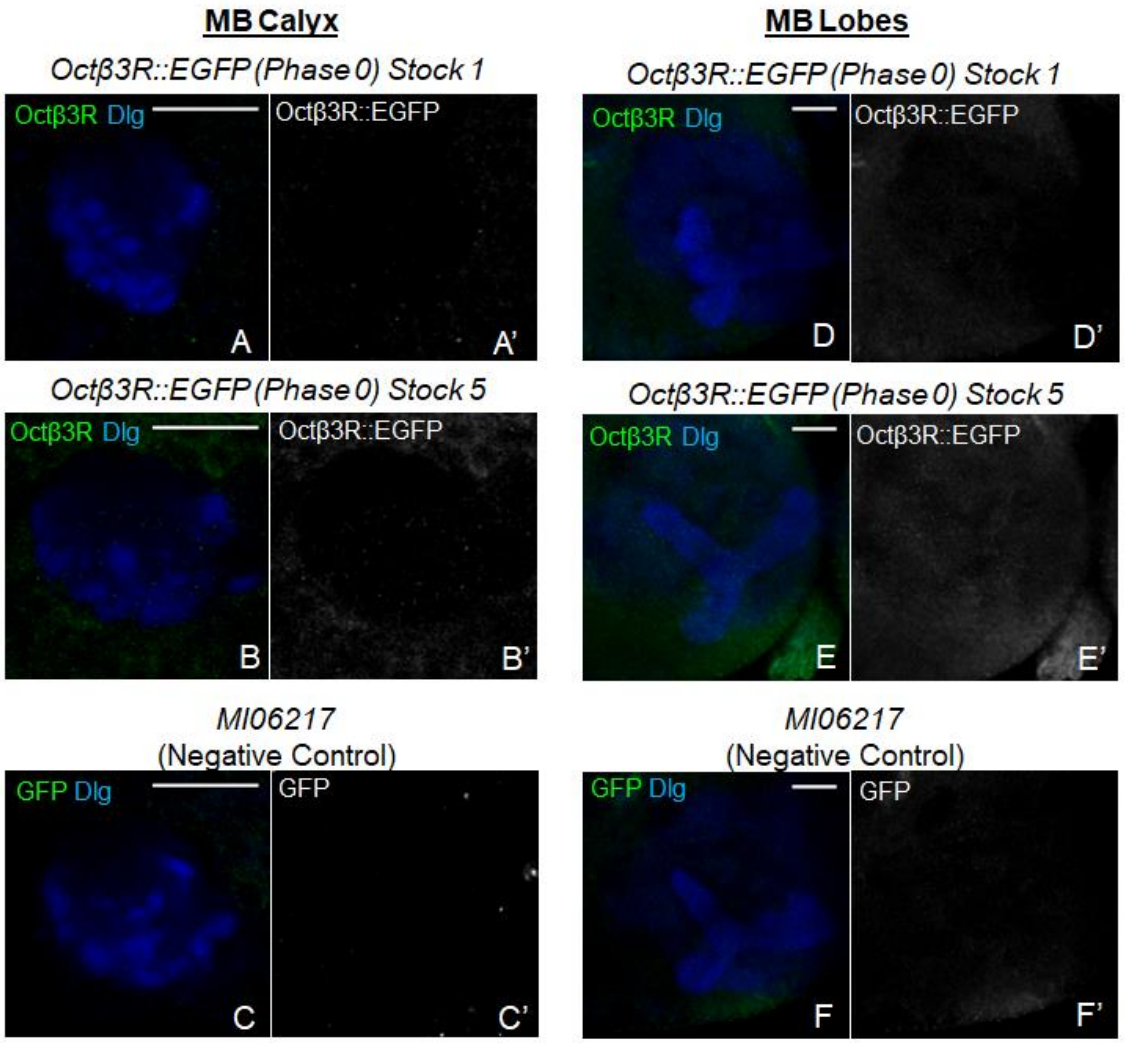

Figure 5.40. No EGFP signal observed in larval MB calyx or lobes in two other *Octβ3R::EGFP (Phase 0)* stocks. Single confocal optical sections of the MB calyx and lobes of *Octβ3R::EGFP (Phase 0) Stock 1* **(A,D)**; *Octβ3R::EGFP (Phase 0) Stock 5* **(B,E)**; and *MI06217* negative control **(C,F)**. Green is chicken anti-GFP and blue is anti-Dlg. Medial (M) is right and posterior (P) is up. Scale bar: 20 μm.

5.3. Discussion

While previous studies have shown that Octβ1R, Octβ2R and Octβ3R were expressed in the larval CNS using *in situ* hybridisation and promoter-*GAL4* lines (Ohhara et al., 2012; El-Kholy et al., 2015), the neuronal types expressing these OctβRs had not been identified. Strong expression of *Octβ3R-GAL4* in both adult and larval MBs (El-Kholy et al., 2015) suggest that Octβ3R localised to calyx-innervating neurons. On the contrary, *Octβ1R-GAL4* and *Octβ2R-GAL4* were expressed in adult but not in larval MBs (El-Kholy et al., 2015), suggesting that Octβ1R and Octβ2R only localised to calyx-innervating neurons but not in larvae. Octβ1R and Octβ2R expression in adult KCs were confirmed in KC-specific RNA sequencing (Crocker et al., 2016) and consistent with anti-Octβ2R labelling in α'β' KCs in the MB lobes (Wu et al., 2013).

In situ hybridisation, cell-type-specific RNA sequencing and *GAL4* expression can only be used to identify neuronal types expressing OctβRs, but not their subcellular localisation, unlike antibody labelling and protein traps. Moreover, promoter-*GAL4* lines may not always faithfully represent endogenous expression of OA receptors (Chapter 4). As specific Octβ1R and Octβ3R antibodies were unavailable and difficult to develop (El-Kholy et al., 2015), and I did not have access to anti-Octβ2R (Wu et al., 2013), the best available method to examine subcellular localisation of OctβRs in calyx-innervating neurons was to use protein traps.

By using the Octβ1R::EGFP fusion (Venken et al., 2011a; Nagarkar-jaiswal et al., 2015), I directly showed Octβ1R subcellular localisation to the larval MB calyx for the first time. This result is consistent with Octβ1R expression in adult KCs (Crocker et al., 2016), but contradicts the lack of *Octβ1R-GAL4* expression in larval MBs (El-Kholy et al., 2015). I also showed Octβ2R::EGFP, and possibly Octβ1R::EGFP, localisation to a subset of olfactory PN cell bodies, which has not been previously explored. I will discuss the implications of these findings on the calyx circuitry in the following sections.

Out of the four OctβR fusion proteins used in this chapter, only Octβ1R::EGFP localised to the neuronal terminals. Octβ2R::EGFP signal localised to cell bodies only, although this is expected to more accurately show Octβ2R-expressing neurons than promoter-*GAL4* lines; and their identities can be verified using molecular markers which would be difficult to conduct with *in*

situ hybridisation. Finally, neither of the Octβ3R::EGFP fusions showed any signal in the larval brain, contrary to the expectations from *in situ* and promoter-*GAL4* results (Ohhara et al., 2012; El-Kholy et al., 2015). This will be further discussed in Section 5.3.6.

5.3.1. Possible extrasynaptic regulation of KCs via Octβ1R

The diffuse pattern of Octβ1R::EGFP localisation in the larval MB calyx best matches that of KC dendrites innervating the calyx, and not the innervation pattern of other calyx-innervating neurons, suggesting that Octβ1R localised to KC dendrites (Fig. 5.41). This may be validated in the future by knocking down Octβ1R::EGFP signal with EGFP RNAi in the calyx with a specific KC driver. Octβ1R::EGFP signal was also detected in small dorsal cell bodies resembling KC cell bodies; but their identity should be verified through colocalisation with a KC marker. This is consistent with Octβ1R transcripts detected in adult KC cell bodies through RNA sequencing (Crocker et al., 2016), and suggest that Octβ1R localisation to KCs may be conserved from larvae to adults.

Octβ1R localisation to KC dendrites suggest that sVUM1 neurons innervating the larval MB calyx could directly target KC dendrites despite the limited KC-sVUM1 synaptic connections based on GRASP results (Chapter 3). Extrasynaptic Octβ1R on KCs would allow for the mass modulation of many KCs without the need for a large amount of synaptic connections.

It is unclear whether Octβ1R would act as an inhibitory or excitatory receptor on KCs; as it has been shown to couple to an increase of cAMP levels which is associated with increase in neuronal excitability (Balfanz et al., 2005; Maqueira et al., 2005), as well as decrease in cAMP levels associated with hyperpolarisation (Koon and Budnik, 2012), in different cell types. Therefore, to determine the effects of sVUM1 signalling on KCs via Octβ1R, it is necessary to investigate how the absence of Octβ1R may impact KC activity using electrophysiological or calcium imaging methods. Nevertheless, this suggests that sVUM1 may directly modulate KC activity via Octβ1R, adjusting the sparseness of odour representations in KCs, and therefore whether odours can be discriminated.

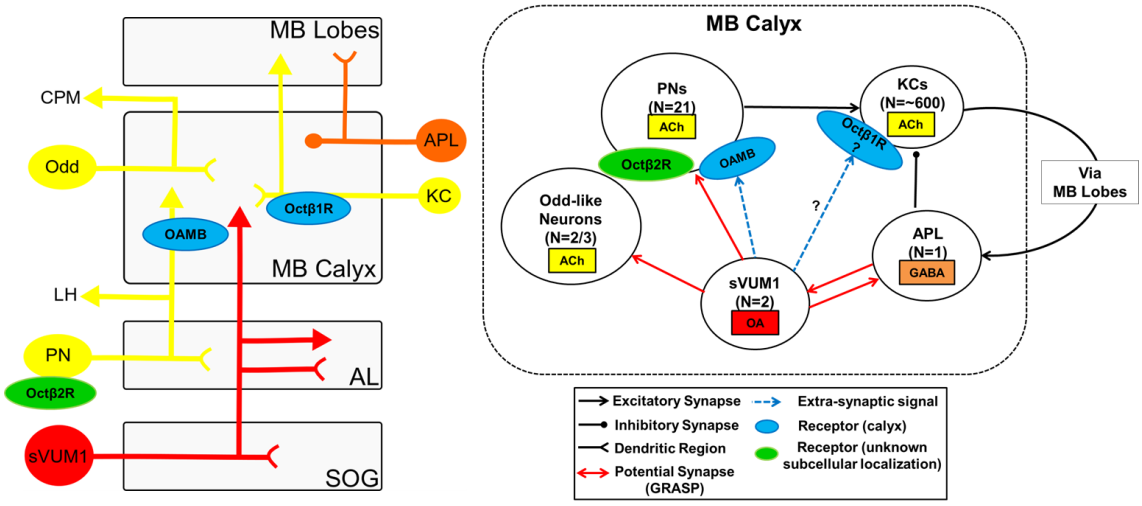

Figure 5.41. Proposed OctβR localisation pattern in larval MB calyx circuitry. Abbreviations: ACh, acetylcholine; AL, antennal lobe; CPM, centroposterior medial compartment; KC, Kenyon Cell; LH, lateral horn; MB, mushroom body; N, number; OA, octopamine; PN, projection neuron.

Octβ2R::EGFP localised to few dorsal cell bodies that may belong to KCs. This remains to be verified through colocalisation with a KC marker, as only a small number of Octβ2R::EGFP-positive cell bodies were observed, compared to the large number of KC cell bodies expected in that region. There is no further evidence that Octβ2R localised to KC dendrites, as the *Octβ2R::EGFP* stock did not show localisation to neuronal processes. This uncertain result is not necessarily contradictory to Octβ2R localisation to adult KCs. While Octβ1R transcripts were observed in α, β and γ KCs, Octβ2R transcripts appeared to more enriched in αβ KCs (Crocker et al., 2016). Moreover, anti-Octβ2R labelling has only been observed in the α'β' MB lobes (Wu et al., 2013), suggesting that Octβ2R may specifically localise to α'β' KCs. Only γ KCs are already born at the L3 stage, while α'β' KCs are beginning to be born at this stage and αβ KCs will not be born until later (Lee et al., 1999). Therefore, the few small dorsal cell bodies expressing Octβ2R::EGFP may belong to newborn α'β' KCs which are not yet fully developed.

5.3.2. Possible co-expression of OA receptors in PNs

In addition to OAMB localisation to the majority of PN terminals in the calyx, I found that around half of the PN cell bodies weakly expressed Octβ2R::EGFP (Fig. 5.41). As Octβ2R::EGFP did not localise to terminals, it is unclear whether OAMB and Octβ2R localised to the same compartments of the PNs they are co-expressed in. If OAMB and Octβ2R both localised to calyx glomeruli, I hypothesise that OAMB and Octβ2R would be activated under different OA concentrations. This would therefore allow PNs co-expressing both receptors at their terminals to respond differently depending on fluctuations of OA concentration. On the other hand, co-expression of OAMB and Octβ2R in different PN compartments would allow PNs to produce a site-specific response to different sources of OA.

Some PN dendrites may also express Octβ1R in the AL. While Octβ1R::EGFP only localised weakly to very few PN cell bodies, there was a medial AL glomerulus where Octβ1R::EGFP was strongly localised. This AL glomerulus may be 35a, 42b, 67b or 74a based on its position (Masuda-Nakagawa et al., 2009). This suggests that Octβ1R localised to the dendrites of a specific PN. As sVUM1 neurons are the only source of OA innervation in the

larval AL (Selcho et al., 2014), it is likely that Octβ1R present on PN dendrites receive OA signalling from sVUM1 neurons. As Octβ1R::EGFP does not appear to localise to discrete calyx glomeruli, Octβ1R is unlikely to localise to presynaptic terminals of PNs in the calyx, and therefore unlikely to mediate sVUM1 signalling there.

As Octβ1R and Octβ2R were expressed in a smaller subset of PNs compared to OAMB, differential OA receptor localisation may present a mechanism for restricting the action of widespread OA signalling to particular neurons. This also suggested that different PNs may respond to OA signalling in different ways based on the types of OA receptors they expressed.

Possible OAMB, Octβ1R and Octβ2R co-expression in PNs is similar to the possible co-expression of Octβ1R and Octβ2R in OA/TA neurons (Koon et al., 2011; Koon and Budnik, 2012), and that of α1- and α2-adrenoceptors in the rat olfactory bulb (Nai et al., 2010). This suggests that receptor co-expression on the same neurons may be a common and important feature in noradrenergic-like neuromodulatory circuitry. This may allow octopamine or noradrenaline to exert a large range of effects on the same neurons depending on the type of receptor activated.

5.3.3. OctβRs unlikely to be OA autoreceptors on sVUM1 neurons

Contrary to expectation, I also did not find any evidence for OA autoreceptors on sVUM1 neurons. Octβ1R did not localise to calyx terminals of sVUM1 neurons, while it was inconclusive whether Octβ2R localised to sVUM1 neurons.

The larval NMJ is the only system in which potential Octβ1R and Octβ2R autoreceptors have been reported in *Drosophila*. The antagonising effects on synaptic growth due to Octβ1R and Octβ2R knockdown in *Tdc2-GAL4* line was used to infer the presence of these receptors on OA Type II motorneurons (Koon et al., 2011; Koon and Budnik, 2012). However, as *Tdc2-GAL4* labelled the majority of OA/TA neurons, it is unknown whether Octβ1R and Octβ2R were expressed on all the OA and TA neurons labelled, only TA neurons or a subset of the neurons labelled. As the authors did not show whether Octβ1R and Octβ2R localised to the presynaptic terminals of OA neurons, it would be useful to explore whether Octβ1R::EGFP and Octβ2R::EGFP signal can be detected

in OA motorneurons in the larval NMJ in the future, to validate whether any of the OctβRs act as autoreceptors on OA neurons.

5.3.4. OctβR localisation to APL or Odd-like neurons not yet identified

I did not manage to determine whether any of the OctβR localised to the calyx terminals of the APL neuron or Odd-like neurons so far. The lack of Octβ1R::EGFP-positive tracts or boutons in the calyx suggest that Octβ1R is unlikely to be localised to the calyx terminals of APL or Odd-like neurons. However, I could not draw a conclusion as to whether Octβ2R or Octβ3R localised to APL or Odd-like neurons.

Identifying Octβ2R colocalisation with calyx-innervating neuron drivers has been challenging thus far. Firstly, the Octβ2R::EGFP protein does not localise to terminals, so Octβ2R localisation can only be identified from Octβ2R::EGFP signal in cell bodies. This is problematic because it is unclear whether Octβ2R is normally localised to the calyx, and thus whether it may be involved in mediating sVUM1 signalling in the calyx circuitry. As the EGFP insertion prevented Octβ2R::EGFP targeting to terminals, it is possible that it also altered Octβ2R::EGFP expression patterns, such that Octβ2R::EGFP may not even be expressed in the same neurons as those expressing Octβ2R. This is possible but unlikely, as Octβ2R::EGFP remains under the control of the same promoter and regulatory elements as the native Octβ2R protein. Instead, Octβ2R::EGFP is probably transcribed and translated in neurons that express Octβ2R, but retained in the ER in the cell body as the EGFP fusion prevents correct folding of the protein.

Next, the background GFP signal detected in the Odd-like neuron cell body labelled in *R68B12>RFP* negative control brains made it difficult to discern whether GFP signal detected in that of *R68B12>RFP, Octβ2R::EGFP* brains was signal or background. It may be possible to eliminate *R68B12>RFP* signal bleedthrough to the GFP channel by using an alternative driver line to label Odd-like neurons, a different red fluorescent reporter, omitting anti-DsRed amplification of the *R68B12>RFP* signal, or adjusting bandpass filters to further restrict the emission frequency range detected by the confocal microscope detector. Instead of using a red fluorescent reporter to label Odd-like neurons in *R68B12-GAL4*, a non-fluorescent epitode tag such as V5 or FLAG together with

a far-red secondary antibody such as Alexa 647, could further ensure that there is minimal spectral overlap between Octβ2R::EGFP and *R68B12* signals to prevent signal bleed through.

Furthermore, the signal from a single copy of Octβ2R::EGFP is weak. Therefore, it is necessary to ensure homozygosity of the *Octβ2R::EGFP* cassette on the third chromosome, as in the Octβ2R-PN colocalisation experiment. However, this limits the use of driver lines only to those on other chromosomes. For the Octβ2R-APL colocalisation, *NP732-GAL4* on the X chromosome (Masuda-Nakagawa et al., 2014) should be used with homozygous *Octβ2R::EGFP*. For Octβ2R-Odd colocalisation, the third chromosome *R68B12-GAL4* construct should be replaced with the second chromosome *R68B12-LexA* driver which also labels a single Odd-like neuron. However, *R68B12-GAL4/LexA* only label one Odd-like cell body, while *OK263-GAL4* cell bodies do not all project to the calyx. Hence, it is currently not possible to validate whether Octβ2R::EGFP localised to all the calyx-innervating Odd-like cell bodies.

Therefore, in the future, measures to maximise Octβ2R::EGFP signal and minimise bleed through together with appropriate negative controls must be used to validate the identity of Octβ2R-positive cell bodies.

5.3.5. Other issues with Octβ1R::EGFP and Octβ2R::EGFP fusions

As there are no Octβ1R antibodies available, the Octβ1R::EGFP fusion protein is currently the best and only tool to identify Octβ1R subcellular localisation. However, as *Octβ1R::EGFP* is homozygous lethal, the Octβ1R::EGFP fusion protein is not fully functional. This suggests that EGFP insertion interferes with Octβ1R function, and it is possible that this may cause Octβ1R::EGFP mislocalisation, such that it may not represent the normal localisation pattern of Octβ1R. This may be because EGFP insertion in Octβ1R::EGFP is within 5 amino acids from a clathrin-associated binding motif which regulates internalisation and lysosomal targeting (Maqueira et al., 2005). However, Octβ1R::EGFP may still be initially targeted to the correct destination, but accumulate at these locations as it is prevented from internalisation and recycling. It is also plausible that Octβ1R::EGFP is non-functional because the EGFP insertion is disrupting other functional binding domains that do not affect

localisation. Ideally, multiple Octβ1R protein traps in which EGFP is inserted at different locations should be compared for consistency to best represent Octβ1R locazation. These may be generated by the existing MiMIC lines *MI06725* and *MI09054* which are inserted in coding region introns of some but not all of the Octβ1R protein isotypes (Venken et al., 2011a; Nagarkar-Jaiswal et al., 2015); or by targeted EGFP knock-in using CRISPR (Xue et al., 2014).

Provided that Octβ1R::EGFP is localised to the same targets as the functional Octβ1R protein, the other challenge is that *Octβ1R::EGFP* must be maintained heterozygously. Unlike OAMB::EGFP and Octβ2R::EGFP fusions, the weak Octβ1R::EGFP signal cannot be further amplified by using homozygous flies that have double the copy number of EGFP fusion proteins. Therefore, alternative methods must be used to increase Octβ1R::EGFP signal (Chapter 9).

As discussed in Section 5.3.4., Octβ2R::EGFP signal is only observed in cell bodies and may also be at risk of misexpression. The lack of Octβ2R::EGFP membrane localisation is probably because the EGFP insertion is only one amino acid away from a TM, and hence affected TM insertion and subsequently membrane targeting. The EGFP insertion is also within 5 amino acids away from a clathrin-associated binding motif which may also affect subcellular localisation. As Octβ2R::EGFP does not reflect subcellular localisation, it may be useful to replace the EGFP cassette with T2A-GAL4 to map the identity of neurons Octβ2R may be expressed in, because T2A-GAL4 shows stronger signals and the full innervation patterns of these neurons (Diao et al., 2015; Gnerer et al., 2015). As T2A-GAL4 is inserted in a coding region intron of *Octβ2R*, its expression is also controlled by the same regulatory elements, which should better represent Octβ2R expression than promoter-*GAL4* lines. The disadvantage for using the T2A-GAL4 system is that a non-GAL4 transcriptional driver must be used for colocalisation experiments with calyx-innervating neurons; and this is not available for the APL neuron. At the moment, the best alternative to map Octβ2R localisation in the larval MB calyx is the Octβ2R antibody (Wu et al., 2013) which I did not manage to obtain for this study.

5.3.6. Lack of Octβ3R::EGFP in the larval brain

The lack of EGFP signals in the larval brain in both *Octβ3R::EGFP (Phase 1)* and *Octβ3R::EGFP (Phase 0)* stocks was unexpected. Between the two EGFP insertion phases, all Octβ3R protein isotopes including the 5 TM Octβ3R-PK isotype should contain the EGFP tag in the correct orientation for expression. It is possible that not all Octβ3R isotypes were expressed; and therefore, Octβ3R::EGFP signal might not be observed for at least one of the stocks. Another reason could be that Octβ3R expression levels in the larval brain were absent or too low to be detected. However, this was contrary to the fact that *Octβ3R* transcripts were detected in the larval brain using *in situ* hybridisation (Ohhara et al., 2012; El-Kholy et al., 2015). Moreover, I did not detect any Octβ3R::EGFP signals in the adult brain (data not shown). However, as *Drosophila* embryos show much higher Octβ3R mRNA levels than larvae or adults (Ohhara et al., 2012), it may be useful to check whether Octβ3R::EGFP signal can be detected at the embryonic stages in the future to confirm whether the problem lies with the *Octβ3R::EGFP* stocks.

The MiMIC insertion site in the *MI06217* stock used to generate these protein traps was not predicted to disrupt TM insertion – one of the most likely causes of protein misfolding and prevention of correct receptor localisation. However, the MiMIC insertion might have disrupted another conserved site that was integral for Octβ3R expression or localisation. Nevertheless, as I cannot determine whether the *Octβ3R::EGFP* stocks are functional or not, another Octβ3R protein trap or antibodies against Octβ3R would be required to show whether Octβ3R proteins are expressed in the larval brain.

Chapter 6. Expression of α2-adrenergic-like Octα2R in calyx-innervating neurons

6.1. Introduction

In addition to excitatory α1- and β-adrenoceptors, NA can also act via inhibitory α2-adrenoceptors, which have been shown to cause hyperpolarisation. In the larval calyx circuitry, I hypothesise that OA signalling from sVUM1 neurons has the flexibility of increasing or decreasing neuronal excitability of different calyx-innervating neurons mediated by both excitatory and inhibitory OA receptors.

It has recently come to our knowledge that the *CG18208* gene encodes a receptor that not only shares strong sequence similarities to the human α2-adrenoceptor, but is also preferentially activated by OA (Qi et al., 2017). Similar to the cellular effects observed upon α2-adrenergic activation, activating the *CG18208*-encoded receptor also decreases intracellular cAMP levels and does not appear to affect intracellular calcium concentration. This receptor has now been renamed as Octα2R (Qi et al., 2017); and is likely to be the main OA receptor that mediates inhibitory functions of OA signalling in *Drosophila*.

As Octα2R is newly cloned and characterised, it is not known where it is expressed in the *Drosophila* adult or larval CNS. As an α2-adrenergic-like receptor, it is probably localised to both pre- and post-synaptic terminals (Aoki et al., 1994; Rosin et al., 1996); where its presynaptic localisation is likely to regulate neurotransmitter release (Hein, 2006). It may also be co-expressed with excitatory OA receptors to mediate opposing functions; similar to the co-expression of α1- and α2-adrenocepters on granule cells of the mammalian olfactory bulb (Nai et al., 2009). In addition, the presence of α2-autoreceptors at the presynaptic terminals of NA neurons (Aoki et al., 1994) suggests that Octα2R may also be localised to presynaptic terminals of sVUM1 neurons in the larval MB calyx.

In this chapter, I aimed to determine whether sVUM1 signalling could be mediated by the inhibitory Octα2R in the larval MB calyx to inhibit particular types of calyx-innervating neurons (Fig. 6.1):

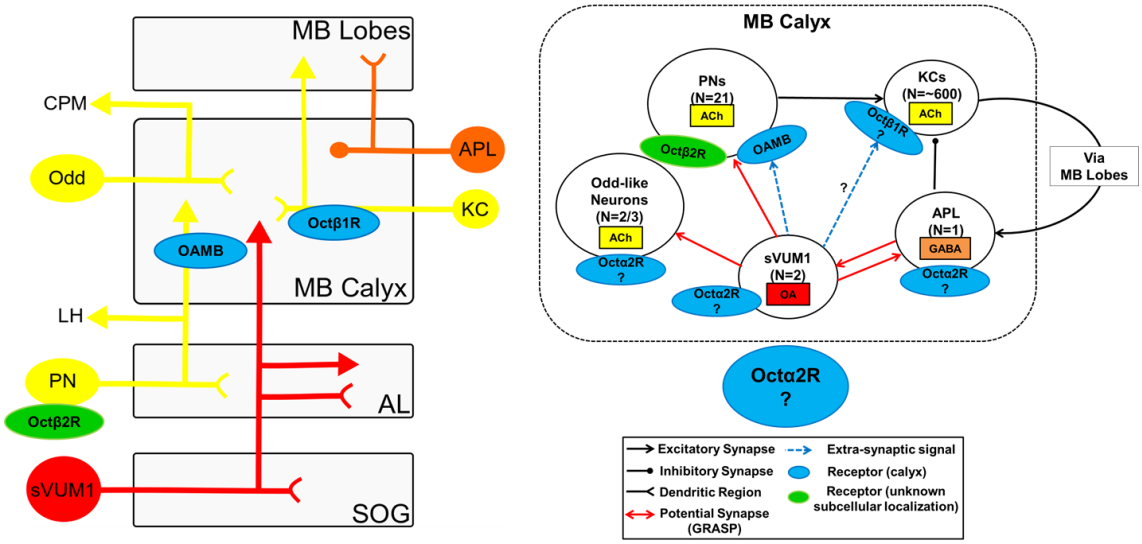

Figure 6.1. Hypothesised Octα2R localisation pattern in larval MB calyx circuitry. Abbreviations: ACh, acetylcholine; AL, antennal lobe; CPM, centroposterior medial compartment; KC, Kenyon Cell; LH, lateral horn; MB, mushroom body; N, number; OA, octopamine; PN, projection neuron.

I hypothesised that Octα2R may be localised to the APL neuron and Odd-like neurons – for which I have yet to identify OA receptors that localise to their calyx terminals. I further hypothesised that Octα2R, similar to its mammalian counterpart α2-adrenoceptor, may act as an autoreceptor for sVUM1 neurons themselves. To explore the endogenous localisation of Octα2R in calyx-innervating neurons, I generated a novel Octα2R::EGFP protein trap in the first attempt to map α2-adrenergic-like receptor expression in insects.

6.2. Results

6.2.1. A novel EGFP-tagged CG18208(Octα2R) line

To visualise the expression of Octα2R in the larval MB calyx, I generated a CG18208(Octα2R)::EGFP protein trap using the *MI10227* line from the MiMIC collection (Venken et al., 2011a; Fig. 6.2).

MI10227 contained the MiMIC cassette in coding region intron 1 of the *CG18208* gene, which corresponded to amino acid position 268 (Fig. 6.3) and thus the extracellular domain between TM IV and V of CG18208 proteins (Fig. 6.4). Therefore, the position of the MI10227 insertion was not expected to disrupt TMs. I confirmed the MI10227 insertion location in the *CG18208* gene by PCR reactions against the 5' and 3' flanking ends of the MI10227 insertion site (Fig. 6.5) and subsequent sequencing of the PCR products (Fig. S8, S9).

Nine recombinant *CG18208::EGFP* stocks were recovered after introducing EGFP cassette to *MI10227*. To identify a recombinant stock that was expected to express EGFP, I conducted PCR reactions for four of the new recombinant stocks. As the MI10227 insertion was in the opposite direction to the *CG18208* gene, PCR products detected for PCR2 and PCR3 reactions indicated the correct EGFP cassette orientation for expression (Fig. 6.6A).

CG18208::EGFP Stock 4 was the only recombinant stock out of the four stocks assayed to show robust bands for PCR2 and PCR3 reactions (Fig. 6.6B), and therefore predicted to express Octα2R::EGFP (Table 6.1). This stock was designated as *CG18208::EGFP*.

Insertion MI10227

Gene Information

Affected Gene(s)
CG18208

Position	CG18208 - coding intron
Phase	CG18208-RA:0, CG18208-RB:0, CG18208-RC:0

Release 6 Annotation

Scaffold	Coordinate	Strand	Site	GBrowse Link
3R	18847297	+	91D2	3R:18847297

FlyBase Annotation	Transposon
FBti0156705	Mi{MIC}

Stock Availability

Donor/Collection	Stockcenter Designation	Stock No.
GDP	Bloomington	53233

Flanking Sequence

MI10227-3' (KG702191)	TATAAAGAAATTGCTGTTGCTATTCAAGTAATTTGAAGATATTTATAAGC CAAGCCGTTGATTATGGTTCGAATAACAGAATTTTATAAAAGTTTAATAA TCTTCCATACTCCACACACATCACACCAGAAAATAGCCAATTGGGCAGCA CACACGATGCTTTTCAATTCCACAACCCGTCTGAATTTTCATTGTTCGAT TGTCGGTGGGGCAACGTCAATTGCCGTCAATTGGCGTCAATTTCGCATGG GATGTGGATTATTGCGCCACTTAGGAGCACCACTTGCCACTTACCTCGCA CTTGGGCAGCGGTCCCTCGGGCATCTTCACCTTCCAGCCGAGGAGCGGCG GTATGCAGATGAGGGCGGACATAATCCAGACCGCCGTGATC
MI10227-5' (KG702192)	AACACTTTGAAACCTAGAATCTCAAGCCAAATATATGTAGTGTTATAAAA ACGTCATACAAGTTAGTAAAAAATTAAAGTGATTAAATTATATGGGTTTC AACTATAAATATGTGGGGTTTA

Figure 6.2. *MI10227* insertion stock listed on the Gene Disruption Project Database. (http://flypush.imgen.bcm.tmc.edu/pscreen/details.php?line=MI10227).

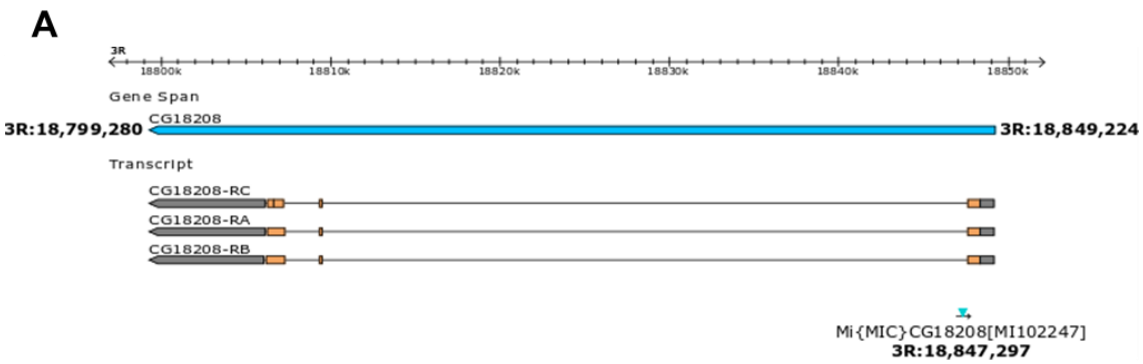

B. CG18208-PA tblastn alignment to *Drosophila* sequences

```
Exon 1
Query:    241   IMSALICIPPLLGWKVKMPEGPLPKCELS         269
                IMSALICIPPLLGWKVKMPEGPLPKCE+S
18847671        IMSALICIPPLLGWKVKMPEGPLPKCEVS         18847585

Exon 2
Query:    259   PEGPLPKCELSEDIGYVLYSALGSFYIPSCIMVFVYIRIYFAAKARARRGIKKHPRKTNN        318
                P       +LSEDIGYVLYSALGSFYIPSCIMVFVYIRIYFAAKARARRGIKKHPRKTNN
18809550        PSSFFDLLQLSEDIGYVLYSALGSFYIPSCIMVFVYIRIYFAAKARARRGIKKHPRKTNN
        18809371
```

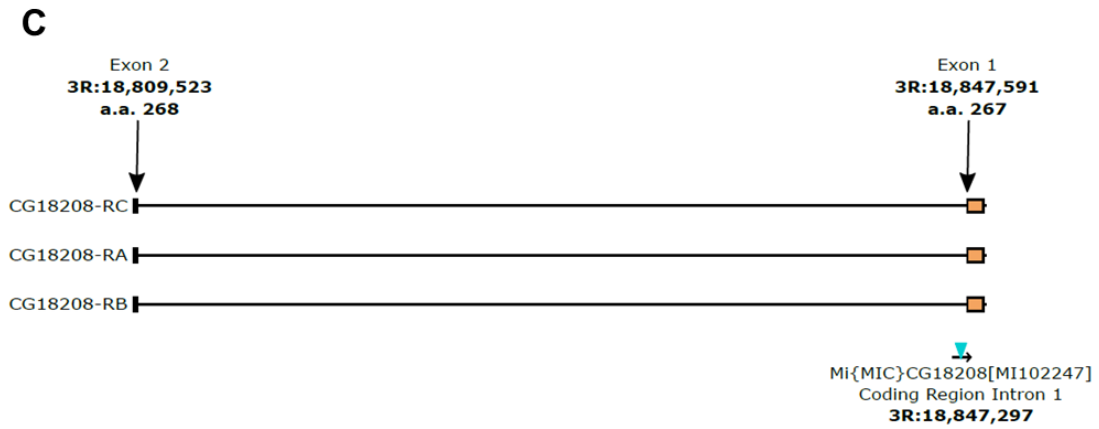

Figure 6.3. MI10227 insertion was in coding region intron 1 of the *CG18208* gene. (A) Map of MI10227 insertion relative to *CG18208* gene and transcripts (Adapted from GBrowse). **(B)** Amino acid coordinates for the MI10227 insertion site based on tblastn alignment with *CG18208* transcripts. **(C)** Magnified map of MI10227 insertion in coding region intron 1 of *CG18208* transcripts with genomic and amino acid coordinates.

CG18208-PA TMHMM Predictions

WEBSEQUENCE	TMHMM2.0	outside	1	116
WEBSEQUENCE	TMHMM2.0	TMhelix	117	139
WEBSEQUENCE	TMHMM2.0	inside	140	151
WEBSEQUENCE	TMHMM2.0	TMhelix	152	174
WEBSEQUENCE	TMHMM2.0	outside	175	188
WEBSEQUENCE	TMHMM2.0	TMhelix	189	211
WEBSEQUENCE	TMHMM2.0	inside	212	231
WEBSEQUENCE	TMHMM2.0	TMhelix	232	254
WEBSEQUENCE	TMHMM2.0	outside	255	273
WEBSEQUENCE	TMHMM2.0	TMhelix	274	296
WEBSEQUENCE	TMHMM2.0	inside	297	625
WEBSEQUENCE	TMHMM2.0	TMhelix	626	648
WEBSEQUENCE	TMHMM2.0	outside	649	662
WEBSEQUENCE	TMHMM2.0	TMhelix	663	685
WEBSEQUENCE	TMHMM2.0	inside	686	699

MI10227 insertion site: a.a. 268

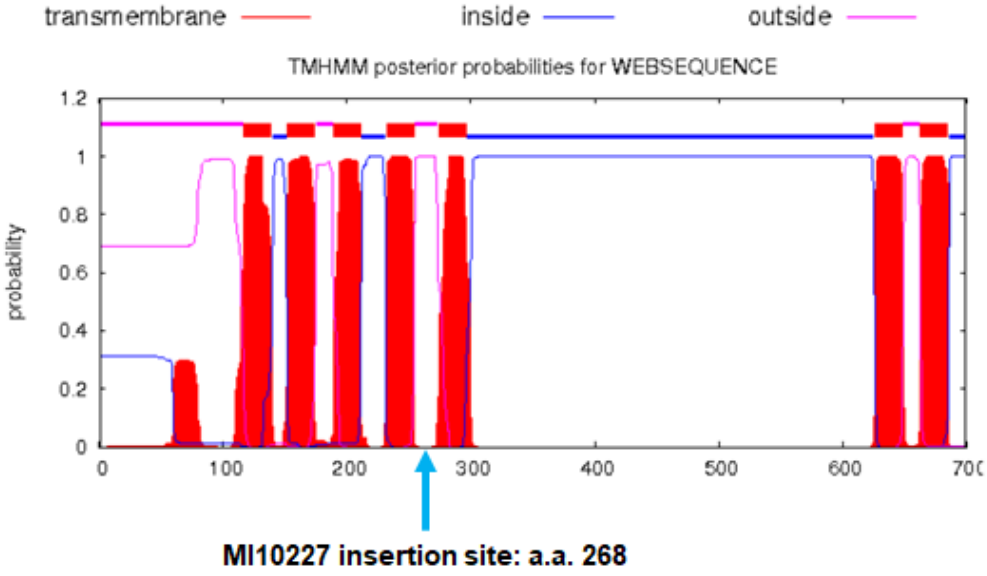

Figure 6.4. MI10227 insertion was between TM IV and V of CG18208/Octα2R proteins. MI10227 insertion site relative to TM predictions (TMHMM) for the CG18208/Octα2R-PA isotype as a representative example.

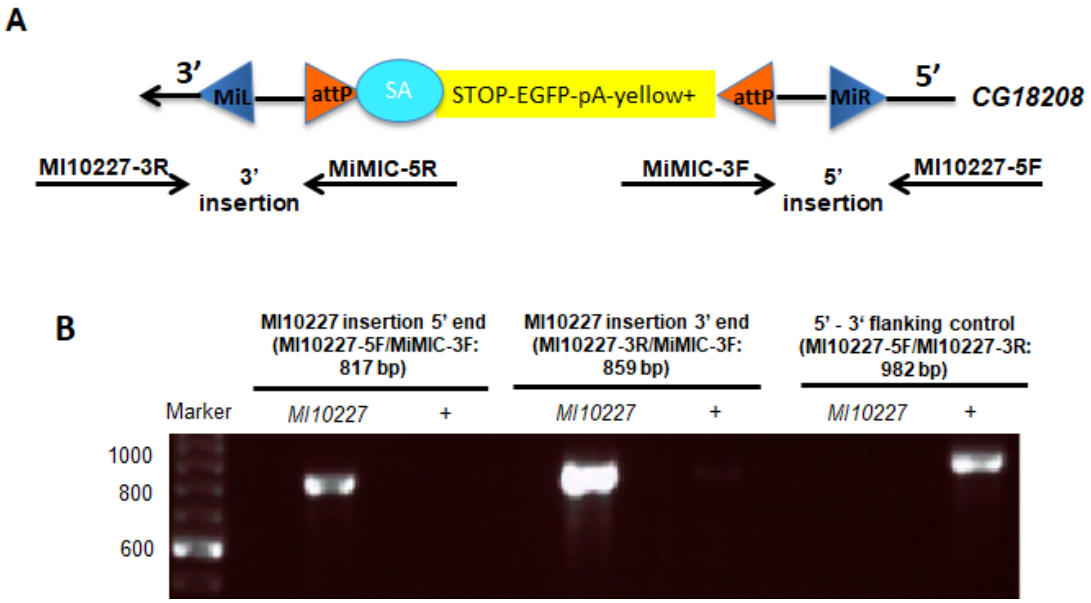

Figure 6.5. PCR verification of MI10227 insertion in the *CG18208* gene. (A) Primers designed against 5' and 3' flanking ends of the MI10227 insertion site in the *CG18208* gene. **(B)** PCR products were detected for 5' and 3' ends of the MI10227 insertion. *CS* (denoted as +) DNA was used as a wild type control.

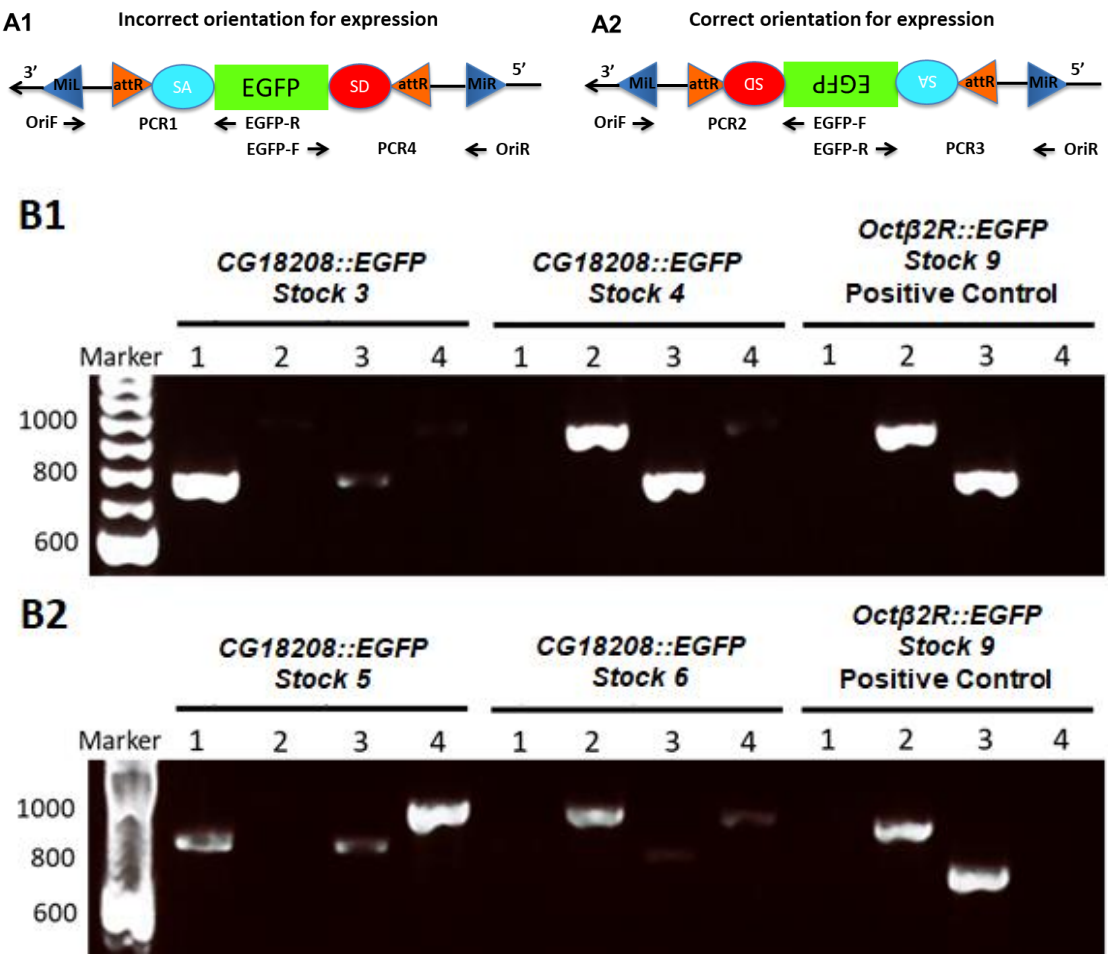

Figure 6.6. PCR validation of EGFP orientation in recombinant *CG18208::EGFP* stocks. **(A1)** Products for PCR1 and PCR 4 indicate EGFP insertion in the incorrect orientation for expression. **(A2)** Products for PCR2 and PCR3 indicate EGFP insertion in the correct orientation for expression. **(B)** Results for PCR reactions 1-4 for *CG18208::EGFP Stocks 3* and *4* **(B1)**; and *Stocks 5* and *6* **(B2)**. *Octβ2R::EGFP Stock 9* was used as a positive control for PCR2 and PCR3 reactions. Abbreviations: MiL/R, MiMIC sequences Left/Right; SA, splice acceptor site; SD, splice donor site; OriF, Orientation-MiL-F; OriR, Orientation-MiL-R; EGFP-F, EGFPdo-Seq-F; EGFP-R, EGFPdo-Seq-R.

Stock	PCR1	PCR2	PCR3	PCR4	Figure (PCR)	Expected expression
CG18208::EGFP Stock 3	+++	-	+	+	6.6B1	No
CG18208::EGFP Stock 4	-	+++	+++	+	6.6B1	Yes
CG18208::EGFP Stock 5	++	-	+	+++	6.6B2	No
CG18208::EGFP Stock 6	-	+++	+	+	6.6B2	Maybe

Table 6.1. One out of four recombinant *CG18208::EGFP* stocks contained EGFP in the correct orientation for expression. PCR products obtained from each of the PCR reactions (PCR1, PCR2, PCR3 and PCR4) were scored as follows: -, no bands observed; +, weak band observed; ++, strong band observed. PCR results were used to determine whether Octα2R::EGFP expression was expected (Expected Expression).

6.2.2. Octα2R::EGFP localised to cell bodies but not to neuropils

Octα2R::EGFP, the fusion protein produced from the *CG18208::EGFP* stock, did not localise to the larval MB calyx. Instead, I observed Octα2R::EGFP signals in cell bodies near the calyx (n=3; Fig. 6.7, arrowheads). The identity of these cell bodies was unclear. Many of them were larger than 5 μm in diameter (Fig. 6.7A-F, empty arrowheads), suggesting that they were not KC cell bodies.

To determine whether the lack of signal in the calyx is due to the retention of Octα2R::EGFP in cell bodies, I examined whether Octα2R::EGFP localised to other neuropils in the larval brain. Octα2R::EGFP localised only to cell bodies; but not to neuropils labelled by anti-Dlg or to any neuronal tracts or processes in the larval brain lobes viewed from both dorsal and frontal orientations (Fig. 6.8). This suggested that Octα2R::EGFP was not targeted to neuronal terminals. However, the *CG18208::EGFP* stock would still be useful for identifying neuronal cell bodies that expressed Octα2R through colocalisation experiments using molecular markers which label calyx-innervating neurons.

6.2.3. Octα2R::EGFP did not localise to KC cell bodies

I identified several Octα2R::EGFP-positive cell bodies immediately dorsal to the larval MB calyx (n=3; Fig. 6.9, arrowheads), where KC cell bodies are normally located (Fig. 4.16A). However, while KC cell bodies are usually 3-5 μm in diameter, most of the Octα2R::EGFP-positive cell bodies in the region were >5μm in diameter (Fig. 6.9, empty arrowheads). This suggested that Octα2R::EGFP was probably not expressed in KCs.

6.2.4. Octα2R::EGFP localised to GABAergic and PN cell bodies near AL

Octα2R::EGFP localised to cell bodies near the AL (Fig. 6.8B, 6.10). To differentiate cholinergic PN cell bodies from the cell bodies of GABAergic AL local neurons, I examined the colocalisation of Octα2R::EGFP with anti-GABA (Fig. 6.10). Anterior to the AL, I identified both Octα2R::EGFP-positive cell bodies that colocalised with anti-GABA (Fig. 6.10E, filled arrowheads) and others that did not (Fig. 6.10E, empty arrowheads). This suggested that Octα2R was expressed in a subset of AL local neurons, as well as in other non-

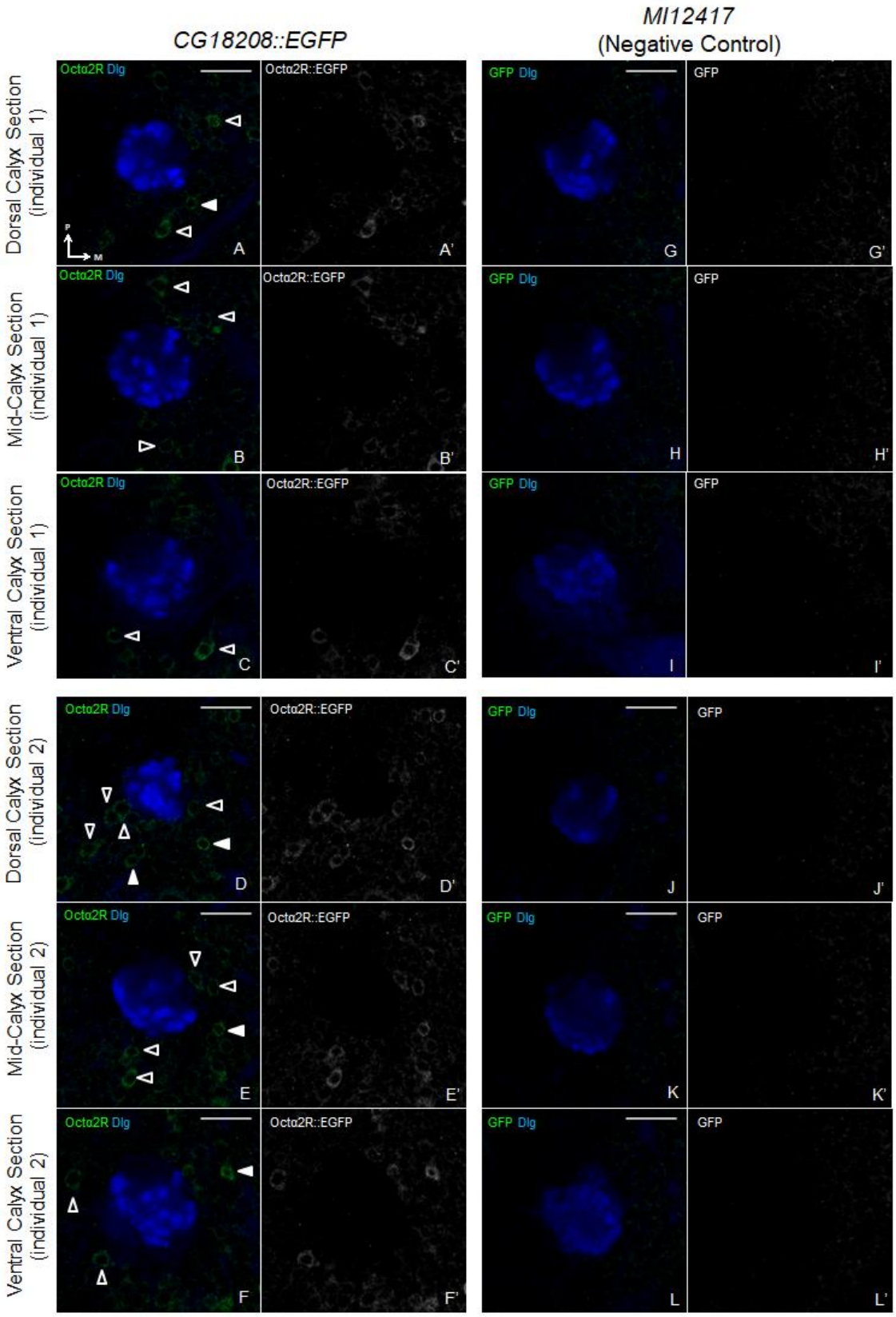

Figure 6.7. Octα2R::EGFP localised to cell bodies but not the larval MB calyx. Confocal optical sections of the calyx from two *CG18208::EGFP* individuals **(A-F)** with corresponding *MI12417* negative controls **(G-L)**. Green is Octα2R::EGFP and blue is anti-Dlg. Cell bodies >5 μm in diameter are indicated with empty arrowheads; cell bodies <5 μm in diameter are indicated with filled arrowheads. Medial (M) is right and posterior (P) is up. Scale bar: 20 μm.

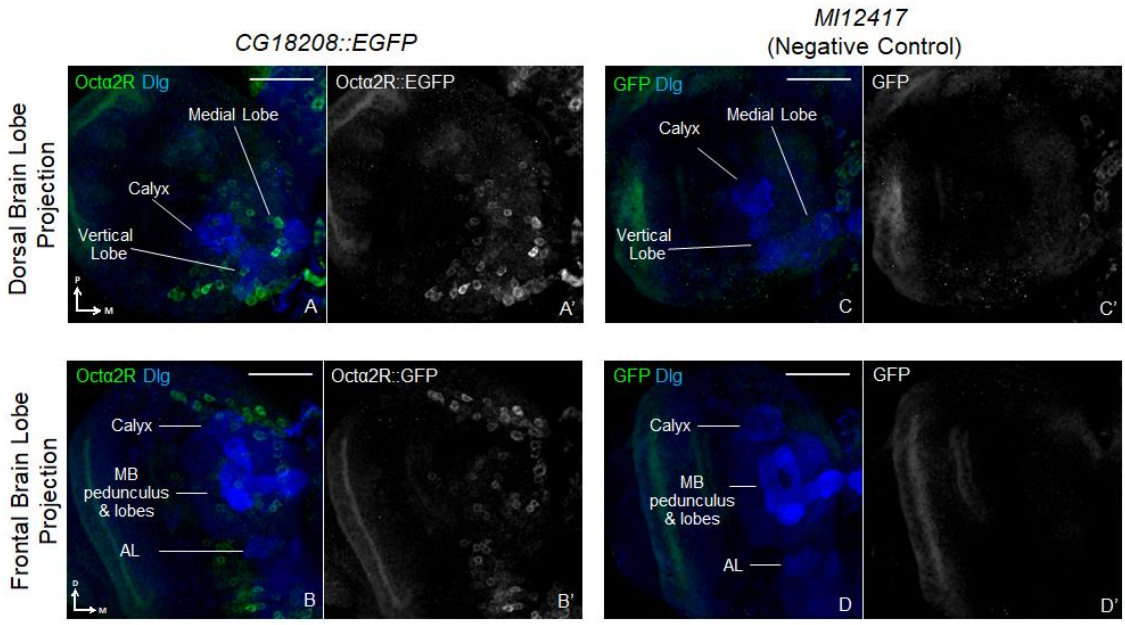

Figure 6.8. Octα2R::EGFP localised to cell bodies but not major neuropils in the larval brain. Confocal projections of the dorsal and frontal brain lobe of *CG18208::EGFP* **(A-B)** with corresponding *MI12417* negative controls **(C-D)**. Green is Octα2R::EGFP and blue is anti-Dlg. Medial (M) is right; posterior (P) is up for **(A,C)** and dorsal (D) is up for **(B,D)**. Scale bar: 50 μm.

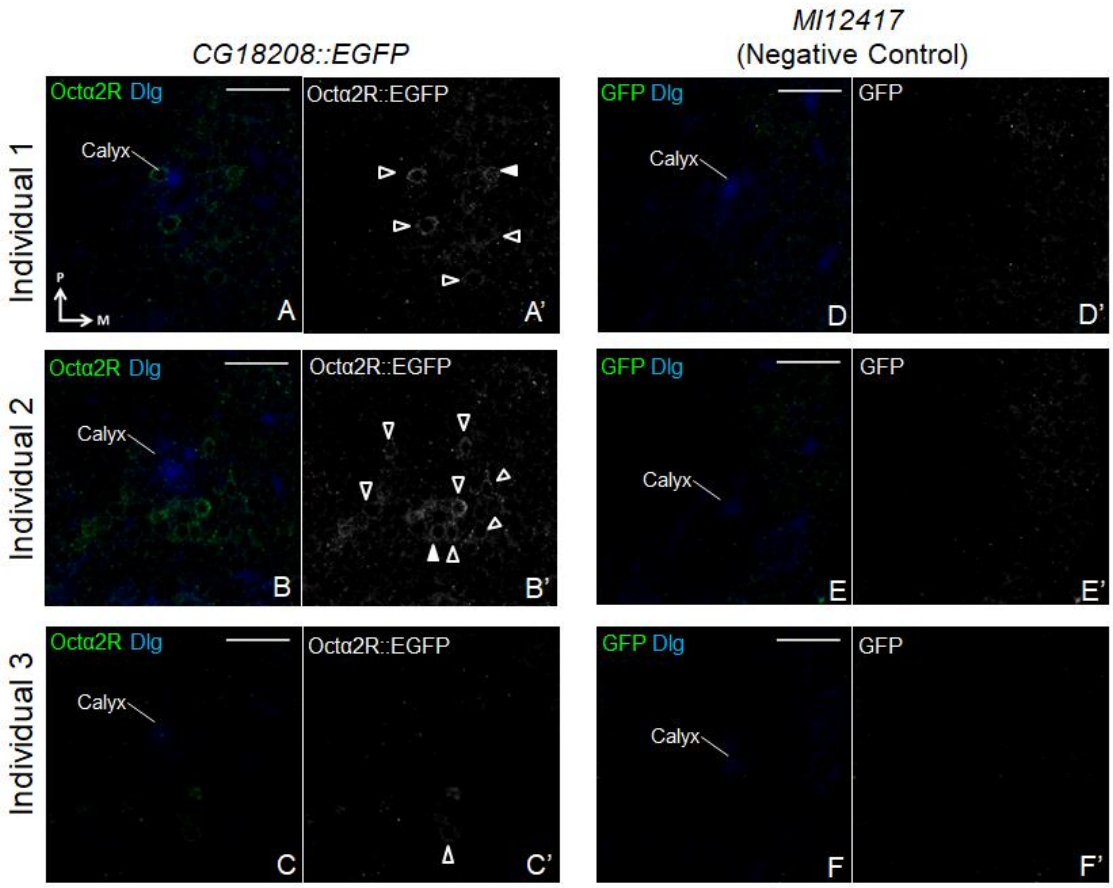

Figure 6.9. Octα2R::EGFP did not localise to KC cell bodies. Confocal optical sections taken immediately dorsal to the first calyx glomerulus (marked with anti-Dlg in blue) of *CG18208::EGFP* larval brains **(A-C)**, with *MI12417* negative controls **(D-F)**. Octα2R::EGFP is green. Many Octα2R::EGFP-positive cell bodies (empty arrowheads) are >5 µm in diameter, larger than KC cell bodies. Cell bodies <5 µm in diameter are indicated with filled arrowheads. Medial (M) is right and posterior (P) is up. Scale bar: 20 µm.

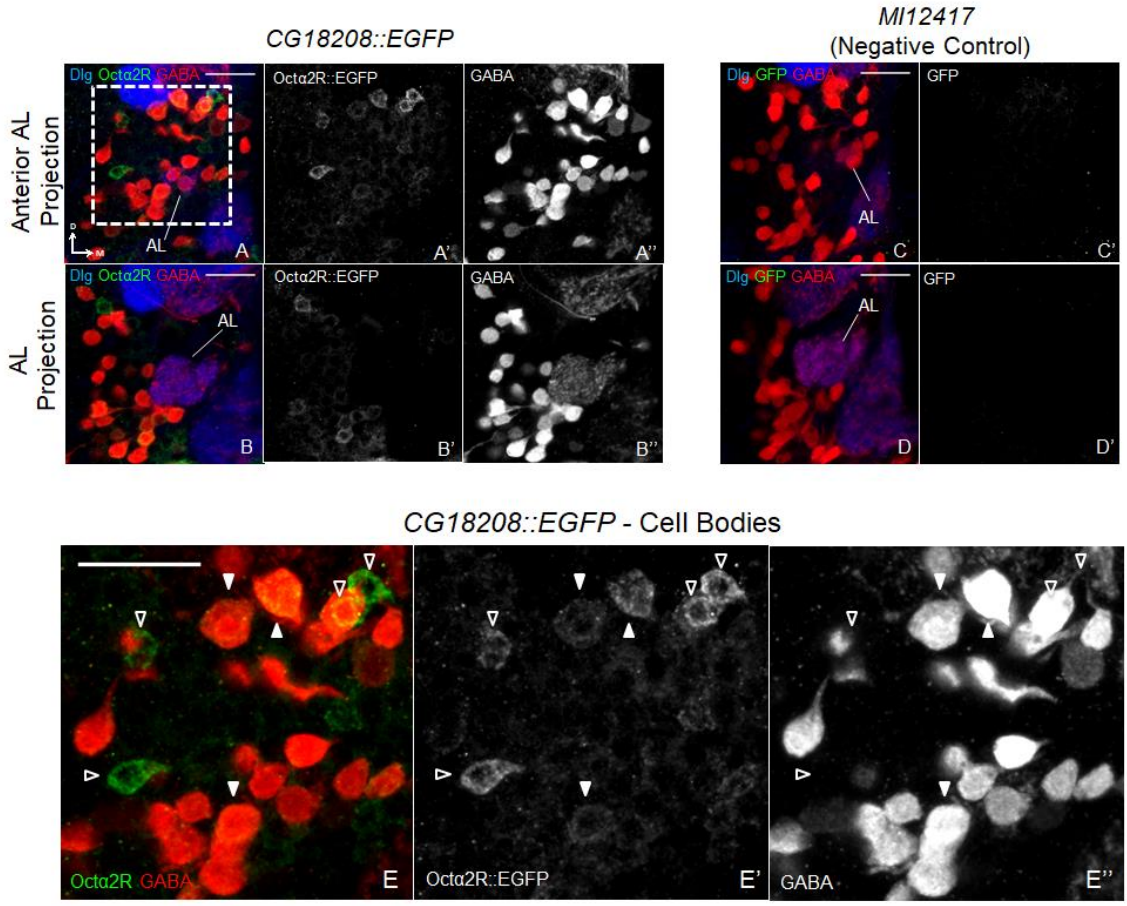

Figure 6.10. Octα2R::EGFP localised to GABA-positive cell bodies near AL. Confocal projections of the AL of *CG18208::EGFP* **(A-B)** with *MI12417* negative control **(C-D)**. **(E)** is an enlarged image of the cell bodies from dotted square in **(A).** Green is Octα2R::EGFP, red is anti-GABA and blue is anti-Dlg. Octα2R-GABA colocalisation indicated with filled arrowheads; Octα2R-positive cell bodies negative for GABA indicated with empty arrowheads. Medial (M) is right and dorsal (D) is up. Scale bar: 20 μm.

GABAergic neurons that may include PNs.

I then examined whether Octα2R::EGFP localised to PN cell bodies labelled by *NP225-GAL4*. 8 ± 2.5 *NP225*-positive cell bodies near the AL co-expressed Octα2R::EGFP (n=3; Fig. 6.11, filled arrows; Table 6.2). There were also many Octα2R::EGFP-positive cell bodies that were *NP225*-negative (Fig. 6.11, empty arrowheads). This is consistent with the Octα2R-GABA data (Fig. 6.10), suggesting that Octα2R::EGFP localised to subsets of both PN and GABAergic cell bodies near the AL.

One out of three larvae showed much lower number of cell bodies co-expressing Octα2R::EGFP and *NP225*>RFP than the two other individuals (Table 6.2). The sample size was too small to determine whether this was an experimental artefact. However, if this variation persisted with a larger sample size, there could be several explanations for it. Third instar larvae may be at a developmental stage where Octα2R expression in PNs is transitioning between an on and off state – such that some individuals have more PNs that express Octα2R. The difference may also be experience-dependent, for example, only PNs that have been previously activated by odourants may express Octα2R. This is less likely as the larvae dissected were raised in the same environment. On the other hand, it could also be due to different levels of bleed through from the *NP225>RFP* construct. In the previous chapter, I observed bleed through from upto three brightly labelled *NP225*-positive cell bodies in the GFP channel in negative control genotypes (Fig. 5.11; Table 5.1, 5.3). This suggested that Octα2R::EGFP may only be localised to around 5 PN cell bodies labelled by *NP225-GAL4*.

6.2.5. Octα2R::EGFP localised to OA cell bodies

As α2-adrenoceptors can act as autoreceptors on NA neurons (Aoki et al., 1994), I examined whether Octα2R was expressed in OA cell bodies in the larval brain. All of the OA-positive cell bodies at the ventral median of the SOG colocalised with Octα2R::EGFP (n=3; Fig. 6.12). This suggested that Octα2R was expressed in all the OA neuron cell bodies at the SOG ventral median midline, where the cell bodies of calyx-innervating sVUM1 neurons are located.

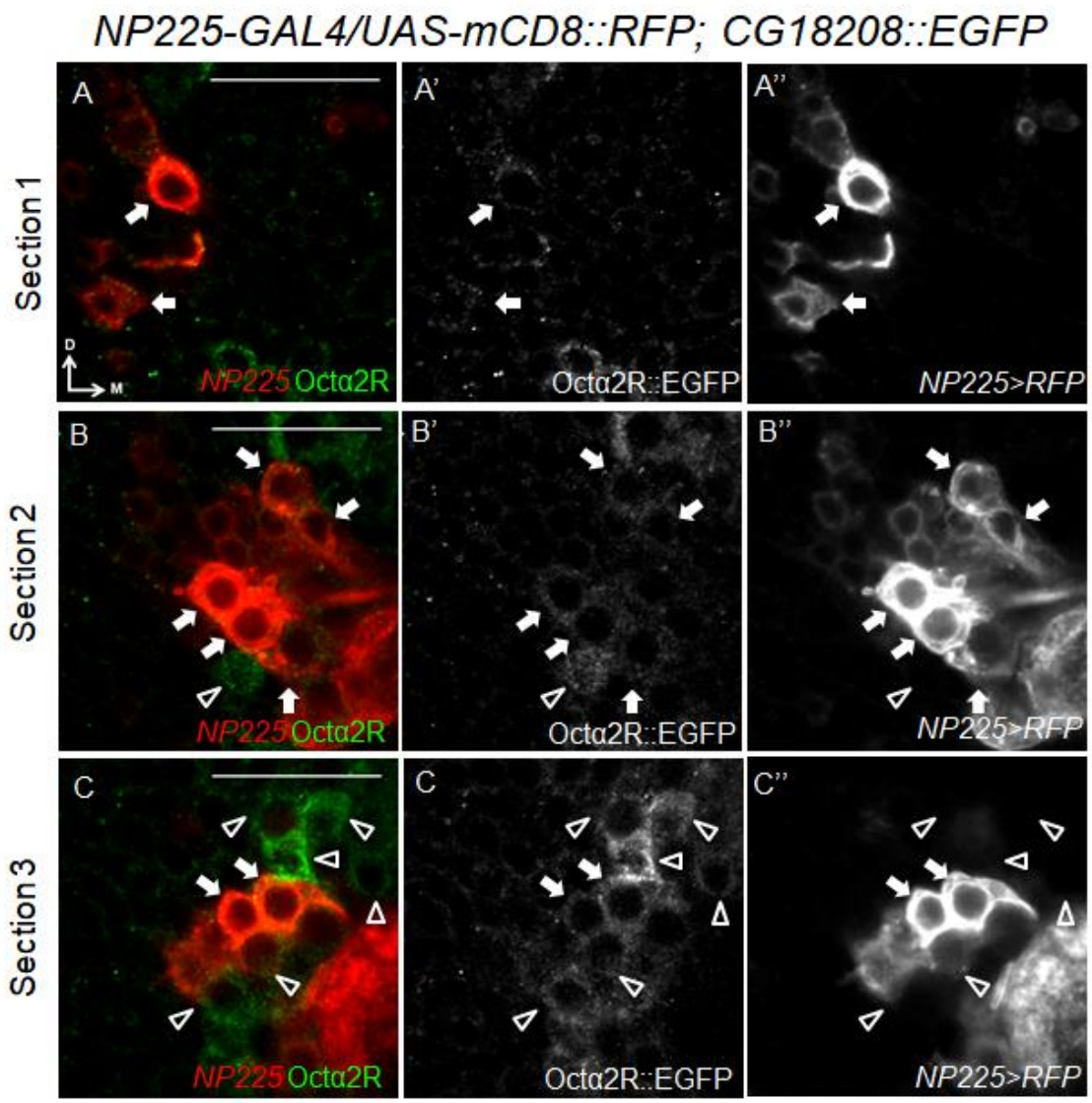

Figure 6.11. Octα2R::EGFP colocalised with some PN cell bodies labelled by *NP225-GAL4*. Single confocal optical sections of the AL of *NP225-GAL4/UAS-mCD8::RFP; CG18208::EGFP*. Green is Octα2R::EGFP and red is *NP225>RFP*. Octα2R-GABA colocalisation indicated with filled arrows; Octα2R-positive cell bodies negative for *NP225>RFP* indicated with empty arrowheads. Medial (M) is right and dorsal (D) is up. Scale bar: 20 μm.

Genotype	Individual	Octα2R+/NP225+
NP225-GAL4/UAS-mCD8::RFP; CG18208::EGFP	Individual 1	10
	Individual 2	3
	Individual 3	11
Statistical Description	N	3
	Mean	8.0
	S.D.	4.4
	S.E.M.	2.5

Table 6.2. Numbers of *NP225-GAL4* cell bodies positive for Octα2R::EGFP. Abbreviations: Octα2R+, Octα2R::EGFP-positive; NP225+, *NP225>RFP*-positive; N, number; S.D., standard deviation; S.E.M., standard error of the mean.

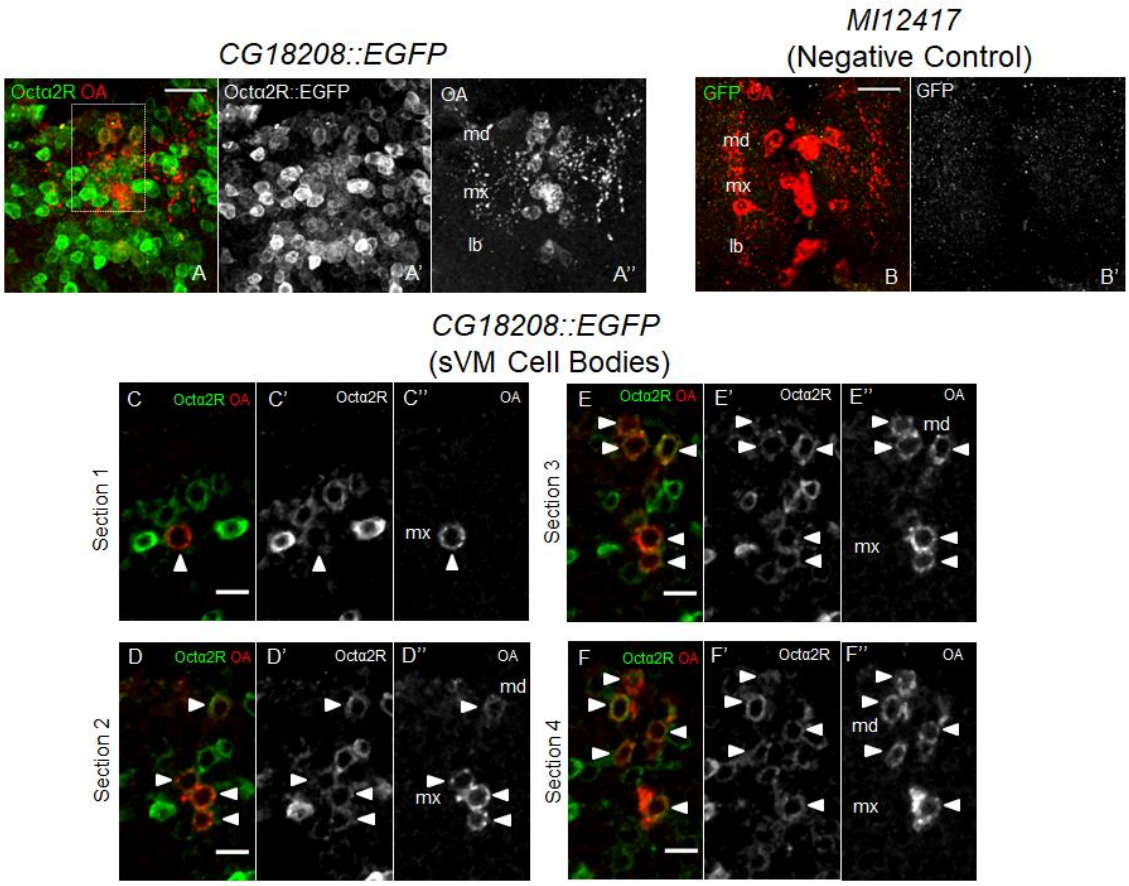

Figure 6.12. Octα2R::EGFP localised to OA-positive cell bodies. Confocal projections of the SOG of *CG18208::EGFP* **(A)** with *MI12417* negative control **(B)**. **(C-F)** are enlarged single confocal optical sections from the dotted box in **(A)** showing all the OA-positive cell bodies at the SOG ventral median. Octα2R-OA colocalisation indicated with arrowheads. Green is Octα2R::EGFP and red is anti-OA. OA cell body clusters are labelled: md (mandibular), mx (maxillary) and lb (labial). Anterior is up and medial is at vertical midline. Scale bar: 20 μm in **(A-B)**; 5 μm in **(C-F)**.

6.2.6. Subcellular localisation of Octα2R::EGFP and OAMB::EGFP

None of the six OA receptor-EGFP fusion proteins generated using the MiMIC recombinase-mediated cassette exchange method appeared to be fully functional: OAMB::EGFP was homozygous infertile (Section 4.2.2.), Octβ1R::EGFP was homozygous lethal (Section 5.2.1.1.), Octβ2R::EGFP and Octα2R::EGFP localised to cell bodies but not to neuropils (Sections 5.2.2.2. & 6.2.2.), and neither Octβ3R::EGFP fusions showed any signals in the larval brain (Sections 5.2.3.2. & 5.3.2.3.). Interestingly, OAMB::EGFP and Octβ1R::EGFP localised to neuropils, while Octβ2R::EGFP and Octα2R::EGFP were retained in cell bodies. This suggested the EGFP cassette insertion disrupted correct protein localisation for Octβ2R and Octα2R, but probably affected other aspects of protein function for OAMB and Octβ1R, such as OA binding or G-protein signalling.

At the endoplasmic reticulum (ER), where proteins are translated and folded, misfolded proteins are recognised, prevented from exiting and eventually degraded (Sitia and Braakman, 2003). As Octβ2R::EGFP and Octα2R::EGFP only localised to cell bodies, this suggested they may be retained in the ER, probably because they were not correctly folded.

To determine whether OA receptor-EGFP fusion proteins accumulated in the ER, I examined whether Octα2R::EGFP colocalised with two ER membrane markers: a mouse monoclonal calnexin (Cnx99a) antibody (Riedel et al., 2016) and a genetically encoded Sec61β::tdTomato fusion protein (Summerville et al., 2016). I also examined whether Octα2R::EGFP colocalised with the plasma membrane marker *10XUAS-IVS-mCD8::RFP* (Pfeiffer et al., 2010). As a comparison, I examined whether OAMB::EGFP colocalised with the same markers, as OAMB::EGFP localised to neuronal terminals despite not being fully functional. As both OAMB::EGFP and Octα2R::EGFP localised to PN and other cell bodies near the AL, I focused on this area of interest and used the PN driver *NP225-GAL4* with the genetically encoded markers.

To visualise the ER structure, I imaged OAMB::EGFP- and Octα2R::EGFP-positive cell bodies at twice the optimal resolution of the confocal microscope at a pixel size of 50 nm, while noting the maximum resolution for the microscope using a 40X lens with a numerical aperture of 1.3 is actually around 150 nm. Nevertheless, this is still not at a sufficiently high

resolution for observing ER structures, which is usually around 30-50 nm in diameter (Schwarz and Blower, 2016). While I only had access to a standard confocal microscope, a microscope with higher resolving power, such as a stimulated emission depletion (STED) microscope with a resolution of 50 nm (Riedel et al., 2016), should ideally be used instead.

I observed anti-Cnx99a labelling in all the cell bodies near the AL (n=6; Fig. 6.13). A few of these cell bodies showed stronger anti-Cnx99a labelling than their neighbours (Fig. 6.13, empty arrowheads). These are probably neurosecretory cells as they contain large amounts of rough ER (Smirle et al., 2013).

Both EGFP fusion proteins colocalised with the Cnx99a ER marker (n=3 each; Fig. 6.13), although the EGFP signal in cell bodies were more punctate and less continuous than ER labelling (Fig. 6.13B,D,E). Some degree of fusion protein-ER colocalisation was expected, as membrane proteins are produced and trafficked through the ER before they reach their target membranes. As there was no observable difference between OAMB::EGFP and Octα2R::EGFP colocalisation with the Cnx99a ER marker in cell bodies, this suggested that either both or neither of these fusion proteins accumulated in the ER. If both of the fusion proteins accumulate in the ER, non-functional OAMB::EGFP must also be recognised by ER quality control mechanisms. On the other hand, if neither of the fusion proteins accumulated in the ER, this suggested that even though Octα2R::EGFP did not localise to neuronal terminals, misfolded Octα2R::EGFP were probably degraded in the ER before it had the opportunity to aggregate. At the current resolving limit, it was difficult to determine whether the EGFP fusion proteins mislocalised to ER structures in the cell body or are in the cytoplasm where ER is also present.

Compared to the Cnx99a ER antibody, the Sec61β::tdTomato ER marker showed stronger signals and more defined ER structures (n=6; Fig. 6.14). OAMB::EGFP signal generally colocalised with the Sec61β::tdTom marker, although OAMB::EGFP again was more punctate and did not perfectly coincide with sites with slightly stronger Sec61β::tdTom signals (n=3; Fig. 6.14A-B). This suggested that OAMB::EGFP and the ER were both present in the cytoplasm, but it was not clear whether OAMB::EGFP accumulated in the ER specifically.

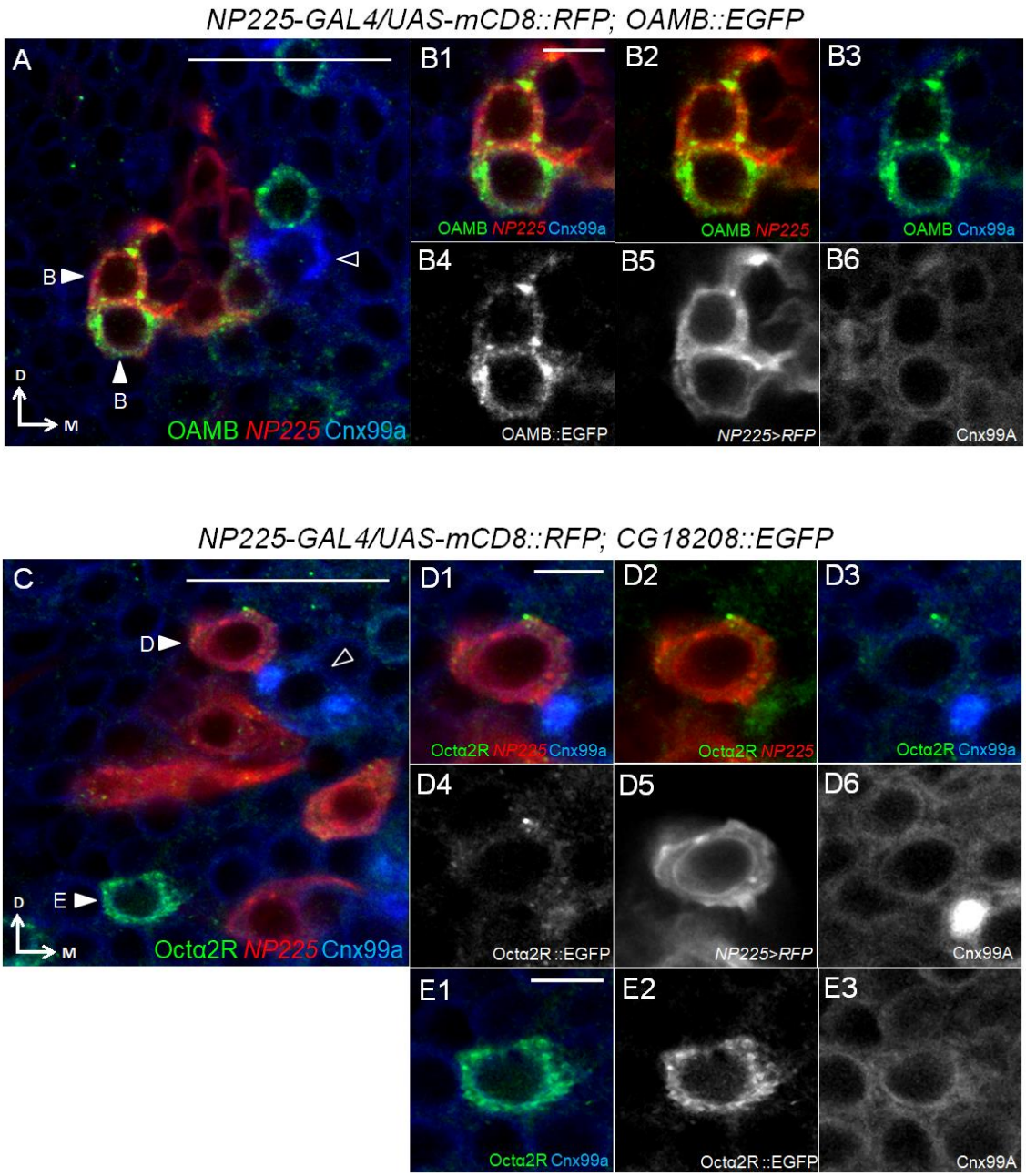

Figure 6.13. OAMB::EGFP and Octα2R::EGFP colocalisation with ER marker anti-calnexin99a. Confocal optical sections of the AL of *NP225-GAL4/UAS-mCD8::RFP; OAMB::EGFP* **(A-B)** and *NP225-GAL4/UAS-mCD8::RFP; CG18208::EGFP* **(C-E)**. **(B)** is an enlarged image of the cell bodies indicated in **(A)**; while **(D,E)** are enlarged images of cell bodies indicated in **(C)**. Red is *NP225>RFP*, blue is anti-calnexin99A (Cnx99a). Green is OAMB::EGFP in **(A-B)** and Octα2R::EGFP in **(C-E)**. Empty arrowheads indicate cell bodies with strong Cnx99a labelling. Medial (M) is right and dorsal (D) is up. Scale bar: 20 µm in **(A,C)**, 5 µm in **(B,D-E)**.

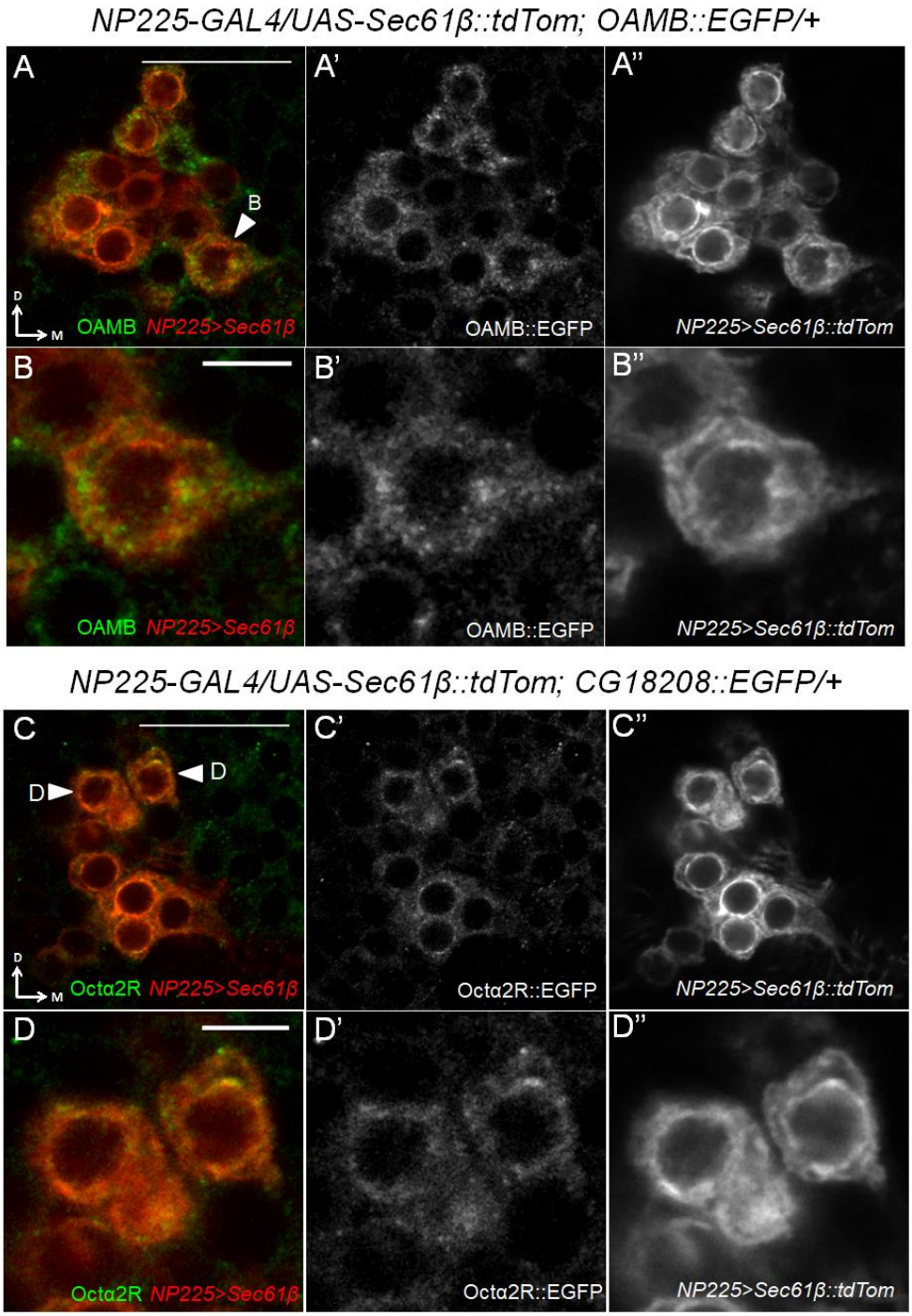

Figure 6.14. OAMB::EGFP and Octα2R::EGFP colocalisation with ER marker Sec61β::tdTom. Confocal optical sections of the AL of *NP225-GAL4/UAS-Sec61β::tdTom; OAMB::EGFP/+* **(A-B)** and *NP225-GAL4/UAS-Sec61β::tdTom; Octα2R::EGFP/+* **(C-D)**. **(B)** and **(D)** are enlarged images of cell bodies indicated by filled arrowheads in **(A)** and **(C)** respectively. Red is *NP225>Sec61β::tdTom*. Green is OAMB::EGFP in **(A-B)** and Octα2R::EGFP in **(C-D)**. Medial (M) is right and dorsal (D) is up. Scale bar: 20 µm in **(A,C)**, 5 µm in **(B,D)**.

Octα2R::EGFP colocalised very well with all *NP225>Sec61β::tdTom*-positive cell bodies (n=3; Fig. 6.14C-D), even better than *NP225>Sec61β::tdTom* colocalisation with OAMB::EGFP (Fig. 6.14A-B). This was unexpected as Octα2R::EGFP only colocalised with a maximum of 11 *NP225*-positive cell bodies (Fig. 6.11; Table 6.2) in a previous experiment to determine Octα2R::EGFP localisation to PN cell bodies. This suggested that some of the Octα2R::EGFP signal observed may be caused by bleed through from the very bright Sec61β::tdTom marker. It was likely that *NP225>Sec61β::tdTom* also bled through in the OAMB::EGFP experiment; but the more robust OAMB::EGFP signal in most of the *NP225*-positive cell bodies obscured some of the bleed through signal. Given the possibility of bleed through, this renders the Octα2R::EGFP-Sec61β::tdTom colocalisation unreliable for interpretation, unless I could show that a *NP225>Sec61β::tdTom* negative control without any GFP constructs did not show any signal in the GFP channel.

Finally, both of the fusion proteins also colocalised with the mCD8::RFP plasma membrane marker in the cytoplasm but not at the plasma membrane of cell bodies (Fig. 6.13B,D). This was unsurprising as I expected OA receptors to localise to the plasma membrane of terminals but not to that of cell bodies. Nevertheless, this was useful for showing that the fusion proteins and Cnx99a ER marker localised to the cytoplasm and not to the plasma membrane.

6.3. Discussion

As the only tool available for Octα2R expression analyses, the newly generated *CG18208::EGFP* is not only useful for identifying Octα2R localisation to larval neuronal cell bodies, but could also be used to identify cells in other *Drosophila* tissues or developmental stages that may express Octα2R. There are currently no data on α2-adrenergic-like OA receptor localisation in other insects – making this the first and only known attempt in mapping α2-adrenergic-like OA receptors in insects.

Similar to Octβ2R::EGFP in Chapter 5, Octα2R::EGFP signal was detected in cell bodies but not membrane terminals, and therefore also shared possible risks of mislocalisation. The reason for Octα2R::EGFP retention in cell bodies is less obvious, as the EGFP insertion site is more than five amino acids away from any TMs or motifs for functional domains (Qi et al., 2017). This suggests that it is difficult to identify the optimal EGFP knock-in site, even when there is a choice such as CRISPR targeting, as a seemingly neutral insertion site could still prevent localisation to membrane terminals. I also used OAMB::EGFP and Octα2R::EGFP as examples to explore whether non-functional fusion proteins accumulated in the endoplasmic reticulum – a subcellular organelle where misfolded proteins are often detected and retained. These results will be discussed in Section 6.3.4.

6.3.1. Octα2R expression in sVUM1 neurons

The localisation of Octα2R to all the OA neurons (Fig. 6.15) was unsurprising, as its homologue α2-adrenoceptor also localised to NA neurons (Aoki et al., 1994). This supports the conservation between Octα2R and mammalian α2-adrenoceptors; while simultaneously suggesting that Octα2R may regulate the activity of OA neurons in the larval brain.

Octα2R would most likely act as an auto-inhibitory receptor which exerts feedback control of OA release at presynaptic terminals, including that of sVUM1 neurons in the larval calyx. Octα2R may also mediate lateral inhibition between OA neurons, for example between sVUMmd1 and sVUMmx1 neurons in the calyx, that is OA signalling from sVUMmd1 may suppress the sVUMmx1 or vice versa. This is consistent with the sVUMmd1-sVUMmx1 connections

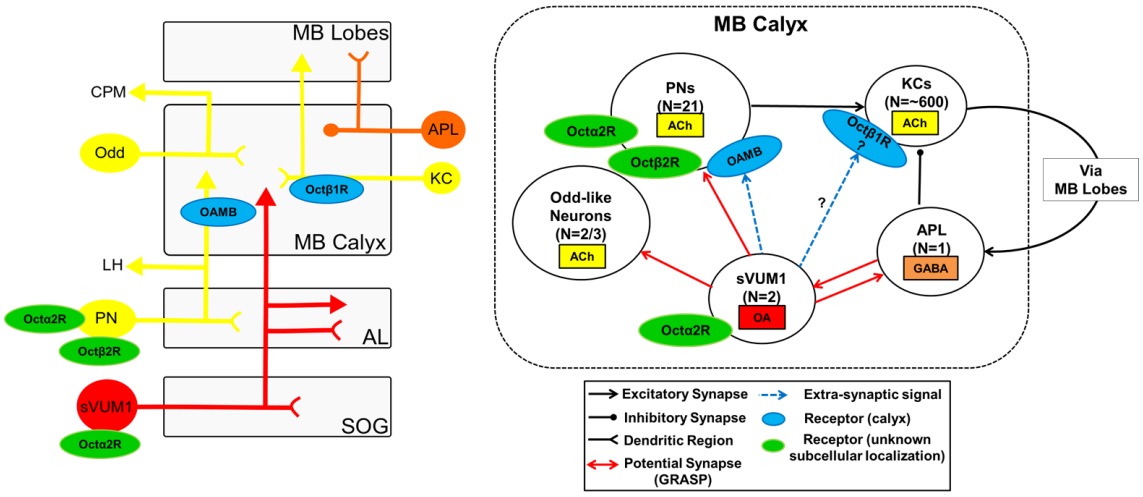

Figure 6.15. Proposed Octα2R localisation pattern in larval MB calyx circuitry. Abbreviations: ACh, acetylcholine; AL, antennal lobe; CPM, centroposterior medial compartment; KC, Kenyon Cell; LH, lateral horn; MB, mushroom body; N, number; OA, octopamine; PN, projection neuron.

observed in the L1 connectomics data (Eichler et al., 2017; NeuroFLP). However, whether Octα2R is localised to pre- and/or post-synaptic terminals of OA neurons remains to be identified through an alternative method, such as anti-Octα2R labelling.

6.3.2. Possible Octα2R expression in some PN cell bodies

Provided this was not an artefact from *NP225>RFP* bleed through, this observation would suggest that a subset of olfactory PN cell bodies of variable number is also positive for Octα2R::EGFP expression (Fig. 6.15). As speculated in Section 6.2.4., this variation may be due to developmental stochasticity or experience-depedent mechanisms.

I did not expect Octα2R to be expressed in PNs, as PNs already expressed OAMB, Octβ2R and possibly Octβ1R (Chapters 4 & 5). It is currently unclear whether the different types of OA receptors are expressed on the same or different subsets of olfactory PNs. It is possible that they are grouped based on the odour quality encoded by individual PNs, as each PN relays olfactory information from a single type of olfactory receptor. Individual PNs can be identified by using specific driver lines that each label single PNs. Alternatively, OA receptors could be tagged with spectrally distinct fluorescent reporters to determine expression in common and distinct neurons, as well as, to explore the possibility of differential subcellular localisation.

Octα2R localisation to PN axons would exert an additional layer of control over PN output by OA signalling depending on the OA signal given by the sVUM1 neurons, provided that different types of OA receptors are activated depending on OA concentration. When OAMB and/or Octβ2R are activated at PN axons, this would likely increase PN inputs to KCs; while Octα2R activation would reduce PN inputs.

6.3.3. Possible Octα2R expression in other calyx-innervating neurons

The lack of Octα2R in KCs could be because Octβ1R localisation to KC dendrites is already fulfilling the role of an inhibitory OA receptor there. While Octβ1R is considered to be mainly coupled to the excitatory G_s pathway, there is one example of its coupling to the inhibitory G_o pathway which decreases

intracellular cAMP levels and act to inhibit synaptic growth at the NMJ (Koon and Budnik, 2012).

Preliminary observations of Octα2R::EGFP localisation in the larval CNS suggest that Octα2R may also be expressed in the APL neuron and Odd-like neurons. Octα2R::EGFP localisation to GABAergic cell bodies near the AL, suggest that Octα2R may be able to modulate GABAergic inhibition. This may extend to the modulation of the GABAergic APL neuron. Octα2R::EGFP signals in dorsal cell bodies near the calyx larger than 5 μm in diameter suggests that Octα2R could be expressed in Odd-like neuron cell bodies as well. However, I have not managed to confirm the identity of Octα2R::EGFP-positive cell bodies yet with molecular markers for these neurons.

Hypothetical Octα2R localisation to APL axons in the calyx might reduce the levels of inhibition from the APL neuron on KCs. This would lead to decreased sparseness of KC activity, increased correlation of odour representations and worse odour discrimination; similar to the effects observed when APL activity is genetically blocked (Lin et al., 2014; Masuda-Nakagawa et al., 2014). On the other hand, Octα2R localisation on Odd-like neurons would probably decrease the output signal carried by cholinergic output neurons from the calyx.

6.3.4. Colocalisation of OAMB::EGFP and Octα2R::EGFP with ER markers

Both OAMB::EGFP and Octα2R::EGFP colocalised with ER but not plasma membrane markers in cell bodies, even though OAMB::EGFP localised to membrane terminals while Octα2R::EGFP was retained in cell bodies. Due to the limited resolving power of the confocal microscope (around 150 nm), compared to the size of rough ER in the cell bodies (around 30-50 nm) (Schwarz and Blower, 2016), it was not possible to determine whether the fusion proteins localised to the ER itself, or if the ER and the fusion proteins merely occupy the cytoplasmic compartment of neuronal cell bodies. Therefore, a higher resolution microscope such as the STED (50 nm resolution) would be required to visualise ER structures.

This was further hindered by the lack of clear and specific ER markers. Anti-Cnx99a signal was observed in the cytoplasm of all cell bodies which made it difficult to control for signal versus background, and only showed strong

labelling for cell bodies that contained a lot of rough ER. On the other hand, the genetically encoded *Sec61β::tdTom* suffered bleed through into the GFP channel, probably due to the wider emission spectrum of the red fluorescent tdTomato protein that displays substantial overlap with the Alexa 488 fluorophore used to amplify GFP signals (ThermoFisher Fluorescence Spectral Viewer: https://www.thermofisher.com/).

OAMB::EGFP and Octα2R::EGFP signal in the cell body appear to be at similar intensities. As most proteins are translated at the ER before they are trafficked to the plasma membrane, a baseline level of fusion proteins are expected to be present at the ER. It is unknown what this baseline would be for OA receptors as it may vary depending on protein turnover rates; and how this correlates to the intensity of EGFP fusion proteins. The lack of OAMB::EGFP and Octα2R::EGFP colocalisation with the plasma membrane marker in the cell body is also expected; as receptor proteins probably localise to the plasma membrane at synaptic terminals but not cell bodies. Moreover, if misfolded proteins are rapidly recognised and degraded in the ER, there will also not be a difference in EGFP signal between fusion proteins that are functional or non-functional. Therefore, it is impossible to quantify whether fusion proteins are accumulating in the ER. Alternatively, it might be useful to explore whether non-functional fusion proteins accumulate in compartments where misfolded proteins are degraded – such as proteasomes or lysosomes; provided there is a baseline control to show that it is different to the turnover and degradation of its functional protein counterpart.

Chapter 7. Expression patterns of GABA receptors in sVUM1 neurons

7.1. Introduction

Putative synaptic connections have been detected between sVUM1 neurons and the GABAergic APL neuron using GRASP in the larval calyx. As the APL neuron is also presynaptic in the larval calyx (Masuda-Nakagawa et al., 2014), it is possible sVUM1 neurons are regulated by GABAergic inhibition by the APL neuron in the larval calyx. In this chapter, I aimed to determine whether sVUM1 neurons expressed any GABA receptors which would allow sVUM1 neurons to respond to APL signalling in the larval MB calyx.

There are four known types of GABA receptors in *Drosophila*: an ionotropic $GABA_AR$, a GABA-gated chloride channel (Hosie et al., 1997); and three metabotropic $GABA_BRs$ – $GABA_BR1$, $GABA_BR2$ and $GABA_BR3$ (Mezler et al., 2001). $GABA_BRs$ are G-protein coupled receptors which generally inhibit neuronal activity by presynaptically downregulating voltage-gated Ca^{2+} channels to inhibit neurotransmitter release (Bettler et al., 1998), or postsynaptically activating inward rectifying K^+ channels resulting in hyperpolarisation (Kaupmann et al., 1998). In *Drosophila*, $GABA_BR1$ and $GABA_BR2$ are functional heterodimers that show co-expression; while $GABA_BR3$ is not co-expressed with the other two receptors (Mezler et al., 2001).

Both $GABA_AR$ and $GABA_BR$ are localised to the adult MBs (Enell et al., 2007; Liu et al., 2007); where the $GABA_AR$ subunit Rdl has been shown to affect olfactory processing in KCs. The overexpression of Rdl in KCs inhibited calcium responses in the MB and impaired memory acquisition; while Rdl knockdown in KCs improved memory formation (Liu et al., 2007). The RNAi-mediated knockdown of Rdl, but not $GABA_BR$, in KCs reduced the sparse and selective activity in KCs required for odour discrimination (Lei et al., 2013). As blocking APL activity results in the same phenotype as Rdl knockdown in KCs (Lei et al., 2013; Lin et al., 2014), this suggests that Rdl is mediating the signalling effects of APL on KCs. On the other hand, the function of $GABA_BR$ in

the MB remains unknown, and may instead function on non-KC neurons in the MB. However, the localisation and requirement of GABA receptors on non-KC neurons innervating the MB calyx are yet to be tested.

In the larval CNS, the localisation of $GABA_AR$ and the $GABA_BR1/GABA_BR2$ complex has previously been visualised using antibodies against the $GABA_AR$ subunit Rdl and $GABA_BR2$ respectively (Enell et al., 2007). This has revealed that $GABA_AR$ and the $GABA_BR1/GABA_BR2$ complex localise to the larval MB calyx (Enell et al., 2007); and KC cell bodies are additionally immunoreactive to Rdl (Enell et al., 2007). On the other hand, it is unclear whether GABA receptors are expressed in sVUM1 neurons as well, as the strong immunoreactivity against both GABA receptors throughout the calyx might be overshadowing other populations of neurons to which these receptors are localised.

To determine whether sVUM1 neurons could be regulated by GABA signalling, here I used Rdl::EGFP and GABA-B-R1::EGFP protein traps to examine whether the $GABA_A$ receptor subunit Rdl and the $GABA_BR1/R2$ complex were expressed in sVUM1 neurons (Fig. 7.1).

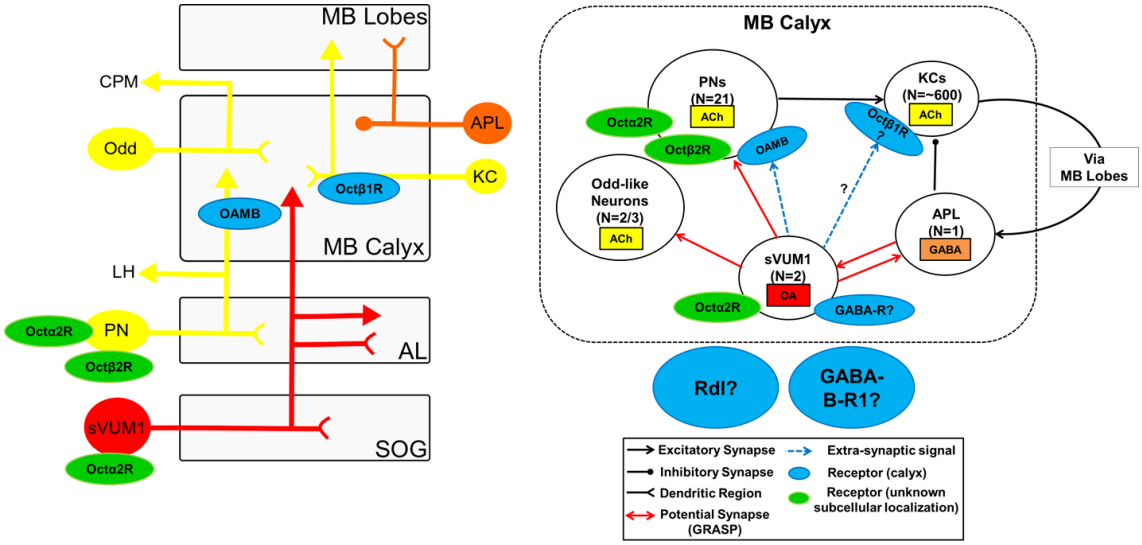

Figure 7.1. Hypothesised GABA receptor localisation pattern in larval MB calyx circuitry. Abbreviations: ACh, acetylcholine; AL, antennal lobe; CPM, centroposterior medial compartment; KC, Kenyon Cell; LH, lateral horn; MB, mushroom body; N, number; OA, octopamine; PN, projection neuron.

7.2. Results

7.2.1. Rdl::EGFP localisation in sVUM1 neurons

To determine whether sVUM1 neurons expressed the ionotropic $GABA_A$ receptor, I used the *Rdl::EGFP* line from the MiMIC RMCE collection (Venken et al., 2011a; Nagarkar-Jaiswal et al., 2015; Fig. 7.2) to visualise the localisation of the $GABA_A$ receptor subunit Rdl.

As expected from immunolabelling data (Enell et al., 2007), *Rdl::EGFP* localised to KC cell bodies dorsal to the calyx (Fig. 7.3A). However, contrary to immunolabelling data, Rdl::EGFP did not localise to the MB calyx (Fig. 7.3B). This suggested that the Rdl::EGFP fusion protein from the *Rdl::EGFP* line was not targeted to synaptic terminals, and could only be used to identify cell bodies that express Rdl.

While I could not determine whether Rdl localised to the calyx terminals of sVUM1 neurons, I detected Rdl::EGFP signal in all the OA-positive cell bodies at the ventral midline of the SOG region (n=4; Fig. 7.4, arrowheads). This suggested that Rdl was expressed in all OA neuronal cell bodies, including sVUM1 cell bodies, although its subcellular localisation is unknown.

7.2.2. GABA-B-R1::EGFP did not localise to presynaptic calyx terminals of sVUM1 neurons

To determine whether sVUM1 neurons expressed the metabotropic $GABA_BR1/R2$, I used a *GABA-B-R1::EGFP* line selected from the MiMIC RMCE collection (Venken et al., 2011a; Nagarkar-Jaiswal et al., 2015; Fig. 7.5) to visualise the localisation of the $GABA_BR1/R2$ heterodimer complex.

Consistent with anti-$GABA_BR2$ immunostaining, I observed strong GABA-B-R1::EGFP signals throughout the calyx (n=4; Fig. 7.6). GABA-B-R1::EGFP localised diffusely in the interglomerular region and showed stronger localised signals in calyx glomeruli (Fig. 7.6A-D). The diffuse localisation pattern suggested that $GABA_BR1$ localised to KCs, while the glomerular localisation pattern suggested $GABA_BR1$ also localised to PNs. However, this requires confirmation with KC and PN markers.

RMCE Line MI02620

Parental MI Line:

Insertion	Gene(s) Affected	Location	Position	Phase
MI02620	Rdl [-]	3L:9167127 [-]	Rdl-coding intron;	Rdl-RA:0, Rdl-RC:0, Rdl-RD:0, Rdl-RE:0, Rdl-RF:0, Rdl-RG:0

Gene Trap	Lethality
YES	lethal

RMCE Line:

Insertion	Gene Target	Phase	Method	Tag
MI02620-GFSTF.0	Rdl	0	injection	EGFP-FlAsH-StrepII-TEV-3xFLAG

Lethality	Fails to Complement
lethal	no (stock used)

BDSC Stock No.
59796

Images (antibody staining)	
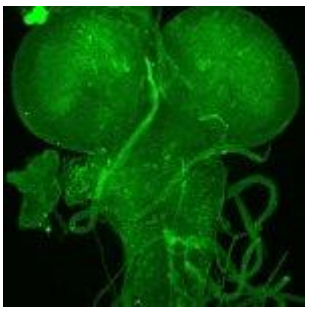	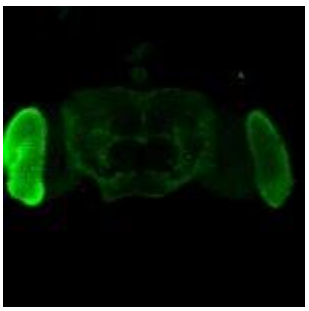

Figure 7.2. *Rdl::EGFP* recombinant stock listed on the Gene Disruption Project Database. (http://flypush.imgen.bcm.tmc.edu/pscreen/rmce/rmce.php?entry=RM00053).

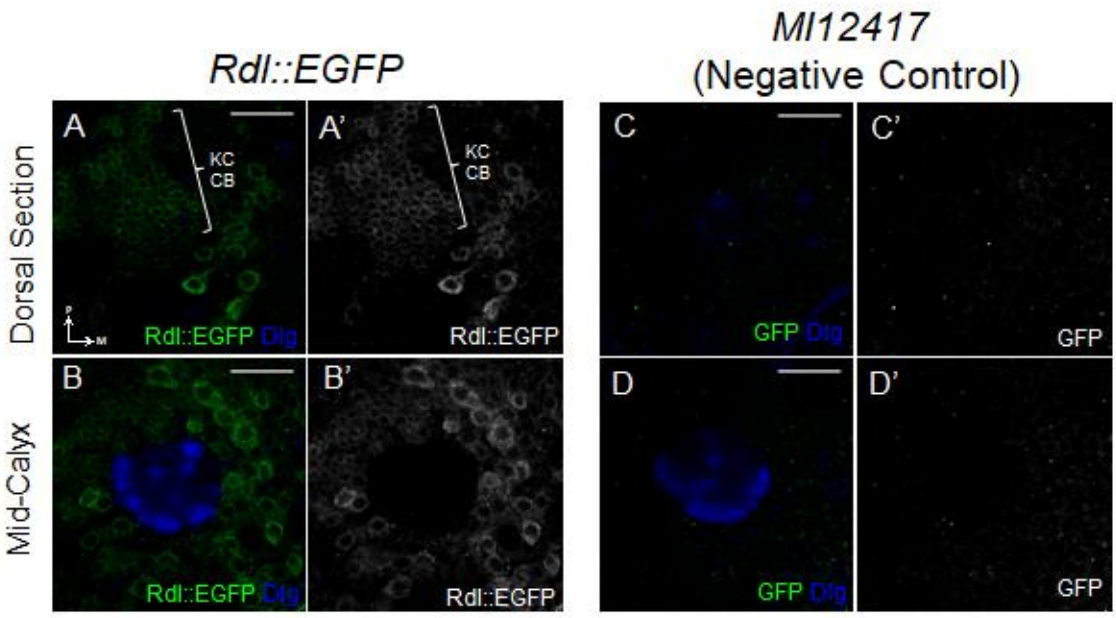

Figure 7.3. Rdl::EGFP localised to KC and other dorsal cell bodies but not to MB calyx. Confocal optical sections of the calyx of *Rdl::EGFP* **(A-B)** with *MI12417* negative control **(C-D)**. Green is Rdl::EGFP and blue is anti-Dlg. Medial (M) is right and posterior (P) is up. Scale bar: 20 μm. Abbreviation: CB, cell bodies.

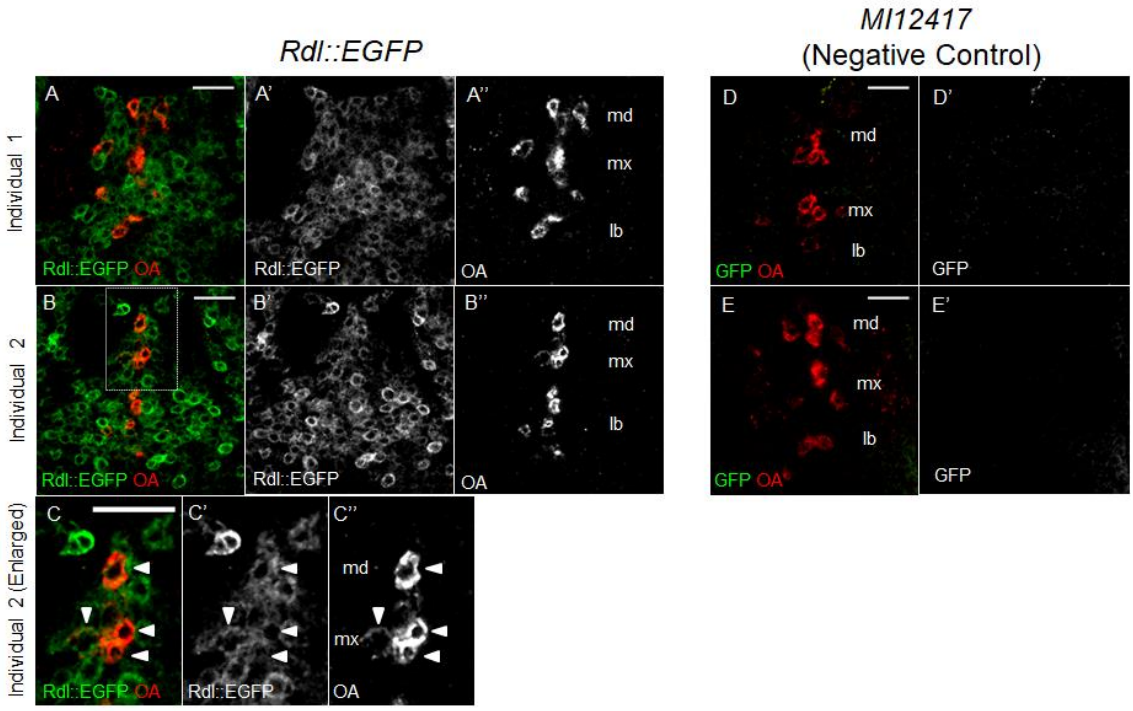

Figure 7.4. Rdl::EGFP signal localised to OA neuron cell bodies at SOG. Confocal optical sections of the SOG from three *Rdl::EGFP* individuals **(A-C)** with *MI12417* negative controls **(D-E)**. Green is Rdl::EGFP and red is anti-OA. **(C)** is enlarged from the dotted box in **(B)**. Arrowheads indicate Rdl::EGFP-OA colocalisation. OA cell body clusters are labelled: md (mandibular), mx (maxillary) and lb (labial). Anterior is up, medial is vertical mid-line. Scale bar: 20 µm.

RMCE Line MI01930

Parental MI Line:

Insertion	Gene(s) Affected	Location	Position	Phase
MI01930	GABA-B-R1 [+]	2L:15024209 [+]	GABA-B-R1-coding intron;	GABA-B-R1-RB:0, GABA-B-R1-RC:0

RMCE Line:

Insertion	Gene Target	Phase	Method	Tag
MI01930-GFSTF.0	GABA-B-R1	0	injection	EGFP-FlAsH-StrepII-TEV-3xFLAG

Lethality	Fails to Complement
viable	

BDSC Stock No.
60522

Images (antibody staining)
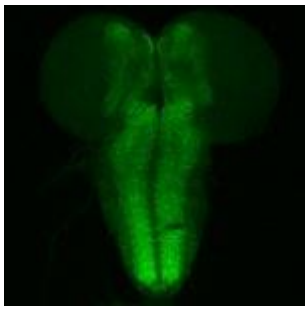

Figure 7.5. *GABA-B-R::EGFP* recombinant stock listed on the Gene Disruption Project Database. (http://flypush.imgen.bcm.tmc.edu/pscreen/rmce/rmce.php?entry=RM00241).

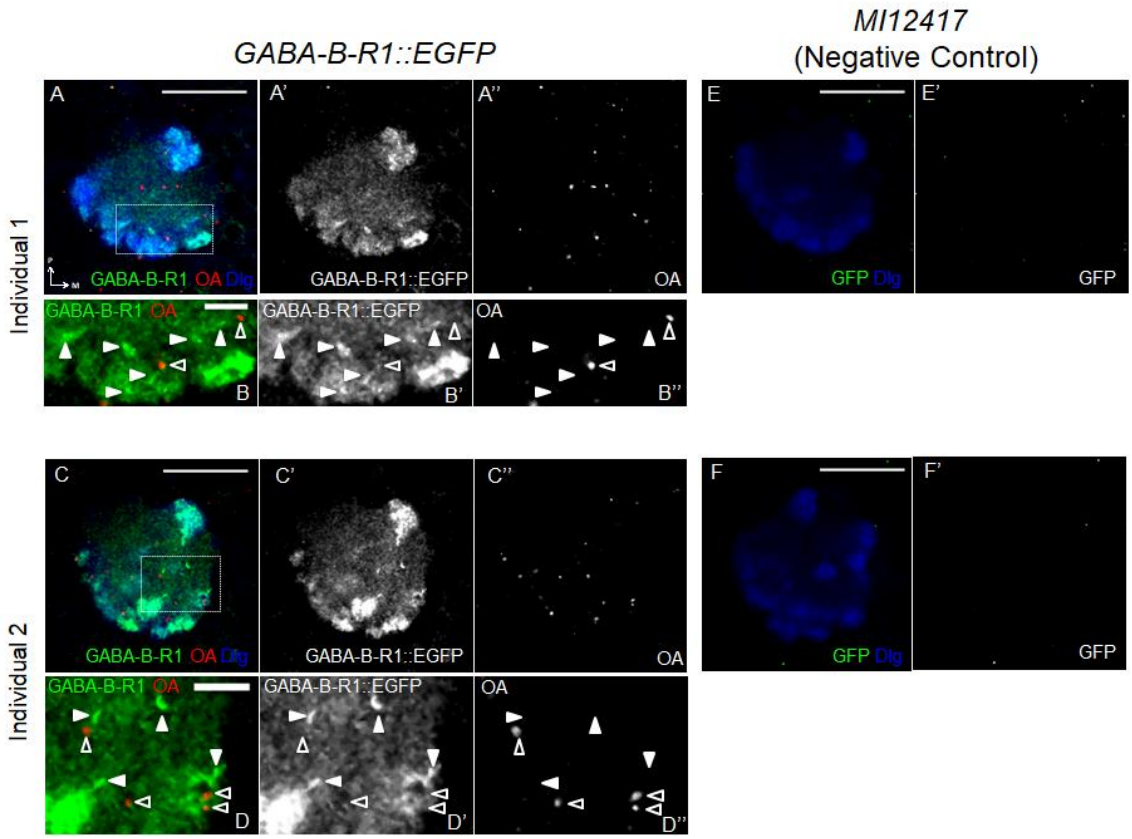

Figure 7.6. GABA-B-R1::EGFP did not colocalise with OA puncta in MB calyx. Confocal optical sections of the calyx from two *GABA-B-R1::EGFP* individuals **(A-D)** with *MI12417* negative controls **(E-F)**. Green is GABA-B-R1::EGFP, red is anti-OA and blue is anti-Dlg. GABA-B-R1::EGFP-positive puncta are indicated with filled arrowheads, while OA puncta are indicated with empty arrowheads. Medial (M) is right and posterior (P) is up. Scale bar: 20 µm in **(A,C,E-F)** and 5 µm in **(B,D)**.

I also observed GABA-B-R1::EGFP-positive puncta in the interglomerular region (n=4; Fig. 7.6B,D, filled arrowheads). This suggested that another type of non-KC, non-PN neuron expresses $GABA_BR1$. None of the GABA-B-R1::EGFP-positive puncta (Fig. 7.6B,D, filled arrowheads) colocalised with OA puncta (Fig. 7.6B,D, empty arrowheads). This suggested that GABA-B-R1 did not localise to the presynaptic OA terminals of the sVUM1 neurons in the larval MB calyx.

On the other hand, some but not all OA-positive cell bodies expressed GABA-B-R1::EGFP at the ventral midline of the SOG region (n=3; Fig. 7.7). While it was not possible to identify whether sVUM1 neurons were among the cell bodies that expressed GABA-B-R1::EGFP, the lack of colocalisation of GABA-B-R1::EGFP signal with OA puncta in the calyx suggested that the metabotropic $GABA_BR1/R2$ heterodimer was not responsible for mediating GABAergic modulation of sVUM1 neurons from the APL neuron in the calyx.

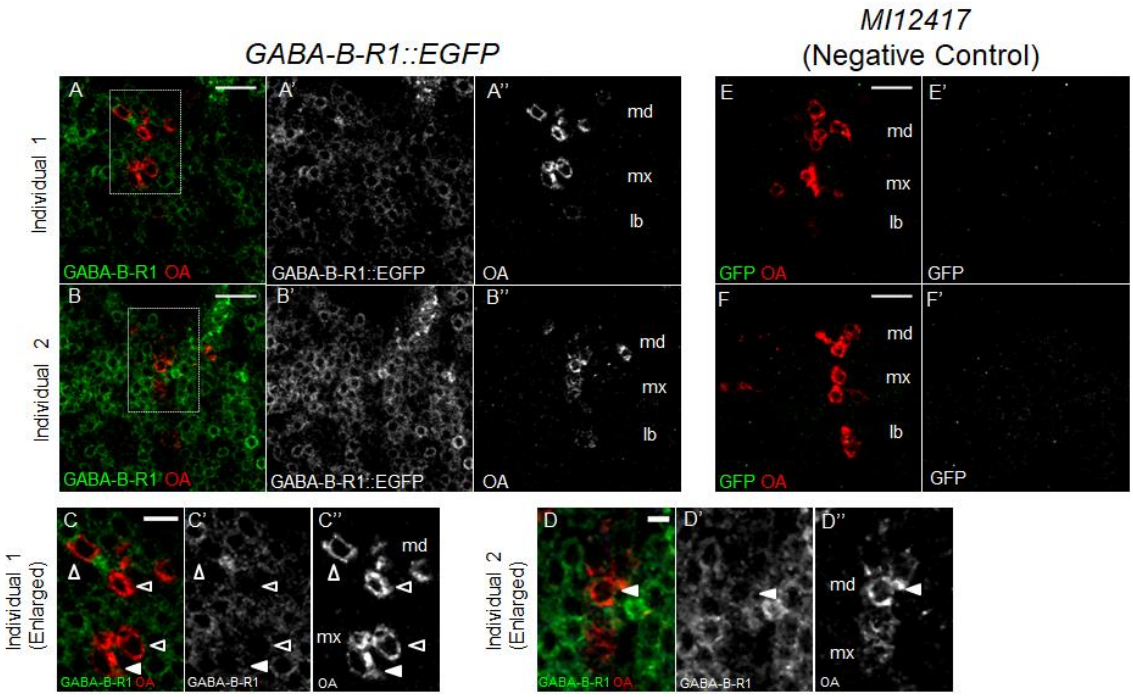

Figure 7.7. GABA-B-R1::EGFP localised to some OA neuron cell bodies at SOG. Confocal optical sections of the SOG from two *GABA-B-R1::EGFP* individuals **(A-D)** with *MI12417* negative controls **(D-E)**. Green is GABA-B-R1::EGFP and red is anti-OA. Some OA cell bodies colocalised with GABA-B-R1::EGFP (filled arrowheads), others did not (empty arrowheads). Anterior is up, medial is vertical midline. OA cell body clusters are labelled: md (mandibular), mx (maxillary) and lb (labial). Scale bar: 20 μm in **(A-B,E-F)** and 10 μm in **(C-D)**.

7.3. Discussion

7.3.1. GABA receptor localisation on sVUM1 neurons

While it is known that Rdl and $GABA_BRs$ localised to the larval MB calyx (Enell et al., 2007), this is the first study to consider GABA receptor localisation on calyx-innervating neurons besides KCs and PNs. I found that Rdl::EGFP was expressed in all OA neuronal cell bodies at the ventral midline of the SOG, suggesting that sVUM1 neurons may express the ionotropic $GABA_AR$ (Fig. 7.8). On the other hand, $GABA_BR1$::EGFP did not localise to the presynaptic terminals of sVUM1 neurons in the larval calyx.

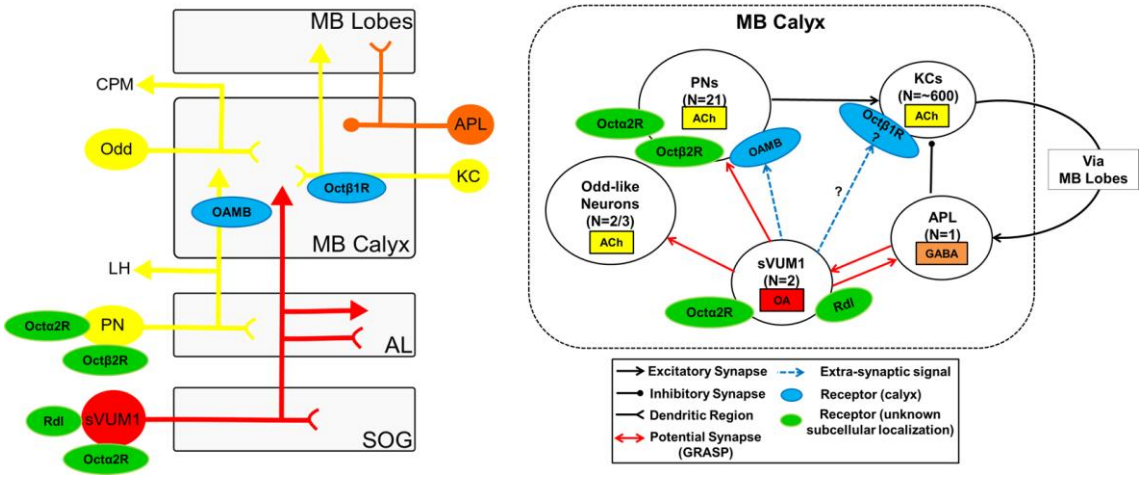

Figure 7.8. Proposed GABA receptor localisation pattern in larval MB calyx circuitry. Abbreviations: ACh, acetylcholine; AL, antennal lobe; CPM, centroposterior medial compartment; KC, Kenyon Cell; LH, lateral horn; MB, mushroom body; N, number; OA, octopamine; PN, projection neuron.

$GABA_AR$ expression suggests that sVUM1 neurons are susceptible to fast and reversible ionotropic inhibition. While my data cannot show where Rdl::EGFP is localised subcelullarly, if Rdl (and therefore $GABA_AR$) is indeed localised to the calyx terminals of sVUM1 neurons, this would suggest that sVUM1 neurons may be subjected to GABAergic signalling from the APL neuron. As the APL neuron receives input from KC axons (Lin et al., 2014; Masuda-Nakagawa et al., 2014), this suggests that if sVUM1 neurons contained calyx-localised $GABA_AR$, they could be indirectly inhibited by KC outputs via the APL neuron. Functionally, this may form a feedback loop where KC outputs

inactivate sVUM1 activity to maintain temporal resolution of OA signalling in the larval MB calyx.

The pharmacological block of $GABA_AR$ neurotransmission in the honeybee MB calyx impairs reversal learning, in which honeybees learn to respond to a change in valence of the same stimulus (Boitard et al., 2015). Unlike the behavioural prediction from knocking down $GABA_AR$ in KCs in the adult fly (Lei et al., 2013), odour discrimination is not impaired when $GABA_AR$ is non-specifically blocked in the honeybee calyx (Boitard et al., 2015). This suggests $GABA_AR$-mediated inhibition on non-KC neurons in the calyx, such as OA neurons, may be involved in reversal learning.

On the other hand, $GABA_AR$ may also localise to the AL terminals of sVUM1 neurons (Selcho et al., 2014), as the AL receives a lot of GABAergic input from AL local neurons (Wilson and Laurent, 2005; Thum et al., 2011); or to sVUM1 dendrites in the SOG region. In this scenario, GABAergic inhibition from outside the MB would be important in controlling the activity of sVUM1 modulation in the larval MB calyx.

Although metabotropic $GABA_BR1/R2$ do not localise to sVUM1 terminals in the larval MB calyx, sVUM1 neurons may still be subjected to slower GABA modulation if the metabotropic $GABA_BR3$ localised to their calyx terminals instead.

7.3.2. GABA-B-R1::EGFP localisation to other calyx-innervating neurons

Although GABA-B-R1::EGPP did not colocalise with OA terminals in the larval MB calyx, its localisation pattern suggested that $GABA_BR1$ may be localised to multiple types of calyx-innervating neurons: including KC dendrites which may be responsible for the diffuse glomerular and interglomerular signal, PN terminals responsible for the stronger labelling in calyx glomeruli, as well as another type of extrinsic neurons, which may account for the GABA-B-R1::EGFP-positive boutons observed in the interglomerular region of the calyx.

This level of detail was probably not visible using anti-$GABA_BR2$, as Enell et al. (2007) had proposed that based on their staining results, $GABA_BR1$ was probably localised to KC dendrites in the calyx but did not discuss whether the receptor may also localise to other cell types in the calyx. Identifying GABA-B-R1::EGFP-positive cell bodies with molecular markers, together with cell-type

specific knockdown of GABA-B-R1::EGFP, could potentially reveal the different types of calyx-innervating neurons that contain $GABA_BR1$ at their calyx terminals.

7.3.3. EGFP-tagged GABA receptors as an alternative to antibodies

The GABA receptor expression patterns in the larval CNS visualised through GABA receptor protein traps are generally in agreement with what was previously observed using antibodies against GABA receptors. For example, anti-$GABA_BR2$ and GABA-B-R1::EGFP both localised to the larval MB calyx; while anti-Rdl and Rdl::EGFP were both observed in KC cell bodies. This suggests that fusion proteins are generally able to recapitulate antibody expression patterns. However, there is always a risk that the EGFP insertion could cause misexpression or mislocalisation of functional receptors, as discussed in previous chapters. The other limitation of protein traps is that the fusion protein it produced, such as from *Rdl::EGFP*, did not always successfully localise to neuronal terminals. In this case, it may be useful to convert EGFP to T2A-GAL4 to visualise the full innervation patterns of neurons expressing Rdl (Diao et al., 2015; Gnerer et al., 2015).

On the other hand, anti-$GABA_BR2$ did not label any cell bodies (Enell et al., 2007). Therefore, it was impossible to confirm the identities of the neurons expressing GABA receptors in a structure which shows strong anti-$GABA_BR2$, such as the larval MB calyx. As GABA-B-R1::EGFP localised to cell bodies as well as neuropils, it is more useful for identifying neurons expressing $GABA_B$ receptors and their subcellular localisation. Here, antibody labelling and protein trapping could be complementary methods for confirming GABA receptor localisation.

Chapter 8. Genetic tools for testing the OA modulatory circuitry of the larval MB calyx

8.1. Introduction

To understand the OA modulatory circuitry in the larval MB calyx, it is necessary to test the functionality of the OA connections identified through anatomical methods. How do neurons expressing the different OA receptors in the calyx respond to OA signalling from the sVUM1 neurons? How are sVUM1 neurons themselves regulated by calyx-innervating neurons? How does sVUM1 signalling modulate odour representations in the calyx; and how does this affect olfactory perception and odour discrimination behaviour in the larvae?

To address these questions, it is essential to have the appropriate tools to isolate each component of the OA modulatory calyx circuitry for genetic manipulation and assay for functionality or behaviour. The binary expression system in *Drosophila* is well-developed for a wide range of genetic manipulations from conditional neuronal activation and silencing, to imaging neuronal activity *in vivo*. The availability of strong and specific transcriptional drivers of the neurons of interest is integral for testing neuronal functions. Such drivers are required to ensure that any phenotypic effects observed are due to the neurons of interest, but not the other neurons labelled in the driver. In this chapter, I aimed to confirm the expression pattern of specific sVUM1 and Odd-like neuron driver lines.

8.1.1. Confirming specific sVUM1 expression in published lines

To investigate the functions of OA signalling in the MB calyx, it is necessary to limit genetic manipulation to the calyx-innervating sVUM1 neurons without affecting other OA neurons.

Traditionally, the *Tdc2-GAL4* line has been used to study OA neurons in *Drosophila*. *Tdc2-GAL4* contains the yeast *GAL4* transcription factor upstream to the coding start of the *Tdc2* gene, which encodes the tyrosine decarboxylase enzyme required for TA and OA biosynthesis (Cole et al., 2005). Two *Tdc2-LexA::VP16* lines were later generated by inserting the regulatory region used in

Tdc2-GAL4 into a *LexA* cloning vector (Burke et al., 2012). In the adult fly brain, *Tdc2-GAL4* and *Tdc2-LexA* label all OA-positive neurons. *Tdc2-LexA* also has additional labelling in the central complex (Burke et al., 2012).

Using clonal analysis, Selcho et al. (2014) has shown that two types of OA neurons innervate the larval MB calyx – sVUMmd1 and sVUMmx1 (collectively known as sVUM1 neurons) – labelled by the *Tdc2-GAL4* line. I have previously confirmed that the calyx-innervating neurons labelled in *Tdc2-GAL4* and *Tdc2-LexA* are responsible for all the anti-OA staining in the larval MB calyx (H.W., MPhil Thesis 2014).

The cell bodies of all 24 OA neurons innervating the *Drosophila* larval brain are located at the SOG region (Selcho et al., 2014). As *Tdc2-GAL4* and *Tdc2-LexA* lines labelled all of the OA-positive cell bodies in the SOG (Selcho et al., 2014; H.W., MPhil Thesis 2014), these lines labelled many other OA neurons in addition to the calyx-innervating sVUM1 neurons. In addition, *Tdc2-GAL4* also labelled OA neurons in the ventral nerve cord, neurons that were solely TA-positive (Selcho et al., 2012, 2014), as well as KCs in the larval calyx (H.W., MPhil Thesis 2014). Although it has not been verified, it is likely that *Tdc2-LexA* also labels OA motorneurons and TA neurons, as its adult expression pattern overlaps with that of *Tdc2-GAL4* (Burke et al., 2012). Therefore, it would be difficult to isolate the functions of sVUM1 neurons from other OA neurons using these lines, which is not ideal for investigating OA signalling in the larval calyx circuitry.

Here, I labelled a selection of Janelia Farm Fly Light *GAL4/LexA* lines (Jenett et al., 2012; L. Masuda-Nakagawa, personal communication) with OA to confirm whether these lines labelled sVUM1 neurons.

8.1.2. Confirming expression of specific Odd-like neuron lines

In addition to a specific sVUM1 line for manipulating OA signalling in the larval calyx, it is also useful to have specific lines to test the functions of potential synaptic partners of sVUM1 neurons in the calyx, such as Odd-like neurons.

The current driver lines available to label Odd-like neurons, *OK263-GAL4* (L. Masuda-Nakagawa, personal communication) and *Odd-GAL4* (Slater et al., 2015), both label a cluster of cell bodies whose tracts merge into a single tract before projecting to the calyx. Therefore, it was difficult to identify the cell bodies

that project to the calyx from those that do not, especially for determining whether Odd-like neurons expressed OA receptors in previous chapters. Here I aimed to confirm the expression patterns of Janelia Farm Fly Light *GAL4/LexA* lines that label single calyx-innervating Odd-like neurons.

8.2. Results

8.2.1. OA labelling of candidate lines that label sVUM1 neurons

Candidate transcriptional driver lines that strongly labelled sVUM1 neurons were identified from the Janelia FlyLight collection (Jenett et al., 2012; Li et al., 2014; L. Masuda-Nakagawa, J. Truman, personal communication). To confirm the innervation pattern of the selected lines, I labelled these lines by crossing them to *UAS-mCD8::GFP* or *LexAOp-mCD8::GFP* and analysed resulting images to find out whether 1) there were OA-immunoreactive cell bodies near the SOG ventral median (sVM) mandibular (md) and sVM maxillary (mx) clusters, where the cell bodies of sVUMmd1 and sVUMmx1 are located respectively (Selcho et al., 2014); and 2) whether there was calyx innervation that colocalised with anti-OA staining. Using these criteria, five out of sixteen candidate lines labelled sVUM1 neurons (Table 8.1).

8.2.1.1. *R34A11-GAL4* and *R34A11-LexA* labelled sVUM1 neurons but few other OA neurons

In the larval MB calyx, anti-OA labelling colocalised with both *R34A11-GAL4>mCD8::GFP* (n=2; Fig. 8.1A) and *R34A11-LexA>mCD8::GFP* (n=2; Fig. 8.1B-C) processes. This confirmed that these lines labelled the OA sVUM1 neurons. In addition to sVUM1 neurons, *R34A11-LexA* also showed diffuse labelling in the larval calyx characteristic of KC dendrites (n=2; Fig. 8.1B-C).

At the sVM, *R34A11-GAL4>mCD8::GFP* colocalised with five OA-positive cell bodies (Fig. 8.2A): 2 sVMmd cell bodies, 2 sVMmx cell bodies, and 1 cell body in the sVM labial (lb) cluster (n=2; Fig. 8.2B-E, arrowheads). *R34A11-GAL4* also labelled many other OA-negative neurons in the SOG region (Fig. 8.2A). Therefore, *R34A11-GAL4* would be a good candidate for generating a more specific sVUM1 line through intersection with *Tdc2-LexA*.

***GAL4/LexA* Line**	**Gene**	**OA Colocalisation**	**sVUM1 labelled**	**Figure**
R34A11-GAL4	*Sema-1a*	Calyx innervation; 2 OA-positive cell bodies each in sVMmd and sVMmx clusters; some OA-negative cell bodies	Yes	8.1, 8.2
R34A11-LexA	*Sema-1a*	Calyx innervation; 1 OA-positive cell body each in sVMmd and sVMmx clusters; 2 OA-negative cell bodies in SOG region; weak KCs	Yes	8.1, 8.3
NP7088-GAL4		Calyx innervation; all OA-positive cell bodies in SOG; some OA-negative cell bodies in SOG	Yes	8.4, 8.5
R76H04-GAL4	*Tβh*	Calyx innervation; all OA-positive cell bodies in SOG; some OA-negative cell bodies in SOG; weak KCs	Yes	8.4, 8.6
R57F09-LexA	*Tdc2*	Calyx innervation; all OA-positive cell bodies in SOG	Yes	8.4, 8.7
R76G06-GAL4	*Tβh*	No calyx innervation; many OA-positive cell bodies in the SOG	No	8.8, 8.9
R76H03-LexA	*Tβh*	No OA-positive neurons	No	8.10
R43E08-GAL4	*dmrt93B*	2 OA-negative cell bodies near sVMlb cluster	No	
R76G07-GAL4	*Tβh*	KCs, no OA-positive neurons	No	
R76G11-GAL4	*Tβh*	KCs, no OA-positive neurons	No	
R76H01-LexA	*Tβh*	No OA-positive neurons	No	
R61E08-GAL4	*DAT*	Few OA-negative cell bodies near sVMlb cluster	No	
R68A08-GAL4	*TyrR*	Several OA-negative cell bodies lateral to sVMmd/mx cell bodies	No	
R77B01-GAL4	*Opa*	Many OA-negative cell bodies near sVM clusters	No	
R83G11-GAL4	*Blimp-1*	1 OA-negative cell body near sVMmx cluster, 2 OA-negative cell bodies near sVMlb cluster	No	
R83H01-GAL4	*Blimp-1*	OA-negative cell bodies near sVM clusters	No	

Table 8.1. Summary of anti-OA labelling of sVUM1 drivers. Reference for stocks: *NP7088-GAL4*: Tanaka et al. (2008); all other stocks: Jennett et al. (2012).

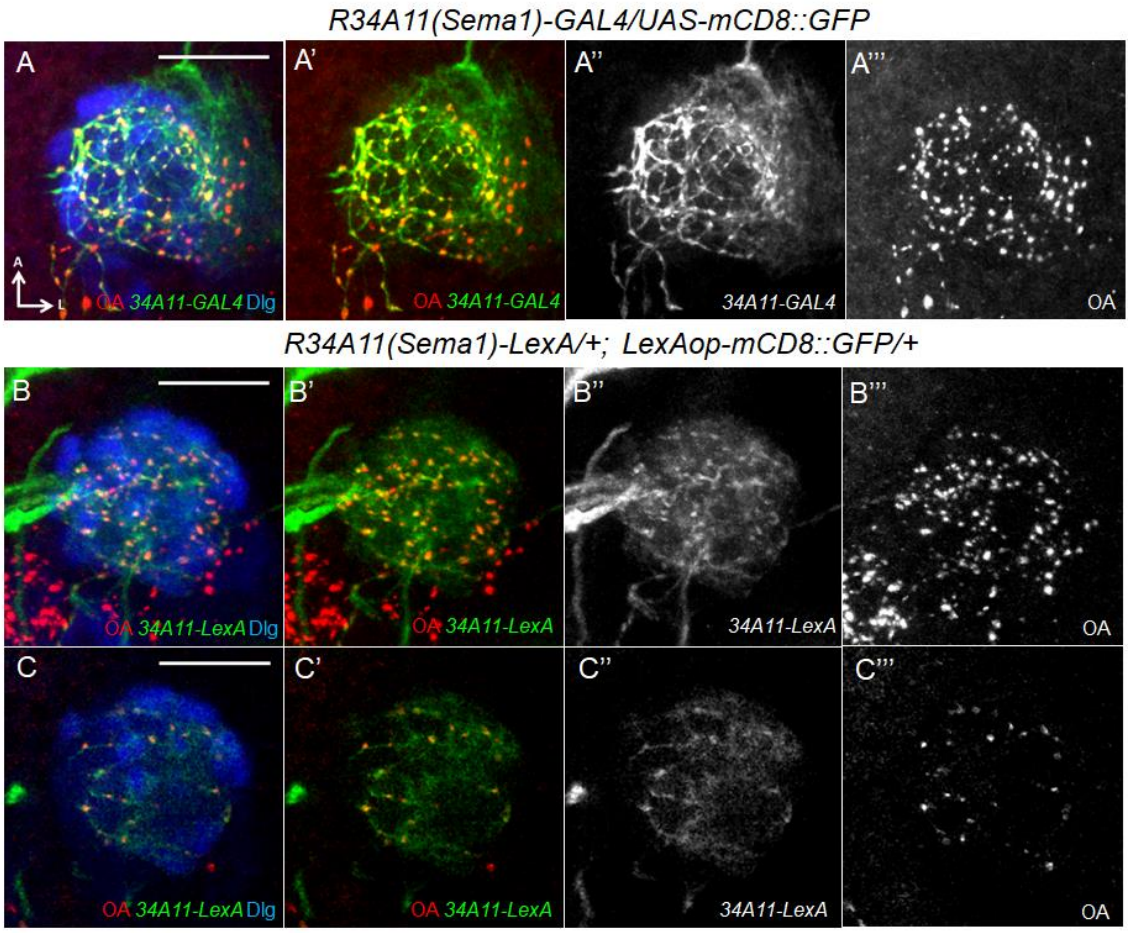

Figure 8.1. *R34A11-GAL4* and *R34A11-LexA* colocalised with anti-OA in the larval calyx. mCD8::GFP is green, anti-OA is red and anti-Dlg is blue. **(A)** Confocal projection of the calyx of *R34A11-GAL4>UAS-mCD8::GFP*. **(B-C)** Confocal projection **(B)** and single confocal optical section **(C)** of the calyx of *R34A11-LexA>LexAOp-mCD8::GFP*. Anterior (A) is up, lateral (L) is right. Scale bar: 20 µm.

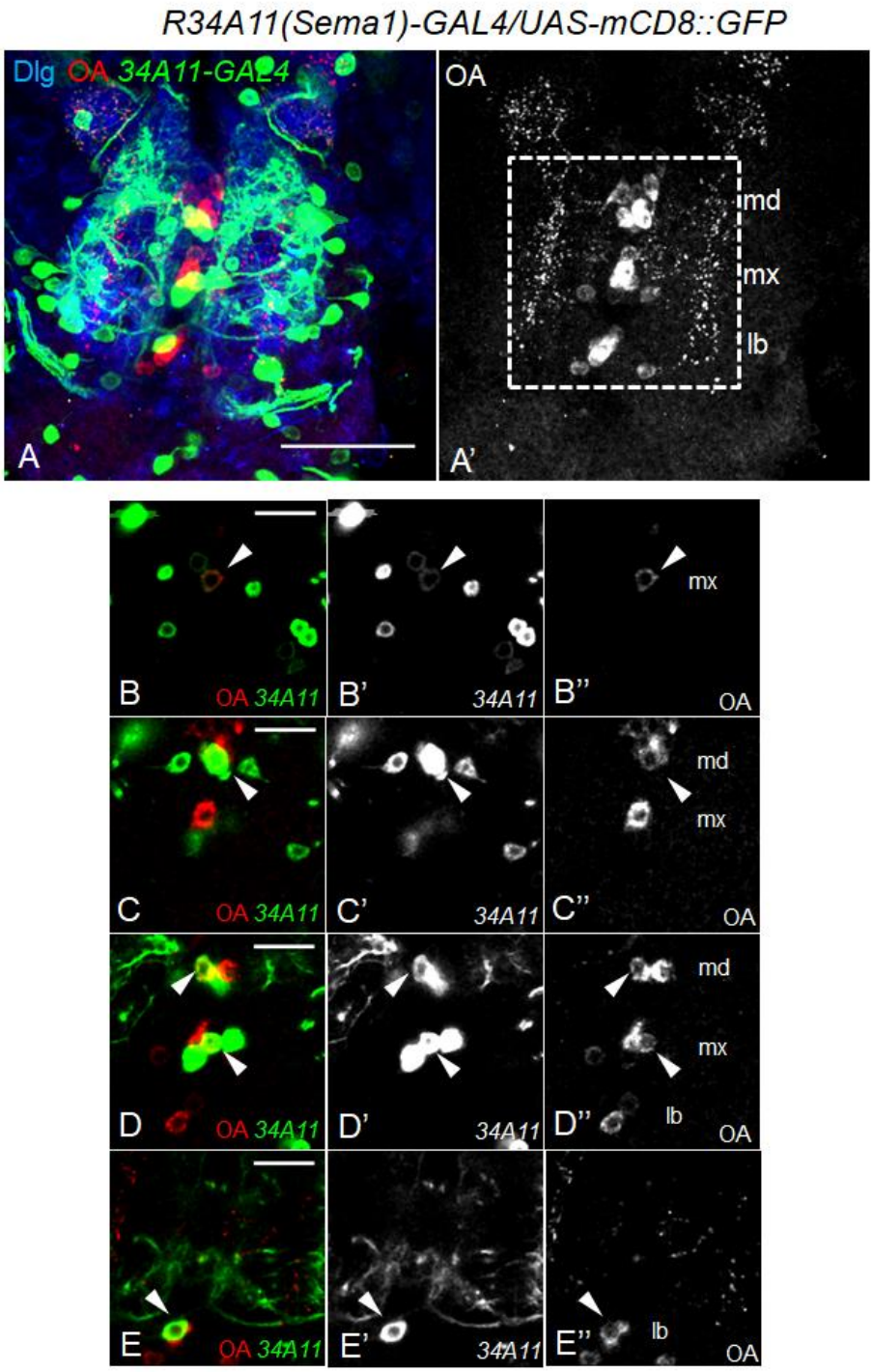

Figure 8.2. *R34A11-GAL4* colocalised with five OA-positive cell bodies in the SOG. *R34A11-GAL4>UAS-mCD8::GFP* is green, anti-OA is red, anti-Dlg is blue. **(A)** Confocal projection of the SOG. **(B-E)** Single confocal optical sections taken from dotted square in **(A)**. *R34A11-GAL4* colocalisation with OA is indicated with arrowheads. Anterior is up, medial is at vertical mid-line. OA cell body clusters are labelled: md (mandibular), mx (maxillary) and lb (labial). Scale bar: 50 µm in **(A)** and 20 µm in **(B-E)**.

R34A11-LexA labelled only two OA-positive cell bodies in the SOG, one each in the sVMmd and sVMmx clusters (n=2; Fig. 8.3, arrowheads). Therefore, the only OA neurons labelled by *R34A11-LexA* were likely to be sVUMmd1 and sVUMmx1. However, as both *R34A11-LexA* (Fig. 8.1B-C) and *Tdc2-GAL4* labelled KCs, the intersection between *R34A11-LexA* and *Tdc2-GAL4* would yield a line that labelled sVUM1 neurons as well as KCs, which could not be used for functional or behavioural studies.

8.2.1.2. *NP7088-GAL4, R76H04-GAL4* and *R57F09-LexA* labelled all OA neurons in SOG

Three other candidate lines – *NP7088-GAL4*, *R76H04(Tβh)-GAL4* and *R57F09(Tdc2)-LexA* – also labelled sVUM1 neurons; as their mCD8::GFP expression colocalised with all the OA-positive puncta in the calyx (Fig. 8.4). These three lines also labelled all the OA-positive cell bodies in the SOG (Fig. 8.5, 8.6, 8.7, arrowheads). Therefore, an intersection of these lines with *Tdc2-GAL4/Tdc2-LexA* would still label all the OA neurons in the SOG.

R76H04-GAL4 could not be used for an intersection with *R34A11-LexA*, as both lines label KCs in addition to sVUM1 neurons in the calyx (Fig. 8.1B-C, 8.4B). *NP7088-GAL4* could possibly be used for an intersection with *R34A11-LexA*; provided that, unlike the *NP7088-GAL4* and *R34A11-LexA* constructs, the *LexAOp-FLP* required for FLP-out intersection is not on the second chromosome. On the other hand, *R57F09-LexA* could be a good alternative to *Tdc2-LexA* for an intersection with *R34A11-GAL4* to generate a more specific sVUM1 line.

8.2.1.3. *R76G06-GAL4* labelled some OA neurons but not sVUM1 neurons

Contrary to expectation, not all of the lines containing *Tβh* regulatory fragments labelled all the OA neurons in the larval brain. *R76G06(Tβh)-GAL4* did not label the calyx-innervating sVUM1 neurons, as *R76G06-GAL4>mCD8::GFP* did not colocalise with anti-OA in the calyx (Fig. 8.8). Instead, *R76G06-GAL4* showed a more diffuse pattern in the calyx, resembling that of KC dendrites.

Even though *R76G06-GAL4* did not label sVUM1 neurons, it labelled a subset of OA neurons in the SOG in all three sVM cell body clusters (Fig. 8.9,

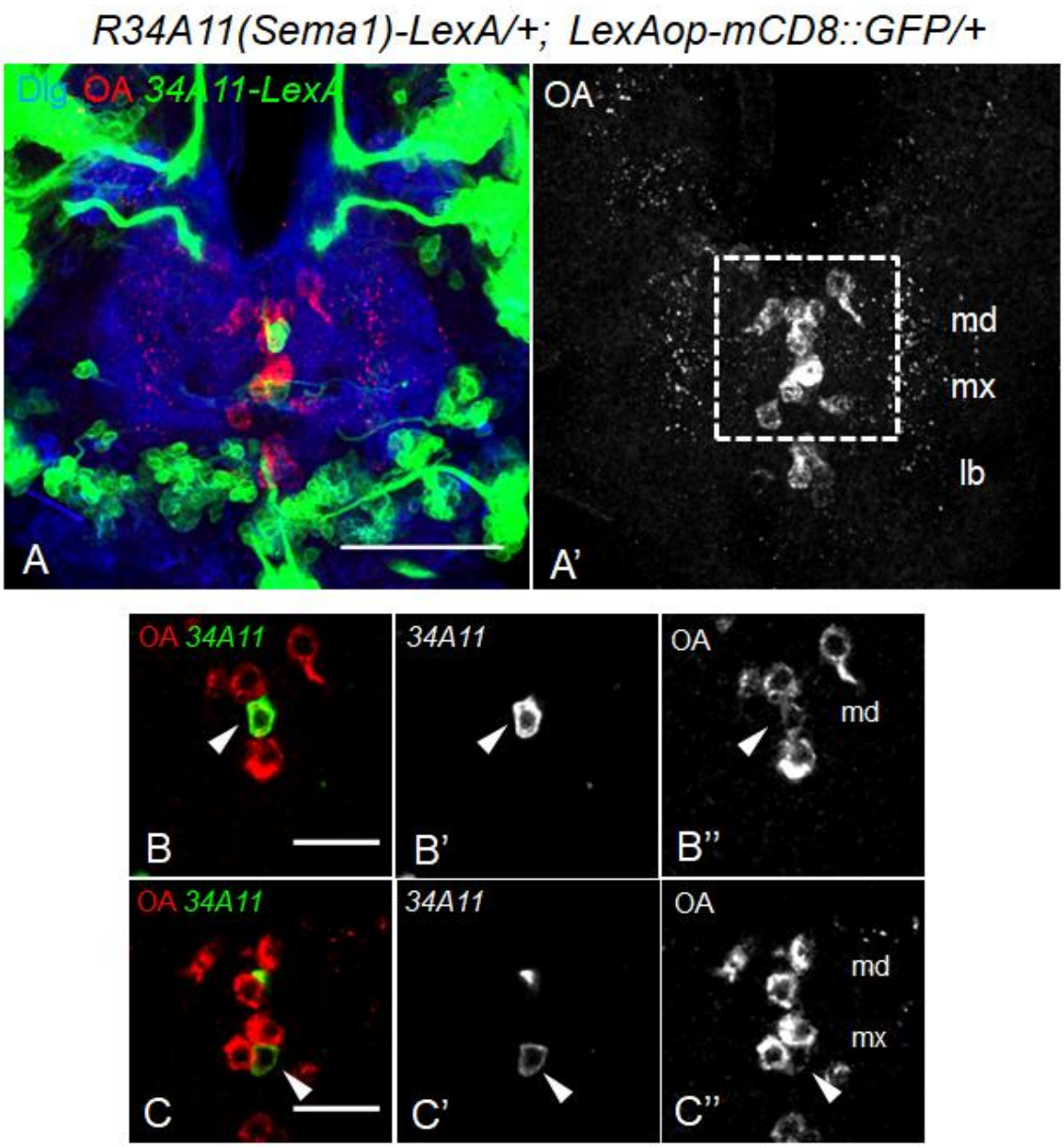

Figure 8.3. *R34A11-LexA* colocalised with two OA-positive cell bodies in the SOG. *R34A11-LexA>LexAOp-mCD8::GFP* is green, anti-OA is red, Dlg is blue. **(A)** Confocal projection of the SOG. **(B-C)** Confocal optical sections taken from dotted box in **(A)**. Anterior is up, medial is at vertical mid-line. *R34A11-LexA* colocalisation with OA indicated with arrowheads. Scale bar: 50 µm in **(A)**, 20 µm in **(B-C)**. Abbreviations as Fig. 8.2.

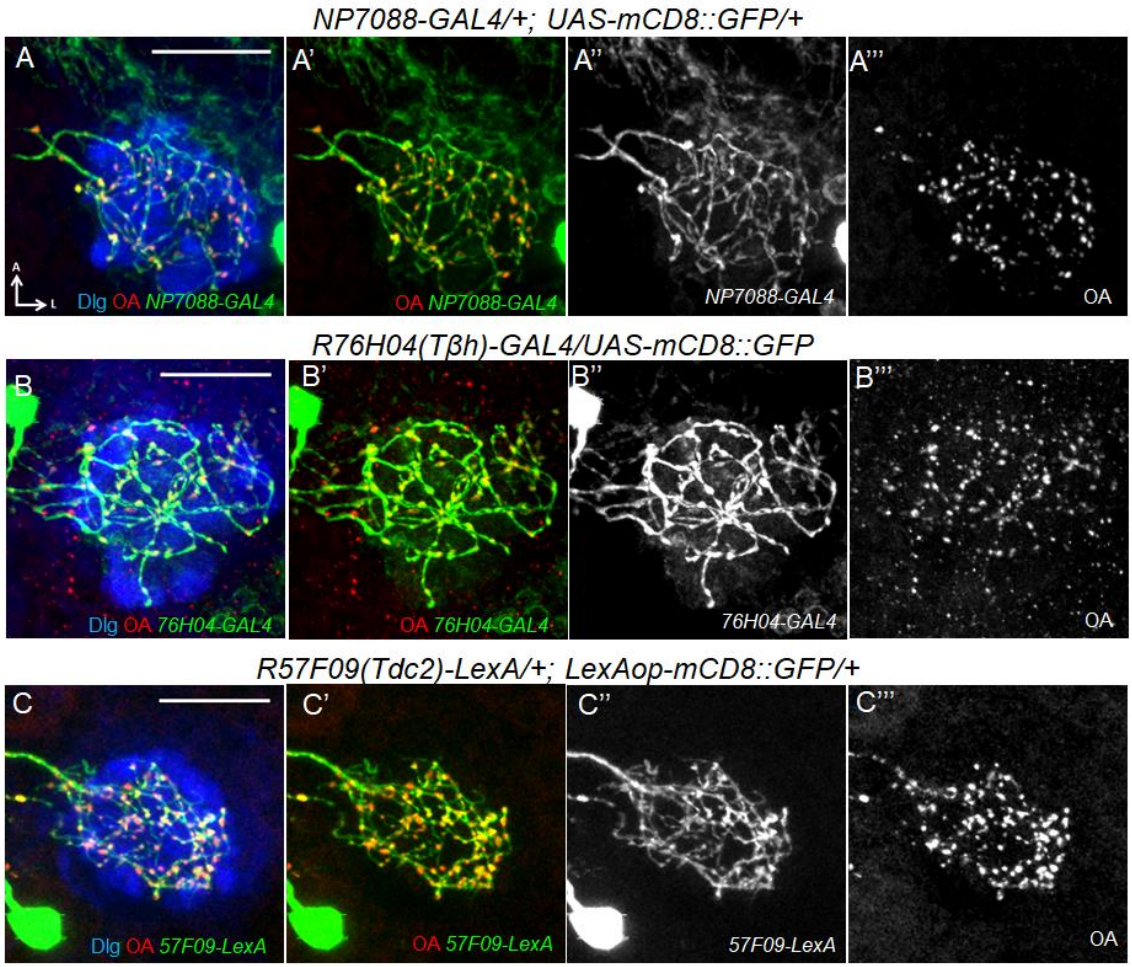

Figure 8.4. *NP7088-GAL4, R76H04-GAL4* and *R57F09-LexA* colocalised with anti-OA in the larval calyx. mCD8::GFP is green, anti-OA is red and anti-Dlg is blue. Confocal projections of the calyx of *NP7088-GAL4>UAS-mCD8::GFP* **(A)**, *R76H04-GAL>UAS-mCD8::GFP* **(B)** and *R57F09-LexA>LexAOp-mCD8::GFP* **(C)**. Anterior (A) is up, lateral (L) is right. Scale bar: 20 µm.

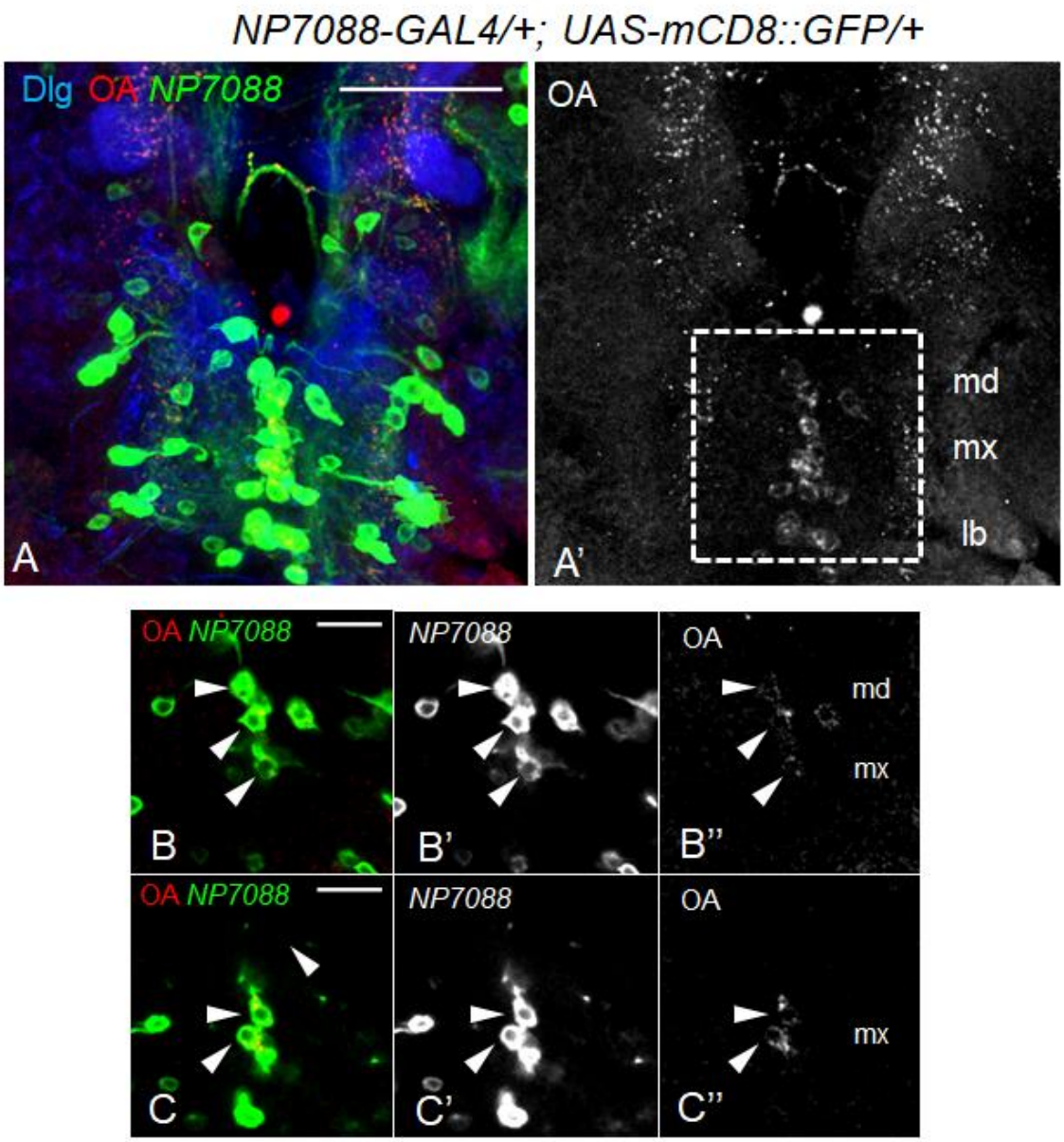

Figure 8.5. *NP7088-GAL4* colocalised with all OA-positive cell bodies in the SOG. *NP7088-GAL4>UAS-mCD8::GFP* is green, anti-OA is red, anti-Dlg is blue. **(A)** Confocal projection of the SOG. **(B-C)** Confocal optical sections of the SOG from the dotted box in **(A)**. *NP7088-GAL4* colocalisation with OA indicated with arrowheads. Anterior is up, medial is at vertical mid-line. Scale bar: 50 µm in **(A)** and 20 µm in **(B-C)**. Abbreviations as Fig.8.2.

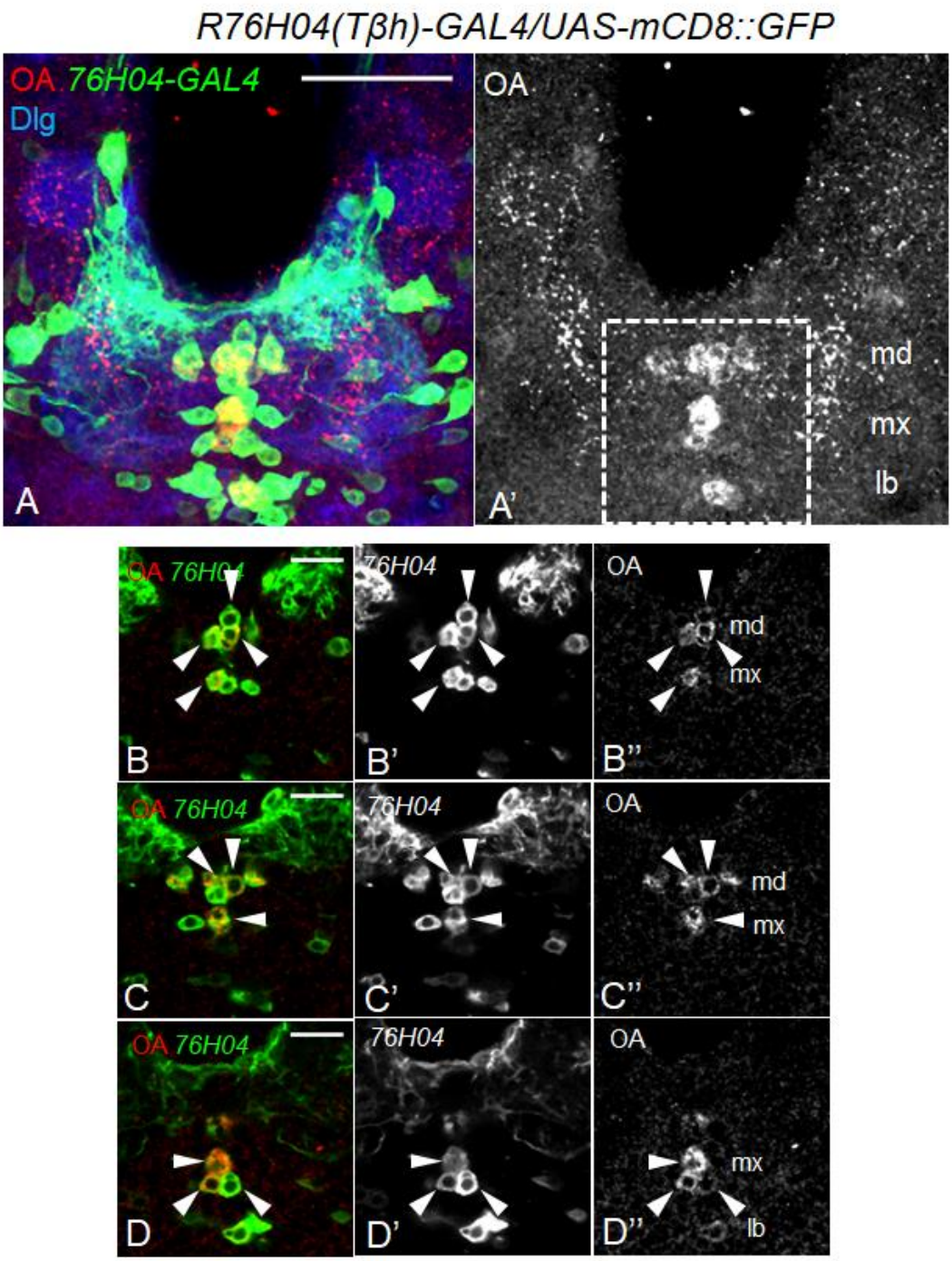

Figure 8.6. *R76H04-GAL4* colocalised with all OA-positive cell bodies in the SOG. *R76H04-GAL4>UAS-mCD8::GFP* is green, anti-OA is red, anti-Dlg is blue. **(A)** Confocal projection of the SOG. **(B-D)** Confocal optical sections of the SOG from the dotted box in **(A)**. *R76H04-GAL4* colocalisation with OA indicated with arrowheads. Anterior is up, medial is at vertical mid-line. Scale bar: 50 µm in **(A)** and 20 µm in **(B-D)**. Abbreviations as Fig.8.2.

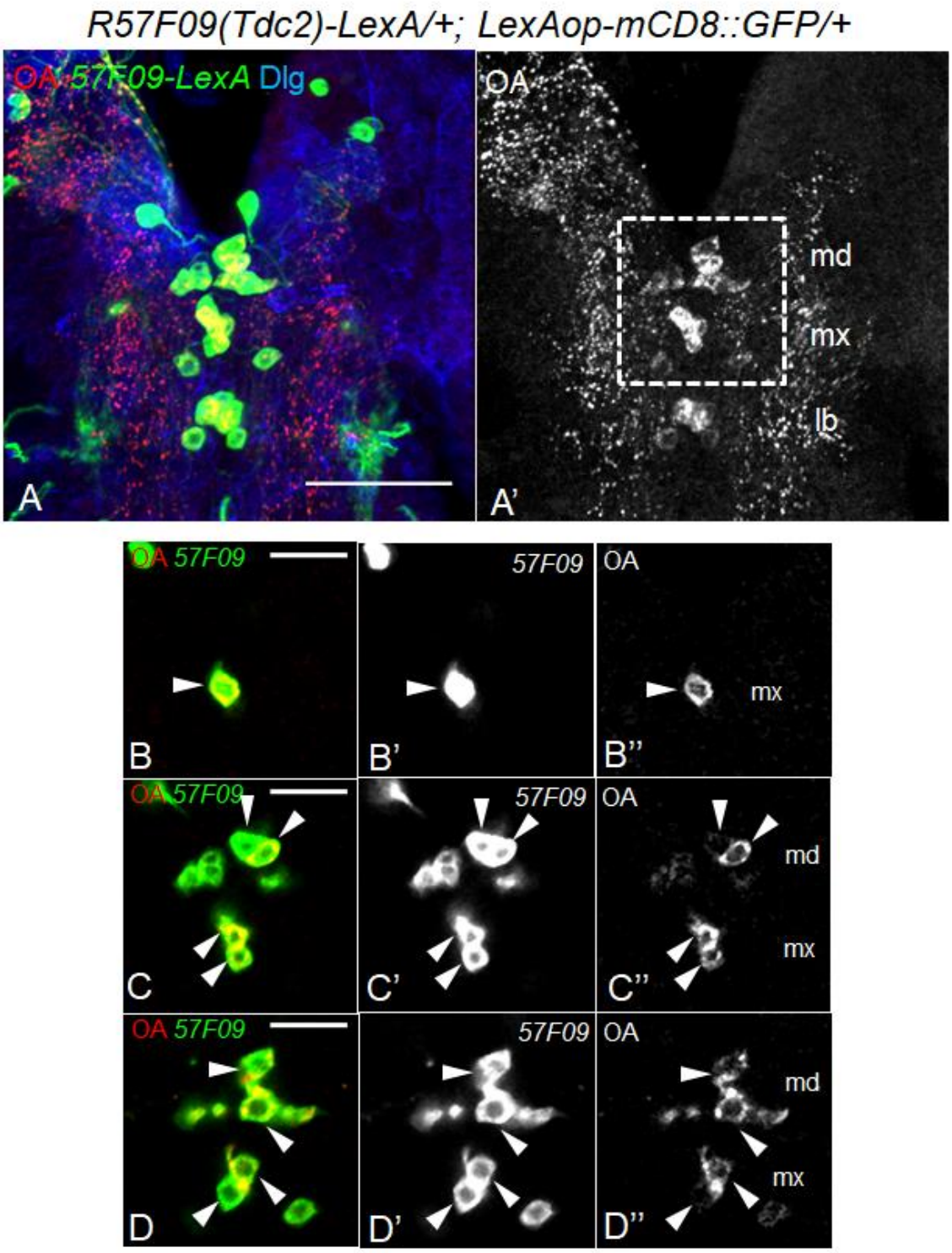

Figure 8.7. *R57F09-LexA* colocalised with all OA-positive cell bodies in the SOG. *R57F09-LexA>LexAOp-mCD8::GFP* is green, anti-OA is red, anti-Dlg is blue. **(A)** Confocal projection of the SOG. **(B-D)** Confocal optical sections of the SOG from the dotted box in **(A)**. *R57F09-LexA* colocalisation with OA indicated with arrowheads. Anterior is up, medial is at vertical mid-line. Scale bar: 50 µm in **(A)** and 20 µm in **(B-D)**. Abbreviations as Fig.8.2.

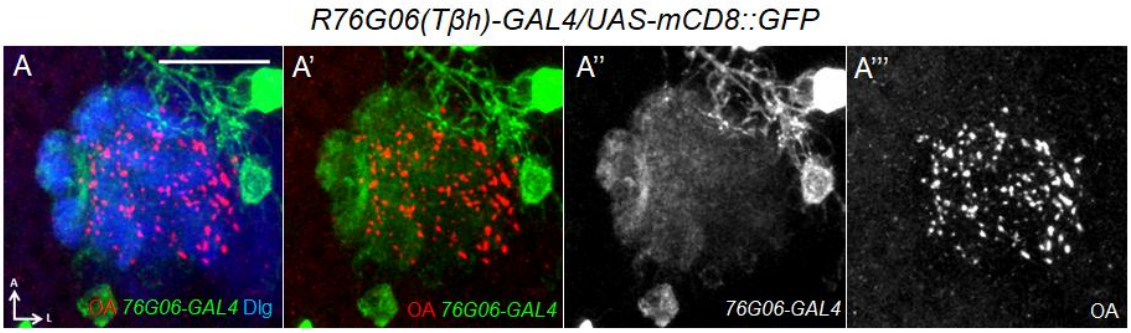

Figure 8.8. *R76G06-GAL4* did not colocalise with anti-OA in the larval calyx. Confocal projection of the calyx of *R76G06-GAL4>UAS-mCD8::GFP* (green). Anti-OA is red and anti-Dlg is blue. Anterior (A) is up, lateral (L) is right. Scale bar: 20 µm.

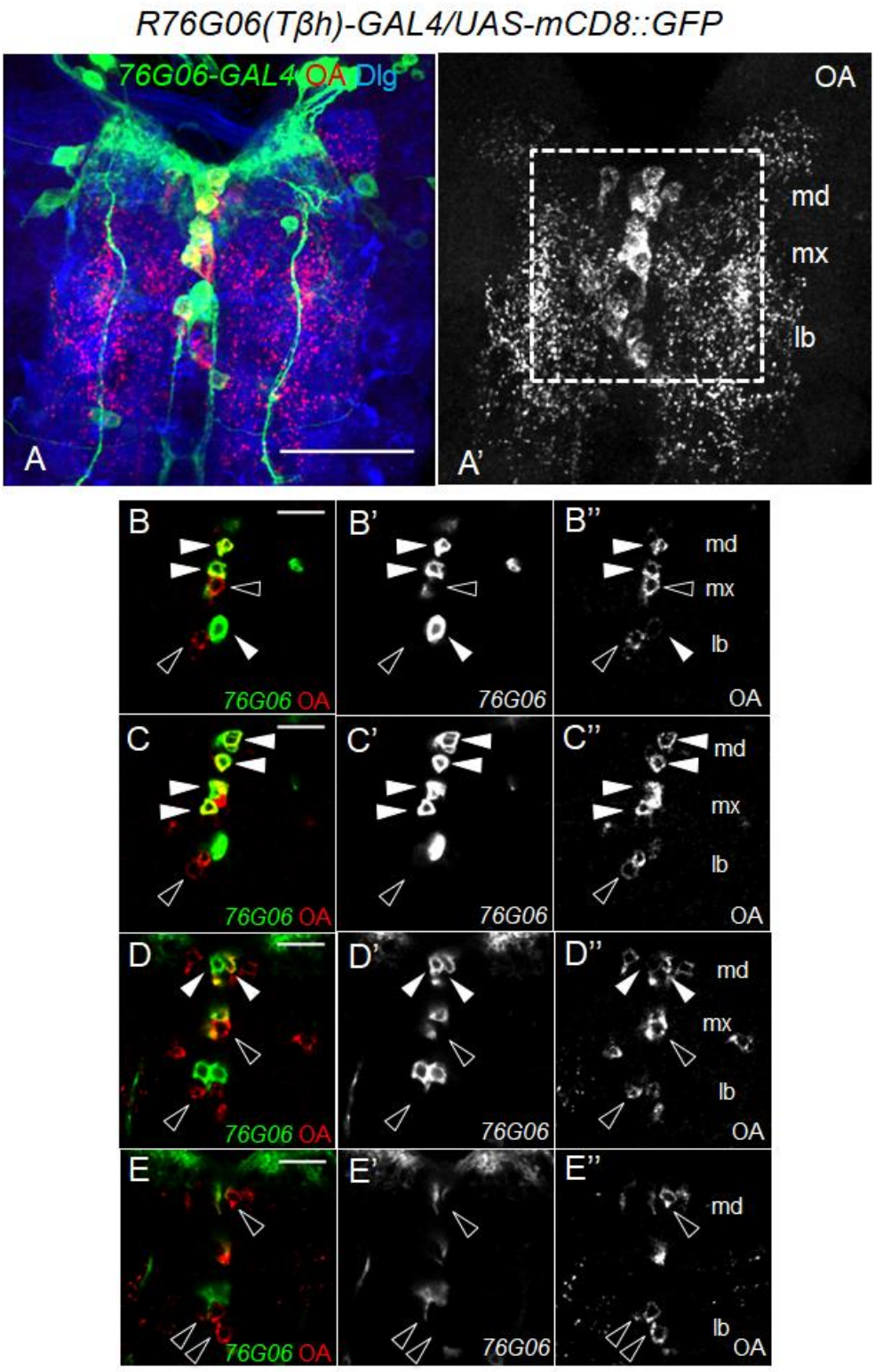

Figure 8.9. *R76G06-GAL4* colocalised with some OA-positive cell bodies in the SOG. *R76G06-GAL4>UAS-mCD8::GFP* is green, anti-OA is red, anti-Dlg is blue. **(A)** Confocal projection of the SOG. **(B-E)** Confocal optical sections of the SOG from the dotted box in **(A)**. *R76G06-GAL4* colocalisation with OA indicated with filled arrowheads, while OA cell bodies that did not colocalise with *R76G06-GAL4* are indicted with empty arrowheads. Anterior is up, medial is at vertical mid-line. Scale bar: 50 µm in **(A)** and 20 µm in **(B-E)**. Abbreviations as Fig.8.2.

filled arrowheads). OA-positive cell bodies that were not labelled by *R76G06-GAL4,* including sVUM1 neurons, are indicated by empty arrowheads (Fig. 8.9).

As *R76G06-GAL4* labelled many OA neurons but not the sVUM1 neurons, it could be used for the alternative FLP-in intersectional approach with *Tdc2-LexA*, which activates the *GAL80* block only in neurons labelled by both parental driver lines (Bohm et al., 2010).

8.2.1.4. Ten candidate lines did not label OA-positive cell bodies in SOG

The ten remaining candidate lines did not label any OA-positive cell bodies in the SOG region (Table 8.1), an example of which is shown in Fig. 8.10. As many of these lines labelled OA-negative SOG cell bodies, they could be useful for generating FLP-in lines if they shared expression with another line that labelled the sVUM1 neurons, for example *R34A11-GAL4*.

Three of the lines that did not label any OA-positive SOG cell bodies were associated with the *Tβh* gene (Fig. 8.10; Table 8.1). This suggested that different fragments taken from the same promoter produced driver lines with very different expression patterns: *R76H04(Tβh)-GAL4* labelled all OA-positive cell bodies (Fig. 8.4, 8.6), *R76G06(Tβh)-GAL4* labelled a subset of OA-positive neurons excluding the sVUM1 neurons (Fig. 8.8, 8.9); and *R76H03(Tβh)-LexA* did not label any OA-positive neurons (Fig. 8.10). This suggested that *GAL4/LexA* lines generated from promoter fragments may not accurately represent gene expression patterns.

8.2.2. Double reporter expression of sVUM1 driver lines

Based on the above results, *R34A11-GAL4 X Tdc2-LexA* and *R34A11-GAL4 X R57F09-LexA* were chosen as two candidate combinations for generating a more specific sVUM1 line through genetic intersection. To compare the expression patterns of *R34A11-GAL4* with *Tdc2-LexA* and *R57F09-LexA*, I used *UAS-mCD8::RFP, LexAOp-mCD8::GFP* (BDSC 32229; Pfeiffer et al., 2010) to simultaneously visualise *GAL4* and *LexA* expression.

R34A11-GAL4>mCD8::RFP, *Tdc2-LexA>mCD8::GFP* colocalized perfectly in the larval calyx (n=4; Fig. 8.11A); confirming that *R34A11-GAL4*

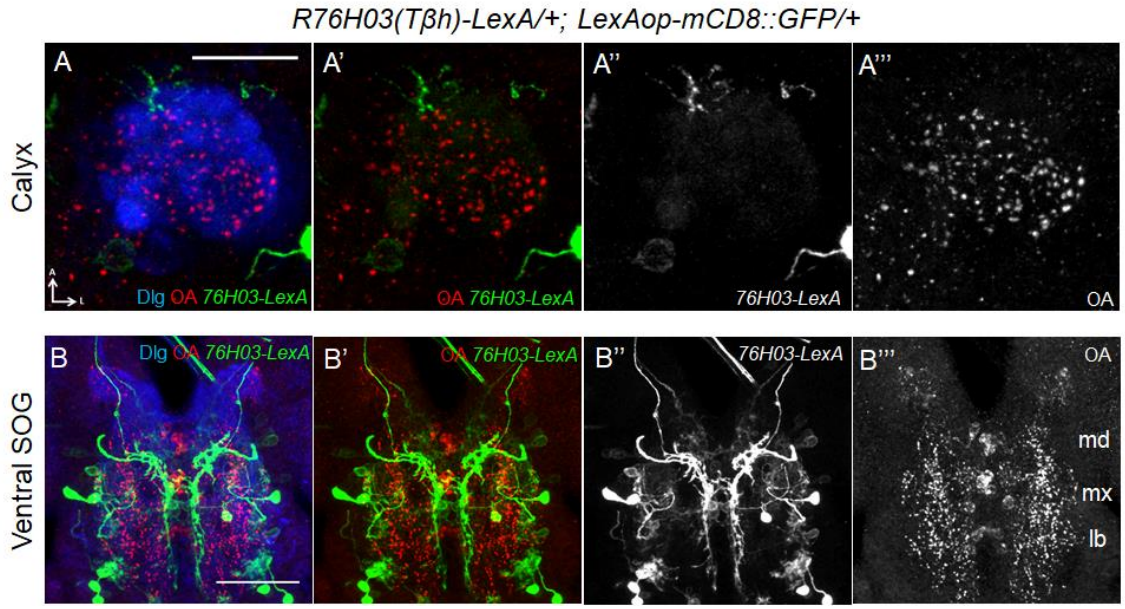

Figure 8.10. *R76H03-LexA* did not label OA-positive neurons. *R76H03-LexA>LexAOp-mCD8::GFP* is green, anti-OA is red, anti-Dlg is blue. **(A)** Confocal projection of the calyx. Anterior (A) is up, lateral (L) is right. **(B)** Confocal projection of the SOG. Anterior is up, medial is at vertical mid-line. Scale bar: 20 µm in **(A)** and 50 µm in **(B)**. Abbreviations as Fig.8.2.

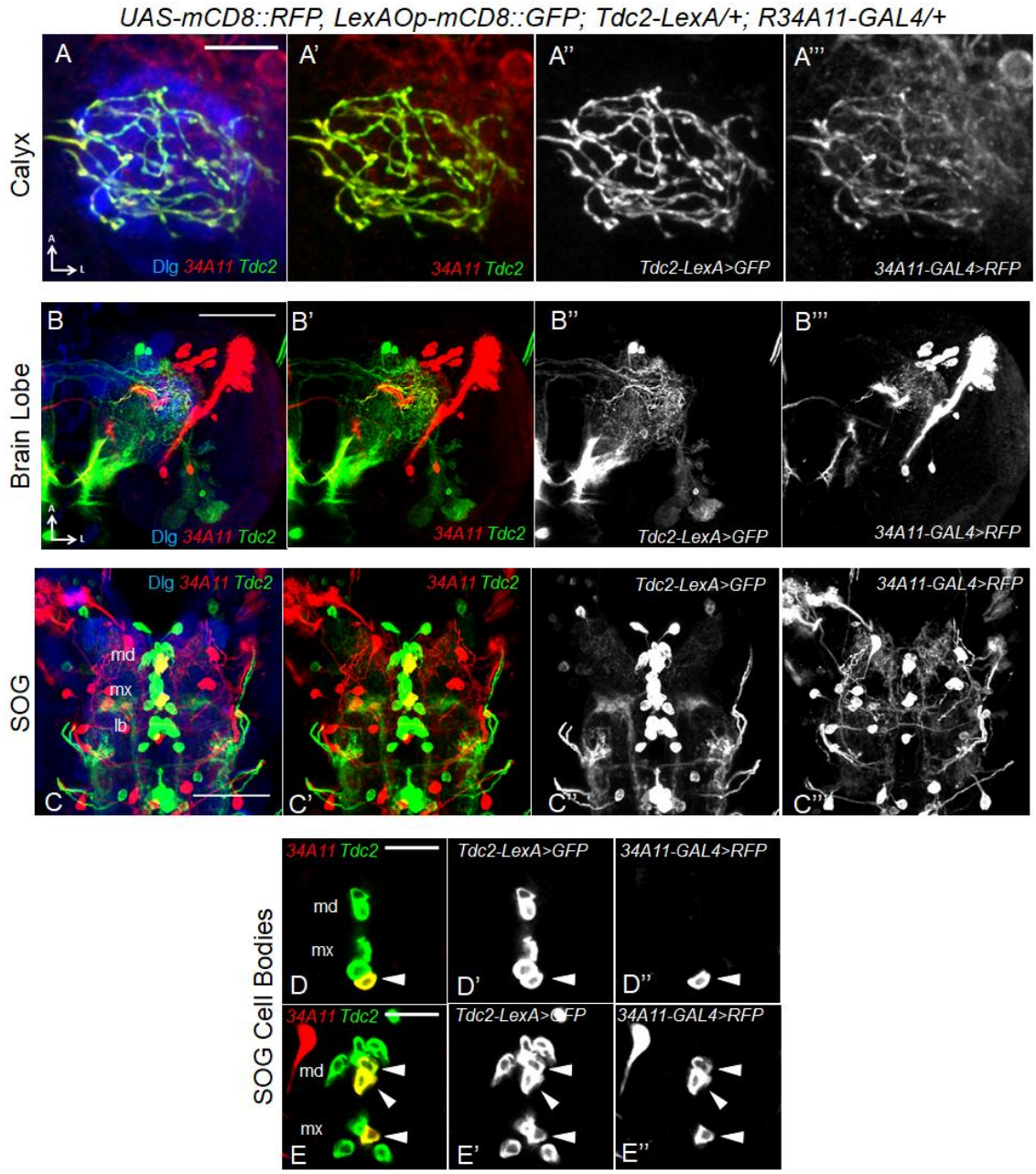

Figure 8.11. *R34A11-GAL4* and *Tdc2-LexA* shared expression in sVUM1 neurons. Confocal projections and optical sections of *UAS-mCD8::RFP, LexAOp-mCD8::GFP; Tdc2-LexA/+; R34A11-GAL4/+*. *Tdc2-LexA>mCD8::GFP* is green, *R34A11-GAL4>mCD8::RFP* is red, anti-Dlg is blue. **(A-C)** Confocal projections of the calyx **(A)**, dorsal brain lobe **(B)** and SOG **(C)**. **(D-E)** Confocal optical sections of the SOG. Anterior (A) is up. Lateral (L) is right in **(A-B)**; medial is at vertical mid-line in **(C-E)**. Scale bar: 20 µm in **(A,D-E)** and 50 µm in **(B-C)**. Abbreviations as Fig.8.2.

labelled the OA sVUM1 neurons. There was limited colocalisation between *R34A11-GAL4* and *Tdc2-LexA* outside the calyx in the brain lobes (Fig. 8.11B) and in the SOG region (Fig. 8.11C). As predicted from anti-OA staining of *R34A11-GAL4*, two cell bodies each in the sVMmd and sVMmx clusters (n=2; Fig. 8.11D-E, arrowheads) and 1 cell body in the sVMlb cluster (n=2; Fig. 8.11C), were co-labelled by *R34A11-GAL4* and *Tdc2-LexA.* This indicated that the intersection between *R34A11-GAL4* and *Tdc2-LexA* should result in a line that labelled five OA-positive neurons, including the sVUM1 neurons, 1 sVUMlb neuron and probably another class of sVUM neurons in the md/mx clusters.

On the other hand, there was greater variability with the double reporter colocalisation of *R57F09-LexA* and *R34A11-GAL4*. Two out of three brains showed perfect colocalisation in the calyx (Fig. 8.12A-B); while neither *R34A11-GAL4>mCD8::RFP* nor *R57F09-LexA>mCD8::GFP* was observed in the third calyx (Fig. 8.12C). Moreover, individual 1 showed denser colocalised innervation in the calyx (Fig. 8.12A) than individual 2 (Fig. 8.12B); suggesting individual 2 might only label one sVUM1 neuron rather than two.

The observation in the calyx matched the number of cell bodies at the ventral midline of the SOG that co-expressed *R34A11-GAL4>mCD8::RFP* and *R57F09-LexA>mCD8::GFP* (Fig. 8.13). Individual 1 labelled four colocalised cell bodies in the SOG – two sVMmd and two sVMmx cell bodies – suggesting that both sVUMmd1 and sVUMmx1 neurons were labelled (Fig. 8.13A-B). Individual 2 labelled three cell bodies that showed colocalisation – one in the sVMmd cluster and two in the sVMmx cluster (Fig. 8.13C-D) – consistent with the lack of expression of one of the sVUM1 neurons in the calyx (Fig. 8.12B), likely to be sVUMmd1. Individual 3 showed colocalisation only in two cell bodies, one each in the sVMmd and sVMmx clusters respectively (Fig. 8.13E-F). This was consistent with the lack of expression in both sVUMmd1 and sVUMmx1 in the calyx (Fig. 8.12C).

This further suggested that there is only one sVUMmd1 neuron and one sVUMmx1 neuron innervating the larval MB calyx with non-overlapping innervation patterns. This was not previously known through clonal analysis, as there were more cell bodies in the sVM clusters than is predicted by the OA

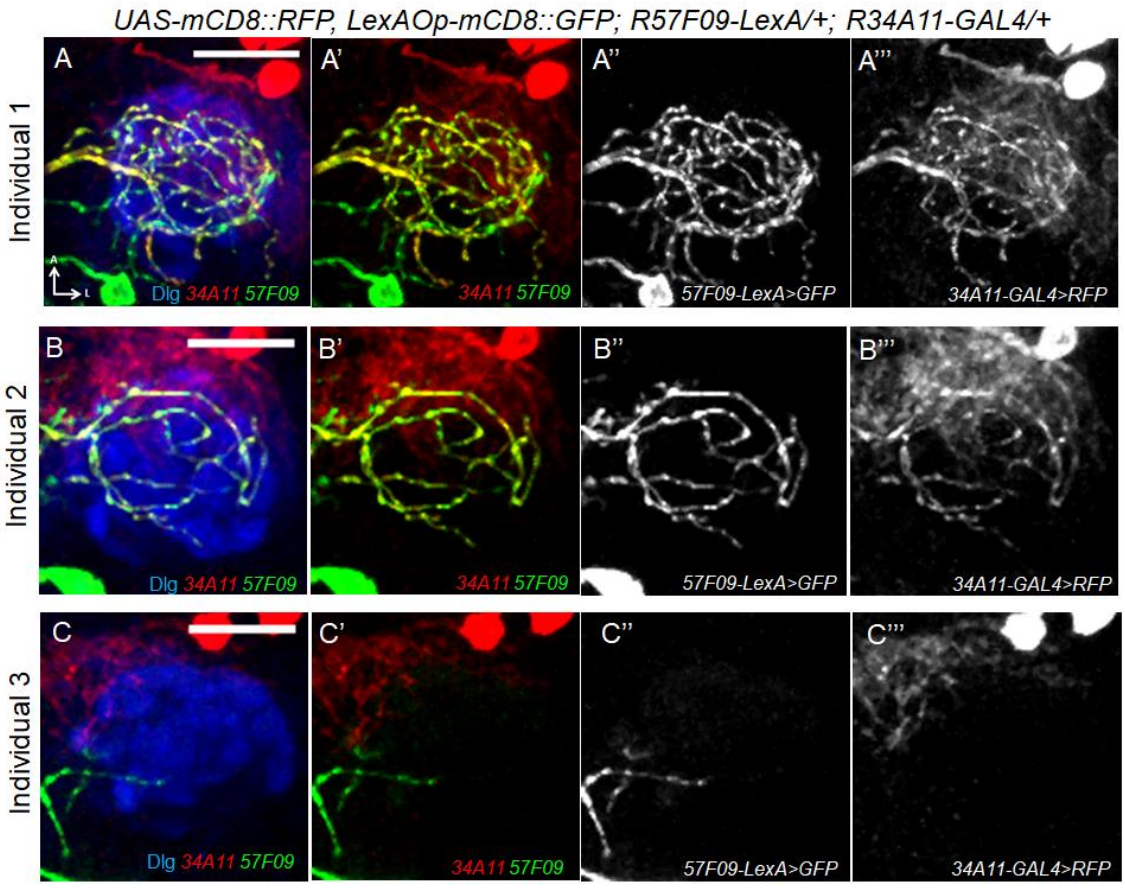

Figure 8.12. *R34A11-GAL4* and *R57F09-LexA* shared expression in sVUM1 neurons inconsistently. Confocal projections of the calyx from three *UAS-mCD8::RFP, LexAOp-mCD8::GFP; R57F09-LexA/+; R34A11-GAL4/+* individuals. *R57F09-LexA>mCD8::GFP* is green, *R34A11-GAL4>mCD8::RFP* is red, anti-Dlg is blue. Anterior (A) is up, lateral (L) is right. Scale bar: 20 µm.

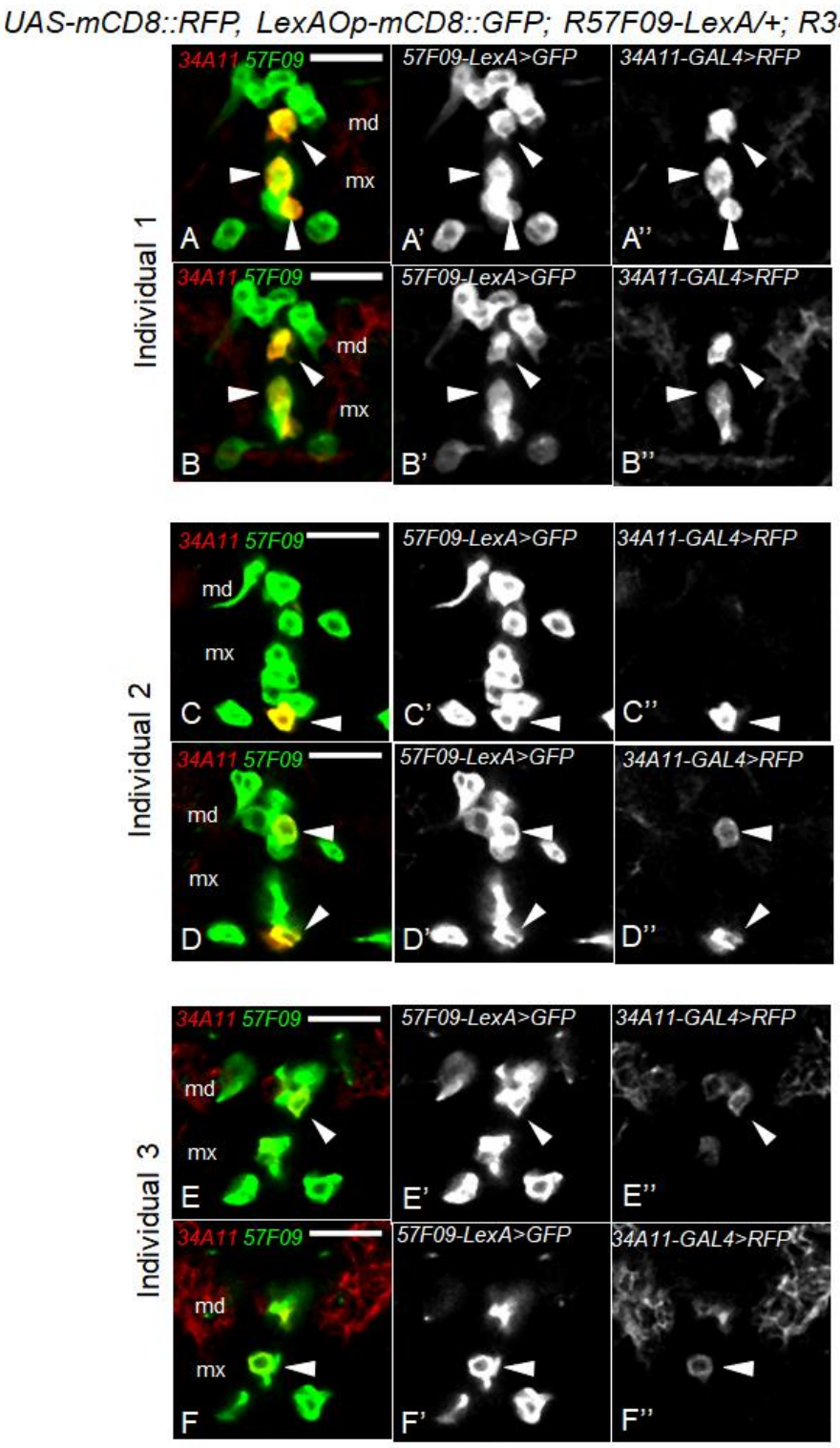

Figure 8.13. *R34A11-GAL4* and *R57F09-LexA* colocalised in a variable number of OA-positive neurons. Confocal optical sections of the SOG from the same three *UAS-mCD8::RFP, LexAOp-mCD8::GFP; R57F09-LexA/+; R34A11-GAL4/+* individuals corresponding to Fig. 8.12. *R57F09-LexA>GFP* is green, *R34A11-GAL4>RFP* is red. **(A-B)** Individual 1; **(C-D)** Individual 2; **(E-F)** Individual 3. Arrowheads indicate colocalisation. Anterior is up, medial is at vertical mid-line. Scale bar: 20 µm. Abbreviations as Fig.8.2.

neuron types, suggesting that there could be more than one neuron for some types of OA neurons (Selcho et al., 2014). Outside of the calyx and ventral midline, there was little colocalisation between *R34A11-GAL4* and *R57F09-LexA* (Fig. 8.14).

Given that the colocalisation outside sVUM1 neurons for the two combinations were similar, *R34A11-GAL4* x *Tdc2-LexA* was more reliable for labelling both sVUM1 neurons in the calyx consistently; and therefore was chosen for generating the specific sVUM1 line using FLP-out intersection.

8.2.3. A *Tdc2-LexA x R34A11-GAL4* sVUM1 intersectional line

A genetic intersection cross between *Tdc2-LexA* and *R34A11-GAL4* was generated (C.O'Kane, personal communication) using the FLP-out intersectional approach (Lee and Luo, 1999). The principle is that *GAL4* inhibitor *GAL80* flanked by *FRT* sites was ubiquitously expressed, preventing *GAL4* expression. *FLP* recombinase was driven in *Tdc2-LexA* neurons, enabling *FLP* recombination at *FRT* sites flanking the *GAL80* sequence. *GAL80* was excised in these neurons, relieving its inhibition of *GAL4* in neurons co-expressing *Tdc2-LexA* and *R34A11-GAL4*. *UAS-Chrimson::mVenus* (Klapoetke et al., 2014) was used as the reporter, as Chrimson would be used to optogenetically activate sVUM1 neurons in future imaging or behavioural experiments.

Five neurons were consistently labelled in the *FRT-GAL80/+; LexAOp-FLP/Tdc2-LexA; UAS-Chrimson::mVenus/R34A11-GAL4* intersection line (n=9; Fig. 8.15A), including two sVUMmd neurons, two sVUMmx neurons and one sVUMlb neuron. This included the two sVUMmd1 and sVUMmx1 neurons as *Tdc2-LexA x R34A11-GAL4* showed innervation in the calyx (Fig. 8.15B) as well as AL (Fig. 8.15C). The additional pattern observed in the brain lobe resembled that of sVUM2 neurons (Selcho et al., 2014), especially as the larval optic neuropil is labelled in the intersection (Fig. 8.15A). This suggested that sVUMmd2 and sVUMmx2 neurons, and a sVUMlb neuron of unknown identity, were likely to be the only other OA neurons strongly and consistently labelled in this line. There are also occasionally very few additional cell bodies weakly labelled in the brain lobe or SOG region. However, they do not appear to send projections or processes.

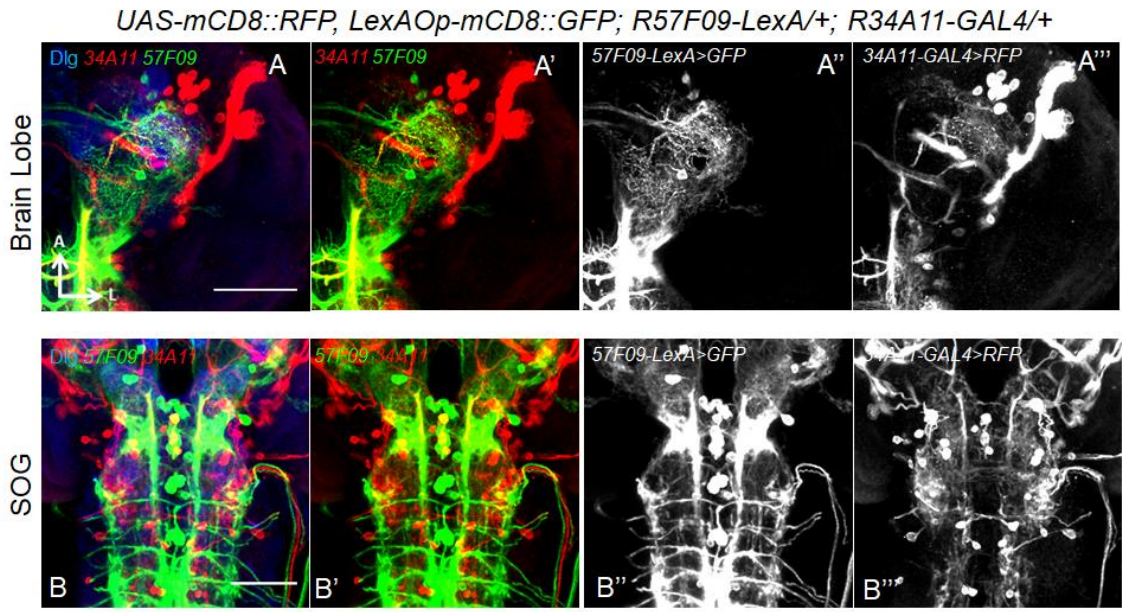

Figure 8.14. *R34A11-GAL4* and *R57F09-LexA* did not share expression outside sVUM neurons. *UAS-mCD8::RFP, LexAOp-mCD8::GFP; R57F09-LexA/+; R34A11-GAL4/+* Individual 1 from Fig. 8.12, 8.13. *Tdc2-LexA>GFP* is green, *R34A11-GAL4>RFP* is red, anti-Dlg is blue. **(A-B)** Confocal projections of the dorsal brain lobe **(A)** and ventral SOG **(B)**. Anterior (A) is up; lateral (L) is right for **(A)** and medial is at vertical mid-line for **(B)**. Scale bar: 50 µm.

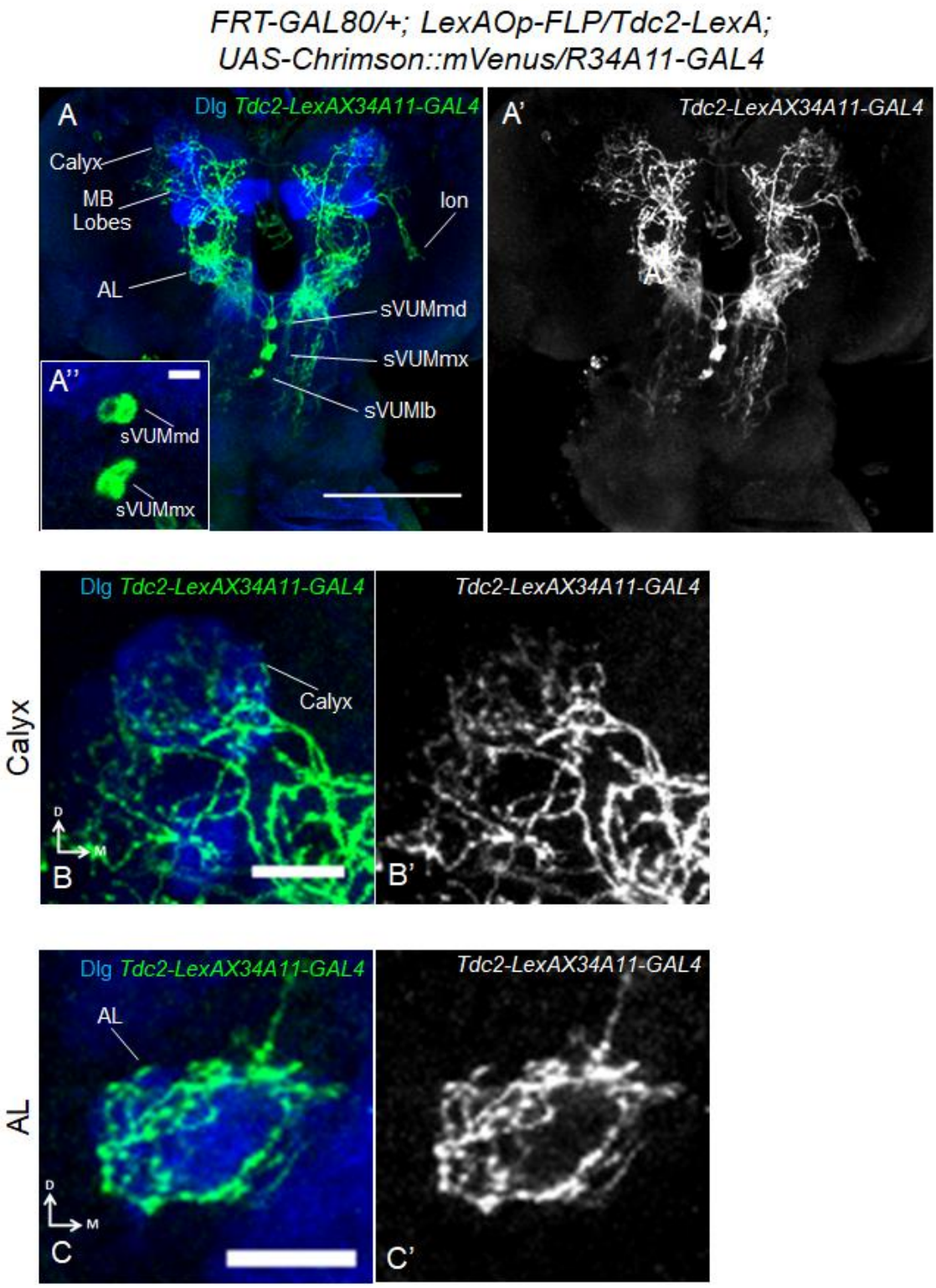

Figure 8.15. *R34A11-GAL4* and *Tdc2-LexA* intersection labelled sVUM1 neurons and 3 other neurons. *FRT-GAL80/+; LexAOp-FLP/Tdc2-LexA; UAS-Chrimson::mVenus/R34A11-GAL4* is green, anti-Dlg is blue. **(A-C)** Confocal projections of the brain lobe and ventral nerve cord **(A)**, calyx **(B)** and AL **(C)**. **(A'')** Inset of sVMmd and sVMmx cell bodies labelled. Dorsal (D) is up; medial (M) is at vertical mid-line for **(A)** and right for **(B-C)**. Scale bar: 100 µm in **(A)**, 10 µm in **(A'',C)** and 50 µm in **(B)**. Abbreviation: lon, larval optic neuropil.

8.2.4. Labelling candidate lines for single neurons innervating the calyx

Six *GAL4/LexA* lines that potentially label single calyx innervating neurons were selected from the Janelia FlyLight collection (Jennett et al., 2012; L. Masuda-Nakagawa, personal communication). Four of these lines labelled one or two neurons innervating the calyx; while two other lines – *R74G04(GABA-B-R1)-GAL4* and *R76B09(GABA-B-R3)-GAL4* labelled only KCs in the calyx (Table 8.2).

R76C06(GABA-B-R3)-GAL4 labelled two cell bodies that innervated the non-glomerular region of the calyx (Fig. 8.16A-D, arrowheads) and around the medial lobes (Fig. 8.16E); similar to Odd-like neurons (Slater et al. 2015). This line also labelled KCs (Fig. 8.16A-B).

R68C01(Octβ2R)-GAL4 and *R68B12(Octβ2R)-GAL4* both labelled one neuron that showed characteristic innervation of the calyx and MB lobes similar to Odd-like neurons (Fig. 8.17, 8.18, arrowheads). Both lines also labelled KCs weakly. Overall, *R68C01(Octβ2R)-GAL4* labelled many more additional neurons (Fig. 8.17A) compared to *R68B12(Octβ2R)-GAL4* (Fig.8.18A).

R68B12(Octβ2R)-LexA, which shared the same promoter fragment as *R68B12(Octβ2R)-GAL4*, strongly labelled one neuron in each brain lobe (Fig. 8.19, arrowhead). This line did not label other neurons in the brain lobes, although additional labelling was observed in the SOG region (Fig. 8.19A). This was the most specific line identified for Odd-like neurons; and would be very useful for functional and behavioural analyses if the SOG and ventral nerve cord expression could be effectively blocked.

***GAL4/LexA* Lines**	**Gene**	**Results**	**Figure**
R76C06-GAL4	*GABA-B-R3*	2 calyx-innervating neurons, KCs	8.16
R68C01-GAL4	*Octβ2R*	1 calyx-innervating neuron, KCs	8.17
R68B12-GAL4	*Octβ2R*	1 calyx-innervating neuron, KCs	8.18
R68B12-LexA	*Octβ2R*	1 calyx-innervating neuron; very few other neurons labelled	8.19
R74G04-GAL4	*GABA-B-R1*	KCs	
R76B09-GAL4	*GABA-B-R3*	KCs	

Table 8.2. Summary of the labelling of specific calyx-innervating neuron drivers.

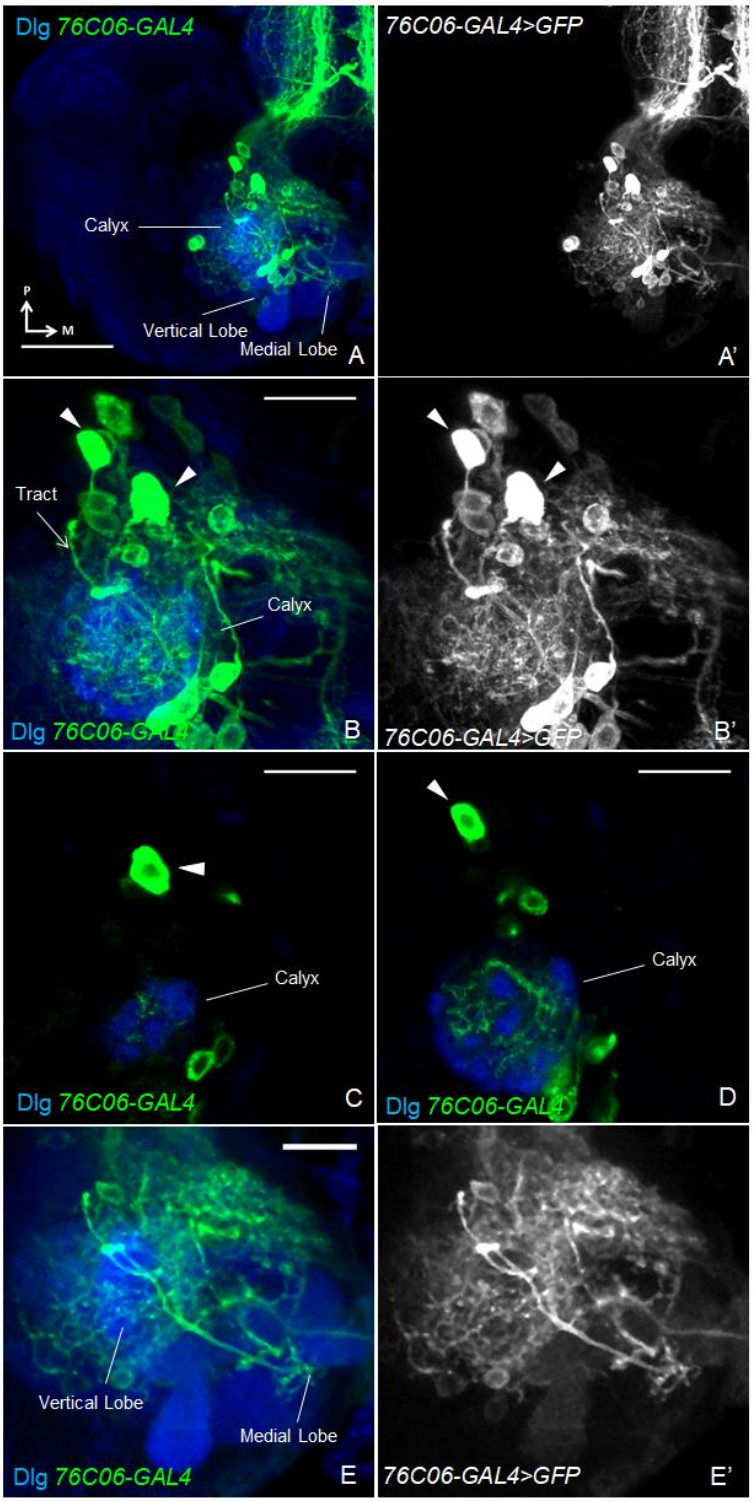

Figure 8.16. *R76C06-GAL4* labelled two calyx-innervating neurons. Confocal projections of the full dorsal brain lobe expression pattern **(A)**, calyx **(B)** and MB lobes **(E)**, and confocal optical sections of the calyx **(C-D)**, of *R76C06-GAL4>UAS-mCD8::GFP* (green). Anti-Dlg is blue. Cell bodies sending projections to calyx indicated with arrowheads. Posterior (P) is up, medial (M) is right. Scale bar: 50 µm for **(A)** and 20 µm for **(B-E).**

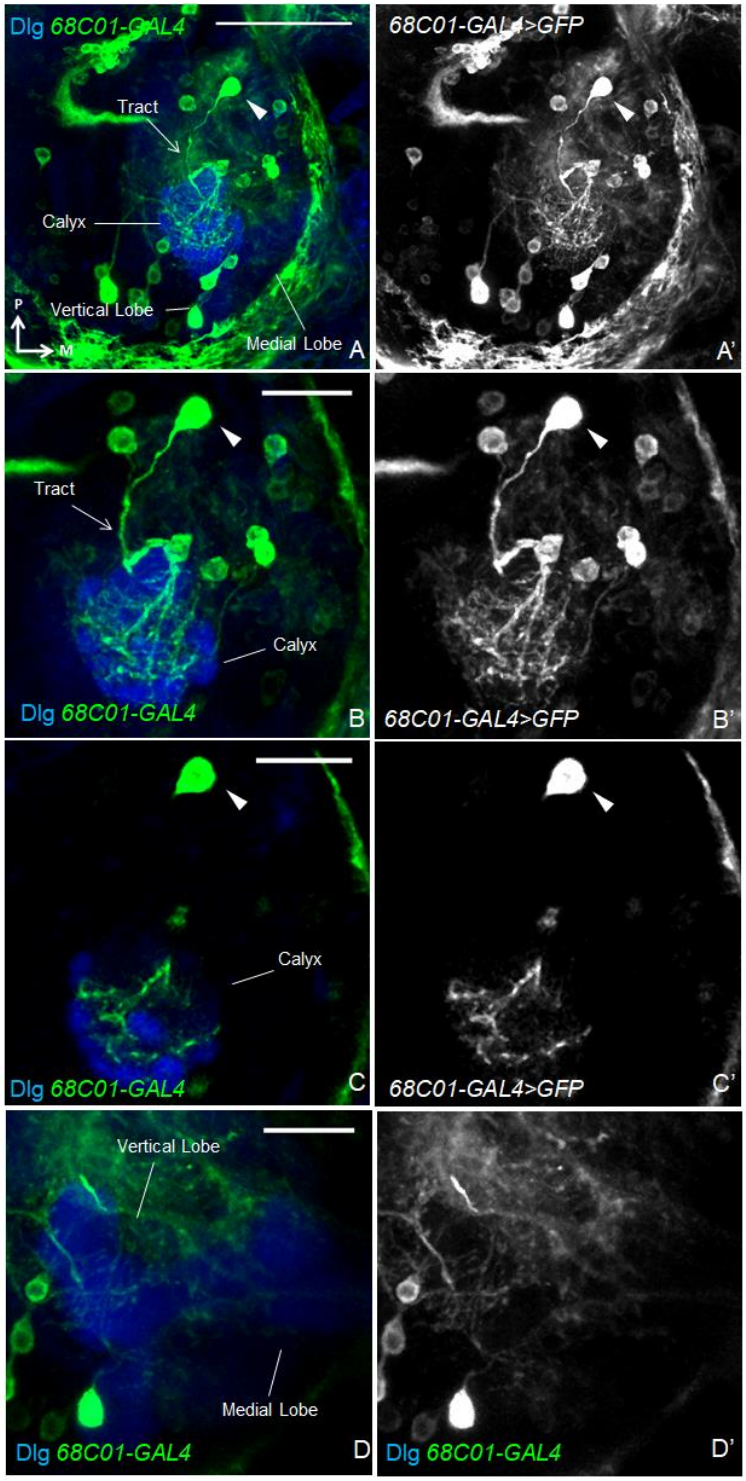

Figure 8.17. *R68C01-GAL4* labelled a single calyx-innervating neuron. Confocal projections of the full dorsal brain lobe expression pattern **(A)**, calyx **(B)** and MB lobes **(D)**, and a confocal optical section of the calyx **(C)**, of *R68C01-GAL4>UAS-mCD8::GFP* (green). Anti-Dlg is blue. Cell body projecting to calyx indicated with arrowhead. Posterior (P) is up, medial (M) is right. Scale bar: 50 µm for **(A)** and 20 µm for **(B-D).**

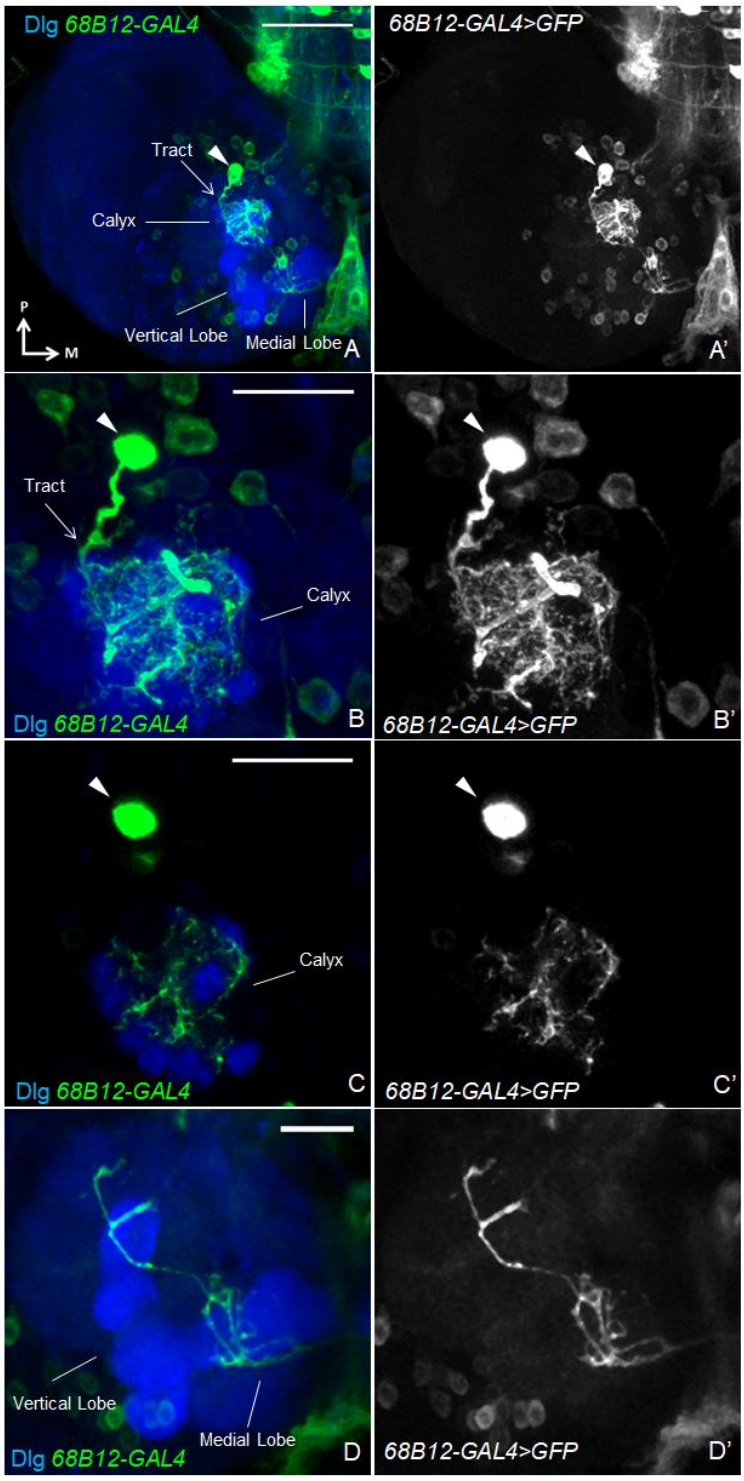

Figure 8.18. *R68B12-GAL4* labelled a single calyx-innervating neuron. Confocal projections of the full dorsal brain lobe expression pattern **(A)**, calyx **(B)** and MB lobes **(D)**, and a confocal optical section of the calyx **(C)**, of *R68B12-GAL4>UAS-mCD8::GFP* (green). Anti-Dlg is blue. Cell body projecting to calyx indicated with arrowhead. Posterior (P) is up, medial (M) is right. Scale bar: 50 µm for **(A)** and 20 µm for **(B-D).**

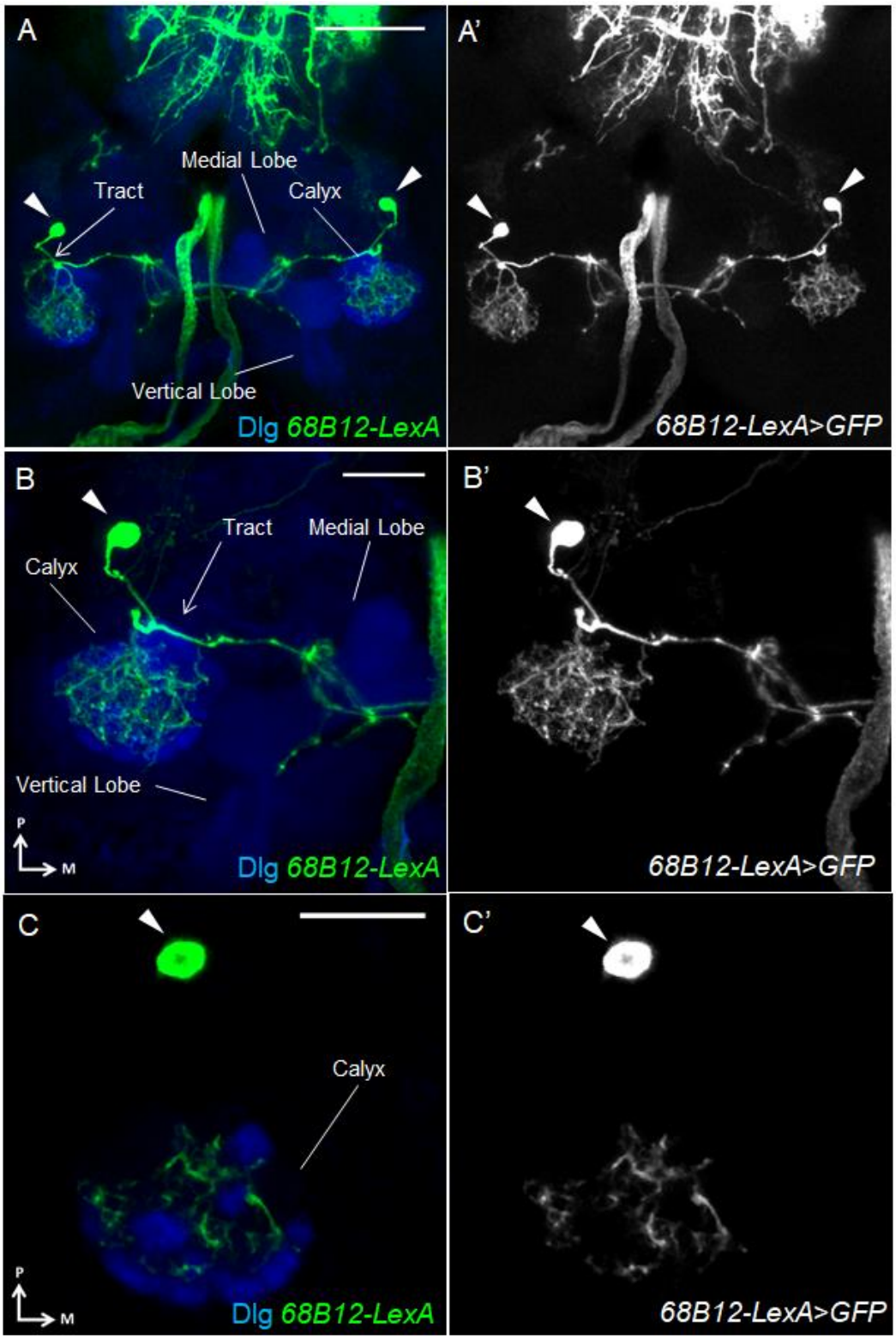

Figure 8.19. *R68B12-LexA* labelled a single calyx-innervating neuron. Confocal projections of the brain lobes from the frontal orientation **(A)** and MB calyx and lobes **(B)**, and a confocal optical section of the calyx **(C)**, of *R68B12-LexA>LexAOp-mCD8::GFP* (green). Anti-Dlg is blue. Cell body projecting to calyx indicated with arrowhead. Ventral is up, medial is at vertical mid-line for **(A)**. Posterior (P) is up and medial (M) is right for **(B-C)**. Scale bar: 50 µm for **(A)** and 20 µm for **(B-C)**.

8.3. Discussion

8.3.1. A more specific sVUM1 driver line

The *Tdc2-GAL4* line, which has traditionally been used to study the functions of OA neurons, labels the majority of OA/TA neurons which project to diverse regions of the adult and larval brains (Busch et al., 2009; Selcho et al., 2014). It is therefore impossible to discern the function of a particular OA neuron within a specific circuit using *Tdc2-GAL4*. Moreover, some effects of OA signalling might be obscured by signalling from neurons which only express TA, also labelled by the *Tdc2-GAL4* line (Selcho et al., 2014). TA itself can act as a neurotransmitter in insects (Roeder, 1999); and has been shown to oppose OA effects in larval locomotion (Saraswati et al., 2004).

To differentiate the effects of OA from TA, some studies have used the *Tβh* mutant which is defective for OA synthesis from TA (Schwaerzel et al., 2003). However, this is also problematic as *Tβh* mutants overexpress TA, which might cause confounding effects for studying OA function.

A previous attempt to restrict expression of *Tdc2-GAL4* by using *tsh-GAL80* to block *GAL4* expression in the ventral nerve cord allowed for the disassociation between OA/TA neurons in the ventral nerve cord from OA/TA neurons in the brain hemisphere and SOG in larval locomotion and memory formation respectively (Selcho et al., 2012, 2014). *NP7088-GAL4* has also been used with *Tdc2-LexA* in intersection to generate an OA neuron line that excluded the calyx-innervating OA-VPM5 neuron amongst others in the adult brain (Busch et al., 2009; Burke et al., 2012). Therefore, the *Tdc2-LexA x R34A11-GAL4* intersectional line from this study is the most specific sVUM1 driver line to date.

However, this intersection line still labels three other OA neurons that do not innervate the calyx or MB. Furthermore, this line does not differentiate between sVUMmd1 and sVUMmx1, which may have different functions, as laser ablation of sVUMmd and sVUMmx neurons resulted in opposing effects in starvation-dependent larval feeding behaviour (Zhang et al., 2013a).

Nevertheless, the *Tdc2-LexA x R34A11-GAL4* intersectional line will be an improvement from using the general OA neuron lines – *Tdc2-GAL4/Tdc2-*

LexA –for more specific manipulations of the sVUM1 neurons in the larval calyx circuitry.

8.3.2. Single calyx-innervating neuron lines

The four single calyx-innervating neuron lines will be useful in dissecting the function of the relatively uncharacterised Odd-like neurons in the calyx circuitry; in particular, how they are potentially modulated by OA signalling. These driver lines label one or two Odd-like neurons whose tracts could be followed to the calyx.

According to Slater et al. (2015), three Odd neurons with distinctive innervation patterns have been identified using clonal analysis from the *Odd-GAL4* line. Two of these neurons extended both ipsilateral and contralateral projections, but the authors did not further elaborate on how they could be distinguished from each other. The third neuron only extended ipsilateral projections. From the new driver lines, there appears to be at least two Odd-like neurons.

The availability of multiple single neuron driver lines for Odd-like neurons that label different populations of neurons is useful for attributing phenotypes to Odd-like neurons, such as their requirements for odour discrimination, rather than to the other neurons that may be labelled as well. The *R68B12-LexA* line is especially useful: not only is it specific, it is also the first and only *LexA* line known to label Odd-like neurons.

8.3.3. Variable expression of promoter-fragment transcriptional drivers

I examined several *GAL4* lines under different promoter fragments of the same gene. For example, only one out of five *Tβh-GAL4* lines screened showed expression in all of the OA neurons, despite containing a promoter fragment for the enzyme required for OA synthesis. Instead, different *Tβh-GAL4* lines displayed a wide range of expression patterns. This has been previously observed for *OAMB-GAL4* lines as well (Jenett et al., 2012; El-Kholy et al., 2015; Watanabe et al., 2017).

On the other hand, *GAL4* and *LexA* lines under the control of the same promoter fragments, for example *R34A11-GAL4/LexA* or *R68B12-GAL4/LexA*, did not show exactly the same expression pattern. For example, *R68B12-LexA*

labelled fewer neurons in the brain lobe compared to *R68B12-GAL4*. There may also be intrinsic variation of *GAL4/LexA* expression. For example, the *R57F09-LexA; R34A11-GAL4* construct sometimes did not label both of the sVUM1 neurons (n=2 out of 3).

This large variation in expression between different promoter fragment driver lines suggests that it is unlikely that a single promoter-fragment transcriptional line can accurately represent the expression pattern of the gene the promoter fragment is associated with. For example, it cannot be inferred that Odd-like neurons expresses the GABA-B-R3 receptor because *76C06(GABA-B-R3)-GAL4* labelled Odd-like neurons, while *R76B09(GABA-B-R3)-GAL4* did not. On the other hand, some *Tβh-GAL4* lines indeed labelled the majority of OA-positive neurons; and Odd-like neurons were labelled in two *Octβ2R-GAL4* lines.

Therefore, promoter fragment *GAL4/LexA* lines should only act as rough guide to gene expression patterns, which must be corroborated with alternative methods such as protein traps or antibody labelling.

Chapter 9. General discussion

To understand the logic of higher brain circuitry, much of the current work has focused on constructing a complete map of the synaptic connections in the brain. Some of these projects, such as the *Drosophila* olfactory connectome of the first instar larva, are beginning to come to fruition (Berck et al., 2016; Eichler et al., 2017). While these projects have revealed many novel connections and network motifs, they do not represent the full extent of neuromodulation, which can often act at long-range targets that would not be detected using EM. It might also be challenging to translate such large-scale reconstruction efforts to functional testing, as many of the neurons are yet to be characterised, and there are no readily available tools to manipulate these neurons.

Here I presented an alternative approach in mapping the neuromodulation circuit of a higher sensory pathway. Through using the already well-characterised *Drosophila* larval MB calyx, I aimed to identify potential postsynaptic partners to the OA sVUM1 neurons and map all the known OA receptors to each of the known calyx-innervating neurons. To date, neuromodulatory receptor maps have only been achieved in lower invertebrates such as *C.elegans* (Bentley et al., 2016); but have not yet been attempted in higher order sensory circuits in *Drosophila*. The goal of this neuromodulatory map would be to identify all potential OA targets in the calyx, and to predict the possible effects of OA signalling based on the receptor expressed. Such a map would provide a framework for testing the effects of OA signalling from sVUM1 neurons on individual neurons via specific types of receptors, and how individual effects could interact to form a complete neuromodulatory network.

In this chapter, I first discuss the extent to which I achieved my aims of developing a preliminary OA neuromodulatory map of the larval MB calyx, evaluate the methods used in this study, and propose alternative approaches in how to continue developing this map. Next, I will focus on my key findings and their implications, how they could be validated and how they fit into our understanding of the MB calyx circuitry in *Drosophila* larvae, adults and other insects. Based on this, I will propose a model on how OA modulates the odour discrimination circuitry in the MB calyx, and how this model can be

experimentally tested. Finally, I will discuss how my findings change our understanding of how neuromodulatory circuitry is organised for modulating sensory processing.

9.1. Mapping sVUM1 targets in the larval MB calyx

To identify potential sVUM1 targets subjected to OA neuromodulation in the larval MB calyx, I used GRASP-OA colocalisation experiments to identify putative postsynaptic partners of sVUM1 neurons, and EGFP-tagged receptors generated from MiMIC insertion lines to visualise the localisation pattern of the five known OA receptors in the calyx and identify the neurons they were present on. I also used EGFP-tagged GABA receptors to determine whether $GABA_AR$ and $GABA_BR$ localised to the sVUM1 terminals in the larval MB calyx for mediating APL signalling to sVUM1 neurons. The full results from this study are summarised in Figure 9.1 and Table 9.1.

Building on my MPhil work (H.W., MPhil Thesis 2014), I found that potential synapses between sVUM1 neurons and PNs, the APL neuron and Odd-like neurons colocalised with OA terminals in the calyx – suggesting that they may be postsynaptic to sVUM1 neurons and probably receive OA neuromodulation (Fig. 9.1). These were consistent with L1 EM connectivity data that became publically available two years after these experiments were completed (Eichler et al., 2017; Https://neuronlp.larva.fruitflybrain.org/). Contrary to L1 EM and adult GRASP results (Zhou et al., 2012; Pech et al., 2013; Eichler et al., 2017), I only detected limited KC-sVUM1 connections in the larval MB calyx; which may be due to developmental reasons. While EM data are better for visualising synapses than GRASP, my data showed GRASP colocalisaton with OA, hence indicating potential postsynaptic sites that are probably modulated by OA signalling. This is important as OA neurons may co-release TA and neuropeptides, and EM data do not directly show the neurotransmitter released at synaptic connections.

My main discoveries from this study centre around the characterisation of expression patterns of OA/GABA receptors in the larval MB calyx, both in terms of cell type and subcellular distribution (Fig. 9.1; Table 9.1). For the first time, I found that 1) the α1-adrenergic-like OAMB broadly localised to the presynaptic

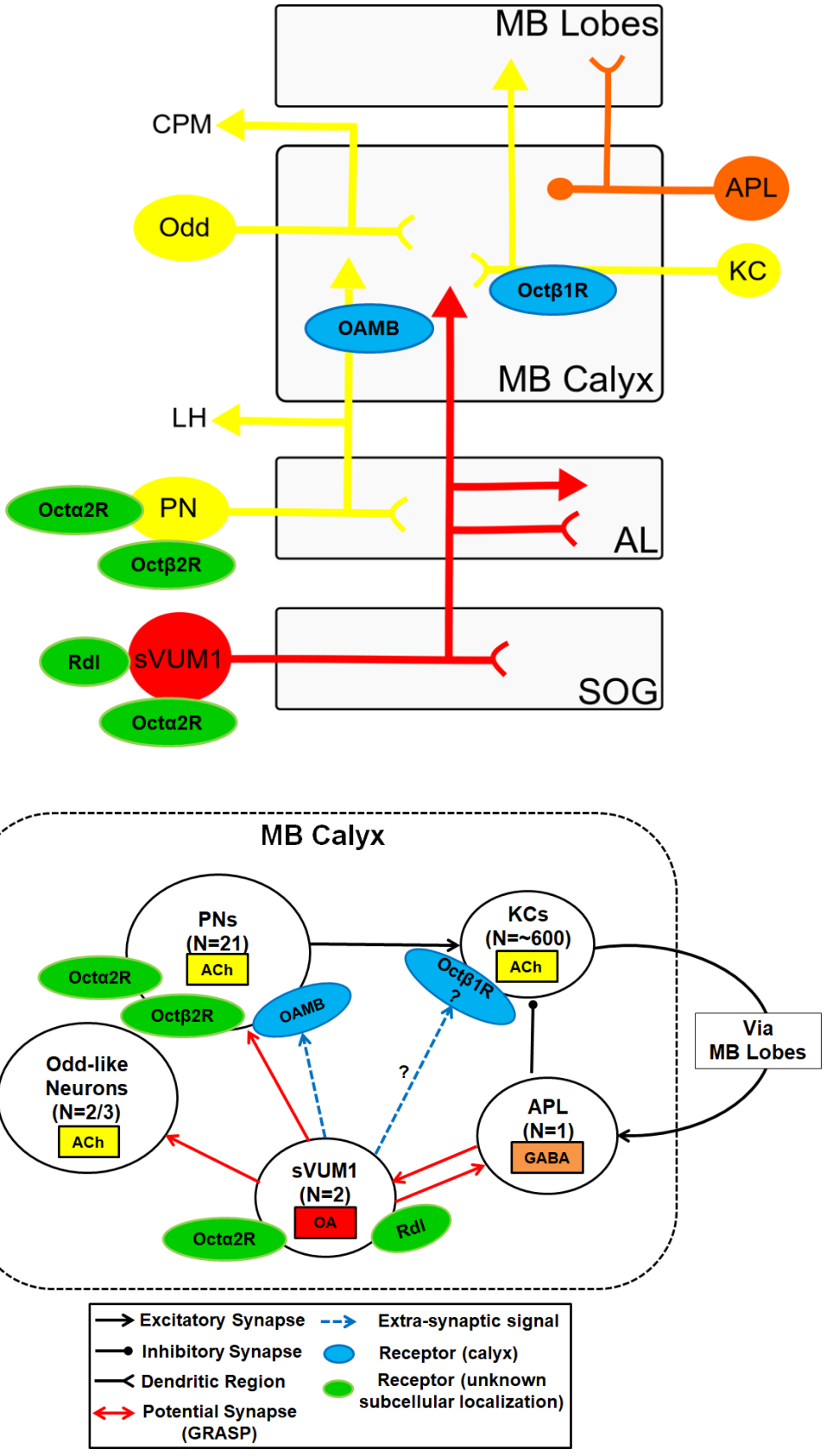

Figure 9.1. Summary diagram of proposed OA and GABA receptor localisation in the larval MB calyx circuitry. Abbreviations: ACh, acetylcholine; AL, antennal lobe; CPM, centroposterior medial compartment; KC, Kenyon Cell; LH, lateral horn; MB, mushroom body; N, number; OA, octopamine; PN, projection neuron.

	KCs	PNs	APL	sVUM1	Odd-like
OAMB	-	+	-	-	-
Octα2R*	-	+*	N/A	+*	N/A
Octβ1R	+ (Likely)	-	-	-	-
Octβ2R*	Inconclusive	+*	Too weak	Inconclusive	Inconclusive
Octβ3R	-	-	-	-	-
Rdl*	+*	Likely	N/A	+*	N/A
$GABA_BR1$	Likely	Likely	N/A	-	N/A

Table 9.1. Summary table of OA and GABA receptor localisation to neurons innervating the larval MB calyx. + indicates the presence of the receptor, - indicates the absence of the receptor, and N/A indicates there are no available data. * indicates that it is unclear whether the receptor is localised to calyx terminals of the neurons they are expressed in.

terminals of olfactory PNs in the larval MB calyx; 2) the β-adrenergic-like Octβ1R probably localised to KC dendrites in the calyx; 3) the α2-adrenergic-like Octα2R and β-adrenergic-like Octβ2R both localised to a subset of the olfactory PN cell bodies, although their subcellular localisation was unclear; and 4) Octα2R and the ionotropic $GABA_AR$ subunit Rdl localised to all OA-positive cell bodies at the SOG, including the sVUM1 neurons, even though again it was unclear whether these receptors localised to their calyx terminals. I will discuss these new findings and their implications in the MB calyx circuitry in detail in Section 9.2.

There are still many gaps to fill in this preliminary map. These mainly arise from technical challenges that have prevented me from systematically mapping all of the known OA receptors to calyx-innervating neurons. Firstly, EGFP fusion proteins generated from MiMIC insertions did not always show subcellular localisation. Octα2R::EGFP, Octβ2R::EGFP and Rdl::EGFP did not localise to membrane terminals (marked with * in Table 9.1); while neither Octβ3R::EGFP fusions showed any signals in the larval brain. Secondly, weak signal to noise ratio, high background labelling, and bleed through from mCD8::RFP to the GFP channel, has led to ambiguous and inconsistent results for receptor localisation. Finally, there is a possibility that the EGFP insertion within receptor proteins could cause receptor mislocalisation. I will discuss these limitations of MiMIC protein traps, possible alternative methods and further validation experiments in the following sections.

Nevertheless, I have developed a preliminary map for OA and GABA receptor localisation of the larval MB calyx; which I hope can form the foundation to build and expand upon for the understanding of how neuromodulatory circuitry is anatomically organised.

9.1.1. Advantages and limitations of mapping connectivity with GRASP

GRASP is an established method for mapping potential synaptic connectivity in the *Drosophila* brain (Gordon and Scott, 2009; Venken et al., 2011b). It is simple and straightforward to conduct, provided that there are suitable *GAL4* and *LexA* lines available to drive split GFP halves in the neuronal populations of interest. Results can be easily replicated to demonstrate experimental consistency or compare individual variation, which is difficult to achieve in time-

consuming and labour-intensive EM reconstruction projects. While EM reconstruction represents a systematic unbiased approach for mapping synaptic connectivity, GRASP provides a more hypothesis- or circuit-based alternative to determine whether specific populations of neurons synapse with each other. GFP reconstitution signals can be detected in unfixed brains with a fluorescence or confocal microscope, and therefore used in live imaging, which is not possible in EM. GRASP can also be detected in fixed and immunolabelled brains, which allow for co-labelling with antibodies labelling neuropils, synaptic proteins, neurotransmitters and other membrane proteins; hence providing additional information about the putative synapses that may not be easily accessible with EM data.

The most pertinent issue of the GRASP method is that it cannot be used to directly visualise synapses, such that non-synaptic membrane contacts may be mistaken for synapses. These false positives may be reduced by comparing GRASP signals with synaptic marker or neurotransmitter labelling, or by fusing spGFP halves to synaptic markers (Karuppudurai et al., 2014), which may also help to determine the direction of synaptic transmission. However, EM remains the best and only method for confirming synaptic connections (Meinertzhagen and Lee, 2012). GRASP also does not reveal extrasynaptic connectivity or volume transmission – a common feature of neuromodulator signalling (Trueta and De-Miguel, 2012). While dense core vesicles associated with volume transmission can be identified in EM sections (Eichler et al., 2017), examining receptor localisation to non-synaptic sites would provide the strongest evidence for extrasynaptic signalling. Finally, GRASP relies on specific transcriptional driver lines, which may not always be available. These lines are not required to map connectivity using systematic EM reconstruction, but will nonetheless hinder functional validation of these connections at a later stage.

9.1.2. Advantages and limitations of mapping receptor localisation with MiMIC protein traps

While there have been other studies that examined OA receptor localisation in the *Drosophila* brain, this is the first study to use EGFP-tagged OA receptors. This method was chosen to visualise native levels of receptor expression and localisation within the neuron, which is difficult to achieve without the availability

of a specific antibody. In one instance, the protein trap proved to be superior to antibody labelling, as the *GABA-B-R1::EGFP* labelled cell bodies expressing $GABA_BR1$ that were previously not observed with the anti-$GABA_BR$ antibody (Enell et al., 2007).

While mRNA localisation and promoter-*GAL4* constructs have been used to identify neurons that express OA receptors (Han et al., 1998; Ohhara et al., 2012; El-Kholy et al., 2015), neither approach can reflect the pattern of subcellular localisation. It is also difficult to determine which promoter-*GAL4* line showed the most accurate expression pattern due to the large variations of expression, as observed in Chapter 8. Even when the full promoter sequence is fused to *GAL4* (El-Kholy et al., 2015), this ignores distal regulatory elements that may affect protein expression patterns.

Moreover, to verify receptor localisation in particular neuronal types, the use of the EGFP-RNAi or deGradFP systems (Caussinus et al., 2011; Neumüller et al., 2012) in conjunction with EGFP-tagged protein receptors, could bypass the need of a strong RNAi line against a specific protein. The EGFP tag can also be used to assay the efficacy of the knockdown, which is more representative of protein levels post-knockdown compared to measuring number of transcripts using qPCR.

While one of the main strengths of protein trapping is the ability to visualise the subcellular localisation of OA receptors, not all of the *MiMIC::EGFP* lines target the receptor protein-EGFP fusion to terminals. In this study, Octα2R::EGFP, Octβ2R::EGFP and Rdl::EGFP signals were retained in cell bodies; and therefore it remains uncertain whether these receptors are normally targeted to the calyx terminals of the neurons they are expressed in. It is also unclear whether the fusion proteins are accumulated and degraded in the ER (Sections 6.2.6. and 6.3.4). Octβ3R::EGFP also did not appear to be expressed in the larval brain, even though Octβ3R transcripts were present (Ohhara et al., 2012). These problems may be due to the random nature of MiMIC insertion, as certain conserved sites of the receptor protein may affect targeting to their membrane locations.

Additionally, neither *OAMB::EGFP* nor *Octβ1R::EGFP* produced functional receptor proteins, as neither stock can be maintained as homozygous. This suggests that even when the EGFP-tagged receptors are

localised to terminals, the EGFP insertion may interfere with normal receptor function without affecting localisation; for example, by obscuring or causing steric hindrance to active domains such as G-protein binding domains or phosphorylation sites. It is also possible that the EGFP insertion rendered these fusion proteins non-functional by preventing their removal from the plasma membrane by endocytosis. In this case, the EGFP-tagged receptors are localised to the same locations as endogenous receptors initially but accumulate at plasma membrane terminals. There is also a slight possibility that the EGFP insertion could actively misdirect subcellular protein localisation in a gain-of-function scenario; but it is more likely that misfolded fusion proteins are recognised in the ER for retention and degradation before they can reach any neuronal terminals.

The other major issue is the intrinsically weak signal from the EGFP-tagged receptors, which together with non-specific polyclonal GFP antibody binding used to amplify these EGFP signals, led to many of the ambiguous results in this study. To enhance the signal to background ratio for visualising receptor fusion proteins, I have tested three different GFP antibodies and introduced an antibody preincubation step for immunolabelling. As I observed that larvae heterozygous for the EGFP-tagged receptors usually have a much weaker signal than that of larvae homozygous for the protein trap, I attempted to maintain homozygosity for EGFP protein traps whenever possible. However, this was not possible for the homozygous lethal *Octβ1R::EGFP* stock, or when there was a lack of appropriate transcriptional drivers in alternative chromosomes for colocalisation experiments.

9.1.3. Alternative methods for mapping OA neuromodulatory circuitry

The main gap in our knowledge of neuromodulatory circuitry organisation is how receptors are distributed within a sensory processing network. This is because synaptic connectomes cannot fully represent the nuances of neuromodulation; most notably, the variable effects caused by differential receptor expression, and potential long-range signalling effects. While I have attempted to bridge this gap by beginning to map OA neuromodulatory circuitry of the larval MB calyx, there is still much work to be done to generate a comprehensive neuromodulatory map. As dicussed in Section 9.1.2, the main problems of the

MiMIC EGFP fusion proteins used in this study were the possibilities of protein misfolding or mislocalisation, disrupted receptor function and weak signal to background ratio. It was also sometimes difficult to isolate specific neurons where fusion proteins are localised. Here I propose modifications to this method and alternative approaches to continue developing the OA neuromodulatory map in the calyx as well as other neuromodulatory circuits in the fly brain.

Currently, the only method for detecting subcellular receptor localisation without compromising protein function or localisation is to use strong and specific antibodies – of which few are available and are difficult to develop (Nagarkar-Jaiswal et al., 2015). From the OA receptors in flies, only anti-OAMB and anti-Octβ2R have been developed; and the signal-to-background ratio for anti-OAMB is poor and inconsistent in the adult fly brain (Han et al., 1998; Kim et al., 2013; Wu et al., 2013). Therefore, it is better to optimise the protein trapping method instead for visualising endogenous protein localisation.

Protein misfolding, mislocalisation or loss-of-function are probably caused by the EGFP insertion within fusion proteins. This can potentially be resolved by targeting the EGFP insertion to a site with a lower probability of interfering with protein localisation or function using the CRISPR/Cas9 method (Gratz et al., 2013). This would commonly be at the C- or N- terminals of proteins (Koles et al., 2016; Kanca et al., 2017) to reduce the risk of protein misfolding or disrupt membrane insertion. However, as these terminals contain motifs that regulate G-protein coupled receptor trafficking (Dong et al., 2007), EGFP insertion at these sites may cause mislocalisation. Therefore, it may be useful to generate multiple protein traps for the same receptor, as EGFP inserted at different locations may maximise the recovery of functional EGFP-tagged receptors. This may be achieved if multiple MiMIC lines for the same receptor were available, or by directing CRISPR/Cas9 knock-in to multiple sites. The rapid improvement in CRISPR/Cas technologies for reporter knock-ins in *Drosophila* suggest that targeted EGFP insertion using CRISPR/Cas methods would be increasingly advantageous in the future (Mohr et al., 2014; Xue et al., 2014).

Another approach to reduce protein misfolding and mislocalisation is to modify the existing protein trap: by increasing the length of flexible peptide linkers flanking the EGFP insertion already used in MiMIC recombinants

(Venken et al., 2011a; Nagarkar-Jaiswal et al., 2015); or using multiple copies of short epitope tags rather than a larger fluorescent protein.

The next challenge is to increase the signal to noise ratio of fusion proteins. In addition to EGFP, the MiMIC fusion proteins used in this study are also tagged with streptavidin and FLAG (Venken et al., 2011a; Nagarkar-Jaiswal et al., 2015); such that concurrent immunolabelling with anti-GFP, biotin and anti-FLAG respectively may be able to maximise fusion protein signal. Using chemical tags with a fluorescent substrate may also be a useful alternative for maximising EGFP signal and reducing background caused by polyclonal GFP antibodies (Kohl et al., 2014).

There are also a series of alternative epitope and fluorescence tag combinations developed for the MiMIC system which may be able to give stronger signals (Venken et al., 2011a). As homozygous larvae with two copies of EGFP showed stronger signals than heterozygous larvae, increasing the number of copies of EGFP inserted in the protein may also maximise signals; although this may simultaneously increase the risk of protein misfolding and mislocalisation. Replacing the MiMIC EGFP reporter with a spaghetti monster fluroscent protein (smFP) may also help increase fusion protein signals. smFP contains 10-15 copies of commonly used epitope tags attached to a fluorescent protein scaffold, and has been shown to strongly label neurons in the multicolour FLP-out approach (Nern et al., 2015; Viswanathan et al., 2015). In this method, the fluorescent protein can also be made non-fluorescent (Nern et al., 2015), which could be used to restrict spectral profile and cross-reactivity in immunolabelling and imaging. However, as smFP requires a fluorescent protein scaffold, it would have similar effects in protein misfolding and function as the EGFP insertion.

There are also alternative approaches directed to uncovering the identity of the neurons expressing OA receptors. T2A-GAL4, T2A-LexA or other T2A-based binary transcription factors can be inserted in receptor genes using RMCE with existing MiMIC lines or targeted CRISPR knockins, such that binary transcriptional systems are placed under the control of the endogenous promoter and regulatory elements of these genes (Diao et al., 2015; Gnerer et al., 2015). These would show more accurate expression patterns than existing promoter-GAL4 lines (Pfeiffer et al., 2010; El-Kholy et al., 2015). T2A is a

ribosomal skipping site that allows transcription factors such as GAL4 and LexA to be translated together but released from the receptor protein and bind to downstream effectors (Diao and White, 2012). Therefore, this method can be used to visualise and manipulate neurons expressing the receptors of interest; although it cannot be used to detect subcellular localisation patterns. Nevertheless, T2A-GAL4/LexA-driven UAS-mCD8::GFP showed stronger signals than the EGFP fusion proteins they are derived from (Diao et al., 2015; Gnerer et al., 2015). T2A-GAL4/LexA can be inserted in the coding region intron to produce a truncated mutant protein; or at the C-terminal to produce a full length and probably functional protein (Diao et al., 2015). Similarly, T2A-EGFP can be inserted at the C-terminal of the receptor protein to produce a full length and more likely functional receptor rather than a fusion protein; but this also cannot be used to reflect subcellular localisation.

It may also be possible to tag or manipulate receptor proteins in specific or even single cells using tissue-specific or conditional tags, which would make it easier to isolate and/or manipulate specific neurons that express neuromodulatory receptors. The majority of tissue-specific and conditional tags use the FLP-FRT recombination system (Chen et al., 2014; Fisher et al., 2017; Nagarkar-Jaiswal et al., 2017; Lee et al., 2018); although alternative recombinases such as Cre-lox or Rippase-RRS can also be used (Koles et al., 2016). The general logic is to include recombinase recognition sites and a transcriptional stop site in the knockin cassette: the EGFP reporter, T2A-GAL4/LexA or other epitope tags; and express the recombinase in a specific population of neurons labelled by transcriptional driver lines or randomly under conditional activation such as heat shock treatments. This allows for knockin tags to be only expressed in neurons which are able to undergo recombinase-mediated excision of the transcriptional stop sites (Chen et al., 2014; Koles et al., 2016; Lee et al., 2018). Tagging receptors in single cells is particularly useful for determining receptor localisation to pre- or post-synaptic terminals, in which presynaptic terminals can also be specifically labelled in the same manner using the synaptic tagging with recombination method (Chen et al., 2014).

The other source of difficulty for mapping receptors to calyx-innervating neurons is the bleed through of mCD8::RFP signal to the GFP channel in

colocalisation experiments. As discussed in detail in Section 5.3.4, this may be resolved by using alternative tools to label calyx-innervating neurons and by restricting spectral overlap detected by the confocal microscope.

9.2. sVUM1 connectivity in the larval MB calyx and their implications

In this study, I have identified candidate neurons that receive OA neuromodulation from sVUM1 neurons in the larval MB calyx, some of the OA receptors they express, and that sVUM1 neurons themselves express OA and GABA receptors. Here I discuss these discoveries in the context of what we know about the MB calyx circuitry in larvae and whether they are likely to be conserved. Based on the known cellular effects of OA receptor and their NA counterparts, I also hypothesise how sVUM1 signalling may affect the activity of each type of calyx-innervating neurons.

It is important to be cautious with these speculations, as the effects of OA receptor activation on the physiology of *Drosophila* neurons *in vivo* are not well-characterised, and the activation of the same receptors could result in different responses dependent on downstream signalling targets expressed in each neuronal type. For example, Octβ1R activation increases cAMP when expressed *in vitro* or in mice hippocampal neurons *in vivo* (Balfanz et al., 2005; Maqueira et al., 2005; Havekes et al., 2014), but decreases cAMP levels of Type II motorneurons at the larval NMJ (Koon and Budnik, 2012). Therefore, I will also discuss how to test these hypotheses.

9.2.1. OA modulation of olfactory PNs

I have shown that olfactory PNs are putative postsynaptic partners to OA terminals of sVUM1 neurons in the larval MB calyx, the majority of which express the α1-adrenergic-like OAMB receptor at their calyx terminals (Fig. 9.1; Table 9.1). OAMB localised to more calyx glomeruli than the number of synapses detected between sVUM1 neurons and PNs in the calyx, and in a broader pattern, indicating possible evidence for extrasynaptic OA signalling. However, it is unknown whether synaptic and extrasynaptic OA signalling to PNs have any functional differences, which may be an interesting question for future investigation.

A subset of olfactory PNs may also express the α2-adrenergic-like Octα2R and β-adrenergic-like Octβ2R, although it is unclear whethere they are localised to the calyx, lateral horn or AL (Fig. 9.1; Table 9.1). The identity of the PNs expressing Octα2R and Octβ2R is also currently unclear, but I hypothesise that they may be grouped based on primary odour qualities conferred by specific PNs. This can be validated by converting Octα2R and Octβ2R fusion proteins to T2A-GAL4/LexA lines (Diao et al., 2015; Gnerer et al., 2015), and mapping them to specific calyx glomeruli, each of which is stereotypically innervated by a PN (Masuda-Nakagawa et al., 2009), or with colocalisation with specific PN driver lines (Masuda-Nakagawa et al., 2010).

Overall, this suggested that olfactory PNs were subjected to OA signalling from sVUM1 neurons via OAMB, and possibly Octα2R and Octβ2R, in the larval MB calyx.

Olfactory PNs as postsynaptic partners of sVUM1 neurons is consistent with L1 connectome data (Eichler et al., 2017; Https://neuronlp.larva.fruitflybrain.org/). OAMB localisation to PNs is consistent with the unpublished data suggesting that OAMB localised to extrinsic neurons in the adult MB calyx (Kim et al., 2013); while cAMP increase observed upon OA application to PN axons in adult flies (Tomchik and Davis, 2009) is in agreement with the possible effects of OAMB and/or Octβ2R activation in PNs. On the contrary, the OAMB homologue in honeybees AmOA1 did not localise to uniglomerular olfactory PN terminals in the honeybee calyx, which instead express the honeybee TA receptor AmTyr1(Sinakevitch et al., 2013, 2017). This suggests PNs are modulated by OA in the fly MB calyx, but possibly by TA in the honeybee calyx.

Pharmacological studies have previously shown that OAMB predominantly increases intracellular calcium, but also shows a cAMP response at higher concentrations (Han et al., 1998; Balfanz et al., 2005; Morita et al., 2006), Octβ2R also increases cAMP levels (Maqueira et al., 2005), while Octα2R instead decreases cAMP levels (Qi et al., 2017).

The calcium-activated potassium channel slowpoke may be one of the downstream targets for controlling PN excitability and presynaptic neurotransmitter release (Warbington et al., 1996). In *Drosophila* pars intercerebralis neurons, OA inhibits slowpoke channels in an OAMB-dependent

manner, resulting in prolonged depolarisation and increased excitability (Crocker et al., 2010). As Octβ2R increases intracellular cAMP levels, this could activate PKA, which would go on to inhibit slowpoke channels through phosphorylation (Zhou et al., 2002). Conversely, this could be counteracted by Octα2R which would decrease intracellular cAMP concentration (Qi et al., 2017). This mechanism could be tested by assaying cAMP levels using epac1-camps (Nikolaev et al., 2004), as well as measuring whole-cell outward currents when slowpoke channels are blocked using the potassium channel blocker tetraethylammonium (Crocker et al., 2010), upon specifically activating or inhibiting OAMB, Octα2R and Octβ2R respectively on PNs.

OAMB activation at PN axons could also increase neurotransmitter release through the PKC activated by the G_q pathway. For example, PKC may increase neurotransmitter release probability, the availability of vesicles for release, as well as open N-type Ca^{2+} channels; all of which were observed for α1-adrenergic-mediated facilitation of glutamatergic release in rat medial prefrontal cortex neurons (Luo et al., 2015). OAMB-mediated increase of intracellular calcium may also facilitate neurotransmitter release from directly interacting with calcium-sensitive components of synaptic vesicles, such as synaptotagmin (Brose et al., 1992; Südhof, 2013). Octβ2R-mediated increase of cAMP could contribute to increased neurotransmitter release at PN axons. For example, this could be mediated by cAMP modulation of voltage-gated K^+/Ca^{2+} ether-a-go-go channels or cyclic nucleotide-gated Ca^{2+} channels which would mediate calcium entry to presynaptic terminals required for vesicle release (Brüggemann et al., 1993; Pavot et al., 2015). Again, Octα2R-mediated decrease of cAMP levels would lead to the opposite effects and probably decrease neurotransmitter release at PN terminals. The individual effects of these OA receptors on acetylcholine release from PN axons in the calyx can be measured using synapto-pHluorin (Ng et al., 2002) when they are specifically activated or inhibited in PNs.

In general, I hypothesise that both OAMB and Octβ2R are likely to have excitatory cellular effects on PNs, which is likely to increase neurotransmitter release at PN axons, and therefore increase inputs from PNs to KCs in the larval MB calyx, while Octα2R would have the opposite effect in a subset of PNs. Therefore, OAMB and Octβ2R activation on PNs is likely to impair odour

discrimination, while Octα2R improves it. This can be tested by manipulating OA receptor signalling selectively in olfactory PNs and examining their consequences on PN activity using electrophysiological methods or functional imaging, such as GCaMP (Tian et al., 2009; Akerboom et al., 2012), and neurotransmitter release using synapto-pHluorin (Ng et al., 2002) at the larval MB calyx; as well as odour discrimination and generalisation behaviour in larvae.

9.2.2. OA modulation of KCs

While I only observed limited GRASP between sVUM1 neurons and KCs in the larval MB calyx, I found that β-adrenergic-like Octβ1R may localise to KC dendrites, although this requires further validation (Fig. 9.1; Table 9.1). This suggested that KC dendrites innervating the larval MB calyx may receive OA signalling extrasynaptically from sVUM1 neurons. The lack of KC-OA connectivity in the larval MB calyx is different to previous observations in the L1 and adult calyces (Zhou et al., 2012; Pech et al., 2013; Eichler et al., 2017) – suggesting that KC-OA connectivity may be plastic over development. However, this may be less significant because larval KCs are still able to receive OA signalling if they expressed Octβ1R. On the other hand, Octβ1R localisation to larval KCs is consistent with Octβ1R transcripts detected in adult KCs (Crocker et al., 2016); suggesting that this may be conserved from larvae to adults.

Octβ1R is predominantly associated with the G_s pathway, which activates the adenyl cyclase production of cAMP (Balfanz et al., 2005; Maqueira et al., 2005). This is consistent with the OA-induced increase of cAMP previously observed in KC dendrites the adult MB calyx (Tomchik and Davis, 2009). The aforementioned cAMP modulation of Na^+, K^+ and Ca^{2+} channels may increase neuronal excitability in KCs (Gordon et al., 1990; Brüggemann et al., 1993; Zhou et al., 2002; Pavot et al., 2015). Octβ1R may also couple to the inhibitory G_o pathway which decreases cAMP production (Koon and Budnik, 2012); resulting in similar cellular effects to the α2-adrenoceptor which is canonically coupled to $G_{i/o}$ pathways. This is likely to result in hyperpolarisation of KCs through inhibiting voltage-gated Ca^{2+} channels, opening K^+ channels and blocking cyclic nucleotide-gated channels (Marzo et al., 2009). The simultaneous coupling to G_s and G_i has been previously observed with

mammalian β2-adrenoceptors in the heart, which appears to have functional roles in compartmentalising cAMP signal (Xiao, 2001). Therefore, Octβ1R may take on a similar role in KCs to maintain site-specific cAMP localisation. Whether Octβ1R in KC dendrites are coupled to increase or decrease of intracellular cAMP, and thus excitability or inhibition respectively, which can be assayed using epac1-camps in KCs (Nikolaev et al., 2004).

The co-application of acetylcholine at KC dendrites (calyx) and OA at KC axons (MB lobes) showed an additive cAMP response in the adult MB calyx (Tomchik and Davis, 2009). However, it is unclear whether co-application of acetylcholine and OA at the calyx would have the same response, as OA application on its own results in spatially-specific cAMP responses in the adult calyx and lobes (Tomchik and Davis, 2009). *In vitro*, the co-application of acetylcholine and OA results in a synergistic increase in calcium responses of cultured KCs (Leyton et al., 2014). This suggests that OA is capable of potentiating acetylcholine responses; but it is unknown whether this effect is mediated by Octβ1R or other OA receptors which may be localised to the MB lobes *in vivo*. This can be tested by measuring the cAMP and GCaMP (Akerboom et al., 2012) response in KC dendrites when KCs and sVUM1 neurons are activated, and compare the difference when Octβ1R is functional versus when it is blocked.

As β-adrenergic signalling and its downstream cAMP effector are closely associated with synaptic plasticity regulation, Octβ1R signalling could also result in long-term synaptic changes at KC dendrites. For example, β-adrenoceptors promote long-term potentiation at mammalian hippocampal neurons by activating postsynaptic glutamate receptors and inhibiting dendritic potassium channels (Thomas et al., 1996; Seol et al., 2007; O'Dell et al., 2015; Liu et al., 2017). At the *Drosophila* NMJ, cAMP signalling via Octβ1R and Octβ2R regulate the structural plasticity of synaptic boutons (Koon et al., 2011; Koon and Budnik, 2012; Maiellaro et al., 2016).

Considering OA application on adult and cultured KCs increases cAMP and potentiates acetylcholine responses, I propose that Octβ1R activation in larval KCs would increase KC excitability and reduce odour discrimination ability. This can be tested by manipulating Octβ1R signalling specifically in KCs, and measuring how this affects KC activity using GCaMP (Akerboom et al.,

2013); especially how this changes the sparseness and correlation of KC activity in a population for different odours (Lin et al., 2014). An odour discrimination assay can also be applied to larvae in which Octβ1R is specifically activated or blocked in KCs, to validate whether their odour discrimination ability is impaired.

9.2.3. Modulation of sVUM1 neurons

I also found that all OA-positive cell bodies, including sVUM1 cell bodies, expressed Octα2R and the ionotropic $GABA_AR$ subunit Rdl (Fig. 9.1; Table 9.1). This suggested that sVUM1 neurons may be subjected to OA and GABA modulation, although it was unclear whether this is at the calyx, AL or SOG region. Nevertheless, this is a novel finding as we currently do now know the inputs to sVUM1 neurons and how sVUM1 activity is regulated. As sVUM1 neurons and the APL neuron show GRASP in the larval MB calyx (H.W., MPhil Thesis 2014), this suggested that the APL neuron could be modulating sVUM1 neurons via Rdl. On the other hand, Octα2R expression suggested that sVUM1 neurons may be subjected to neuromodulation from themselves, each other, or other OA neurons. L1 connectivity data show that the APL neuron has reciprocal synapses with sVUM1 neurons, while sVUM1 neurons also synapse with each other (Eichler et al., 2017; Https://neuronlp.larva.fruitflybrain.org/); but cannot reveal whether sVUM1 neurons are autoregulated.

I predict that Octα2R localised to the presynaptic terminals of sVUM1 neurons in the larval calyx, similar to the presynaptic localisation of α2-adrenocepters on NA neurons (Aoki et al., 1994). This suggests that Octα2R could act as an autoreceptor inhibiting OA release from sVUM1 neurons presynaptically in the calyx – constituting a negative feedback mechanism for OA release. Octα2R could also mediate local inhibition of OA release between the two types of sVUM1 neurons innervating the calyx – sVUMmd1 and sVUMmx1. This can be validated by measuring neuronal activity of sVUM1 neurons using GCaMP and neurotransmitter release using synapto-pHluorin when sVUM1 activity and Octα2R signalling on sVUM1 neurons are manipulated respectively. It would be particularly valuable if sVUMmd1 and sVUMmx1 neurons can be individually manipulated and visualised to determine whether the effects are autoinhibitory or local inhibitory. I predict that OA-

mediated feedback is a homeostatic mechanism and does not have a profound effect in odour discrimination – which should be validated using odour discrimination assays. On the other hand, dendritic localisation of Octα2R would suggest that sVUM1 neurons receive inhibitory OA inputs that may possibly underlie the context-dependent activity of sVUM1 neurons. However, it is currently unclear whether sVUM1 neurons are subjected to other sources of OA modulation outside the calyx.

Rdl expression in sVUM1 neurons suggests that the APL neuron provides fast inhibitory GABAergic inputs to sVUM1 neurons in the calyx and/or reflect context-depedent inhibitory inputs to sVUM1 neurons at the AL and SOG, depending on the subcellular localisation of the $GABA_AR$. As the APL is activated by KC output (Lin et al., 2014; Masuda-Nakagawa et al., 2014), this suggests that KC outputs could indirectly inhibit sVUM1 activity via the APL neuron, forming a feedback inhibitory loop between KCs and sVUM1 neurons. This can be tested by activating or blocking APL activity and determining its effects on sVUM1 activity visualised using GCaMP in the calyx, and whether this affects OA release using synapto-pHluorin. Rdl signalling can also be manipulated in these experiments to validate its potential role in sVUM1 neurons.

9.2.4. OA modulation of the APL and Odd-like neurons

Using OA-GRASP colocalisation, I identified APL and Odd-like neurons are also putative postsynaptic partners to sVUM1 neurons in the larval MB calyx (Fig. 9.1). This is consistent with L1 connectivity data. However, I have yet to identify an OA receptor that localised to these neurons (Table 9.1). While there are no data in the adult or larval fly yet to show whether these types of neurons express OA receptors, the honeybee counterparts of the APL neuron express AmOA1 – the honeybee homologue of OAMB (Sinakevitch et al., 2013).

While it is clear that OAMB and Octβ1R do not localise to the calyx terminals of the APL or Odd-like neurons, it remains possible that these neurons could express Octα2R or Octβ2R (Table 9.1). This has not yet been tested due to technical challenges and the lack of available tools; but should be attempted in the future using the modified approaches proposed in Section 9.1.3. OA modulation of the APL and Odd-like neurons can also be functionally

validated by optogentically manipulating sVUM1 signalling using the sVUM1 intersectional line (Chapter 8), and measuring neuronal activity using GCaMP in the APL neuron and Odd-like neurons. However, given that I do not know the type of OA receptors expressed in these neurons, I cannot predict what the possible effects would be and how this may impact on odour discrimination. Moreover, this method cannot differentiate sVUM1 modulation from OA or other neurotransmitters that are co-released by sVUM1 neurons. The most likely examples being TA, a precursor to OA present in OA neurons that is a neurotransmitter in its own right (Saraswati et al., 2004), or neuropeptides. Therefore, it is possible that the APL neuron or Odd-like neurons postsynaptic to sVUM1 neurons may express one of the three types of TA receptors, which could also be activated by OA at a high concentration (Arakawa et al., 1990; Saudou et al., 1990; Bayliss et al., 2013), or neuropeptide receptors.

It is also possible that OA signalling from sVUM1 neurons does not modulate the APL or Odd-like neurons despite the GRASP results for the below reasons. Firstly, the GRASP signal observed between sVUM1 neurons and these neurons may be false positives indicative of membrane contacts but not synapses; suggesting that these neurons are not synaptic partners of sVUM1 neurons in the calyx. This is unlikely due to colocalisation observed at OA terminals. Secondly, the sVUM1-APL neuron may not be reciprocal; and that GRASP colocalised with OA because the APL neuron is presynaptic to sVUM1 terminals where OA is released (Section 9.2.3). This does not apply to Odd-like neurons which are predominantly postsynaptic in the MB calyx (L.M.N., unpublished).

9.2.5. Tools for validating OA neuromodulatory circuitry

In addition to mapping the OA neuromodulatory circuitry in the larval MB calyx, I examined and tested tools that would be useful for validating the hypotheses for OA neuromodulation mechanisms discussed above. This includes selecting and verifying more specific transcriptional drivers for sVUM1 neurons and Odd-like neurons, as well as testing OAMB knockdown lines.

The new sVUM1 intersectional line, which consistently labels the sVUM1 neurons with only three extra neurons, is currently the most specific line available for manipulating sVUM1 neuronal activity. This line can be used to

conditionally activate or knock down sVUM1 neurons using optogenetic or thermogenetic methods. On the other hand, the Odd-like neuron lines would be useful for confirming the presence of receptor localisation to Odd-like neuron cell bodies, especially when the protein trap signal is restricted only to cell bodies and not to terminals. In this study, I also identified the first *LexA* line that only labels one Odd-like neuron in each brain – which would be valuable to use in a dual binary transcriptional system in conjunction with another neuronal type labelled in a *GAL4* line to understand their interactions. None of these lines have been reported in the most recent single-cell functional study of MB extrinsic neurons in L3 larvae (Saumweber et al., 2018).

To examine the function of OAMB signalling in PNs, I found that the most efficient OAMB-RNAi knockdown line showed around 50% OAMB::EGFP signal compared to that of the non-knockdown control, while the other lines did not show observable knockdown. This level of efficacy may be further optimised by the use of *UAS-Dicer* to increase processing of dsRNA into siRNA; or increasing *GAL4/UAS* expression by raising the temperature. I also found that it was more desirable to knock down functionally intact EGFP-tagged OA receptors using EGFP-shRNA or deGradFP, which targets GFP-tagged protein for ubiquitination and degradation (Caussinus et al., 2011; Neumüller et al., 2012; Nagarkar-jaiswal et al., 2015). The *EGFP-shRNA.3* construct (Neumüller et al., 2012) tested in this study showed the strongest and most consistent knockdown of OAMB::EGFP signal in calyx glomeruli labelled by *NP225-GAL4*, compared to the three other *OAMB-RNAi* lines tested, with around 80% of the OAMB::EGFP signal knocked down. However, this method cannot be applied to the fusion proteins in this study as they are not fully functional.

The deGradFP system is also theoretically superior to RNAi knockdown, as it directly targets proteins rather than transcripts. This system uses NSlmb-vhhGFP4, a fusion protein made of a F-box domain required for ubiquitination and a single-domain antibody fragment against GFP, under *UAS* control (Caussinus et al., 2011). It may be possible to repurpose this system by using antibody fragments against OA receptors instead to facilitate the degradation of OA receptor proteins in the ubiquitination system.

9.3. Organisation of OA neuromodulatory circuitry in the MB calyx

GRASP and receptor localisation data suggest that all of the known calyx-innervating neurons, including KCs, PNs, the APL neuron, Odd-like neurons, and even sVUM1 neurons themselves, are probably targets of OA signalling from sVUM1 neurons. OA connectivity in L3 larvae is consistent with the L1 connectivity data recently made public on the NeuroNLP server (https://neuronlp.larva.fruitflybrain.org/; Berck et al., 2016; Eichler et al., 2017). Compared to previous studies that have largely focused on how OA directly modulates KCs (Burke et al., 2012; Kim et al., 2013; Pech et al., 2013), this provides new insights into how OA modulation is also indirectly regulating KC activity through a strongly interconnected network of multiple cell types all subjected to OA neuromodulation.

While this is the first study to examine OA receptor localisation in non-KC neurons innervating the fly MB calyx, OA/TA receptor localisation patterns have been previously examined in the honeybee calyx. While OAMB and its honeybee homologue AmOA1 both localised to the MB calyx, they are expressed on different types of neurons: OAMB in uniglomerular PNs versus AmOA1 in GABAergic interneurons and multiglomerular PNs (Sinakevitch et al., 2011, 2013). It is even more interesting that the honeybee α2-adrenergic-like TA receptor AmTyr1 – homologous to the fly TA receptor Oct-TyrR – appears to share similar localisation patterns to the larval fly OAMB receptor: both of which localised to uniglomerular olfactory PN axons, and probably KC axons but not KC dendrites (Sinakevitch et al., 2017). This suggests that TA/AmTyr1 in honeybees and OA/OAMB in fruitfly larvae may have similar roles in modulating their corresponding MB calyx circuitries. However, the lack of connectivity and functional data in the honeybee, and receptor localisation data in the adult fly and other insects have made it difficult to assess to what extent MB calyx neuromodulatory circuitry is conserved.

9.3.1. Distribution of OA receptor types in the larval MB calyx

From the five known types of OA receptors in *Drosophila*, OAMB and Octβ1R localised to the larval MB calyx; while Octβ2R and Octα2R are expressed in the cell bodies of calyx-innervating neurons, and may therefore localise to the calyx as well. This demonstrates that multiple types of OA receptors are involved in

the larval MB calyx circuitry. This is expected as this allows for a single source of OA to differentially modulate different targets to generate a coordinated effect within the circuit – an example being the mammalian olfactory bulb which requires α- and β-adrenoceptors for odour discrimination behaviours (Mandairon et al., 2008).

Co-expression of OA receptors was also observed in PNs. A subset of PNs appeared to express Octα2R and/or Octβ2R, in addition to the widely expressed OAMB. Similarly, preliminary data show that Octβ1R and OAMB may both be expressed in KCs, although unlike Octβ1R, OAMB appeared to only localise to KC axons in the MB lobes but not to KC dendrites in the calyx. As the subcellular localisation of Octβ2R is unclear, it might be localised to a different subcellular compartment to the calyx-localised OA receptors. The differential subcellular localisation of OA receptors in a single neuron could facilitate compartment-specific effects of OA signalling.

Alternatively, if more than one type of OA receptor localised to the same neuronal terminals in the larval calyx, they could allow differential effects of OA modulation depending on the concentration of OA in the environment. For example, the co-expression of Octβ1R and Octβ2R on OA neurons at the larval NMJ regulates synaptic growth antagonistically (Koon et al., 2011; Koon and Budnik, 2012). In the mammalian NA system, different dosages of NA is required to activate the different types of adrenoceptors; and this is proposed to generate different behaviours suitable for the context (Atzori et al., 2016). Similarly, OA could also have different affinities for OA receptors in *Drosophila*. In HEK-cells transfected with OA receptors in culture, Octα2R appear to have the highest affinity to OA ($EC_{50}=10^{-10}M$), followed by Octβ1R ($EC_{50}=3x10^{-8}M$) and OAMB ($10^{-8}M$ for Ca^{2+} response and $EC_{50}=6x10^{-7}M$ for cAMP response) (Han et al., 1998; Balfanz et al., 2005; Qi et al., 2017).

The concentration-dependent activation of OA receptors should be tested in *Drosophila* neurons *in vivo*. This may be done in a mutant receptor background, in which individual OA receptor types are rescued by cDNA and assayed for activation with variable injected OA concentrations to the calyx or with increasing intensities of optogenetic stimulation of sVUM1 neurons.

9.3.2. Extrasynaptic targets of OA signalling in the larval MB calyx

The other interesting feature of the OA neuromodulatory circuitry in the larval MB calyx is the possibility of extrasynaptic OA receptors in KCs and PNs. While extrasynaptic receptors are common for neuromodulators and OA extrasynaptic receptors have been detected in *C.elegans* (Trueta and De-Miguel, 2012; Bentley et al., 2016), this is the first study to explore the possibility of extrasynaptic OA receptors in *Drosophila*. However, this matches with the large dense core vesicles associated with volume transmission that have been identified in OA neurons (Eichler et al., 2017).

It is currently unknown whether there are differences between synaptic and non-synaptic neuromodulation; although there is evidence that changing the distribution of *Drosophila* vesicular monoamine transporter in synaptic vesicles and large dense core vesicles involved in extrasynaptic release in OA neurons impaired larval locomotion (Grygoruk et al., 2014). Additionally, there could be differences in OA dosages required or the timescale of the modulation, or potential co-release of OA with another peptidergic modulator.

The observation of extrasynaptic receptors in the larval MB calyx circuitry confirms that OA released from sVUM1 neurons is likely to reach longer-range non-synaptic targets in the calyx. However, it is still unknown how far reaching OA signalling in the larval CNS could be, which would depend on its active concentration, the localisation of degradation enzymes and reuptake transporters, as well as the presence of diffusion barriers such as glia surrounding the larval calyx (Omoto et al., 2015).

9.4. Possible functions of OA neuromodulation in the MB calyx

9.4.1. A proposed model for sVUM1 signalling in the larval MB calyx

The different patterns of OA signalling, as a result of a behavioural state or external cue, could lead to the activation of different OA receptors in the calyx. Based on mammalian models of NA activation (Atzori et al., 2016) and the affinity of OA receptors towards OA (Han et al., 1998; Balfanz et al., 2005; Maqueira et al., 2005; Qi et al., 2017), I hypothesise that low levels of OA signalling would activate Octα2R, intermediate levels would recruit OAMB, and high levels would further activate OctβRs (Fig. 9.2).

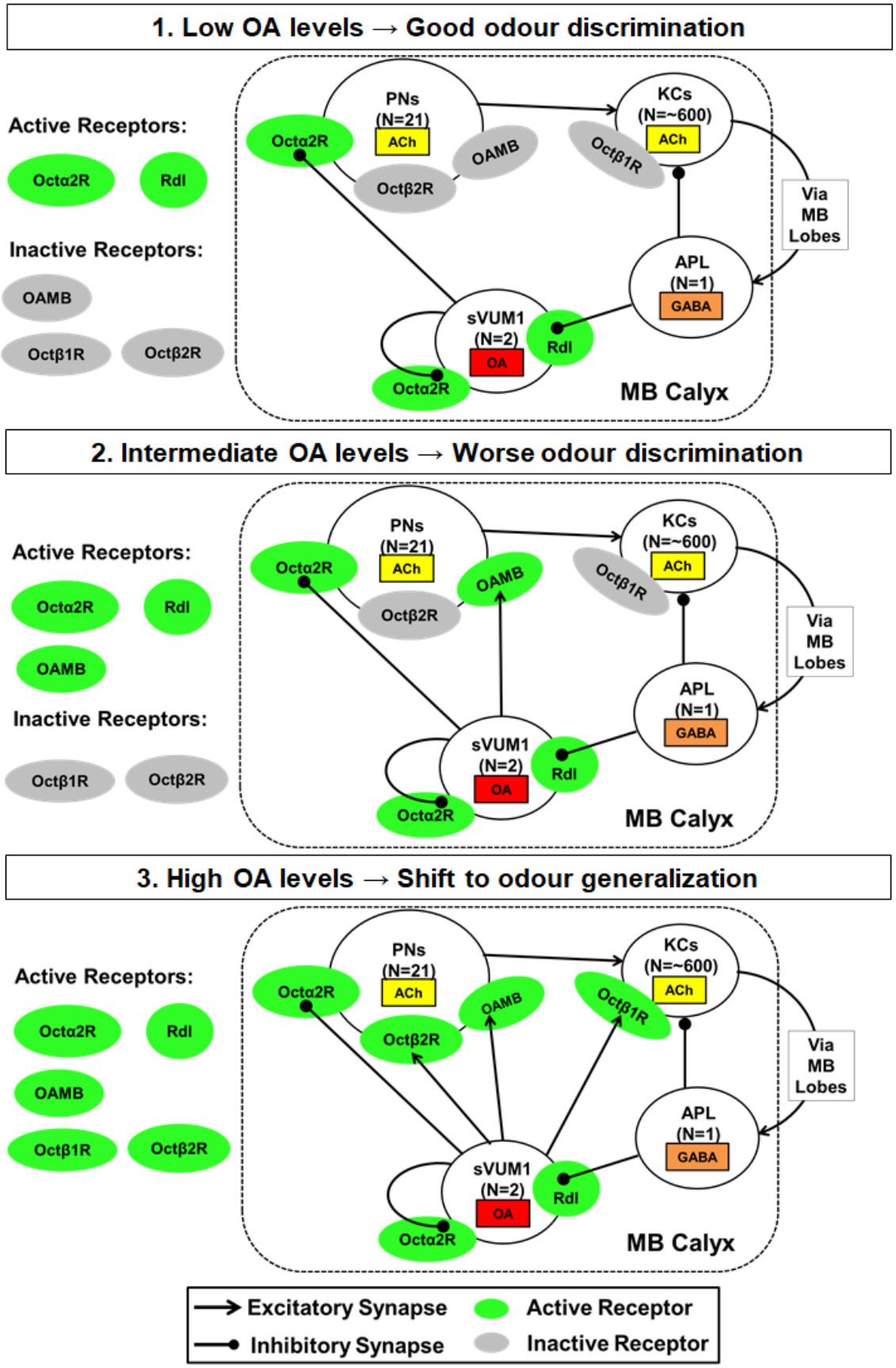

Figure 9.2. Proposed model of OA neuromodulation in the *Drosophila* larval MB calyx. Abbreviations: ACh, acetylcholine; KC, Kenyon Cell; MB, mushroom body; N, number; OA, octopamine; PN, projection neuron.

At low levels of OA signalling, I propose that OA is self-inhibitory and also inhibit the activity of a subset of PNs via Octα2R, and therefore restrict PN inputs to KCs. Odour-evoked activation of KCs would further suppress OA activity via Rdl mediating GABAergic inhibition from the APL neuron. This would ensure decorrelated odour representations in KCs for odour discrimination. Upon intermediate levels of OA signalling, OA inhibition on PNs via Octα2R would be counteracted by OAMB activation in most olfactory PNs, in which their olfactory inputs to KCs are increased. This would increase the number of active KCs, resulting in more overlap in odour representations and a decrease in odour discrimination. The highest level of OA signalling would increase neuronal excitability in both PNs via OAMB and Octβ2R, and KC dendrites via Octβ1R, through a feedforward loop, further increasing overlap between odour representations and impairing odour discrimination, and may mediate a shift to odour generalisation. This model is illustrated in Fig. 9.2.

In this model, the feedback inhibition from the APL neuron is decisive as to whether sparse odour representations can be maintained under increased PN and KC activity. If APL activity is sufficient to maintain sparseness in KCs, then sVUM1 signalling is likely to increase the sensitivity of odour detection, allowing the detection of previously subthreshold stimuli, but without losing odour discrimination. If the APL fails to generate adequate inhibition on KCs, this would impair odour discrimination. APL activity may be suppressed by sVUM1 signalling as well, possibly through the inhibitory Octα2R, which is yet to be tested. This would then reduce KC sparseness and selectivity and impair odour discrimination.

9.4.2. sVUM1 regulation of odour discrimination-generalisation balance

Depending on how two similar odours are presented in olfactory learning tasks, *Drosophila* larvae are capable of producing either a discriminatory or a generalised response (Mishra et al., 2010; Barth et al., 2014; Chen and Gerber, 2014). The perceptual distance between odours in discrimination and generalisation tasks are correlated (Chen and Gerber, 2014); suggesting that there may be an external input to shift the balance between discrimination and generalisation. Studies in adult *Drosophila* also suggest that both discrimination and generalisation depends on odour representations in KCs (Campbell et al.,

2013). While it is important for animals to be able to learn to discriminate between two similar odours, odour generalisation can also confer benefits to the animal's survival. When faced with a novel odour, the ability to generalise allows the animal to compute the most appropriate behavioural response based on similar odours that it has previously encountered. For example, the conditioned fear response in rodents, which is important for responding to potential dangerous stimuli, can be generalised (Ito et al., 2009; Chen et al., 2011b). Generalisation is also important to allow the animal to recognise biologically relevant stimulus from a noisy and variable background. An example being adult flies learning to generalise across different visual contexts to identify the conditioned pattern – an ability that requires the MBs (Liu et al., 1999). While not necessarily advantageous, stressful contexts also impair odour discrimination. In rodents, this involves NA modulation of the olfactory bulb (Manella et al., 2013).

As mathematical modelling has shown that the trade-off between discrimination and generalisation is dependent on the sparseness of randomly connected neurons in a network (Barak et al., 2013); based on my model, I hypothesise that increasing OA signalling from sVUM1 neurons will reduce sparseness and increase correlation in KC odour responses, and therefore promote generalisation over discrimination (Fig. 9.2).

9.4.3. Testing proposed model for sVUM1 regulation of odour discrimination

Testing this model for OA neuromodulation in the larval MB calyx circuitry requires several critical steps. Firstly, the effects of OA modulation on each of their target neuronal types must be validated. This can be achieved by measuring the change in the electrical properties of neurons such as membrane potentials or firing frequencies using electrophysiological methods, neuronal activity using functional calcium imaging (GCaMP) and neurotransmitter release using synapto-pHluorin in these neuronal types when sVUM1 and/or OA receptor signalling is specifically manipulated – the details of which have been discussed in Section 9.2.

Next, it is necessary to establish the relationship between OA concentration or sVUM1 activity and OA receptor activation in the MB calyx.

This may be done be injecting increasing concentrations of OA into the calyx, or increasing electrical or optogenetic stimulation of sVUM1 neurons, and measuring how the electrical or calcium responses changes in the different neuronal types. Responses should only be seen in neurons that express the corresponding receptor types and should disappear if the receptors are mutated or blocked. Alternatively, this could also be conducted in a background where all receptors are mutated and only one type is rescued at a time. This can reveal the concentrations or sVUM1 activation required to activate individual receptor types on the neurons they are normally expressed on.

Finally, the net output of different levels of OA signalling on KC activity and odour discrimination behaviour should be assayed. OA signalling levels should be controlled by manipulating sVUM1 activity (electrically, thermogenetically or optogenetically), manipulating receptor signalling on individual neurons or by varying injected OA concentrations. Functional GCaMP imaging can be used to measure the activation of KCs as a population and how the sparseness and correlation of perceptually similar odour representations varies with OA activity (Lin et al., 2014) – in which KC responses are expected to be less sparse and less decorrelated with increasing levels of OA signalling. Behavioural phenotypes associated with variable OA activity can be assayed using odour discrimination and generalisation assays. In brief, larvae can be trained to associate odours with reward. In generalisation tasks, they would be tested for their response to an untrained but perceptually similar odour; while in discrimination tasks, they would be presented with a choice between the paired odour and a similar but explicitly unpaired odour (Mishra et al., 2010; Chen et al., 2011a). I would expect that larvae exposed to low levels of OA signalling to perform better at discrimination tasks, while those exposed to high levels of OA signalling to perform better at generalisation tasks.

9.4.4. Possible contexts conveyed by sVUM1 neurons

Another question integral to this model is the type of signals that sVUM1 neurons are bringing to the larval MB calyx to elicit the changes in odour representations in KCs. As neuromodulatory neurons, it is likely that OA sVUM1 neurons show variable firing patterns depending on context. Mammalian NA neurons show both tonic and phasic activation patterns: tonic activation is

associated with arousal and behavioural states; while phasic activation is associated with novel, unexpected or salient stimuli (Rajkowski et al., 1994; Vankov et al., 1995). In the context of associative learning, NA neurons are active specifically during the presentation of the CS+, especially with food reinforcement; or when there is a change in stimulus contingency, such as in reversal learning (Sara and Segal, 1991; Rajkowski et al., 1994; Aston-Jones et al., 1997).

The honeybee counterpart of sVUM1 neurons, the VUMmx1 neuron, shows phasic activation in response to sucrose and odours and that VUMmx1 odour response increases after forward odour pairing (Hammer, 1993). This suggests that similar to NA neurons, OA neurons in insects can respond to salient stimuli and show plasticity in learning.

It is likely that sVUM1 neurons may also convey arousal or satiety states. The OA receptor Octβ2R was required for the formation of artificial reward memories only in satiated but not hungry flies (Burke et al., 2012). Moreover, four of the known OA receptors were differentially expressed in the antennae of starved versus fed flies (Ko et al., 2015). This suggested that OA might provide a link between satiety signals and the olfactory pathway. As OA also controls arousal and starvation-induced locomotion in *Drosophila* (Crocker et al., 2010; Koon et al., 2011; Yang et al., 2015); this suggests that OA may be able to regulate sensory circuits depending on arousal and satiety states of the animal.

Nevertheless, to understand the signals that may be regulating odour discrimination in the larval MB calyx, future experiments are required to validate the type of stimuli that can activate sVUM1 neurons, identify the inputs to sVUM1 neurons and determine how sVUM1 activity varies with behavioural states.

9.4.5. Tyraminergic and peptidergic signalling from sVUM1 neurons

In addition to OA, activation of sVUM1 neurons may also release TA and possibly neuropeptides in the larval MB calyx – both of which may add additional layers to sVUM1 regulation of olfactory processing circuitry.

TA is an OA precursor which also acts as a neurotransmitter in *Drosophila* and preferentially activates TA receptors (Arakawa et al., 1990; Saudou et al., 1990; Saraswati et al., 2004; Bayliss et al., 2013). High

concentrations of OA can activate TA receptors, and high concentrations of TA can activate OA receptors (Arakawa et al., 1990; Saudou et al., 1990; Han et al., 1998; Maqueira et al., 2005; Qi et al., 2017). Recent reports revealed that VUMmd1 and VUMmx1 neurons project tyraminergic inputs to the honeybee MB calyx, which is strongly immunoreactive against a honeybee TA receptor AmTyr1/AmTAR1; and that AmTyr1 is localised to the axons of honeybee uniglomerular olfactory PNs in the calyx (Sinakevitch et al., 2017; Thamm et al., 2017). This suggests that sVUM1 neurons, their *Drosophila* larval counterparts, may also mediate tyraminergic signalling in the larval MB calyx. So far, I have found that the TyrRII::EGFP fusion from the Gene Disruption Project (Nagarkar-jaiswal et al., 2015) did not show any signal in the larval CNS (H.W., unpublished observations). However, it is uncertain whether this is because TyrRII expression was disrupted by the EGFP cassette insertion. In the future, it would be useful to investigate whether TA is released at the larval calyx and whether calyx-innervating neurons express corresponding TA receptors.

The presence of dense core vesicles in *Drosophila* sVUM1 neurons not only suggest the possibility of volume transmission of OA, but also the possibility of co-transmission of neuropeptides (Nässel, 2009; Grygoruk et al., 2014; Eichler et al., 2017). Neuropeptides including NPF and tachykinin have been implicated in appetitive olfactory and satiety behaviours in fruit flies (Root et al., 2011; Wang et al., 2013; Zhang et al., 2013a; Ko et al., 2015); suggesting that their pathways may intersect with OA neurons which also modulate relevant behaviours. Therefore, it would also be interesting to determine what type of neuropeptides, if any, are co-expressed in sVUM1 neurons to understand how this may further modulate the larval MB calyx circuitry.

9.5. Implications on the organisation of neuromodulatory circuitry

The preliminary OA neuromodulatory map of the larval MB calyx I developed in this study reveal three major design features that enable effective neuromodulation of sensory discrimination pathways:

Firstly, I found that OA neuromodulation targets several interconnected neuronal types in the larval MB calyx. As neuromodulatory innervation is usually widespread and distributed (Bargmann and Marder, 2013), their effects can be optimised by having multiple targets within the same pathway. This reiterates

the need to investigate neuromodulation in the context of a circuit in order to understand its output behaviour.

Secondly, I demonstrated the possibility of extrasynaptic OAMB and Octβ1R receptors in PNs and KCs respectively. Although it is well-known that neuromodulation can act extrasynaptically, this is the first evidence to my knowledge of extrasynaptic OA receptors in *Drosophila*. This is functionally useful as it allows neuromodulators to exert long-distance effects without the need to form physical synapses; and also economical, as it reduces the need for numerous synapses provided the appropriate receptors are expressed. This also demonstrates why it is important to consider neuromodulation beyond the synaptic connectome. It will also be interesting to explore whether there are functional differences between synaptic and extrasynaptic transmission by neuromodulators.

Thirdly, and most importantly, I have shown that different types of OA receptors are distributed among their putative targets; such that a single source of OA in the larval MB calyx is able to differentially modulate multiple neuronal types within the same circuit. Based on the model I proposed, the distribution of OA receptors with variable affinities to OA on different types of calyx-innervating neurons is integral in mediating the context-dependent changes in OA signalling by sVUM1 neurons in the larval MB calyx. This model remains to be validated (Section 9.4.3), and it remains to be seen whether this is conserved across other neuromodulatory circuits in different organisms. Differential receptor distribution supports the mechanisms behind how phasic and tonic neuromodulatory activities can have different effects on their target neurons, a phenomenon previously observed for NA modulation of the rodent somatosensory cortex (Devilbiss and Waterhouse, 2011). This suggests that the pattern of receptor expression can form the framework in understanding how circuits as a whole can respond to changing levels of neuromodulator signalling in a coordinated manner, and how this may affect how we perceive sensory stimuli and behavioural response under different circumstances.

9.6. Concluding remarks

To understand the anatomical organisation of higher brain neuromodulatory circuits, I studied the OA modulatory circuitry in the fly larval MB calyx by

identifying putative postsynaptic partners of OA neurons and mapping OA and GABA receptors to calyx-innervating neurons. While this map is by no means complete, I hope this preliminary receptor localisation data can guide future experiments in investigating the mechanisms and effects of OA on their various targets in the MB calyx, and how this translates to the coordinated modulation of odour discrimination behaviour.

Appendix 1 – Supplemental Figures

A. Sequenced PCR product for MI12417 5' flanking end

NTCTTTATTCGCATAATATAAATCACATGGCTCAAAGAAGAAGTCACGCATCATAATTAG
CATTATATTCCAAGTTGGGCAAAAACAAGAAATCGATAAACGCTGAGGAAGCACATCAAA
CAAATCGGCTTAGATAAAATTGAGGTTGGGATTAAATAGGAGCGGGATTCCAGCCAGAAA
ATGGCAGACATGAAAGCGAGCCATCGGCTAAAACGAAATAAAATATACGAGCCCCAACCA
CTATTAATTCGAACAGCATGTTTTTTTGCAGTGCGCAATGTTTAACACACTATATTATCA
ATACTACTAAAGATAACACATACCAATGCATTTCGTCTCAAAGAGAATTTTATTCTCTTC
ACGACGAAAAAAAAAGTTTTGCTCTATTTCCAACAACAACAAAAATATGAGTAATTTATT
CAAACGGTTTGCTTAAGAGATAAGAAAAAAGTGACCACTATTAATTCGAACGCGGCGTAA
GCTACTAAATCTCTCANGAA

B. MI12417 5' flanking end alignment with MiMIC sequences

Synthetic construct MIMIC transposable element, complete sequence
Sequence ID: GU370067.1 Length: 7267 Number of Matches: 2

Range 1: 102 to 370 GenBank Graphics ▼ Next Match ▲ Previous Match

Score	Expect	Identities	Gaps	Strand
484 bits(262)	7e-133	267/269(99%)	1/269(0%)	Plus/Plus

```
Query  226  TACGAGCCCCAACCACTATTAATTCGAACAGCATGttttttGCAGTGCGCAATGTTTAA  285
            ||||||||||||||||||||||||||||||||||||||||||||||||||||||||||
Sbjct  102  TACGAGCCCCAACCACTATTAATTCGAACAGCATGTTTTTTTGCAGTGCGCAATGTTTAA  161

Query  286  CACACTATATTATCAATACTACTAAAGATAACACATACCAATGCATTTCGTCTCAAAGAG  345
            ||||||||||||||||||||||||||||||||||||||||||||||||||||||||||||
Sbjct  162  CACACTATATTATCAATACTACTAAAGATAACACATACCAATGCATTTCGTCTCAAAGAG  221

Query  346  AATTTTATTCTCTTCACGACGaaaaaaaaaGTTTTGCTCTATTTCCAACAACAACAAAAA  405
            |||||||||||||||||||||||||||||||||||||||||||||||||||||||||||
Sbjct  222  AATTTTATTCTCTTCACGACGAAAAAAAAAAGTTTTGCTCTATTTCCAACAACAACAAAAA  281

Query  406  TATGAGTAATTTATTCAAACGGTTTGCTTAAGAGATAAGAAAAAAGTGACCACTATTAAT  465
            ||||||||||||||||||||||||||||||||||||||||||||||||||||||||||||
Sbjct  282  TATGAGTAATTTATTCAAACGGTTTGCTTAAGAGATAAGAAAAAAGTGACCACTATTAAT  341

Query  466  TCGAACGCGGCGTAAGCTAC-TAAATCTC  493
            |||||||||||||||||| | ||||||
Sbjct  342  TCGAACGCGGCGTAAGCTACCTTAATCTC  370
```

C. MI12417 5' flanking end alignment with *OAMB* sequences

Drosophila melanogaster chromosome 3R
Sequence ID: AE014297.3 Length: 32079331 Number of Matches: 1

Range 1: 20697058 to 20697273 GenBank Graphics ▼ Next Match ▲ Previous Match

Score	Expect	Identities	Gaps	Strand
394 bits(213)	1e-105	216/217(99%)	1/217(0%)	Plus/Minus

Features: octopamine receptor in mushroom bodies, isoform D
octopamine receptor in mushroom bodies, isoform G

```
Query  11        GCATAATATAAATCACATGGCTCAAAGAAGAAGTCACGCATCATAATTAGCATTATATTC  70
                 |||||||||||||||| ||||||||||||||||||||||||||||||||||||||||||
Sbjct  20697273  GCATAATATAAATCACATG-CTCAAAGAAGAAGTCACGCATCATAATTAGCATTATATTC  20697215

Query  71        CAAGTTGGGCAAAAACAAGAAATCGATAAACGCTGAGGAAGCACATCAAACAAATCGGCT  130
                 ||||||||||||||||||||||||||||||||||||||||||||||||||||||||||||
Sbjct  20697214  CAAGTTGGGCAAAAACAAGAAATCGATAAACGCTGAGGAAGCACATCAAACAAATCGGCT  20697155

Query  131       TAGATAAAATTGAGGTTGGGATTAAATAGGAGCGGGATTCCAGCCAGAAAATGGCAGACA  190
                 ||||||||||||||||||||||||||||||||||||||||||||||||||||||||||||
Sbjct  20697154  TAGATAAAATTGAGGTTGGGATTAAATAGGAGCGGGATTCCAGCCAGAAAATGGCAGACA  20697095

Query  191       TGAAAGCGAGCCATCGGCTAAAACGAAATAAAATATA  227
                 |||||||||||||||||||||||||||||||||||||
Sbjct  20697094  TGAAAGCGAGCCATCGGCTAAAACGAAATAAAATATA  20697058
```

Figure S1. MI12417 5' PCR product aligned to MiMIC and *OAMB* sequences. (A) Sequenced PCR product for MI12417 5' flanking end. Alignment to MiMIC sequences is indicated in yellow, alignment to *OAMB* sequences in grey and overlapping alignment at the MiMIC insertion site (TA) in red. **(B-C)** Alignment of MI12417 5' PCR products to MiMIC **(B)** and *Drosophila melanogaster* **(C)** sequences using Nucleotide BLAST.

A. Sequenced PCR product for MI12417 3' flanking end

GCGGGAGTCGCGACTACGCCCCCACTGAGAGACTCAAAGGTTTACCCCAGTTGGGGCACT
ACTCCCGAAAACCGCTTCTGACCTGGGCCGCGGGGGAAATTAATTAAATTATTGTTTTAA
GTATGATAGTAAATCACATTACGCCGCGTTCGAATTAATAGTGGTCACTTTTTTCTTATC
TCTTAAGCAAACCGTTTGAATAAATTACTCATATTTTTGTTGTTGTTGGAAATAGAGCAA
AACTTTTTTTTTCGTCGTGAAGAGAATAAAATTCTCTTTGAGACGAAATGCATTGGTATG
TGTTATCTTTAGTAGTATTGATAATATAGTGTGTTAAACATTGCGCACTGCAAAAAAAAC
ATGCTGTTCGAATTAATAGTGGTTGGGGCTCGTAATATGTCTTCCCTGTTAGCATGTTCT
GTTTGCAATTTTCTATTTTCTTAGGTTTTTGTCGTTTCAGGCCTCACTGGTCCCCAAAGA
CTCTGTGGGGCCGGATAATCGGCTTTGTTCTGACAGCCGTTTTTTTGCTGGGCTGAATGT
TTAACACACTGGACCATCAGTTTGACTCAGGACTCACGGACCAGTGGCTCCTCCTCTCAA
AGAGAGTTTTATTCTCCTCGCCACAGCAAGGAAGGCCCTGCACGATGTCGAACAGGACCC
CGTGTGGCTCATCTCTTGCTTCTGTGGGAGGCAAGTCTAACCCAGTGTGACCTCCATGAA
GTCGAGAACAAGTAACTCAATCTCCCATCCCACCCTTATGCTGCGCCAGACCCGTGAGGA
GCCCACCTCCGGTGGACAC

B. MI12417 3' flanking end alignment with MiMIC sequences

Synthetic construct MIMIC transposable element, complete sequence
Sequence ID: GU370067.1 **Length:** 7267 **Number of Matches:** 2

Range 1: 6823 to 7204 GenBank Graphics ▼ Next Match ▲ Previous Match

Score	Expect	Identities	Gaps	Strand
688 bits(372)	0.0	380/383(99%)	3/383(0%)	Plus/Plus

```
Query  14    CTACGCCCCC-ACTGAGAG-ACTCAAAGGTTTACCCCAGTTGGGGCACTACTCCCGAAAA  71
             ||||||||| |||||||| |||||||| ||||||||||||||||||||||||||||||
Sbjct  6823  CTACGCCCCCAACTGAGAGAACTCAAAGG-TTACCCCAGTTGGGGCACTACTCCCGAAAA  6881

Query  72    CCGCTTCTGACCTGGGCCGCGGGGGAAATTAATTAAATTATTGTTTTAAGTATGATAGTA  131
             ||||||||||||||||||||||||||||||||||||||||||||||||||||||||||||
Sbjct  6882  CCGCTTCTGACCTGGGCCGCGGGGGAAATTAATTAAATTATTGTTTTAAGTATGATAGTA  6941

Query  132   AATCACATTACGCCGCGTTCGAATTAATAGTGGTCACTTTTTTCTTATCTCTTAAGCAAA  191
             ||||||||||||||||||||||||||||||||||||||||||||||||||||||||||||
Sbjct  6942  AATCACATTACGCCGCGTTCGAATTAATAGTGGTCACTTTTTTCTTATCTCTTAAGCAAA  7001

Query  192   CCGTTTGAATAAATTACTCATATTTTTGTTGTTGTTGGAAATAGAGCAAAACtttttttt  251
             ||||||||||||||||||||||||||||||||||||||||||||||||||||||||||||
Sbjct  7002  CCGTTTGAATAAATTACTCATATTTTTGTTGTTGTTGGAAATAGAGCAAAACTTTTTTTT  7061

Query  252   tCGTCGTGAAGAGAATAAAATTCTCTTTGAGACGAAATGCATTGGTATGTGTTATCTTTA  311
             ||||||||||||||||||||||||||||||||||||||||||||||||||||||||||||
Sbjct  7062  TCGTCGTGAAGAGAATAAAATTCTCTTTGAGACGAAATGCATTGGTATGTGTTATCTTTA  7121

Query  312   GTAGTATTGATAATATAGTGTGTTAAACATTGCGCACTGCaaaaaaaaCATGCTGTTCGA  371
             ||||||||||||||||||||||||||||||||||||||||||||||||||||||||||||
Sbjct  7122  GTAGTATTGATAATATAGTGTGTTAAACATTGCGCACTGCAAAAAAAACATGCTGTTCGA  7181

Query  372   ATTAATAGTGGTTGGGGCTCGTA  394
             |||||||||||||||||||||||
Sbjct  7182  ATTAATAGTGGTTGGGGCTCGTA  7204
```

C. MI12417 3' flanking end alignment with *OAMB* sequences

Drosophila melanogaster chromosome 3R
Sequence ID: AE014297.3 **Length:** 32079331 **Number of Matches:** 1

Range 1: 20696953 to 20697059 GenBank Graphics ▼ Next Match ▲ Previous Match

Score	Expect	Identities	Gaps	Strand
176 bits(95)	8e-40	104/108(96%)	1/108(0%)	Plus/Minus

Features: octopamine receptor in mushroom bodies, isoform D
octopamine receptor in mushroom bodies, isoform G

```
Query  393       TAATATGTCTTCCCTGTTAGCATGTTCTGTTTGCAATTTTCTATTTTCTTAGGTTTTTGT  452
                  ||||||||||||||||||||||||||||||||||||||||||||||||||||||||||||
Sbjct  20697059  TAATATGTCTTCCCTGTTAGCATGTTCTGTTTGCAATTTTCTATTTTCTTAGGTTTTTGT  20697000

Query  453       CGTTTCAGGCCTCACTGGTCCCCAAAGACTCTGTGGGGCCGGATAATC  500
                  ||||||||||||||||||||||||||||| |||||| | || ||||||
Sbjct  20696999  CGTTTCAGGCCTCACTGGTCCCCAAAGACGCTGTGGTGGCG-ATAATC  20696953
```

Figure S2. MI12417 3' PCR product aligned to MiMIC and *OAMB* sequences. (A) Sequenced PCR product for MI12417 3' flanking end. Alignment to MiMIC sequences is indicated in yellow, alignment to *OAMB* sequences in grey and overlapping alignment at the MiMIC insertion site (TA) in red. **(B-C)** Alignment of MI12417 3' PCR products to MiMIC **(B)** and *Drosophila melanogaster* **(C)** sequences using Nucleotide BLAST.

A. Sequenced PCR product for MI05807 5’ flanking end

TCTGACCACACTATTATTCGAACAGCATGTTTTTTTGCAGTGCGCAATGGTTTAACACAC
TATATTATCAATACTACTAAAGATAACACATACCAATGCATTTCGTCTCAAAGAGAATTT
TATTCTCTTCACGACGAAAAAAAAAGTTTTGCTCTATTTCCAACAACAACAAAAATATGA
GTAATTTATTCAAACGGTTTGCTTAAGAGATAAGAAAAAAGTGACCACTATTAATTCGAA
CGCGGCGTAAGCTACTTAAATCTCAAGCATAGCTTATCCAGTTCACTTCTCTGGTGCTTT
TTTCGTATCTCTGAGCAGACCGTTGAATAACTTACTCAATCTTTGTTGTTGTTGGAAATA
CACACACTTTTTTTTTCTCTTGAAGGAATAAAATTCGTTTGACCCCAAATGATTGGTGGG
GTTATCTTTATTAATATGATTGATACGGGGCTAAAATTGGCCTGCAAAAAAAATGACGTC
CAAGAAATAGGTTCGGACTATGTAGTGAACGGTCTCAAAGTAAAGGACGGAATCCGCGAC
GCCATCGAAGATTGAAGCGTCAAACACCCCAACCAGTACCGTCCGAGCTCCCCCAACAGA
CACGGACGCTTGCTGCTGCCAGTCCACCTCGACCTGAGTTCCAGTCCGCCCTGCCAATAA
CGGGTCACTAAGCGCGTTCCAGGTCCTGCTGGAGTCCAGACTCCCTCTGATTCCTCTCGA
CATCGACGAGCTGATCATTTTACTCGTCGCACTATTAACTGCAAGAGTCAATCTCGTCGC
TGCATCTAGAGAAGATCGAATGACGAGTAGCTTATCTACAATGATAAGTTACAATCAATG
ATCATTGCTAAATCTTCACCGATGTTTATTGCAGCATTAATGCTGCAGGAGCACGCTAAC
ACTACATGGCGTACGACTATGTACCCGTTCAGGGAGTGAGGCAGATTCATCATTGAAGTT
GCCAGGTCGGTGATTGTACTGAACAAACTATCGTCCCATGCAATAAGTAATACTGCTGTC
CTAAGAATGATGCCGGGCCA

B. MI05807 5’ flanking end alignment with MiMIC sequences

Synthetic construct MIMIC transposable element, complete sequence

Sequence ID: GU370067.1 **Length:** 7267 **Number of Matches:** 2

Range 1: 115 to 373 GenBank Graphics ▼ Next Match ▲ Previous Match

Score	Expect	Identities	Gaps	Strand
457 bits(247)	4e-124	256/260(98%)	2/260(0%)	Plus/Plus

```
Query  9    CACTATT-ATTCGAACAGCATGttttttttGCAGTGCGCAATGGTTTAACACACTATATTA  67
            ||||||| ||||||||||||||||||||||||||||||||| ||||||||||||||||||
Sbjct  115  CACTATTAATTCGAACAGCATGTTTTTTTTGCAGTGCGCAAT-GTTTAACACACTATATTA  173

Query  68   TCAATACTACTAAAGATAACACATACCAATGCATTTCGTCTCAAAGAGAATTTTATTCTC  127
            ||||||||||||||||||||||||||||||||||||||||||||||||||||||||||||
Sbjct  174  TCAATACTACTAAAGATAACACATACCAATGCATTTCGTCTCAAAGAGAATTTTATTCTC  233

Query  128  TTCACGACGaaaaaaaaaGTTTTGCTCTATTTCCAACAACAACAAAAATATGAGTAATTT  187
            ||||||||||||||||||||||||||||||||||||||||||||||||||||||||||||
Sbjct  234  TTCACGACGAAAAAAAAAAGTTTTGCTCTATTTCCAACAACAACAAAAATATGAGTAATTT  293

Query  188  ATTCAAACGGTTTGCTTAAGAGATAAGAAAAAAGTGACCACTATTAATTCGAACGCGGCG  247
            ||||||||||||||||||||||||||||||||||||||||||||||||||||||||||||
Sbjct  294  ATTCAAACGGTTTGCTTAAGAGATAAGAAAAAAGTGACCACTATTAATTCGAACGCGGCG  353

Query  248  TAAGCTACTTAAATCTCAAG  267
            |||||||| | |||||||||
Sbjct  354  TAAGCTACCTTAATCTCAAG  373
```

Figure S3. MI05807 5’ PCR product aligned to MiMIC sequences. (A) Sequenced PCR product for MI05807 5’ flanking end. Alignment to MiMIC sequences is indicated in yellow. **(B)** Alignment of MI05807 5’ PCR products to MiMIC sequences using Nucleotide BLAST. *Drosophila* genomic sequences could not detected because the primer used against the *Octβ1R* sequences was too close (5 bp) to the MiMIC insertion site, and therefore not reported in the sequenced product.

A. Sequenced PCR product for MI05807 3' flanking end

GGGGTCCGTCGGCGACCTACGCCCCAACTGAGAGAACTCAAAGGTTACCCCAGTTGGGGC
ACTACTCCCGAAAACCGCTTCTGACCTGGGCCGCGGGGGAAATTAATTAAATTATTGTTT
TAAGTATGATAGTAAATCACATTACGCCGCGTTCGAATTAATAGTGGTCACTTTTTTCTT
ATCTCTTAAGCAAACCGTTTGAATAAATTACTCATATTTTTGTTGTTGTTGGAAATAGAG
CAAAACTTTTTTTTTCGTCGTGAAGAGAATAAAATTCTCTTTGAGACGAAATGCATTGGT
ATGTGTTATCTTTAGTAGTATTGATAATATAGTGTGTTAAACATTGCGCACTGCAAAAAA
AACATGCTGTTCGAATTAATAGTGGTTGGGGCTCGTATAATCGGCTTTTGGGTAACGCCT
CAATAACATTTTCGTGTTGCCTCTGATGCGGGTGTTTTGCCTTTGTACTTTTTGGGCGCT
TTAAGCTTGCTCCAAAAATGTAGACCTTTCGGGGCGTCAGTTTGTGGCCGTAATTAGGTT
TGCGGGAGATGGTTTAATGTCCCAGTGAAATATGGCAAAATGGCGAGCGATGTTTAACGA
GA

B. MI05807 3' flanking end alignment with MiMIC sequences

Transposon mutagenesis vector pMiET
Sequence ID: AM711972.1 Length: 7819 Number of Matches: 2

Range 1: 7462 to 7762 GenBank Graphics ▼ Next Match ▲ Previous Match

Score	Expect	Identities	Gaps	Strand
556 bits(301)	8e-157	301/301(100%)	0/301(0%)	Plus/Plus

```
Query  97    GGGAAATTAATTAAATTATTGTTTTAAGTATGATAGTAAATCACATTACGCCGCGTTCGA  156
             ||||||||||||||||||||||||||||||||||||||||||||||||||||||||||||
Sbjct  7462  GGGAAATTAATTAAATTATTGTTTTAAGTATGATAGTAAATCACATTACGCCGCGTTCGA  7521

Query  157   ATTAATAGTGGTCACTTTTTTCTTATCTCTTAAGCAAACCGTTTGAATAAATTACTCATA  216
             ||||||||||||||||||||||||||||||||||||||||||||||||||||||||||||
Sbjct  7522  ATTAATAGTGGTCACTTTTTTCTTATCTCTTAAGCAAACCGTTTGAATAAATTACTCATA  7581

Query  217   TTTTTGTTGTTGTTGGAAATAGAGCAAAACtttttttttCGTCGTGAAGAGAATAAAATT  276
             ||||||||||||||||||||||||||||||||||||||||||||||||||||||||||||
Sbjct  7582  TTTTTGTTGTTGTTGGAAATAGAGCAAAACTTTTTTTTTCGTCGTGAAGAGAATAAAATT  7641

Query  277   CTCTTTGAGACGAAATGCATTGGTATGTGTTATCTTTAGTAGTATTGATAATATAGTGTG  336
             ||||||||||||||||||||||||||||||||||||||||||||||||||||||||||||
Sbjct  7642  CTCTTTGAGACGAAATGCATTGGTATGTGTTATCTTTAGTAGTATTGATAATATAGTGTG  7701

Query  337   TTAAACATTGCGCACTGCaaaaaaaaCATGCTGTTCGAATTAATAGTGGTTGGGGCTCGT  396
             ||||||||||||||||||||||||||||||||||||||||||||||||||||||||||||
Sbjct  7702  TTAAACATTGCGCACTGCAAAAAAAACATGCTGTTCGAATTAATAGTGGTTGGGGCTCGT  7761

Query  397   A  397
             |
Sbjct  7762  A  7762
```

C. MI05807 3' flanking end alignment with *Octβ1R* sequences

Drosophila melanogaster chromosome 3R
Sequence ID: AE014297.3 Length: 32079331 Number of Matches: 1

Range 1: 22511815 to 22512020 GenBank Graphics ▼ Next Match ▲ Previous Match

Score	Expect	Identities	Gaps	Strand
370 bits(200)	1e-100	204/206(99%)	0/206(0%)	Plus/Plus

Features: octopamine beta1 receptor, isoform E
octopamine beta1 receptor, isoform A

```
Query  396       TATAATCGGCTTTTGGGTAACGCCTCAATAACATTTTCGTGTTGCCTCTGATGCGGGTGT  455
                  ||||||||||||||||||||||||||||||||||||||||||||||||||||||||||||
Sbjct  22511815  TATAATCGGCTTTTGGGTAACGCCTCAATAACATTTTCGTGTTGCCTCTGATGCGGGTGT  22511874

Query  456       TTTGCCTTTGTACTTTTTGGGCGCTTTAAGCTTGCTCCAAAAAATGTAGACCTTTCGGGGC  515
                  ||||||||||||||||||||||||||||||||||||||||||||||||||||||||||||
Sbjct  22511875  TTTGCCTTTGTACTTTTTGGGCGCTTTAAGCTTGCTCCAAAAAATGTAGACCTTTCGGGGC  22511934

Query  516       GTCAGTTTGTGGCCGTAATTAGGTTTGCGGGAGATGGTTTAATGTCCCAGTGAAATATGG  575
                  ||||||||||||||||||||||||||||||||||||||||||||||||||||||||||||
Sbjct  22511935  GTCAGTTTGTGGCCGTAATTAGGTTTGCGGGAGATGGTTTAATGTCCCAGTGAAATATGG  22511994

Query  576       CAAAATGGCGAGCGATGTTTAACGAG  601
                  |||||||||||||||| |||||||||
Sbjct  22511995  CAAAATGGCGAGCGATTGTTAACGAG  22512020
```

Figure S4. MI05807 3' PCR product aligned to MiMIC and *Octβ1R* sequences. (A) Sequenced PCR product for MI05807 3' flanking end. Alignment to MiMIC sequences is indicated in yellow, alignment to *Octβ1R* sequences in grey, and overlapping alignment at the MiMIC insertion site (TA) in red. **(B-C)** Alignment of MI05807 3' PCR products to MiMIC **(B)** and *Drosophila melanogaster* **(C)** sequences using Nucleotide BLAST.

A. Sequenced PCR product for MI13416 3’ flanking end

GCGGGTTCGCGACCTACGCCCCACTGAGAGACTCAAAGGTTACCCCAGTTGGGGCACTAC
TCCCGAAAACCGCTTCTGACCTGGGCCGCGGGGGAAATTAATTAAATTATTGTTTTAAGT
ATGATAGTAAATCACATTACGCCGCGTTCGAATTAATAGTGGTCACTTTTTTCTTATCTC
TTAAGCAAACCGTTTGAATAAATTACTCATATTTTTGTTGTTGTTGGAAATAGAGCAAAA
CTTTTTTTTTCGTCGTGAAGAGAATAAAATTCTCTTTGAGACGAAATGCATTGGTATGTG
TTATCTTTAGTAGTATTGATAATATAGTGTGTTAAACATTGCGCACTGCAAAAAAAACAT
GCTGTTCGAATTAATAGTGGTTGGGGCTCGTATCTATCATAATAAATAAATAAATAAATA
TGTATATTTAGCAAGGGATATACAAAAAATATTTTTCATTTATAAAGTTAACTTGAATGA
AATTATTCGGTCGGTATATTACCATAATCGAGCAAAAGTTTTCGAGAGCAGTAAATGCTC
AATTTTGATTGCAAACTTTTCCCATTTGGCTTAGTCAAAATGGTGAATGAAAGGCGGCCA
CCTGGAGTTCTGGAAGGGAACAAAAAATTTAACGGGGGCTTAATTTTCCGCCATGAAACT
TGTTCCTTGCCATATTAGAACCAGACGAGTGCTGCTCCTTAACCCATGATCTCCATACGA
ACTTCACGCGAGATTGAAGCACGTCTCATGTAGCAGAGCGTTAGCCTCGCATCTATGTCG
ACGGATATCTTTCTCCTGCGATCAGCACAGTCAATGCCGGAGCCTGCACGCGCGAAAGAT
CACCGATTCGCACTAGTGGAACTCCTTGCTAAGTTGGCATAACGTGCAATGTGATTACTA
CACGCACAACGGACGTTGCCCGCAGCCGCGCCTCGCCGCTATCAGATTGATCAGGATGCT
GTCACGCTCCATACGCCACGAAGATGAGGAAAGATGCGACACTTCGCCAGTCATGCTGTA
TCTCGGCGGGACGCAGGCCATCCTTGCAGACCTCTCGGTGGGGATCGGAAGCCACGGTGA
GGCTGGAAGAGACCGGGACTTCCGTGCCTACTGGGGATGCGACGGCGTGCTCGTCCACGC
TTAGCGCGCGGATCTAACGCCTAAGGCCTCTGGGAATCG

B. MI13416 3’ flanking end alignment with MiMIC sequences

Synthetic construct MIMIC transposable element, complete sequence

Sequence ID: GU370067.1 **Length:** 7267 **Number of Matches:** 2

Range 1: 6817 to 7204 GenBank Graphics ▼ Next Match ▲ Previous Match

Score	Expect	Identities	Gaps	Strand
691 bits(374)	0.0	384/388(99%)	4/388(1%)	Plus/Plus

```
Query  9     GCGA-CCTACG-CCCC-ACTGAGAG-ACTCAAAGGTTACCCCAGTTGGGGCACTACTCCC  64
             |||| |||||| |||| ||||||| ||||||||||||||||||||||||||||||||||
Sbjct  6817  GCGACCCTACGCCCCCAACTGAGAGAACTCAAAGGTTACCCCAGTTGGGGCACTACTCCC  6876

Query  65    GAAAACCGCTTCTGACCTGGGCCGCGGGGGAAATTAATTAAATTATTGTTTTAAGTATGA  124
             ||||||||||||||||||||||||||||||||||||||||||||||||||||||||||||
Sbjct  6877  GAAAACCGCTTCTGACCTGGGCCGCGGGGGAAATTAATTAAATTATTGTTTTAAGTATGA  6936

Query  125   TAGTAAATCACATTACGCCGCGTTCGAATTAATAGTGGTCACTTTTTTCTTATCTCTTAA  184
             ||||||||||||||||||||||||||||||||||||||||||||||||||||||||||||
Sbjct  6937  TAGTAAATCACATTACGCCGCGTTCGAATTAATAGTGGTCACTTTTTTCTTATCTCTTAA  6996

Query  185   GCAAACCGTTTGAATAAATTACTCATATTTTTGTTGTTGTTGGAAATAGAGCAAAACttt  244
             ||||||||||||||||||||||||||||||||||||||||||||||||||||||||||||
Sbjct  6997  GCAAACCGTTTGAATAAATTACTCATATTTTTGTTGTTGTTGGAAATAGAGCAAAACTTT  7056

Query  245   tttttCGTCGTGAAGAGAATAAAATTCTCTTTGAGACGAAATGCATTGGTATGTGTTAT  304
             |||||||||||||||||||||||||||||||||||||||||||||||||||||||||||
Sbjct  7057  TTTTTCGTCGTGAAGAGAATAAAATTCTCTTTGAGACGAAATGCATTGGTATGTGTTAT  7116

Query  305   CTTTAGTAGTATTGATAATATAGTGTGTTAAACATTGCGCACTGCaaaaaaaaCATGCTG  364
             ||||||||||||||||||||||||||||||||||||||||||||||||||||||||||||
Sbjct  7117  CTTTAGTAGTATTGATAATATAGTGTGTTAAACATTGCGCACTGCAAAAAAAACATGCTG  7176

Query  365   TTCGAATTAATAGTGGTTGGGGCTCGTA  392
             |||||||||||||||||||||||||||
Sbjct  7177  TTCGAATTAATAGTGGTTGGGGCTCGTA  7204
```

C. MI13416 3’ flanking end alignment with *Octβ2R* sequences

Drosophila melanogaster chromosome 3R
Sequence ID: AE014297.3 Length: 32079331 Number of Matches: 1

Range 1: 12557568 to 12557760 GenBank Graphics ▼ Next Match ▲ Previous Match

Score	Expect	Identities	Gaps	Strand
346 bits(187)	9e-91	191/193(99%)	0/193(0%)	Plus/Minus

Features: octopamine beta2 receptor, isoform F
octopamine beta2 receptor, isoform C

```
Query  418       atatgtatatttagcaagggatatacaaaaaatatttttcatttataaAGTTAACTTGAA  477
                  ||||||||||||||||||||||||| |||||||||||||||||||||||||||||||||
Sbjct  12557760  ATATGTATATTTAGCAAGGGATATACAACAAATATTTTTCATTTATAAAGTTAACTTGAA  12557701

Query  478       TGAAATTATTCGGTCGGTATATTACCATAATCGAGCAAAAGTTTTCGAGAGCAGTAAATG  537
                  ||||||||||||||||||||||||||||||||||||||||||||||||||||||||||||
Sbjct  12557700  TGAAATTATTCGGTCGGTATATTACCATAATCGAGCAAAAGTTTTCGAGAGCAGTAAATG  12557641

Query  538       CTCAATTTTGATTGCAAACTTTTCCCATTTGGCTTAGTCAAAATGGTGAATGAAAGGCGG  597
                  ||||||||||||||||||||||||||||||||||||| ||||||||||||||||||||
Sbjct  12557640  CTCAATTTTGATTGCAAACTTTTCCCATTTGGCTTAGTGAAAATGGTGAATGAAAGGCGG  12557581

Query  598       CCACCTGGAGTTC  610
                  |||||||||||||
Sbjct  12557580  CCACCTGGAGTTC  12557568
```

Figure S5. MI13416 3’ PCR product aligned to MiMIC and *Octβ2R* sequences. (A) Sequenced PCR product for MI13416 3’ flanking end. Alignment to MiMIC sequences is indicated in yellow, alignment to *Octβ2R* sequences in grey, overlapping alignment at the MiMIC insertion site (TA) in red, and an unidentified sequence indicated in green. **(B-C)** Alignment of MI13416 3’ PCR products to MiMIC **(B)** and *Drosophila melanogaster* **(C)** sequences using Nucleotide BLAST.

A. Sequenced PCR product for MI06217 5’ flanking end

AGATCGATGGTCGCGTTTCACCAGTTCCGCAAGTGAGTAGTCATCCATTTGGTCATTGTG
TAGACTGTATAGCTCGTGCTTGATTTAAGTAGCTCTTTTAAGACAATTTATATCTGCCCC
AGAGAAATTCGTTCTGTTTTTGTCAGTTTTCCACGAAAAGTTCAAGTGTTTCAATGTTTG
ACTTAACTTTTTCGCACATTCTTTTGTCCTTGTTTTTTTGAGGAGTAATTGGCCTGAATT
CGGGTTTAACATAAGGAATCTGGTCTTACTAGAATTTTGATCTTAAAATAAAGATACGAA
CTTTTACCATATTTAAATATAGTTCTTACCTTGAAGAAAACTGTGAATTGTGTATTTAAG
TTCCTTTCAAAAGCGGTGCGAATTTCTGAAAAATCATACAGTGTTTTAAAATGTATAGAA
CCTATAAACCCTCATTGGAAAAGTAATACTCAAATGCTTCGAATGAAACTTTAGTTAACT
AGCTTACTATACGAGCCCCAACCACTATTAATTCGAACAGCATGTTTTTTTGCAGTGCGC
AATGTTTAACACACTATATTATCAATACTACTAAAGATAACACATACCAATGCATTTCGT
CTCAAAGAGAATTTTATTCTCTTCACGACGAAAAAAAAAGTTTTGCTCTATTTCCAACAA
CAACAAAAATATGAGTAATTTATTCAAACGGTTTGCTTAAGAGATAAGAAAAAAGTGACC
ACTATTAATTCGAACGCGGCGTAAGTTTCCTACATCGTCATTAGGTTCTTGCCTAGGGAT
CATTGGGGTTGCCCTGACCTCTGGTGAGTAACCTCATTTAAACTTATC

B. MI06217 5’ flanking end alignment with MiMIC sequences

Synthetic construct MIMIC transposable element, complete sequence

Sequence ID: GU370067.1 **Length:** 7267 **Number of Matches:** 2

Range 1: 102 to 357 GenBank Graphics ▼ Next Match ▲ Previous Match

Score	Expect	Identities	Gaps	Strand
473 bits(256)	3e-129	256/256(100%)	0/256(0%)	Plus/Plus

```
Query  490  TACGAGCCCCAACCACTATTAATTCGAACAGCATGttttttGCAGTGCGCAATGTTTAA  549
            ||||||||||||||||||||||||||||||||||||||||||||||||||||||||||
Sbjct  102  TACGAGCCCCAACCACTATTAATTCGAACAGCATGTTTTTTTGCAGTGCGCAATGTTTAA  161

Query  550  CACACTATATTATCAATACTACTAAAGATAACACATACCAATGCATTTCGTCTCAAAGAG  609
            ||||||||||||||||||||||||||||||||||||||||||||||||||||||||||||
Sbjct  162  CACACTATATTATCAATACTACTAAAGATAACACATACCAATGCATTTCGTCTCAAAGAG  221

Query  610  AATTTTATTCTCTTCACGACGaaaaaaaaaGTTTTGCTCTATTTCCAACAACAACAAAAA  669
            |||||||||||||||||||||||||||||||||||||||||||||||||||||||||||
Sbjct  222  AATTTTATTCTCTTCACGACGAAAAAAAAAGTTTTGCTCTATTTCCAACAACAACAAAAA  281

Query  670  TATGAGTAATTTATTCAAACGGTTTGCTTAAGAGATAAGAAAAAAGTGACCACTATTAAT  729
            ||||||||||||||||||||||||||||||||||||||||||||||||||||||||||||
Sbjct  282  TATGAGTAATTTATTCAAACGGTTTGCTTAAGAGATAAGAAAAAAGTGACCACTATTAAT  341

Query  730  TCGAACGCGGCGTAAG  745
            ||||||||||||||||
Sbjct  342  TCGAACGCGGCGTAAG  357
```

C. MI06217 5’ flanking end alignment with *Octβ3R* sequences

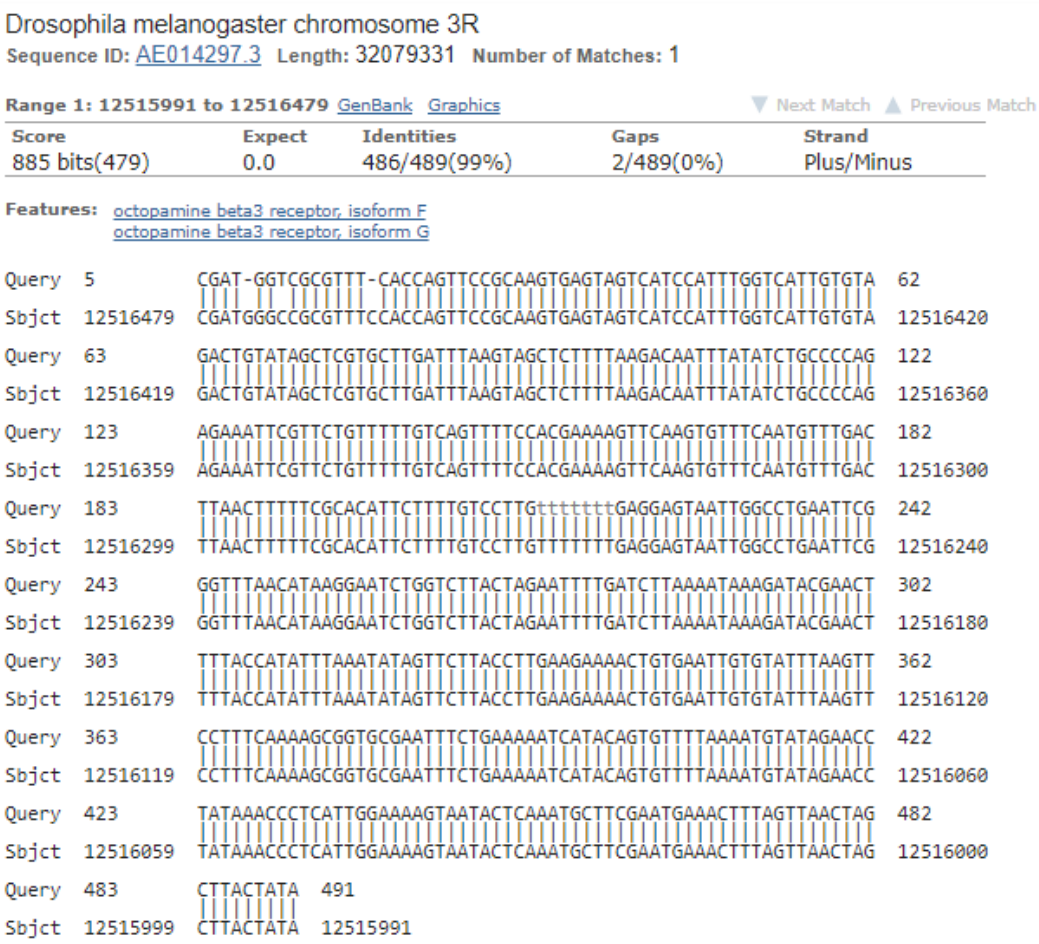

Figure S6. MI06217 5’ PCR product aligned to MiMIC and *Octβ3R* sequences. (A) Sequenced PCR product for MI06217 5’ flanking end. Alignment to MiMIC sequences is indicated in yellow, alignment to *Octβ3R* sequences in grey, and overlapping alignment at the MiMIC insertion site (TA) in red. **(B-C)** Alignment of MI06217 5’ PCR products to MiMIC **(B)** and *Drosophila melanogaster* **(C)** sequences using Nucleotide BLAST.

A. Sequenced PCR product for MI06217 3’ flanking end

NGCGTGTGCCGGCAACCTACCGCCCCACTGAGAGGACTCAAAGGTTACCCCAGTTGGGGC
ACTACTCCCGAAAACCGCTTCTGACCTGGGCCGCGGGGGAAATTAATTAAATTATTGTTT
TAAGTATGATAGTAAATCACATTACGCCGCGTTCGAATTAATAGTGGTCACTTTTTTCTT
ATCTCTTAAGCAAACCGTTTGAATAAATTACTCATATTTTTGTTGTTGTTGGAAATAGAG
CAAAACTTTTTTTTTCGTCGTGAAGAGAATAAAATTCTCTTTGAGACGAAATGCATTGGT
ATGTGTTATCTTTAGTAGTATTGATAATATAGTGTGTTAAACATTGCGCACTGCAAAAAA
AACATGCTGTTCGAATTAATAGTGGTTGGGGCTCGTATATATATAATATAATGTATAGCA
TTTAGTTAGTTGCACCTGCAAACGAAGACAGAAAGGGACGACCTACTTCAGGAAGACAGG
AAGGAAAAAAAAAAAAAAAATTATTATATTGGTGAAAGGG

B. MI06217 3’ flanking end alignment with MiMIC sequences

Synthetic construct MIMIC transposable element, complete sequence

Sequence ID: GU370067.1 **Length:** 7267 **Number of Matches:** 2

Range 1: 6812 to 7204 GenBank Graphics ▼ Next Match ▲ Previous Match

Score	Expect	Identities	Gaps	Strand
686 bits(371)	0.0	386/393(98%)	2/393(0%)	Plus/Plus

```
Query  7     TGCCGGC-AACCTACCGCCCC-ACTGAGAGGACTCAAAGGTTACCCCAGTTGGGGCACTA  64
             || |||| | |||||  |||| ||||||| ||||||||||||||||||||||||||||
Sbjct  6812  TGTCGGCGACCCTACGCCCCCAACTGAGAGAACTCAAAGGTTACCCCAGTTGGGGCACTA  6871

Query  65    CTCCCGAAAACCGCTTCTGACCTGGGCCGCGGGGGAAATTAATTAAATTATTGTTTTAAG  124
             ||||||||||||||||||||||||||||||||||||||||||||||||||||||||||||
Sbjct  6872  CTCCCGAAAACCGCTTCTGACCTGGGCCGCGGGGGAAATTAATTAAATTATTGTTTTAAG  6931

Query  125   TATGATAGTAAATCACATTACGCCGCGTTCGAATTAATAGTGGTCACTTTTTTCTTATCT  184
             ||||||||||||||||||||||||||||||||||||||||||||||||||||||||||||
Sbjct  6932  TATGATAGTAAATCACATTACGCCGCGTTCGAATTAATAGTGGTCACTTTTTTCTTATCT  6991

Query  185   CTTAAGCAAACCGTTTGAATAAATTACTCATATTTTTGTTGTTGTTGGAAATAGAGCAAA  244
             ||||||||||||||||||||||||||||||||||||||||||||||||||||||||||||
Sbjct  6992  CTTAAGCAAACCGTTTGAATAAATTACTCATATTTTTGTTGTTGTTGGAAATAGAGCAAA  7051

Query  245   ACttttttttCGTCGTGAAGAGAATAAAATTCTCTTTGAGACGAAATGCATTGGTATGT  304
             ||||||||||||||||||||||||||||||||||||||||||||||||||||||||||||
Sbjct  7052  ACTTTTTTTTTCGTCGTGAAGAGAATAAAATTCTCTTTGAGACGAAATGCATTGGTATGT  7111

Query  305   GTTATCTTTAGTAGTATTGATAATATAGTGTGTTAAACATTGCGCACTGCaaaaaaaaCA  364
             ||||||||||||||||||||||||||||||||||||||||||||||||||||||||||||
Sbjct  7112  GTTATCTTTAGTAGTATTGATAATATAGTGTGTTAAACATTGCGCACTGCAAAAAAAACA  7171

Query  365   TGCTGTTCGAATTAATAGTGGTTGGGGCTCGta  397
             |||||||||||||||||||||||||||||||
Sbjct  7172  TGCTGTTCGAATTAATAGTGGTTGGGGCTCGTA  7204
```

C. MI06217 3’ flanking end alignment with *Octβ3R* sequences

Drosophila melanogaster chromosome 3R

Sequence ID: AE014297.3 **Length:** 32079331 **Number of Matches:** 1

Range 1: 12515906 to 12515992 GenBank Graphics ▼ Next Match ▲ Previous Match

Score	Expect	Identities	Gaps	Strand
139 bits(75)	7e-29	84/88(95%)	1/88(1%)	Plus/Minus

Features: octopamine beta3 receptor, isoform F
octopamine beta3 receptor, isoform G

```
Query  396       tatatatataatataATGTATAGCATTTAGTTAGTTGCACCTGCAAACGAAGACAGAAAG  455
                  ||||||||||||||||||||||||||||||||||||||||||||||||||||||||||||
Sbjct  12515992  TATATATATAATATAATGTATAGCATTTAGTTAGTTGCACCTGCAAACGAAGACAGAAAG  12515933

Query  456       GGACGACCTACTTCAGGAAGACAGGAAG  483
                  |||||||||||||  || ||||||  ||
Sbjct  12515932  GGACGACCTACTTCCAGA-GACAGGGAG  12515906
```

Figure S7. MI06217 3’ PCR product aligned to MiMIC and *Octβ3R* sequences. (A) Sequenced PCR product for MI06217 3’ flanking end. Alignment to MiMIC sequences is indicated in yellow, alignment to *Octβ3R* sequences in grey, and overlapping alignment at the MiMIC insertion site (TA) in red. **(B-C)** Alignment of MI06217 3’ PCR products to MiMIC **(B)** and *Drosophila melanogaster* **(C)** sequences using Nucleotide BLAST.

A. Sequenced PCR product for MI10227 5’ flanking end

CCCGCATCTGCTACCGCCGCTCCTCGGCTGGAGGTGAAGATGCCCGAGGGACCGCTGCCC
AAGTGCGAGGTAAGTGGCAAGTGGTGCTCCTAAGTGGCGCAATAATCCACATCCCATGCG
AAATTGACGCCAATTCGACGGCAATTCGACGTTGCCCCACCGACAATCGAACAATGAAAA
TTCAGACGGGTTGTGGAATTGAAAAGCATCGTGTGTGCTGCCCAATTGGCTATTTTCTGG
TGTGATGTGTGTGGAGTATGGAAGATTATTAAACTTTTATAAAATTCTGTTATTCGAACC
ATAATCAACGGCTTGGCTTATAAATATCTTCAAATTACTTGAATAGCAACAGCAATTTCT
TTATACGAGCCCCAACCACTATTAATTCGAACAGCATGTTTTTTTTGCAGTGCGCAATGT
TTAACACACTATATTATCAATACTACTAAAGATAACACATACCAATGCATTTCGTCTCAA
AGAGAATTTTATTCTCTTCACGACGAAAAAAAAAGTTTTGCTCTATTTCCAACAACAACA
AAAATATGAGTAATTTATTCAAACGGTTTGCTTAAGAGATAAGAAAAAAGTGACCACTAT
TAATTCGAACGCGGCGTAATGTGATTTACTATCATACTTAAAACAATAATTTAATTAATT
TCCCCCGCGGCCCAGGTCAGAAGCGGTTTTCGGGAGTAGTGCCCCAACTGGGGTAACCTT
TGAGTTCTCTCAGTTGGGGGCGTAGGGTCGCCGACATGACACAAGGGTGCGCCCCCCCCC
CCCACACAAAAAAAGGCCTGGCGAAGCAACCCTCAAAAAGGGAACCCCCCAGCACTCTGA
ATATCAGCATCTGATCAGACTGAGAAGTCTTCAGATCTTGT

B. MI10227 5’ flanking end alignment with MiMIC sequences

Synthetic construct MIMIC transposable element, complete sequence

Sequence ID: GU370067.1 Length: 7267 Number of Matches: 2

Range 1: 6801 to 7208 GenBank Graphics ▼ Next Match ▲ Previous Match

Score	Expect	Identities	Gaps	Strand
749 bits(405)	0.0	407/408(99%)	0/408(0%)	Plus/Minus

```
Query  360   TTTATACGAGCCCCAACCACTATTAATTCGAACAGCATGtttttttGCAGTGCGCAATG  419
Sbjct  7208  TTTCTACGAGCCCCAACCACTATTAATTCGAACAGCATGTTTTTTTTGCAGTGCGCAATG  7149
Query  420   TTTAACACACTATATTATCAATACTACTAAAGATAACACATACCAATGCATTTCGTCTCA  479
Sbjct  7148  TTTAACACACTATATTATCAATACTACTAAAGATAACACATACCAATGCATTTCGTCTCA  7089
Query  480   AAGAGAATTTTATTCTCTTCACGACGaaaaaaaaaGTTTTGCTCTATTTCCAACAACAAC  539
Sbjct  7088  AAGAGAATTTTATTCTCTTCACGACGAAAAAAAAAGTTTTGCTCTATTTCCAACAACAAC  7029
Query  540   AAAAATATGAGTAATTTATTCAAACGGTTTGCTTAAGAGATAAGAAAAAAGTGACCACTA  599
Sbjct  7028  AAAAATATGAGTAATTTATTCAAACGGTTTGCTTAAGAGATAAGAAAAAAGTGACCACTA  6969
Query  600   TTAATTCGAACGCGGCGTAATGTGATTTACTATCATACTTAAAACAATAATTTAATTAAT  659
Sbjct  6968  TTAATTCGAACGCGGCGTAATGTGATTTACTATCATACTTAAAACAATAATTTAATTAAT  6909
Query  660   TTCCCCCGCGGCCCAGGTCAGAAGCGGTTTTCGGGAGTAGTGCCCCAACTGGGGTAACCT  719
Sbjct  6908  TTCCCCCGCGGCCCAGGTCAGAAGCGGTTTTCGGGAGTAGTGCCCCAACTGGGGTAACCT  6849
Query  720   TTGAGTTCTCTCAGTTGGGGGCGTAGGGTCGCCGACATGACACAAGGG  767
Sbjct  6848  TTGAGTTCTCTCAGTTGGGGGCGTAGGGTCGCCGACATGACACAAGGG  6801
```

C. MI10227 5’ flanking end alignment with *CG18208* sequences

Figure S8. MI10227 5’ PCR product aligned to MiMIC and *CG18208* sequences. (A) Sequenced PCR product for MI10227 5’ flanking end. Alignment to MiMIC sequences is indicated in yellow, alignment to *CG18208* sequences in grey, and overlapping alignment at the MiMIC insertion site (TA) in red. **(B-C)** Alignment of MI10227 5’ PCR product to MiMIC **(B)** and *Drosophila melanogaster* **(C)** sequences using Nucleotide BLAST.

A. Sequenced PCR product for *MI10227* 3’ flanking end

TGCGATTAGGCGCGGGATGTGAATGTGGTTTGGAAACCAACAGCCAAGGCATCGCCGAAT
CATCTGACAATCGTGCCGACAACTCGCCAAATTTGCATAGAAAGAGGCCGCAATTTTGCG
CTTTGCATGTTGCTAGCCGAGCTTTTGCCAGCATTTTAGCCATTCACCGCTTTATTGTTA
GCAAATGTAAGTACTCGGCAGCGATGGCATCTATTGACGTGCAAAAAGTGGCTACATCGG
GCTAGAAAATATTGCTTAAAATAGCCACGGTAAATTATTAAGACATTACGGAAATAATTT
ATGTATACATTTGCCCTATTTTTATACAGATGTTCCTAGACTGGTAAGAAAATGAAAATG
CCATTATATGCCATAACATCTTTTTTATACCAAGCCTTTTCTTGTAAACACTTTGAAACC
TAGAATCTCAAGCCAAATATATGCCGTGTTATAAAAACGTCAAGCAAGTTCGTAAAAAAT
TAAAGTGCTTAAATTCTATGGGTTTCAACTATAAATATGTGGGGTTTACGAGCCCCAACC
ACTATTAATTCGAACAGCATGTTTTTTTGCAGTGCGCAATGTTTAACACACTATATTATC
AATACTACTAAAGATAACACATACCAATGCATTTCGTCTCAAAGAGAATTTTATTCTCTT
CACGACGAAAAAAAAAGTTTTGCTCTATTTCCAACAACAACAAAAATATGAGTAATTTAT
TCAAACGGTTTGCTTAAAGAGATAAAAAAAAAAGTGACCACTATTAATTCGAACGCGGCG
TAGTTCTTTTTTTCTCTCGGGGGGGGGGG

B. MI10227 3’ flanking end alignment with MiMIC sequences

Synthetic construct MIMIC transposable element, complete sequence

Sequence ID: GU370067.1 **Length:** 7267 **Number of Matches:** 2

Range 1: 102 to 355 GenBank Graphics ▼ Next Match ▲ Previous Match

Score	Expect	Identities	Gaps	Strand
455 bits(246)	1e-123	253/256(99%)	2/256(0%)	Plus/Plus

```
Query  527  TACGAGCCCCAACCACTATTAATTCGAACAGCATGttttttGCAGTGCGCAATGTTTAA  586
            ||||||||||||||||||||||||||||||||||||||||||||||||||||||||||
Sbjct  102  TACGAGCCCCAACCACTATTAATTCGAACAGCATGTTTTTTTGCAGTGCGCAATGTTTAA  161

Query  587  CACACTATATTATCAATACTACTAAAGATAACACATACCAATGCATTTCGTCTCAAAGAG  646
            ||||||||||||||||||||||||||||||||||||||||||||||||||||||||||||
Sbjct  162  CACACTATATTATCAATACTACTAAAGATAACACATACCAATGCATTTCGTCTCAAAGAG  221

Query  647  AATTTTATTCTCTTCACGACGaaaaaaaaaGTTTTGCTCTATTTCCAACAACAACAAAAA  706
            ||||||||||||||||||||||||||||||||||||||||||||||||||||||||||||
Sbjct  222  AATTTTATTCTCTTCACGACGAAAAAAAAAGTTTTGCTCTATTTCCAACAACAACAAAAA  281

Query  707  TATGAGTAATTTATTCAAACGGTTTGCTTAAAGAGATaaaaaaaaaGTGACCACTATTA  766
            |||||||||||||||||||||||||||| ||||||||| ||||||||||||||||||||
Sbjct  282  TATGAGTAATTTATTCAAACGGTTTGCTT-AAGAGATAAG-AAAAAAGTGACCACTATTA  339

Query  767  ATTCGAACGCGGCGTA  782
            ||||||||||||||||
Sbjct  340  ATTCGAACGCGGCGTA  355
```

C. MI10227 3’ flanking end alignment with *CG18208* sequences

Drosophila melanogaster chromosome 3R
Sequence ID: AE014297.3 Length: 32079331 Number of Matches: 1

Range 1: 18846784 to 18847297 GenBank Graphics ▼ Next Match ▲ Previous Match

Score	Expect	Identities	Gaps	Strand
854 bits(462)	0.0	497/514(97%)	1/514(0%)	Plus/Plus

Features: uncharacterized protein, isoform B
uncharacterized protein, isoform C

```
Query  14        GGGATGTGAATGTGGTTTGGAAACCAACAGCCAAGGCATCGCCGAATCATCTGACAATCG  73
                 ||||||||||||||||||| ||||||||||||||||||||||||||||||||||||||
Sbjct  18846784  GGGATGTGAATGTGGTTTGGATACCAACAGCCAAGGCATCGCCGAATCATCTGACAATCG  18846843

Query  74        TGCCGACAACTCGCCAAATTTGCATAGAAAGAGGCCGCAATTTTGCGCTTTGCATGTTGC  133
                 ||||||||||||||||||||||||||||||||||||||||||||||||||||||||||||
Sbjct  18846844  TGCCGACAACTCGCCAAATTTGCATAGAAAGAGGCCGCAATTTTGCGCTTTGCATGTTGC  18846903

Query  134       TAGCCGAGCTTTTGCCAGCATTTTAGCCATTCACCGCTTTATTGTTAGCAAATGTAAGTA  193
                 |||||||||||||||||||||||||||||||||||||||||||| ||||||||||||||
Sbjct  18846904  TAGCCGAGCTTTTGCCAGCATTTTAGCCATTCACCGCTTTATTGTTCGCAAATGTAAGTA  18846963

Query  194       CTCGGCAGCGATGGCATCTATTGACGTGCAAAAAGTGGCTACATCGGGCTAGAAAATATT  253
                 |||||||||||||||||||||||||||||||||||| |||||||||||| ||||||||||
Sbjct  18846964  CTCGGCAGCGATGGCATCTATTGACGTGCAAAAAGTGGCTAAATCGGGCTAGAAAATTTT  18847023

Query  254       GCTTAAAATAGCCACGGTAAATTATTAAGACATTACGGAAATAATTTATGTATACATTTG  313
                 ||||||||||||||||||||||||||||||||||||||||||||||||||||||||||||
Sbjct  18847024  GCTTAAAATAGCCACGGTAAATTATTAAGACATTACGGAAATAATTTATGTATACATTTG  18847083

Query  314       CCCTATTTTTATACAGATGTTCCTAGACTGGTAAGAAAATGAAAATGCCATTATATGCCA  373
                   |||||||||||||||||||||||||||||||||||||||||||||||||||||||||
Sbjct  18847084  ACCTATTTTTATACAGATGTTCCTAGACTGGTAAGAAAATGAAAATGCCATTATATGCCA  18847143

Query  374       TAACATCTTTTTTATACCAAGCCTTTTCTTGTAAACACTTTGAAACCTAGAATCTCAAGC  433
                 |||||||||||||||||||||||||||||||||||| |||||||||| ||||| ||||
Sbjct  18847144  TAACATCTTTTTTATACCAAGCCTTTTCTTGTAAACATTTTGAAACCTAAAATCTGAAGC  18847203

Query  434       CAAATATATGCCGTGTTATAAAAACGTCAAGCAAGTTCGTAAAAAATTAAAGTGCTTAAA  493
                 |||||||||||||||||||||||| |||||||||||||||||| |  ||||||||||
Sbjct  18847204  CAAATATATGCCGTGTTATAAAAACATCAAGCAAGTTCGTAAAAAATAATTGTGCTTAAA  18847263

Query  494       TTCTATGGGTTTCAACTATAAATATGTGG-GGTT  526
                  ||| || |||||||||||||| ||||| ||||
Sbjct  18847264  GTCTGTGCGTTTCAACTATAAATCTGTGGAGGTT  18847297
```

Figure S9. MI10227 3’ PCR product aligned to MiMIC and *CG18208* sequences. (A) Sequenced PCR product for MI10227 3’ flanking end. Alignment to MiMIC sequences is indicated in yellow, alignment to *CG18208* sequences in grey, and overlapping alignment at the MiMIC insertion site (TA) in red. **(B-C)** Alignment of MI10227 3’ PCR products to MiMIC **(B)** and *Drosophila melanogaster* **(C)** sequences using Nucleotide BLAST.

References

Adamo, S.A., Linn, C.E., and Hoy, R.R. (1995). The role of neurohormonal octopamine during "fight or flight" behaviour in the field cricket Gryllus bimaculatus. J. Exp. Biol. 198, 1691–1700.

Agnati, L.F., Zoli, M., Strömberg, I., and Fuxe, K. (1995). Intercellular communication in the brain: Wiring versus volume transmission. Neuroscience 69, 711–726.

Akerboom, J., Chen, T.-W., Wardill, T.J., Tian, L., Marvin, J.S., Mutlu, S., Calderon, N.C., Esposti, F., Borghuis, B.G., Sun, X.R., et al. (2012). Optimization of a GCaMP Calcium Indicator for Neural Activity Imaging. J. Neurosci. 32, 13819–13840.

Akerboom, J., Carreras Calderón, N., Tian, L., Wabnig, S., Prigge, M., Tolö, J., Gordus, A., Orger, M.B., Severi, K.E., Macklin, J.J., et al. (2013). Genetically encoded calcium indicators for multi-color neural activity imaging and combination with optogenetics. Front. Mol. Neurosci. *6*, 2.

Altschul, S.F., Gish, W., Miller, W., Myers, E.W., and Lipman, D.J. (1990). Basic local alignment search tool. J. Mol. Biol. 215, 403–410.

Andrews, J.C., Fernández, M.P., Yu, Q., Leary, G.P., Leung, A.K.W., Kavanaugh, M.P., Kravitz, E. a., and Certel, S.J. (2014). Octopamine Neuromodulation Regulates Gr32a-Linked Aggression and Courtship Pathways in *Drosophila* Males. PLoS Genet. 10.

Aoki, C., Go, C.G., Venkatesan, C., and Kurose, H. (1994). Perikaryal and synaptic localisation of α2A-adrenergic receptor-like immunoreactivity. Brain Res. 650, 181–204.

Arakawa, S., Gocayne, J.D., McCombie, W.R., Urquhart, D.A., Hall, L.M., Fraser, C.M., and Venter, J.C. (1990). Cloning, localisation, and permanent expression of a *Drosophila* octopamine receptor. Neuron 4, 343–354.

Aso, Y., Siwanowicz, I., Bräcker, L., Ito, K., Kitamoto, T., and Tanimoto, H. (2010). Specific dopaminergic neurons for the formation of labile aversive memory. Curr. Biol. 20, 1445–1451.

Aso, Y., Hattori, D., Yu, Y., Johnston, R.M., Iyer, N.A., Ngo, T.T.B., Dionne, H., Abbott, L.F., Axel, R., Tanimoto, H., et al. (2014). The neuronal architecture of the mushroom body provides a logic for associative learning. Elife 3, e04577.

Aso, Y., and Rubin, G.M. (2016). Dopaminergic neurons write and update memories with cell-type-specific rules. Elife 5, 1–15.

Aston-Jones, G., Rajkowski, J., and Kubiak, P. (1997). Conditioned responses of monkey locus coeruleus neurons anticipate acquisition of discriminative behavior in a vigilance task. Neuroscience 80, 697–715.

Aton, S.J. (2013). Set and setting: How behavioral state regulates sensory function and plasticity. Neurobiol. Learn. Mem. 106, 1–10.

Atzori, M., Cuevas-Olguin, R., Esquivel-Rendon, E., Garcia-Oscos, F., Salgado-Delgado, R.C., Saderi, N., Miranda-Morales, M., Treviño, M., Pineda, J.C., and Salgado, H. (2016). Locus ceruleus norepinephrine release: A central regulator of cns spatio-temporal activation? Front. Synaptic Neurosci. 8.

Baldassi, S., and Simoncini, C. (2011). Reward sharpens orientation coding independently of attention. Front. Neurosci. 5, 1–11.

Balfanz, S., Strünker, T., Frings, S., and Baumann, A. (2005). A family of octopamine receptors that specifically induce cyclic AMP production or Ca2+ release in *Drosophila* melanogaster. J. Neurochem. 93, 440–451.

Barak, O., Rigotti, M., and Fusi, S. (2013). The Sparseness of Mixed Selectivity Neurons Controls the Generalization-Discrimination Trade-Off. J. Neurosci. 33, 3844–3856.

Bargmann, C.I., and Marder, E. (2013). From the connectome to brain function. Nat. Methods 10, 483–490.

Barnstedt, O., Owald, D., Felsenberg, J., Brain, R., Moszynski, J.P., Talbot, C.B., Perrat, P.N., and Waddell, S. (2016). Memory-Relevant Mushroom Body Output Synapses Are Cholinergic. Neuron 89, 1237–1247.

Barth, J., Dipt, S., Pech, U., Hermann, M., Riemensperger, T., and Fiala, A. (2014). Differential associative training enhances olfactory acuity in *Drosophila* melanogaster. J. Neurosci. 34, 1819–1837.

Bayliss, A., Roselli, G., and Evans, P.D. (2013). A comparison of the signalling properties of two tyramine receptors from *Drosophila*. J. Neurochem. 125, 37–48.

Bentley, B., Branicky, R., Barnes, C.L., Chew, Y.L., Yemini, E., Bullmore, E.T., Vértes, P.E., and Schafer, W.R. (2016). The Multilayer Connectome of Caenorhabditis elegans. PLoS Comput. Biol. 12.

Berck, M.E., Khandelwal, A., Claus, L., Hernandez-nu, L., Si, G., Tabone, C.J., Li, F., Truman, J.W., Fetter, R.D., Louis, M., et al. (2016). The wiring diagram of a glomerular olfactory system. bioRxiv 1–21.

Best, A.R., and Wilson, D.A. (2004). Coordinate Synaptic Mechanisms Contributing to Olfactory Cortical Adaptation. J. Neurosci. 24, 652–660.

Bettler, B., Kaupmann, K., and Bowery, N. (1998). GABAB receptors: drugs meet clones. Curr. Opin. Neurobiol. 8, 345–350.

Blundon, J.A., Roy, N.C., Teubner, B.J.W., Yu, J., Eom, T.Y., Sample, K.J., Pani, A., Smeyne, R.J., Han, S.B., Kerekes, R.A., et al. (2017). Restoring auditory cortex plasticity in adult mice by restricting thalamic adenosine signaling. Science (80-.). 356, 1352–1356.

Bohm, R. a, Welch, W.P., Goodnight, L.K., Cox, L.W., Henry, L.G., Gunter, T.C., Bao, H., and Zhang, B. (2010). A genetic mosaic approach for neural circuit mapping in *Drosophila*. Proc. Natl. Acad. Sci. U. S. A. 107, 16378–16383.

Boitard, C., Devaud, J.-M., Isabel, G., and Giurfa, M. (2015). GABAergic feedback signaling into the calyces of the mushroom bodies enables olfactory reversal learning in honey bees. Front. Behav. Neurosci. 9, 1–13.

Bouret, S., and Sara, S.J. (2002). Locus coeruleus activation modulates firing rate and temporal organization of odour-induced single-cell responses in rat piriform cortex. Eur. J. Neurosci. 16, 2371–2382.

Boyden, E.S., Zhang, F., Bamberg, E., Nagel, G., and Deisseroth, K. (2005). Millisecond-timescale, genetically targeted optical control of neural activity. Nat. Neurosci. 8, 1263–1268.

Bräcker, L.B., Siju, K.P., Arela, N., So, Y., Hang, M., Hein, I., Vasconcelos, M.L., and Grunwald Kadow, I.C. (2013). Essential role of the mushroom body in context-dependent CO2 avoidance in *Drosophila*. Curr. Biol. 23, 1228–1234.

Brand, a H., and Perrimon, N. (1993). Targeted gene expression as a means of altering cell fates and generating dominant phenotypes. Development 118, 401–415.

Bräunig, P., and Burrows, M. (2004). Projection patterns of posterior dorsal unpaired median neurons of the locust subesophageal ganglion. J. Comp. Neurol. 478, 164–175.

Brezina, V. (2010). Beyond the wiring diagram: signalling through complex neuromodulator networks. Philos. Trans. R. Soc. B Biol. Sci. 365, 2363–2374.

Brose, N., Petrenko, A., Sudhof, T., and Jahn, R. (1992). Synaptotagmin: a calcium sensor on the synaptic vesicle surface. Science (80-.). 256, 1021–1025.

Brüggemann, A., Pardo, L.A., Stühmer, W., and Pongs, O. (1993). Ether-à-go-go encodes a voltage-gated channel permeable to K+ and Ca2+ and modulated by cAMP. Nature 365, 445–448.

Bücheler, M.M., Hadamek, K., and Hein, L. (2002). Two alpha(2)-adrenergic receptor subtypes, alpha(2A) and alpha(2C), inhibit transmitter release in the brain of gene-targeted mice. Neuroscience 109, 819–826.

Burke, C.J., Huetteroth, W., Owald, D., Perisse, E., Krashes, M.J., Das, G., Gohl, D., Silies, M., Certel, S., and Waddell, S. (2012). Layered reward signalling through octopamine and dopamine in *Drosophila*. Nature 492, 433–437.

Busch, S., Selcho, M., Ito, K., and Tanimoto, H. (2009). A map of octopaminergic neurons in the *Drosophila* brain. J. Comp. Neurol. 513, 643–667.

Busch, S., and Tanimoto, H. (2010). Cellular configuration of single octopamine neurons in *Drosophila*. J. Comp. Neurol. 518, 2355–2364.

Campbell, R. a a, Honegger, K.S., Qin, H., Li, W., Demir, E., and Turner, G.C. (2013). Imaging a population code for odor identity in the *Drosophila* mushroom body. J. Neurosci. 33, 10568–10581.

Caron, S.J.C., Ruta, V., Abbott, L.F., and Axel, R. (2013). Random convergence of olfactory inputs in the *Drosophila* mushroom body. Nature 497, 113–117.

Caussinus, E., Kanca, O., and Affolter, M. (2011). Fluorescent fusion protein knockout mediated by anti-GFP nanobody. Nat. Struct. Mol. Biol. 19, 117–121.

Chen, Y.C., Mishra, D., Schmitt, L., Schmuker, M., and Gerber, B. (2011a). A behavioral odor similarity “space” in larval *Drosophila*. Chem. Senses 36, 237–249.

Chen, C.-F.F., Barnes, D.C., and Wilson, D.A. (2011b). Generalized vs. stimulus-specific learned fear differentially modifies stimulus encoding in primary sensory cortex of awake rats. J. Neurophysiol. 106, 3136–3144.

Chen, Q., Li, D.-P., and Pan, H.-L. (2006). Presynaptic alpha1 adrenergic receptors differentially regulate synaptic glutamate and GABA release to hypothalamic presympathetic neurons. J. Pharmacol. Exp. Ther. 316, 733–742.
Chen, Y., Akin, O., Nern, A., Tsui, C.Y.K., Pecot, M.Y., and Zipursky, S.L. (2014). Cell-type-specific labeling of synapses in vivo through synaptic tagging with recombination. Neuron 81, 280–293.
Cheung, U., Atwood, H.L., and Zucker, R.S. (2006). Presynaptic effectors contributing to cAMP-induced synaptic potentiation in *Drosophila*. J. Neurobiol. 66, 273–280.
Cohn, R., Morantte, I., and Ruta, V. (2015). Coordinated and Compartmentalized Neuromodulation Shapes Sensory Processing in *Drosophila*. Cell 163, 1742–1755.
Cole, S.H., Carney, G.E., McClung, C. a, Willard, S.S., Taylor, B.J., and Hirsh, J. (2005). Two functional but noncomplementing *Drosophila* tyrosine decarboxylase genes: distinct roles for neural tyramine and octopamine in female fertility. J. Biol. Chem. 280, 14948–14955.
Colomb, J., Grillenzoni, N., Ramaekers, A., and Stocker, R.F. (2007). Architecture of the primary taste center of *Drosophila* melanogaster larvae. J. Comp. Neurol. 502, 834–847.
Crocker, A., Shahidullah, M., Levitan, I.B., and Sehgal, A. (2010). Identification of a neural circuit that underlies the effects of octopamine on sleep:wake behavior. Neuron 65, 670–681.
Crocker, A., Guan, X.J., Murphy, C.T., and Murthy, M. (2016). Cell-Type-Specific Transcriptome Analysis in the *Drosophila* Mushroom Body Reveals Memory-Related Changes in Gene Expression. Cell Rep. 15, 1580–1596.
Dacks, A.M., Christensen, T. a., Agricola, H.J., Wollweber, L., and Hildebrand, J.G. (2005). Octopamine-immunoreactive neurons in the brain and subesophageal ganglion of the hawkmoth Manduca sexta. J. Comp. Neurol. 488, 255–268.
Das, A., Gupta, T., Davla, S., Prieto-Godino, L.L., Diegelmann, S., Reddy, O.V., Raghavan, K.V., Reichert, H., Lovick, J., and Hartenstein, V. (2013). Neuroblast lineage-specific origin of the neurons of the *Drosophila* larval olfactory system. Dev. Biol. 373, 322–337.
Davenport, A. and Evans, P. (1984). Stress-induced changes in the octopamine levels of insect haemolymph. Insect Biochemistry, 14(2), pp.135-143.
Deady, L.D., and Sun, J. (2015). A Follicle Rupture Assay Reveals an Essential Role for Follicular Adrenergic Signaling in *Drosophila* Ovulation. PLoS Genet. 11, 1–21.
Descarries, L., Watkins, K.C., and Lapierre, Y. (1977). Noradrenergic axon terminals in the cerebral cortex of rat. III. Topometric ultrastructural analysis. Brain Res. 133, 197–222.
Devilbiss, D.M., and Waterhouse, B.D. (2011). Phasic and Tonic Patterns of Locus Coeruleus Output Differentially Modulate Sensory Network Function in the Awake Rat. J. Neurophysiol. 105, 69–87.
Diao, F., and White, B.H. (2012). A novel approach for directing transgene expression in *Drosophila*: T2A-Gal4 in-frame fusion. Genetics 190, 1139–1144.
Diao, F., Ironfield, H., Luan, H., Diao, F., Shropshire, W.C., Ewer, J., Marr, E., Potter, C.J., Landgraf, M., and White, B.H. (2015). Plug-and-play genetic access to *Drosophila* cell types using exchangeable exon cassettes. Cell Rep. 10, 1410–1421.
Dietzl, G., Chen, D., Schnorrer, F., Su, K., Barinova, Y., Fellner, M., Gasser, B., Kinsey, K., Oppel, S., Scheiblauer, S., et al. (2007). A genome-wide transgenic RNAi library for conditional gene inactivation in *Drosophila*. Nature 448, 151–156.
Domyancic, a V, and Morilak, D. a (1997). Distribution of alpha1A adrenergic receptor mRNA in the rat brain visualized by in situ hybridization. J. Comp. Neurol. 386, 358–378.
Dong, C., Filipeanu, C.M., Duvernay, M.T., and Wu, G. (2007). Regulation of G protein-coupled receptor export trafficking. Biochim. Biophys. Acta - Biomembr. 1768, 853–870.
Doucette, W., Milder, J., and Restrepo, D. (2007). Adrenergic modulation of olfactory bulb circuitry affects odor discrimination. Learn Mem 14, 539–547.
Eichler, K., Li, F., Litwin-Kumar, A., Park, Y., Andrade, I., Schneider-Mizell, C.M., Saumweber, T., Huser, A., Eschbach, C., Gerber, B., et al. (2017). The complete connectome of a learning and memory centre in an insect brain. Nature 548, 175–182.
El-Kholy, S., Stephano, F., Li, Y., Bhandari, A., Fink, C., and Roeder, T. (2015). Expression analysis of octopamine and tyramine receptors in *Drosophila*. Cell Tissue Res.
Enell, L., Hamasaka, Y., Kolodziejczyk, A., and Nässel, D.R. (2007). γ-Aminobutyric acid (GABA) signaling components in *Drosophila* : Immunocytochemical localisation of GABA B receptors in relation to the GABA A receptor subunit RDL and a vesicular GABA transporter. J. Comp. Neurol. 505, 18–31.
Evans, P.D., and Maqueira, B. (2005). Insect octopamine receptors: a new classification scheme based on studies of cloned *Drosophila* G-protein coupled receptors. Invert.

Neurosci. 5, 111–118.
Feinberg, E.H., Vanhoven, M.K., Bendesky, A., Wang, G., Fetter, R.D., Shen, K., and Bargmann, C.I. (2008). GFP Reconstitution Across Synaptic Partners (GRASP) defines cell contacts and synapses in living nervous systems. Neuron 57, 353–363.
Feng, L., Kwon, O., Lee, B., Oh, W.C., and Kim, J. (2014). Using mammalian GFP reconstitution across synaptic partners (mGRASP) to map synaptic connectivity in the mouse brain. Nat. Protoc. 9, 2425–2437.
Fisher, Y.E., Yang, H.H., Isaacman-Beck, J., Xie, M., Gohl, D.M., and Clandinin, T.R. (2017). FlpStop, a tool for conditional gene control in *Drosophila*. Elife 6, 1–33.
Fletcher, M.L., and Wilson, D.A. (2002). Experience modifies olfactory acuity: acetylcholine-dependent learning decreases behavioral generalization between similar odorants. J. Neurosci. 22, RC201.
Franks, K.M., and Isaacson, J.S. (2006). Strong single-fiber sensory inputs to olfactory cortex: Implications for olfactory coding. Neuron 49, 357–363.
Gaucher, Q., and Edeline, J.-M. (2015). Stimulus-specific effects of noradrenaline in auditory cortex: implications for the discrimination of communication sounds. J. Physiol. 593, 1003–1020.
Gnerer, J.P., Venken, K.J.T., and Dierick, H. a. (2015). Gene-specific cell labeling using MiMIC transposons. Nucleic Acids Res.
Gohl, D.M., Silies, M.A., Gao, X.J., Bhalerao, S., Luongo, F.J., Lin, C.-C., Potter, C.J., and Clandinin, T.R. (2011). A versatile in vivo system for directed dissection of gene expression patterns. Nat. Methods 8, 231–237.
Goosey, M.W., and Candy, D.J. (1980). The d-octopamine content of the haemolymph of the locust, Schistocerca Americana gregaria and its elevation during flight. Insect Biochem. 10, 393–397.
Gordon, M.D., and Scott, K. (2009). Motor control in a *Drosophila* taste circuit. Neuron 61, 373–384.
Gramates, L.S., Marygold, S.J., Dos Santos, G., Urbano, J.M., Antonazzo, G., Matthews, B.B., Rey, A.J., Tabone, C.J., Crosby, M.A., Emmert, D.B., et al. (2017). FlyBase at 25: Looking to the future. Nucleic Acids Res. 45, D663–D671.
Gratz, S.J., Cummings, A.M., Nguyen, J.N., Hamm, D.C., Donohue, L.K., Harrison, M.M., Wildonger, J., and O'connor-Giles, K.M. (2013). Genome engineering of *Drosophila* with the CRISPR RNA-guided Cas9 nuclease. Genetics 194, 1029–1035.
Gruntman, E., and Turner, G.C. (2013). Integration of the olfactory code across dendritic claws of single mushroom body neurons. Nat. Neurosci. 16, 1–11.
Grygoruk, A., Chen, A., Martin, C.A., Lawal, H.O., Fei, H., Gutierrez, G., Biedermann, T., Najibi, R., Hadi, R., Chouhan, A.K., et al. (2014). The Redistribution of *Drosophila* Vesicular Monoamine Transporter Mutants from Synaptic Vesicles to Large {Dense-Core} Vesicles Impairs {Amine-Dependent} Behaviors. 34, 69246937.
Gutnisky, D.A., Hansen, B.J., Iliescu, B.F., and Dragoi, V. (2009). Attention Alters Visual Plasticity during Exposure-Based Learning. Curr. Biol. 19, 555–560.
Hammer, M. (1993). An identified neuron mediates the unconditioned stimulus in associative olfactory learning in honeybees. Nature 366, 59–63.
Hammer, M., and Menzel, R. (1998). Multiple sites of associative odor learning as revealed by local brain microinjections of octopamine in honeybees. Learn. Mem. 5, 146–156.
Han, K. a, Millar, N.S., and Davis, R.L. (1998). A novel octopamine receptor with preferential expression in *Drosophila* mushroom bodies. J. Neurosci. 18, 3650–3658.
Hanson, J.L., and Hurley, L.M. (2014). Context-dependent fluctuation of serotonin in the auditory midbrain: the influence of sex, reproductive state and experience. J. Exp. Biol. 217, 526–535.
Harley, C.W., Darby-king, A., Mccann, J., and Mclean, J.H. (2006). B1-Adrenoceptor or a1-adrenoceptor activationinitiates early odor preference learning in rat pups : Support for the mitral cell / cAMP model of odor preference learning. Learn. Mem. 8–13.
Hasselmo, M.E., Linster, C., Patil, M., Ma, D., and Cekic, M. (1997). Noradrenergic suppression of synaptic transmission may influence cortical signal-to-noise ratio. J. Neurophysiol. 77, 3326–3339.
Hayashi, S., Ito, K., Sado, Y., Taniguchi, M., Akimoto, A., Takeuchi, H., Aigaki, T., Matsuzaki, F., Nakagoshi, H., Tanimura, T., et al. (2002). GETDB, a database compiling expression patterns and molecular locations of a collection of Gal4 enhancer traps. Genesis 34, 58–61.
Hein, L. (2006). Adrenoceptors and signal transduction in neurons. Cell Tissue Res. 326, 541–

551.
Hein, L., Altman, J.D., and Kobilka, B.K. (1999). Two functionally distinct alpha2-adrenergic receptors regulate sympathetic neurotransmission. Nature 402, 181–184.
Heisenberg, M., Borst, A., Wagner, S., and Byers, D. (1985). *Drosophila* mush- room body mutants are deficient in olfactory learning. J. Neurogenet. 2, 1–30
Heisenberg, M. (2003). Mushroom body memoir: from maps to models. Nat. Rev. Neurosci. 4, 266–275.
Heuer, C.M., Kollmann, M., Binzer, M., and Schachtner, J. (2012). Neuropeptides in insect mushroom bodies. Arthropod Struct. Dev. 41, 199–226.
Hige, T., Aso, Y., Modi, M.N., Rubin, G.M., and Turner, G.C. (2015). Heterosynaptic Plasticity Underlies Aversive Olfactory Learning in *Drosophila*. Neuron 88, 985–998.
Honjo, K., and Furukubo-Tokunaga, K. (2009). Distinctive neuronal networks and biochemical pathways for appetitive and aversive memory in *Drosophila* larvae. J. Neurosci. 29, 852–862.
Honjo, K., Hwang, R.Y., and Tracey, W.D. (2012). Optogenetic manipulation of neural circuits and behavior in *Drosophila* larvae. Nat. Protoc. 7, 1470–1478.
Howell, K.M., and Evans, P.D. (1998). The characterization of presynaptic octopamine receptors modulating octopamine release from an identified neurone in the locust. J. Exp. Biol. 201, 2053–2060.
Huetteroth, W., Perisse, E., Lin, S., Klappenbach, M., Burke, C., and Waddell, S. (2015). Sweet Taste and Nutrient Value Subdivide Rewarding Dopaminergic Neurons in *Drosophila*. Curr. Biol. 751–758.
Huser, A., Rohwedder, A., Apostolopoulou, A. a., Widmann, A., Pfitzenmaier, J.E., Maiolo, E.M., Selcho, M., Pauls, D., von Essen, A., Gupta, T., et al. (2012). The Serotonergic Central Nervous System of the *Drosophila* Larva: Anatomy and Behavioral Function. PLoS One 7.
Inagaki, H.K., Ben-Tabou De-Leon, S., Wong, A.M., Jagadish, S., Ishimoto, H., Barnea, G., Kitamoto, T., Axel, R., and Anderson, D.J. (2012). Visualizing neuromodulation in vivo: TANGO-mapping of dopamine signaling reveals appetite control of sugar sensing. Cell 148, 583–595.
Inagaki, H.K., Panse, K.M., and Anderson, D.J. (2014). Independent, Reciprocal Neuromodulatory Control of Sweet and Bitter Taste Sensitivity during Starvation in *Drosophila*. Neuron 84, 806–820.
Ito, W., Pan, B.-X., Yang, C., Thakur, S., and Morozov, A. (2009). Enhanced generalization of auditory conditioned fear in juvenile mice. Learn. Mem. 16, 187–192.
Jenett, A., Rubin, G.M., Ngo, T.T.B., Shepherd, D., Murphy, C., Dionne, H., Pfeiffer, B.D., Cavallaro, A., Hall, D., Jeter, J., et al. (2012). A GAL4-Driver Line Resource for *Drosophila* Neurobiology. Cell Rep. 2, 991–1001.
Kanca, O., Bellen, H.J., and Schnorrer, F. (2017). Gene Tagging Strategies To Assess Protein Expression, Localisation, and Function in *Drosophila*. Genetics 207, 389–412.
Karuppudurai, T., Lin, T.Y., Ting, C.Y., Pursley, R., Melnattur, K. V., Diao, F., White, B.H., Macpherson, L.J., Gallio, M., Pohida, T., et al. (2014). A Hard-Wired Glutamatergic Circuit Pools and Relays UV Signals to Mediate Spectral Preference in *Drosophila*. Neuron 81, 603–615.
Kaupmann, K., Schuler, V., Mosbacher, J., Bischoff, S., Bittiger, H., Heid, J., Froestl, W., Leonhard, S., Pfaff, T., Karschin, a, et al. (1998). Human gamma-aminobutyric acid type B receptors are differentially expressed and regulate inwardly rectifying K+ channels. Proc. Natl. Acad. Sci. U. S. A. 95, 14991–14996.
Kim, J.-H., Jung, A.-H., Jeong, D., Choi, I., Kim, K., Shin, S., Kim, S.J., and Lee, S.-H. (2016). Selectivity of Neuromodulatory Projections from the Basal Forebrain and Locus Ceruleus to Primary Sensory Cortices. J. Neurosci. 36, 5314–5327.
Kim, S.M., Su, C.-Y., and Wang, J.W. (2017). Neuromodulation of Innate Behaviors in *Drosophila*. Annu. Rev. Neurosci. 40, 327–348.
Kim, Y.-C., Lee, H.-G., Lim, J., and Han, K.-A. (2013). Appetitive learning requires the alpha1-like octopamine receptor OAMB in the *Drosophila* mushroom body neurons. J. Neurosci. 33, 1672–1677.
Kirkhart, C., and Scott, K. (2015). Gustatory learning and processing in the *Drosophila* mushroom bodies. J. Neurosci. 35, 5950–5958.
Kitamoto, T. (2001). Conditional modification of behavior in *Drosophila* by targeted expression of a temperature - sensitive shibire allele in defined neurons. J. Neurobiol.
Klapoetke, N.C., Murata, Y., Kim, S.S., Pulver, S.R., Birdsey-Benson, A., Cho, Y.K., Morimoto,

T.K., Chuong, A.S., Carpenter, E.J., Tian, Z., et al. (2014). Independent optical excitation of distinct neural populations. Nat. Methods 11, 338–346.
Ko, K.I., Root, C.M., Lindsay, S.A., Zaninovich, O.A., Shepherd, A.K., Wasserman, S.A., Kim, S.M., and Wang, J.W. (2015). Starvation promotes concerted modulation of appetitive olfactory behavior via parallel neuromodulatory circuits. Elife 4, 1–17.
Kohl, J., Ng, J., Cachero, S., Ciabatti, E., Dolan, M.-J., Sutcliffe, B., Tozer, A., Ruehle, S., Krueger, D., Frechter, S., et al. (2014). Ultrafast tissue staining with chemical tags. Proc. Natl. Acad. Sci. 111, E3805–E3814.
Koles, K., Yeh, A.R., and Rodal, A.A. (2016). Tissue-specific tagging of endogenous loci in *Drosophila* melanogaster. Biol. Open 5, 83–89.
Koon, A.C., and Budnik, V. (2012). Inhibitory Control of Synaptic and Behavioral Plasticity by Octopaminergic Signaling. J. Neurosci. 32, 6312–6322.
Koon, A.C., Ashley, J., Barria, R., DasGupta, S., Brain, R., Waddell, S., Alkema, M.J., and Budnik, V. (2011). Autoregulatory and paracrine control of synaptic and behavioral plasticity by octopaminergic signaling. Nat. Neurosci. 14, 190–199.
Krashes, M.J., and Waddell, S. (2008). Rapid Consolidation to a radish and Protein Synthesis-Dependent Long-Term Memory after Single-Session Appetitive Olfactory Conditioning in *Drosophila*. J. Neurosci. 28, 3103–3113.
Krashes, M.J., DasGupta, S., Vreede, A., White, B., Armstrong, J.D., and Waddell, S. (2009). A Neural Circuit Mechanism Integrating Motivational State with Memory Expression in *Drosophila*. Cell 139, 416–427.
Kreher, S.A., Mathew, D., Kim, J., and Carlson, J.R. (2008). Translation of Sensory Input into Behavioral Output via an Olfactory System. Neuron 59, 110–124.
Kreissl, S., Eichmüller, S., Bicker, G., Rapus, J., and Eckert, M. (1994). Octopamine-like immunoreactivity in the brain and subesophageal ganglion of the honeybee. J. Comp. Neurol. 348, 583–595.
Lai, S.-L., and Lee, T. (2006). Genetic mosaic with dual binary transcriptional systems in *Drosophila*. Nat. Neurosci. 9, 703–709.
Langer, S.Z. (1980). Presynaptic receptors and modulation of neurotransmission: pharmacological implications and therapeutic relevance. Trends Neurosci. 3, 110–112.
Lee, T., and Luo, L. (1999). Mosaic analysis with a repressible cell marker for studies of gene function in neuronal morphogenesis. Neuron 22, 451–461.
Lee, H.-G., Seong, C.-S., Kim, Y.-C., Davis, R.L., and Han, K.-A. (2003). Octopamine receptor OAMB is required for ovulation in *Drosophila* melanogaster. Dev. Biol. 264, 179–190.
Lee, H.-G., Rohila, S., and Han, K.-A. (2009). The octopamine receptor OAMB mediates ovulation via Ca2+/calmodulin-dependent protein kinase II in the *Drosophila* oviduct epithelium. PLoS One 4, e4716.
Lee, P.-T., Zirin, J., Kanca, O., Lin, W.-W., Schulze, K.L., Li-Kroeger, D., Tao, R., Devereaux, C., Hu, Y., Chung, V., et al. (2018). A gene-specific T2A-GAL4 library for *Drosophila*. Elife 7, 1–24.
Lee, T., Lee, A., and Luo, L. (1999). Development of the *Drosophila* mushroom bodies: sequential generation of three distinct types of neurons from a neuroblast. Development 126, 4065–4076.
Lei, Z., Chen, K., Li, H., Liu, H., and Guo, A. (2013). The GABA system regulates the sparse coding of odors in the mushroom bodies of *Drosophila*. Biochem. Biophys. Res. Commun. 436, 35–40.
Leyton, V., Goles, N.I., Fuenzalida-Uribe, N., and Campusano, J.M. (2014). Octopamine and dopamine differentially modulate the nicotine-induced calcium response in *Drosophila* mushroom body kenyon cells. Neurosci. Lett. 560, 16–20.
Lin, A.C., Bygrave, A.M., de Calignon, A., Lee, T., and Miesenböck, G. (2014). Sparse, decorrelated odor coding in the mushroom body enhances learned odor discrimination. Nat. Neurosci. 17, 559–568.
Linster, C., and Hasselmo, M.E. (2001). Neuromodulation and the functional dynamics of piriform cortex. Chem. Senses 26, 585–594.
Linster, C., Johnson, B. a, Yue, E., Morse, a, Xu, Z., Hingco, E.E., Choi, Y., Choi, M., Messiha, a, and Leon, M. (2001). Perceptual correlates of neural representations evoked by odorant enantiomers. J. Neurosci. 21, 9837–9843.
Linster, C., Johnson, B.A., Morse, A., Yue, E., and Leon, M. (2002). Spontaneous versus reinforced olfactory discriminations. J. Neurosci. 22, 6842–6845.
Linster, C., and Cleland, T.A. (2016). Neuromodulation of olfactory transformations. Curr. Opin.

Neurobiol. 40, 170–177.
Liu, L., Wolf, R., Ernst, R., and Heisenberg, M. (1999). Context generalization in *Drosophila* visual learning requires the mushroom bodies. Nature 400, 753–756.
Liu, X., Krause, W.C., and Davis, R.L. (2007). GABAA Receptor RDL Inhibits *Drosophila* Olfactory Associative Learning. Neuron 56, 1090–1102.
Liu, Y., Cui, L., Schwarz, M.K., Dong, Y., and Schl??ter, O.M. (2017). Adrenergic Gate Release for Spike Timing-Dependent Synaptic Potentiation. Neuron 93, 394–408.
Livet, J., Weissman, T.A., Kang, H., Draft, R.W., Lu, J., Bennis, R.A., Sanes, J.R., and Lichtman, J.W. (2007). Transgenic strategies for combinatorial expression of fluorescent proteins in the nervous system. Nature 450, 56–62.
Luo, F., Li, S.H., Tang, H., Deng, W.K., Zhang, Y., and Liu, Y. (2015). Phenylephrine enhances glutamate release in the medial prefrontal cortex through interaction with N-type Ca2+ channels and release machinery. J. Neurochem. 132, 38–50.
Luo, J., Lushchak, O. V., Goergen, P., Williams, M.J., and Nässel, D.R. (2014). *Drosophila* insulin-producing cells are differentially modulated by serotonin and octopamine receptors and affect social behavior. PLoS One 9.
Maiellaro, I., Lohse, M.J., Kittel, R.J., Correspondence, D.C., and Calebiro, D. (2016). cAMP Signals in *Drosophila* Motor Neurons Are Confined to Single Synaptic Boutons Cell Reports Report cAMP Signals in *Drosophila* Motor Neurons Are Confined to Single Synaptic Boutons. Cell Rep. 17, 1238–1246.
Mandairon, N., Peace, S., Karnow, A., Kim, J., Ennis, M., and Linster, C. (2008). Noradrenergic modulation in the olfactory bulb influences spontaneous and reward-motivated discrimination, but not the formation of habituation memory. Eur. J. Neurosci. 27, 1210–1219.
Manella, L.C., Alperin, S., and Linster, C. (2013). Stressors impair odor recognition memory via an olfactory bulb-dependent noradrenergic mechanism. Front. Integr. Neurosci. 7, 1–12.
Maqueira, B., Chatwin, H., and Evans, P.D. (2005). Identification and characterization of a novel family of *Drosophila* beta-adrenergic-like octopamine G-protein coupled receptors. J. Neurochem. 94, 547–560.
Marder, E. (2012). Neuromodulation of Neuronal Circuits: Back to the Future. Neuron 76, 1–11.
Marzo, A., Bai, J., and Otani, S. (2009). Neuroplasticity regulation by noradrenaline in mammalian brain. Curr. Neuropharmacol. 7, 286–295.
Masuda-Nakagawa, L.M., Tanaka, N.K., and O'Kane, C.J. (2005). Stereotypic and random patterns of connectivity in the larval mushroom body calyx of *Drosophila*. Proc. Natl. Acad. Sci. U. S. A. 102, 19027–19032.
Masuda-Nakagawa, L.M., Gendre, N., O'Kane, C.J., and Stocker, R.F. (2009). Localised olfactory representation in mushroom bodies of *Drosophila* larvae. Proc. Natl. Acad. Sci. U. S. A. 106, 10314–10319.
Masuda-Nakagawa, L.M., Awasaki, T., Ito, K., and O'Kane, C.J. (2010). Targeting expression to projection neurons that innervate specific mushroom body calyx and antennal lobe glomeruli in larval *Drosophila*. Gene Expr. Patterns 10, 328–337.
Masuda-Nakagawa, L.M., Ito, K., Awasaki, T., and O'Kane, C.J. (2014). A single GABAergic neuron mediates feedback of odor-evoked signals in the mushroom body of larval *Drosophila*. Front. Neural Circuits 8, 35.
Meinertzhagen, I. a, and Lee, C.-H. (2012). The genetic analysis of functional connectomics in *Drosophila*. (Elsevier).
Mezler, M., Müller, T., and Raming, K. (2001). Cloning and functional expression of GABA(B) receptors from *Drosophila*. Eur. J. Neurosci. 13, 477–486.
Michels, B., Chen, Y.-C., Saumweber, T., Mishra, D., Tanimoto, H., Schmid, B., Engmann, O., and Gerber, B. (2011). Cellular site and molecular mode of synapsin action in associative learning. Learn. Mem. 18, 332–344.
Mishra, D., Louis, M., and Gerber, B. (2010). Adaptive adjustment of the generalization-discrimination balance in larval *Drosophila*. J. Neurogenet. 24, 168–175.
Mitrano, D.A., Schroeder, J.P., Smith, Y., Cortright, J.J., Bubula, N., Vezina, P., and Weinshenker, D. (2012). alpha-1 Adrenergic receptors are localised on presynaptic elements in the nucleus accumbens and regulate mesolimbic dopamine transmission. Neuropsychopharmacology 37, 2161–2172.
Mohr, S.E., Smith, J. a, Shamu, C.E., and Neumüller, R. a (2014). RNAi screening comes of age : improved techniques and complementary approaches. Nat. Publ. Gr. 15, 591–600.
Morita, M., Susuki, J., Amino, H., Yoshiki, F., Moizumi, S., and Kudo, Y. (2006). Use of the

exogenous *Drosophila* octopamine receptor gene to study Gq-coupled receptor-mediated responses in mammalian neurons. Neuroscience 137, 545–553.
Morrison, G.L., Fontaine, C.J., Harley, C.W., and Yuan, Q. (2013). A role for the anterior piriform cortex in early odor preference learning: evidence for multiple olfactory learning structures in the rat pup. J. Neurophysiol. 110, 141–152.
Nadim, F., and Bucher, D. (2014). Neuromodulation of neurons and synapses. Curr. Opin. Neurobiol. 29, 48–56.
Nagarkar-Jaiswal, S., Lee, P.-T., Campbell, M.E., Chen, K., Anguiano-Zarate, S., Cantu Gutierrez, M., Busby, T., Lin, W.-W., He, Y., Schulze, K.L., et al. (2015). A library of MiMICs allows tagging of genes and reversible, spatial and temporal knockdown of proteins in *Drosophila*. Elife 4, 1–28.
Nagarkar-Jaiswal, S., Manivannan, S.N., Zuo, Z., and Bellen, H.J. (2017). A cell cycle-independent, conditional gene inactivation strategy for differentially tagging wild-type and mutant cells. Elife 6, 1–15.
Nai, Q., Dong, H.-W., Hayar, A., Linster, C., and Ennis, M. (2009). Noradrenergic Regulation of GABAergic Inhibition of Main Olfactory Bulb Mitral Cells Varies as a Function of Concentration and Receptor Subtype. J Neurophysiol 101, 2472–2484.
Nai, Q., Dong, H.W., Linster, C., and Ennis, M. (2010). Activation of alpha1 and alpha2 noradrenergic receptors exert opposing effects on excitability of main olfactory bulb granule cells. Neuroscience 169, 882–892.
Nässel, D.R. (2009). Neuropeptide signaling near and far: How localised and timed is the action of neuropeptides in brain circuits? Invertebr. Neurosci. 9, 57–75.
Nässel, D.R., Enell, L.E., Santos, J.G., Wegener, C., and Johard, H.A. (2008). A large population of diverse neurons in the *Drosophila* central nervous system expresses short neuropeptide F, suggesting multiple distributed peptide functions. BMC Neurosci. 9, 90.
Nern, A., Pfeiffer, B.D., and Rubin, G.M. (2015). Optimized tools for multicolor stochastic labeling reveal diverse stereotyped cell arrangements in the fly visual system. Proc. Natl. Acad. Sci. U. S. A. 112, E2967–E2976.
Neumüller, R. a., Wirtz-Peitz, F., Lee, S., Kwon, Y., Buckner, M., Hoskins, R. a., Venken, K.J.T., Bellen, H.J., Moh, S.E., and Perrimon, N. (2012). Stringent analysis of gene function and protein-protein interactions using fluorescently tagged genes. Genetics 190, 931–940.
Ng, M., Roorda, R.D., Lima, S.Q., Zemelman, B. V., Morcillo, P., and Miesenböck, G. (2002). Transmission of olfactory information between three populations of neurons in the antennal lobe of the fly. Neuron 36, 463–474.
Ni, J.-Q., Markstein, M., Binari, R., Pfeiffer, B., Liu, L.-P., Villalta, C., Booker, M., Perkins, L., and Perrimon, N. (2008). Vector and parameters for targeted transgenic RNA interference in *Drosophila* melanogaster. Nat. Methods 5, 49–51.
Ni, J.-Q., Zhou, R., Czech, B., Liu, L.-P., Holderbaum, L., Yang-Zhou, D., Shim, H.-S., Tao, R., Handler, D., Karpowicz, P., et al. (2011). A genome-scale shRNA resource for transgenic RNAi in *Drosophila*. Nat. Methods 8, 405–407.
Nicholas, a. P., Pieribone, V. a., and Hokfelt, T. (1993). Cellular localisation of messenger RNA for beta-1 and beta-2 adrenergic receptors in rat brain: An in situ hybridization study. Neuroscience 56, 1023–1039.
Nicolaï, L.J.J., Ramaekers, A., Raemaekers, T., Drozdzecki, A., Mauss, A.S., Yan, J., Landgraf, M., Annaert, W., and Hassan, B. a (2010). Genetically encoded dendritic marker sheds light on neuronal connectivity in *Drosophila*. Proc. Natl. Acad. Sci. U. S. A. 107, 20553–20558.
Nikolaev, V.O., Bünemann, M., Hein, L., Hannawacker, A., and Lohse, M.J. (2004). Novel single chain cAMP sensors for receptor-induced signal propagation. J. Biol. Chem. 279, 37215–37218.
O'Dell, T.J., Connor, S.A., Guglietta, R., and Nguyen, P. V. (2015). β-Adrenergic receptor signaling and modulation of long-term potentiation in the mammalian hippocampus. Learn. Mem. 22, 461–471.
Oettl, L.L., Ravi, N., Schneider, M., Scheller, M.F., Schneider, P., Mitre, M., da Silva Gouveia, M., Froemke, R.C., Chao, M. V., Young, W.S., et al. (2016). Oxytocin Enhances Social Recognition by Modulating Cortical Control of Early Olfactory Processing. Neuron 90, 609–621.
Ohhara, Y., Kayashima, Y., Hayashi, Y., Kobayashi, S., and Yamakawa-Kobayashi, K. (2012). Expression of β-adrenergic-like octopamine receptors during *Drosophila* development. Zoolog. Sci. 29, 83–89.
Omoto, J.J., Yogi, P., and Hartenstein, V. (2015). Origin and development of neuropil glia of the

Drosophila larval and adult brain: Two distinct glial populations derived from separate progenitors. Dev. Biol. 404, 2–20.
Papadopoulou, M., Cassenaer, S., Nowotny, T., and Laurent, G. (2011). Normalization for sparse encoding of odors by a wide-field interneuron. Science 332, 721–725.
Pauls, D., von Essen, a., Lyutova, R., van Giesen, L., Rosner, R., Wegener, C., and Sprecher, S.G. (2014). Potency of Transgenic Effectors for Neurogenetic Manipulation in *Drosophila* Larvae. Genetics 199, 25–37.
Pavot, P., Carbognin, E., and Martin, J. (2015). PKA and cAMP / CNG Channels Independently Regulate the Cholinergic Ca 2+ -Response of *Drosophila* Mushroom Body Neurons. eNeuro 2, 1–22.
Pech, U., Pooryasin, A., Birman, S., and Fiala, A. (2013). Localisation of the contacts between Kenyon cells and aminergic neurons in the *Drosophila* melanogaster brain using SplitGFP reconstitution. J. Comp. Neurol. 521, 3992–4026.
Pedarzani, P., and Storm, J.F. (1995). Protein kinase A-independent modulation of ion channels in the brain by cyclic AMP. Proc. Natl. Acad. Sci. U. S. A. 92, 11716–11720.
Perez-Orive, J., Mazor, O., Turner, G.C., Cassenaer, S., Wilson, R.I., and Laurent, G. (2002). Oscillations and sparsening of odor representations in the mushroom body. Science 297, 359–365.
Perkins, L.A., Holderbaum, L., Tao, R., Hu, Y., Sopko, R., McCall, K., Yang-Zhou, D., Flockhart, I., Binari, R., Shim, H.S., et al. (2015). The transgenic RNAi project at Harvard medical school: Resources and validation. Genetics 201, 843–852.
Pfeiffer, B.D., Ngo, T.-T.B., Hibbard, K.L., Murphy, C., Jenett, A., Truman, J.W., and Rubin, G.M. (2010). Refinement of tools for targeted gene expression in *Drosophila*. Genetics 186, 735–755.
Poo, C., and Isaacson, J.S. (2009). Odor representations in olfactory cortex: “sparse” coding, global inhibition, and oscillations. Neuron 62, 850–861.
Python, F., and Stocker, R.F. (2002). Immunoreactivity against choline acetyltransferase, γ-aminobutyric acid, histamine, octopamine, and serotonin in the larval chemosensory system of *Drosophila* melanogaster. J. Comp. Neurol. 453, 157–167.
Qi, Y., Xu, G., Gu, G., Mao, F., Ye, G., Liu, W., and Huang, J. (2017). A new *Drosophila* octopamine receptor responds to serotonin. Insect Biochem. Mol. Biol. 90, 61–70.
Quian Quiroga, R., Reddy, L., Kreiman, G., Koch, C., and Fried, I. (2005). Invariant visual representation by single neurons in the human brain. Nature 435, 1102–1107.
Rajkowski, J., Kubiak, P., and Aston-Jones, G. (1994). Locus coeruleus activity in monkey: Phasic and tonic changes are associated with altered vigilance. Brain Res. Bull. 35, 607–616.
Ramaekers, A., Magnenat, E., Marin, E.C., Gendre, N., Jefferis, G.S.X.E., Luo, L., and Stocker, R.F. (2005). Glomerular maps without cellular redundancy at successive levels of the *Drosophila* larval olfactory circuit. Curr. Biol. 15, 982–992.
Ramos, B.P., and Arnsten, A.F.T. (2007). Adrenergic pharmacology and cognition: Focus on the prefrontal cortex. Pharmacol. Ther. 113, 523–536.
Rice, M.E., and Cragg, S.J. (2008). Dopamine spillover after quantal release: Rethinking dopamine transmission in the nigrostriatal pathway. Brain Res. Rev. 58, 303–313.
Riedel, F., Gillingham, A.K., Rosa-Ferreira, C., Galindo, A., and Munro, S. (2016). An antibody toolkit for the study of membrane traffic in *Drosophila* melanogaster. Biol. Open 5, 987–992.
Roeder, T. (1999). Octopamine in invertebrates. Prog. Neurobiol. 59, 533–561.
Rohwedder, A., Selcho, M., Chassot, B., and Thum, A.S. (2015). Neuropeptide F neurons modulate sugar reward during associative olfactory learning of *Drosophila* larvae. J. Comp. Neurol. 523, 2637–2664.
Rohwedder, A., Wenz, N.L., Stehle, B., Huser, A., Yamagata, N., Zlatic, M., Truman, J.W., Tanimoto, H., Saumweber, T., Gerber, B., et al. (2016). Four Individually Identified Paired Dopamine Neurons Signal Reward in Larval *Drosophila*. Curr. Biol. 26, 661–669.
Root, C.M., Ko, K.I., Jafari, A., and Wang, J.W. (2011). Presynaptic facilitation by neuropeptide signaling mediates odor-driven food search. Cell 145, 133–144.
Rosenzweig, M., Brennan, K.M., Tayler, T.D., Phelps, P.O., Patapoutian, A., and Garrity, P.A. (2005). The *Drosophila* ortholog of vertebrate TRPA1 regulates thermotaxis. Genes Dev. 19, 419–424.
Rosin, D.L., Talley, E.M., Lee, a, Stornetta, R.L., Gaylinn, B.D., Guyenet, P.G., and Lynch, K.R. (1996). Distribution of alpha 2C-adrenergic receptor-like immunoreactivity in the rat central nervous system. J. Comp. Neurol. 372, 135–165.

Sara, S.J., and Segal, M. (1991). Plasticity of sensory responses of locus coeruleus neurons in the behaving rat: Implications for cognition. Prog. Brain Res. 88, 571–585.
Sara, S.J., and Bouret, S. (2012). Orienting and Reorienting: The Locus Coeruleus Mediates Cognition through Arousal. Neuron 76, 130–141.
Saraswati, S., Fox, L.E., Soll, D.R., and Wu, C.F. (2004). Tyramine and Octopamine Have Opposite Effects on the Locomotion of *Drosophila* Larvae. J. Neurobiol. 58, 425–441.
Saudou, F., Amlaiky, N., Plassat, J.L., Borrelli, E., and Hen, R. (1990). Cloning and characterization of a *Drosophila* tyramine receptor. EMBO J. 9, 3611–3617.
Saumweber, T., Rohwedder, A., Schleyer, M., Eichler, K., Chen, Y.C., Aso, Y., Cardona, A., Eschbach, C., Kobler, O., Voigt, A., et al. (2018). Functional architecture of reward learning in mushroom body extrinsic neurons of larval *Drosophila*. Nat. Commun. 9, 1–19.
Sayin, S., Boehm, A.C., Kobler, J.M., De Backer, J.-F., and Grunwald Kadow, I.C. (2018). Internal State Dependent Odor Processing and Perception—The Role of Neuromodulation in the Fly Olfactory System. Front. Cell. Neurosci. 12, 1–17.
Scheibner, J., Trendelenburg, A., Hein, L., and Starke, K. (2001). a 2 -Adrenoceptors modulating neuronal serotonin release: a study in a 2 -adrenoceptor subtype-de®cient mice 1. Br. J. Pharmacol. 925–933.
Scherer, S., Stocker, R.F., and Gerber, B. (2003). Olfactory learning in individually assayed *Drosophila* larvae. Learn. Mem. 10, 217–225.
Schlegel, P., Texada, M.J., Miroschnikow, A., Schoofs, A., H??ckesfeld, S., Peters, M., Schneider-Mizell, C.M., Lacin, H., Li, F., Fetter, R.D., et al. (2016). Synaptic transmission parallels neuromodulation in a central food-intake circuit. Elife 5, 1–28.
Schneider, D., and Woolley, S.M.N. (2013). Sparse and Background-Invariant Coding of Vocalizations in Auditory Scenes. Neuron 79, 141–152.
Schneider, A., Ruppert, M., Hendrich, O., Giang, T., Ogueta, M., Hampel, S., Vollbach, M., Büschges, A., and Scholz, H. (2012). Neuronal basis of innate olfactory attraction to ethanol in *Drosophila*. PLoS One 7, e52007.
Schroll, C., Riemensperger, T., Bucher, D., Ehmer, J., Völler, T., Erbguth, K., Gerber, B., Hendel, T., Nagel, G., Buchner, E., et al. (2006). Light-Induced Activation of Distinct Modulatory Neurons Triggers Appetitive or Aversive Learning in *Drosophila* Larvae. Curr. Biol. 16, 1741–1747.
Schwaerzel, M., Monastirioti, M., Scholz, H., Friggi-Grelin, F., Birman, S., and Heisenberg, M. (2003). Dopamine and octopamine differentiate between aversive and appetitive olfactory memories in *Drosophila*. J. Neurosci. 23, 10495–10502.
Schwarz, D.S., and Blower, M.D. (2016). The endoplasmic reticulum: Structure, function and response to cellular signaling. Cell. Mol. Life Sci. 73, 79–94.
Selcho, M., Pauls, D., El Jundi, B., Stocker, R.F., and Thum, A.S. (2012). The role of octopamine and tyramine in *Drosophila* larval locomotion. J. Comp. Neurol. 520, 3764–3785.
Selcho, M., Pauls, D., Huser, A., Stocker, R.F., and Thum, A.S. (2014). Characterization of the octopaminergic and tyraminergic neurons in the central brain of *Drosophila* larvae. J. Comp. Neurol. 522, 3485–3500.
Seol, G.H., Ziburkus, J., Huang, S., Song, L., Kim, I.T., Takamiya, K., Huganir, R.L., Lee, H.K., and Kirkwood, A. (2007). Neuromodulators Control the Polarity of Spike-Timing-Dependent Synaptic Plasticity. Neuron 55, 919–929.
Shafer, O.T., Kim, D.J., Dunbar-Yaffe, R., Nikolaev, V.O., Lohse, M.J., and Taghert, P.H. (2008). Widespread Receptivity to Neuropeptide PDF throughout the Neuronal Circadian Clock Network of *Drosophila* Revealed by Real-Time Cyclic AMP Imaging. Neuron 58, 223–237.
Shakhawat, A.M., Gheidi, A., MacIntyre, I.T., Walsh, M.L., Harley, C.W., and Yuan, Q. (2015). Arc-Expressing Neuronal Ensembles Supporting Pattern Separation Require Adrenergic Activity in Anterior Piriform Cortex: An Exploration of Neural Constraints on Learning. J. Neurosci. 35, 14070–14075.
Shakiryanova, D., Zettel, G.M., Gu, T., Hewes, R.S., and Levitan, E.S. (2011). Synaptic neuropeptide release induced by octopamine without Ca2+ entry into the nerve terminal. Proc. Natl. Acad. Sci. U. S. A. 108, 4477–4481.
Shang, Y., Griffith, L.C., and Rosbash, M. (2008). Light-arousal and circadian photoreception circuits intersect at the large PDF cells of the *Drosophila* brain. Proc. Natl. Acad. Sci. 105, 19587–19594.
Shipley, M.T., and Ennis, M. (1996). Functional organization of olfactory system. J. Neurobiol. 30, 123–176.

Sinakevitch, I., and Strausfeld, N.J. (2006). Comparison of octopamine-like immunoreactivity in the brains of the fruit fly and blow fly. J. Comp. Neurol. 494, 460–475.
Sinakevitch, I., Niwa, M., and Strausfeld, N.J. (2005). Octopamine-like immunoreactivity in the honey bee and cockroach: Comparable organization in the brain and subesophageal ganglion. J. Comp. Neurol. 488, 233–254.
Sinakevitch, I., Mustard, J. a, and Smith, B.H. (2011). Distribution of the octopamine receptor AmOA1 in the honey bee brain. PLoS One 6, e14536.
Sinakevitch, I.T., Smith, A.N., Locatelli, F., Huerta, R., Bazhenov, M., and Smith, B.H. (2013). Apis mellifera octopamine receptor 1 (AmOA1) expression in antennal lobe networks of the honey bee (Apis mellifera) and fruit fly (*Drosophila* melanogaster). Front. Syst. Neurosci. 7, 70.
Sinakevitch, I.T., Daskalova, S.M., and Smith, B.H. (2017). The biogenic amine tyramine and its receptor (AmTyr1) in olfactory neuropils in the honey bee (Apis mellifera) brain. Front. Syst. Neurosci. 11, 1–19.
Sitia, R., and Braakman, I. (2003). Quality control in the endoplasmic reticulum protein factory. Nature 426, 891–894.
Slater, G., Levy, P., Chan, K.L. a., and Larsen, C. (2015). A Central Neural Pathway Controlling Odor Tracking in *Drosophila*. J. Neurosci. 35, 1831–1848.
Smirle, J., Au, C.E., Jain, M., Dejgaard, K., Nilsson, T., and Bergeron, J. (2013). Cell biology of the endoplasmic reticulum and the Golgi apparatus through proteomics. Cold Spring Harb. Perspect. Biol. 5, a015073.
Sonnhammer, E.L., von Heijne, G., and Krogh, A. (1998). A hidden Markov model for predicting transmembrane helices in protein sequences. Proceedings 6, 175–182.
States, D.J., and Gish, W. (1994). Combined use of sequence similarity and codon bias for coding region identification. J. Comput. Biol. 1, 39–50.
Stettler, D.D., and Axel, R. (2009). Representations of Odor in the Piriform Cortex. Neuron 63, 854–864.
Stevenson, P.A., and Pflüger, H.J. (1994). Colocalisation of octopamine and FMRFamide related peptide in identified heart projecting (DUM) neurones in the locust revealed by immunocytochemistry. Brain Res. 638, 117–125.
Südhof, T.C. (2013). A molecular machine for neurotransmitter release: synaptotagmin and beyond. Nat. Med. 19, 1227–1231.
Summerville, J.B., Faust, J.F., Fan, E., Pendin, D., Daga, A., Formella, J., Stern, M., and McNew, J.A. (2016). The effects of ER morphology on synaptic structure and function in *Drosophila* melanogaster. J. Cell Sci. 129, 1635–1648.
Sweeney, S.T., Broadie, K., Keane, J., Niemann, H., and O'Kane, C.J. (1995). Targeted expression of tetanus toxin light chain in *Drosophila* specifically eliminates synaptic transmission and causes behavioral defects. Neuron 14, 341–351.
Taghert, P.H., and Nitabach, M.N. (2012). Peptide Neuromodulation in Invertebrate Model Systems. Neuron 76, 82–97.
Takemura, S. ya, Aso, Y., Hige, T., Wong, A., Lu, Z., Xu, C.S., Rivlin, P.K., Hess, H., Zhao, T., Parag, T., et al. (2017). A connectome of a learning and memory center in the adult *Drosophila* brain. Elife 6, 1–43.
Turner, G.C., Bazhenov, M., and Laurent, G. (2008). Olfactory Representations by *Drosophila* Mushroom Body Neurons. J. Neurophysiol. 734–746.
Tanaka, N.K., Awasaki, T., Shimada, T., and Ito, K. (2004). Integration of Chemosensory Pathways in the *Drosophila* Second-Order Olfactory Centers. Curr. Biol. 14, 449–457.
Tanaka, N.K., Tanimoto, H., and Ito, K. (2008). Neuronal assemblies of the *Drosophila* mushroom body. J. Comp. Neurol. 508, 711–755.
Thamm, M., Scholl, C., Reim, T., Grübel, K., Möller, K., Rössler, W., and Scheiner, R. (2017). Neuronal distribution of tyramine and the tyramine receptor AmTAR1 in the honeybee brain. J. Comp. Neurol. 525, 2615–2631.
Thomas, M.J., Moody, T.D., Makhinson, M., and O'Dell, T.J. (1996). Activity-dependent beta-adrenergic modulation of low frequency stimulation induced LTP in the hippocampal CA1 region. Neuron 17, 475–482.
Thum, A.S., Leisibach, B., Gendre, N., Selcho, M., and Stocker, R.F. (2011). Diversity, variability, and suboesophageal connectivity of antennal lobe neurons in D. melanogaster larvae. J. Comp. Neurol. 519, 3415–3432.
Tian, L., Hires, S.A., Mao, T., Huber, D., Chiappe, M.E., Chalasani, S.H., Petreanu, L., Akerboom, J., McKinney, S. a, Schreiter, E.R., et al. (2009). Imaging neural activity in

worms, flies and mice with improved GCaMP calcium indicators. Nat. Methods 6, 875–881.
Ting, M. (2015). University of Cambridge Part II Genetics Project Report.
Tomchik, S.M., and Davis, R.L. (2009). Dynamics of Learning-Related cAMP Signaling and Stimulus Integration in the *Drosophila* Olfactory Pathway. Neuron 64, 510–521.
Treviño, M., Frey, S., and Köhr, G. (2012). Alpha-1 adrenergic receptors gate rapid orientation-specific reduction in visual discrimination. Cereb. Cortex 22, 2529–2541.
Trueta, C., and De-Miguel, F.F. (2012). Extrasynaptic exocytosis and its mechanisms: A source of molecules mediating volume transmission in the nervous system. Front. Physiol. 3 SEP, 1–19.
Vadodaria, K.C., Yanpallewar, S.U., Vadhvani, M., Toshniwal, D., Liles, L.C., Rommelfanger, K.S., Weinshenker, D., and Vaidya, V.A. (2017). Noradrenergic regulation of plasticity marker expression in the adult rodent piriform cortex. Neurosci. Lett. 644, 76–82.
Vankov, A., Hervé - Minvielle, A., and Sara, S.J. (1995). Response to Novelty and its Rapid Habituation in Locus Coeruleus Neurons of the Freely Exploring Rat. Eur. J. Neurosci. 7, 1180–1187.
Venken, K.J.T., Schulze, K.L., Haelterman, N. a, Pan, H., He, Y., Evans-Holm, M., Carlson, J.W., Levis, R.W., Spradling, A.C., Hoskins, R. a, et al. (2011a). MiMIC: a highly versatile transposon insertion resource for engineering *Drosophila* melanogaster genes. Nat. Methods 8, 737–743.
Venken, K.J.T., Simpson, J.H., and Bellen, H.J. (2011b). Genetic manipulation of genes and cells in the nervous system of the fruit fly. Neuron 72, 202–230.
Viswanathan, S., Williams, M.E., Bloss, E.B., Stasevich, T.J., Speer, C.M., Nern, A., Pfeiffer, B.D., Hooks, B.M., Li, W.P., English, B.P., et al. (2015). High-performance probes for light and electron microscopy. Nat. Methods 12, 568–576.
Vitzthum, H., and Homberg, U. (1998). Immunocytochemical demonstration of locustatachykinin-related peptides in the central complex of the locust brain. J. Comp. Neurol. 390, 455–469.
Vogt, K., Aso, Y., Hige, T., Knapek, S., Ichinose, T., Friedrich, A.B., Turner, G.C., Rubin, G.M., and Tanimoto, H. (2016). Direct neural pathways convey distinct visual information to *Drosophila* mushroom bodies. Elife 5, e14009.
Walkinshaw, E., Gai, Y., Farkas, C., Richter, D., Nicholas, E., Keleman, K., and Davis, R.L. (2015). Identification of genes that promote or inhibit olfactory memory formation in *Drosophila*. Genetics 199, 1173–1182.
Wan, B. A. (2015). University of Cambridge MPhil Thesis.
Wang, Y., Pu, Y., and Shen, P. (2013). Neuropeptide-gated perception of appetitive olfactory inputs in *Drosophila* larvae. Cell Rep. 3, 820–830.
Warbington, L., Hillman, T., Adams, C., and Stern, M. (1996). Reduced transmitter release conferred by mutations in the slowpoke-encoded Ca2+-activated K+ channel gene of *Drosophila*. Invertebr. Neurosci. 2, 51–60.
Watanabe, K., Chiu, H., Pfeiffer, B.D., Wong, A.M., Hoopfer, E.D., Rubin, G.M., and Anderson, D.J. (2017). A Circuit Node that Integrates Convergent Input from Neuromodulatory and Social Behavior-Promoting Neurons to Control Aggression in *Drosophila*. Neuron 95, 1112–1128.e7.
Williams, J.T., Henderson, G., and North, R.A. (1985). Characterization of a2-adrenoreceptors which increase potassium conducance in rat locus coeruleus neurones. Neuroscience 14, 95–101.
Wilson, D. a., and Stevenson, R.J. (2003). Olfactory perceptual learning: The critical role of memory in odor discrimination. Neurosci. Biobehav. Rev. 27, 307–328.
Wilson, D. a., and Sullivan, R.M. (2011). Cortical processing of odor objects. Neuron 72, 506–519.
Wilson, R.I., and Laurent, G. (2005). Role of GABAergic inhibition in shaping odor-evoked spatiotemporal patterns in the *Drosophila* antennal lobe. J. Neurosci. 25, 9069–9079.
Wong, A.M., Wang, J.W., and Axel, R. (2002). Spatial representation of the glomerular map in the *Drosophila* protocerebrum. Cell 109, 229–241.
Wong, J.Y.H. (2014). University of Cambridge MPhil Thesis.
Wu, C.L., Shih, M.F.M., Lee, P.T., and Chiang, A.S. (2013). An octopamine-mushroom body circuit modulates the formation of anesthesia-resistant memory in *Drosophila*. Curr. Biol. 23, 2346–2354.
Wu, S.F., Xu, G., Qi, Y.X., Xia, R.Y., Huang, J., and Ye, G.Y. (2014). Two splicing variants of a novel family of octopamine receptors with different signaling properties. J. Neurochem. 129,

37–47.
Xiao, R.-P. (2001). β-Adrenergic Signaling in the Heart: Dual Coupling of the 2-Adrenergic Receptor to Gs and Gi Proteins. Sci. Signal. 2001, re15-re15.
Xue, Z., Ren, M., Wu, M., Dai, J., Rong, Y.S., and Gao, G. (2014). Efficient Gene Knock-out and Knock-in with Transgenic Cas9 in *Drosophila*. G3: Genes|Genomes|Genetics 4, 925–929.
Yagi, R., Mabuchi, Y., Mizunami, M., and Tanaka, N.K. (2016). Convergence of multimodal sensory pathways to the mushroom body calyx in *Drosophila* melanogaster. Sci. Rep. 6, 29481.
Yang, Z., Yu, Y., Zhang, V., Tian, Y., Qi, W., and Wang, L. (2015). Octopamine mediates starvation-induced hyperactivity in adult *Drosophila*. Proc. Natl. Acad. Sci. 201417838.
Yi, F., Liu, S.-S., Luo, F., Zhang, X.-H., and Li, B.-M. (2013). Signaling mechanism underlying α 2A -adrenergic suppression of excitatory synaptic transmission in the medial prefrontal cortex of rats. Eur. J. Neurosci. 38, 2364–2373.
Yu, Z., Chen, H., Liu, J., Zhang, H., Yan, Y., Zhu, N., Guo, Y., Yang, B., Chang, Y., Dai, F., et al. (2014). Various applications of TALEN- and CRISPR/Cas9-mediated homologous recombination to modify the *Drosophila* genome. Biol. Open 3, 271–280.
Zhang, T., Branch, A., and Shen, P. (2013a). Octopamine-mediated circuit mechanism underlying controlled appetite for palatable food in *Drosophila*. Proc. Natl. Acad. Sci. U. S. A. 110, 15431–15436.
Zhang, Z., Cordeiro Matos, S., Jego, S., Adamantidis, A., and Séguéla, P. (2013b). Norepinephrine Drives Persistent Activity in Prefrontal Cortex via Synergistic α1 and α2 Adrenoceptors. PLoS One 8.
Zhang, J., Tan, L., Ren, Y., Liang, J., Lin, R., Feng, Q., Zhou, J., Hu, F., Ren, J., Wei, C., et al. (2016). Presynaptic Excitation via GABAB Receptors in Habenula Cholinergic Neurons Regulates Fear Memory Expression. Cell 166, 716–728.
Zheng, Z., Lauritzen, J.S., Perlman, E., Saalfeld, S., Fetter, R.D., and Bock Correspondence, D.D. (2018). A Complete Electron Microscopy Volume of the Brain of Adult *Drosophila* melanogaster. Cell 174, 1–14.
Zhou, C., Huang, H., Kim, S., and Lin, H. (2012). Molecular genetic analysis of sexual rejection: roles of octopamine and its receptor OAMB in *Drosophila* courtship conditioning. J. Neurosci. 32, 14281–14287.
Zhou, Y., Wang, J., Wen, H., Kucherovsky, O., and Levitan, I.B. (2002). Modulation of *Drosophila* Slowpoke Calcium-Dependent Potassium Channel Activity by Bound Protein Kinase A Catalytic Subunit. J. Neurosci. 22, 3855–3863.
Zhu, P.C., Thureson-Klein, Å., and Klein, R.L. (1986). Exocytosis from large dense cored vesicles outside the active synaptic zones of terminals within the trigeminal subnucleus caudalis: A possible mechanism for neuropeptide release. Neuroscience 19, 43–54.